

**Palaeosalinity change in the Taw Estuary, south-west England:
response to late Holocene river discharge
and relative sea-level change**

*submitted by Glenn Michael Havelock to the University of Exeter
as a thesis for the degree of Doctor of Philosophy in Geography,
January 2009.*

*This thesis is available for Library use on the understanding that it is copyright
material and that no quotation from the thesis may be published without
proper acknowledgment.*

*I certify that all material in this thesis which is not my own work has been identified and
that no material is included for which a degree has previously been conferred upon me.*

Glenn Havelock

.....

ABSTRACT

Present models of Holocene estuary evolution are driven largely by changes in relative sea-level (RSL) with little reference to long-term changes in fluvial regime and regional climate. Recent US studies of estuarine sequences have shown that decadal-centennial scale fluctuations in river discharge and freshwater inflow can be inferred by changes in estuarine palaeosalinity and that the timing of these events reflect changes in regional precipitation. It is therefore becoming apparent that estuarine sequences may hold an archive of mid-late Holocene climate change information, as well as being recorders of RSL change.

The principal aim of this study is to produce a palaeosalinity-based climate record for southern England during the late Holocene, based on changes in climate-driven freshwater influx into the estuarine environment. The late Holocene palaeosalinity record of the inner Taw Estuary will be reconstructed using diatom salinity index as a proxy for salinity. Nine periods of below-average or above-average palaeosalinity have been recognised in the Taw Estuary since 300 cal.yr.BC. Four intervals of high river discharge are identified at 520-780, 850-1030, 1215-1315, and 1420-1900 cal.yr.AD. Five intervals of low river discharge are identified at 300-520, 780-850, 1030-1215, 1315-1420, and 1900-2000 cal.yr.AD. This shows that there has been significant climatic variation in southern Britain since *c.*300 cal.yr.AD, with climatic shifts evident in the estuarine record. In order to validate this record, the fluvial geomorphic history of the lower Taw valley was also investigated. There is a strong correspondence between the dry and wet climatic periods identified in the estuary and the geomorphic fluvial history and flood record of the lower Taw valley. Comparisons with other proxy climate records in the UK and Europe show a high degree of correspondence with the Taw Estuary palaeosalinity-based climate record.

As the inner estuary environment will also be influenced by RSL change during the late Holocene, RSL change since *c.*6600 cal.yr.BP was successfully reconstructed in the Taw Estuary, with eleven new validated SLIPs providing evidence of former MSL. The magnitude and rates of RSL rise in north Devon are compared with other RSL records in southern Britain, suggesting that the isostatic history is similar to other areas bordering the Bristol Channel and with the central south coast of England. Fluctuations in palaeosalinity in the late Holocene are seen to be mainly controlled by centennial-scale changes in climate-driven river discharge, rather than RSL change.

ACKNOWLEDGMENTS

My research at the University of Exeter (Department of Geography) could not have happened without the very considerable support of many individuals, in so many ways.

My supervisors Prof Tony Brown and Dr Jason Jordan gave valuable professional help and encouragement throughout for which I am truly grateful. Personal advice and helpful discussions came from Prof John Allen (University of Reading) and Prof Antony Long (University of Durham). I would like to thank the technical staff in the Department of Geography at Exeter, for their valuable advice and technical assistance, especially from Jim Grapes, Sue Frankling, Angela Elliot, Neville England, Mike Rouillard (Department of Archaeology) and Terry Bacon. I would also like to thank Helen Jones and Tracey Reeves for their administrative support throughout my time at Exeter.

I would like to thank the University of Exeter for the provision of a three-year departmental scholarship, for which I am truly grateful. Much appreciated funding for the OSL dating programme came via grants awarded from the QRA-RLAHA Luminescence Dating Award (this award is run collaboratively by the Quaternary Research Association and the Research Laboratory for Archaeology and the History of Art at Oxford University) and the British Society for Geomorphology Postgraduate Research Fund. Much appreciated funding for the radiocarbon dating programme came via the substantial support from a NERC Radiocarbon Dating grant (Allocation Number: 1213.0207) and from funding by Devon County Council Archaeological Service (this fund was used for rangefinder dates; many thanks to Frances Griffith, County Archaeologist, and her colleague Bill Horner). Special thanks go to Dr Jean-Luc Schwenninger, at the University of Oxford RLAHA Luminescence Dating Laboratory, for his support, encouragement and provision of additional OSL dates. I also thank Jean-Luc and his technician David Peat for the training given in OSL sample preparation and for their help in OSL sample recovery from the UH1 field site.

I would like to thank Dr Kevin White (Department of Geography, University of Reading) for the use of their Mineral Magnetism Laboratory and for the practical training, advice and support that he gave. Thanks again go to Frances Griffith for access to the Devon County Council Archaeological Service aerial photograph collection

(invaluable in the early desk study) and the Devon Sites and Monuments Register. I thank Edina Digimap/Ordnance Survey for supply of digitised map data and I am also grateful to the NERC British Isles GPS Archive Facility (BIGF) for supply of archive GPS RINEX data (used in the modern estuary survey).

In terms of field work, I am very grateful for the generous time and help (coring in all weather!) given by so many Exeter colleagues. Many thanks go to Jason Jordan, Mark Dinnin, Laura Basell, Chris Carey, Rob Stroud, Phil Allen, Ben Thomas, Jenny Bennett, Paul Clark, Naomi Holmes, Lucy Clarke, Steve Davis, and Lynda Yorke (University of Aberystwyth). Of these, I thank Laura Basell, Chris Carey and also Chris Smart (Department of Archaeology) for help with the differential GPS survey and post-processing, and thank Chris Carey and Phil Allen for the help with the Geoprobe (much fun!). And most especially, my thanks go to the various landowners who generously allowed me access to their land in the lower Taw Valley, especially Colonel Maxse who took particular interest in the project.

I would also like to thank Dr Klaus Kuhn for taking me on as his teaching assistant for so many years, and for his general support and good humour; and I thank my work colleagues at the University of Exeter Library (the shelving team!) for the many good hours together.

I owe a particular debt and thanks to my parents, for their invaluable support throughout my education. And last but by no means least, my heartfelt gratitude to my wife Caryn, who together with our sons Samuel and Jacob, was so patient, supportive and enduring throughout.

G.M.H.

CONTENTS LIST

	<i>Page</i>
ABSTRACT	2
ACKNOWLEDGMENTS	3
LIST OF CONTENTS	5
LIST OF FIGURES	12
LIST OF TABLES	17
1. INTRODUCTION.....	18
1.1 BACKGROUND TO RESEARCH	18
1.2 AIMS AND OBJECTIVES	19
1.3 STUDY AREA	22
2. ESTUARINE EVOLUTION AND PALAEO-SALINITY	26
3. METHODOLOGY	32
3.1 GEOMORPHOLOGICAL MAPPING	32
3.2 STRATIGRAPHIC TRANSECTS	32
3.3 CORE RECOVERY AND FIELD SAMPLING	34
3.4 CORE ANALYSIS	34
3.4.1 Core description	34
3.4.2 Sediment sub-sampling	35
3.4.3 Organic matter and carbonate content	35
3.4.4 Magnetic susceptibility	36
3.4.5 Magnetic remanence	39
3.4.6 Diatom analysis	42
3.5 CHRONOLOGICAL FRAMEWORK	43
3.5.1 Radiocarbon dating	43
3.5.2 Optically stimulated luminescence (OSL) dating	46
3.6 RELATIVE SEA-LEVEL RECONSTRUCTION	50
3.7 CONTEMPORARY DIATOM DISTRIBUTION	53
3.8 DATA ANALYSIS	56
3.8.1 Analysis of the modern dataset	56
3.8.2 Analysis of the Holocene dataset	56

4	CONTEMPORARY DIATOM DISTRIBUTION IN THE TAW ESTUARY AND THE LOWER TAW VALLEY	58
4.1	INTRODUCTION	58
4.1.1	Taw Estuary survey	58
4.1.2	River Taw survey	60
4.2	TAW ESTUARY	61
4.2.1	Taw Estuary transect	61
4.2.2	Contemporary diatom distribution and environmental variables	69
4.2.3	Altitude and diatom salinity index	80
4.3	RIVER TAW	82
4.3.1	River Taw transect	82
4.3.2	Salinity	89
4.3.3	Sedimentary environmental variables	91
4.3.4	Contemporary diatom distribution	94
4.3.5	Limitations of River Taw dataset in palaeosalinity reconstruction	98
5	LITHO- AND BIO-STRATIGRAPHY OF THE INNER TAW ESTUARY: A HOLOCENE RECORD OF GEOMORPHIC AND ENVIRONMENTAL CHANGE	100
5.1	INTRODUCTION	100
5.1.1	Chapter objectives	100
5.1.2	Floodplain sediment units	102
5.1.3	Geomorphology of the inner Taw Estuary and location of transects ..	103
5.1.4	Legends for sedimentary sections and core logs	106
5.1.5	Radiocarbon and luminescence dates	106
5.2	GEOMORPHOLOGY AND STRATIGRAPHY OF THE PILL LANE REACH	110
5.2.1	Reach geomorphology	110
5.2.2	Lithostratigraphy of the Pill Lane transect	112
5.2.3	PL1 core	115
	Sedimentology	115
	Geochronology	119
	Magnetic properties	120
	Diatom analysis	128
5.2.4	PL2 core	151

	Sedimentology and magnetic properties	151
	Geochronology	152
	Diatom analysis	153
5.2.5	PL3core	156
	Sedimentology and magnetic properties	156
	Geochronology	157
	Diatom analysis	158
5.2.6	PL4 core	160
	Sedimentology and magnetic properties	160
5.2.7	PL5 core	162
	Sedimentology and magnetic properties	162
5.2.8	Phases of geomorphic and environmental change in the Pill Lane reach	164
5.3	GEOMORPHOLOGY AND STRATIGRAPHY OF THE TAWSTOCK REACH	172
5.3.1	Reach geomorphology	172
5.3.2	Lithostratigraphy of the Tawstock transect	172
5.3.3	TS1 core	176
	Sedimentology	176
	Geochronology	178
	Magnetic properties	179
	Diatom analysis	186
5.3.4	TS2 core	193
	Sedimentology and magnetic properties	193
	Geochronology	195
	Diatom analysis	195
5.3.5	TS3 core	199
	Sedimentology and magnetic properties	199
5.3.6	CF1 core	201
	Sedimentology and magnetic properties	201
	Geochronology	202
	Diatom analysis	203
5.3.7	CF2 core	205
	Sedimentology and magnetic properties	205
	Geochronology	207

	Diatom analysis	207
5.3.8	CH1 core	211
	Sedimentology and magnetic properties	211
	Geochronology	213
5.3.9	Phases of geomorphic and environmental change in the Tawstock reach	213
5.4	GEOMORPHOLOGY AND STRATIGRAPHY OF THE NEW BRIDGE REACH	219
5.4.1	Reach geomorphology	219
5.4.2	Lithostratigraphy of the Straypark Wood transect	219
5.4.3	SW1 core	223
	Sedimentology	223
	Geochronology	225
	Magnetic properties	225
	Diatom analysis	230
5.4.4	SW2 core	235
	Sedimentology and magnetic properties	235
	Geochronology	237
	Diatom analysis	237
5.4.5	SW3 core	241
	Sedimentology and magnetic properties	241
	Geochronology	243
	Diatom analysis	243
5.4.6	SW4 core	245
	Sedimentology and magnetic properties	245
	Geochronology	247
	Diatom analysis	247
5.4.7	Lithostratigraphy of the New Bridge transect	250
5.4.8	NB1 core	252
	Sedimentology and magnetic properties	252
	Diatom analysis	254
5.4.9	NB2 core	257
	Sedimentology and magnetic properties	257
	Geochronology	258
	Diatom analysis	258

5.4.10 NB3 core	261
Sedimentology and magnetic properties	261
Geochronology	263
Diatom analysis	263
5.4.11 NB4 core	266
Sedimentology and magnetic properties	266
Geochronology	267
Diatom analysis	268
Phases of geomorphic and environmental change in the New Bridge reach	270
Straypark Wood transect	270
New Bridge transect	273
6. LITHO- AND BIO-STRATIGRAPHY OF THE NON-TIDAL TAW VALLEY: A HOLOCENE RECORD OF GEOMORPHIC AND ENVIRONMENTAL CHANGE UPSTREAM OF THE TIDAL HEAD	277
6.1 INTRODUCTION	277
6.1.1 Chapter objectives	277
6.1.2 Geomorphology of the non-tidal River Taw and location of transects	278
6.1.3 Legend for sedimentary sections	280
6.1.4 Radiocarbon and luminescence dates	280
6.2 GEOMORPHOLOGY AND STRATIGRAPHY OF THE BRIDGETOWN REACH	283
6.2.1 Reach geomorphology	283
6.2.2 Lithostratigraphy of the Bridgetown transect	286
6.2.3 BT1 core	288
Sedimentology and magnetic properties	288
Geochronology	288
Diatom analysis	289
6.2.4 BT2 core	291
Sedimentology and magnetic properties	291
6.2.5 Lithostratigraphy of the Chapelton transect	292
6.2.6 CT1 core	294
Sedimentology and magnetic properties	294

	Geochronology	294
	Diatom analysis	296
6.2.7	Brackish groundwater intrusion in the Bridgetown reach	298
6.3	GEOMORPHOLOGY AND STRATIGRAPHY OF THE YEOTOWN REACH	300
6.3.1	Reach geomorphology	300
6.3.2	Lithostratigraphy of the Yeotown transect	302
6.3.3	YW1 core	305
	Sedimentology and magnetic properties	305
	Geochronology	305
	Diatom analysis	305
6.3.4	YE1 core	308
	Sedimentology and magnetic properties	308
	Geochronology	309
	Diatom analysis	309
6.3.5	YE2 core	311
	Sedimentology and magnetic properties	311
	Geochronology	311
	Diatom analysis	312
6.3.6	Brackish groundwater intrusion in the Yeotown reach	314
6.4	GEOMORPHOLOGY AND STRATIGRAPHY OF THE UMBERLEIGH HOUSE REACH	315
6.4.1	Reach geomorphology	315
6.4.2	Lithostratigraphy of the Horestone transect	317
6.4.3	HS1 core	320
	Sedimentology and magnetic properties	320
	Geochronology	321
	Diatom analysis	321
6.4.4	HS2 core	323
	Sedimentology and magnetic properties	323
	Geochronology	324
	Diatom analysis	324
6.4.5	Lithostratigraphy of the Umberleigh House transect	326
6.4.6	UH1 core	328
	Sedimentology and magnetic properties	328

Geochronology	330
6.4.7 UH2 core	330
Sedimentology and magnetic properties	330
Diatom analysis	331
6.4.7 Brackish groundwater intrusion in the Umberleigh House reach	333
7. RESULTS SYNTHESIS: STRATIGRAPHY, CHANNEL CHANGE HISTORY, RELATIVE SEA-LEVEL CHANGE AND PALAEOSALINITY	334
7.1 STRATIGRAPHIC ARCHITECTURE	334
7.2 LATE HOLOCENE PERIODS OF FLUVIAL FLOODING AND CHANNEL CHANGE	344
7.3 RELATIVE SEA-LEVEL CHANGE IN THE TAW ESTUARY DURING THE MID-LATE HOLOCENE	345
7.4 ESTUARINE PALAEOSALINITY CHANGE DURING LATE HOLOCENE	349
8. DISCUSSION	357
8.1 MID-LATE HOLOCENE RELATIVE SEA-LEVEL CHANGE IN THE TAW ESTUARY	357
8.2 LATE HOLOCENE PALAEOSALINITY CHANGE: IMPLICATIONS FOR RIVER DISCHARGE AND CLIMATE CHANGE	366
9. CONCLUSIONS	384
APPENDIX	389
BIBLIOGRAPHY	390

LIST OF FIGURES

	<i>Page</i>
Figure 1.1	Map of the lower River Taw catchment and Taw Estuary 24
Figure 2.1	Dalrymple <i>et al.</i> (1992) model of a tide-dominated estuary 27
Figure 2.2	Schematic section along the axis of a tide-dominated estuary 28
Figure 2.3	Core log from the San Francisco Estuary showing changes in Diatom Salinity Index 29
Figure 3.1	Hand coring and recovery of the PL1 core 35
Figure 3.2	Geoprobe with raised hydraulic hammer 47
Figure 3.3	Excavated OSL pit at UH1 palaeochannel site 48
Figure 3.4	Following removal of the OSL sample from section face, moisture content sample was recovered 48
Figure 3.5	TS1 core showing transgressive overlap with salt-marsh silty clay deposited on top of fenwood peat 50
Figure 4.1	Location of the Taw Estuary transects, 3 km west of Barnstaple .. 62
Figure 4.2	Photographs of the middle and high saltmarsh zones, Estuary South transect 63
Figure 4.3	Photographs of the Estuary North transect and low saltmarsh zone, Estuary South transect 64
Figure 4.4	Photograph of the Taw Estuary study site 65
Figure 4.5	Profile of Estuary South transect with location of sampling stations 66
Figure 4.6	Profile of Estuary North transect with location of sampling stations 67
Figure 4.7	Diatom diagram for the Taw Estuary transects (>3%TDV spp.)... 70
Figure 4.8	Diatom diagram for the Taw Estuary transects (>3%TDV spp.)... 76
Figure 4.9	Diatom salinity index and tidal frame position in Taw Estuary transects 81
Figure 4.10	Location of sampling stations R1 to R11 in the tidal River Taw zone upstream of Barnstaple 83
Figure 4.11	Location of sampling stations R11 to R17 in the largely non-tidal River Taw zone 84
Figure 4.12	Photographs of contemporary River Taw sampling stations 86
Figure 4.13	Longitudinal section of the lower River Taw showing relation- ship between sampling station altitudes (R1 to R17) and tidal

	frame levels	88
Figure 4.14	Longitudinal section of the lower River Taw showing relationship between sampling station location (R1 to R17) and maximum salinity	90
Figure 4.15	Diatom diagram for the River Taw transect (>3% TDV spp.) showing assemblage changes with up-river distance from Barnstaple Long Bridge	93
Figure 5.1	Geomorphology of the tidal River Taw zone upstream of Barnstaple	104
Figure 5.2	(a) Legend for diatom and magnetics diagram lithology logs; (b) Legend for lithostratigraphic transect sections; (c) Legend for core lots	107
Figure 5.3	Geomorphology of the Pill Lane reach	111
Figure 5.4	Lithostratigraphy of the Pill Lane transect	113
Figure 5.5	Detailed lithostratigraphy of the western end of transect A (Pill Lane transect)	114
Figure 5.6	PL1 core log	116
Figure 5.7	Magnetic characteristics of PL1 core	121
Figure 5.8	Diatom diagram for PL1 core (>5% TDV spp.)	129
Figure 5.9	PL2 core log	152
Figure 5.10	Diatom diagram for PL2 core (>3% TDV spp.)	154
Figure 5.11	PL3 core log	157
Figure 5.12	Diatom diagram for PL3 core	159
Figure 5.13	PL4 core log	161
Figure 5.14	PL5 core log	162
Figure 5.15	Transect A (Pill Lane transect)	164
Figure 5.16	Floodplain Sediment Units in the vicinity of PL1 (Transect A)....	165
Figure 5.17	Geomorphology of the Tawstock reach	173
Figure 5.18	Lithostratigraphy of transect B (Tawstock transect)	174
Figure 5.19	TS1 core log	176
Figure 5.20	Magnetic characteristics of TS1 core	180
Figure 5.21	Diatom diagram for TS1 core (>3% TDV spp.)	187
Figure 5.22	TS2 core log	194
Figure 5.23	Diatom diagram for TS2 core (>3% TDV spp.)	196
Figure 5.24	TS3 core log	200

Figure 5.25	CF1 core log	202
Figure 5.26	Diatom diagram for CF1 core (>3% TDV spp.)	204
Figure 5.27	CF2 core log	206
Figure 5.28	Diatom diagram for CF2 core (>3% TDV spp.)	208
Figure 5.29	TS3 core log	212
Figure 5.30	Transect B (Tawstock transect)	214
Figure 5.31	Geomorphology of the New Bridge reach	220
Figure 5.32	Lithostratigraphy of transect C (Straypark Wood transect)	221
Figure 5.33	SW1 core log	224
Figure 5.34	Magnetic characteristics of SW1 core and resulting magnetic zones	226
Figure 5.35	Diatom diagram for SW1 core (>3% TDV spp.)	231
Figure 5.36	SW2 core log	236
Figure 5.37	Diatom diagram for SW2 core (>3% TDV spp.)	238
Figure 5.38	SW3 core log	242
Figure 5.39	Diatom diagram for SW3 core (>3% TDV spp.)	244
Figure 5.40	SW4 core log	246
Figure 5.41	Diatom diagram for SW4 core (>3% TDV spp.)	248
Figure 5.42	Lithostratigraphy of transect D (New Bridge transect)	251
Figure 5.43	NB1 core log	253
Figure 5.44	Diatom diagram for NB1 core (>3% TDV spp.)	255
Figure 5.45	NB2 core log	257
Figure 5.46	Diatom diagram for NB2 core (>3% TDV spp.)	259
Figure 5.47	NB3 core log	262
Figure 5.48	Diatom diagram for NB3 core (>3% TDV spp.)	264
Figure 5.49	NB4 core log	267
Figure 5.50	Diatom diagram for NB4 core (>3% TDV spp.)	269
Figure 5.51	Transect C (Straypark Wood transect) Floodplain Sediment Units	271
Figure 5.52	Transect D (New Bridge transect) Floodplain Sediment Units.....	274
Figure 6.1	Geomorphology of the non-tidal River Taw zone	279
Figure 6.2	Legend for lithostratigraphic transect sections in Chapter 6	280
Figure 6.3	Geomorphology of the Bridgetown reach	284
Figure 6.4	Lithostratigraphy of the Bridgetown transect	287
Figure 6.5	BT1 core log	289
Figure 6.6	Diatom diagram for BT1 core (>3% TDV spp.)	290

Figure 6.7	BT2 core log	292
Figure 6.8	Lithostratigraphy of the Chapelton transect	293
Figure 6.9	CT1 core log	295
Figure 6.10	Diatom diagram for CT1 core (3% TDV spp.)	297
Figure 6.11	Geomorphology of the Yeotown reach	301
Figure 6.12	Lithostratigraphy of the Yeotown transect	303
Figure 6.13	YW1 core log	306
Figure 6.14	Diatom diagram for YW1 core (>3% TDV spp.)	307
Figure 6.15	YE1 core log	308
Figure 6.16	Diatom diagram for YE1 core (>3% TDV spp.)	310
Figure 6.17	YE2 core log	312
Figure 6.18	Diatom diagram for YE2 core (>3% TDV spp.)	313
Figure 6.19	Geomorphology of the Umberleigh House reach	316
Figure 6.20	Lithostratigraphy of the Horestone transect	318
Figure 6.21	HS1 core log	320
Figure 6.22	Diatom diagram for HS1 core (>3% TDV spp.)	322
Figure 6.23	HS2 core log	323
Figure 6.24	Diatom diagram for HS2 core (>3% TDV spp.)	325
Figure 6.25	Lithostratigraphy of the Umberleigh House transect	327
Figure 6.26	UH1 core log	329
Figure 6.27	UH2 core log	331
Figure 6.28	Diatom diagram for UH2 core (>3% TDV spp.)	332
Figure 7.1	Stratigraphic units for the lower Taw Valley and inner Taw Estuary	335
Figure 7.2	Presence of stratigraphic units in each of the nine litho- stratigraphic valley sections (transects A to I)	336
Figure 7.3	Chrono-stratigraphic distribution of late Holocene radiocarbon And OSL dates	337
Figure 7.4	Stratigraphy of transects A, B and C	338
Figure 7.5	Stratigraphy of transects D, E and F	339
Figure 7.6	Stratigraphy of transects G, H and I	340
Figure 7.7	Late Holocene flood record for the Taw valley	344
Figure 7.8	Relative sea-level curve for the Taw estuary showing changes in the altitude of MHWST	348
Figure 7.9	Late Holocene DSI-based palaeosalinity change in transect A ...	352

Figure 7.10	Late Holocene DSI-based palaeosalinity change in transect B ...	353
Figure 7.11	Late Holocene DSI-based palaeosalinity change in transect C ...	354
Figure 7.12	DSI-based palaeosalinity change in the Taw Estuary during the Late Holocene (transects A, B and C)	355
Figure 7.13	Late Holocene periods of high (more marine) and low (less marine) palaeosalinity in the Taw Estuary	356
Figure 8.1	Sea-level index points for the Taw Estuary and Bristol Channel/ Severn Estuary plotted against mean sea-level.	358
Figure 8.2	DSI-based palaeosalinity change in the Taw Estuary during the Late Holocene (transects A, B and C) and inferred palaeoclimate periods	367
Figure 8.3	Regional composite water table record for northern Britain during the last 4500 yrs	371
Figure 8.4	Comparison between the number of Irish Scots pine, oak tree populations and mean bog oak ages	372
Figure 8.5	Holocene proxy climate records from the North Atlantic and Europe	375

LIST OF TABLES

		<i>Page</i>
Table 3.1	Magnetic domains and typical grain size	38
Table 3.2	Interpretation of frequency dependent susceptibility values	38
Table 3.3	Mineral magnetic parameters used in identification of magnetic components	41
Table 3.4	Indicative range and indicative meaning for commonly dated materials	52
Table 4.1	Tidal frame levels for Barnstaple	68
Table 4.2	Planktonic diatom salinity tolerance classification	91
Table 5.1	Radiocarbon dates for transects A to D, tidal River Taw	108
Table 5.2	OSL dates for transects A to D, tidal River Taw	109
Table 5.3	Dominant diatom species in PL1	130
Table 6.1	Radiocarbon dates for transects E to I, the non-tidal River Taw	281
Table 6.2	OSL dates for transects E to I, the non-tidal River Taw	282
Table 7.1	Sea-level index points (SLIPs) for the inner Taw Estuary	346
Table 7.2	Indicative meaning and indicative range of overlaps encountered in Taw Estuary stratigraphy	347
Table 7.3	Errors associated with determining elevation and indicative meaning of SLIPS in this study	347
Table 7.4	Samples used in palaeosalinity reconstruction	350
Table 8.1	Taw Estuary SLIPs (MSL) with tidal range corrections	360
Table 8.2	Late Holocene river discharge levels and associated climatic periods inferred from the DSI palaeosalinity record	368
Table 8.3	Holocene river flooding episodes in Great Britain since 2500 cal.yr.BP	372

1 INTRODUCTION

1.1 BACKGROUND TO RESEARCH

Models of Holocene estuary evolution have so far been driven largely by changes in relative sea-level (RSL) (*e.g.* Allen, 1990, 2003; Fletcher *et al.*, 1990; Long, 2000), with little reference, if any, to long-term changes in fluvial regime. This is surprising as estuarine deposition is known to be controlled by both marine and fluvial processes (Dalrymple *et al.*, 1992; Allen and Posamentier, 1993). Centennial scale climate change has been shown to have a major control on Holocene river behaviour, with fluvial records showing evidence for a high sensitivity of flood occurrence to changing climate (*e.g.* Knox, 1985, 1993, 2003; Rumsby and Macklin, 1996; Brown, 1998; Macklin and Lewin, 1993, 2003; Maddy *et al.*, 2003; Macklin *et al.*, 2005, 2006). For example, Macklin *et al.* (2005) identified sixteen major periods of flooding in the UK since 11,160 cal.yr.BP, with a strong correspondence between flood episodes and climatic deteriorations inferred from proxy climate records (*e.g.* mire wet shifts). It follows that the changes in river discharge associated with these climatic fluctuations and periods of fluvial instability or stability should have an important bearing on estuarine hydrology, sedimentology and stratigraphy, especially in the inner estuarine zone. Indeed, recent studies in San Francisco Bay (Ingram *et al.*, 1996; Bryne *et al.*, 2001, Malamud-Roam *et al.*, 2006) and Chesapeake Bay (Cronin *et al.*, 2000, 2005) in the US and in the Pearl River Estuary, southern China (Zong *et al.*, 2006) have shown that Holocene changes in river discharge and freshwater influx can be inferred by changes in estuarine palaeosalinity and that the timing of these events reflect changes in regional precipitation. It is therefore becoming apparent that estuarine sequences may hold an archive of mid/late Holocene climate change information, as well as being recorders of RSL change.

The only significant palaeosalinity reconstruction done in a UK estuary is the diatom-based study by Juggins (1992) in the Thames Estuary. However, this study was based on a limited number of archaeological samples and the tentative conclusions related salinity to RSL change and human induced changes in tidal range (bridges and embankments), ignoring possible river discharge changes. There is therefore an opportunity to undertake the first palaeosalinity reconstruction in a UK estuary, with the

aim of extracting a precipitation-driven river discharge record of climate change during the late Holocene. Other proxy climate records (*e.g.* mire wet shifts and tree ring records) have shown that the late Holocene has been climatically unstable on a centennial scale, containing such periods as the Little Ice Age and the Medieval Warm Period. Processes such as the North Atlantic Oscillation (NAO) are also a major source of multidecadal (*c.*60-70 years; Delworth and Mann, 2000) climate variability in the North Atlantic region. Improvements in our knowledge of natural climate variability (multi-decadal to centennial scale) from the last 2000 years would therefore put recent 20th Century climate variability into context. As estuarine palaeosalinity is also effected by changes in RSL, a UK investigation of discharge-driven palaeosalinity changes during the last 2000-3000 years benefits from relatively low rates of RSL rise during this period. For example, in southwest England, where the present study takes place, there has been *c.*2.0 m of RSL rise during this period (Massey *et al.*, 2008).

There is also a need to improve our understanding of the geomorphic effect of centennial scale changes in river discharge on the stratigraphy and sedimentary record of the inner estuarine environment. Current sequence stratigraphic facies models of Holocene estuary evolution (*e.g.* Dalrymple *et al.*, 1992) do not incorporate sedimentary responses to cyclic long-term changes in river discharge, despite acknowledging that estuaries are effected by both marine and fluvial processes.

1.2 AIMS AND OBJECTIVES

The principal aim of this study is to produce a palaeosalinity based climate record for the late Holocene, based on changes in climate-driven freshwater influx into the estuarine environment. The late Holocene palaeosalinity record of the inner Taw Estuary will be reconstructed using diatom salinity index (ratio of fresh and brackish species to marine species) as a proxy for salinity (Bryne *et al.*, 2001). In addition to freshwater river discharge, estuarine palaeosalinity will be controlled by centennial-millennial scale changes in RSL. This study will therefore also investigate correlations between RSL change and palaeosalinity. This will be done by reconstructing RSL change in the Taw Estuary using the traditional qualitative litho-stratigraphic approach (Shennan, 1982, 1986; Tooley, 1982; Shennan *et al.*, 1983), with diatom biostratigraphy providing evidence of changes in marine influence at transgressive and

regressive overlaps. Examples of qualitative RSL studies using diatoms include Shennan *et al.* (1995, 2000a); Hemphill-Haley (1995); Zong and Tooley (1996); Zong (1997, 1998); Long *et al.* (1998, 2008); Smith *et al.* (2003); Gehrels *et al.* (2006); Selby and Smith (2007). Correlations between estuarine palaeosalinity and the local fluvial geomorphic record will also be determined so as to identify palaeosalinity-climate correlations. This investigation will identify (and date) phases of active channel change during the late Holocene (*e.g.* Rumsby and Macklin, 1996; Brown, 1998; Taylor *et al.*, 2000; Howard *et al.*, 2004) and will be the first study of its kind in the River Taw catchment. The palaeosalinity record will also be compared with other proxy climate records from Britain and Europe (*e.g.* Nesje *et al.*, 2000; Bond *et al.*, 2001; Leuschner *et al.*, 2002; Magney *et al.*, 2003; Macklin *et al.*, 2005, 2006; Turney *et al.*, 2005; Charman *et al.*, 2006)

A secondary aim of this study is to investigate the influence of RSL rise and centennial-scale changes in river discharge on the geomorphic evolution of an inner estuarine and fluvio-estuarine environment (see Blum and Tornqvist, T.E., 2000 for a review of the effects of climate and RSL on the lower fluvial zone).

In order to meet these aims, the objectives of this study are as follows:

1. Contemporary zonation of diatoms and environmental variables in the tidal frame

(1a) Determine the relationship between contemporary diatom assemblages and tidal frame position in the Taw Estuary. This will provide a local qualitative contemporary analogue of diatom species distribution and altitudinal zonation. The development of a quantitative transfer function, to statistically quantify the relationship between modern diatom assemblages and elevation (*e.g.* Zong and Horton, 1999; Gehrels *et al.*, 2001; Sawai, *et al.*, 2004; Hamilton and Shennan, 2005; Horton *et al.*, 2006, 2007; Szkornik *et al.*, 2006; Hill *et al.*, 2007; Nelson *et al.*, 2008; Kemp *et al.*, 2009) was deemed beyond the scope of this multi-faceted study and was not attempted.

(1b) Determine the relationship between elevation in the tidal frame and a range of environmental variables, including salinity, vegetation cover, pH, sediment organic matter content, sediment mineralogy (specifically carbonate and magnetic mineral concentration), and sediment grain size (*e.g.* Rijk and Troelstra, 1997; Zong and Horton,

1998; Horton, 1999; Horton *et al.*, 1999; Sawai, *et al.*, 2004).

(1c) Explore the relationship between DSI (diatom salinity index) and elevation in the tidal frame. DSI is not to be used as an indicator of elevation in the core records. The purpose is to determine which environmental zones (*e.g.* high saltmarsh) in the tidal frame show very similar DSI (*i.e.* the least variation). This is to reduce errors in the palaeosalinity reconstruction (see objective 4d) when these zones will be compared for salinity changes.

2. Relative sea-level reconstruction

(2a) Identify inner estuarine marsh deposits that have high potential in RSL reconstruction and recover one or two sediment cores for analysis.

(2b) Determine the age of all transgressive and regressive overlaps (Shennan, 1982; Tooley, 1982) in these cores using radiocarbon dating.

(2c) Reconstruct mid-late Holocene RSL change in the Taw Estuary using the traditional qualitative litho-stratigraphic method (Shennan, 1982, 1986; Tooley, 1982; Shennan *et al.*, 1983), with diatom bio-stratigraphy providing evidence of changes in marine influence at transgressive and regressive overlaps.

3. The contemporary salinity gradient and diatom distribution

(3a) Determine the high tide salinity gradient for the inner Taw Estuary and determine the up-valley limits of marine influence, including the limit of saline tidal water (salinity front), the tidal head (limit to freshwater tidal zone) during HAT (highest astronomical tide) conditions, and the up-valley limits of saline groundwater intrusion. This framework would enable the late Holocene palaeosalinity record to be put into context.

(3b) Determine the contemporary distribution of diatom species along the salinity gradient of the Taw Estuary, including upstream of the tidal head. In the tidal zone, samples would be taken from a similar elevation in the tidal frame to ensure salinity, rather than elevation, was the major control on assemblage composition.

(3c) Establish the relationship between location in the salinity gradient and a range of sedimentary variables, including organic matter content, carbonate content and magnetic mineral concentration.

4. Palaeosalinity reconstruction

4(a) Recover a series of sediment cores from different locations along the salinity gradient of the inner Taw Estuary, and from the lower fluvial zone (as this zone may have experienced former marine incursions and may record changes in marine groundwater intrusion). These cores would also be used in objective 5 (see below).

(4b) Determine the age of these cores using radiocarbon and optically stimulated luminescence (OSL) methods.

(4c) Identify former tidal frame elevations within the core stratigraphy. This would be done for all cores in the tidal zone and would be based on diatom assemblage composition. The interpretation of former elevation would be based on the diatom zonation seen in the Taw Estuary and in other UK estuaries. Sedimentary evidence of former tidal frame elevation would be used to support this task.

(4d) Reconstruct late Holocene temporal and spatial changes in palaeosalinity, using DSI as a proxy for salinity. Specific tidal frame environments (*e.g.* high saltmarsh or mid saltmarsh) would be analysed separately for changes in palaeosalinity. This would ensure that differences in DSI reflect differences in salinity, rather than tidal frame position.

(4e) Use magnetic mineral assemblage characteristics in sediment cores as a proxy indicator of marine influence and sediment source. This will provide information about location in the salinity gradient at the time of deposition (Oldfield *et al.*, 2003).

5. Geomorphic evolution and fluvial flood record

(5a) Map the geomorphology of the inner estuary and lower fluvial zones.

(5b) Determine the Holocene litho-stratigraphy of the inner estuary and lower fluvial zones through a series of cross-valley auger transects.

(5c) Investigate Holocene geomorphic and environmental change in the inner estuarine and fluvio-estuarine (transitional) zones.

(5d) Identify (and date) phases of active channel change and fluvial instability during the late Holocene.

1.3 STUDY AREA

The initial phase of this study involved the search for a suitable study area in one of the

coastal river valleys of southwest England. Many of the rivers in the region were assessed, including the rivers Exe, Tamar, Otter, Teign, Dart, Fowey, Fal, Camel, Parrett, Torridge and Taw. The potential study reach needed to encompass the inner estuarine and lower fluvial zones, contain a sedimentary record covering the whole of the mid-late Holocene, and contain geomorphological evidence of phases of channel change and instability (*e.g.* Holocene river terraces and palaeochannels) during this period. The inner or middle estuary also needed to contain areas of un-reclaimed saltmarsh that could be used in the investigation of contemporary diatom distribution. As the preservation potential of older deposits is reduced in smaller confined valleys with actively migrating channels (Lewin and Macklin, 2003), the three largest rivers were prioritised. These were the Rivers Exe, Torridge and Taw. The River Exe has a non-tidal catchment area of 601 km², the Torridge catchment is 663 km², and the freshwater River Taw catchment is 826 km². However, the tidal zone of the Torridge is constrained in a narrow, steep sided valley, with only narrow areas of floodplain and tidal marsh, so this site was discounted. The rivers Exe and Taw both have relatively wide floodplains and as they both drain upland areas with high precipitation, Dartmoor and Exmoor, they have discharges that are sensitive to changes in climate. However, the River Exe has several disadvantages, compared to the Taw. Large parts of the tidal floodplain have been built on near Exeter, preventing the exploration of the underlying stratigraphy, unlike the more rural Taw valley which has largely unhindered access. The tidal zone of the River Exe is heavily engineered with several weirs and diversions of flow into new flood channels and canals, and has significant sections where the channel is contained within flood walls. The inner and middle estuary tidal marshes of the Exe Estuary have also been largely reclaimed. This poses problems for both contemporary surveys of diatom distribution (salinity gradient and intertidal elevation). The River Taw was therefore chosen for this study.

The River Taw is located in North Devon and drains both Dartmoor and Exmoor. The underlying geology of the lowland areas of the catchment mainly consist of Carboniferous Culm measures (shales and sandstones), with a smaller Permian sandstone outcrop. Exmoor is underlain by Devonian sandstones and shales, whilst the Dartmoor Block is largely formed of granite. The river drains into Bideford Bay, and the Atlantic via the Taw Estuary, with the River Torridge entering the estuary at Appledore near the mouth. Figure 1.1 shows a map of the lower Taw catchment and Taw Estuary. The first weir is located at Umberleigh, 5 km upstream of HAT. Flow has

been measured for the River Taw at a gauging station at Umberleigh since 1958. For the period 1958 to 2000, the mean flow was $18.48 \text{ m}^3\text{s}^{-1}$, the highest monthly mean flow was $82 \text{ m}^3\text{s}^{-1}$, and the highest daily mean flow was $363 \text{ m}^3\text{s}^{-1}$. The average rainfall in the catchment during this period was 1180mm.

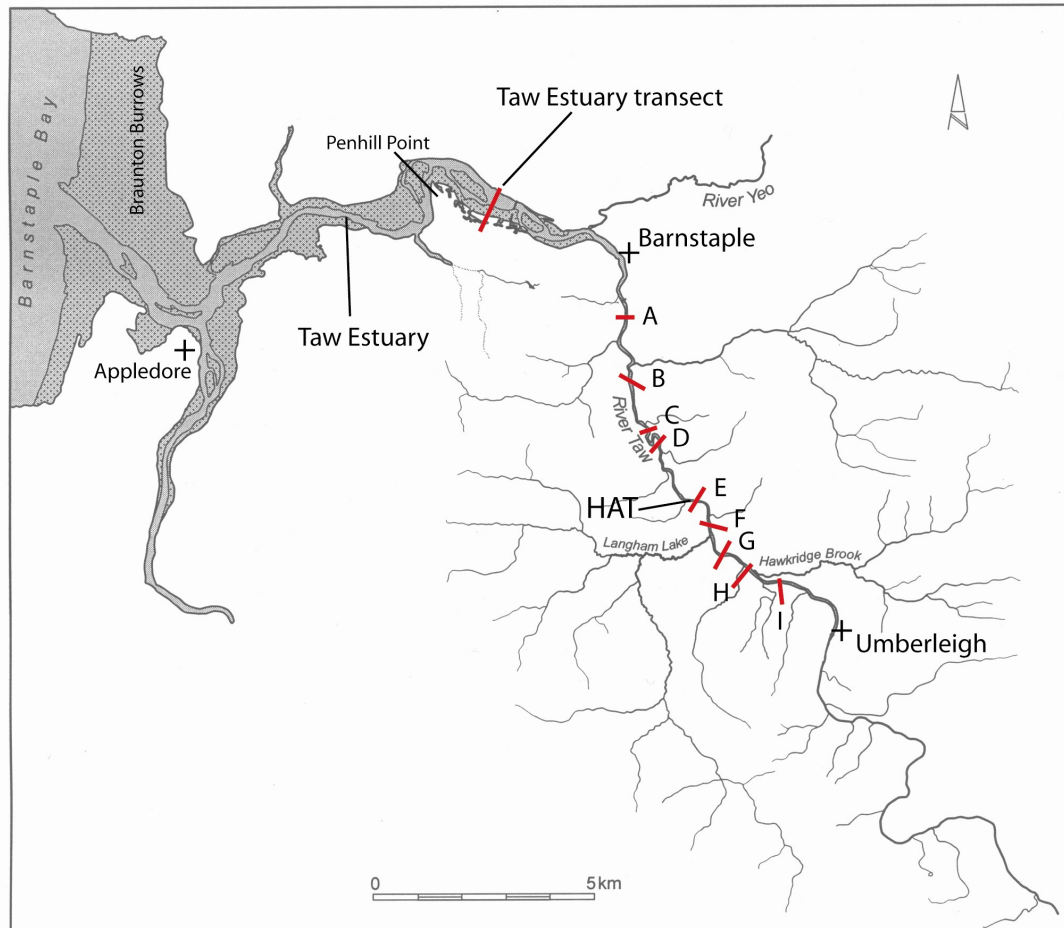


Figure 1.1 Map of the lower River Taw catchment and Taw Estuary. The estuary opens into Barnstaple Bay and the Bristol Channel. The location of all core transects and the contemporary environment Taw Estuary transect is indicated. HAT = highest astronomical tide (*i.e.* tidal head).

The Taw Estuary is macro-tidal, and at Appledore near its mouth, has a tidal range of 7.3m (MHWST to MLWST). This falls to 3.8m at Barnstaple in the inner estuary (Admiralty Tide Tables, 2008). However, this decrease in tidal range is largely caused by the up-estuary rise in bed elevation, with drying heights east of Penhill Point (5km west of Barnstaple) exceeding MLWST, so that the estuary is entirely intertidal (Pethick, 2007). MHWST actually increases slightly up-estuary from 4.32m OD at

Appledore to 4.70m OD at Barnstaple (Admiralty Tide Tables, 2008). Between Fremington in the middle estuary and Barnstaple, tidal curves indicate a marked flood tidal asymmetry (HR Wallingford, 1990; Kirby, 1996). The estuary is generally quite sandy west of Penhill Point, but landward of Penhill Point sediments become finer grained, with extensive areas of saltmarsh located on the southern side of the estuary between the Point and Barnstaple. These marshes have grown significantly since the 19th Century, corresponding with a progressive siltation of the channel at Barnstaple, which was abandoned as a trading port in the 19th Century (Pethick, 2007).

The mouth of the Taw-Torridge Estuary is constrained to the north by the 6km long barrier and coastal dune system of Braunton Burrows, one of the three largest dune systems on the west coast of Britain where individual dunes can exceed 30m OD. Remarkably little research has been done on the origin and age of this barrier but it is thought to be at least 2000 years old (Packham and Willis, 2001), and based on cartographic evidence, there has been very little change in its dimensions during the last 150 years (May and Hansom, 2003). On the estuary side of the barrier, Braunton Marsh was once the site of extensive saltmarshes but these were reclaimed in 1811 (Manning, 2007).

The study area for this investigation is located along a 10 km reach of the tidal and non-tidal River Taw between Barnstaple and the village of Umberleigh (figure 1.1). This reach encompasses 6km of inner estuarine tidal river and a further 4km of freshwater non-tidal river. The location of all core transects (A to I) are indicated in figure 1.1, as is the upstream limit of the highest astronomical tides (HAT). Surveys of contemporary diatom distribution were located along the salinity gradient of this reach and along a transect across intertidal environments (saltmarsh and tidal flat) in the middle Taw Estuary, 3 km west of Barnstaple.

2 ESTUARINE EVOLUTION AND PALEOSALINITY

Estuaries have been defined as occupying the seaward portion of drowned valley systems which receive sediment from both fluvial and marine sources. The nature and organisation of facies within them is controlled by the interplay between marine processes (waves and tides), which generally decrease in intensity up-estuary, and fluvial processes, which decrease in strength down-estuary (Dalrymple *et al.*, 1992). Dalrymple *et al.* (1992) proposed two end-member models of estuaries, the wave-dominated estuary and the tide-dominated estuary (figure 2.1). These models have been widely used to describe modern and ancient estuarine systems (Yang *et al.*, 2007). Unlike earlier models that defined the up-valley boundary of an estuary as either the transition to freshwater salinities of <0.1‰ (Pritchard, 1967), or the upper limit of tidal influence (Fairbridge, 1980). Dalrymple *et al.* (1992) defined it as the facies boundary between marine/tidally-influenced and fluvial sediments. This enabled the boundary to be recognised in the geological record. The Taw Estuary is a macro-tidal tide-dominated estuary. As shown in figure 2.1, tidal current energy exceeds wave energy at the mouth in these estuaries and gradually dissipates in the middle and inner estuary up to the tidal head. Conversely, river current energy dissipates with down-estuary distance. This results in a tripartite division of the estuary into an outer marine-dominated zone, a middle mixed-energy zone and an inner river-dominated zone. The ‘inner’ Taw Estuary is defined in this study as the area between the tidal head and Barnstaple, where the estuarine channel opens out into expanses of marine-dominated tidal flat. In the Dalrymple *et al.* (1992) model, the inner Taw Estuary would cover the river-dominated and mixed-energy zones. The ‘tidal-fluvial’ sediments seen in figure 2.1 are also generally called fluvio-estuarine in this study.

Despite this pivotal position between the fluvial and marine environment, models of Holocene estuary evolution have so far been driven largely by changes in relative sea-level (RSL) and ocean processes (*e.g.* Devoy, 1979; Allen, 1990, 2003; Fletcher *et al.*, 1990; Long, 2000), with little reference, if any, to long-term changes in fluvial regime. In the USA and Canada, sequence stratigraphic models of facies distribution in estuaries are prolific (*e.g.* Frey & Howard, 1986; Allen and Posamentier, 1993; Dalrymple *et al.*, 1992; Dalrymple & Zaitlin, 1994), but this is not the case in the UK. These models illustrate how rising RSL during the Holocene has caused the upward accretion and

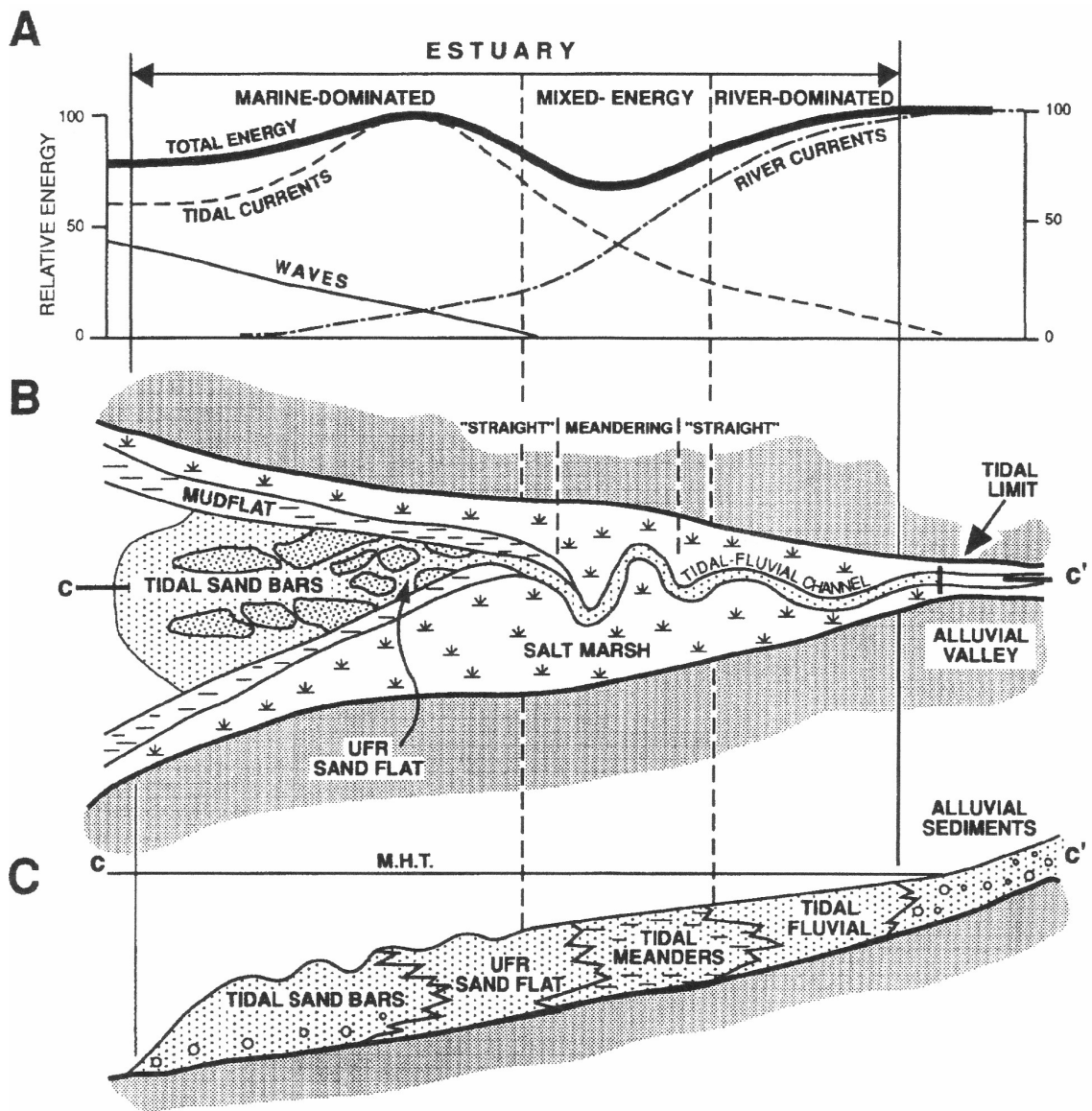


Figure 2.1 Dalrymple *et al.* (1992) model of a tide-dominated estuary. Distribution of A) energy types, B) morphological elements in plan view, and C) sedimentary facies in longitudinal section. UFR = upper flow regime; MHT = mean high tide (from Dalrymple *et al.*, 1992).

landward progradation of estuarine facies under transgressive systems tract (TST) conditions. Estuaries in southern England have experienced a Holocene RSL rise of at least 30m (Long *et al.*, 2000), although most of this rise occurred in the early-middle Holocene, with a general slowdown in RSL rise occurring at *c.*7000-5000 cal.yr.BP (Shennan and Horton, 2002). These facies models indicate this slowdown with the down-estuary migration of fluvial and fluvio-estuarine sedimentation during the later Holocene, when the rate of RSL rise slowed and estuaries began to fill up with sediment under highstand systems tract (HST) conditions (figure 2.2).

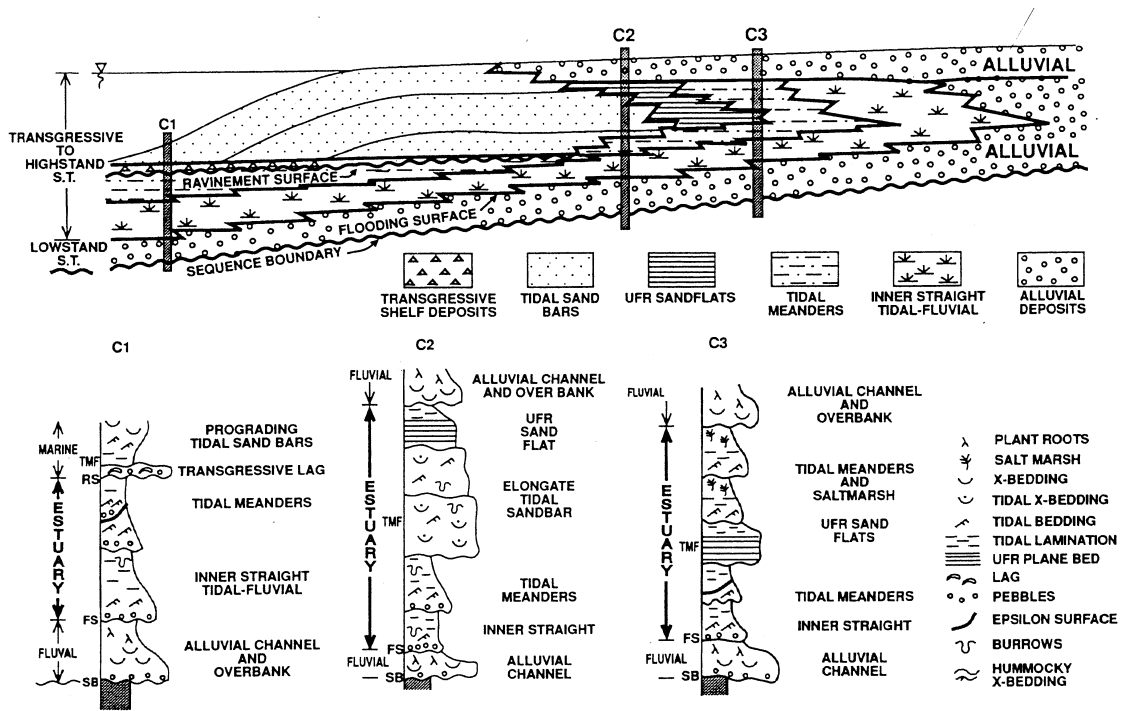


Figure 2.2 Schematic section along the axis of a tide-dominated estuary, showing the distribution of lithofacies resulting from transgression of the estuary, followed by estuary filling and progradation of sand bars, tidal flats, marsh and alluvial deposits (from Dalrymple *et al.*, 1992).

Prior to the late 1990's the importance of river discharge as a driver of estuarine change was occasionally surmised (*e.g.* Shennan & Waller, 1994) but saw little evaluation, certainly in the UK, because of the difficulties in determining temporal changes. However, with the development of new carbon isotope (*e.g.* Chmura and Aharon, 1995; Bryne *et al.*, 2001; Malamud-Roam & Ingram, 2004; Lamb *et al.*, 2006), oxygen isotope (*e.g.* Ingram *et al.*, 1996; Cronin *et al.*, 2005), pollen (*e.g.* Bryne *et al.*, 2001; Willard *et al.*, 2003; Malamud-Roam & Ingram, 2004) and microfossil (*e.g.* Cronin *et al.*, 2000; Bryne *et al.*, 2001; Zong *et al.*, 2006; Leorri and Cerreta, 2009) techniques that allowed estuarine palaeosalinities to be reconstructed, it has become apparent that there have been significant decadal-centennial scale fluctuations in river discharge during the mid to late Holocene (*e.g.* Cronin *et al.*, 2000, 2005; Malamud-Roam & Ingram, 2004; Malamud-Roam *et al.*, 2006).

Records of stable carbon isotopes ($\delta^{13}\text{C}$) in marsh sediments can be used as a proxy for estuary salinity because the majority of terrestrial plants use the C_3 photosynthetic pathway, while certain saltmarsh grasses (*e.g.* *Spartina spp.*) have evolved the C_4 pathway as an adaption to water stress. C_3 plants are isotopically lighter ($\delta^{13}\text{C} \sim -29\text{‰}$) than C_4 plants ($\delta^{13}\text{C} \sim -12\text{‰}$) so that measurements of the $\delta^{13}\text{C}$ value of sedimentary

organic matter in marsh cores can be used to infer changes in terrestrial and saltmarsh vegetation. This can therefore be used as a proxy for salinity (and Malamud-Roam & Ingram, 2004). Recent studies in the San Francisco Bay estuary by Bryne *et al.* (2001) and Malamud-Roam & Ingram (2004) have used records of stable carbon isotopes ($\delta^{13}\text{C}$) from sediment cores to infer changes in marsh vegetation (C_3 vs. C_4 plants) over the last 3000 years. Their results show significant late Holocene fluctuations in salinity, relating to changes in fresh water inflow from the Sacramento-San Joaquin catchment. A comparison of the timing of these events with regional climate records showed that the palaeosalinity variations reflected regional precipitation (Malamud-Roam *et al.*, 2006). This indicates that one of the main controls of estuarine palaeosalinity is river discharge and regional climate.

Pollen records in coastal sediment sequences can be used to reconstruct changes in marsh vegetation. This can then be used to infer changes in estuarine salinity, and this method has been widely used, though often in combination with other palaeosalinity proxies (*e.g.* Bryne *et al.*, 2001; see figure 2.3 for an example). Several authors have used normalised ratios of salt-tolerant to salt-intolerant marsh pollen as an indicator of changing salinity (*e.g.* Davis, 1992; May, 1999; Bryne *et al.*, 2001; Malamud-Roam and Ingram, 2004).

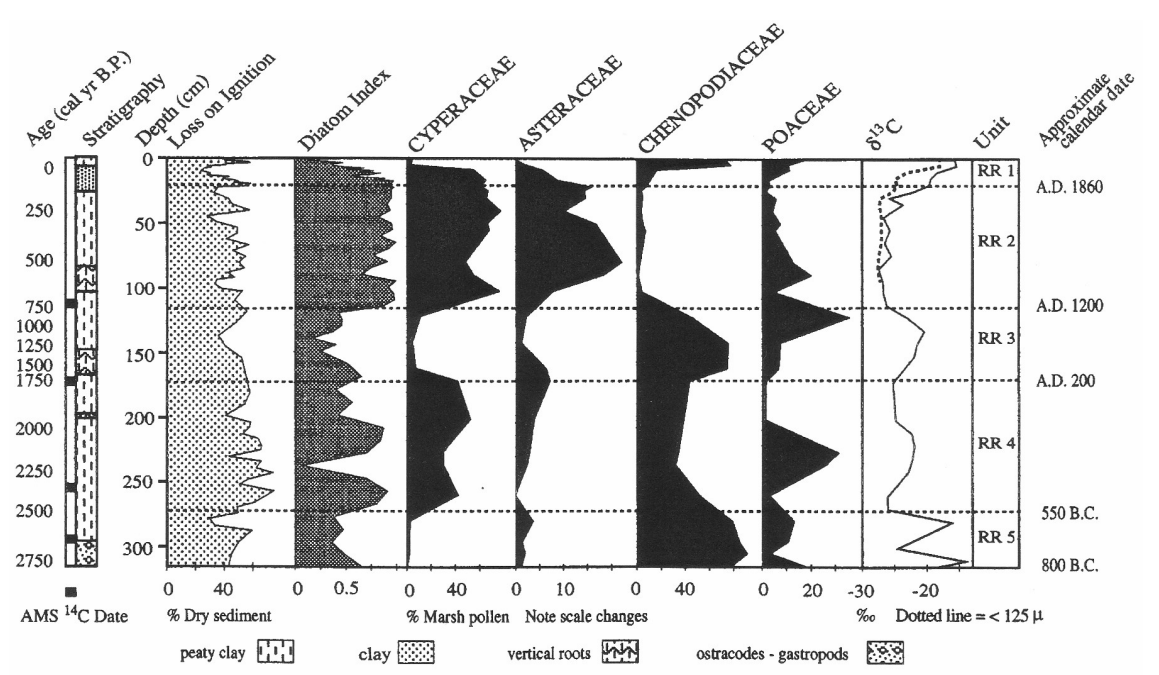


Figure 2.3 Core log from the San Francisco Estuary showing changes in Diatom Salinity Index, selected pollen taxa and $\delta^{13}\text{C}$ values (Bryne *et al.*, 2001).

Cronin *et al.* (2000; 2005) used a method of palaeosalinity reconstruction that entails calibrating $\delta^{13}\text{O}_{\text{water}}$ in Chesapeake Bay to salinity and applying this relationship to calculate trends in palaeosalinity from the $\delta^{13}\text{O}_{\text{foram}}$ in the dominant benthic foram *Elphidium selseyense*, correcting for changes in water temperature estimated from ostracode Mg/Ca ratios. This work was based on cores from the mainstem channel of Chesapeake Bay and the most sensitive core to salinity change was interestingly in the shallowest water at the mouth of the Patuxent Estuary, near Solomons Island. This suggests that an even more sensitive record may be found within the confines of a smaller estuary or an inner estuarine environment, where the proximity to a freshwater source and the smaller cross-sectional area will allow a higher river discharge : tidal prism ratio. Cronin *et al.* (2005) used the instrumental record of Susquehanna River discharge for the period 1900-1990 as a means to verify down core $\delta^{13}\text{O}_{\text{foram}}$ patterns as estimates of palaeosalinity. In the Susquehanna River, a previous study by Najjar (1999) has shown that discharge is positively correlated with regional precipitation for the period 1900-1990. This verification exercise showed how changes in $\delta^{13}\text{O}_{\text{foram}}$ were directly correlated with decadal-scale changes in discharge.

No study in Europe has yet taken this palaeosalinity-based approach to palaeo-climate reconstruction, but there are indications that this is about to change, with a recent study by Leorri and Cerrata (2009) in northern Spain on the potential of foraminifera in salinity reconstruction, indicative of the growing interest in this field. Their study quantitatively assessed the relationship between foraminifera species and relative distance from the estuary mouth (RDEM), which was used as a proxy for palaeosalinity. This study demonstrated a good correlation between benthic foraminiferal species and RDEM, and show that there are potentially several micro-fossil techniques that can be used in palaeosalinity reconstruction

Diatoms are found in all salinities, from freshwater, through brackish to fully marine. They are very sensitive to changes in salinity and therefore make an excellent proxy for changes in palaeosalinity (Cooper, 1999). Diatom species have been classified into several broad salinity groups (Hustedt, 1953; Denys, 1991) and this scheme has been used to qualitatively reconstruct palaeosalinity in various estuarine studies (e.g. Siddell *et al.*, 2000; Bryne *et al.*, 2001). However, this method is qualitative in nature and does not account for local and regional differences in diatom salinity preferences and tolerances. Brynne *et al.* (2001) developed the use of 'diatom salinity index' (DSI) as a

proxy for salinity. This index is essentially a ratio of freshwater and brackish diatom species to marine species. It was found in their multi-proxy study in San Francisco Bay Estuary to be more sensitive to variations in former estuarine salinity than carbon isotope or pollen methods. The DSI method is to be used in this study to reconstruct palaeosalinity in the Taw Estuary.

3 METHODOLOGY

3.1 GEOMORPHOLOGICAL MAPPING

Once the potential study reach in the lower Taw valley had been designated (which contains both inner estuarine and non-tidal fluvial river environments), an initial geomorphological assessment of the valley was made using aerial photographs obtained from Devon County Council (DCC) Archaeological Service. A geomorphological map of the study reach was constructed by viewing aerial photographs from several surveys taken between 1945 and 2000. Analogue prints were viewed using a lens stereoscope. The primary resource was the 2000 *Millennium* aerial survey of Devon. Photographs from this survey have been digitised and photomosaiced (by DCC) into a rectified and spatially referenced format suitable for viewing in *ArcGIS* (or image viewer software such as *ER Viewer*). Landform elements visible in the aerial photographs (*e.g.* palaeochannels, river terraces, scroll bars) were mapped onto a 1:5000 topographic base map.

Geomorphological field mapping was then done for the entire 9 km valley reach between Umberleigh and Barnstaple, at a scale of 1:5000. A hand level was used to help identify several Holocene river terraces, with older Pleistocene terraces mapped up to the level of ‘Terrace 2’ in the British Geological Survey map produced by Edmonds *et al.* (1979). Field mapping revealed the existence of many more palaeochannels than those visible in the aerial photographs (approximately 50% of palaeochannels are visible in the aerial survey).

Completed geomorphological field maps were then scanned and imported into *ArcGIS* where they were georeferenced and mosaiced. All landform elements were then on-screen digitised to produce a new GIS map of the lower Taw valley.

3.2 STRATIGRAPHIC TRANSECTS

The modern tidal limit of the River Taw was assessed prior to any stratigraphic investigation to ascertain the up-valley limits to the inner estuarine environment. This

was done by referring to published topographic maps which indicate the Normal Tidal Limit (NTL) and by field observations of a spring-neap tidal cycle. An exploratory stratigraphic survey was then done of the study reach using a 30mm gouge hand corer. This was done to assess the palaeo-environmental potential of former tidal wetlands (now protected from flooding by embankments) and tidal/non-tidal palaeochannels to contain datable records of estuarine or fluvio-estuarine (*i.e.* mixed) deposition.

Nine core transects were located across the valley at high potential sites. An attempt to incorporate a range of middle-late Holocene age deposits was done by locating each transect, where possible, across several floodplain sedimentary units (*e.g.* river terraces). Four transects (A – D) are located in the inner estuarine tidal river valley, one (E) is in the vicinity of HAT (highest astronomical tide, 20 year cycle) and four (F – I) are in the non-tidal river valley. The River Taw at Transect I is 3.0 km upstream of HAT and has a typical low flow water surface of 9.5 m OD (*c.*3.7m above HAT). This upstream extension of the field investigation above HAT was done for several reasons: (a) it may include the upstream limit to saline groundwater intrusion; (b) storm surges can raise the water surface 1-2 m above HAT, when coinciding with a high spring tide (Kidson, 1986); (c) the tidal limits during the late Holocene may have been higher than modern limits due to higher RSL or a larger tidal range; (d) the upstream deposits may contain examples of pure freshwater diatom assemblages, unaffected by marine influence.

Transect lines were surveyed using a prism sighting compass with distances between boreholes measured with a 50m tape or by pacing (30-40m typical interval). The average transect length was 590m with 15-25 stratigraphic cores per transect in the inner estuary zone and 8-15 cores per transect in the non-tidal fluvial zone. The stratigraphy was investigated with a 30mm gouge at each core location and described in the field with the aid of a x10 hand lens and grain size card. Sediment texture, fabric, colour and type of contact was recorded using standard geological nomenclature (Jones *et al.*, 1999; Tucker, 1996). In addition, organic deposits were described using a modified Troels-Smith system (Troels-Smith, 1955; Aaby and Berglund, 1986).

Altitude and coordinate data were surveyed at all core points and along each transect line with a differential GPS (Leica GPS1200). This GPS system has an accuracy of +/- 2cm. All points were referenced to Ordnance Datum by the surveying of two local OS

benchmarks. Post-processing was done using the interface software *Leica Geo Office*. All x, y, z coordinate-altitude data was exported into the GIS.

3.3 CORE RECOVERY AND FIELD SAMPLING

Following appraisal of the stratigraphy, 10 core sites located along the salinity gradient were re-visited and sediment cores recovered (Figure 3.1) for laboratory analysis (see 3.4). Cores were recovered with a 50mm gouge hand corer, placed in 1m lengths of plastic guttering and wrapped in cling film and foil. They were then stored in a refrigerated cold room at 5°C prior to sub-sampling at 2cm intervals. Two of these cores, Pill Lane 1 (PL1) and Tawstock 1 (TS1), were used for RSL reconstruction (see 3.6).

Nineteen additional stratigraphic core points were also re-visited and sampled in the field with a 30mm gouge corer. A stratified random sampling approach was used (Birks and Birks, 1980) with several 20g samples taken from each major stratigraphic unit, resulting in a mean sampling interval of *c.*40cm, for later analysis of diatoms, magnetic susceptibility (low frequency and dual frequency), organic matter content and carbonate content (see 3.4 for methods). Additional organic samples (*e.g.* plant macrofossils, seeds, wood) were taken for possible AMS radiocarbon dating (see 3.5.1). Core sites were chosen so as to sample a range of deposit ages at each transect. This was particularly important in the inner estuarine tidal reach where spatial and temporal changes in diatom-inferred estuarine palaeosalinity would be analysed. All core points were re-surveyed with a differential GPS.

3.4 CORE ANALYSIS

3.4.1 Core description

The recovered cores were described in the laboratory with the aid of a x10 hand lens and grain size card. Sediment texture, fabric, colour and type of contact was recorded using standard geological nomenclature (Jones *et al.*, 1999; Tucker, 1996) and presented as graphic logs using the software program *Rockworks* (Rockware

Incorporated, 2004). Peats were classified according to organic matter content. The following division was made: peaty clay/silt = 15-25% organic matter; clayey/silty peat = 25-40% organic matter; peat = >40% organic matter. In addition, each core was described using the semi-quantitative Troels-Smith method (Troels-Smith, 1955; Aaby and Berglund, 1986).



Figure 3.1 Hand coring and recovery of the PL1 core. This core was to be used for sea-level reconstruction.

3.4.2 Sediment sub-sampling

Each of the 10 recovered cores was sub-sampled at 2cm intervals. All samples were then tested for moisture content, organic matter and carbonate content (see 3.4.3). Samples were then freeze dried and tested for magnetic susceptibility (see 3.4.5) and a sub-sample used in diatom analysis (3.4.7).

3.4.3 Organic matter and carbonate content

Moisture content, organic matter content and carbonate content were measured using

the loss on ignition method (Dean, 1974). Samples with a wet weight of *c.* 2g were dried in an oven for 24 hours at 105°C and then re-weighed. The percentage weight loss gives an estimate of moisture content. The samples were then ignited in a muffle furnace at 500°C for 4 hours and then re-weighed. The percentage weight loss equates to organic matter content. Samples were then placed in the muffle furnace at 850°C for 1 hour. The percentage weight loss gives an estimate of carbonate content. However, with the carbonate estimate, any weight loss $\leq 1.5\%$ may be due to dehydration of clay minerals (Dearing, 1986).

3.4.4 Magnetic susceptibility

Magnetic susceptibility (χ_{fr}) gives information about the total concentration of ferrimagnetic minerals (*e.g.* magnetite and greigite) in a sediment. If ferrimagnetic minerals are present in low concentrations, it can give information about the total concentration of paramagnetic and canted antiferrimagnetic minerals (Dearing, 1999). All samples were tested for magnetic susceptibility with a Bartington MS2 susceptibility meter.

The purpose of the magnetic susceptibility (χ_{fr}) measurements in this study was to aid core correlation (Dearing, 1986) and to make inferences on the source of sediment deposited in the inner estuarine zone. Sediment in this zone can be derived from the catchment via river currents or from the middle and outer estuary via tidal currents, with the model of Dalrymple *et al.* (1992) indicating an up-estuary gradient caused by decreasing tidal energy and increasing river current energy (figure 2.1). It has been found in previous studies (Oldfield, 1994; Gibbs, 2000) that high concentrations of secondary magnetite and greigite often exist in estuarine saltmarsh and mudflat sediments. These ferrimagnetic minerals show much higher susceptibility than ferromagnetic minerals such as haematite. Therefore, high χ_{fr} values may indicate that sediment is sourced from the extensive mudflats and saltmarshes of the middle and outer Taw Estuary. However, for inferences to be made on sediment source with a higher degree of confidence, the magnetic minerals and their grain sizes need to be identified. This can be done through further magnetic remanence measurements (see 3.4.5).

Sample preparation involved placing a known weight (typically 8-10 g) of freeze-dried sample into a cling film lined 10 cm³ plastic pot. Freeze drying (or drying at temperatures below 40°C) is necessary as higher temperatures can cause changes in the magnetic mineralogy (Walden, 1999). Samples were freeze dried relatively quickly after collection as it has also been found that long-term storage of wet samples can cause changes in their magnetic properties due to continuing biological activity (*e.g.* Snowball and Thompson, 1988). As samples dry out over a long period they also tend to lose both susceptibility and remanence, with the finest magnetic grains being particularly prone. The loss of magnetic minerals is thought to be caused by oxidation of greigite (Snowball and Thompson, 1988; Hilton, 1990) and conversion of fine grained magnetite to non-ferrimagnetic phases (Oldfield *et al.*, 1992).

Sample pots were placed into a Bartington MS2B dual frequency susceptibility sensor at the low frequency (LF) setting (0.46 kHz) and measured for low field (0.1 mT) volume susceptibility (κ_{lf}). This value was converted to mass specific susceptibility (χ_{lf}), in SI units of 10⁻⁶ m³ kg⁻¹. Samples were then measured at the high frequency (HF) setting (4.6 kHz). Frequency dependent susceptibility was calculated and expressed as a percentage of the original LF value ($\kappa_{fd\%}$ or $\chi_{fd\%}$) using the equation:

$$\kappa_{fd\%} = \{(\kappa_{lf} - \kappa_{hf}) / \kappa_{lf}\} \times 100 \quad \text{eq. 3.1}$$

Measurements made at two frequencies are used to detect the presence of ultrafine (or fine viscous) ferrimagnetic grains with a magnetic grain size of *c.* 0.02 μm . Magnetic grain size is related to magnetic domain size (see Smith, 1999; Evans and Heller, 2003) and table 3.1 gives the approximate grain sizes for each domain state. Samples where fine viscous grains are present will show slightly lower values when measured on the HF range. $\chi_{fd\%}$ is derived from this difference (eq.3.1) and gives the relative proportion of fine viscous grains (lying at the SSD/SP boundary, *c.* 0.02 μm) to the total ferrimagnetic assemblage (Dearing, 1999). A guide to the interpretation of frequency dependent susceptibility measurements is given in table 3.2.

Fine viscous and SP ferrimagnetic grains often occur as crystals produced by bacteria or by chemical processes in soil. This means that they are often a significant contributor to total susceptibility in soils and weathered horizons (Oldfield *et al.*, 1983; Maher, 1986, 1988). $\chi_{fd\%}$ values of between 4% and 10% can indicate a significant contribution by

soil-derived fine viscous grains in a magnetic assemblage, and values can be as high as 14% in samples of fertile topsoil. $\chi_{fd\%}$ measurements can therefore give important environmental and palaeo-environmental information. In this study these measurements have been used on modern and core samples from the inner estuarine and transitional fluvio-estuarine zones to infer sediment source as sediment sourced from catchment soils (especially cultivated fields) is expected to show higher $\chi_{fd\%}$ values than sediment transported on tidal currents from the middle and outer estuary. Up-estuary gradients in $\chi_{fd\%}$ have been found in several previous studies (Oldfield *et al.*, 1985, 1989, 2003).

Magnetic grain sizes (domains)		
MD	Multi-domain	>110 μm
PSD	Pseudo-single domain	0.4 - 110 μm
SSD	Stable single domain	0.02 – 0.4 μm
SP	Super-paramagnetic	<0.02 μm

Table 3.1 Magnetic domains and typical grain size. Exact size boundaries vary depending upon mineral type and grain shape (Dearing, 1999; Walden, 1999).

Interpretation of frequency dependent susceptibility values		
Low $\chi_{fd\%}$	<2.0	Virtually no SP grains
Medium $\chi_{fd\%}$	2.0-8.0	Admixture of SP and coarser grains, or SP grains <0.005 μm
High $\chi_{fd\%}$	8.0-14.0	Virtually all SP grains
Very high $\chi_{fd\%}$	>14.0	Erroneous measurement, anisotropy, weak sample or contamination

Table 3.2 Interpretation of frequency dependent susceptibility values (Dearing, 1999; Oldfield, 1999).

A high degree of accuracy and precision is required during high frequency testing. This means that samples containing very low concentrations of ferrimagnetic minerals are too weak for dual frequency measurements. Dearing (1999) advises that samples with κ_{if} values <10 should not be measured at HF as they cannot provide useful dual frequency data and even samples with κ_{if} values of 10-25 are prone to large errors. For weak samples, the mean value of 10 measurements should be used. In view of the large number of samples to be tested (approximately 2200), only core samples with κ_{if} values >25 were tested for frequency dependent susceptibility. However, the contemporary surface samples (see 3.7) were prioritised. For these samples the mean value of 10 HF measurements was used for κ_{if} values between 10 and 25.

3.4.5 Magnetic remanence

Magnetic remanence measurements were done on samples from three cores, located along the salinity gradient of the inner estuary. The mean sampling interval in all cores was 6cm. All remanence measurements were performed at the University of Reading (Department of Geography) magnetics laboratory. Remanence measurements differ from susceptibility measurements, which measure the induced magnetisation of a sample held in a magnetic field, in two main areas. First, much larger magnetic fields are applied, which can permanently alter the magnetic properties of some minerals. Secondly, after samples have been exposed to a magnetic field of known strength, they are removed from that field and then the remanence (or remanent magnetisation) acquired in that field is measured. Only ferrimagnetic (or ferromagnetic) minerals such as iron oxides (*e.g.* magnetite or haematite) or iron sulphides (*e.g.* greigite) can retain a permanent remanence (Walden, 1999a).

Magnetic remanence measurements can provide detailed information on the mineral composition, concentration and grain size of a sediments magnetic mineral assemblage. Remanence measurements were used in this study to determine the source of sediment deposited in the inner estuarine zone during the late Holocene. As stated in 3.4.4, sediment in this zone can be derived from the catchment or middle/outer estuary, and the identification of magnetic minerals associated with the estuarine environment (*e.g.* biogenic magnetite and authigenic greigite) can give an indication of the predominant sediment source. When up-estuary trends in estuary sourced minerals are compared with down-estuary trends in catchment derived minerals such as soil-derived magnetite (distinguished from biogenic saltmarsh magnetite by its smaller magnetic grain size), an estimate of depositional location in the salinity gradient can be given (*e.g.* Oldfield *et al.*, 2003).

Sample preparation is similar to that described for magnetic susceptibility (see 3.4.4). However, the rim of each plastic pot lid was removed to allow placement into the various sample holders. This is because the equipment was originally designed for palaeomagnetic analysis on one-inch cylindrical rock samples (Walden, 1999b). The measurement process is described in Walden (1999a) and consists of three stages:

(1) Anhysteretic remanent magnetisation (ARM or χ_{arm})

An ARM was induced in each sample with a Molspin a.f. demagnetiser with ARM attachment. This is achieved by placing the sample within an alternating field and also applying a small constant biasing field. The ARM was then measured by placing the sample in a Molspin magnetometer and spinning for 6 seconds. This generates an electric current in the surrounding coil as defined by Faraday's Law. The size of the current is proportional to the size of the remanence held by the sample.

(2) Demagnetisation

The sample was then demagnetised by placing in a Molspin a.f. demagnetiser. The sample was rotated while an alternating magnetic field was applied so that the effects of the field are randomised and the sample is demagnetised.

(3) Isothermal remanent magnetisation (IRM)

A series of known magnetic fields was then applied to the sample using a Molspin pulse magnetiser, with each field inducing an IRM (isothermal remanent magnetisation) that could be measured with the magnetometer. IRM acquisition was measured after exposure to a small field initially (20 mT), and then after progressively larger fields (60, 100, 300, 500, 800 and 1000 mT). Saturation isothermal remanent magnetisation (SIRM) was measured after the 1000 mT field and is the highest remanence that can be produced in a sample. Once saturated, the sample was exposed to a number of backfields (20, 40, 100 and 300 mT) to enable comparisons with older work reported in the literature.

The completion of these stages resulted in a range of IRM and ARM values for each sample which when supplemented by the magnetic susceptibility data, allowed detailed information to be gained about the magnetic mineral assemblage of each sample. Table 3.3 presents a summary of the various magnetic parameters (including ratios and quotients) that can be used in the identification of magnetic mineral composition, concentration and grain size (Maher, 1986; Oldfield, 1991; Oldfield, 1999; Walden, 1999b; Evans and Heller, 2003).

Concentration-related measurements	
X_{if}	Concentration of ferrimagnetic minerals (less proportional to magnetite concentrations in fine or mixed grain size assemblages, <i>i.e.</i> more proportional in uniformly coarse grained assemblages) or the concentration of paramagnetic and antiferromagnetic minerals if ferrimagnetic minerals are present in very low concentrations.
SIRM	Combined concentration of all remanence carrying minerals in a sample. However, the value is also dependent upon the assemblage of mineral types and their magnetic grain size. Relatively large quantities of coarse grained magnetite and, in particular, antiferromagnetic minerals (<i>e.g.</i> haematite) can be masked by the presence of much lower concentrations of fine grained SSD ferrimagnets (<i>e.g.</i> magnetite) as ferrimagnetic SSD grains give a much higher contribution to SIRM compared to coarse grains.
X_{arm}	Concentration of SSD ferrimagnetic grains (<i>e.g.</i> magnetite) at 0.02-0.4 μ m.
IRM_{soft} (IRM_{20mT})	Concentration of ferrimagnets (<i>e.g.</i> magnetite).
IRM_{hard} ($SIRM-IRM_{500mT}$)	Concentration of haematite.
IRM_{int} ($IRM_{100mT}-IRM_{60mT}$)	High values of IRM acquisition at intermediate fields can indicate the presence of greigite (see below).
Relative proportions of magnetic components	
$X_{fd\%}$ (X_{fd}/X_{if})	Gives the relative proportion of fine viscous grains (lying at the SSD/SP boundary, <i>c.</i> 0.02 μ m) to the total ferrimagnetic assemblage. Such fine grains are a significant contributor to total susceptibility in soils and weathered horizons.
IRM_{20mT}/IRM_{300mT}	Estimates the relative contribution of either MD or fine viscous SD ferrimagnetic grains to IRM.
<i>Note: where fine viscous grains dominate, the two quotients above will be positively correlated. Where MD grains dominate, the quotients will be unrelated or negatively correlated.</i>	
SIRM/X	Values will be reduced by: (i) increased ferrimagnetic versus imperfect antiferromagnetic contributions; (ii) by increased mean grain size from SD upwards (<i>e.g.</i> MD dominated assemblages have low values); (iii) by increased SP contributions; (iv) by the increased relative importance of the paramagnetic contribution to X_{if} .
IRM_{20mT}/X_{arm}	High values point to MD, low values to SSD dominance.
$SIRM-IRM_{300mT}/SIRM$	Estimates the relative contribution of imperfect antiferromagnets to IRM.
X_{arm}/X	Both parameters increase linearly with magnetite. Therefore, if the sample is dominated by magnetite, this ratio can be used to determine grain size with high values indicating fine SSD grains. (The parameters are often plotted as a "King plot", with X_{arm} as the ordinate.)
$X_{arm}/SIRM$	High values indicate the dominance of fine grained (SSD or less) ferrimagnets. This often indicates a strong bacterial magnetite (magnetosome) contribution, but can also indicate soil-derived ferrimagnets (SSD/SP boundary grains) when accompanied by high $X_{fd\%}$.
$SIRM/X_{arm}$	Particularly high values can indicate the presence of greigite (see below).
Reverse field ratios	Back field IRM/SIRM ratios have a range from +1 to -1 (-1 indicating saturation of the sample in the opposite direction to the application of the original forward field). The $IRM_{-100mT}/SIRM$ ratio (often termed the "S-ratio") is important as the majority of magnetite is fully saturated in fields of 100mT so that magnetite dominated samples produce $IRM_{-100mT}/SIRM$ ratios very close to -1. Samples containing magnetically harder mineral types (<i>e.g.</i> haematite) have higher ratios and can be positive if ferrimagnetic minerals are virtually absent. A divergence in reverse field ratios can indicate the presence of greigite.
Greigite identification	
Yes to all indicates greigite	(1) High SIRM, SIRM/X and $SIRM/X_{arm}$? (2) Reverse field divergence? (3) Relatively low IRM_{hard} ? (4) High IRM_{int} acquisition?

Table 3.3 Mineral magnetic parameters used in the identification of magnetic components and in the identification of relative proportions of components in a magnetic assemblage (Maher, 1986; Oldfield, 1991, 1999; Walden, 1999; Evans and Heller, 2003).

3.4.6 Diatom analysis

Diatom slides were prepared using a modified version of the method described by Battarbee (1986). Oxidation and removal of organic matter was achieved by placing a sub-sample of 0.5 cm³ of sediment in a beaker and adding 25 ml of 30% H₂O₂. The sample was heated on a hotplate for 2-3 hours until the chemical reaction ceased. In order to remove clay and fine silt particles, the sample was transferred to a centrifuge tube, topped up with distilled water and centrifuged at 1500 rpm for 5 minutes (higher speeds may cause breakage of fragile pennate diatom frustules). The sample was centrifuged and washed with distilled water at least three times (typically 3 – 5 times) until the supernatant was clear. The sample was then transferred to a labelled phial and suspended in distilled water. After sample mixing, a few drops of suspension were pipetted onto a cover slip. Distilled water was then carefully pipetted to achieve complete sample coverage of the cover slip. A second more dilute sub-sample was prepared by pipetting a smaller amount of suspension onto an adjacent cover slip. Diatoms were then allowed to settle and the water evaporate at room temperature for 24 hours. Once dry, the two cover slips were mounted onto a microscope slide with the mounting resin Naphrax, which has a high refractive index.

Diatoms were examined with a Leitz Dialux 20 EB microscope at 1000x and 1250x magnification, using an oil immersion objective. A minimum of 300 diatom valves were counted per sample and identified using Hustedt (1930), Hendey (1964), Barber and Haworth (1981), Krammer and Lange-Bertalot (1986, 1988, 1991a, 1991b) and Hartley *et al.* (1996). A count number of 300 has been shown to give a reasonable approximation of both frequency of individual taxa and the number of taxa in the sample (Battarbee, 1986; Palmer and Abbott, 1986). Fragments of diatom valves were included in the count but to avoid the possibility of double or multiple counting, only fragments that included the valve centre or a single characteristic feature of the valve were counted. However, some taxa (*e.g.* some *Synedra* species) do not possess recognizable centres, and with these the system used was to only count fragments that included a valve end and divide the total by 2 (Battarbee, 1986). Of the 430 slides prepared approximately 20% (85 samples) had no diatoms, very rare diatoms or very poor preservation (very fragmented). From the remaining 345 slides, 225 were selected (typically those with good diatom preservation and diatom numbers) for full counts.

These included 50 samples from the core used in RSL reconstruction (PL1), 130 samples from the other cores and 45 modern analogue surface samples.

Using the ecological information provided by Denys (1991), Vos and de Wolf (1993a) and Van Dam *et al.* (1994) each diatom species can be assigned to one of the halobian salinity categories of Hustedt (1953; 1957), shown as follows:

Halobian group	Salinity preference
Polyhalobian	>30 g l ⁻¹
Mesohalobian	0.2 – 30 g l ⁻¹
Oligohalobian halophilous	optimum in slightly brackish water
Oligohalobian indifferent	optimum in fresh water but tolerant of slightly brackish water
Oligohalobian halophilous	restricted to freshwater environments and intolerant of brackish and marine waters

For each count, diatom frequencies were expressed as percentages of total diatom valves (%TDV). The diatom results for each core and surface transect were presented as diatom diagrams constructed using the software programs *TGView* (Grimm, 2004) and *Tilia* (Grimm, 1993). The complete set of raw diatom counts are presented in the Appendix (attached CD).

3.5 CHRONOLOGICAL FRAMEWORK

3.5.1 Radiocarbon dating

During core description and sampling (in the laboratory and field), a variety of terrestrial plant macrofossils (seeds, fruits, leaves, stems, small twigs) were picked out for potential AMS (accelerator mass spectrometry) radiocarbon dating. These samples were wrapped in foil and stored in a freezer. Individual macrofossils were also extracted from peat samples by wet sieving (0.5 mm mesh) and picking under a binocular microscope. These samples were dried at 110°C and stored in small glass bottles. Twenty samples were submitted to the NERC Radiocarbon Laboratory in East Kilbride for AMS ¹⁴C dating. Another five samples were sent to the Beta Analytic Radiocarbon

Laboratory in Miami, Florida for conventional radiometric ^{14}C dating (four samples) and AMS dating (one sample).

Samples to be used in relative sea-level reconstruction were stratigraphically located at organic-minerogenic boundaries representing transgressive or regressive overlaps (Shennan, 1982; Tooley 1982; see 3.6). Samples from palaeochannel sequences were located at the base of the infill to give a date for channel abandonment. One sample was from a flooding surface at the base of a floodbasin sequence.

Conventional and AMS samples underwent a standard acid-alkali-acid pre-treatment process to remove secondary organic and mineral components (Switsur, 1994). Samples were digested in 2M HCl (80°C, 8 hours), washed free from mineral acid with deionised water then digested in 1M KOH (80°C, 2 hours). The digestion was repeated using deionised water until no further humics were extracted. The residue was rinsed free of alkali, digested in 1M HCl (80°C, 2 hours) then rinsed free of acid, dried and homogenised.

For AMS ^{14}C dating, the total carbon in a known weight of the pre-treated sample was recovered as CO_2 by heating with CuO in a sealed quartz tube. The gas was converted to graphite by Fe/Zn reduction and samples were mounted on a metal disc in the AMS. The isotope ratio of ^{14}C relative to that of the stable forms of carbon (^{13}C or ^{12}C) was measured in the spectrometer to determine the residual ^{14}C content. This was compared with a modern standard of known ^{14}C activity (NBS oxalic acid held by the American Bureau of Standards) to give a sample/modern ratio from which a radiocarbon age can be calculated in years BP. The radiocarbon age is expressed as a mean determination with a +/- value of one standard deviation ($1\ \sigma$) to reflect statistical uncertainties associated with the precise measurement of the ^{14}C decay curve (Lowe and Walker, 1997; Walker, 2005). Further details of the AMS dating process are given in Bowman (1990).

For conventional ^{14}C dating, the liquid scintillation counting technique was used. This involves pre-treated samples being combusted to CO_2 , reacted with molten lithium metal to produce lithium carbide, mixed with water to release acetylene and finally polymerised to benzene. A phosphoric scintillant was added which emits pulses of light (photons) in response to radioactive disintegrations (β particle emission) which can be

counted photoelectrically. The residual ^{14}C activity of the sample was determined from the rate of emissions and compared to the activity of a modern reference standard (NBS oxalic acid). As with AMS dating, the radiocarbon age was expressed with a +/- value of 1σ to reflect uncertainty associated with determining activity (Lowe and Walker, 1997; Walker, 2005).

The AMS ^{14}C particle counting technique was preferentially used instead of 'conventional' beta decay counting because it needs much smaller amounts of carbon (>1mg for AMS dating; >1g for conventional dating) and can date individual macrofossils from a discrete sediment layer or lamination. Where the conventional ^{14}C dating technique was used (principally for cost reasons), samples consisted of single pieces of wood showing minimal erosion.

Reworked older organic material (*e.g.* wood) is often found within alluvial units and is a potential source of error in radiocarbon dating (*e.g.* Blong and Gillespie, 1978; Stanley, 2001). To minimise this risk, when wood samples were used for AMS ^{14}C dating, small sub-aerial twigs showing minimal erosion were chosen. Seed, fruit or leaf samples were used wherever possible as these contain carbon produced in a single year, unlike wood samples which can represent several years growth. They also have a guaranteed sub-aerial source. No aquatic plant macrofossils were used for dating purposes as they can give erroneously old dates due to hard-water reservoir effects (Bjorck and Wohlfarth, 2001). Root samples were not used and all samples were checked under the microscope for root penetration.

All radiocarbon ages were calibrated to calendar years using the program OxCal (Bronk Ramsey, 2001) based on the IntCal04 calibration curve (Reimer *et al.*, 2004) and expressed as a 2σ range in 'cal years AD/BC'.

It has been established that atmospheric ^{14}C activity has fluctuated throughout the Holocene (de Vries, 1958; Pearson *et al.*, 1986), resulting in several plateaux in the ^{14}C calibration curve caused by periods of reduced atmospheric ^{14}C concentration. A radiocarbon date that coincides with one of these plateaux may have more than one calendar (or calibrated) age and a relatively large 2σ range (Walker, 2005). For example, the calibration curve runs fairly level with the calendar axis between 750 cal.BC and 400 cal.BC. This means that a radiocarbon age of about 2450 ± 50 BP

would have a very wide calibrated date range. To help overcome this problem, the OxCal program was also used to produce a probability distribution along the calendar axis for each calibrated date range. The calendar axis is divided into small periods of time and the distribution is in the form of a histogram of the probabilities of the date being in a particular period (Switsur, 1994). The probability distribution therefore enabled the statistically most likely date range(s) to be identified within the distribution.

3.5.2 Optically stimulated luminescence (OSL) dating

Minerals such as quartz and feldspar are able to trap and accumulate charge derived from ionizing radiation sourced from surrounding naturally occurring radionuclides in the sediment matrix, and cosmic rays. The trapped charge can be released by exposure to light and, in the process of recombination, a fraction of the trapped charge is released as light (Madsen *et al.*, 2005). This release of light is termed optically stimulated luminescence (OSL). OSL dating dates the last time that sediment quartz grains were exposed to daylight. It works on the principle that any trapped charge is emptied by exposure to daylight during transport and deposition. This process is known as resetting, zeroing or bleaching.

Following a stratigraphic investigation with a gouge auger, OSL samples were recovered in the field from units of sandy quartz rich sediment. The sediments to be dated varied from thick units of estuarine sand, formed by migrating sandbars, to thinner (*c.*40cm thick) units of fluvial and fluvio-estuarine sand found at the base of palaeochannel fills. The majority (14 out of 16) samples were recovered in sediment cores, recovered by percussion driving a 5 cm diameter, 125 cm long, black plastic pipe into the ground using a Geoprobe drilling rig (figure 3.2). End caps were attached to the pipe and they were then wrapped in cling film (to retain moisture) and tin foil (to help ensure no exposure to sunlight), and stored in a refrigerated cold store. This store was located in the University of Oxford Luminescence Dating Laboratory.

In addition to the Geoprobe core samples, two samples were recovered from the side wall of an excavated pit (figures 3.3 and 3.4). This was only possible because the samples were located at a relatively shallow depth. Sample tubes (6.5cm diameter, 16 cm long) were hammered in to the cleaned section face, and then



Figure 3.2 Geoprobe with raised hydraulic hammer ready for attachment of core chamber.

recovered and end caps fitted. The tubes were then wrapped in black plastic bags. From the sample site in the section face, an auger was used to remove another 30cm of sediment (figure 3.4) and a smaller sample was retrieved from the back of the hole for later water content testing. A field gamma spectrometer probe was then inserted into the augered hole. This was used to measure external gamma-dose.

In the laboratory at Oxford, the core tubes were split open using a circular saw and the surface core sediment was scraped off. 6cm long samples of sediment were removed from the desired stratigraphic locations. Subsamples were taken for water content and radionuclide concentration testing (measured using ICP-MS). All samples were wet sieved into size fractions. Either the 125-180 μm or preferentially the 90-125 μm (if enough) fraction was selected for pre-treatment and OSL testing. All samples were soaked in 37% HCl to remove carbonates, washed twice, then treated to concentrated HF and left on a shaker for 45 mins to remove feldspar and etch the surface of the quartz grains. The sample was then washed four times with water and then once with 10% HCl to remove any remaining soluble fluorides. Samples were then washed twice more with water, once with methylated spirits and once with acetone to help remove water. The residual material was then oven dried at 50°C and sieved again with a 90 μm mesh to remove finer etched grains. The fines were retained and the 90-125 μm sand poured into a micro-tube. Two samples needed 'SPT' or heavy mineral removal. This involved



Figure 3.3 Excavated OSL pit at UH1 palaeochannel site.



Figure 3.4 Following removal of the OSL sample from the section face, a moisture content sample was recovered from the back of the sample hole with a hand auger.

putting the sample into a centrifuge tube and half filling with Sodium polytungstate (has a very high density). The sample was centrifuged at 3000rpm for 5 mins, and the quartz grains were decanted off the top carefully. This was repeated two or three times. All the samples were then mounted onto 11mm diameter aluminium disks for OSL testing. This was done by applying a very thin layer of silica gel to the centre of each disc. The sand was put into a pile on some foil and the disc was dropped onto the sand, picked up with tweezers and the excess sand removed. This should result in a mono-layer of grains sticking to the gel.

The disc-mounted samples were then all OSL tested for equivalent dose (D_e) using a Risø OSL reader. In order to calculate age, the total annual dose rate was calculated from sediment radionuclide concentration (U, Th and K), water content and estimated cosmic ray contribution (based on sample depth, elevation and assumed burial history) using the methods of Aitken (1998) and Prescott and Hutton (1994). It was assumed that all sediment samples had been fully zeroed prior to deposition.

All OSL ages were initially expressed as years before 2000 AD, rounded to the nearest 10 years. A 2σ uncertainty was attached to all dates. This value is based on random and systematic errors from beta-source calibration, dose rate determination, sub-sampling for chemical data, and optical measurement errors following methods in Aitken and Allred (1972) and Aitken (1976, 1985). OSL ages are also expressed in calendar years AD/BC for easier comparison with radiocarbon age results.

A potential problem with OSL dating is partial bleaching. This is where the grains are not exposed to enough light to be completely zeroed. This can result in an overestimate of depositional age (Duller, 2004). Quartz, rather than feldspar grains were tested for OSL as it is known that quartz bleaches faster than feldspar. Sediments deposited in water suffer from the problem that water attenuates the blue end of the spectrum (the most efficient bleaching wave-lengths), and any turbidity can attenuate the daylight spectrum (Berger, 1990). 10 of the OSL samples in this study were deposited in a fluvial or fluvio-estuarine environment, 6 were from a more fully estuarine channel environment. However, despite initial concerns over the partial bleaching issue, there have been many recent studies where fluvial sediments (*e.g.* Wallinga *et al.*, 2001; Wallinga, 2002; Rittenour *et al.*, 2003, 2005, 2007; Rittenour, 2008), and more recently, intertidal sediments (*e.g.* Madsen, *et al.*, 2005; Roberts and Plater, 2007; Jacobs, 2008),

have been successfully OSL dated, with validation of OSL ages by other dating techniques. The measurement of quartz is much less prone to dating error, as the OSL dating of feldspar grains has been shown to give underestimates of age for young sediments and overestimates of age for old sediments (Wallinga *et al.*, 2001).

3.6 RELATIVE SEA-LEVEL RECONSTRUCTION

Holocene RSL changes in the Taw Estuary were reconstructed using the traditional qualitative litho-stratigraphic approach (Shennan, 1982, 1986; Tooley, 1982; Shennan *et al.*, 1983) with diatom bio-stratigraphy providing evidence of changes in marine influence at transgressive and regressive overlaps (Shennan, 1982; Tooley, 1982; Palmer and Abbott, 1986; Vos and de Wolf, 1988). These overlaps were located at core litho-stratigraphic boundaries between organic (peat) and minerogenic (silt-clay) layers (see figure 3.5 for an example), and represent changes in former marsh surface elevation and sedimentation style around MHWST. Organic material (*e.g.* plant macro-remains) from these overlaps was radiocarbon dated to determine the age of deposition and these



Figure 3.5 TS1 core showing transgressive overlap with salt-marsh silty clay deposited on top of fenwood peat. Some bioturbation has occurred in the upper 3 cm of the peat.

ages were used as sea level index points (SLIPs) on an age-altitude plot. This required the present altitude (m OD) of the SLIP to be accurately determined by surveying the top of the core site with a dGPS, and required the indicative meaning of the SLIP to be determined. The indicative meaning is the height of deposition of the sample on the palaeo-marsh surface relative to a reference tide level (Van de Plassche, 1977, 1986; Shennan, 1986; Gehrels 1999). The reference tide level used in this study was MHWST at Barnstaple, derived from Admiralty Tide Tables (2008). The vertical position of a SLIP, relative to MHWST, can therefore be calculated as

$$\text{SLIP (m MHWST)} = H - D - I. \quad \text{eq. 3.2}$$

H is the height of the marsh surface at the core site relative to MHWST, D is the depth of the dated sample in the core (located at an overlap in the stratigraphy), I is the height of deposition of the sample (indicative meaning) on the palaeo-marsh surface relative to MHWST (Gehrels, 1999). Shennan (1982, 1986) presented a table showing the indicative meaning of various overlap types (*e.g.* *Phragmites* peat overlying a saltmarsh silt). This is shown in table 3.4 and formed the basis for determining indicative meaning in the Taw Estuary stratigraphy. However, in this study, all SLIP samples were referenced to a single reference tide level, MHWST, and the altitude of the transition from saltmarsh silt to marsh border peat was determined locally in the Taw Estuary (occurs at MHWST – 0.27cm, not the MHWST – 0.20cm given in table 3.4).

A significant factor that can lead to errors in the determination of SLIP altitude is autocompaction, that is, compression of a sedimentary package by its own weight (Kaye and Barghoorn, 1964; Bloom, 1964; Pizzuto and Schwendt, 1997; Allen, 1999). As the determination of former marsh surface altitude is fundamental in the reconstruction of RSL, post-depositional compaction and consolidation of sediments should be an important consideration. However, because of the problems associated with calculating it, it has often been ignored in sea-level studies. However, it is an important factor as it has been known in certain circumstances to reduce the thickness of organic peats to 10% of their original thickness (Greensmith and Tucker, 1986; Shennan and Waller, 1994). If the problem of compaction is ignored, sea-level index points can be assigned lower altitudes than their ‘true’ depositional altitude, which can result in an overestimation of the rate and magnitude of relative sea-level rise and also affect crustal

models by increasing the apparent trend of subsidence in subsiding areas (Haslett *et al.*, 1998; Allen, 1999).

Table 3.4 Indicative range and indicative meaning for commonly dated materials (Shennan, 1982, 1986).

Dated Material	Indicative range* (cm)	Indicative meaning**
<i>Phragmites</i> or monocot peat:		
Directly above salt-marsh deposit	± 20	[(MHWST + HAT)/2] – 20cm
Directly below salt-marsh deposit	± 20	MHWST – 20cm
Directly above fen wood deposit	± 20	MHWST – 10cm
Directly below fen wood deposit	± 20	[(MHWST + HAT)/2] – 10cm
Directly above & below salt-marsh deposit	± 40	MHWST
Middle of layer	± 70	Infer from stratigraphy
Fen wood peat:		
Directly above <i>Phragmites</i> or salt-marsh deposit	± 20	(MHWST + HAT)/2
Directly below <i>Phragmites</i> or salt-marsh deposit	± 20	MHWST
Basal peat***:		
Directly below <i>Phragmites</i> or salt-marsh deposit	± 20	MHWST
Directly below fen wood deposit	± 80	MTL to MHWST

* The Indicative range (given as a maximum) is the most probable vertical range in which the sample was originally deposited.

** The indicative meaning is the height of deposition of the sample on the palaeo-marsh surface relative to a reference tide level.

*** A basal peat is formed as the result of a rising water-table.

There are several methods used to correct for compaction in sea-level studies. A soil mechanics approach has occasionally been used (*e.g.* Cullingford *et al.*, 1980; Smith, 1985; Pizzuto and Schwendt, 1997; Paul and Barras, 1998; Rybczyk *et al.*, 1998; Allen, 1999; Tovey and Paul, 2002; Williams, 2003; Bird *et al.*, 2004; Massey *et al.*, 2006) to estimate the original thickness of peat and clay layers. In this method a compaction correction factor is applied to each sediment type. Cullingford *et al.* (1980) proposed a correction factor of 40-68% for peats and this value has since been used in various sea-level studies (*e.g.* Smith *et al.*, 2003; Selby and Smith, 2007).

The most reliable method for overcoming the compaction problem, that is less prone to error, is to only use sea-level index points from thin basal peats (*e.g.* Gehrels *et al.*, 1996; Gehrels, 1999; Donnelly *et al.*, 2004; Tornqvist *et al.*, 2004) deposited on non-

deformable basement (sand and gravel or bedrock) as the sediment here is compaction-free and not vertically displaced over time.

A basal peat sequence was not found in the inner Taw Estuary, but a good core site was found that contained a 6 m sequence of intercalated peats and minerogenic silts. This core was used for RSL reconstruction and the approach of Haslett *et al.* (1998) was followed with regard to compaction. This method requires sediment to be onlapping non-deformable basement as it is based on the principle that intercalated peats will become compaction-free when they onlap a sloping basement surface. The maximum altitude of each peat layer surface, as it onlaps the valley side, would therefore give an approximation of the pre-compaction altitude for that palaeo-surface. This method depends on the assumption that prior to compaction, the organic deposits accumulated upwards in a uniform manner to produce a synchronous upper surface with a common altitude. An alternative hypothesis would be that the peat surface topography represents a largely unaltered sloping palaeo-surface which was formed diachronously by rising sea-level. This latter hypothesis could be tested by dating the peat surface at a separate location, higher up the slope.

To follow this method, a series of closely spaced boreholes (0.4 m to 2.0 m intervals) was cored with a gouge auger along the western end of the transect that contained the RSL core (Transect A). This increased stratigraphic resolution enabled any altitudinal changes in the upper surfaces of the peat layers to be investigated. However, funds could not be found for the radiocarbon dating of additional non-SLIP peat samples. The assumption was therefore made that the upper surfaces of peat layers were synchronous, unless any sedimentary evidence suggested otherwise.

3.7 CONTEMPORARY DIATOM DISTRIBUTION

The modern distribution of diatom species was investigated by the collection of a set of modern analogue samples located along various environmental gradients in the Taw Estuary and River Taw valley. These gradients were related to altitude (flooding duration) in the estuary survey and salinity in the river survey. This involved sampling the surface 1 cm of sediment at 34 sampling stations located along two transects:

(1) Taw Estuary transverse transect

Sampling stations were established along a 1.1 km transect located transversely across the middle Taw estuary, 3.0 km west of Barnstaple. This transect covers a large part of the intertidal zone from below MTL (Mean Tide Level) to above MHWST (Mean High Water of Spring Tides) with depositional environments including tidal flat, low and high salt-marsh, and a brackish mire at the landward edge.

(2) Tidal and non-tidal River Taw longitudinal transect

Sampling stations were located along a 10 km stretch of mainly inner estuarine tidal river, between Barnstaple and Umberleigh. All samples were taken from the vegetated channel edge, with samples located close to MHWST in the tidal reach.

Six environmental variables were recorded at each sampling station. Altitude and pH were measured in the field. Water samples were taken for later salinity measurement and sediment samples were taken for analysis of organic matter content, carbonate content and magnetic susceptibility. In addition, the flora was described at each station in the Estuary transect. The methods used are as follows:

Altitude

Altitude was measured with a differential GPS.

Salinity (conductivity)

Pore-water samples were collected at each field station (ponded surface water was collected in the river survey) and measured in the laboratory with a Portland Electronics conductivity meter, which was adjusted for temperature. Conductivity was converted to salinity using the algorithms of Fofonoff and Millard (1983). Conductivity readings were also made in the field using a Hanna Instruments Primo5 conductivity meter. However, this meter can only measure conductivities under 2.0 mS/cm (approx. 1.2 ppt salinity) and was therefore primarily used to locate the brackish – freshwater transition.

pH

The pH of a 2:1 slurry (by volume) of distilled water and soil was measured in the field using an electrometric Hanna Instruments Checker pH meter. The meter was first calibrated using pH 4 and pH 7 buffer solutions.

Organic matter content

The loss on ignition method was used to measure the organic matter content of a 2 g sediment sample (3.4.3).

Carbonate content

Carbonate content was also analysed via the loss on ignition method (see 3.4.3).

Magnetic susceptibility

Magnetic susceptibility (low frequency and frequency dependent) was measured in the laboratory with a Bartington MS2 susceptibility meter and MS2B dual frequency sensor (see 3.4.4).

Flora

At each sampling station in the Estuary transect the floral assemblage within a 4 m radius was identified and quantified as percentage cover for each species. This allowed the salt-marsh to be divided into floral assemblage zones.

In both the estuary and river surveys, sediment and water samples were collected immediately after a range of tides between MHWST and HAT (during 2005-2007). This was done to investigate variation in sedimentary characteristics such as carbonate content and to investigate variations in salinity. These repeat surveys were especially relevant to the river survey where changes in the position of the salinity front could be monitored at several high tides. Diatoms were analysed from samples collected after a more typical MHWST tide.

The tidal frame levels at Barnstaple Quay were derived from consultation of Admiralty Tide Tables (2008). Important tidal frame positions include MHWNT (Mean High Water of Neap Tides), MHWST (Mean High Water of Spring Tides), and HAT (Highest Astronomical Tide). The up-river spatial limit to HAT was determined by observing and tracking the highest tide during 2007. The altitude that this tide reached near its up-river limit was determined by marking and surveying the high water level with a differential GPS. This enabled any up-river tidal slope to be ascertained (caused by up-river changes in tidal range).

3.8 DATA ANALYSIS

3.8.1 Analysis of the modern dataset

Constrained incremental sum of squares cluster analysis (CONISS) was performed on the modern diatom assemblages so as to group them into relatively homogenous clusters. These clusters related to depositional altitude in the Taw Estuary survey and to distance upstream from Barnstaple in the longitudinal river survey. Cluster analysis was done using the program *Tilia* (Grimm, 1993) and presented as a dendrogram. Only species that reach 3%TDV were included.

3.8.2 Analysis of the Holocene dataset

The diatom assemblage data (>3%TDV species) from each of the cores was analysed for zonation using constrained incremental sum-of-squares cluster analysis (CONISS). This was done using the program *Tilia* (Grimm, 1993) and presented as a dendrogram. The resulting diatom zones were interpreted in terms of depositional altitude in the tidal frame. This qualitative interpretation was based on the modern analogue of diatom altitudinal zonation in the middle Taw Estuary (chapter 4) and on previous studies of diatom distribution in the UK and elsewhere. In the cores used in RSL reconstruction, this provided bio-stratigraphic evidence of changes in marine influence across each transgressive and regressive overlap (Tooley, 1982; Shennan, 1982; Shennan *et al.*, 1983).

A Diatom Salinity Index (DSI) was developed for each diatom assemblage (sample) using the method of Bryne *et al.* (2001) in order to give a semi-quantitative measure of palaeosalinity. This index requires taxa to be classified according to the salinity classification of Van der Werff (1958) and Van der Werff and Huls (1957-1974). This was done using the species check-list of Denys (1991). This classification groups diatom species into those with a similar salinity preference. These preferences are freshwater (F; 0-2‰ salinity), both freshwater and brackish (FB; 0-30‰ salinity), brackish (B; 2-30‰ salinity), brackish and marine (BM; 2-35‰ salinity), and marine (M; 30-35‰ salinity). The DSI of an assemblage summarises the proportions of taxa that prefer freshwater, brackish, and marine salinities and is calculated as follows:

$$\text{DSI} = (\text{F} + \text{FB} + 0.5\text{B}) / (\text{F} + \text{FB} + \text{B} + \text{BM} + \text{M}) \quad \text{eq. 3.3}$$

The index ranges from 0.00 to 0.30 for samples dominated by marine taxa, 0.31 to 0.70 for samples dominated by a mixture of taxa, and 0.71 to 1.00 for samples dominated by freshwater taxa (Bryne *et al.*, 2001).

Constrained cluster analysis (CONISS) was performed on the magnetic data, using the five concentration-related parameters X_{lf} , SIRM, X_{arm} , IRM_{soft} and IRM_{hard} and presented as a dendrogram. A square root transformation was performed on all data prior to this analysis. Other ratio, percentage and quotient parameters were not used in the analysis as it has been shown (*e.g.* Maher, 1986) that these other parameters do not help the classification. This shows that there is inter-correlation between many magnetic parameters (Lees, 1999). The resulting magnetics zones were interpreted in terms of magnetic mineral composition, concentration and grain size using the semi-quantitative approach outlined in tables 3.2 and 3.3.

4 CONTEMPORARY DIATOM DISTRIBUTION IN THE TAW ESTUARY AND THE LOWER TAW VALLEY

4.1 INTRODUCTION

This chapter will describe the results of two surveys of contemporary diatom distribution in the Taw Estuary and the lower Taw valley.

4.1.1 Taw Estuary survey

The estuary survey was carried out during 2005, with samples collected along an intertidal transect which incorporated tidal flat, pioneer, low middle and high saltmarsh, and marsh border environments. The transect was located in the middle estuary as no suitable site was found in the tidal river environment of the inner estuary (upstream of Barnstaple) that showed the required altitudinal succession of depositional zones. This was due to the presence of flood embankments on each side of the tidal river causing the absence of a natural succession into marsh border at the upper end of the tidal frame close to HAT, and due to the steep nature of the channel banks in the tidal river.

The aims of the estuary survey were as follows:

- (1) To establish the relationship between contemporary diatom assemblages and tidal frame position (*e.g.* Nelson and Kashima, 1993; Hemphill-Haley, 1995a, 1995b; Shennan *et al.*, 1995, 1996; Zong, 1997; Zong and Horton, 1998, 1999; Sherrod, 1999; Gehrels *et al.*, 2001; Sawai, *et al.*, 2004; Hamilton and Shennan, 2005; Patterson *et al.*, 2000, 2005; Horton *et al.*, 2006, 2007; Szkornik *et al.*, 2006; Hill *et al.*, 2007; Nelson *et al.*, 2008; Kemp *et al.*, 2009).
- (2) To establish the relationship between tidal frame position and a range of environmental variables, including salinity, vegetation cover, pH, sediment organic matter content, sediment mineralogy (specifically carbonate and magnetic mineral concentration), and sediment grain size (*e.g.* Rijk and Troelstra, 1997; Zong and Horton, 1998; Horton, 1999; Horton *et al.*, 1999; Sawai, *et al.*, 2004).

(3) To establish the relationship between diatom assemblage DSI (diatom salinity index) and tidal frame position.

The purpose of the first aim is to provide a local contemporary analogue of diatom species distribution and altitudinal zonation (relating to tidal cycle submergence duration: Gehrels, 2000) that can be used in the qualitative interpretation of fossil core assemblages. This will allow diatom assemblages from a series of inner Taw Estuary sediment cores (chapter 5) to be interpreted in terms of former depositional altitude in the tidal frame. In the cores used in RSL reconstruction, the qualitative identification of tidal frame position will provide bio-stratigraphical evidence of down-core changes in marine influence, enabling the validation of sea-level index points at transgressive and regressive overlaps (*e.g.* Haggart, 1986; Long, 1992; Plater and Shennan, 1992; Healey, 1995; Shennan *et al.*, 1995, 1996, 2000a; Zong and Tooley, 1996; Zong, 1997, 1998; Long *et al.*, 1998; Smith *et al.*, 2003; Gehrels *et al.*, 2006; Selby and Smith, 2007). In the full suite of inner estuary cores, diatom assemblage DSI values can be used to give a semi-quantitative measure of palaeosalinity (Bryne *et al.*, 2001). Once depositional altitudes have been identified in the Holocene core records, spatial and temporal variations in palaeosalinity for individual depositional environments (*e.g.* high saltmarsh) can be investigated (chapter 7).

The second aim will provide a contemporary analogue of sedimentary and vegetation changes along an intertidal altitudinal gradient. This analogue can be used to support the qualitative identification of former depositional altitude in the core records of the inner estuary (Chapter 5).

The objective of the third aim is to investigate DSI changes along an intertidal altitudinal gradient in a middle estuarine setting and to ascertain the degree of DSI variation that occurs within specific intertidal zones (*e.g.* high saltmarsh or middle saltmarsh zones). Those tidal frame zones that show the least internal DSI variation will be used in the palaeosalinity analysis presented in chapter 7. This will enable smaller uncertainties to be attached to fossil assemblage DSI values.

4.1.2 River Taw survey

The River Taw survey was carried out during 2007, with samples collected from the river-bank along an up-river longitudinal transect from Barnstaple, through the inner estuarine tidal reach, to the top of the non-tidal freshwater reach (1.5 km downstream of Umberleigh). Up-river salinity measurements were made during several spring tides (including the HAT for 2007). The aims of this survey are as follows:

- (1) To determine the salinity gradient for the inner estuary and to clarify the HAT limits of surface and groundwater saltwater intrusion in the Taw valley.
- (2) To establish the relationship between contemporary diatom assemblages and an up-river salinity gradient, with samples in the inner estuarine tidal reach taken from a similar tidal frame position.
- (3) To establish the relationship between location in the salinity gradient and a range of sedimentary environmental variables, including organic matter content, carbonate content and magnetic mineral concentration.

The first aim will provide an estimate of the maximum up-stream location of the salinity front (boundary between brackish tidal zone and freshwater tidal zone) and the freshwater tidal head (HAT). This can be used as a benchmark in the investigation of former late Holocene salinity front location, as seen in the core diatom records.

The second aim will provide a local contemporary analogue of diatom species distribution and up-river location for a specific high inter-tidal zone. This will aid qualitative interpretation of the fossil diatom records, and the modern assemblage DSI values can be used as a contemporary layer in the temporal-spatial analysis of estuarine palaeosalinity change during the late Holocene.

The third aim will provide a contemporary analogue of changes in specific sedimentary variables along an up-river salinity gradient. This will aid interpretation of the core records, in terms of location along the fluvio-estuarine facies transition.

4.2 TAW ESTUARY

4.2.1 Taw Estuary transect

Figure 4.1 shows a map of the middle Taw Estuary, 3 km west of Barnstaple, where an inter-tidal saltmarsh has developed on the southern side of the estuary. The location of two transects, Estuary South and Estuary North, are indicated. A smaller transect, Estuary South extension, incorporates an area of upper high saltmarsh and a thin marsh border strip, unseen in the main Estuary South transect. A dendritic network of tidal channels has formed on the middle and lower high saltmarsh platform, indicative of a mature marsh (Pye and French, 1993). Steel and Pye (1997) have shown that following marsh inception, drainage density may quickly reach a maximum in about 100 years. This seems to be the case with the Taw Estuary marsh, as the 1905 Ordnance Survey map of the area shows that the former marsh edge was located at the current mid saltmarsh – high saltmarsh boundary (currently defined by a line of marsh creeks). This indicates that the middle and low saltmarsh zones have developed and accreted in the last 100 years. Studies of saltmarsh development and long-term accretion rates confirm that a mid saltmarsh elevation can be reached in this time-frame (Pethick, 1981; French, 1993). In the middle and high saltmarsh zones, numerous elongate saltpans (Bayliss-Smith *et al.*, 1979) have developed at the ends of abandoned first order creeks, with isolated saltpans (usually permanently full of water) located at sub-catchment hydraulic boundaries. A similar pattern of saltpans has also been observed in other UK saltmarshes, for example, in the North Norfolk saltmarshes by Pye (1992), Havelock (2001) and Lawrence *et al.* (2004). Photographs of the Taw saltmarsh and tidal flat zones (see figure 4.1 for zone locations) are shown in figures 4.2 and 4.3, indicating a typical flat marsh platform, dissected by U-shaped creeks.

Figure 4.4 shows the transverse profile of the Taw Estuary, along the combined Estuary North and Estuary South transect lines. Figures 4.5 and 4.6 show the profiles of the individual transect lines and the location of 17 sampling stations. The Estuary South extension, on the landward edge of the saltmarsh, has been incorporated into the Estuary South transect profile. The saltmarsh has been divided into several zones, based on the altitudinal zonation of the marsh vegetation. The dominant plant species are given in figure 4.5. The pioneer saltmarsh zone is dominated by *Spartina anglica* (English Cordgrass). The low saltmarsh zone is dominated by *Spartina anglica* and *Puccinellia*

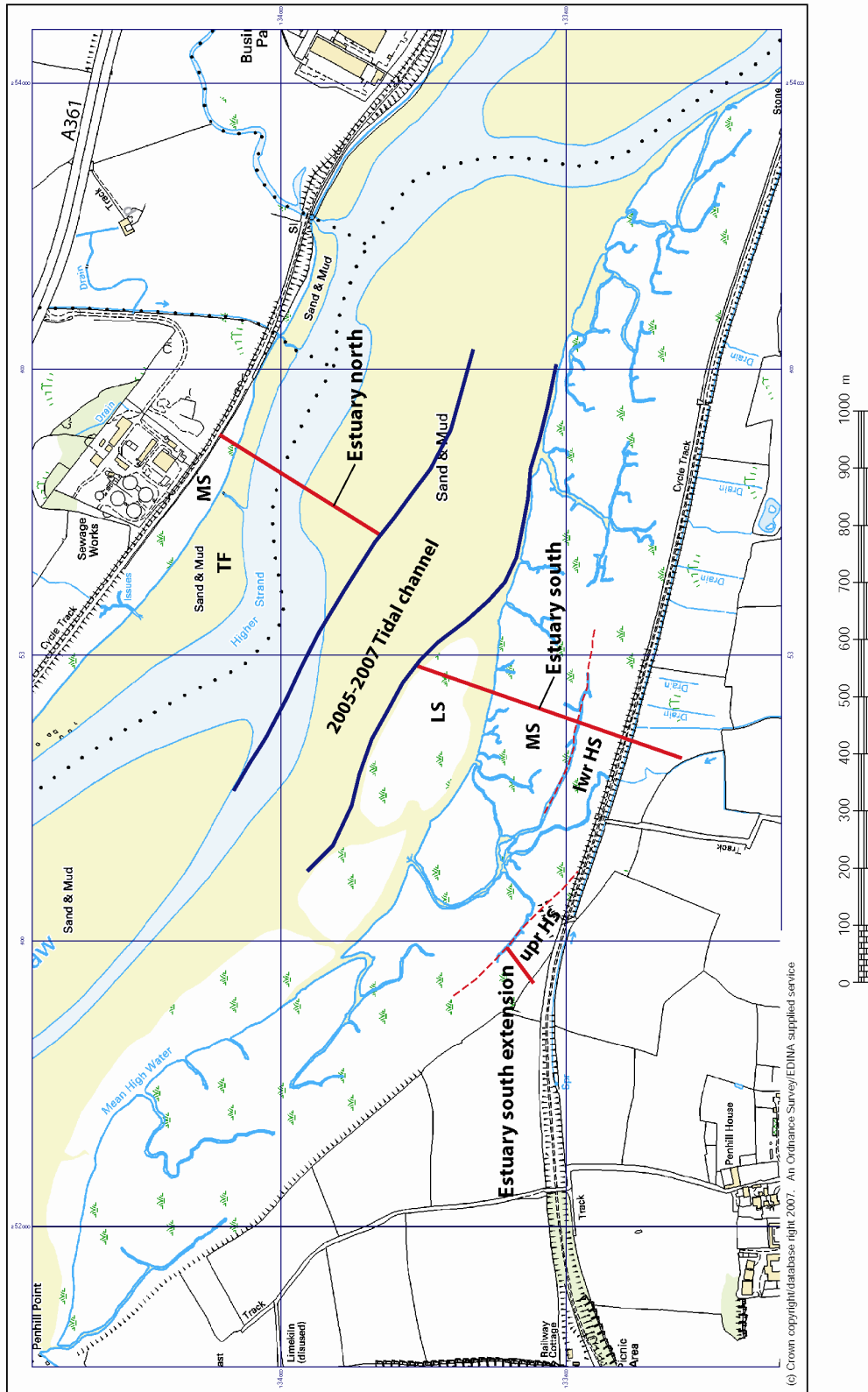
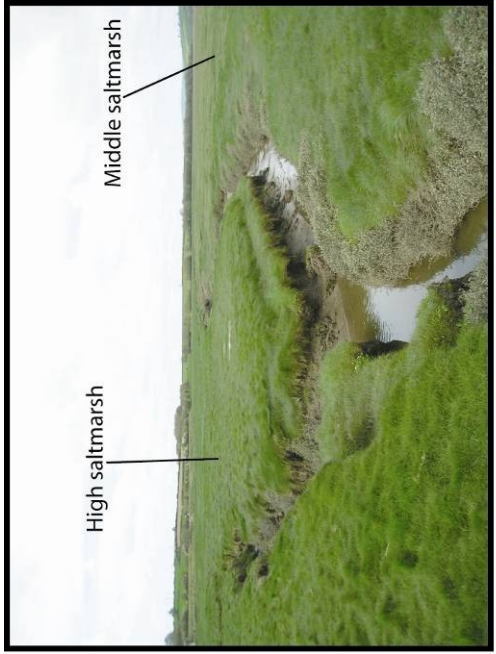


Figure 4.1 Location of the Taw Estuary transects, 3 km west of Barnstaple. Upr HS = upper High saltmarsh; lwr HS = lower High saltmarsh; MS = Middle saltmarsh; LS = Lower saltmarsh; TF = Tidal flat. The 1:10,000 base map was supplied by Ordnance Survey/EDINA Digimap. GB National Grid lines are shown.

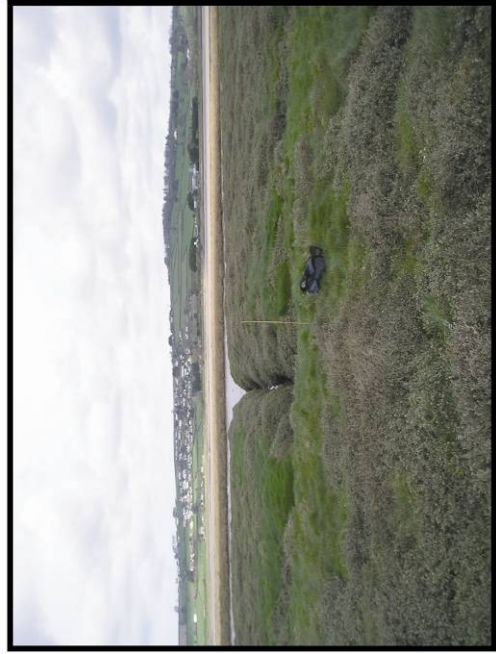
incorporates and OS 10,000 colour raster layers (supplied by Ordnance Survey/EDINA Digimap).



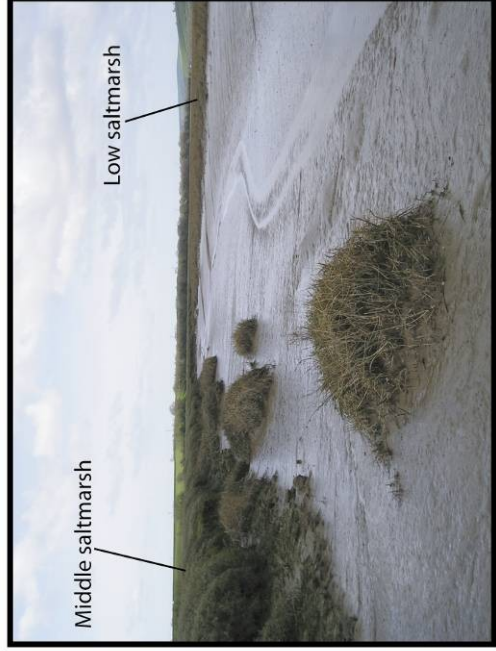
(a) High saltmarsh (Estuary South)



(b) *Puccinellia maritima* zone of middle saltmarsh (Estuary South)

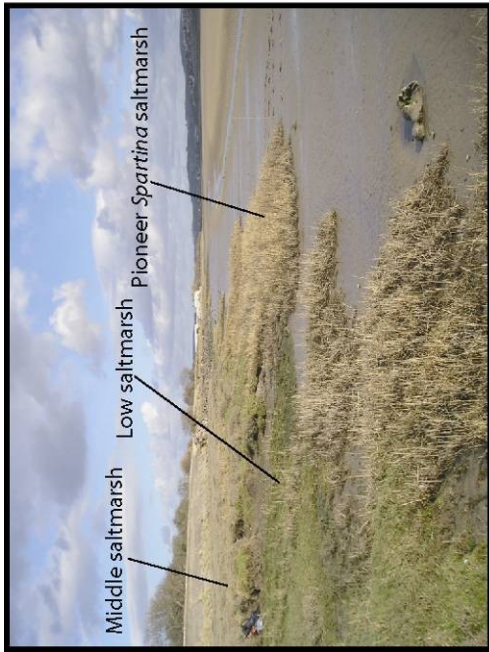


(c) *Atriplex portulacaoides* zone of middle saltmarsh (Estuary South)



(d) Tidal channel separating middle and low saltmarsh (Estuary South)

Figure 4.2 Photographs of the middle and high saltmarsh zones in the Estuary South transect (see figure 4.5 for location of vegetation zones).



(a) Saltmarsh edge in Estuary North transect at low tide



(b) View south along Estuary North transect line at start of flood tide



(c) Eroding estuarine cutbank in Estuary South transect



(d) Low *Spartina* saltmarsh in Estuary South transect

Figure 4.3 Photographs of the Estuary North transect and low saltmarsh zone of the Estuary South transect.

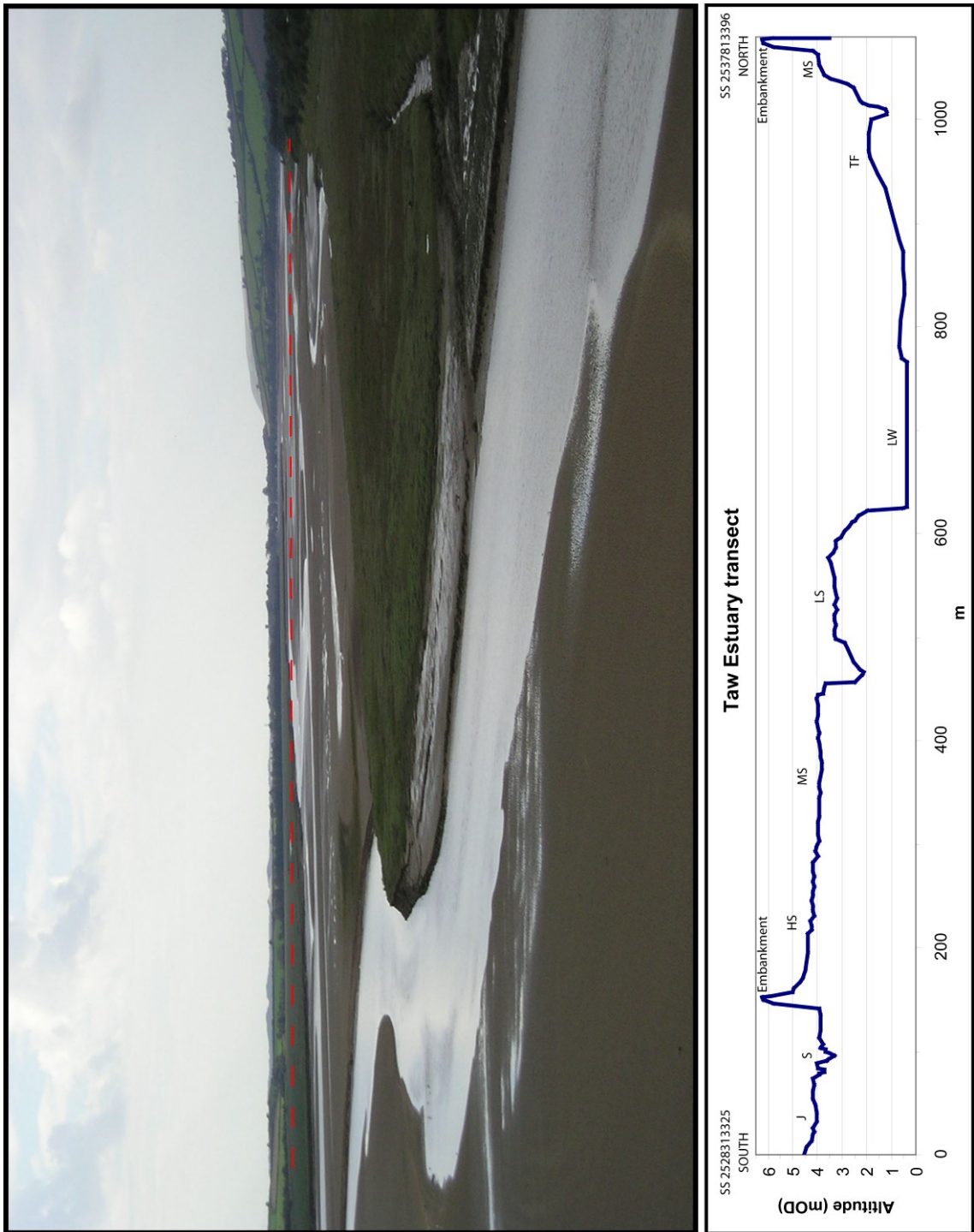


Figure 4.4 Photograph of the Taw Estuary study site, taken from Taw Bridge (Barnstaple western bypass). The location of the combined transect line is indicated on the photograph and given as a transverse estuary profile in the lower diagram. UK National Grid references are given for the ends of the transect line. The flood embankments on either side of the estuary are also the site of former railway lines. HS = High saltmarsh; MS = Mid saltmarsh; LS = Low saltmarsh; TF = Tidal flat; LW = low water level; J = *Juncus* marsh; S = *Scirpus* marsh.

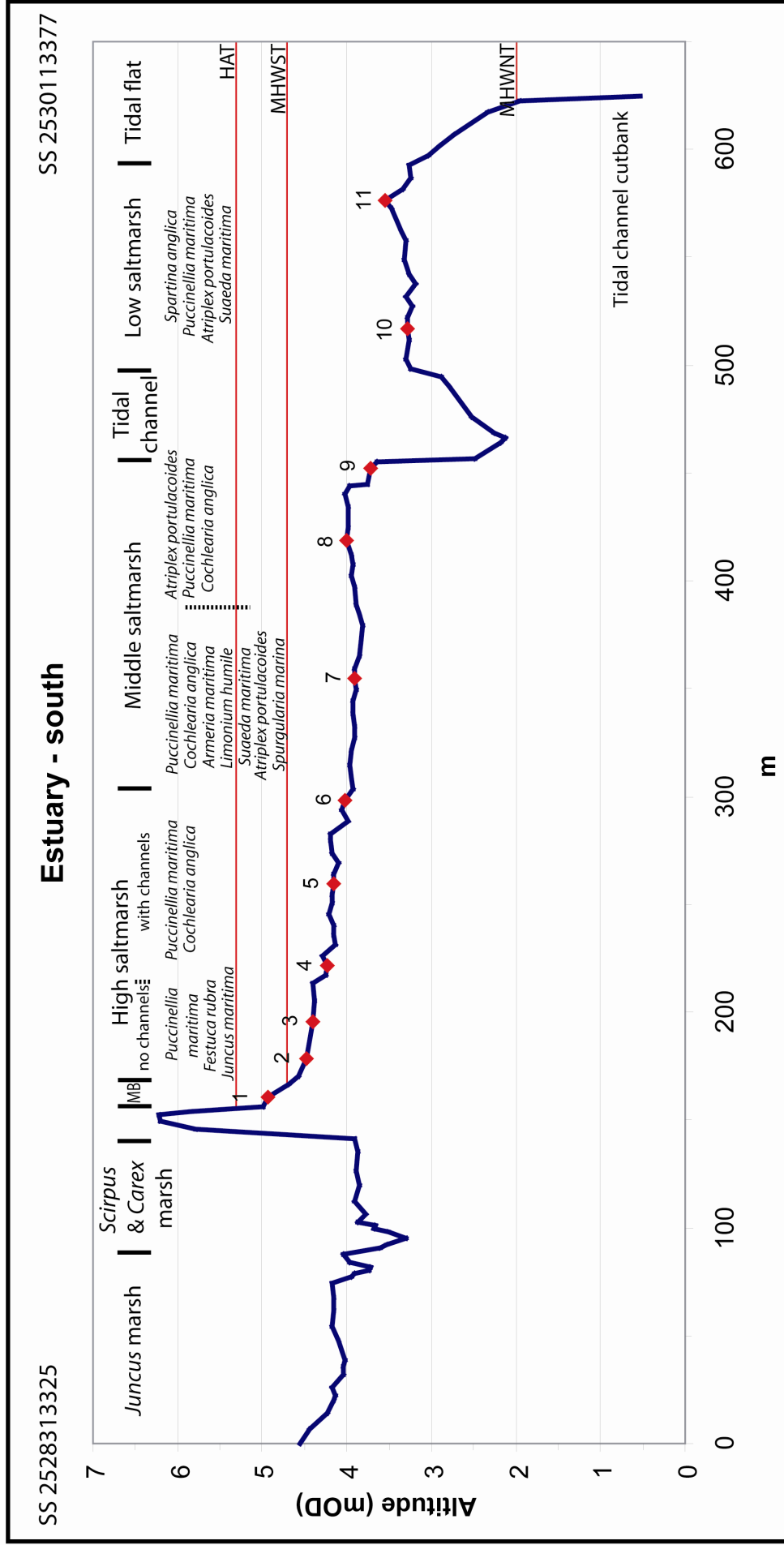


Figure 4.5 Profile of the Estuary South transect with location of sampling stations. The vegetation zones are indicated, and associated dominant vascular plant species. The upper high saltmarsh subzone corresponds with the area where tidal channels are absent and was incorporated into this profile from the Estuary South extension transect. Tidal frame levels are indicated. MB = Marsh border zone. UK National Grid references are given for the ends of the transect line. See figure 4.1 for transect location.

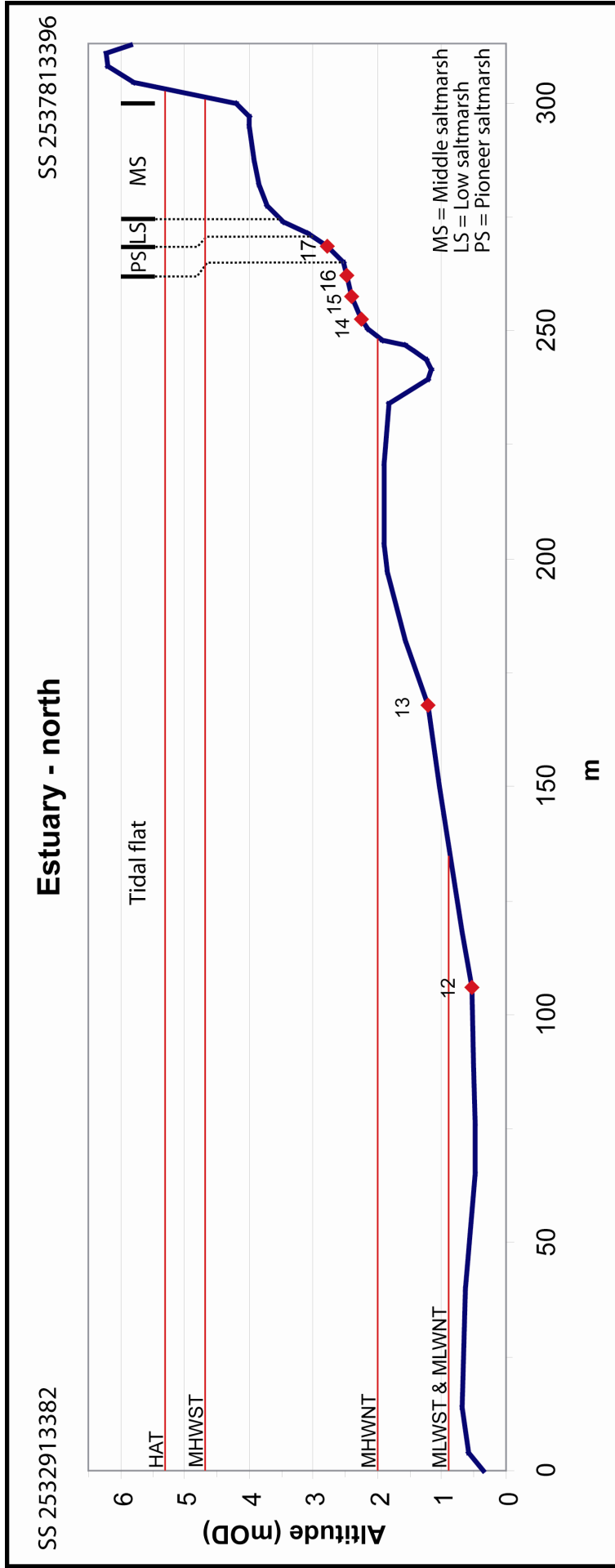


Figure 4.6 Profile of the Estuary North transect with location of sampling stations. Tidal frame levels are indicated. UK National Grid references are given for the ends of the transect line. See figure 4.1 for transect location.

maritima (Saltmarsh Grass). The middle saltmarsh zone is divided into two subzones, with the area nearest the saltmarsh edge dominated by *Atriplex portulacoides* (Sea Purslane) and *Puccinellia maritima*. The landward area of the middle saltmarsh is dominated by a diverse saltmarsh flora, including *Puccinellia maritima*, *Cochlearia anglica* (English Scurvy Grass), *Armeria maritima* (Thrift), *Limonium vulgare* (Common Sea Lavender) and *Suaeda maritima* (Annual Seablite). The high saltmarsh is also divided onto two subzones with the lower high saltmarsh subzone dominated by *Puccinellia maritima* and *Cochlearia anglica*. The upper high saltmarsh is dominated by *Puccinellia maritima*, *Festuca rubra* (Red Fescue) and *Juncus maritimus* (Sea Rush). The first appearance of *Juncus maritimus* has been recorded in other UK studies at the landward edge of saltmarshes at MHWST or just below (e.g. Tramaig Bay and Nith Estuary: Zong and Horton, 1998, 1999), or just above MHWST (e.g. Roudsea Marsh: Zong, 1997; Zong and Horton, 1998, 1999). Figure 4.5 also shows that the Estuary South transect extends at its landward end into a brackish *Juncus-Scirpus* marsh. This area was not sampled for diatoms as its location behind a flood embankment has resulted in artificial salinity-altitude and submergence duration-altitude relationships. Before embanking, this area would have been a high saltmarsh environment that was regularly flooded. However, since embanking, a *Scirpus* marsh has developed in a former saltmarsh creek, with partial tidal submergence caused by some tidal water making its way through cracks in an embankment sluice gate. A small freshwater stream also helps maintain lower salinities.

The tidal frame levels (e.g. MHWST) for the inner Taw Estuary (indicated in figures 4.5 and 4.6) are given in table 4.1. These are for Barnstaple and are derived from Admiralty Tide Tables (2008). The shallow water effect of the inner estuary has resulted in a restricted tidal range with MLWNT and MLWST both at 0.9m OD. This is the mean level of residual non-tidal flow from the River Taw at Barnstaple. At the transect site, this level was recorded at c.0.5m OD. This may have been because of a low river discharge on the survey date, or it may represent the fluvial water surface slope between Barnstaple and the transect site (2 km).

Tidal frame level	HAT	MHWST	MHWNT	MLWNT	MLWST
Altitude (m OD)	5.3	4.7	2.0	0.9	0.9

Table 4.1 Tidal frame levels for Barnstaple (Admiralty Tide Tables, 2008)

4.2.2 Contemporary diatom distribution and environmental variables

Environmental variation in the Taw Estuary transects

As discussed in chapter 2, diatom distribution in estuaries has two major controls, flooding duration/frequency and salinity. Flooding duration is strongly linked with elevation in the tidal frame and it has been shown in many studies that diatom distribution can be related to elevation (*e.g.* Nelson and Kashima, 1993; Hemphill-Haley, 1995a, 1995b; Shennan *et al.*, 1995, 1996; Zong, 1997; Zong and Horton, 1998, 1999; Sherrod, 1999; Gehrels *et al.*, 2001; Sawai, *et al.*, 2004; Hamilton and Shennan, 2005; Patterson *et al.*, 2000, 2005; Horton *et al.*, 2006, 2007; Szkornik *et al.*, 2006; Hill *et al.*, 2007; Nelson *et al.*, 2008; Kemp *et al.*, 2009). A number of environmental variables (*e.g.* organic matter content, grain size, vegetation cover and pH) have also been shown to be associated with elevation in the tidal frame, *i.e.* flooding duration (Horton *et al.*, 1999, 2003; Zong and Horton, 1999; Sawai *et al.*, 2004; Horton and Edwards, 2005). The relationship between marsh surface elevation and a number of environmental variables was explored in the Taw Estuary transects. These variables were sediment texture (or grain size, described in the field), organic matter content, carbonate content, magnetic susceptibility (a measure of magnetic mineral concentration), pH and vegetation. In addition to the diatom data, figure 4.7 records changes in these environmental variables along an altitudinal tidal frame gradient from 0.5m OD (the low tide level of residual fluvial drainage) to 5.0m OD (30cm below the 2008 HAT).

In terms of sediment characteristics, the tidal sandflat is composed of fine-medium sand with a low organic matter content of 1-2%. Sand-grade comminuted shell debris make up a significant component of this sand, resulting in carbonate content values of 8-20% (early diagenetic carbonate crystals may also be present, Allen (1987)). Carbonate grains have also been found to be an important component of the sediments found in the nearby Severn Estuary where they represent up to 10% of the sediment (Allen 1987). The tidal mudflat is composed of planar inter-laminated shelly sand and silt with an organic matter content of 3-5% and a carbonate content of 9-12%. The pioneer saltmarsh zone (which is absent in some areas, where it is replaced by tidal mudflat) is also composed of planar inter-laminated shelly sand and silt with an organic matter content of 7% and a carbonate content of 5%. The low saltmarsh zone is composed of

silty/sandy clay with an organic matter content of 10-11% and a carbonate content of 4-6%. The mid saltmarsh zone is composed of clayey silt with an organic matter content of 10-12% and a carbonate content of 2-4%. The lower high saltmarsh zone is composed of clayey silt with an organic matter content of 13-15% and a carbonate content of 2%. The upper high saltmarsh zone is composed of peaty silt with an organic matter content of 18-26% and a carbonate content of 1-2%. The marsh border zone is composed of silty peat with an organic matter content of 29% and a carbonate content of 1%. The sharp rise in organic matter content occurs at approximately MHWST-27cm. The indicative meaning of a silt-peat transgressive overlap given in Table 3.4 (chapter 3) was MHWST-20cm (Shennan, 1982). Using the local field evidence for the Taw Estuary, this will be modified to MHWST-27cm for use in RSL reconstruction (chapter 7).

Magnetic susceptibility (X_{if}) values are very low ($0.04-0.08 \times 10^{-6} \text{ m}^3 \text{ kg}^{-1}$) in the tidal sandflat, indicating low concentrations of detrital magnetic grains. X_{if} values rise through the tidal mudflat to reach $0.30 \times 10^{-6} \text{ m}^3 \text{ kg}^{-1}$ in the pioneer saltmarsh zone. Peak values ($0.33-0.58 \times 10^{-6} \text{ m}^3 \text{ kg}^{-1}$) are seen in the low and mid saltmarsh zones, and the base of the lower high saltmarsh zone. X_{if} values then fall to $0.20-0.32$ in the rest of the high saltmarsh zone, and fall to $0.14 \times 10^{-6} \text{ m}^3 \text{ kg}^{-1}$ in the marsh border peat. The high X_{if} values of the low, mid and lower high saltmarsh sediments are thought to be due to the presence of secondary magnetite in the form of magnetosomes produced by magnetotactic bacteria. Previous studies have shown that bacterial magnetite makes a significant contribution to magnetic assemblages in inter-tidal saltmarsh environments (Oldfield and Yu, 1994; Gibbs, 2000). The high X_{if} values may also be due to the presence of authigenic greigite. The chemical precipitation of this ferrimagnetic iron sulphide at the sediment-water interface has been reported in both brackish-marine and lacustrine anoxic environments (Snowball and Thompson, 1988; Snowball, 1991; Oldfield, 1994).

It was found that pH values are very similar (7.1-7.8) throughout the minerogenic tidal flat and saltmarsh zones, but in the peaty silt and silty peat of the upper high saltmarsh and marsh border, values gradually fall to a more acidic 5.8.

Salinity is the other main control on diatom distribution in estuaries. However, this mainly controls the spatial distribution of diatoms up the axis of the estuary along the

salinity gradient (e.g. Juggins, 1992; Sidell *et al.*, 2000). Changes in salinity with elevational change have been found to be much less pronounced (Horton *et al.*, 1999, 2003; Zong and Horton, 1999; Sawai *et al.*, 2004; Horton and Edwards, 2005). For example, the study by Zong and Horton (1998) of six UK saltmarshes revealed trends of relatively little change in porewater salinity, when measured across a marsh transect after a spring tide. However, their work recorded significant variations in salinity between different high tides. This was also seen in a study by Rijk (1995a, 1995b) and Rijk and Troelstra (1997) in the Great Marshes in Massachusetts (USA), where their daily records of marsh salinity over a 50 day period recorded changes in salinity that correlated with the higher spring tides and with heavy rainfall days. At Roudsea Marsh, in the UK, a record of seasonal variation in marsh salinity recorded by Zong (1997) was attributed to changes in freshwater discharge from the catchment.

Salinity was measured in pore-water samples at each of the sampling stations in the Taw Estuary transect and the results are shown in figure 4.7. Salinity was measured twice, once immediately after a 5.3m OD spring tide (equal to the 2008 HAT), and again after a 5.1m OD spring tide. However, the upper high saltmarsh and marsh border sampling stations (Estuary South extension transect in figure 4.1) were not sampled during this latter survey. After the 5.3m OD tide, salinities were found to be quite similar right across the inter-tidal zone with values ranging from 26‰ to 36‰. Highest values were found in the low and mid saltmarsh zones (34-36‰). Values of 32‰ were typical for the tidal mudflat, while in the tidal sandflat, values gradually decreased to 28‰ at 0.53m OD, where the water chemistry is more affected by residual fluvial flow at low tide. In the upper part of the tidal frame, values were seen to fluctuate between 26‰ and 32‰ in the high saltmarsh and marsh border zones. After the 5.1m OD tide, somewhat more variation was seen in salinity across the transect, and the salinity of most tidal zones fell significantly, despite the modest decrease in high water level, with values ranging from 15‰ to 33‰. Highest values were again found in the low saltmarsh zone (32-33‰). Salinities in the pioneer saltmarsh and tidal mudflat zones ranged from 26‰ to 28‰, and then gradually decreased to 15‰ at the base of the sandflat zone, where it was affected by fluvial outflow. In the upper parts of the tidal frame, values fluctuated at 21-28‰ in the mid saltmarsh zone, before declining from 25‰ to 15‰ up through the lower high saltmarsh zone, where infrequent tidal inundation and groundwater seepage from the adjacent upland (Rijk, 1995b) will reduce salinity values.

The results of the Taw Estuary salinity survey show some agreement with trends in other UK estuaries, with relatively small amounts of variation in salinity occurring over most of the inter-tidal transect. The fall in salinity close to MHWST and in the marsh border is typical, relating to infrequent tides and groundwater seepage. The fall in salinity in the tidal flat zone is not so typical and probably relates to the location of the transect in the inner part of the middle estuary, where freshwater influx from the residual flow of the River Taw is significant at low tide. The relatively large change in salinity after only a 20cm fall in high tide level shows agreement with other studies (Rijk, 1995a, 1995b; Rijk and Troelstra, 1997; Zong and Horton, 1998) which show significant changes in salinity between different tides. In retrospect, the Taw Estuary survey would have benefited from a series of salinity measurements taken throughout the spring-neap cycle, and from different seasons of the year. This would have shown the full range of salinities effecting each marsh surface elevation. However, the purpose of the middle Taw Estuary survey was to create a modern analogue of diatom distribution relating to elevation in the tidal frame. This could then be used to infer former marsh surface elevation in the analysed core records. The purpose was not to relate diatom assemblages to altitudinal salinity ranges, therefore a full suite of salinity measurements from throughout the tidal cycle was not deemed necessary.

Contemporary diatom distribution (salinity groups)

Figure 4.7 shows a diatom diagram for PL1. All 37 species which exceed 3% TDV (*i.e.* >3% total diatom valves counted) are shown, along with the diatom sums for the different halobian salinity groups (sums of >3% spp). Changes in assemblage DSI (based on total diatom count) are also shown. Zonation of the diatom diagram was completed using constrained cluster analysis (CONISS; no data transformation was applied) based on species records exceeding 3%TDV. This analysis resulted in four diatom zones (E1 to E4), some of which were divided into subzones. Diatom valves were abundant and well preserved throughout the estuary transects. A total of 158 diatom taxa were recorded in the contemporary samples, with 37 species exceeding 3%TDV.

Polyhalobous species (especially planktonic and tycho planktonic taxa) are seen to dominate (53-80%) the tidal flat (E1) and pioneer to mid saltmarsh zones (E2), with

Delphineis surirella, *Odontella mobiliensis* and *Podosira stelligera* all exceeding >10%TDV. Polyhalobous species remain dominant, but in reduced numbers (42-56%), in the high saltmarsh E3 zone, with *Actinocyclus octonarius* and *Delphineis surirella* at >10%TDV. Above MHWST, in the marsh border E4 zone, numbers fall significantly (12%), with no species present at >5%TDV. However, *Paralia sulcata* and *Podosira stelligera* are both present at 3%TDV in E4. The general dominance by allochthonous planktonics and tycho planktonics (planktonics are by definition allochthonous: Simonsen, 1969) throughout most of the transect is a reflection of the strong tidal currents (Vos and de Wolf, 1993a, 1993b) present in the macro-tidal Taw Estuary. This dominance has been seen in other UK macro-tidal environments such as the Severn Estuary (Hill *et al.*, 2007).

Mesohalobous species are generally rare in the tidal sandflat (2-4%). However, numbers rise to 9% in the basal E(i) subzone due to the influence of low tide fluvial drainage. The mesohalobous sum remains at *c.*10% throughout the tidal mudflat (upper E1(ii)) and pioneer-mid saltmarsh zones (E2), with *Navicula phyllepta* and *Navicula avenacea* present at >5%TDV. In the high saltmarsh (E3) and marsh border (E4) zones, mesohalobous numbers reach 19% and 18% respectively, with *Navicula phyllepta* dominating the high saltmarsh (>10%TDV) and *Navicula peregrina* dominating the marsh border above MHWST (>10%TDV).

The halophilous sum remains <5% throughout the transect up to the lower high saltmarsh zone (E3(i)). However, in the upper high saltmarsh (E3(ii)), numbers increase to 9-11% and reach 16% in the marsh border (E4). *Navicula pusilla* and *Navicula cincta* are present at >5%TDV in both of these zones.

The oligohalobous indifferent sum remains at 6% for most of the tidal sandflat, and then rises in the tidal mudflat to 10-13%, with similar numbers recorded through the saltmarsh zones up to the lower high saltmarsh. The freshwater assemblage will be allochthonous throughout these zones. In the upper high saltmarsh (E3 (ii)), freshwater indifferent species numbers increase to 17%, and rise significantly to 39% in the marsh border (E4), with *Pinnularia subcapitata* present at >10%TDV and *Gomphonema angustum* and *Hantzschia amphioxys* present at >5%TDV.

Contemporary diatom distribution (tidal frame zone groups)

Instead of grouping diatoms into salinity groups (polyhalobous *etc.*), Zong (1997, 1998) grouped diatom species according to their optimum distribution in the tidal frame. This approach has been used in several other qualitative studies (*e.g.* Nelson and Kashima, 1993; Hemphill-Haley, 1995a, 1996; Shennan *et al.*, 1995, 1996) but the study by Zong (1998) probably showed the most successful application of this method to fossil core sequences, prior to the application of quantitative methods in the late 1990s. This approach has been followed here and figure 4.8 shows the common (>3%TDV) diatom species grouped according to their optimum distribution. This resulted in four groups, named in relation to an elevational environment. These groups are tidal flat, low-mid saltmarsh (group includes pioneer saltmarsh), high saltmarsh and marsh border. The boundary between the high saltmarsh and marsh border groups is approximate to MHWST.

Zone E1 (0.50m OD to 2.52m OD)

Zone E1 (figure 4.8) is dominated by the tidal flat diatom group (42-60%). This group is almost entirely composed of polyhalobous planktonic and tychoplanktonic species with *Delphineis surirella* present at >10%TDV, along with *Actinoptychus senarius*, *Coscinodiscus radiatus*, *Cymatosira belgica*, *Paralia sulcata*, and *Rhaphoneis ampiceros* all at >5%TDV. Other dominant tidal flat species in this zone include the polyhalobous epipelics *Pleurosigma normanii* and *Nitzschia panduriformis* (both >5%TDV). The dominant *Delphineis surirella* species has been frequently recorded in optimum numbers within tidal flats (*e.g.* Hustedt and Aleem, 1951; Sullivan, 1975; Hemphill-Haley, 1995a; Shennan *et al.*, 1996; Zong, 1997; Zong and Horton, 1998; Hill *et al.*, 2007). *Paralia sulcata* has also been widely associated with tidal flats (*e.g.* Nelson and Kashima, 1993; Hill *et al.*, 2007), although this species is also widely recorded in significant numbers up to the marsh border environment (*e.g.* Nelson and Kashima, 1993; Zong and Horton, 1998; Gehrels *et al.*, 2001; Hill *et al.*, 2007). In the Severn Estuary, Hill *et al.* (2007) recorded a similar tidal flat optimum for *Rhaphoneis ampiceros* and *Actinoptychus senarius*. The only non-polyhalobous tidal flat group taxa are exclusively found in subzone E(i), which is influenced by low tide fluvial drainage where less marine allochthonous diatoms will be transported into the middle estuary. These species are the mesohalobous planktonic *Cyclotella striata* (4%TDV), the mesohalobous epipellic *Nitzschia navicularis* (3%TDV), and the halophilous epipellic

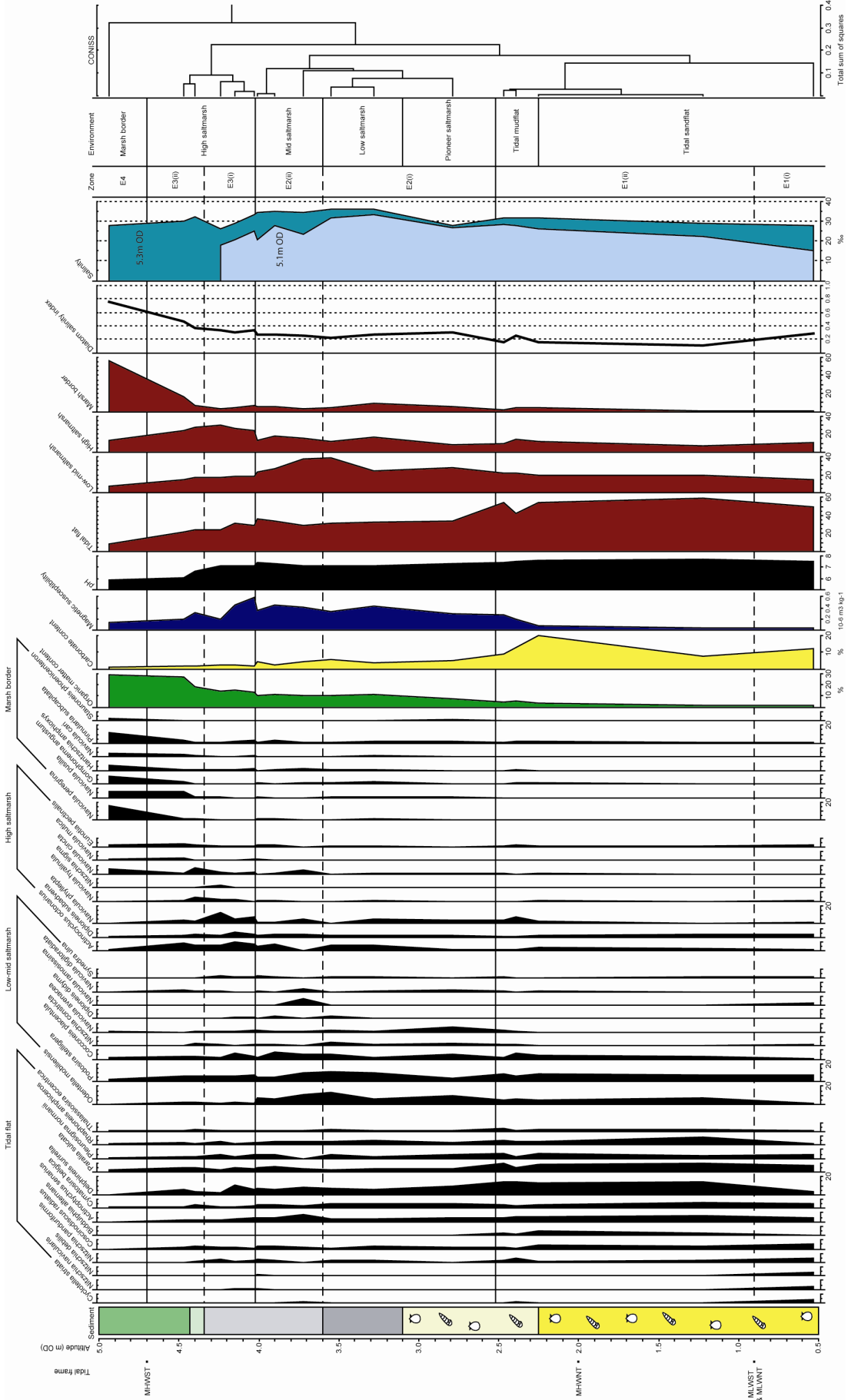


Figure 4.8 Diatom diagram for the Taw Estuary transects ($\geq 3\%$ TDV spp.). Taxa are grouped into four assemblages: tidal flat, low-mid saltmarsh, high salt-marsh and marsh border. Organic matter, carbonate content, pH, X_{fr} , salinity (5.3m OD & 5.1m OD tides) and DSI is also shown.

See figure 5.2 for lithology key.

Nitzschia debilis (4%TDV). Significant numbers of low-mid saltmarsh group taxa (15-22%) are also present in zone E1, with dominance by the polyhalobous planktonic *Podosira stelligera* and tychoplanktonic *Odontella mobiliensis*, along with the freshwater indifferent epiphyte *Cocconeis placentula* (all at >5%TDV). A small high saltmarsh assemblage is also present in E1, with *Navicula phyllepta* present at >5%TDV in the upper tidal mudflat.

Zone E2 (2.52m OD to 4.02m OD)

Zone E2 is dominated by both low-mid saltmarsh group taxa (23-39%) and wide ranging tidal flat taxa (29-36%). The low-mid saltmarsh assemblage is dominated by the polyhalobous planktonic-tychoplanktonics *Podosira stelligera* and *Odontella mobiliensis* (both >10%TDV) with other dominant species including the mesohalobous epipellic *Navicula avenacea* and the freshwater epiphyte *Cocconeis placentula* salt-tolerant (both >5%TDV). Shennan *et al.* (1996) also recorded *Navicula avenacea* in a low marsh environment below MHWST (within a tidal river setting similar to the Taw). Hill *et al.* (2007) gave an optimum for this species at MHWST. This suggests a wide range, and in the Taw transect, *Navicula avenacea* is present in the high saltmarsh and marsh border. Although *Cocconeis placentula* is classified in this study as Oligohalobous indifferent (following Denys, 1991), Vos and de Wolf (1993a) placed it in a brackish-freshwater group, suggesting it is salt-tolerant.

Some of the low-mid saltmarsh group taxa are more prevalent in subzone E(ii) (mid saltmarsh). These are all epipellic species, and include polyhalobous *Navicula ramosissima* (>5%TDV), and mesohalobous *Diploneis didyma* and *Navicula digitoradiata* (both 3%TDV). The tidal flat group in zone E2 is dominated by the marine planktonics-tychoplanktonics *Delphineis surirella*, *Actinocyclus senarius*, *Cymatosira belgica* and *Paralia sulcata* (all >5%TDV, with *Delphineis surirella* >10%TDV in the Pioneer saltmarsh). High saltmarsh group taxa become more prevalent (8-18%) in E2, with dominance by the polyhalobous planktonic *Actinocyclus octonarius* and the mesohalobous epipellic *Navicula phyllepta* (both >5%TDV).

Zone E3 (4.02m OD to 4.70m OD)

Subzone E3(i) (located in the lower high saltmarsh from MHWST-68cm to MHWST-36cm) has a mixed assemblage with a high saltmarsh group sum of 24-31%, a low-mid saltmarsh group sum of 17-19% and a tidal flat group sum of 29-31%. The high

saltmarsh group is dominated by the polyhalobous planktonic *Actinocyclus octonarius* and the mesohalobous epipellic *Navicula phyllepta* (both >10%TDV), along with the polyhalobous epipellic *Diploneis subadvena* (>5%TDV). Although *Navicula phyllepta* has its optimum in the high saltmarsh, it was recorded at >5%TDV in both the tidal mudflat and pioneer to mid saltmarsh zones, suggesting a wide range. A similar wide range was recorded by Zong and Horton (1998), with significant numbers recorded from the tidal flat up to MHWST. The mesohalobous epipellic *Nitzschia sigma* is also present in E(i) at 3%TDV. Hill *et al.* (2007) and Shennan *et al.* (1996) both recorded the highest numbers of this species lower in the tidal frame, equivalent to the Taw mudflat and low-mid saltmarsh zones, although they also recorded >5%TDV levels up to MHWST. However, Shennan *et al.* (1996) and Gehrels *et al.* (2001) also recorded significant above MHWST, suggesting a wide range. The low-mid saltmarsh group assemblage is dominated by the marine planktonic *Podosira stelligera* and the freshwater epiphyte *Cocconeis placentula* (both >5%TDV). The tidal flat group assemblage is dominated by *Delphineis surirella* (>10%TDV) and *Paralia sulcata* (>5%TDV). E(i) sees the emergence of the marsh border freshwater species *Pinnularia subcapitata* at 4%TDV, suggesting it is salt-tolerant, despite its oligohalobous indifferent classification.

Subzone E3(ii) (located in the upper high saltmarsh from MHWST-36cm to MHWST) also has a mixed assemblage but sees the emergence of the marsh border group at 6-17%. The high saltmarsh group is dominant at 24-28%, with the low-mid saltmarsh sum falling to 14-16% and the tidal flat sum falling to 21-24%. The high saltmarsh group is dominated by the polyhalobous species *Actinocyclus octonarius* and *Navicula hyalinula*, along with the epipellic halophile *Navicula cincta* (all at >5%TDV). *Navicula cincta* has been recorded with a similar optimum close to MHWST in several other studies (*e.g.* Zong, 1997; Zong and Horton, 1998, 1999; Hill *et al.*, 2007). Other high saltmarsh group species include the aerophilous halophile *Navicula mutica* and the freshwater indifferent epiphyte *Eunotia pectinalis* (both >3%TDV). *Navicula mutica* has been widely recorded in saltmarshes with an optimum between MHWST and HAT (*e.g.* Nelson and Kashima, 1993; Zong, 1997; Shennan *et al.*, 1996; Zong and Horton, 1998, 1999). However, many of these studies also show significant numbers just below MHWST, equivalent to the Taw subzone E3(ii). The low-mid saltmarsh and tidal flat group marine planktonics *Podosira stelligera*, *Paralia sulcata* and *Delphineis surirella* all persist into the upper high saltmarsh at >5%TDV. Marsh border species present in

the upper high saltmarsh include the aerophilous halophile *Navicula pusilla* (>5%TDV) and the oligohalobous indifferent benthics *Navicula cari* and *Pinnularia subcapitata* (both 3%TDV). Shennan *et al.* (1995), Zong and Horton (1998, 1999), and Nelson and Kashima (1993) all reported the optimum elevation for *Navicula pusilla* in the marsh border zone between MHWST and HAT. Its range in the Taw Estuary appears to be slightly larger, with a >5%TDV presence at MHWST-23cm. Gehrels *et al.* (2001) recorded the emergence of *Navicula pusilla* within a *Puccinellia maritima*-*Juncus maritimus* vegetation zone, which is identical to the upper high saltmarsh of the Taw transect. Like *Pinnularia subcapitata*, the emergence of *Navicula cari* in the high saltmarsh suggests it is somewhat more salt-tolerant than other oligohalobous indifferent species. The emergence of aerophilous species in subzone E(ii) reflects the dryer conditions, with less frequent tidal inundation, present just below MHWST.

Zone E4 (4.70m OD to 5.0m OD)

Zone E4 (located above MHWST) is dominated by the marsh border group (56%) while the high saltmarsh sum falls to 13%, and the low-mid saltmarsh and tidal flat group sums fall to 7% and 8% respectively. The marsh border group assemblage is dominated by the mesohalobous epipellic *Navicula peregrina* and the oligohalobous indifferent species *Pinnularia subcapitata* (both >10%TDV). Zong and Horton (1998) recorded the highest abundance of *Navicula peregrina* in the zones either side of MHWST (*i.e.* marsh border and upper high saltmarsh in the Taw Estuary), while Shennan *et al.* (1995) recorded the maximum abundance in an assemblage 14cm below MHWST. Although not seen in the Taw transect, Zong and Horton (1999) suggest a range that would extend down to the mid saltmarsh zone. Other marsh border species in zone E4 include the aerophilous halophile *Navicula pusilla*, the aerophilous indifferent *Hantzschia amphioxys*, and the freshwater indifferent benthics *Gomphonema angustum* and *Navicula cari* (all >5%TDV). *Hantzschia amphioxys* was also recorded by Zong and Horton (1998, 1999), Sherrod (1999) and Hill *et al.* (2007) in the marsh border zone, with the highest numbers appearing nearer HAT, rather than MHWST. Vos and de Wolf (1993a) included this species in their brackish-freshwater aerophilous ecological group (which includes *Navicula pusilla* and *Navicula mutica*), indicating it is salt-tolerant. The smaller high saltmarsh group is dominated by *Navicula cincta*, with the low-mid saltmarsh and tidal flat group planktonics *Podosira stelligera* and *Paralia sulcata* persisting at 3%TDV each.

4.2.3 Altitude and diatom salinity index

Figure 4.9 shows changes in assemblage DSI through the tidal frame, from the base of the intertidal sandflat at 0.53m OD to the marsh border at 4.94m OD (MHWST+24cm). Below 4.02m OD, DSI values from the tidal flat and the pioneer to mid saltmarsh zones (*i.e.* zones E1 and E2) are all below 0.3, indicating assemblages dominated by marine taxa (Bryne *et al.*, 2001). Within these zones, there is a general trend of decreasing DSI value with decrease in elevation. However, there is a rise in DSI in the basal E(i) subzone which is influenced by low tide fluvial discharge. Above 4.02m OD (the mid-high saltmarsh boundary), a mixed brackish-marine assemblage is indicated in the lower high saltmarsh (E3(i)) by DSI values of 0.30-0.34. A linear increase in DSI is seen through the organic upper high saltmarsh (E3(ii)) and marsh border (E4) zones, reaching 0.76 in the marsh border assemblage at MHWST+24cm, indicative of an assemblage dominated by freshwater taxa.

It should be stated that the purpose of this DSI investigation is not to produce a modern analogue of DSI values in the intertidal zone that can be used to quantitatively identify tidal frame position in the palaeo-records. A quantitative analysis such as this would not work in this study as the ‘training set’ is located in the middle estuary, while the cores are located in the less saline inner estuary where DSI values will be higher (less marine) for each elevation zone. A modern analogue transect (or preferably several transects) located in the inner estuary would have overcome this problem but, as stated earlier, a suitable inner estuary site was not found.

The purpose of exploring the relationship between DSI and elevation in the tidal frame is to determine which environmental zones (*e.g.* high saltmarsh) in the tidal frame show very similar DSI (*i.e.* the least variation). Three DSI clusters have been highlighted in figure 4.9 as A, B and C. These relate to three separate tidal frame zones where there is relatively low DSI variation. Cluster A largely relates to the lower high saltmarsh organic silts with DSI values ranging from 0.30 to 0.37 (range = 0.07, n = 4). Cluster B largely relates to the mid saltmarsh clayey silts, with DSI values ranging from 0.22 to 0.27 (range = 0.05, n = 4). Cluster C relates to the tidal sandflat component of E1(ii) where DSI values are at their lowest (most marine), with values ranging from 0.11 to 0.16 (range = 0.05, n = 2).

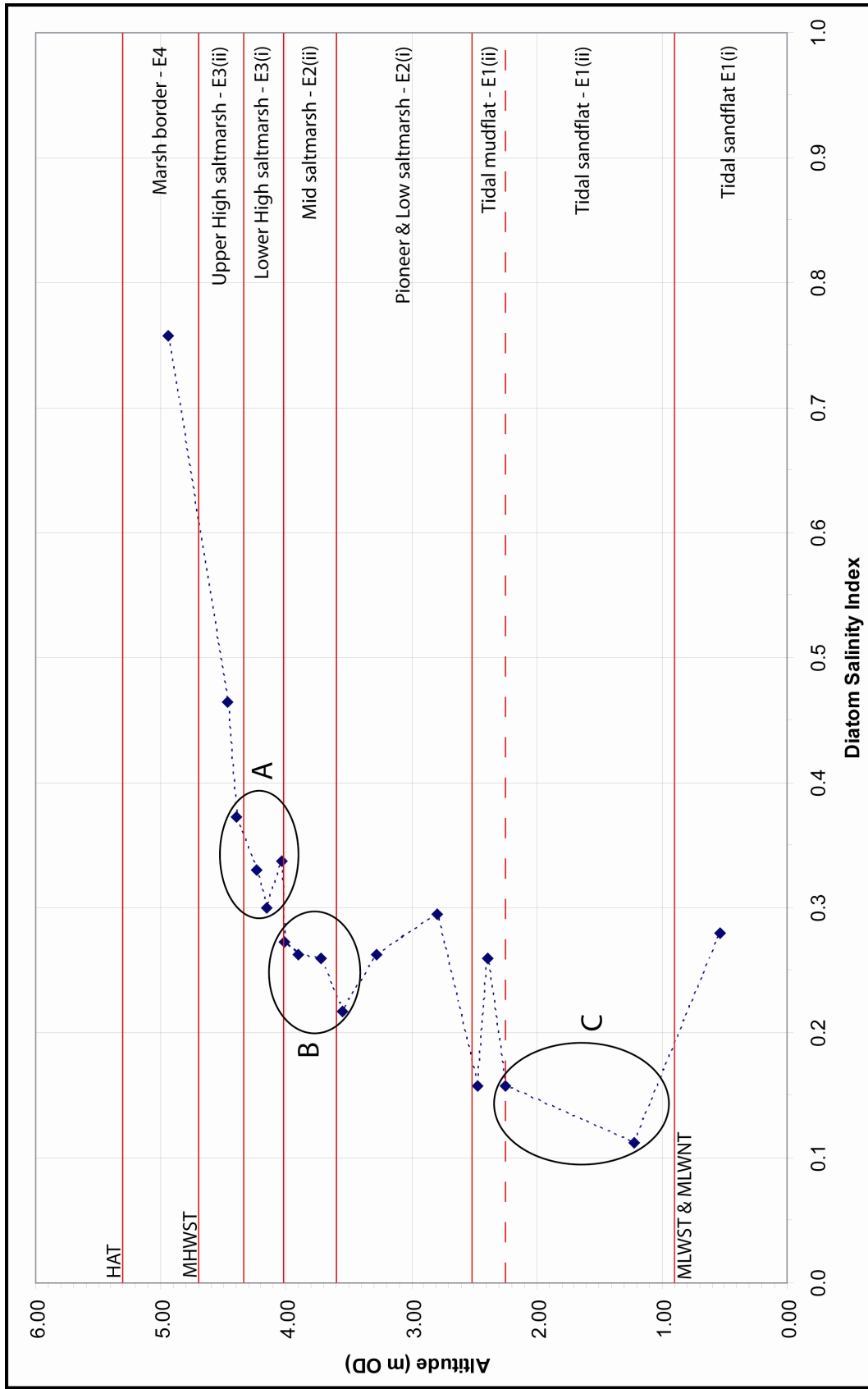


Figure 4.9 Diatom salinity index and tidal frame position in the Taw Estuary transects. Tidal frame zones of relative DSI stability are highlighted (A, B, C).

Diatom and sedimentary evidence will be used to identify these three tidal frame zone environments in the core stratigraphy of the inner Taw Estuary (chapter 5). These specific environments will then be analysed separately for spatial and temporal changes in palaeosalinity (chapter 7), with DSI changes reflecting differences in salinity, rather than tidal frame position. For each of the three analysed zones, the DSI uncertainty attached to core assemblages will equal the contemporary DSI range for that zone, e.g, the DSI uncertainty for high saltmarsh samples will be ± 0.07 , for middle saltmarsh samples ± 0.05 and for tidal flat samples ± 0.05 .

Figure 4.9 shows that the upper high saltmarsh subzone, pioneer/low saltmarsh zone and tidal mudflat subzone, all show larger DSI ranges, and would therefore have greater uncertainty attached (± 0.09 , ± 0.08 and ± 0.10 respectively) if they were used in the palaeosalinity analysis. The marsh border zone only has one sample, so the possible range of DSI values in this zone is unknown.

4.3 RIVER TAW

4.3.1 River Taw transect

Figures 4.10 and 4.11 show the location of 17 contemporary sampling stations (R1 to R17) within the tidal inner estuary and non-tidal lower Taw valley. These figures also show how the modern sample locations relate to the core transects (A to I) and the geomorphology described in chapters 5 and 6. Stations were located along 11.25 km of river channel, starting 0.75 km upstream of Barnstaple Long Bridge and ending 1.5 km downstream of Umberleigh. This reach encompasses *c.*4 km of the inner estuary that is fully tidal during mean high tide conditions (R1-R7), a further *c.*3 km of tidal river between the mean tidal limit (MTL) and extreme HAT tide conditions (R7-R12), and a further *c.*4 km of non-tidal river (R12-R17). Yearly HAT elevations are typically 5.3m OD at Barnstaple (*e.g.* Admiralty Tide Tables, 2008). However, an exceptionally high HAT of 5.7m OD was predicted in 2007 and this was tracked during the flood tide to its tidal head (figure 4.11). The elevation that this tide reached was surveyed at R11, giving an elevation of 5.56m OD, 14cm short of the predicted height for Barnstaple. This would suggest a slight fall in elevation as tides travel up-river. However, as predicted tidal frame levels are rounded to the nearest 10cm, and can be affected by

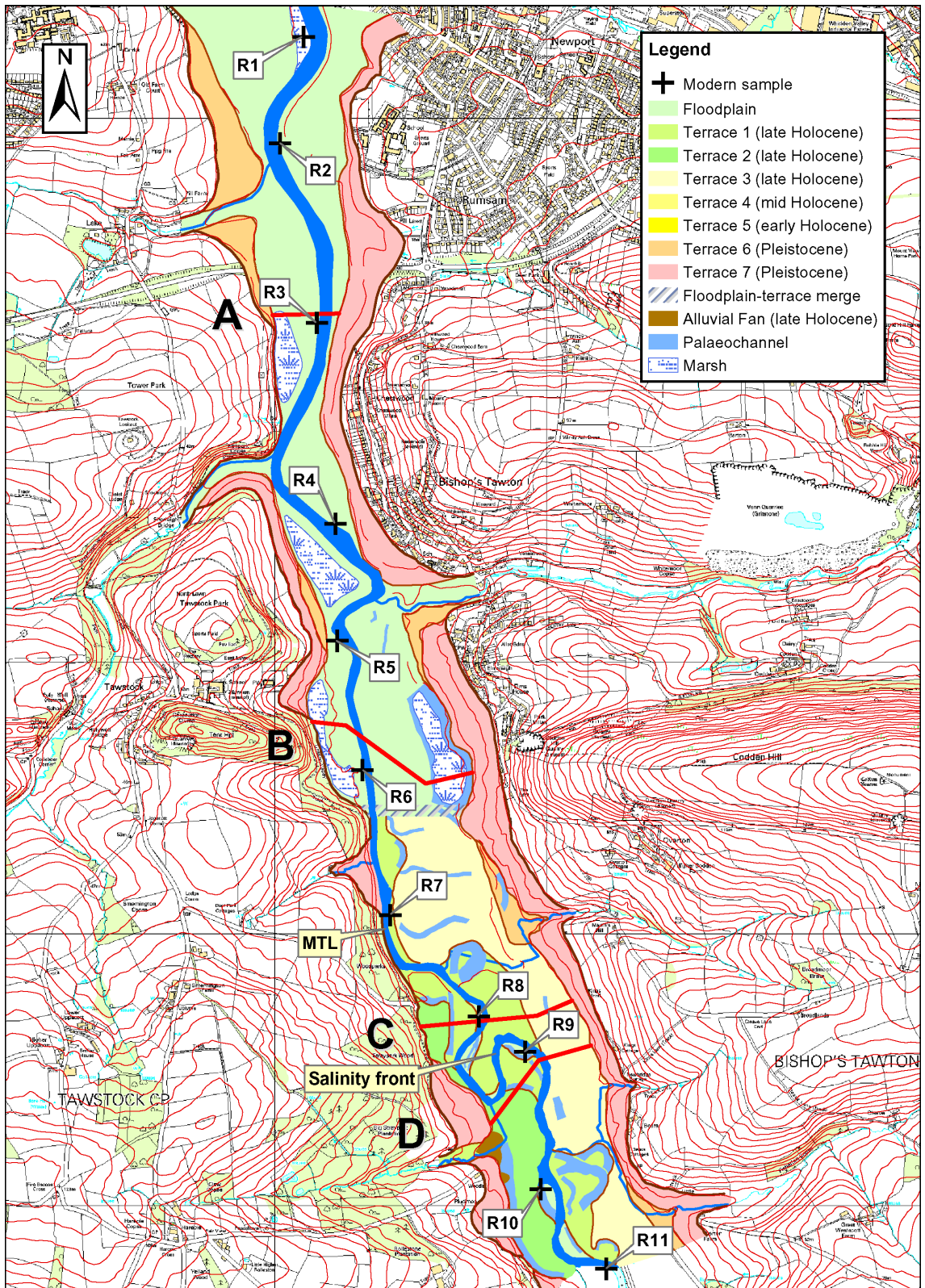


Figure 4.10 Location of sampling stations R1 to R11 in the tidal River Taw zone upstream of Barnstaple. MTL (mean tidal limit) corresponds to NTL (normal tidal limit), as shown on the Ordnance Survey 1:25 000 Explorer 127 sheet (Revised edition A, 1997). The salinity front corresponds with the boundary between the brackish and the freshwater tidal zones. The geomorphology and core transects A to D will be discussed in chapter 5. This map was produced in a GIS and incorporates OS Landform Profile (5m contours) and OS 10,000 colour raster layers (supplied by Ordnance Survey/EDINA Digimap).

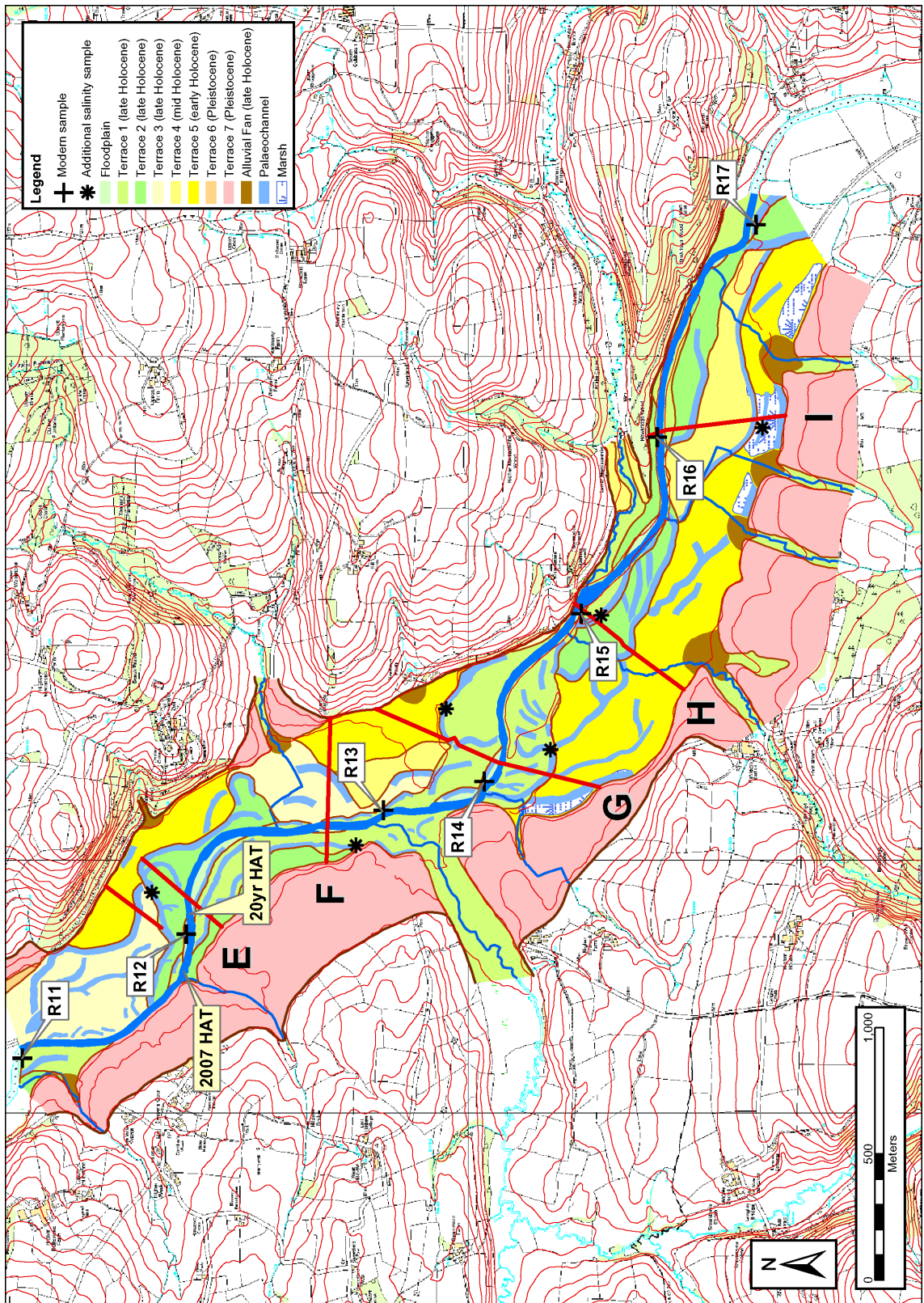


Figure 4.11 Location of sampling stations R11 to R17 in the largely non-tidal River Taw zone. The location of the observed 2007 HAT is indicated (5.7m OD). The estimated location of the highest predicted 20yr HAT (2000 to 2020) is also shown (5.9m OD). The geomorphology and core transects E to I will be discussed in chapter 6. This map was produced in a GIS and incorporates OS Landform Profile (5m contours) and OS 10,000 colour raster layers (supplied by Ordnance Survey/EDINA Digimap).

meteorological conditions, a horizontal water surface is presumed for this study. Figure 4.11 also shows the location of the tidal head for a predicted 5.9m OD 20 year HAT (relating to the 18.61yr lunar-nodal cycle: Oost *et al.*, 1993). This is an estimate based on the location of the 2007 5.7m OD tidal head and the local gradient of the river (there is a steeper riffle in the vicinity of the suggested 5.9m OD HAT limit).

Samples were taken from the vegetated channel bank/floodplain edge, with an attempt made to locate all inner estuarine samples at the same tidal frame position by locating samples at approximately equal distances above the start of vascular plant growth. Photographs of most inner estuarine tidal river sampling stations, and some freshwater stations, are shown in figure 4.12.

Figure 4.13 shows a longitudinal section of all sampling station altitudes, and how each sample elevation relates to tidal frame levels. This reveals that stations R1 to R9 are submerged at MHWST, with most stations located in the middle Taw Estuary high saltmarsh zone (R5 and R6 are located at low-mid saltmarsh elevations). R10 becomes tidally submerged during higher spring tides, while R11 would be submerged by a 20yr HAT. However, during storms with strong onshore wind, tides will be higher than predicted by several decimetres and if the atmospheric pressure is particularly low, the resulting storm surge can typically raise the tide in British waters by *c.*1.0m (Lennon, 1963a, 1963b; Suthons, 1963; McIntyre, 1979). A documented coastal flood that affected Barnstaple (and the wider south-west) in 1607 AD has been postulated by Haslett and Bryant (2004) as either an extreme storm surge or a tsunami (Ridson, 1620; Gray, 1998; Bryant and Haslett, 2002). The initial wave of this flood, which coincided with a 5.7m OD spring tide, reached up to 7.53m OD at Barnstaple, translating into a 1.83m increase in the predicted tide. Haslett and Bryant (2004) favour a tsunami origin, as a storm surge of this magnitude would require hurricane strength 80 mph winds (of which there is no documented evidence). The tidal head of a 7.53m OD tide would have reached close to R14 (figure 4.11). Although such an event must be considered as extremely rare, other storm surges that may have coincided with HAT tides may have increased, for example a 5.7m OD tide by *c.*1.0m to *c.*6.7m OD. In this scenario, the tidal head would reach close to R13 (core transect F).



(a) R1



(b) R1



(c) R2



(d) R3



(e) R4



(f) R5

Figure 4.12 (Continued on next page) Photographs of contemporary River Taw sampling stations. (a) R1 saltmarsh with saltpan, view north; (b) R1, view north; (c) R2, with area of *Scirpus* marsh in foreground, view north; (d) R3 beside stand of *Phragmites*, view south-east; (e) R4, view west; (f) R5, beside tidal mudflat, view south-east; (g) R6, with *Phragmites* at water's edge, view north; (h) R8, back of vegetated gravel point bar with tidal mud drape, view north-west; (i) R8 sample site submerged at 5.2m OD high tide (at slack water), view north; (j) R9, vegetated bench, view north-west; (k) R10, vegetated bank attached bar and recent palaeochannel (now a slough channel), view south; (l) R11, vegetated bench with sample located at 5.83m OD (would be submerged by 20yr 5.9m HAT), view south-east; (m) R12, close to location of 20 yr HAT tidal head, view west; (n) R15, vegetated bank attached bar, view south-east.



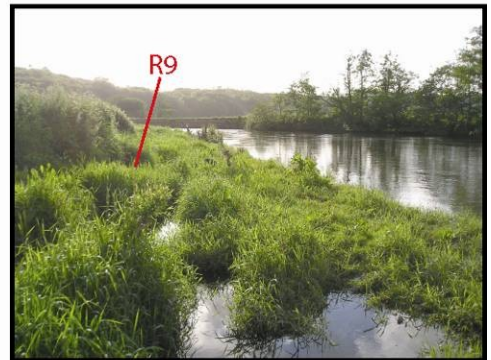
(g) R6



(h) R8



(i) R8 at 5.2m OD high tide



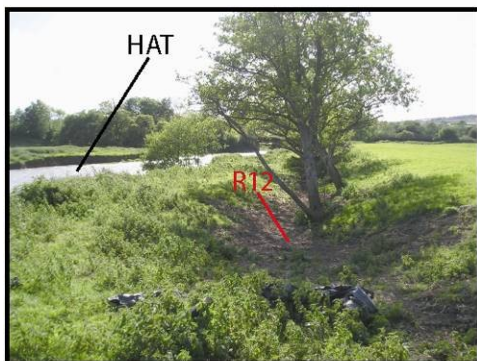
(j) R9



(k) R10



(l) R11



(m) R12



(n) R15

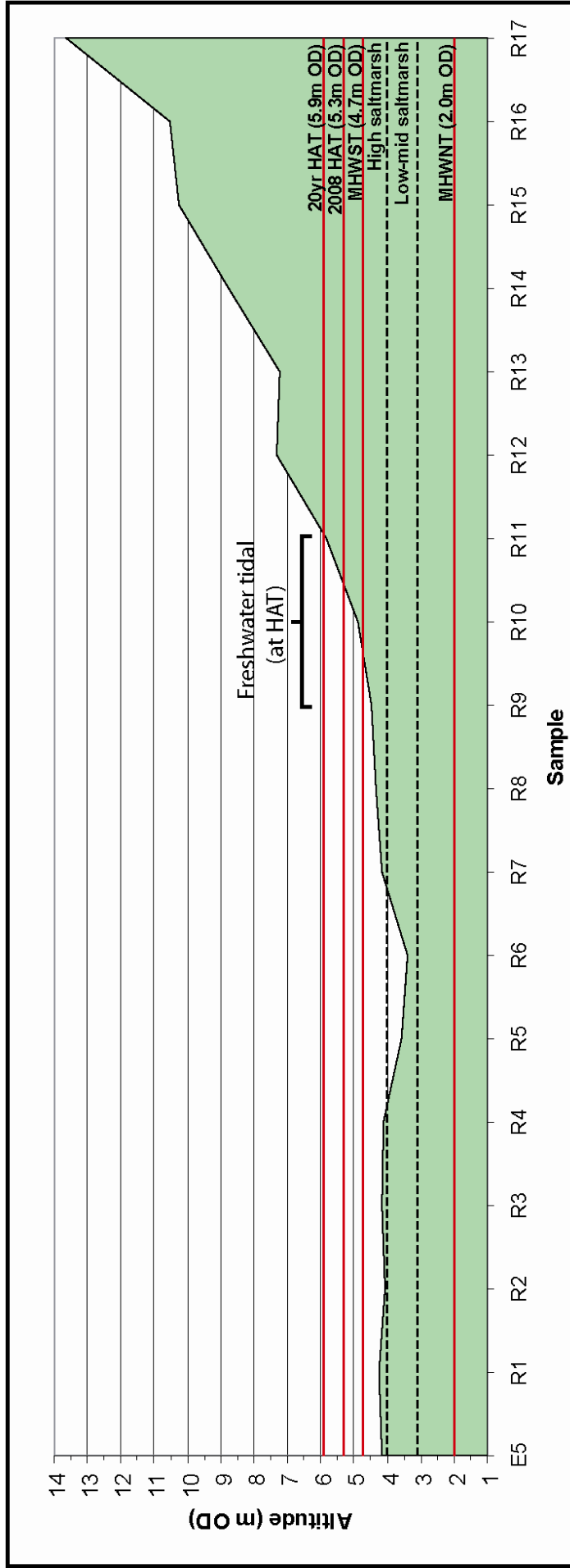


Figure 4.13 Longitudinal section of the lower River Taw showing relationship between sampling station altitudes (R1 to R17) and tidal frame levels. The high saltmarsh and low-mid saltmarsh tidal frame zones are also indicated, with most of the tidal sampling station altitudes lying within the high saltmarsh estuary zone (MHWST-68cm to MHWST). Sampling station E5 is located in the lower high saltmarsh of the Taw Estuary transect and has been included for comparison.

4.3.2 Salinity

Surface water salinity was measured at each of the sampling stations (R1-R17) after a 5.3m OD tide during 2007 (the 2007 HAT was 5.7m OD). The results of these measurements are shown in figure 4.14. Measurements were made on ponded tidal water at stations R1-R11, and on overbank (or channel bench) waterlogged/ponded depressions at stations R12 to R17. Salinity was also measured at stations located on either side of the salinity front (the boundary between the brackish tidal zone and freshwater tidal zone) immediately after a 5.4m OD tide and a 5.5m OD tide (figure 4.14).

The 5.3m OD tide results show that salinity only falls by 6‰ (from 29‰ to 23‰) between the estuary transect and river station R3 (the location of transect A), an up-estuary distance of 5.0 km. This suggests only minor high tide fluvial-estuarine mixing in the tidal prism downstream of R4. These salinities would correspond with marine conditions (figure 4.11), in terms of diatom salinity tolerance (table 4.2). Brackish salinity values were recorded at R4 (16-18‰) and R5 (5-7‰) during both the 5.3m and 5.5m OD tides. The sharp fall in salinity (by 13‰) between R4 and R5 indicates the maximum up-estuary location of the halocline, where the fluvial and estuarine water's meet and mix. This coincides with the turbidity maximum, a feature of partially mixed estuaries where there is a peak in suspended load concentration (Dyer, 1972; Pethick, 1984). Brackish-fresh salinity values (Vos and de Wolf, 1993a) are recorded at R6 (2-4‰), R7 (2-3‰) and R8 (0.5-1.2‰) during 5.3m, 5.4m and 5.5m tides. This indicates the tidal prism is increasingly dominated by fluvial mixing in this zone. Freshwater salinities (<0.2‰) were recorded at R9 during all three tides, indicating the start of freshwater tidal conditions. Salinity was measured at this key site both at high tide slack water (from river water samples), and from ponded samples after the tide had ebbed. Both sets of measurements gave similar freshwater values. The salinity front for each of these tides is therefore located between R8 and R9 (approximate to core transect D), and marks the boundary between the freshwater tidal zone and the brackish-fresh tidal zone. As stated earlier, the 20yr HAT for the Taw is 5.9m OD. As this is 40cm higher than the measured 5.5m OD tide, the salinity front may be located just upstream of R9 during these conditions. It is also expected that the location of the salinity front will vary, depending on the river discharge rate, with the salinity front located further downstream during high-stage floods. High discharges would also cause increased dilution of the

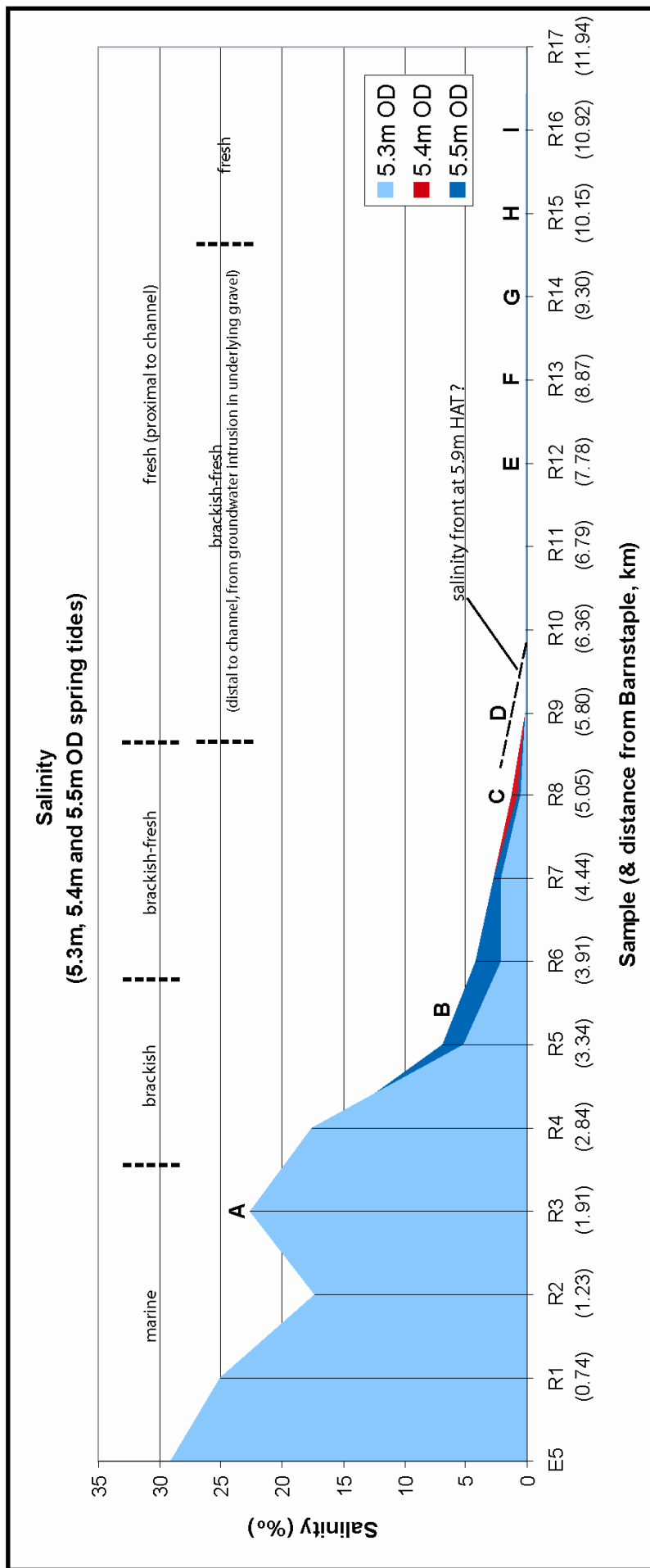


Figure 4.14 Longitudinal section of the lower River Taw showing relationship between sampling station location (R1 to R17) and maximum salinity. Water samples were taken after three high tides (5.3m, 5.4m and 5.5m OD) during 2007 (the 2007 HAT was 5.7m OD). Samples were taken from all stations (R1-R17) after the 5.3m OD tide (which is equal to the 2007 HAT). After the 5.4m OD tide, only stations R7-R10 were sampled and after the 5.5m OD tide, only stations R4-R10 were sampled. Quoted distances (km) are from Barnstaple Long Bridge, where the estuary opens out. Regions of the salinity gradient corresponding with the diatom salinity tolerance classification of Vos and de Wolf (1993a) are also shown (see table 4.2). Salinity data from a lower high saltmarsh Estuary transect station (E5, measured after a 5.3m OD spring tide) has also been included for comparison.

tidal prism, resulting in a down-estuary translation of the brackish-fresh and brackish zones.

Salinity	>20‰	4-20‰	0.2-4.0‰	<0.2‰
Diatom group (planktonics)	Polyhalobous	Mesohalobous		Oligohalobous
	Marine	Brackish	Brackish-freshwater	Freshwater

Table 4.2 Planktonic diatom salinity tolerance classification (adapted from Vos and de Wolf, 1988, 1993a). The salinity boundaries (e.g. 4‰) are similar for other life form groups (e.g. epiphytes). However, the terms vary (e.g. brackish plankton = marine/brackish epiphytes).

Upstream of R9, freshwater salinities of 0.07-0.12‰ were found at all sampling stations, including the freshwater tidal sites at R10 and R11. Salinities were also tested in ponded palaeochannel settings, at six floodplain locations set back away from the channel (figure 4.11). These measurements were taken approximately 24 hours after the 2007 5.7m OD HAT. The four sites located between transects E and G registered water salinities of 0.16-0.29‰. These values are all higher than those found at the sampling stations proximal to the river channel and indicate border line brackish-fresh (>0.2‰) conditions at floodplain localities away from the channel. This may suggest a zone upstream of the surface HAT that is influenced by marine groundwater intrusion (figure 4.14). Freshwater salinities of 0.10-0.13‰ were measured at the two sites upstream of transect H.

4.3.3 Sedimentary environmental variables

Sediment samples from each of the sampling stations were also tested for organic matter content, carbonate content and magnetic susceptibility (X_{lf} and $X_{fd\%}$). The results of these tests are included in figure 4.15. Carbonate content, X_{lf} and $X_{fd\%}$ was measured after two separate tides, a typical spring tide (4.8m OD) and the 2007 HAT (5.7m OD). Organic matter content values are very variable throughout the river transect, ranging from 4% to 21%. The variation appears to be partly controlled by the elevation of the

sample above the average water-level of the river. For example, in the inner estuarine tidal zone, R5 and R6 were taken from low-mid saltmarsh elevations and have organic matter content values under 10%. The low values of upstream stations R15-R17 (4-5%) may be due to reduced organic matter production (and preservation) rates due to a lower water table distal to the estuary.

Carbonate values (figure 4.15) for stations R10 to R17 are typically 0.9-1.2% at all freshwater tidal zone and non-tidal zone sampling stations. These appear to be typical values for freshwater riverine environments in the River Taw with sediment sourced from the catchment. Downstream of R10, carbonate values are significantly higher (up to 8%) and reflect the presence of carbonate sand (comminuted shell debris) that has been sourced from the estuary. Some important differences are seen between sediment collected after the 4.8m OD tide and after the 5.7m OD HAT tide. After the lower 4.8m OD tide, carbonate values of 2-8% are recorded at stations R1 to R7. However, after the 5.7m OD tide, carbonate values of 2-8% are seen between R1 and R9, indicating that the higher tide has transported estuarine sediment 1.0-1.5 km further upstream. The 2% carbonate value (5.7m OD tide) at a station (R9) that recorded freshwater conditions at a 5.5m OD tide suggests some estuarine sediment becomes mixed into the freshwater tidal zone, upstream of the salinity gradient. Both tides show a peak in carbonate values of 5-8% between stations R4 and R6. Salinity measurements identified this zone as the area immediately upstream of the halocline where there is the most fluvial and estuarine mixing. The peaks in carbonate give support to this zone corresponding with a turbidity maximum where tidally pumped sediment is transported up river and deposited at slack water. The decline in carbonate values downstream of this zone suggests flood-dominated tidal asymmetry in the inner Taw estuary, with the R4-R6 area acting as a sedimentary sink for estuarine sediment. This form of tidal asymmetry is typical in inner estuaries, where the flood tide duration can last only 2-3 hours out of a total 12.4 hour tidal period (Pethick, 1984) and flood tidal asymmetry has indeed been confirmed

Figure 4.15 (Next page) Diatom diagram for the River Taw transect (>3%TDV spp.) showing assemblage changes with up-river distance from Barnstaple Long Bridge. Transect data for altitude, salinity (after three separate tides), organic matter content, carbonate content, X_{lf} , $X_{fd}\%$ and DSI is also shown. Carbonate content, X_{lf} and $X_{fd}\%$ was measured after two separate tides, a typical spring tide (4.8m OD) and the 2007 HAT (5.7m OD). The location of core transects A to I are indicated on the altitude profile. Magnetics measurements were not made on the R8 sample after the 4.8m OD tide. At the non-tidal R17 station, the X_{lf} value (measured during the 4.8m OD tide survey) was $1.3 \cdot 10^{-6} \text{ m}^3 \text{ kg}^{-1}$. This is off the scale of the chart given below.

from the tide curves of the middle Taw Estuary by HR Wallingford (1990) and Kirby (1996).

Figure 4.15 shows that X_{fr} values remain at similar levels ($0.24\text{--}0.45 \times 10^{-6} \text{ m}^3 \text{ kg}^{-1}$) throughout the river transect during both tides. However, a general up-river trend of declining X_{fr} value is seen between R1 and R16, with mean values falling from $c.0.43 \times 10^{-6} \text{ m}^3 \text{ kg}^{-1}$ at R1 to $c.0.21 \times 10^{-6} \text{ m}^3 \text{ kg}^{-1}$ at R16. Chapter 5 will show that this is related to an upriver trend of decline in estuarine biogenic and authigenic ferrimagnetic minerals (magnetite and greigite) and a rise in catchment derived antiferromagnetic minerals (haematite) which carry a lower magnetic susceptibility (Dearing, 1999).

Dual-frequency susceptibility results ($X_{\text{fd}\%}$) show low values (1-7%) for stations R1 to R8, indicative of low concentrations of ferrimagnetic fine viscous SD/SP grains of a $c.0.02 \mu\text{m}$ grain (Dearing, 1999, Oldfield, 1999). Results for the 4.8m OD tide show $X_{\text{fd}\%}$ values rising to $c.10\%$ at R9 and generally remaining at this level for all upstream stations. The 5.7m OD tide results show a similar pattern, except the rise in $X_{\text{fd}\%}$ occurs further upstream at R10. The 10% $X_{\text{fd}\%}$ values indicates the magnetic assemblages are dominated by fine viscous grains upstream of R9 or R10. These grains are often derived from weathered soils (Oldfield *et al.*, 1983; Maher, 1986, 1988), and this suggests that fine viscous secondary magnetite derived from catchment soils is an important part of the sediment magnetic assemblage in the freshwater tidal and fluvial zones. As with the carbonate results, the low $X_{\text{fd}\%}$ values upstream of the salinity front at R9 during the 5.7m OD tide suggests some tidally transported estuarine sediment becomes mixed into the freshwater fluvial zone, although this may be derived from reworked channel bank sediment during freshwater tidal back-up. Down-estuary trends of decreasing soil derived magnetite and increasing dominance by estuarine bacterial magnetite has also been observed in some US estuaries by Oldfield *et al.* (1985, 1989).

4.3.4 Contemporary diatom distribution

Figure 4.15 includes a diatom diagram for the River Taw transect. All 36 species which exceed 3% TDV are shown, along with the diatom sums for the different halobian salinity groups (sums of $>3\%$ spp). Changes in assemblage DSI (based on total diatom count) are also shown. Zonation of the diatom diagram was completed using

constrained cluster analysis (CONISS; no data transformation was applied) based on species records exceeding 3%TDV. This analysis resulted in four diatom zones (Riv 1 to Riv 4), some of which were divided into subzones. A total of 178 diatom taxa were recorded in the contemporary samples, with 36 species exceeding 3%TDV.

Zone Riv 1 (R1 to R2)

This zone is associated with sampling stations R1 and R2. These stations are elevated at 4.24m OD and 4.07m OD respectively, placing them in the lower high saltmarsh tidal frame zone. The DSI values of 0.54-0.64 indicate a mixed assemblage of marine-brackish and freshwater taxa. This is reflected in the diatom group sums with a polyhalobous sum of 26-32%, a mesohalobous sum of 9-13%, a halophile sum of 11-17% and a oligohalobous indifferent sum of 22-30%. The polyhalobous group is dominated by marine planktonics with *Actinocyclus octonarius*, *Paralia sulcata* and *Podosira stelligera* all present at >5%TDV. The mesohalobous group is dominated by the epipellic *Navicula avenacea* (>5%TDV), and the halophile group is dominated by epipellic *Navicula cincta* (>5%TDV) and aerophilous *Navicula mutica* (>10%TDV). These halophiles are both from the estuary transect high saltmarsh group. Dominant freshwater indifferent species are *Cocconeis placentula* and *Gomphonema angustum* (both >5%TDV).

Zone Riv 2 (R3 to R8)

This zone corresponds with stations R3 to R8, incorporating stations up to the high spring tide and HAT salinity front (located between R8 and R9). All stations apart from R5 and R6 were located in the high saltmarsh tidal frame zone, with R5 and R6 located in the low-mid saltmarsh zone. Riv 2 has been divided into two subzones, with Riv 2(i) associated with station R3, and Riv 2(ii) associated with stations R4-R8. The principal difference between these subzones is that Riv 1(i) contains a peak in polyhalobous taxa abundance and a smaller mesohalobous sum.

The lowest DSI values in zone Riv 1 are located between stations R3 and R6 where they fall to 0.36-0.48, indicating marine-brackish species dominance. These values are lower (more marine) than that seen in the downstream Riv 1 zone. This is thought to be because these stations correspond with the turbidity maximum (with highest estuarine carbonate) where the allochthonous component, derived largely from the mid/outer estuary, will be at its maximum.

In subzone Riv 2 (i), the DSI value of 0.36 indicates marine species dominance. The polyhalobous sum rises to 46% with the mesohalobous and halophile sums falling to 6% and 3% respectively. The oligohalobous indifferent sum remains similar to Riv 1 at 21%. The polyhalobous group is dominated by planktonic and tycho planktonic species with the tidal flat group species *Delphineis surirella* reaching >10%TDV, along with *Actinocyclus octonarius*, *Actinoptychus senarius* and *Podosira stelligera* all at >5%TDV. The mesohalobous group remains dominated by the epipelagic *Navicula avenacea*, while the only >5%TDV freshwater species present is the epiphyte *Cocconeis placentula* (>10%TDV).

In subzone Riv 2(ii), DSI values gradually rise from 0.44 to 0.60, indicating a gradual decline in marine species. This is seen in the diatom group sums, with the polyhalobous sum falling from 31% at R4 to 19-24% at R7 and R8. This group remains dominated by allochthonous marine planktonics and tycho planktonics with *Actinocyclus octonarius*, *Delphineis surirella* and *Podosira stelligera* all present at >5%TDV for most of the subzone. The tycho planktonic *Cymatosira belgica* is present at >5%TDV at R4. This species was recorded by Vos and de Wolf (1993b) to be the most prominent allochthonous tycho planktonic in the Holocene coastal deposits of the Netherlands. In the mesohalobous group, *Navicula avenacea* is joined by the high saltmarsh species (Taw Estuary transect) *Navicula phyllepta* at >5%TDV. In the oligohalobous indifferent group, *Cocconeis placentula* (>10%TDV) is joined by the marsh border benthic *Pinnularia subcapitata* at >5%TDV, which was also found at high saltmarsh elevations in the Taw Estuary.

Zone Riv 3 (R9 to R13)

This zone has been divided into two subzones with Riv 3(i) corresponding with stations R9 and R10, and Riv 3 (ii) associated with stations R11 to R13. Riv 3(i) stations are situated in the freshwater tidal zone identified in section 4.3.2. Riv 3(ii) stations are located at elevations above HAT (R11 is situated downstream of the HAT tidal head but the riverbank bench would only be submerged during 20yr HAT conditions).

Subzone Riv 3(i) sees DSI values rise from 0.64 at R9 to 0.79 at R10, indicating this subzone includes an up-river threshold where mixed assemblages change to freshwater dominated (>0.7 DSI) assemblages. This is seen in the polyhalobous sum which falls from 11.5% at R9 to 0% at R10. The R9 marine component includes the planktonic

Actinocyclus octonarius and the tychoplanktonics *Cymatosira belgica* and *Delphineis surirella* all at >2%TDV. R9 is elevated below MHWST at 4.49m OD (in the upper high saltmarsh tidal frame zone) and although it is situated above the salinity front identified for HAT tides below 5.5m OD, the presence of marine planktonics-tychoplanktonics indicates some estuarine sediment does become mixed into the start of the freshwater tidal zone (supporting the carbonate and $X_{fd\%}$ evidence). The mesohalobous group rises to 23-26% in Riv 3(i) due to the continuing presence of *Navicula avenacea* at >5%TDV and a rise in *Navicula phyllepta* to >10%TDV numbers. Figure 4.15 shows that the up-river transect optimum for *Navicula phyllepta* is reached in this subzone. The altitudinal optimum for this species was located in the high saltmarsh zone in the estuary transect, indicating it can withstand long periods of emergence and drying out. Despite its mesohalobous classification, its presence in Riv 3(i) (and Riv 3 (ii)) indicates it is also freshwater tolerant. The continuing presence of *Navicula avenacea* indicates that this mesohalobous species is also particularly freshwater tolerant and can withstand a wide range of submergence levels by both tidal and fluvial water. The oligohalobous indifferent group is dominated in Riv 3(i) by *Cocconeis placentula* (>10%TDV), *Gomphonema angustum* and *Pinnularia subcapitata* (both at >5%TDV). Subzone Riv 3(i) also sees the emergence of *Nitzschia palea* at >5%TDV abundance.

Subzone Riv 3(ii) sees DSI values consistently remain at 0.83 at all stations (R11 to R13), indicating freshwater dominated assemblages with a minor brackish component. The mesohalobous sum (22-27%) remains at similar levels to Riv 3(ii), and the oligohalobous indifferent sum rises slightly to 57-59%. The only mesohalobous species present (>2%TDV) are the epipelics *Navicula avenacea* and *Navicula phyllepta* (both >10%TDV), with figure 4.15 showing *Navicula avenacea* has reached its optimum in the river transect. Riv 3(i) and Riv 3(ii) are located in the zone thought to be affected by slightly saline groundwater intrusion (0.16-0.29‰, section 4.3.2). This may account for the continuing presence and optimums for these two mesohalobous species. Some marine/brackish epipelics are known to be able to withstand salinities down to the freshwater boundary at 0.2‰ (Vos and de Wolf, 1993a), so this supports the intrusion of some saline groundwater upstream of HAT. The presence of these species in channel marginal settings also suggests some brackish groundwater penetrates the soil/sediment proximal to the channel. The oligohalobous indifferent group is dominated by the epiphytes *Cocconeis placentula* and *Nitzschia palea*, both at >10%TDV. *Nitzschia palea*

is classified as a freshwater epiphyte by Vos and de Wolf (1993a). However, Van de Werff and Huls (1957-1974) classified this species as fresh-brackish. This may account for its optimum abundance in zone Riv 3 (numbers fall to <3%TDV in Riv 4).

Zone Riv 4 (R14 to R17)

This zone has been divided into two subzones with Riv 4(i) corresponding with stations R14 and R16, and Riv 4(ii) associated with station R17. DSI values rise to 0.94-0.96 in Riv 4(i), indicative of a freshwater assemblage with some rare brackish taxa. In Riv 4(ii), the DSI value rises to 0.98 indicating a relatively pure freshwater assemblage.

In subzone Riv 4(i), the mesohalobous sum falls to 8-11% and the oligohalobous indifferent sum rises to 73-76%. The continuing presence of the mesohalobous species *Navicula avenacea* (>10%TDV) and the disappearance of *Navicula phyllepta* to <2%TDV levels suggests this subzone experiences some marine groundwater intrusion, but at very low diluted salinities (not recorded during the salinity survey), which is beyond the tolerance of *Navicula phyllepta*. In the oligohalobous indifferent group, the steady decline in *Nitzchia palea* from 2.5%TDV at R14 to 1%TDV at R16 would also support this. The oligohalobous indifferent group is dominated by *Cocconeis placentula*, *Gomphonema angustum* and *Pinnularia subcapitata* all at >10%TDV, along with *Gomphonema angustatum* at >5%TDV.

In subzone Riv 4(ii), the mesohalobous sum falls to 2.5% and the oligohalobous indifferent sum rises to 82%. This subzone sees a sharp decline in *Navicula avenacea* to 2%TDV. This suggests that this subzone is now beyond the up-valley limit of groundwater intrusion, with the limit occurring between R16 and R17. The freshwater assemblage is dominated by *Cocconeis placentula* and *Pinnularia subcapitata* at >10%TDV, along with *Eunotia pectinalis*, *Gomphonema angustum* and *Hantzschia amphioxys* all at >5%TDV.

4.3.5 Limitations of River Taw dataset in palaeosalinity reconstruction

The limited number of high tide salinity measurements and the analysis of diatoms from only a single high tide has put some limitations on the use of the contemporary dataset in any palaeosalinity reconstruction. This salinity gradient survey of diatom distribution

would have certainly benefited from a series of salinity measurements taken throughout the spring-neap tide cycle, and from different seasons of the year. This would have given a better estimate of the full range of salinities effecting each sampling station. The identification of contemporary diatom assemblages at various times in the tidal cycle and during various seasons would also have given a much better understanding about both seasonal and tidal cycle changes in diatom distribution and assemblage composition.

However, the palaeosalinity reconstruction in this study is not a quantitative exercise (*e.g.* Juggins, 1992) based on a statistically significant predictive transfer function (ter Braak, 1987; ter Braak and Prentice, 1988) to quantify the relationship between contemporary diatoms and salinity. This approach would indeed have required a large contemporary training set with diatoms sampled during a range of seasonal discharge and tidal cycle conditions. Instead, this study is using assemblage DSI as a proxy for salinity (Bryne *et al.*, 2001). The DSI of an assemblage is based on the salinity classification scheme of Van der Werff (1958) and Van der Werff and Huls (1957-1974), and as such is semi-quantitative at best, and is not based on a local training set or modern analogue. This is its main drawback, as it does not account for local species optimums and preferences.

The purpose of the contemporary survey (as laid out in 4.1.2) is to firstly provide a modern framework of inner estuarine hydrology in terms of the high tide salinity gradient and tidal limits. Secondly, to provide a modern analogue of diatom distribution along the salinity gradient of the inner Taw estuary and lower fluvial zone. This second aim will allow additional qualitative interpretation of the core records, which will supplement the DSI analysis. These two aims will therefore allow the Holocene palaeo records to be put into context, in terms of diatom species distribution and hydrology. Additional salinity measurements and diatom samples from different tides and seasons would have certainly given a more comprehensive understanding about diatom distribution in the inner estuary, but would not have significantly effected the DSI-based palaeosalinity reconstruction. The scope of the survey undertaken is therefore justified.

5 LITHO- AND BIO-STRATIGRAPHY OF THE INNER TAW ESTUARY: A HOLOCENE RECORD OF GEOMORPHIC AND ENVIRONMENTAL CHANGE

5.1 INTRODUCTION

5.1.1 Chapter objectives

This chapter will describe the geomorphology, litho- and bio-stratigraphy of the inner Taw Estuary, from Barnstaple (where salinities reach *c.*25‰) upstream to the freshwater tidal zone and the vicinity of the modern tidal head. Extreme high tides (*e.g.* HAT tides) occasionally penetrate upstream into the fluvial zone described in chapter 6.

The aims of this chapter are as follows:

1. To identify sediment core(s) in the inner Taw Estuary that can be used to reconstruct RSL during the mid-late Holocene, using the traditional lithostratigraphic method of Shennan (1982).
2. In the identified RSL cores (cores PL1 and TS1), to provide bio-stratigraphic (diatom) evidence of down-core changes in marine influence and RSL movement. This evidence will be used to validate a series of sea-level index points located at dated transgressive or regressive overlaps (Shennan, 1982; Tooley, 1982) within the core lithostratigraphy. The qualitative assessment of changes in marine influence will be done by comparing the fossil core assemblages with the contemporary altitudinal zonation of diatom species in the Taw Estuary (presented in chapter 4), and with previous studies of intertidal diatom distribution, especially from the UK (*e.g.* Shennan *et al.*, 1995; Zong, 1997; Zong and Horton, 1998, 1999; Gehrels *et al.*, 2001; Hill *et al.*, 2007).
3. To establish down-core changes in depositional environment, in terms of tidal frame zone (tidal flat/channel, mid saltmarsh, high saltmarsh *etc.*), for a series of dated sediment cores located along the salinity gradient of the inner estuary. As in ‘aim 2’, the identification of depositional altitude will be done qualitatively by comparing the fossil

diatom core assemblages with the contemporary altitudinal zonation of diatom species in the Taw Estuary and elsewhere. The purpose of this aim is to obtain a semi-quantitative measure of palaeosalinity, in the form of DSI (diatom salinity index) values (Bryne *et al.*, 2001), for each of the identified depositional environments (*e.g.* high saltmarsh) at different locations along the salinity gradient. This will allow (in chapter 7) late Holocene temporal and spatial changes in palaeosalinity to be investigated for a series of separate altitudinal environments. Inter-core DSI comparisons based on diatom assemblages from similar depositional altitudes will ensure that salinity, not tidal frame position, is the principal environmental control on DSI (*i.e.* differences in diatom assemblage composition will be caused by differences in salinity regime).

Sedimentary, plant macro-fossil and mineral magnetic evidence of depositional environment will be used to support the above diatom-based identification of palaeoenvironment and tidal frame position. For example, saltmarsh sediments often contain high concentrations of bacterial magnetite (Gibbs, 2000) and authigenic greigite (Oldfield, 1994).

4. To use magnetic mineral assemblage characteristics as a proxy indicator of marine influence and sediment source. Magnetic mineral assemblages can provide information about location in the salinity gradient (Oldfield *et al.*, 1985, 1989, 2003) at the time of deposition by showing the relative contribution of estuarine sourced minerals such as bacterial magnetite and authigenic greigite to catchment derived minerals such as soil derived secondary magnetite (Oldfield *et al.*, 1983; Maher, 1986) and possibly detrital haematite (if this is shown to be sourced from the catchment by an up-estuary increase in concentration).

5. To investigate Holocene geomorphic and environmental change in the estuarine and fluvio-estuarine (transitional) zones of the inner Taw Estuary.

To accomplish these aims the inner estuarine zone will be divided into several reaches, centred around one or two cross-valley auger transects. The geomorphology of each reach will be introduced and described. The location of transects and analysed cores will be shown and valley-wide 2-D lithostratigraphic sections will be constructed to reveal the Holocene alluvial fill. The geochronology of the deposits will be determined through radiocarbon and OSL dating. For each transect, the lithostratigraphy will be

analysed for sedimentary and stratigraphic evidence of geomorphic change. Individual cores will be analysed for diatom assemblage evidence of depositional environment, in terms of depositional altitude in the tidal frame, and relative proximity to the salinity front. This will be supported by sedimentary, plant macro-fossil and mineral magnetic evidence of depositional environment.

Finally, the stratigraphy of each reach will be divided into discrete zones of sediment deposition (termed ‘floodplain sediment units’ or ‘FSUs’; see 5.1.2), related to separate periods of floodplain development and formation. The geomorphic and environmental history of the reach will be summarised, through the interpretation of each FSU. In chapter 7, these FSUs will also form the basis of further stratigraphic division and correlation of the entire inner estuary valley-fill.

5.1.2 Floodplain sediment units

In fluvial environments, terrace and sub-terrace units of floodplain development have been routinely identified (*e.g.* Macklin and Lewin, 1986; Brown, 1987; Taylor and Macklin, 1997; Howard and Macklin, 1999; Moores *et al.*, 1999; Passmore and Macklin, 2001; Johnstone, 2004; Lewin *et al.*, 2005). Needham (1989) phrased these units as ‘alluvial parcels’, each generally separated by a vertical boundary.

Discrete phases of sedimentation have also been identified in some estuarine sequences. For example, phases of Holocene estuarine development and sedimentation were identified in the Humber Estuary by Rees *et al.* (2000), and in the coastal wetland and estuarine deposits of the south-west Netherlands, Vos and Heeringen (1997) identified several phases of mid-late Holocene sedimentation. However, the 3D division of estuarine sequences into parcels of sedimentation remains quite rare, and units are generally millennial-scale, rather than centennial. There is also an inherent bias in Holocene studies to interpret estuarine deposits in terms of RSL change, with little reference to geomorphic change caused by climate-induced changes in river regime (sediment flux and discharge).

The inner estuarine tidal river location of the Taw valley site offers an opportunity to identify phases of alluviation which are influenced by both catchment changes, and

equally influenced by centennial-millennial changes in RSL.

The fluvial approach to stratigraphic division has been replicated in this study, with the stratigraphy of each of the four tidal transects divided into parcels, here called Floodplain Sediment Units (FSUs). The FSU division of transects A to D will enable each unit to be summarised and interpreted in terms of geomorphic/environmental change, and this division will then be incorporated in the stratigraphic division of the whole study area (tidal and non-tidal zones), given in chapter 7.

5.1.3 Geomorphology of the inner Taw Estuary and location of transects

The geomorphology of the inner Taw Estuary is presented in figure 5.1, along with the location of auger transects A to D and the location of analysed cores. The inner estuary is seen to be a tidal river environment with a single-thread meandering channel planform. This environment represents the mixed-energy and river-dominated sections of the Dalrymple *et al* (1992) model of a tide-dominated estuary (see figure 2.1) where both river currents and tidal currents are significant agents of sediment transport. The tidal channel opens out into the tidal flats and sand bars of the middle and outer Taw Estuary at Barnstaple, 1.0km north of the mapped study area. The zone downstream of Barnstaple represents the marine-dominated section of the Dalrymple *et al* (1992) model (figure 2.1) where tidal currents are dominant and wave energy becomes more significant.

Seven late Quaternary river terraces (T1 to T7) were identified within the entire inner estuarine and fluvial zone study area. However, the early-mid Holocene terraces T4 and T5 are only present in the surface geomorphology of the non-tidal fluvial zone (chapter 6). In the geomorphological map of the inner estuary (figure 5.1), the most recent valley floor deposits are labelled 'floodplain' and south of transect B mainly occupy the inside of meander bends, being formed by relatively recent channel migration. T1 to T3 are late Holocene in age, while T6 and T7 are of late Pleistocene Devensian origin (Edmonds *et al.*, 1979). With reference to the geological map produced by Edmonds *et al.* (1979), their youngest terrace (Terrace 1) equates to T7 in this study. However, field mapping has shown some significant errors in the original map extent of this terrace

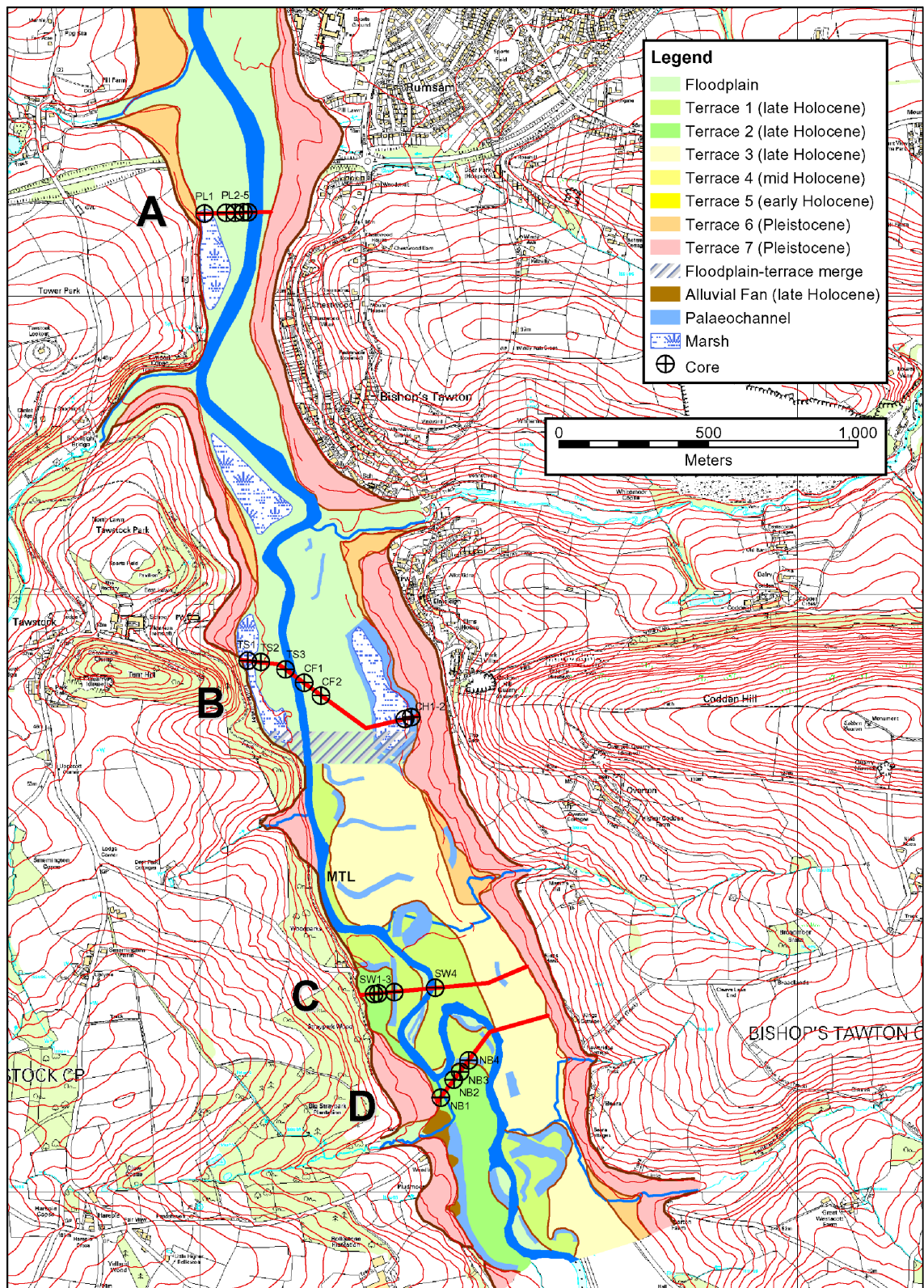


Figure 5.1 Geomorphology of the inner Taw Estuary (a tidal river environment) upstream of Barnstaple. The location of transects A to D and all cores are indicated. MTL (mean tidal limit) corresponds to NTL (normal tidal limit), as shown on the Ordnance Survey 1:25 000 Explorer 127 sheet (Revised edition A, 1997). HAT (highest astronomical tide) is located *c.*800m upstream of the southern map margin, within the non-tidal River Taw zone (Chapter 6). This map was produced in a GIS and incorporates OS Landform Profile (5m contours) and OS 10,000 colour raster layers (supplied by Ordnance Survey/EDINA Digimap).

with Edmonds *et al.* (1979) ascribing 'Terrace 1' status to areas of significantly lower Holocene terrace.

Figure 5.1 shows the Pleistocene (Devensian) terraces preserved on the valley edges, with T6 typically elevated *c.*1.5-2.0m above the Holocene terraces and T7 elevated *c.*8.0m above the highest Holocene alluvium (T3). Occasional exposures of these terraces reveal rounded framework river gravels capped by thin (0.50-0.75m) fine grained sands and silts. This is typical of braided-channel river deposits (dominated by gravel bars) that are representative of a cold climate with sparse vegetation, thin soils and high sediment input (Collinson, 1996). This is consistent with fluvial activity in the Taw valley during the Devensian being fluvio-periglacial in nature, with the Taw catchment located south of the Devensian ice limit (Bowen *et al.*, 1986). Several higher terraces (above T7) were deposited prior to the late Devensian, and were mapped by Edmonds *et al.* (1979). These terraces are not relevant to this study and were therefore not re-mapped or shown in figure 5.1.

Figure 5.1 shows a zone south of transect B where the floodplain and terrace merge. This is the approximate location of the inner estuary bayline (Allen and Posamentier, 1993; Dalrymple and Zaitlin, 1994), where the alluvial floodplain slope meets the estuarine coastal plain at approximately MHWST (4.7m OD) and shows no further significant decrease in altitude with down-estuary distance. Following the facies models of Dalrymple *et al.* (1992) and Allen and Posamentier (1993), the bayline should also be the location where transgressive estuarine tidal sediments overlap the fluvial sediments of the alluvial floodplain.

To the south of the bayline, the altitude of all floodplain and Holocene terrace surfaces begin to rise, giving the typical river valley long-profile. However, in the brackish and freshwater tidal zone there is very little relative elevational difference between the floodplain, T1, T2 and T3. This means that the Holocene terraces essentially behave as a single modern floodplain during overbank floods. It was observed that this area was prone to flooding both during high stage river floods and after very high spring tides. In some areas, particularly in meander cores (*e.g.* in transect D), there is an inverse relationship between 'terrace' surfaces with T1 having a higher elevation than T2. This is thought to be because T1 deposits are proximal to the river channel within a levee environment (with higher rates of deposition during overbank floods) and because T1

deposits are significantly coarser grained, deposited during a period of channel bed aggradation when overbank flooding would have been more frequent. Upstream in the non-tidal fluvial zone (chapter 6), the Holocene terraces are seen to diverge, with altitudinal differences becoming more apparent. This shows that the terrace surfaces have slightly different down-valley gradients, with the slope angle generally increasing with age. Within the tidal zone, this has resulted in terrace surfaces merging and coalescing between transects D and B. The differences in long profile gradients may relate to Holocene changes in RSL and base-level, but are more likely to be relate to late Holocene changes in river discharge and sediment supply (Dawson and Gardiner, 1987). Because of the similarity in terrace elevation between transects B and D, the mapping of terraces in this zone was partly based on sediment characteristics and thickness of alluvium (above the basal gravel). This was explored through subsurface investigation, both in the transects and through exploratory augering between transects. Additional surface evidence for terrace fronts included palaeochannel position and differences in micro-topography.

The inner Taw Estuary was divided into three reaches with the Pill Lane reach centred around transect A, the Tawstock reach centred around transect B, and the New Bridge reach centred around transects C and D. The geomorphology will be described in more detail, in relation to each of these reaches, in sections 5.2, 5.3 and 5.4.

5.1.4 Legends for sedimentary sections and core logs

The legends for sediment types used in many of the figures in this chapter and chapter 6 are given in figure 5.2. Separate legends are presented for (a) diatom and magnetics diagram lithology logs, (b) lithostratigraphic cross-valley section diagrams, and (c) core log figures.

5.1.5 Radiocarbon and luminescence dates

The age results for all radiocarbon samples taken from cores in the inner estuary (transects A to D) are presented in table 5.1. A variety of terrestrial plant macrofossils were submitted for AMS radiocarbon dating. These included seeds, tree and grass

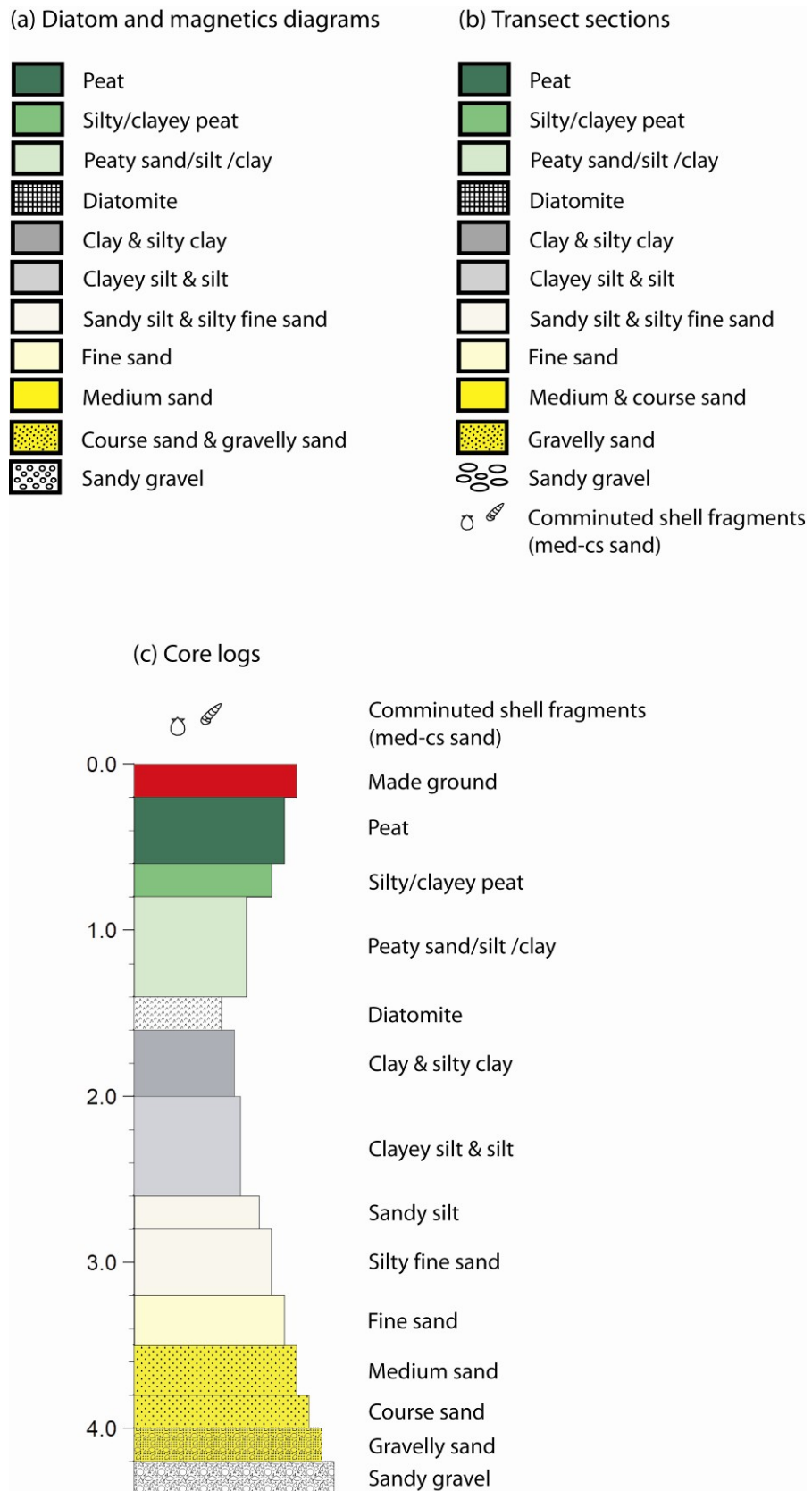


Figure 5.2 (a) Legend for diatom and magnetics diagram lithology logs. (b) Legend for lithostratigraphic transect sections. (c) Legend for core logs.

Tidal River Taw Radiocarbon Dates

Thesis code	Sample code	Laboratory code	Dating method	Sample material	¹⁴ C enrichment (% Modern ±1)	Carbon content (% by wt.)	δ ¹³ C _{VPOB} ‰ ±0.1	Conventional ¹⁴ C Age (years BP ±1)	2σ Calibrated Age (Cal.yr.BP)	1σ Calibrated Age (Cal.yr.AD/BC)	2σ Calibrated Age (Cal.yr.AD/BC)
Transect A											
A1	PL1-26	SUERC-15747	AMS	Gramineae	124.00 ±0.57	31.4	-30.1	modern	modern	modern	modern
A2	PL1-65	SUERC-15748	AMS	Gramineae	85.49 ±0.40	47.0	-29.4	1260 ±/ 37	1283-1081	684-777 AD	668-869 AD
A3	PL1-106	SUERC-15749	AMS	Phragmites	75.96 ±0.35	22.2	-29.4	2209 ±/ 37	2334-2135	360-206 BC	385-186 BC
A4	PL1-250	SUERC-15750	AMS	Phragmites	64.41 ±0.30	33.0	-26.0	3534 ±/ 38	3913-3697	1927-1776 BC	1964-1748 BC
A5	PL1-279	SUERC-18363	AMS	Wood (twig)	62.85 ±0.29	52.3	-29.3	3730 ±/ 38	4228-3975	2199-2043 BC	2279-2026 BC
A6	PL1-358	SUERC-15765	AMS	Wood (twig)	59.26 ±0.28	57.0	-25.7	4203 ±/ 38	4849-4617	2890-2702 BC	2900-2668 BC
A7	PL1-398	SUERC-15766	AMS	Wood (twig)	56.31 ±0.27	47.0	-29.9	4614 ±/ 38	5468-5086	3498-3353 BC	3519-3137 BC
A8	PL1-422	SUERC-15767	AMS	Wood (twig)	55.21 ±0.26	54.0	-27.4	4773 ±/ 38	5593-5331	3636-3525 BC	3644-3382 BC
A9	PL1-557	Beta-217022	Radiometric	Wood (branch)	na	na	-29.2	5390 ±/ 120	6403-5922	4342-4055 BC	4454-3973 BC
A10	PL1-594	SUERC-15768	AMS	Wood (twig)	48.44 ±0.24	58.0	-30.5	5822 ±/ 40	6733-6504	4726-4611 BC	4784-4555 BC
Transect B											
B1	TS1-34	SUERC-18364	AMS	Wood	62.85 ±0.29	52.3	-29.3	3730 ±/ 38	534-328	1433-1485 AD	1417-1623 AD
B2	TS1-84	SUERC-15753	AMS	Seed	89.58 ±0.42	28.2	-25.0	884 ±/ 37	912-729	1051-1213 AD	1038-1221 AD
B3	TS1-484	Beta-216121	Radiometric	Wood (branch)	na	na	-28.8	1590 ±/ 60	1615-1348	415-540 AD	336-603 AD
B6	CF2-161	SUERC-15774	AMS	Wood	71.09 ±0.31	33.0	-29.0	2741 ±/ 35	2925-2761	912-837 BC	976-812 BC
B7	CH1-386	Beta-216111	AMS	Wood (twig)	na	na	-26.9	11470 ±/ 40	13408-13237	11411-11321 BC	11459-11288 BC
Transect C											
C2	SW1-202	Beta-217839	Radiometric	Wood (branch)	na	na	-26.0	680 ±/ 50	694-549	1274-1387 AD	1257-1401 AD
C5	SW4-313	SUERC-15754	AMS	Leaf	93.38 ±0.41	40.6	-29.0	515 ±/ 35	630-503	1403-1438 AD	1320-1448 AD
Transect D											
D1	NB2-420	SUERC-15775	AMS	Wood (twig)	84.68 ±0.39	58.0	-27.0	1335 ±/ 37	1309-1178	650-764 AD	642-773 AD
D2	NB3-309	SUERC-15758	AMS	Leaf	85.52 ±0.40	49.0	-29.4	1257 ±/ 37	1281-1081	683-779 AD	670-870 AD

Table 5.1 Radiocarbon dates for transects A to D, the inner Taw Estuary (na = data not available).

Tidal River Taw OSL Dates

Thesis code	Sample code	Oxford Lab code	Depth (m)	Altitude (m OD)	Grain size (μm)	H ₂ O content (%)	U (ppm)	Th (ppm)	K (wt.%)	External gamma-dose (Gy/ka)	Total dose rate (Gy/ka)	D _e (Gy)	OSL age (yrs)	OSL age (yr.AD/BC)
Transect A														
A11	PL2-311	X3249	3.11	0.76	125-180	39.25	1.6	5.2	1.1	not available	1.23 +/-0.08	2.38 +/-0.11	1930 +/-160	70 +/-160 AD
A12	PL3-238	X3248	2.38	1.58	125-180	35.75	2.3	6.5	1.2	not available	1.53 +/-0.10	1.18 +/-0.07	770 +/-70	1230 +/-70 AD
Transect B														
B4	TS2-297	X3252	2.97	1.14	125-180	44.1	1.9	6.8	1.3	not available	1.34 +/-0.09	1.20 +/-0.04	900 +/-70	1100 +/-70 AD
B5	CF1-276	X3253	2.76	1.98	125-180	55.29	2.8	9.3	1.8	not available	1.47 +/-0.10	1.63 +/-0.12	1110 +/-110	890 +/-110 AD
B8	CH2-262	X3250	2.62	2.44	125-180	31.29	3.4	11.5	2.0	not available	2.56 +/-0.18	33.14 +/-3.05	12960 +/-1490	10960 +/-1490 BC
Transect C														
C1	SW1-175	X2917	1.75	3.58	90-125	65.87	2.1	6.6	1.3	not available	0.89 +/-0.08	0.80 +/-0.08	900 +/-120	1100 +/-120 AD
C3	SW1-336	X3255	3.36	1.97	125-180	54.95	3.1	9.0	1.4	not available	1.31 +/-0.08	1.74 +/-0.16	1330 +/-150	670 +/-150 AD
C4	SW2-125	X2918	1.25	3.96	90-180	34.17	3.4	9.8	1.6	not available	2.13 +/-0.16	0.28 +/-0.04	130 +/-20	1870 +/-20 AD
Transect D														
D3	NB4-120	X3254	1.2	4.36	125-180	36.74	4.2	9.9	1.8	not available	2.21 +/-0.17	2.27 +/-0.46	1030 +/-220	970 +/-220 AD

Table 5.2 OSL dates for transects A to D, the inner Taw Estuary.

leaves, fragments of *Phragmites* stem and sub-aerial wood. Where possible, wood samples consisted of small twigs that showed little sign of abrasion or bark removal. Larger sections of tree branch, penetrated by the gouge auger, were submitted for conventional radiometric dating. Again, no samples with obvious abrasion or signs of reworking were used. Table 5.1 includes the sample $\delta^{13}\text{C}\text{‰}$ values. The results show values typical for wood and terrestrial C_3 plants, though most samples do show some depletion in the $^{14}\text{C}:^{13}\text{C}$ ratio caused by isotopic fractionation. A correction was made to the measured ^{14}C activity because of this. All ^{14}C ages were calibrated to calendar years using the OxCal program (Bronk Ramsey, 2001) and expressed as a 2σ (95% probability) range in ‘cal.yr.AD/BC’. Ages in ‘cal.yrs.BP’ are also given in table 5.1 as this format will sometimes be used in the RSL reconstruction given in chapter 7.

The age results for all OSL samples taken from cores in the tidal zone are presented in table 5.2. The total annual dose rate was calculated from sediment radionuclide concentration (U, Th and K), water content and estimated cosmic ray contribution (based on sample depth, elevation and assumed burial history) using the methods of Aitken (1998) and Prescott and Hutton (1994). The depth related necessity for samples in the tidal zone to be recovered by coring precluded the use of a field gamma detector. The gamma-dose was therefore determined from radionuclide concentrations (Aitken, 1998). It was assumed that the light-sensitive trapped charge of each grain in the sample was zeroed prior to deposition. All OSL ages (table 5.2) were initially expressed as years before 2000 AD, rounded to the nearest 10 years. A 2σ uncertainty is attached to all dates. This value is based on random and systematic errors from beta-source calibration, dose rate determination, subsampling for chemical data, and optical measurement errors following methods in Aitken and Alldred (1972) and Aitken (1976, 1985). OSL ages are also expressed in calendar years AD/BC (table 5.2) for easier comparison with radiocarbon age results.

5.2 GEOMORPHOLOGY AND STRATIGRAPHY OF THE PILL LANE REACH

5.2.1 Reach geomorphology

The geomorphology of the Pill Lane reach is shown in figure 5.3. The Taw valley is

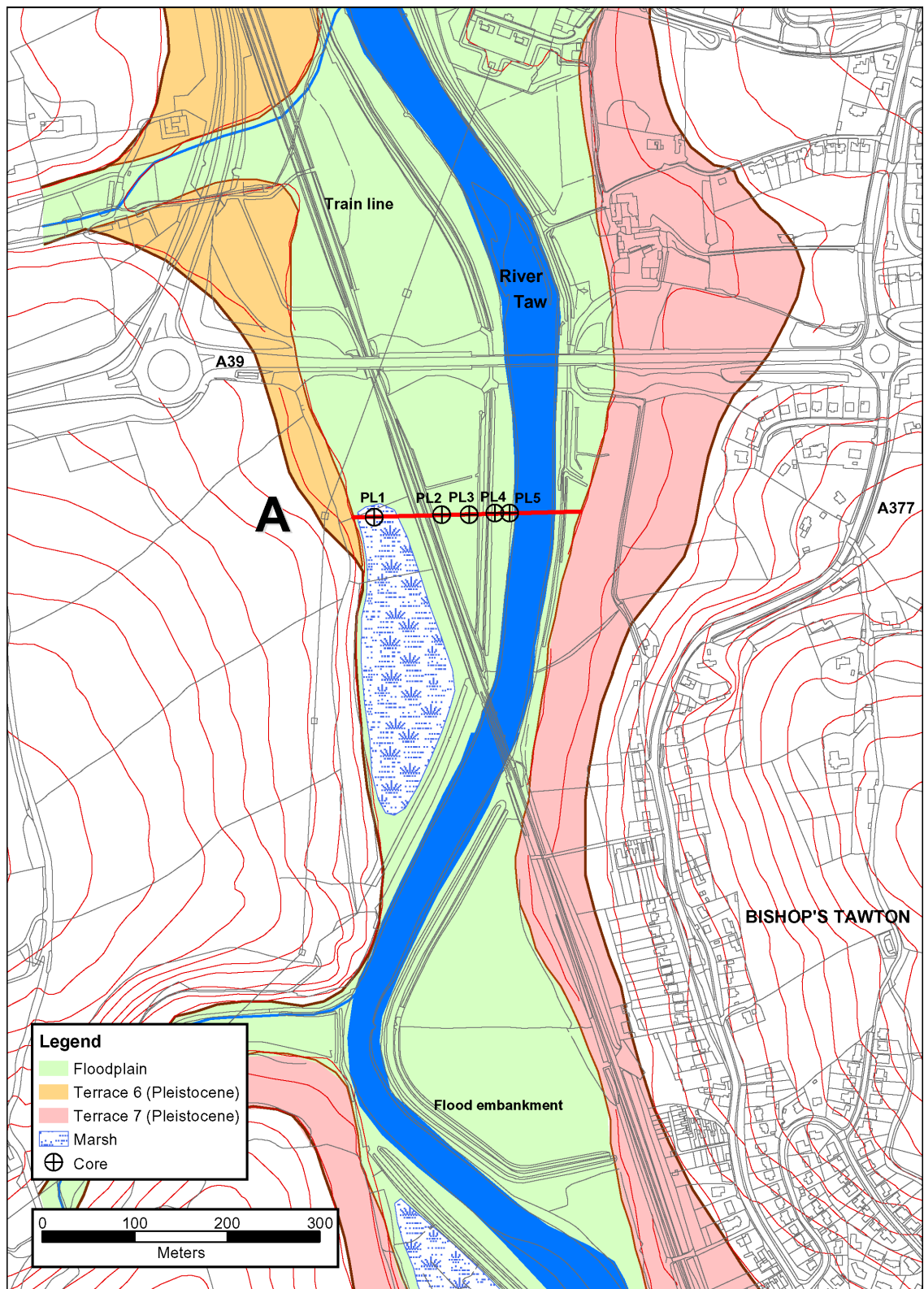


Figure 5.3 Geomorphology of the Pill Lane reach. The location of transect A (Pill Lane transect) and associated cores are indicated. This map was produced in a GIS and incorporates OS Landform Profile (5m contours) and OS MasterMap layers (supplied by Ordnance Survey/EDINA Digimap).

relatively narrow (c.300-400m) in this reach as the river passes through a very resistant geological unit of chert (Edmonds *et al.*, 1979). The location of Transect A (Pill Lane

transect) is shown, along with associated cores PL1 to PL5. Transect A is located *c.*160m south of the A39 road bridge, with the western end of the transect (at PL1) located only 10m south of a man-made slope (fill) that rises up to the western end of the bridge. The river is tidal throughout this reach and is bounded by flood embankments, built to prevent tidal water from flooding the enclosed fields and train line.

Late Pleistocene terraces (T6 and T7) are preserved on both valley sides. No Holocene terraces can be observed in this reach due to burial by onlapping estuarine marsh sediment, deposited during progressive late Holocene RSL rise. Neither are there any surface expressions of palaeochannels. In addition to burial, this may be due to the nature of channel migration in this reach with channel change taking place by lateral migration rather than avulsion or cut-off. The channel planform shows regular meanders with a wavelength of *c.*1200m and relatively low sinuosity ($S = 1.14$).

5.2.2 Lithostratigraphy of the Pill Lane transect

Figure 5.4 shows the lithostratigraphy of transect A, interpreted from the gouge transect. The floodplain surface has an elevation of *c.*4.0m OD outside of the embankments, rising to *c.*4.3m OD within the embanked area. The deposits below PL1 are seen to be much older than the rest of the valley-fill, with a basal age of 4784-4555 cal.yr.BC. This buried mid-late Holocene terrace fragment consists of intercalated organic layers (peaty silt - peat) and minerogenic silt/silty fine sand layers. These changes in depositional environment are thought to be driven by changes in the rate of sea-level rise during the mid and late Holocene and PL1 was quickly identified as having a high potential for use in RSL reconstruction. This reconstruction is presented in chapter 7. Because of this aim, the stratigraphic resolution (distance between transect cores) was increased in the vicinity of PL1 and a more detailed lithostratigraphy is shown in figure 5.5. The primary aim of this additional coring was to investigate the amount of compaction that had occurred in the peats, revealed by altitudinal changes in the peat layer upper surfaces as they onlap the valley side, and to use this information in the RSL reconstruction (chapter 7). However, the additional palaeoenvironmental information derived from figure 5.5 will also be discussed in section 5.2.8.

In the vicinity of PL2, the channel is incised to a depth of -2.1m OD to -3.3m OD and

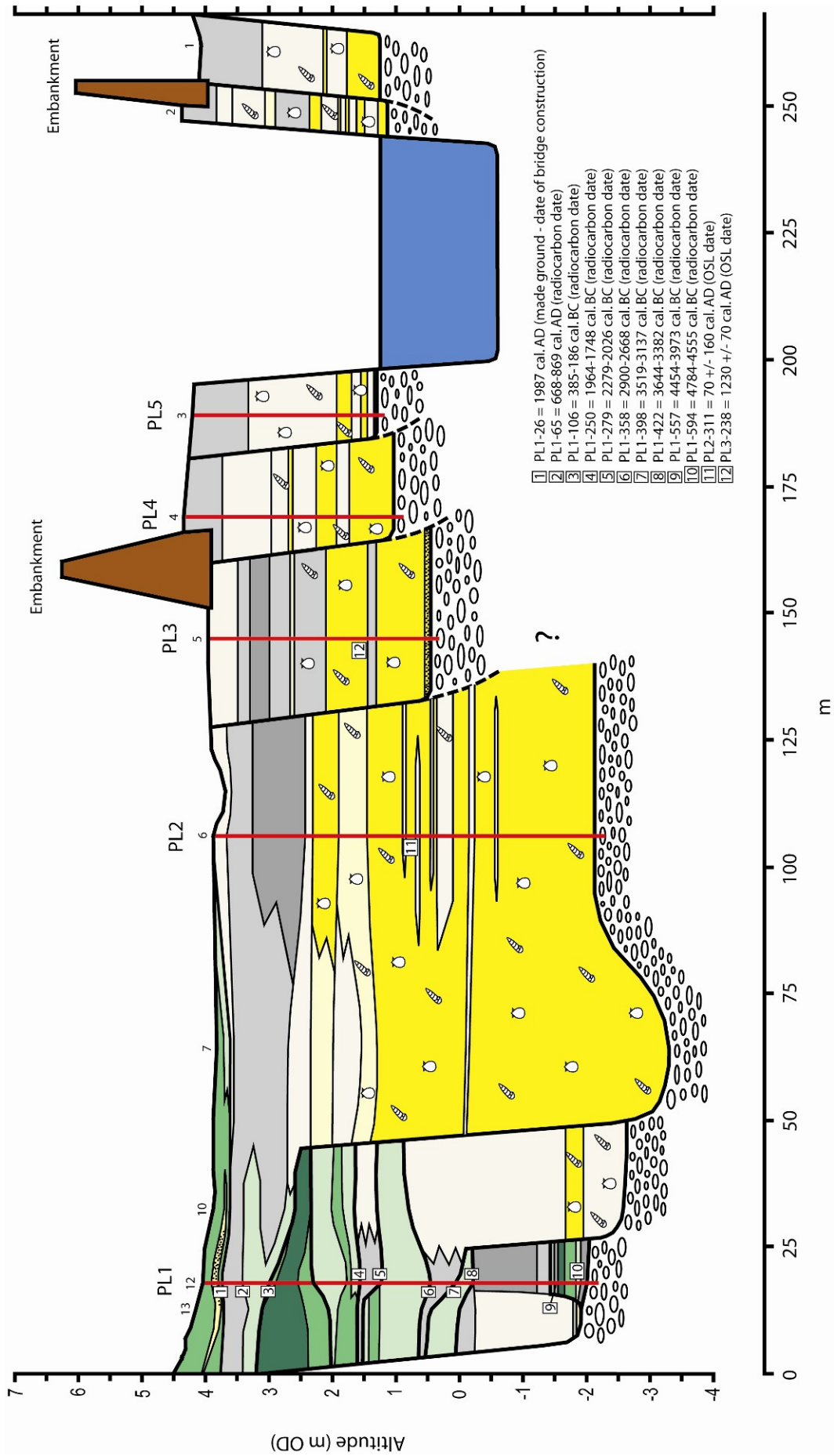


Figure 5.4 Lithostratigraphy of the Pill Lane transect. The location of analysed cores, stratigraphic cores (1-7, 10, 12, 13) and radiocarbon/OSL samples (see tables 5.1 and 5.2) is shown. See figure 5.2 for legend.

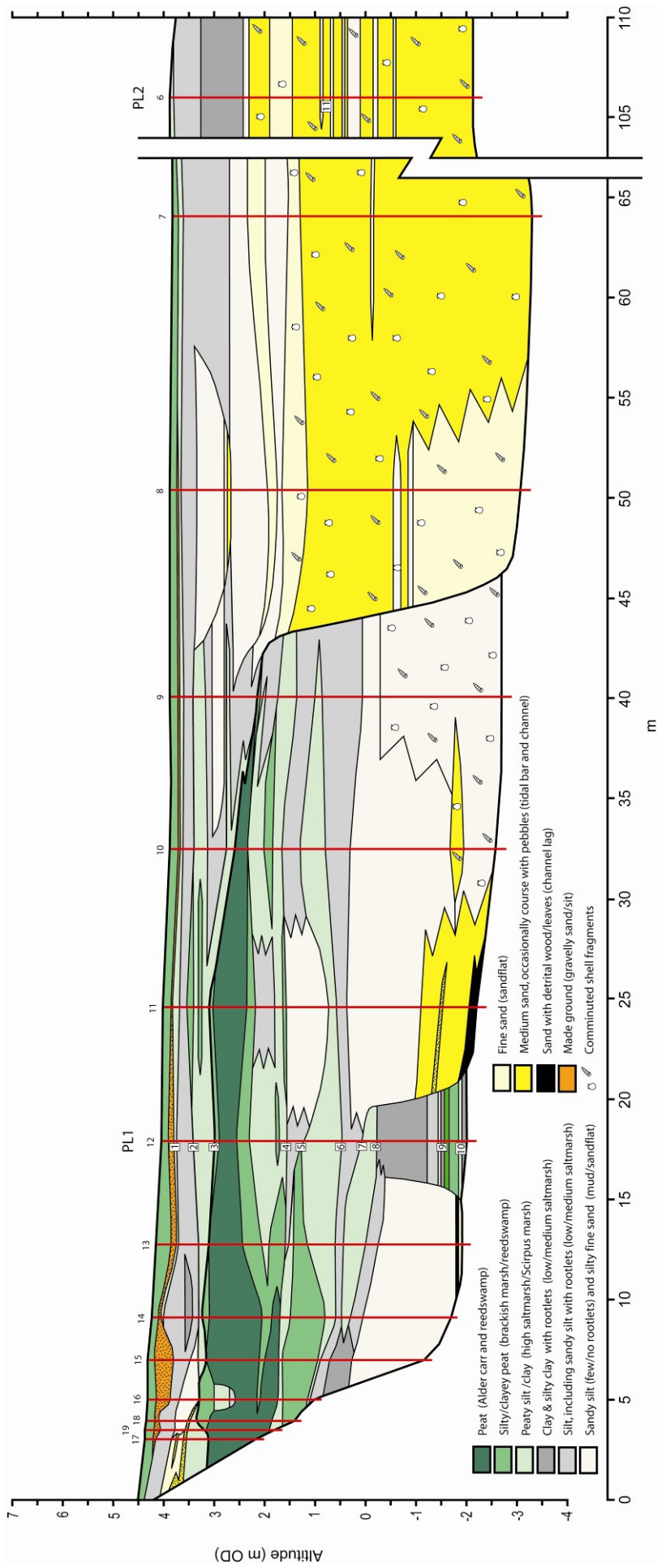


Figure 5.5 Detailed lithostratigraphy of the western end of transect A (Pill Lane transect) . The location of analysed cores PL1 and PL2, stratigraphic cores(6-19) and radiocarbon/OSL samples (see tables 5.1 and 5.2) is shown.

is infilled with shelly estuarine channel sands, capped by marsh silts. These sands were OSL dated, giving an age of 70 +/- 160 cal.yr.AD. The stratigraphy shows an erosive contact between these channel deposits and the mid-Holocene marsh deposits to the west.

The lithostratigraphic interpretation of the core records east of PL2 (figure 5.4) shows a series of near-vertical erosion surfaces separating fining-up estuarine deposits of shelly fine-medium channel sand, each overlain by tidal flat sandy silts and saltmarsh silts and silty clays. These erosion surfaces represent cut-banks formed after a series of sequential meander oscillations or translations on the eastern side of the valley. Reasons for this interpretation are given in section 5.2.8. The channel zone and meander belt has therefore become increasingly constrained to the eastern side of the valley since the first century AD, suggesting a gradual decrease in channel sinuosity.

The stratigraphy also shows a significant period of channel bed aggradation to the east of PL2, with the basal gravel at PL3 rising to 0.45m OD. The shelly channel sands deposited above this gravel were OSL dated, giving an age of 1230 +/- 70 cal.yr.AD. Further periods of minor channel bed aggradation occur in the younger deposits east of PL3.

5.2.3 PL1 core

Sedimentology

Figure 5.6 shows the core log for PL1. This figure shows down-core changes in sediment lithology, organic matter and carbonate content, X_{lf} (low frequency magnetic susceptibility) and $X_{fd\%}$ (frequency dependent susceptibility). In addition, the magnetic zones and diatom zones are indicated (see below), and FSUs (Floodplain Sediment Units, see section 5.2.8) and stratigraphic units (see chapter 7) are shown.

Figure 5.6 shows the sequence of intercalated organic layers (peaty silt - peat) and minerogenic silt layers referred to earlier. The organic layers have been labelled Peat I to Peat V.

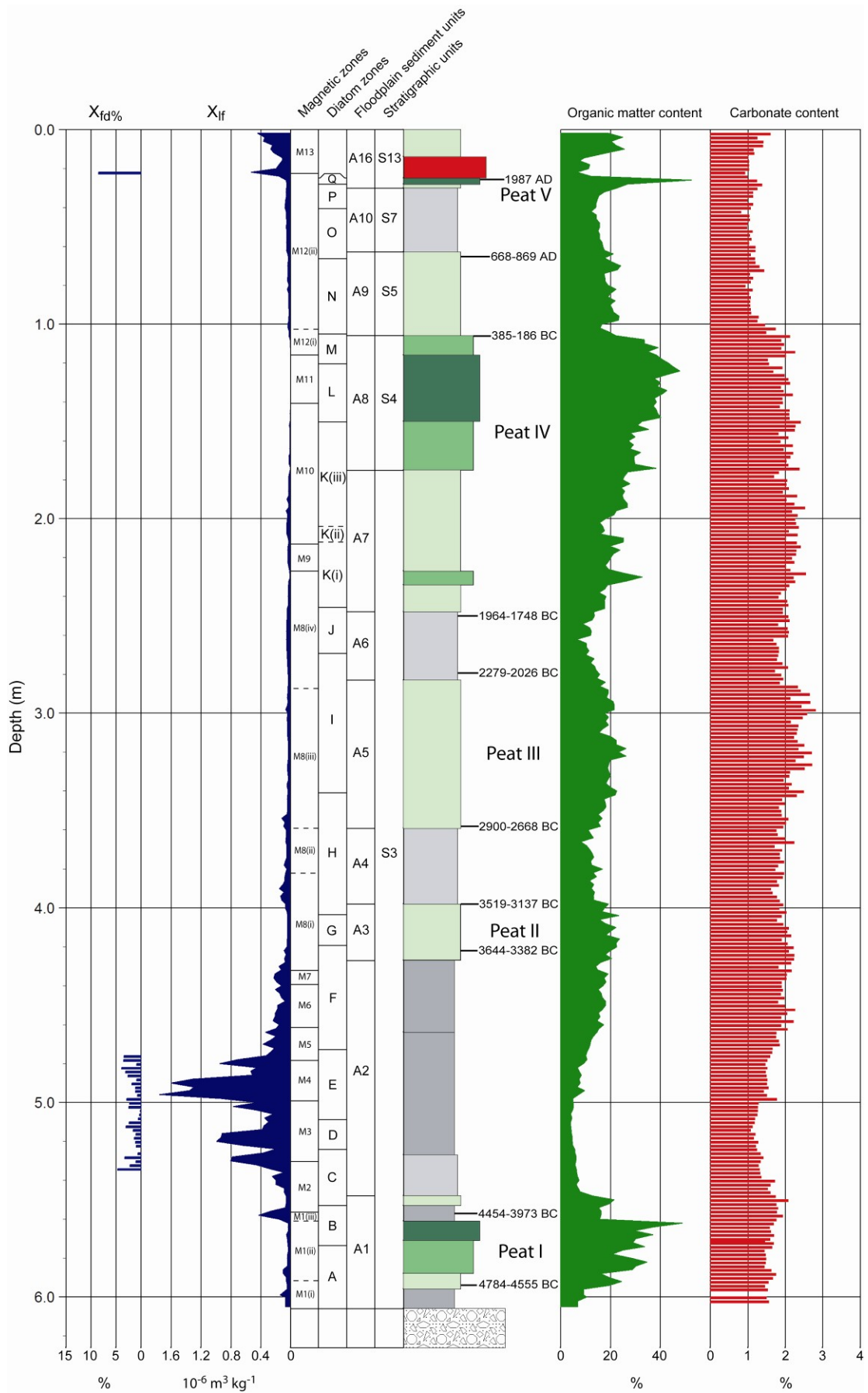


Figure 5.6 PL1 core log. See figure 5.2 for lithology legend. Magnetic zones are derived from figure 5.7, diatom zones are derived from figure 5.8. Floodplain sediment units (FSUs) are discussed in section 5.2.8. Stratigraphic units are discussed in chapter 7.

The basal gravel surface has a depth of 6.06m and above this is a 10cm layer of light grey silty clay. This clay contains many small detrital wood fragments (twigs), giving an overall organic matter content of 7-9%. Carbonate values are low (c.1.5%). Above the clay, Peat I largely consists of black humified wood detritus in a clayey silt matrix. There is a progressive rise in organic matter content from c.20% to c.50% with carbonate values remaining low. At 5.61m, there is a sharp erosive contact which is followed by deposition of a 13cm layer of organic silty clay (15% organic matter content) and peaty silt (c.20% organic matter content). This layer contains many wood fragments (twigs), acorn shell fragments, and nuts/seeds (including a hazelnut), and many fine rootlets.

At 5.48m, Peat I is truncated by another erosion surface, and a change to minerogenic deposition of light grey clayey silt and silty clay (4.95m – 5.48m) with a low organic matter content of 4-7%. The sediment contains occasional fine rootlets and the basal 2cm contains some plant detritus, possibly eroded from the peat below. Between 4.95m and 4.64m, silty clay continues to be deposited but shows a gradual rise in organic matter content, rising to 14%. This is caused by increasing amounts of wood and plant fragments (and occasional seeds and acorn shell fragments) and an increase in the number of rootlets. Carbonate content remains low (c.1.5%). Between 4.64m and 4.27m the carbonate content rises slightly to c.2% and a silty organic clay containing lots of wood (including *Alnus* twigs) and many rootlets is deposited. Other organic components include a *Fagus* seed and a desiccated berry (possibly *Sorbus* or *Crataegus*). Organic matter content remains at 14-17%.

At 4.27m, organic matter content rises to 20% and a dark grey peaty clay (Peat II) persists up to 3.98m, with organic matter content remaining at 19-24%, and carbonate values of c.2%. Organic components include *Phragmites* and *Juncus* stems, occasional twigs (including *Alnus*) and many roots.

Between 3.98m and 3.59m, sedimentation reverts to a minerogenic nature with the deposition of a grey clayey silt unit, bounded by gradational contacts. Organic matter content falls to 10-13% and carbonate content is maintained at 1.8-2.0%. The sediment contains fine rootlets throughout with occasional twigs (possibly including *Fraxinus*) and *Phragmites* fragments.

Following a gradational contact at 3.59m, sedimentation becomes more organic and Peat III is deposited between 3.59m and 2.83m. This deposit is a grey-brown peaty clay with organic matter content values of 17-26%. Above 3.42m carbonate content rises to c.2.5%. The sediment contains rootlets, plant fragments (including *Phragmites*) and occasional twigs. Other components include occasional seeds and acorn shell fragments and a possible hazelnut (*Corylus*).

Between 2.83m and 2.48m, sedimentation reverts to a minerogenic nature with the deposition of a grey clayey silt unit, bounded by gradational contacts. The sediment contains some detrital plant fragments and rootlets and occasional twigs. Organic matter content values range from 8% to 13% and carbonate values fall to 1.7-2.0%.

The sediment becomes more organic at 2.48m and this organic nature persists up to 0.63m with the formation of Peat IV. Between 2.48m and 1.75m, organic matter content gradually rises from 17% to 27%, with the formation of a grey-brown peaty clay with some plant fragments and occasional wood. Rootlets are found throughout, some being 2-6mm thick, possibly from herbaceous marsh plants. However there are two exceptions to this trend of increasing organic matter content. At 2.27-2.34m there is a spike in organic matter content with values reaching 33%. This corresponds to a brown detrital clayey peat. Between 2.10m and 2.00m organic matter content values temporarily fall to 15-18% and the sediment is more minerogenic.

There is a rise in organic matter content (to c.30%) at 1.75m, with a brown clayey peat accumulating between 1.75m and 1.50m. This peat contains many vertical 2-6mm thick herbaceous roots and plant fragments (including *Phragmites*), with occasional wood, suggesting a reedswamp environment. A 6cm thick tree branch is penetrated at 1.62m. Between 1.50m and 1.16m organic matter content values reach 37-48% and a brown peat accumulates with low to moderate humification. Like the clayey peat below, this contains many herbaceous roots and plant fragments (*Cyperaceae* and *Phragmites*), with a slight increase in wood (possibly *Alnus*), suggesting a sedge-reedswamp environment with intermittent Alder. The peat remains similar in nature between 1.16m and 1.06m, but a fall in organic matter to c.35% is seen. Peat IV carbonate content values are maintained at c.2% between 2.48m and 1.06m.

At 1.06m there is fall in carbonate content to c.1.0% and a steep drop in organic matter

content to 16%. A brown peaty silt accumulates between 1.06m and 0.63m with organic matter content values of 17-24% and carbonate values of 1.0-1.4%. This sediment contains many fine rootlets throughout, and many 2-6mm herbaceous roots below 0.84m. A crude minerogenic-organic lamination is visible with individual laminations ranging from 4 to 16mm in thickness.

Above a sharp contact at 0.63m sedimentation becomes more minerogenic, and organic matter content values fall to 12-15%. A grey-brown clayey silt accumulates, containing many fine grass rootlets and carbonate values of *c.* 1.0%. The density of rootlets sharply increases at 0.30m and a thin peat (Peat V) accumulates between 0.30m and 0.25m. Organic matter content values rapidly increase to reach 52% at 0.26cm, with moss becoming an important organic component above 0.28m.

Above a sharp erosive contact at 0.25m, a 9cm layer of poorly sorted silty gravel is found with mottled grey and orange-brown coloration. Gravel clasts are subrounded to subangular of weathered sandstone. This deposit is thought to be made ground, relating to the construction area around the building of the man-made area of fill located 10m to the north, that rises up to the western end of the A39 road bridge. Above another sharp contact at 0.14m, a grey-brown peaty clay has accumulated in the upper 14cm of PL1. This layer contains many grass stems and roots, and occasional leaf detritus, and represents a recent soil developed above the made ground.

Geochronology

As the PL1 core was the principal core used in RSL reconstruction, a relatively large number of samples were submitted for radiocarbon dating (see table 5.1, samples A1 to A10). Figure 5.6 shows the stratigraphic location of these samples in the PL1 core. Samples are located at the top and base of each peat layer so as to date the transitions from minerogenic to organic deposition that occurs around MHWST. These lithostratigraphic boundaries relate to transgressive and regressive overlaps (Shennan, 1982; Tooley, 1982; Shennan *et al.*, 1983) and the dated samples from these depths provide a series of sea-level index points for the Taw Estuary (chapter 7).

The base of Peat I is dated at 4784-4555 cal.yr.BC, and a wood sample in the organic clay horizon near the top of this peat gives an age of 4454-3973 cal.yr.BC. Following a

period of minerogenic deposition, the base of Peat II has a radiocarbon age of 3644-3382 cal.yr.BC. The top of Peat II is dated at 3519-3137 cal.yr.BC. Following a further period of minerogenic deposition, a twig at the base of Peat III gives an age of 2900-2668 cal.yr.BC. A detrital twig at the base of the silt that proceeds Peat III gives an age of 2279-2026 cal.yr.BC for the gradational organic-minerogenic transition. The transition back to organic deposition and the start of Peat IV accumulation is dated from a *Phragmites* stem fragment located 2cm below the silt-peat boundary, giving an age of 1964-1748 cal.yr.BC. Within Peat IV, a *Phragmites* sample located at 1.06m gives an age of 385-186 cal.yr.BC for the abrupt transition from organic peat to more minerogenic peaty clay above. A grass sample at the top of this peaty clay gives an age of 668-869 cal.yr.BC for Peat IV cessation and the start of minerogenic organic silt deposition.

A grass sample located 1cm below the made ground layer, within the thin *Gramineae-Bryophyte* peat, was radiocarbon dated and gave an absolute % modern ^{14}C value of 124.00 +/-0.57 (table 5.1), giving a post-1950 AD 'modern' age. A relative age for this sample horizon can be estimated from its relationship with the made ground immediately above. This made ground is thought to be associated with construction of the A39 road bridge, which was built between 1987 and 1989 AD. Therefore, if the top of the thin peat represents the soil surface at the time of made ground placement, and no erosion took place, an age of 1987 AD can be given for this horizon.

Magnetic properties

Figure 5.6 shows X_{ir} values for PL1 (at 2cm resolution) and $X_{\text{fd}\%}$ for those samples that had a K_{ir} value of $>25.0 \cdot 10^{-5} \text{ m}^3 \text{ kg}^{-1}$. A suite of mineral magnetic remanence measurements were also done on 84 samples from PL1 (*i.e.* at *c.*7cm resolution). The results of these measurements and derived parameter ratios/quotients are shown in figure 5.7. Tables 3.2 and 3.3 were used in the identification of magnetic mineral components and constrained cluster analysis (CONISS) was used to divide the core into 13 magnetic zones (M1 to M13).

Zone M1 (5.57m – 6.06m)

M1 has been divided into three subzones, with M1(i) corresponding to the basal clay layer, M1(ii) corresponding with most of Peat I, and M1(iii) corresponding with the thin

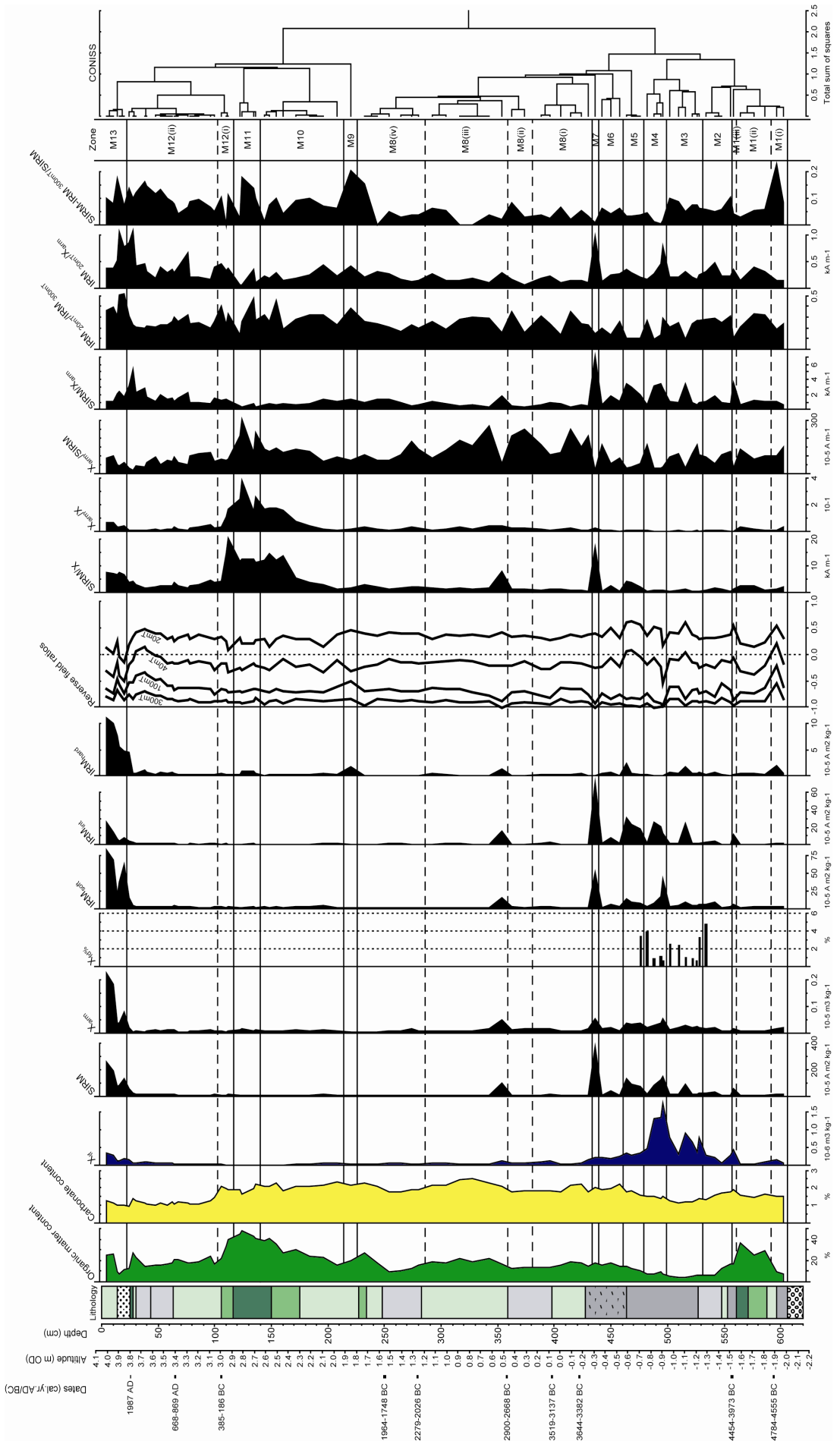


Figure 5.7 Magnetic characteristics of PL1 core and resulting magnetic zones.

organic clay near the top of Peat I. There is a small peak in X_{lf} and IRM_{hard} at the top of the M1(i) basal clay suggesting the presence of haematite. The haematite contribution is seen to gradually increase up-river between PL1, through SW1 (5.3.3) to SW1 (5.4.3), indicating a predominantly catchment provenance. The basal PL1 clay may therefore include a significant proportion of overbank fluvial sedimentation. With lower sea-levels at this time, this is not surprising. The dominance of antiferromagnets in the M1(i) assemblage is confirmed by a peak in $SIRM-IRM_{300mT}/SIRM$ and a corresponding peak in the back field S-ratio ($IRM_{100mT}/SIRM$).

In M(ii), low X_{lf} and SIRM values show very low concentrations of ferrimagnetic and antiferromagnetic minerals. A peak in X_{lf} (and minor peak in SIRM) in the M(iii) clay indicates an increase in ferrimagnetic minerals. This horizon corresponds to a small peak in IRM_{int} , field divergence in the reverse field ratios and a peak in $SIRM/X_{arm}$. This suggests the presence of the ferrimagnetic mineral greigite, although probably in small amounts. However, there is not the expected rise in $SIRM/X$, normally associated with greigite. This may be because $SIRM/X$ is also influenced by grain size, suggesting that any greigite present is dominated by MD grains (*e.g.* Snowball and Thompson, 1988).

Zone M2 (5.31m – 5.57m)

M2 corresponds with the uppermost peaty silt in Peat I and the lower 25cm of proceeding silt deposition. X_{lf} values are generally quite low (0.07 to $0.25 \cdot 10^{-6} \text{ m}^3 \text{ kg}^{-1}$) with the higher values, found in the silt, corresponding with a small rise in X_{arm} and IRM_{soft} . This suggests a rise in SSD magnetite. The contribution by SSD magnetite in the PL1, TS1 and SW1 cores shows a down-river increase, suggesting it is mainly sourced from the estuary. Previous studies have shown that bacterial magnetite makes a significant contribution to magnetic mineral assemblages in inter-tidal saltmarsh environments (Oldfield and Yu, 1994; Gibbs, 2000). Magnetotactic bacteria normally produce magnetosomes of an SSD grain size (Frankel and Blakemore, 1989; Moskowitz *et al.*, 1993), so the rise in SSD magnetite in the silts of zone M2 suggest the palaeo-surface is now located in an upper inter-tidal saltmarsh environment, below MHWST. If the magnetite has a bacterial origin, this may have either been formed in-situ, or it could have been tidally transported from reworked saltmarsh deposits further out in the estuary. Either way, the environment appears more prone to tidal inundation.

Zone M3 (4.99m – 5.31m)

This zone lies towards the base of the minerogenic sediment between Peat I and Peat II, where organic matter content values are at their lowest. A significant rise in ferrimagnetic concentration is seen by the increase in X_{if} . Moderate X_{arm} values suggest the presence of SSD magnetite (as does low IRM_{20mT}/X_{arm} values), with low (<3%) $X_{fd\%}$ values indicating this is above the SSD/SP boundary. This may therefore show a decreasing tidal frame position with a greater contribution by SSD bacterial magnetite. The Taw Estuary survey recorded highest X_{if} values in a zone from the mudflat-pioneer saltmarsh border up the start of the lower high saltmarsh. In the middle of the zone, peaks in IRM_{int} , SIRM, $SIRM/X_{arm}$ correspond with a reverse field divergence. This suggests the presence of MD greigite ($SIRM/X$ values remain low, suggesting MD grains). The chemical precipitation of this iron sulphide at the sediment-water interface has been reported in both brackish-marine and lacustrine anoxic environments (Snowball and Thompson, 1988; Snowball, 1991; Oldfield, 1994). The presence of this authigenic secondary mineral in zone M3 suggests either a saltmarsh environment existed at the PL1 site, or frequent tidal inundation at this site has introduced re-worked estuarine greigite to the marsh surface. An antiferromagnetic (haematite) contribution to the assemblage is suggested by a small rise in IRM_{hard} and high $SIRM-IRM_{300mT}/SIRM$ values. This suggests a fluvial component in marsh alluviation, possibly due to high river discharges at this time causing overbank flooding at the PL1 site.

Zone M4 (4.79m – 4.99m)

This zone is located within the middle of the silty clay between Peat I and Peat II. High X_{if} values (reaching $1.76 \cdot 10^{-6} \text{ m}^3 \text{ kg}^{-1}$) and a rise in SIRM, corresponding with lows in IRM_{hard} , S-ratio and $SIRM-IRM_{300mT}/SIRM$ values, indicate an increase in ferrimagnetic mineral concentration with very little antiferromagnetic (haematite) contribution. Moderate X_{arm} values and generally low (<2%) $X_{fd\%}$ values suggest that SSD magnetite contributes towards the high X_{if} values, with little contribution from fine viscous SD grains. A peak in IRM_{20mT}/X_{arm} near the base of the zone corresponds with the highest IRM_{soft} values suggesting that detrital MD magnetite makes a significant contribution to IRM at this horizon. A peak in IRM_{int} and $SIRM/X_{arm}$ in the middle of the zone, combined with a minor reverse field divergence, high SIRM values and low $SIRM/X$ values all suggest that MD greigite is present at this horizon. MD magnetite may be detrital (primary) in origin or it may be authigenic (Hilton, 1987), which would indicate an estuarine environment. In summary, the high X_{if} values are derived from an increase

in the concentration of MD magnetite and greigite (possibly both authigenic), with a smaller contribution by SSD magnetite, with the very high concentrations suggesting a low or mid saltmarsh environment.

Zone M5 (4.61m – 4.79m)

This zone corresponds with the start of an increase in organic matter within the silty clay beneath Peat II. This zone sees X_{lf} values fall to moderate levels ($0.3 \cdot 10^{-6} \text{ m}^3 \text{ kg}^{-1}$). A peak in SIRM, IRM_{int} , SIRM/X and SIRM/ X_{arm} values, combined with a reverse field divergence and low IRM_{hard} values, all suggest that greigite is the main contributor to X_{lf} and IRM. Moderate X_{arm} and IRM_{20mT}/X_{arm} values suggest a mixed MD and SSD grain size assemblage. A minor peak in IRM_{soft} suggests that SSD magnetite is also a contributing magnetic component. The low IRM_{hard} , S-ratio and SIRM- $IRM_{300mT}/SIRM$ values suggest little antiferromagnetic mineral content. This all suggests an estuarine saltmarsh environment.

Zone M6 (4.39m-4.61m)

This zone corresponds with the organic silty clay below Peat II. X_{lf} values fall to $0.2 \cdot 10^{-6} \text{ m}^3 \text{ kg}^{-1}$, indicating the sediment contains a relatively low concentration of ferrimagnetic minerals. All other concentration-related parameters (SIRM, IRM_{soft} , IRM_{int} , IRM_{hard} and X_{arm}) have low values. The low S-ratio and SIRM- $IRM_{300mT}/SIRM$ values indicate an assemblage dominated by ferrimagnetic minerals. In terms of magnetic grain size, the low X_{arm} values suggest minor SSD magnetite, while other grain size parameters are inconclusive, although the rise in $X_{arm}/SIRM$ at the top of the zone may indicate some SSD bacterial magnetite. It is therefore proposed that the assemblage is dominated by low concentrations of SSD bacterial magnetite. The Taw Estuary transect saw X_{lf} values fall in the lower high saltmarsh subzone. This may suggest that zone M6 was deposited at a high saltmarsh elevation.

Zone M7 (4.33m – 4.39m)

This zone is located at the top of the organic silty clay, 5cm below the start of Peat II. X_{lf} values remain relatively low at $0.2 \cdot 10^{-6} \text{ m}^3 \text{ kg}^{-1}$. However, there is a significant peak in SIRM, indicating a sharp rise in the concentration of remanence carrying minerals. There are also large peaks in IRM_{int} , SIRM/X, and SIRM/ X_{arm} , which when combined with negligible IRM_{hard} and a minor field divergence, point to greigite being a dominant magnetic component. The very low S-ratio confirms the dominance by a ferrimagnetic

mineral. A very high IRM_{20mT}/X_{arm} and very low $X_{arm}/SIRM$ indicates that the assemblage is dominated by MD grains, although a small peak in X_{arm} suggests a minor amount of SSD grains. A large peak in IRM_{soft} indicates that greigite is not the only important ferrimagnetic present, and that magnetite is likely to be equally significant in the assemblage. This may indicate that the assemblage is dominated by low levels of authigenic greigite and bacterial magnetite, deposited in a high saltmarsh environment.

Zone M8 (2.26m – 4.33m)

This large zone starts at 4.33m, 5cm below Peat II, and ends at 2.26m near the base of Peat IV (figure 5.7). Although magnetic characteristics are quite similar throughout cluster analysis divides the zone into four, with M8(i) approximate with Peat II, M8(ii) approximate with the preceding minerogenic layer, M8(iii) coinciding with Peat III, and M8(iv) approximate with the minerogenic silt between Peat III and Peat IV. Very low X_{if} and SIRM values show that the concentration of both ferrimagnetic and antiferromagnetic minerals remain low throughout most of zone M8, suggesting a high tidal frame position in the high saltmarsh or marsh border zones. There are two exceptions to this. At the start of silt deposition, between Peats II and III, there is a minor peak in X_{if} (see figure 5.6). This small rise in ferrimagnets is shown by a corresponding reduction in the S-ratio and minor rise in IRM_{soft} values.

At the start of Peat III deposition, there is a similar small rise in ferrimagnetic minerals, with a small rise in X_{if} and decrease in S-ratio. However, this horizon also has significant peaks in many other parameters. Peaks in SIRM, IRM_{int} , SIRM/X and $SIRM/X_{arm}$, with a corresponding small reverse field divergence, suggest the presence of the ferrimagnet mineral greigite. With no indication of a major MD contribution, this greigite may be sourced from bacterial magnetosomes (Fassbinder and Stanjek, 1994), although authigenic greigite is also often found at this grain size (Roberts, 1995). Rises in X_{arm} and IRM_{soft} indicate a significant SSD magnetite presence. A corresponding low in $X_{arm}/SIRM$ indicates that neither of these ferrimagnetic minerals have a significant fine viscous or SP component. Although a small peak in IRM_{hard} suggests the presence of haematite, the low $SIRM-IRM_{300mT}/SIRM$ value indicates that this gives a relatively minor contribution to IRM. Conditions at the start of Peat III appear to have been particularly conducive for authigenic/biogenic greigite and bacterial magnetite formation. This was also seen at the start of Peat II (zone M7).

Although concentration-related parameters remain very low throughout the majority of zone M8, there are clues to the identity of the magnetic assemblage present. The S-ratio and $\text{SIRM-IRM}_{300\text{mT}}/\text{SIRM}$ values remain low, suggesting a lack of haematite and dominance by ferrimagnetic minerals. Low $\text{IRM}_{20\text{mT}}/X_{\text{arm}}$ values suggest SSD dominance, and a distinct rise in $X_{\text{arm}}/\text{SIRM}$ throughout most of this zone indicates that fine viscous SSD or SP bacterial magnetite may be the main contributor to IRM. This supports a high tidal frame position where the small magnetic assemblage is dominated by secondary bacterial magnetite, formed within the organic high saltmarsh and marsh border sediments.

Zone M9 (2.14m – 2.26m)

This zone is located in peaty clay, immediately above the thin detrital peat near the base of Peat IV. The main concentration-related parameters (X_{lf} and SIRM) remain low in this zone. However, there is a peak in IRM_{hard} and a corresponding rise in the S-ratio and a large rise in $\text{SIRM-IRM}_{300\text{mT}}/\text{SIRM}$ values. This all suggests that there was an influx of antiferromagnetic haematite at this horizon. This may have been caused by an increase in river discharge at this time causing overbank alluviation. The detrital peat at the base of this zone supports this hypothesis. Moderate $\text{IRM}_{20\text{mT}}/X_{\text{arm}}$ values suggest a mixed MD and SSD grain size assemblage, while a minor peak in $\text{IRM}_{20\text{mT}}/\text{IRM}_{300\text{mT}}$ suggests some contribution by fine viscous SSD/SP grains.

Zone M10 (1.40m – 2.14m)

This zone corresponds with a period of sustained rise in organic matter content in Peat IV. All concentration-related parameters (X_{lf} , SIRM, X_{arm} , IRM_{soft} , IRM_{int} and IRM_{hard}) remain low in this zone, suggesting a high tidal frame position. However, above 1.75m (coincident with the start of clayey peat deposition) there are large rises in SIRM/X and X_{arm}/X . This suggests that the small quantities of magnetic minerals present are dominated by SSD bacterial magnetite, with the low S-ratio giving confirmation of this ferrimagnetic origin. The more organic nature of the sediment may have been more conducive for bacterial activity.

Zone M11 (1.17m – 1.40m)

This zone corresponds with the peak in organic matter within Peat IV. Very low X_{lf} and SIRM values show that the concentration of magnetic minerals remains very low, suggesting a high marsh border environment. The continuing presence of bacterial SSD

magnetite is indicated by high SIRM/X and X_{arm}/X values. However, this zone does show a rise in IRM_{hard} values, which when combined with a peak in SIRM- $IRM_{300mT}/SIRM$, suggest that detrital haematite gives a significant contribution to IRM. This suggests that despite the elevated tidal frame position and estuarine location, the marsh surface was periodically inundated by high-stage fluvial floods, indicating a particularly unstable climate at this time. A corresponding rise in $X_{arm}/SIRM$ and decline in IRM_{20mT}/X_{arm} values indicate that both the magnetite and haematite components have an SSD and SP grain size. The S-ratio remains low, suggesting that bacterial magnetite is the largest contributor to IRM, but as ferrimagnetic minerals give a significantly higher IRM, relative to antiferromagnetic minerals (Thompson and Oldfield, 1986), this does not mean that haematite is present in smaller concentrations.

Zone M12 (0.22m – 1.17m)

Cluster analysis (figure 5.7) suggests that this zone can be divided into two, with M12(i) corresponding to the clayey peat between 1.16m and 1.06m, and M12(ii) corresponding to the sediment above the sharp decline in organic matter content at 1.06m. M12(ii) incorporates the peaty silt at the top of peat IV, the minerogenic organic silt above this, and the thin Peat V. Both M12(i) and M12(ii) contain small concentrations of remanence carrying mineral, as shown by the very low X_{ir} and SIRM values, suggesting the tidal frame position did not fall below the high saltmarsh zone. Despite the cluster analysis results, M12(i) shows more similarity to the preceding M11 zone, with bacterial magnetite remaining a significant magnetic component (although SIRM/X and X_{arm}/X values do decline at the top of the subzone). In M12(ii), low SIRM/X and X_{arm}/X values indicate a reduction in bacterial magnetite above the peat/clayey silt transition. This may indicate that the more minerogenic silty nature of the sediment was less conducive for bacterial activity. Within M12(ii), the three sedimentary environments (peaty silt, minerogenic silt and organic Peat V) show corresponding changes in their magnetic parameters. The peaty silt has a low S-ratio, indicating ferrimagnetic dominance. The overlying organic silt shows a steady increase in the S-ratio, a small but significant rise in IRM_{hard} value, and a rise in SIRM- $IRM_{300mT}/SIRM$ values, all indicating an increase in antiferromagnetic mineral concentration (haematite). This suggests an increase in catchment sourced sediment, possibly due to increasing river discharges. The thin Peat V between 0.30m and 0.25m shows a drop in the S-ratio and a steep rise in IRM_{20mT}/X_{arm} values, indicating a change to MD magnetite dominance.

Zone M13 (0.00m – 0.22m)

This zone corresponds with the made ground layer and waterlogged organic soil at the top of PL1. A steep rise in all concentration-related parameters is seen in this zone. High IRM_{soft} and IRM_{hard} values in the made ground layer indicate a mixed ferrimagnetic and antiferromagnetic assemblage, with a variation in grain size shown by increased X_{arm} values (SSD ferrimagnetic grains), high IRM_{20mT}/IRM_{300mT} values (fine viscous SSD/SP boundary grains) and high IRM_{20mT}/X_{arm} values (indicative of MD grains). The base of the surface soil (at 0.14m) shows a temporary decline in IRM_{soft} and X_{arm} values, combined with high IRM_{hard} values, a rise in the S-ratio and a peak in $SIRM-IRM_{300mT}/SIRM$ value. This suggests an influx of haematite during the open ground phase after made ground placement and before the recent soil development. The surface soil layer shows high $SIRM$, IRM_{soft} and IRM_{hard} values, suggesting a mix of ferrimagnetic and antiferromagnetic minerals. The very high X_{arm} values and reduced S-ratio indicate SSD magnetite dominance in this assemblage. However, the high IRM_{hard} values show that haematite is still an important magnetic component.

Diatom analysis

As the diatom record of PL1 is being used to validate the potential sea-level index points located at transgressive and regressive overlaps, the PL1 diatom zones will be described in some detail (relative to other cores) for evidence of changes in marine influence.

Figure 5.8 shows a diatom diagram for PL1. All species with counts of $>5\%$ TDV ($>5\%$ total diatom valves counted) are shown, along with the diatom sums for the different halobian salinity groups (sums of $>5\%$ spp; the final diatom sum in figure 5.8 gives the sum of all $>5\%$ TDV spp, as a percentage of the total diatom count). Changes in diatom salinity index (DSI; based on total diatom count) are also shown. Zonation of the diatom diagram was completed using stratigraphically constrained cluster analysis (CONISS; no data transformation was applied) based on species records exceeding 5%TDV. This analysis resulted in 17 diatom zones (A to Q). Apart from in Peat I, where diatom concentrations were very low, diatoms were well preserved and abundant in PL1. A total of 275 diatom species (277 taxa) were identified, with 39 species exceeding 5%TDV. The dominant species in each zone ($>10\%$ TDV and $>5\%$ TDV) are shown in table 5.3.

Zone	>10%TDV diatom species	>5%TDV diatom species
A	Cocconeis placentula (OI)	Paralia Sulcata (P) Podosira stelligera (P) Cyclotella striata (M) Navicula peregrina (M) Navicula pusilla (OH) Pinnularia viridis (OI) Synedra ulna (OI)
B	Epithemia turgida (OH) Cocconeis placentula (OI) Cymbella silesiaca (OI) Pinnularia viridis (OI) Synedra ulna (OI)	Eunotia pectinalis (OI) Pinnularia major (OI)
C	Cocconeis placentula (OI) Tabellaria fenestrata (OI)	Epithemia turgida (OH) Cymbella silesiaca (OI) Eunotia pectinalis (OI) Pinnularia abaujensis (OI) Synedra ulna (OI)
D	Cocconeis placentula (OI)	Epithemia turgida (OH) Navicula pusilla (OH) Synedra ulna (OI)
E	Cocconeis placentula (OI)	Actinocyclus octonarius (P) Actinoptychus senarius (P) Paralia sulcata (P) Podosira stelligera (P) Cyclotella meneghiniana (M) Cyclotella striata (M) Synedra ulna (OI)
F	Paralia sulcata (P) Navicula peregrina (M) Cocconeis placentula (OI)	Cymatosira belgica (P) Delphineis surirella (P) Podosira stelligera (P) Navicula pusilla (OH) Synedra ulna (OI)
G	Navicula peregrina (M) Cocconeis placentula (OI)	Paralia sulcata (P) Podosira stelligera (P) Navicula pusilla (OH) Synedra ulna (OI)
H	Paralia sulcata (P) Navicula peregrina (M) Navicula pusilla (OH)	Actinoptychus senarius (P) Podosira stelligera (P) Cyclotella meneghiniana (M) Cyclotella striata (M) Nitzschia obtusa (M) Navicula eidrigeana (OH) Cocconeis placentula (OI) Navicula variostrata (OI) Pinnularia borealis (OI)
I	Nitzschia obtusa (M) Navicula cari (OI)	Cymatosira belgica (P) Paralia sulcata (P) Navicula peregrina (M) Nitzschia vitrea (M) Navicula eidrigeana (OH) Navicula mutica (OH) Navicula pusilla (OH) Fragilaria famelica (OI) Navicula variostrata (OI)
J	Paralia sulcata (P)	Podosira stelligera (P) Rhaphoneis amphiceros (P) Navicula peregrina (M) Nitzschia vitrea (M) Caloneis lauta (OI)

Zone	>10%TDV diatom species	>5%TDV diatom species
K(i)	Navicula eidrigeana (OH)	Paralia sulcata (P) Navicula peregrina (M) Nitzschia obtusa (M) Navicula mutica (OH) Navicula pusilla (OH) Caloneis lauta (OI) Navicula cari (OI) Navicula variostrata (OI)
K(ii)	Nitzschia obtusa (M)	Paralia sulcata (P) Podosira stelligera (P) Navicula peregrina (M) Navicula phyllepta (M) Navicula eidrigeana (OH)
K(iii)	Navicula peregrine (M) Nitzschia obtusa (M) Navicula eidrigeana (OH)	Paralia sulcata (P) Navicula phyllepta (M) Nitzschia sigma (M) Staurosira elliptica (OH) Fragilaria famelica (OI) Navicula cari (OI) Navicula tripunctata (OI) Navicula variostrata (OI)
L	Navicula peregrine (M) Navicula pusilla (OH)	Paralia sulcata (P) Cyclotella striata (M) Diploneis interrupta (M) Navicula eidrigeana (OH) Caloneis lauta (OI) Diploneis elliptica (OI) Pinnularia major (OI) Pinnularia viridis (OI) Stauroneis producta (OI)
M	Navicula peregrine (M) Nitzschia obtusa (M) Navicula variostrata (OI)	Navicula eidrigeana (OH) Navicula pusilla (OH) Diploneis elliptica (OI) Pinnularia major (OI) Pinnularia viridis (OI)
N	Diploneis interrupta (M) Navicula peregrina (M) Navicula pusilla (OH)	Paralia sulcata (P) Podosira stelligera (P) Cyclotella striata (M) Navicula avenacea (M) Nitzschia obtusa (M) Navicula eidrigeana (OH) Caloneis lauta (OI) Diploneis elliptica (OI) Navicula variostrata (OI) Pinnularia major (OI)
O	Navicula peregrine (M) Navicula variostrata (OI)	Diploneis interrupta (M) Nitzschia obtusa (M) Navicula pusilla (OH) Diploneis elliptica (OI) Pinnularia major (OI)
P	Diploneis interrupta (M) Navicula peregrina (M) Nitzschia commutata (M) Nitzschia terrestris (OI)	Nitzschia obtusa (M) Navicula pusilla (OH)
Q	Nitzschia commutata (M) Nitzschia terrestris (OI)	Pinnularia borealis (OI)

Table 5.3 Dominant diatom species in PL1. P = Polyhalobous; M = Mesohalobous; OH = Oligohalobous halophilous; OI = Oligohalobous indifferent.

Zone A (5.74m – 6.06m)

This zone corresponds with both the basal organic clay and the lower peaty clay/silty peat part of Peat I. A regressive overlap, dated at 4784-4555 cal.yr.BC, is located between the basal clay and the peaty clay. Zone A has a mixed assemblage of polyhalobous/mesohalobous taxa (28-41%) and oligohalobous taxa (33-43%). The polyhalobous component is dominated by the planktonic species *Paralia sulcata* and *Podosira stelligera*, with mesohalobous taxa represented by planktonic *Cyclotella striata* and epipellic *Navicula peregrina*. The assemblage also contains large numbers (>10%TDV) of the oligohalobous indifferent salt-tolerant epiphyte *Cocconeis placentula* and smaller numbers of the indifferent epiphyte *Synedra ulna*. The zone shows an upwards increase in aerophilous taxa (the halophile *Navicula pusilla* and indifferent *Pinnularia viridis*), suggesting reduced periods of tidal submergence in the upper peaty clay. Evidence for a regressive overlap and a reduction in marine influence between the basal clay and peaty clay is confirmed by a decline in polyhalobous planktonics and a corresponding rise in oligohalobous indifferent and halophilous species (although there is evidence for renewed estuarine inundation higher up in the silty peat).

Organic matter content values suggest the basal clay (7-10% organic matter) was deposited at a tidal frame position that corresponds with the lower high saltmarsh subzone in the Taw Estuary transect (*i.e.* 40-60cm below MHWST). Organic matter content values gradually rise to 30% in the peaty clay and silty peat, which is similar to that seen in the Taw Estuary marsh border zone, 20-30cm above MHWST. This indicates an increase in depositional altitude and reduction in marine influence above the regressive overlap. This is supported by a reduction in the number of marine planktonics and tycho planktonics across the clay-peat boundary from 24% to 16%. The dominant marine planktonic species in the basal clay are *Paralia sulcata* and *Podosira stelligera* (both >5%TDV). Although *Paralia sulcata* was found in the Taw Estuary to have its optimum in the tidal flat zone (also seen by Nelson and Kashima, 1993, and Hill *et al.*, 2007), numbers were seen to increase again in the middle and high saltmarsh zones. A similar rise in *Paralia sulcata* numbers in the high marsh zone, close to MHWST, was reported by Nelson and Kashima (1993). This supports the other evidence for a high saltmarsh depositional environment for the basal clay.

In the Taw Estuary, *Paralia sulcata* and *Podosira stelligera* were also seen insignificant (3%TDV each) but reduced numbers above MHWST in the marsh border zone. Hill *et al.* (2007) recorded significant numbers of *Paralia sulcata* all the way up to HAT. This justifies the presence of these species in the peaty clay, which is thought to be deposited in the lower part of the marsh border zone. The later rise in marine planktonics within the middle of the silty peat suggests deposition at this horizon coincided with a period of particularly high tides, possibly caused by a period of increased storminess.

Evidence of deposition occurring close to MHWST, on both sides of the regressive overlap, is also found in the mesohalobous and halophilous groups. In the Taw Estuary, both *Navicula peregrina* and *Navicula pusilla* are only present in significant numbers in the upper high saltmarsh and in the marsh border above MHWST. Studies by Shennan *et al.* (1995) and Zong and Horton (1998, 1999) recorded the highest abundance of *Navicula peregrina* in the zones either side of MHWST. Shennan *et al.* (1995) and Nelson and Kashima (1993) both reported the optimum elevation for *Navicula pusilla* in the marsh border zone between MHWST and HAT.

Zone B (5.53m – 5.74m)

This zone corresponds with the organic wood peat and thin organic clay near the top of Peat I. Figure 5.8 shows a change to a freshwater environment with a sharp increase in oligohalobous indifferent species, with *Cocconeis placentula*, *Cymbella silesiaca*, *Pinnularia viridis* and *Synedra ulna* all present at >10%TDV, and *Eunotia pectinalis* and *Pinnularia major* present at >5%TDV. The presence of the halophile *Epithemia turgida* at >10%TDV and small numbers of polyhalobous (1-5%) and mesohalobous (2-3%) taxa suggests a brackish environment with rare tidal inundation.

The environment is thought to be a fen wood with the silty clay layer suggesting an increased propensity to freshwater flooding in the later stage. The abundance of epiphytes (*Cocconeis placentula*, *Epithemia turgida*, *Synedra ulna* and *Eunotia pectinalis*) and aerophilous (*Pinnularia viridis*) taxa are typical of this boggy wet subaerial environment. In terms of tidal frame, this zone may be located just below HAT. Zong (1997) reported *Eunotia pectinalis* and *Synedra ulna* at the level of HAT and although the modern Taw Estuary transect does not reach HAT, it does see the appearance of *Eunotia pectinalis* at MHWST and above, and large numbers of *Cocconeis placentula* above MHWST.

Zone C (5.23m – 5.53m)

This zone corresponds with the thin peaty silt at the top of Peat I and the lower 25cm of proceeding minerogenic silt. A transgressive overlap, dated at 4454-3973 cal.yr.BC, is located between the peaty silt and minerogenic silt above. The sedimentary evidence suggests a marked change in depositional environment, with minerogenic accretion rates quickly outpacing organic accumulation rates. However, the salinity regime, shown by the diatom record, is seen to only change slightly in this zone. Although still a predominantly freshwater environment, the salinity is seen to gradually increase through this zone with polyhalobous taxa increasing from 2.3% to 4.7%, mesohalobous taxa increasing from 0% to 2.7%, oligohalobous halophilous taxa increasing from 6.0% to 6.7% and oligohalobous indifferent taxa decreasing from 56% to 51%. These small shifts do therefore show a gradual increase in marine influence, supporting a transgressive overlap interpretation for the peat-silt boundary, especially since the zones above this (D and E) show a progressively more marine environment. A depositional altitude close to MHWST (suggested by the overlap) can be given if zone C is interpreted as a change to a freshwater-brackish tidal floodplain environment. This would signify that the PL1 site was located higher up the salinity gradient at this time, suggesting that the salinity front at 4454-3973 cal.yr.BC was situated further downstream than its current location.

A drop in depositional altitude and change to a slightly brackish tidal floodplain environment is supported by the abrupt appearance of the tychoplanktonic salt-tolerant (indifferent) diatom *Tabellaria fenestrata* in large numbers (>10%). This species has been reported in similar numbers at MHWST by Shennan *et al.* (1996), and Sherrod (1999) reported its only appearance to be in a low high marsh setting corresponding with MHWST. The other species found at >10%TDV levels in zone C is the oligohalobous indifferent species *Cocconeis placentula*. This species is found at all tidal frame levels in the Taw Estuary, up to above MHWST, with Sherrod (1999) reporting a similarly wide distribution.

Zone D (5.08m – 5.23m)

This zone corresponds with the period of minimum organic matter deposition in the minerogenic phase between Peat I and Peat II. A gradual continuation of increasing marine influence is seen with the appearance, in low numbers (<5%TDV), of many polyhalobous and mesohalobous planktonic taxa, with the combined polyhalobous and

mesohalobous sum rising from 7 to 13%. The oligohalobous halophilous sum rises from 7% to 12%. This is largely caused by an increased abundance of the epiphyte *Epithemia turgida* and the reappearance of *Navicula pusilla* at >5%TDV levels (not seen since zone A). The salt-tolerant oligohalobous indifferent epiphytes *Cocconeis placentula* and *Synedra ulna* remain in similar high numbers (>10%TDV and >5%TDV respectively). The large numbers of epiphytes within an inorganic sediment, combined with the presence of marine planktonic species, suggests a strong tidal influence with most of the assemblage being tide-transported and allochthonous in nature. This large allochthonous component, within a brackish floodplain environment, indicates quite frequent tidal submergence, suggesting the floodplain surface was slightly below MHWST. In this environment, the aerophilous *Navicula pusilla* is likely to be an autochthonous part of the assemblage. In the Taw Estuary, *Navicula pusilla* was found to appear in >5%TDV numbers at c.25cm below MHWST. This supports a zone D palaeo-surface level of just under MHWST.

Zone E (4.73m – 5.08m)

This zone corresponds to the middle of the silty clay between Peat I and Peat II, with organic matter content remaining low. There is a large sustained rise in marine and brackish species in this zone, with a corresponding decline in freshwater taxa. The polyhalobous sum reaches 37% at the top of the zone and mesohalobous species total 9%, while oligohalobous indifferent forms fall from their zone D levels of 42% to 18% in zone E. The planktonic polyhalobous and mesohalobous taxa that appeared in zone D all become more abundant with many species accounting for >5%TDV. These include the polyhalobous planktonics *Paralia sulcata* and *Podosira stelligera*, the polyhalobous tycho planktonics *Actinocyclus octonarius* and *Actinoptychus senarius*, and the mesohalobous planktonics *Cyclotella striata* and *Cyclotella meneghiniana*. The oligohalobous indifferent epiphytes *Cocconeis placentula* and *Synedra ulna* both remain abundant (>10%TDV and >5%TDV respectively) at the start of the zone but both show a decline thereafter, with *Synedra ulna* falling to 2%TDV at the end of the zone. The DSI value (based on the total count) falls from 0.83 (freshwater dominated) in zone D to 0.44 at the end of zone E, indicating a switch to marine and brackish species dominance.

In the Taw Estuary, *Actinoptychus senarius* and *Paralia sulcata* show highest abundance in the tidal flat environment. However, both species are present in significant numbers (>5%TDV) up to the high saltmarsh and MHWST (also seen by Hill *et al.*, 2007, for both species), so a tidal flat depositional environment cannot be presumed. Three of the dominant species in zone E (*Podosira stelligera*, *Cocconeis placentula* and *Synedra ulna*) have their Taw Estuary optimums in the low-mid marsh zone and this zone seems the most likely depositional environment. The presence of occasional rootlets suggests a sparse vegetation cover, as seen in a low saltmarsh environment, and the fine-grained sediment texture (silty clay) suggests deposition higher in the tidal frame than the tidal flat or pioneer marsh environments. Indeed, based in sediment texture alone, a silty clay grain size corresponds with the low saltmarsh subzone in the Taw Estuary transect. Zone E therefore represents a significant fall in tidal frame position and depositional altitude from the upper high saltmarsh level in zone D to a low saltmarsh altitude.

Zone F (4.19m – 4.73m)

This zone corresponds with the organic silty clay below Peat II. At the start of the zone, the abundance of polyhalobous and mesohalobous plankton species stabilises, and then falls to *c.*25-28% levels. This sees many of the marine and brackish plankton species prolific in zone E (*Actinocyclus octonarius*, *Actinoptychus senarius*, *Cyclotella striata* and *Cyclotella meneghiniana*) all fall to <5%TDV levels. *Podosira stelligera* remains at >5%TDV abundance, and the planktonic *Paralia sulcata* increases to >10%TDV. New tychoplanktonic polyhalobous species (*Cymatosira belgica* and *Delphineis surirella*) appear at >5%TDV levels. *Delphineis surirella* has its optimum abundance in the tidal flat zone of the taw estuary, but in common with other planktonics, is seen in large numbers up to MHWST. A similar distribution has been recorded by Zong (1997) and Zong and Horton (1998), with Hill *et al.* (2007) reporting >5%TDV levels right up to HAT.

The mesohalobous sum is seen to remain at zone E levels (*c.*15%). However, the planktonic *Cyclotella spp.* are largely replaced by the appearance of the epipellic *Navicula perigrina*, which quickly becomes a dominant species (>10%TDV) in the assemblage. As previously stated in zone A, *Navicula peregrina* only appears in the Taw Estuary at MHWST (also seen by Shennan *et al.*, 1995; Zong and Horton, 1998,

1999). This suggests that zone F was deposited close to MHWST. This interpretation is supported by the reappearance of *Navicula pusilla* at >5%TDV levels and the increase in *Paralia sulcata* to >10%TDV levels, correlating with the similar increase recorded in the Taw Estuary high saltmarsh just below MHWST (also seen in the high marsh by Nelson and Kashima, 1993). The organic matter content of c.15% in zone F is similar to that seen in Taw Estuary lower high saltmarsh subzone, with the large quantities of detrital twigs present in zone F suggesting proximity to the frequent tidal trashlines observed in the vicinity of MHWST. The large numbers of oligohalobous epiphytes (*Cocconeis placentula* and *Synedra ulna*) and aerophilous taxa (*Navicula pusilla*) give further support to a vegetated high saltmarsh environment, with frequent periods of subaerial emergence.

Zone G (4.03m – 4.19m)

This zone corresponds with peaty clay of Peat II and sees a rise in DSI to 0.71, indicating a mixed assemblage with brackish-freshwater dominance. A regressive overlap, dated at 3644-3382 cal.yr.BC, is located at the base of Peat II. A further decrease in polyhalobous taxa (falling to 18%) is seen with *Paralia sulcata* and *Podosira stelligera* being the only marine planktonics at >5%TDV. In the Taw Estuary, these two species are the only marine taxa to remain in significant numbers (>3%TDV) at MHWST and above. The aerophilous halophile *Navicula pusilla* abundance rises to 7%TDV, suggesting longer periods of exposure and a rise in tidal frame position. This is supported by the emergence of an oligohalobous indifferent aerophilous taxa, *Pinnularia borealis*, at 4%TDV levels. Nelson and Kashima (1993) reported *Pinnularia borealis* in the marsh border zone at MHWST levels and above, which suggests that zone G was deposited at an altitude slightly above MHWST. This is supported by the brackish marsh border species *Navicula peregrina* remaining the dominant taxa (>10%TDV) in the assemblage, along with the indifferent epiphyte *Cocconeis placentula* (>10%TDV). An increase in oligohalobous indifferent species is more widely observed, with numbers of the epiphyte *Synedra ulna* rising to 7%TDV. Organic matter content rises in zone G to c.19-24% levels, a value only seen in the Taw Estuary near MHWST and above. The presence of *Phragmites* and *Juncus* stems in the sediment, and the abundance of epiphytic and aerophilous taxa, suggests a brackish reedswamp environment. Zone G therefore sees a reduction in marine influence, giving support to the regressive overlap at its base.

Zone H (3.41m – 4.03m)

This zone includes both the minerogenic clayey silt between Peats II and Peat III and the basal part of Peat III deposition. A transgressive overlap, dated at 3519-3137 cal.yr.BC, is located at the lower boundary between the zone H silts and the underlying peat clay of Peat II. There is also a regressive overlap near the top of the zone, dated at 2900-2668 cal.yr.BC, between the silt and peaty clay of Peat III. Polyhalobous and mesohalobous taxa become more abundant in this zone with oligohalobous indifferent species showing a decline in numbers. *Paralia sulcata* returns to >10%TDV levels and the polyhalobous planktonic *Podosira stelligera* rises to 9%TDV at the start of the zone, supporting an increase in marine influence above the transgressive overlap. The start of the zone also sees a temporary rise in other marine planktonics, most notably the tycho planktonic *Actinoptychus senarius* species (>5%TDV). Mesohalobous planktonics become more frequent, with *Cyclotella meneghiniana* reaching 9%TDV in the middle of the zone. *Navicula peregrina* remains a dominant species (>10%TDV) throughout zone H, indicating deposition remains close to MHWST. However, the abundance of marine-brackish planktonics, especially *Paralia sulcata*, and the fall in organic matter content to c.10-13% levels suggest a high saltmarsh environment. Organic clayey silt deposition is typical of the lower high saltmarsh subzone in the Taw Estuary, suggesting further support for this environment and a general lowering of the palaeo-surface in the tidal frame at the start of zone H. Other evidence for a decrease in tidal frame position includes a decline in *Navicula pusilla* to 2.7%TDV in the middle of the zone.

In the top half of zone H, *Navicula pusilla* becomes more abundant, reaching 10%TDV at the top of the silt. This aerophilous species is indicative of an upper high saltmarsh and marsh border environment (MHWST-25cm and above) in the Taw Estuary and has been shown in several studies to also start gaining prominence in the zone just below MHWST (Nelson and Kashima, 1993; Shennan *et al*, 1996). The upper part of the silt may therefore have been deposited at a slightly higher tidal frame position in the upper high saltmarsh environment.

A reduction in marine influence is seen across the regressive overlap at the top of zone H, with a number of assemblage changes indicating a rise in depositional altitude. The combined polyhalobous and mesohalobous sum falls from 54% to 38%, with replacement by oligohalobous halophilous and oligohalobous indifferent species. Aerophilous taxa become more prominent with the indifferent *Pinnularia borealis*

reappearing (>5%TDV) and a continuing increase in *Navicula pusilla* abundance. This suggests very limited tidal submergence, with both species having their optimums above MHWST. *Navicula variostriata*, an oligohalobous indifferent species appears at >5%TDV levels at the start of Peat III, and the benthic halophile *Navicula eidrigeana* gains >5%TDV prominence. In the mesohalobous community, there is a decline in *Navicula peregrina* (to c.6%TDV) and appearance of the benthic *Nitzschia obtusa* (>5%TDV). These assemblage changes indicate a rise in tidal frame position to the marsh border zone between MHWST and HAT. The mixed assemblage suggests a brackish environment at the start of Peat III deposition, with the presence of *Phragmites* suggesting reedswamp. However, using the Taw Estuary as an analogue, the relatively low organic matter content values of 15-18% at the base of Peat III suggests the marsh palaeo-surface was only slightly above MHWST.

Zone I (2.68m – 3.41m)

This zone corresponds with the bulk of Peat III and the lower half of the overlying minerogenic silt layer. A transgressive overlap, dated at 2279-2026 cal.yr.BC, is located between the top of Peat III and the overlying silt. The start of zone I sees a continuing reduction in marine influence, with a significant fall in polyhalobous species (to 8-13% in Peat III) and a corresponding rise in oligohalobous taxa.

In Peat III, the DSI ranges from 0.65 to 0.77, indicating a mixed assemblage with brackish-freshwater species dominance. All polyhalobous planktonics fall to <5%TDV levels. The assemblage is dominated by benthic diatoms, many of which are aerophilous, e.g. the halophiles *Navicula mutica* and *Navicula pusilla*, and mesohalobous *Nitzschia vitrea* (all >5%TDV). As stated earlier, *Navicula pusilla* has its optimum between MHWST and HAT. Hill *et al.* (2007) reported *Nitzschia vitrea* appearing in this zone, and *Navicula mutica* has been widely recorded between MHWST and HAT (Nelson and Kashima, 1993; Zong, 1997; Shennan *et al.*, 1996; Zong and Horton, 1999). In the Taw Estuary, *Navicula mutica* was recorded at >3%TDV levels above MHWST-25cm, while the highest abundance of *Nitzschia vitrea* recorded was 2%TDV at MHWST+24cm (the highest sampling station).

The two dominant species in zone I (>10%TDV) are the mesohalobous species *Nitzschia obtusa*, and the salt-tolerant indifferent species *Navicula cari*. In the Taw Estuary, *Navicula cari* was recorded around MHWST and above, and the only recorded

count of *Navicula obtusa* was from the highest station at MHWST+24cm. *Navicula peregrina* remains common (>5%TDV) in zone I. As stated earlier, this species becomes abundant in the Taw Estuary above MHWST. Other important species (>5%TDV) in zone I include the halophile *Navicula eidrigeana* and freshwater indifferent species *Fragilaria famelica* and *Navicula variostriata*. The freshwater epiphyte *Synedra ulna* becomes more abundant and is found at 3.0-4.7%TDV levels.

Collectively, this assemblage shows that the main part of zone I, within Peat III, was deposited in a brackish marsh environment (with some *Phragmites* present) above MHWST. However, the palaeo-surface was probably only 10-30cm above MHWST, with mesohalobous taxa remaining ubiquitous and low numbers of marine planktonic taxa being present throughout the zone. The maximum organic matter content in zone I is 26%. This is similar to the organic content at the MHWST+24cm station (29%) in the Estuary transect.

The uppermost part of zone I, corresponding with the start of minerogenic deposition above the transgressive overlap, provides evidence of an increase in marine influence and fall in tidal frame position. The polyhalobous sum abruptly rises from 13% to 24%, caused by an increase in marine planktonics, most notably *Paralia sulcata*. The indifferent species *Navicula variostriata*, common in Peat III (5-9%TDV), shows a sharp decline above the peat-silt boundary. The diatom and sedimentary evidence suggest a fall in depositional altitude caused the replacement of the organic brackish marsh by a minerogenic saltmarsh environment.

Zone J (2.44m – 2.68m)

This zone corresponds to the rest of the minerogenic silt between Peat III and Peat IV. Zone J sees the DSI value fall to its lowest level in PL1 (0.39), indicating an assemblage change to dominance by marine and brackish species. The rapid rise in polyhalobous species continues, reaching 34% in zone J. Oligohalobous indifferent species fall to a PL1 low of 12%, with oligohalobous halophilous taxa falling to 7%. The assemblage is dominated by polyhalobous planktonic species *Paralia sulcata* (>10%TDV) and *Podosira stelligera* (>5%TDV), and tycho planktonic *Rhaphoneis amphiceros* (>5%TDV). A rise is also seen in the mesohalobous planktonics *Cyclotella striata* and *Cyclotella meneghiniana*.

Like *Paralia sucata*, *Rhaphoneis ampiceros* has its Taw Estuary optimum in the tidal flat zone, but is also found at >5%TDV levels in the low saltmarsh, with >3%TDV values recorded up to the lower high saltmarsh subzone. A similar distribution was recorded by Hill *et al.* (2007) in the Severn Estuary, with optimum abundance occurring in the upper tidal flat and low saltmarsh environments. The quantitative study of diatom distribution (based on six UK saltmarshes) by Zong and Horton (1999) placed the optimum SWLI (standardised water level index; as sampling altitudes at different sites differ with respect to local tidal range, they need to be standardised) for *Rhaphoneis ampiceros* at a level that equates to the low saltmarsh zone in the Taw Estuary. This was deduced by finding a Taw Estuary tidal frame altitude that when used in the SWLI equation used by Zong and Horton (1999), equates to their optimum SWLI for *Rhaphoneis ampiceros*.

The mesohalobous component is dominated by the epiphyte *Navicula peregrina* (>5%TDV) and the aerophilous species *Nitzschia vitrea*. These diatoms are associated with altitudes of MHWST and above in the Taw Estuary transect. However, Shennan *et al.* (1995) recorded the maximum abundance just below MHWST, equivalent to the Taw high saltmarsh zone with some numbers also recorded from tidal frame levels comparable with the mid saltmarsh in the Taw Estuary. A large vertical range is also given in Zong and Horton (1999). The oligohalobous indifferent taxa are dominated by *Navicula cari* (reaching 4.5%TDV) in the middle of the zone (seen in the Taw Estuary high saltmarsh and marsh border) with *Caloneis lauta* becoming prevalent (>5%TDV) at the top of the zone.

The assemblage is therefore a mix of marine planktonics with optima in the tidal flat to mid saltmarsh zones, mesohalobous benthics with optimums in the high saltmarsh zone, and salt-tolerant indifferent species seen in the estuary high saltmarsh. On balance, a mid saltmarsh depositional environment is therefore likely. This is supported by a zone J organic matter content of 6-12%, equivalent to the Taw Estuary low and middle saltmarsh, and by the clayey silt sediment grain size which is associated with the mid to high saltmarsh estuary zones.

Zone K (1.50m – 2.44m)

This zone corresponds with the peaty clay and clayey peat that accumulated in Peat IV prior to the organic matter high found in zone L. A regressive overlap, dated at 1964-

1748 cal.yr.BC, is located at the start of zone K, at the silt – peaty clay boundary. Zone K has been divided into three subzones (figure 5.8), largely due to the changes occurring in the middle of the zone (Kii). Subzones K(i) and K(iii) have similar DSI values and diatom group sums, suggesting a similar tidal frame position and depositional environment. Subzone K(ii) sees a temporary rise in mesohalobous species and fall in oligohalobous taxa, indicative of a rise in marine influence.

There is a significant fall in marine influence above the regressive overlap at the start of subzone K(i) with a large fall in polyhalobous taxa (to 13%), a minor drop in mesohalobous taxa (to 14%), and corresponding rises in oligohalobous halophilous (to 16%) and indifferent (to 28%) species. This corresponds with a large rise in DSI value to 0.68, indicating a change to a mixed assemblage dominated by freshwater-brackish species.

In subzones K(i) and K(iii), *Paralia sulcata* is the only marine or brackish planktonic species to remain at >5%TDV numbers, suggesting a decrease in tidal inundation and rise in tidal frame position. Benthic species that are most prevalent in the marsh border zone above MHWST (Taw Estuary and other studies) become more prevalent in all three subzones. These include the mesohalobous epipellic *Navicula peregrina* (>5%TDV in K(i) and K(ii); >10%TDV in K(iii)), the mesohalobous *Nitzschia obtusa* (>5%TDV in K(i); >10%TDV in K(ii) and K(iii)), the aerophilous halophiles *Navicula mutica* and *Navicula pusilla* (both >5%TDV in K(i)), and the salt-tolerant indifferent species *Navicula cari* (>5% in K(i)).

Freshwater species that were prevalent in Peat III (zone I) re-appear in zone K. These taxa include *Navicula eidgeana* (>10%TDV in K(i) and K(iii); >5%TDV in K(ii)), *Fragilaria famelica* (>5%TDV in K(iii)), and the aerophilous taxa *Navicula variostrata* (>5%TDV in K(i) and K(iii)). Several other species, that were present in Peat III in low numbers, reappear at >5%TDV levels. The mesohalobous epipellic species *Nitzschia sigma*, which was present at 2.5-3.5%TDV levels throughout Peat III returns in similar numbers throughout K(i) and K(ii), peaking at 5%TDV at the base of K(iii). This species was recorded in the high saltmarsh zone in the Taw Estuary. The oligohalobous indifferent species *Navicula tripunctata* becomes more common in K(iii), as does the halophile *Staurosira elliptica* (both at >5%TDV). The aerophilous species

Nitzschia terrestris appears in small numbers (3.5%TDV maximum) for the first time in PL1, indicating increasing subaerial exposure.

The diatom assemblages present in subzones K(i) and K(iii) indicate a significant rise in tidal frame position, with the scarcity of planktonics and the prevalence of species usually found above MHWST suggesting deposition in a brackish marsh, slightly above MHWST. The assemblage species composition is very similar to zone I (Peat III), with K(i) also having a similar organic matter content (c.20%). In K(iii), a slight increase in freshwater indifferent species abundance, and a rise in organic matter content to c.27%, suggests a slightly higher position in the tidal frame. It is likely, therefore, that K(i) was deposited at a similar elevation to Peat III, *i.e.* 10-30cm above MHWST, and the K(iii) palaeo-surface may have been 20-40cm above MHWST.

As referred to earlier, subzone K(ii) sees a temporary rise in marine-brackish species abundance and decline in freshwater taxa. The polyhalobous planktonic *Podosira stelligera* gains prominence and most indifferent and halophilous species become less prevalent. A rise in the mesohalobous taxa is the most notable change, and this group is dominated by *Nitzschia obtusa*, *Navicula peregrina* (both associated with MHWST and above) and *Navicula phyllepta*. The epipellic species *Navicula phyllepta* was observed in the Taw Estuary to have a wide range from the tidal mudflat up to MHWST. However, its optimum was in the high saltmarsh zone, just below MHWST, where levels reached 12.5%TDV. Its presence here, along with marsh border species and planktonics that are known to be frequent up to MHWST suggests that K(ii) was deposited in an upper high saltmarsh environment, just below MHWST. The organic matter content in this subzone falls to 16-17%. This is similar to the 17% value found at MHWST-30cm in the estuary transect, giving further support for an upper high saltmarsh environment.

Zone L (1.20m – 1.50m)

This zone corresponds with the organic peat in the middle of Peat IV, with plant macrofossils suggesting a mixed sedge-reedswamp and Alder carr environment. DSI values (0.66-0.71) are seen to remain at K(iii) levels, indicating a mixed assemblage is maintained, with brackish-freshwater species dominance. The polyhalobous sum falls to a mean of 9%, the lowest zone average since zone C. The marine planktonic species *Paralia sulcata* starts the zone at %5TDV, but quickly declines in frequency to 2%TDV. However, the polyhalobous planktonic *Podosira stelligera* becomes more

abundant, rising from 1.5%TDV in zone K(iii) to 4.5%TDV in zone L. This zone also sees a rise in the mesohalobous planktonic species *Cyclotella striata* (>5%TDV), indicating that the marsh is still frequently flooded, though now by more brackish flood-water, as evidenced by the general decline in marine planktonics.

The mesohalobous taxa dominate zone L, with the group sum rising to 33-41%. The most notable change is the increase in *Navicula peregrina*, which reaches 28%TDV in the middle of the zone. This frequency suggests it is autochthonous and living at its optimum elevation, situated between MHWST and HAT. The other dominant assemblage species (>10%TDV), *Navicula pusilla*, is also associated with this tidal frame zone. The mesohalobous aerophilous species *Diploneis interrupta* is seen to be present in >5%TDV numbers for the first time. This taxa has been recorded in a saltmarsh at Kentra Bay, Scotland, to be dominant (>10%TDV) at the MHWST level (Shennan *et al.*, 1995; Zong and Horton, 1998, 1999), suggesting that the zone L palaeo-surface was still relatively close to MHWST. The halophile *Navicula eidrigeana* stays at zone K abundance levels (>5%TDV), suggesting a similar tidal frame elevation is maintained.

The oligohalobous indifferent group remains at similar abundance (26% mean), but shows a significant change in species composition. The >5%TDV component of K(iii) is completely replaced by different >5%TDV species. *Caloneis lauta* and *Stauroneis producta*, present in low numbers throughout zone K, now reach >5%TDV abundance. Two *Pinnularia* species, aerophilous *P.viridis* and epipellic *P.major*, emerge at >5%TDV levels not seen since Peat I. Another epipellic freshwater species, *Diploneis elliptica*, becomes present at >5%TDV levels for the first time.

The similar DSI value to zone K, and dominance by mesohalobous and halophilous species associated with the MHWST-HAT zone, combined with an increase in aerophilous taxa (*e.g.* *Diploneis interrupta*, *Navicula pusilla*, *Pinnularia viridis*) suggest only a minor increase in tidal frame position, within the MHWST-HAT zone. The marsh surface was still prone to tidal flooding, but the planktonic dominance by *Cyclotella striata* together with the disappearance of freshwater species known to be slightly more salt-tolerant (*Navicula cari* and *Navicula tripunctata*), suggests the tidal environment was less saline.

The age of this organic peat can be estimated from the radiocarbon dates at the base of Peat IV (2.50m) and at 1.06m. If a constant accretion rate is presumed, the peat between these two dates would have accreted at 0.92mm/yr. This means it was accreting slightly faster than the 0.76mm/yr RSL rise rate estimated for the Bristol Channel by Shennan and Horton (2002), in agreement with the trend of emergence between 2.50m and 1.06m. This would give an estimated age for the period of zone L peat accumulation at between 820 cal.yr.BC and 394 cal.yr.BC.

Zone M (1.05m – 1.20m)

This zone corresponds with the top of the organic peat in the middle of Peat IV, where organic matter content values fall slightly to c.34%. There is a further decline in the polyhalobous sum down to 3.5%, with the virtual disappearance of all polyhalobous and mesohalobous planktonic species, suggesting that the marsh palaeo-surface has risen to an elevation where only the highest spring tides occasionally reach. DSI values rise to 0.79, indicating an assemblage with increased freshwater dominance. This is seen in the oligohalobous indifferent sum which rises to 43%. However, the mesohalobous and halophilous sums remain at similar levels to zone L, indicating a continuing proximity to brackish water.

Although still dominant, *Navicula peregrina* numbers fall to 11%TDV, suggesting it is now above its optimum elevation (close to MHWST). This is also seen in *Diploneis interrupta*, which disappears in this zone, suggesting that the palaeo-surface is now some distance above MHWST. *Navicula peregrina* is largely replaced by another mesohalobous species, *Nitzschia obtusa* which becomes a dominant taxa (>10%TDV). As stated earlier, the only recorded count of *Navicula obtusa* in the Taw Estuary was from the highest station at MHWST+24cm, suggesting its optimum may be above this level. Its rise in zone M, in the absence of typical saltmarsh species, suggests that its optimum is indeed higher in the tidal frame than that reached in the estuary transect.

The halophilous component is similar to zone L, with *Navicula pusilla* and *Navicula eidrigeana* remaining dominant (both >5%TDV). However, *Navicula pusilla* has been recorded from a wide range of elevations, from just below MHWST (Taw Estuary) all the way up to HAT (Nelson and Kashima, 1993; Shennan *et al.*, 1995). The new freshwater species that emerged in zone L (*Diploneis elliptica*, *Pinnularia major*, *Pinnularia viridis*), remain in zone M in similar numbers (>5%TDV), and freshwater

species dominance is seen by the sharp rise in *Navicula variostrata* to 17%TDV. The likely depositional environment of this zone was a brackish marsh, located at an elevation close to HAT.

Zone N (0.67m – 1.05m)

This zone corresponds with the more minerogenic peaty silt at the top of Peat IV. A transgressive overlap, dated at 385-186 cal.yr.BC, is located at the boundary between the organic peat below 1.06m and the peaty silt of zone N. In terms of organic matter content, this zone has two parts. At the start of zone N (1.06m – 0.98m), organic matter values fall to 16%, but then quickly rise again to remain at *c.*20% for the rest of the zone.

Polyhalobous taxa are seen to become more abundant in this zone (10-19%), with the return of marine planktonics *Paralia sulcata* and *Podosira stelligera* to >5%TDV numbers, suggesting an upper high saltmarsh maximum for the palaeo-surface (just below MHWST). This indicates a rise in marine influence across the transgressive overlap. The mesohalobous planktonic *Cyclotella striata* also returns at >5%TDV, with the marine planktonic *Actinoptychus senarius* present at 2.5%TDV. *Actinoptychus senarius* was recorded in the Taw Estuary at a similar abundance in the upper high saltmarsh subzone, which was the upper limit to its range. The three dominant species (>10%TDV) are the mesohalobous taxa *Navicula peregrina* and *Diploneis interrupta*, and the halophile *Navicula pusilla*. As we have seen, all three taxa are associated with upper high saltmarsh (just below MHWST) and marsh border environments (above MHWST). The prevalence of aerophilous species (*Diploneis interrupta* and *Navicula pusilla*) suggests a high tidal frame position with significant periods of subaerial exposure. The presence of mesohalobous *Nitzschia obtusa* at >5%TDV suggests again deposition around MHWST or above. The halophile *Navicula eidrigeana*, which in previous core zones has been associated with both high saltmarsh and marsh border assemblages, reaches >5%TDV numbers in the lower half of zone N.

The above account of polyhalobous, mesohalobous and halophilous species would suggest deposition at just below MHWST in an upper high saltmarsh environment. The organic matter content values would support this, as would the lack of *Phragmites* and the presence of some tidal lamination in the sediment. However, the species composition of the oligohalobous indifferent group suggests a slightly higher tidal

frame position. *Pinnularia major* and *Pinnularia viridis*, previously associated with brackish marsh above MHWST are present at >5%TDV and 4%TDV respectively, and *Diploneis elliptica* remains at the >5%TDV level seen in zones L and M. *Caloneis lauta* reaches >5%TDV in the middle of the zone, although this species was present in the marine dominated assemblage of zone J. On balance, it is proposed therefore that most of zone N was deposited at, or very close to MHWST, equivalent to the high saltmarsh – marsh border boundary in the Taw Estuary transect.

The initial more minerogenic layer in zone N, at 1.06m to 0.98m, has a somewhat different diatom assemblage. The assemblage is dominated by mesohalobous taxa (53%), resulting in the DSI fall to 0.53, a value usually associated with the lower high saltmarsh environment (zones F and H). The oligohalobous species found elsewhere in the zone are here recorded in very low numbers, with the otherwise dominant halophile *Navicula pusilla* (>10%TDV) present at <3%TDV in this layer. The *Pinnularia* species are virtually absent, with *Diploneis elliptica* being the only oligohalobous indifferent taxa present at >5%TDV. This suggests a distinctly more saline environment and lower tidal frame position. The polyhalobous and mesohalobous planktonics *Paralia sulcata*, *Podosira stelligera* and *Cyclotella striata* are present in the numbers seen elsewhere in the zone, but this layer also sees a peak in the mesohalobous planktonic *Cyclotella meneghiniana* (>3%TDV) and in the polyhalobous tycho planktonic *Rhaphoneis ampiceros* (>3%TDV). In the Taw Estuary, *Rhaphoneis ampiceros* was only found at this level in the lower high saltmarsh zone and below (tidal flat optimum). The dominant species (>10%TDV) are all mesohalobous, with *Navicula peregrina* and *Diploneis interrupta* present at levels similar to the rest of the zone, suggesting deposition close to MHWST. However, *Navicula avenacea* is also present in this layer at >10%TDV abundance. This benthic species had its Taw Estuary optimum in the pioneer saltmarsh, but was also present at >2%TDV up to the lower high saltmarsh subzone. Shennan *et al.* (1996) also recorded this species in a low marsh environment below MHWST (within an inner estuarine tidal river setting similar to the Taw).

It is therefore proposed that this initial phase of zone N was deposited at a tidal frame position equivalent to the lower high saltmarsh zone seen in the middle estuary transect. The estuary transect recorded organic matter content values peaking at *c.*15% in this subzone, so the core values of *c.*16% support this proposal. The change in depositional altitude between zones M and zone N is substantial, from a possible MHWST+70cm

level in zone M, to a MHWST-40cm level at the start of zone N. There is no evidence of erosion at the peat/peaty silt zone boundary in the PL1 core, or in neighbouring stratigraphic cores. Rather, a rapid change in environment is evident, with an abrupt change from brackish marsh to salt-marsh deposition at 385-186 cal.yr.BC. Following the period corresponding to the start of zone N, the marsh palaeo-surface appears to have accreted up through the tidal frame and remained at a new equilibrium elevation of MHWST for the rest of this zone (*i.e.* until 668-869 cal.yr.AD).

Zone O (0.41m – 0.67m)

This zone corresponds with the base of the organic clayey silt deposited on top of Peat IV. A transgressive overlap, dated at 668-869 cal.yr.AD, is located at the base of the zone at the peaty silt – clayey silt boundary. The organic matter contents values of 14-15% are typical for the lower high saltmarsh subzone in the Taw Estuary, suggesting a *c.*40-60cm fall in tidal frame position from the former MHWST level. However, the diatom record does not fully support this. The mesohalobous and halophilous sums remain similar to zone N values, with the oligohalobous sum also remaining at a similar level to that recorded in the middle and very top (0.64m) of zone N, suggesting maintenance of a similar tidal frame position. The polyhalobous sum actually falls to *c.*5%, suggesting a rise in tidal frame position. The DSI value rises to values (0.69-0.74) typical of marsh border environments above MHWST (the marsh border assemblage in the Taw Estuary had a DSI of 0.76). However there are no organic macrofossils such as *Phragmites* or *Juncus* that would support this. Instead, the sediment contains the density of fine rootlets associated with a saltmarsh grass (*Puccinellia maritima*) dominated high saltmarsh. Tidal lamination, associated with saltmarsh rather than marsh border environments, is also present.

As in zone N, the mesohalobous taxa form the dominant diatom group. The dominant species in this group are *Navicula peregrina* (>10%TDV), *Diploneis interrupta* (>5%TDV), and *Nitzschia obtusa* (>5%TDV). These are joined by the halophile *Navicula pusilla* (>5%TDV). As we have seen, these four species are known to be abundant in the zone just below MHWST and above. Shennan *et al.* (1995) recorded highest numbers of *Navicula peregrina* in an assemblage 14cm below MHWST. The optimum for *Navicula peregrina* in the Taw Estuary was in the zone above MHWST. However, samples were not taken between MHWST-23cm and MHWST+24cm so the true optimum may have been lower in the tidal frame. In previous core zones, *Nitzschia*

obtusa has been found in assemblages representing upper high saltmarsh (K(ii)) and above. However, in the study by Shennan *et al.* (1996), this species was usually associated in core assemblages representing deposition below MHWST, suggesting it has a wide range.

It is therefore proposed that zone O was deposited at around the upper and lower high saltmarsh boundary (30-40cm below MHWST). This is based on the dominance of the four brackish species named above and the supporting organic matter content and sedimentary evidence. The decline in allochthonous planktonics may be because of the lack of proximity to the contemporaneous tidal river channel at the time of deposition. Figure 5.5 shows that Peats II to IV thin to the east with a “feather-edge” of intercalated silts and fine sands suggesting close proximity to the palaeo-river. However, the zone O and P horizon shows fine marsh silts extending to PL2 and beyond, suggesting that the river channel was on the east side of the valley at this time.

Zone P (0.27m – 0.41m)

This zone corresponds with both the top of the organic silt below Peat V and the basal 3cm of Peat V. Organic matter content remains at 14-15% between 0.42m and 0.33m, then rises sharply to reach 28% at 0.28m. This zone sees a rise in mesohalobous taxa to 46%, with a corresponding fall in oligohalobous indifferent taxa to 21%. Gradual declines are seen in both the polyhalobous and halophilous groups, reaching 2.5% and 7.5% respectively at end of the zone.

The marine and brackish planktonics remain at very low levels in this zone, with *Podosira stelligera* being the only species to reach 2%TDV. The silt component of the zone is dominated by the mesohalobous taxa *Navicula peregrina* (>10%TDV), *Diploneis interrupta* (>10%TDV), *Nitzschia obtusa* (>5%TDV) and the euryhaline species *Nitzschia commutata* (>5%TDV). The halophilous species *Navicula pusilla* remains at >5%TDV abundance. No freshwater indifferent species are present in the silt at >5%TDV.

The combined decline in freshwater species and continuing dominance by brackish species associated with the zones around MHWST suggests a very minor fall in tidal frame position at the start of zone P (possibly only 10cm). This would bring the marsh palaeo-surface into the lower high saltmarsh subzone, possibly 40-50cm below MHWST, with organic matter content values remaining typical for this environment.

The small numbers of planktonics suggests the marsh remains distal to the estuarine river channel.

The top of zone P, corresponding with the peaty clay at the base of Peat V, sees some important species changes occurring in the mesohalobous group with a substantial decline in *Navicula peregrina* to 3.5%TDV and a corresponding rise in *Nitzschia commutata* to 16%TDV. *Diploneis interrupta* and *Navicula pusilla* remain dominant species and the aerophilous freshwater species *Nitzschia terrestris* emerges at >10%TDV abundance. This change to a more organic depositional environment that remains brackish, but prone to much less tidal submergence, would suggest the marsh surface has accreted above MHWST into the marsh border zone. The presence of some marine and brackish planktonics (*Paralia sulcata*, *Podosira stelligera* and *Cyclotella striata*, totalling 4%TDV) in a relatively subaerial environment, suggests that the River Taw remains un-embanked.

Zone Q (0.25m – 0.27m)

This zone corresponds with the upper thin *Poaceaea-Bryophyte* peat in Peat V, just below the made ground which is speculated to have been laid down in 1987 AD. One sample was taken from 0.26m. The DSI value rises to 0.82, indicating dominance by freshwater taxa. This is seen in the oligohalobous indifferent sum which rises sharply to 48%. The polyhalobous and mesohalobous planktonic component falls to 2.5%, the lowest value seen since the base of zone C. The assemblage is dominated by the euryhaline mesohalobous benthic *Nitzschia commutata* (18%TDV), and the freshwater aerophilous species *Nitzschia terrestris* (36%TDV) and *Pinnularia borealis* (5%TDV). The dominance by aerophilous species indicates the marsh surface is now rarely submerged by water. The modern age of this palaeosoil indicates that it accumulated after the River Taw was contained within flood embankments. The residual autochthonous planktonic component is probably derived from occasional ponding of the PL1 site. This is seen to occur today after high tides (from ground water flow and through leaking drainage ditch sluice gates in the embankment) and after periods of prolonged rainfall.

The change to subaerial organic deposition in Peat V is therefore likely to have commenced after the embanking of the River Taw. It is not known when the Taw was

first embanked, but first series Ordnance Survey maps do show it was embanked before the mid 19th century.

5.2.4 PL2 core

Sedimentology and magnetic properties

Figure 5.9 shows the core log for PL2. This figure shows down-core changes in sediment lithology, X_{ir} , organic matter and carbonate content. In addition, the diatom zones (see later), FSUs (see section 5.2.8) and stratigraphic units (see chapter 7) are indicated.

Below 1.45m the core consists of shelly fine-medium sand, intercalated with thin layers of shelly silty fine sand and sandy silt. The core is underlain by gravel at 6.00m (-2.13m OD). The coarser units often show tidal lamination (especially above 4.47m) with couplets of fine-medium sand (2mm thick) and sandy silt (1mm thick). The finer laminae will have been deposited at slack water. The shell material consists of comminuted calcareous shell fragments (probably from bivalves and gastropods) of medium to very coarse sand size and this is the source of the high carbonate content values of *c.*10-12%. The uppermost sand layer (1.55m –1.97m) contains clayey silt mud drapes, consistent with slack water fines deposited in the troughs of ripple bedforms. The carbonate content value falls to *c.*6%. The sandy facies below 1.45m represents estuarine channel deposits which have laterally accreted during channel migration.

Overlying the sand, between 0.62m and 1.45m, carbonate content values fall to *c.*1.5% and a blue-grey mottled brown silty clay is deposited, with faint planar lamination and occasional rootlets and rootlet traces. This is thought to represent a vertically accreting low-mid saltmarsh deposit that is contemporaneous with the peaty clay at the top of Peat IV in the PL1 core (see figure 5.5). Above the silty clay unit, the sediment coarsens slightly and *c.*40cm of grey mottled orange-brown clayey silt is deposited, with faint planar lamination and some rootlets. The stratigraphy suggests that this silt is contemporaneous with the silt above Peat IV in PL1 and was deposited in a similar high saltmarsh environment. The upper 21cm consists of grey sandy silt, with many grass rootlets in the surface 6cm.

The X_{lf} values remain relatively low ($0.1 \cdot 10^{-6} \text{ m}^3 \text{ kg}^{-1}$) throughout the core, suggesting a low concentration of ferrimagnetic minerals and a similar sediment source (in this case, the outer estuary).

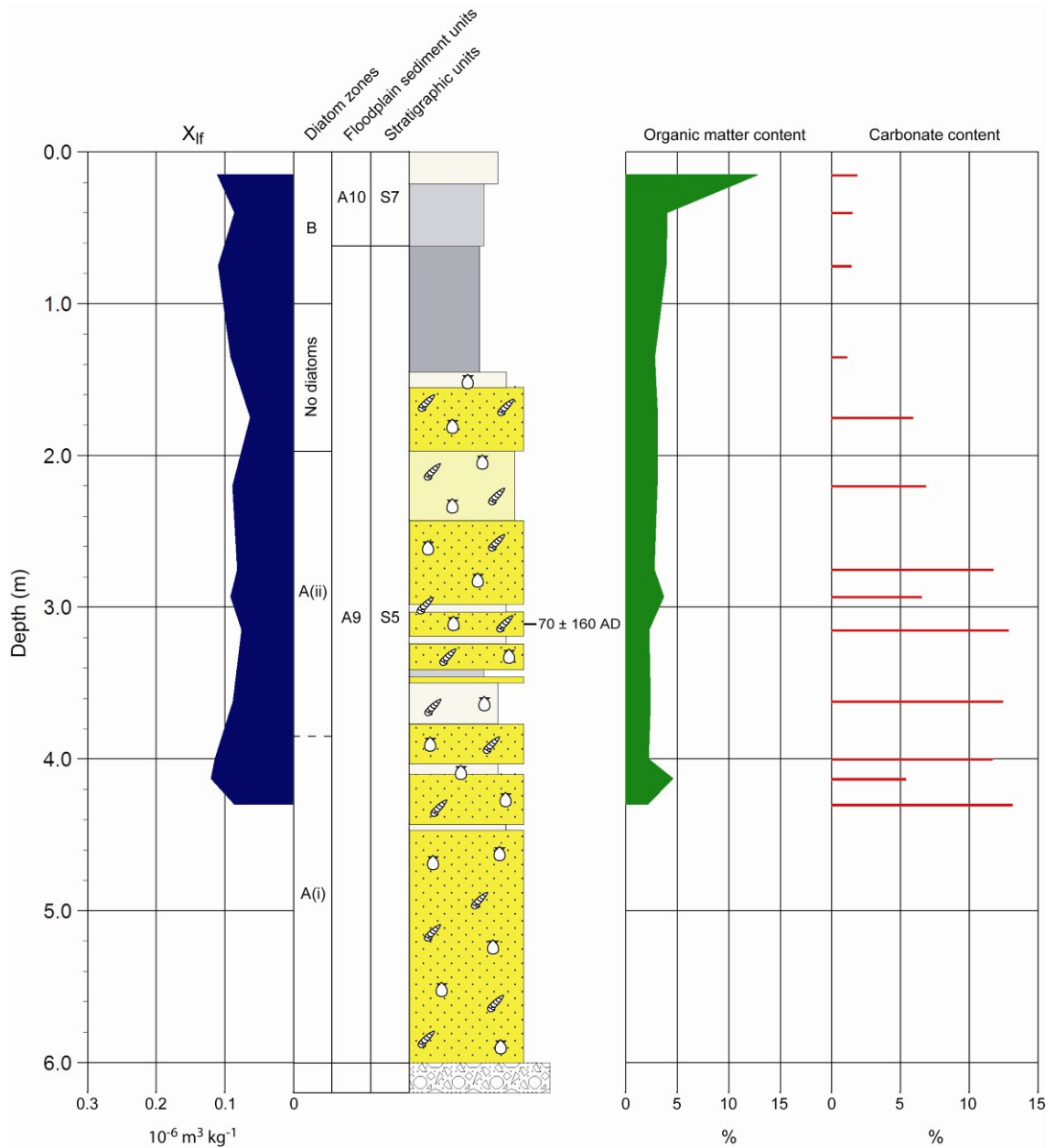


Figure 5.9 PL2 core log. See figure 5.2 for lithology legend. Diatom zones are derived from figure 5.10. Floodplain sediment units (FSUs) are discussed in section 5.2.8. Stratigraphic units are discussed in chapter 7.

Geochronology

An OSL date from 3.11m, in the upper part of the shelly sand, gives a depositional age of $70 \pm 160 \text{ cal.yr.AD}$. The stratigraphy (figure 5.4) suggests the estuarine channel migrated to the east after this date. As the upper silt is thought to be contemporaneous

with the silt above Peat IV in PL1, an age of 684-777 cal.yr.AD (1-sigma) can be given to the lower silt boundary at 0.62m.

Diatom analysis

Figure 5.10 shows a diatom diagram for PL2. All species with counts of >3%TDV are shown, along with the diatom sums. Cluster analysis resulted in 2 diatom zones (A and B). Diatom valves were found to be quite sparse in this core, with none present between c.1.0m and 2.0m. Valves were also significantly fragmented in the channel sands, indicative of abrasion in the high-energy channel environment.

Zone A (6.00m to 1.97m)

This zone corresponds with the shelly channel sands below 1.45m. In the more massive shelly sands below 3.77m (subzone A(i)), the DSI value of 0.70 indicates a mixed assemblage dominated by freshwater species. This is shown in the diatom sums with a value of 45% for the dominant oligohalobous indifferent group, 23% for the polyhalobous taxa and only 2% for the mesohalobous group. The dominant freshwater species are the epiphyte *Cocconeis placentula* (>10%TDV) and *Achnanthes exilis* (>10%TDV). In a tidal river channel, deposition at the base of the channel will be much more effected by the residual fluvial discharge, unlike higher up the channel banks, where deposition is much more influenced by incursions of estuarine water at high tide. This is the likely reason for the freshwater dominance seen at the base of PL2. The diatom valves will be allochthonous, with *Cocconeis placentula* being particularly robust and the very small size of *Achnanthes exilis* allowing it to be transported long distances in suspension at lower velocities. The rest of the assemblage is dominated by polyhalobous planktonics with *Paralia sulcata* and *Delphineis surirella* at >5%TDV, indicative of an estuarine environment.

Above 3.77m, in the channel sands with tidal lamination (subzone A(ii)), the assemblage is dominated by polyhalobous species (65%), indicated by very low DSI values of 0.14-0.21. *Paralia sulcata* dominates the group, reaching 30%TDV, with other dominant (>5%TDV) species being the planktonics *Actinoptychus senarius* and *Podosira westii*, the tychoplanktonics *Cymatosira belgica*, *Delphineis surirella* and *Rhaphoneis amphiceros*, and the benthic *Diploneis subadvena*. Mesohalobous and freshwater indifferent taxa are present in very low numbers (both c.6%) throughout the

zone, with the brackish planktonic *Cyclotella striata* being most abundant (5.5%TDV) at the top of the zone. This subzone therefore indicates deposition in a low-intertidal estuarine environment, with the dominance by marine planktonics indicating that most sediment is sourced from the middle and outer estuary.

Zone B (1.00m – 0.00m)

This zone corresponds with the silty clay and clayey silt that has accreted above the channel facies sands. Zone B is dominated by both polyhalobous taxa (21-31%) and mesohalobous species (44-56%). The polyhalobous group is dominated by marine planktonics and tycho planktonics with *Coscinodiscus radiatus*, *Paralia sulcata*, *Podosira stelligera* and *Rhaphoneis amphicerus* all present at >5%TDV. *Paralia sulcata* and *Podosira stelligera* were present at this level up to the upper high saltmarsh in the Taw Estuary.

At the base of zone B, the most abundant species is the mesohalobous epipellic *Nitzschia navicularis* (23%TDV), suggesting that it is autochthonous in the fine grained siltyclay sediment. In the Taw Estuary, this species was most abundant in the lower tidal flat subzone associated with residual river flow and was therefore probably allochthonous in this setting. However, a rise in numbers was also seen around the mid-high saltmarsh boundary where it may have been autochthonous. This is supported by the study by Hill *et al.* (2007) in the Severn Estuary which recorded an optimum at a similar saltmarsh position in the tidal frame. Zong and Tooley (1996) also found *Nitzschia navicularis* to be associated with core assemblages that were stratigraphically placed on the minerogenic side of overlaps suggesting deposition in the zone below MHWST. A mid to lower high saltmarsh depositional environment in the lower part of zone B is also supported by the rise in *Caloneis westii* to >5%TDV. This species was given an optimum by Zong and Horton (1999) not far under MHWST.

The upper part of zone B is dominated by the mesohalobous species *Navicula peregrina* and *Diploneis interrupta* (both >10%TDV), both associated with the high saltmarsh zone and above. Zone B shows several similarities with the minerogenic PL1 zones O and P where the assemblages were also dominated by the mesohalobous group and also contained high numbers of *Navicula Peregrina* and *Diploneis interrupta*. A similar lower high saltmarsh environment is proposed for the clayey silt at the top of zone B.

The higher numbers of marine planktonics in PL2 may be due to proximity to the estuarine river channel at time of deposition.

5.2.5 PL3 core

Sedimentology and magnetic properties

Figure 5.11 shows the core log for PL3. This figure shows down-core changes in sediment lithology, X_{lf} , organic matter and carbonate content. In addition, the diatom zones (see later), FSUs (see section 5.2.8) and stratigraphic units (see chapter 7) are indicated.

The lower half of the core, below 1.87m, consists of shelly fine-medium sand and an intercalated layer of tidal laminated clayey silt and shelly sand. The uppermost sand layer (1.87m – 2.53m) contains clayey silt mud drapes, deposited at slack water. At the base of the core is a 10cm lag of gravelly shelly sand overlying the gravel channel bed at 3.52m (0.45m OD). The sandy facies below 1.87m represents estuarine channel deposits which have laterally accreted during channel migration. The 11-14% carbonate content of this unit is similar to that seen in the Taw Estuary sandflat zone.

Above the sand is a unit of slightly shelly grey-brown mottled orange brown clayey silt (1.37m – 1.87m) with sporadic lenses and laminae (2-8mm) of shelly fine-medium sand. The sediment contains some long rootlets and rootlet traces. This deposit is somewhat similar to that seen in the Taw Estuary pioneer saltmarsh zone with the 4.5% carbonate content value typical of this environment. Above a thin layer of shelly sand is another layer of clayey silt (0.98m – 1.31m), similar to that seen below. However, here, the shelly sand laminae are absent and this is reflected in the carbonate content which falls to 1.3%. This suggests a rise in the palaeo-surface into the lower or middle saltmarsh zones. Above the silt, the sediment fines into a brown mottled orange brown silty clay unit (0.68m – 0.98m) with occasional rootlets. Faint planar lamination is visible with some sandy partings suggesting tidal deposition on the saltmarsh platform. This is overlain by a clayey silt identical to that seen at 0.98m – 1.31m. Above 0.68m, the sediment coarsens into an upper unit of sandy silt containing occasional rootlets and some silty sand laminae.

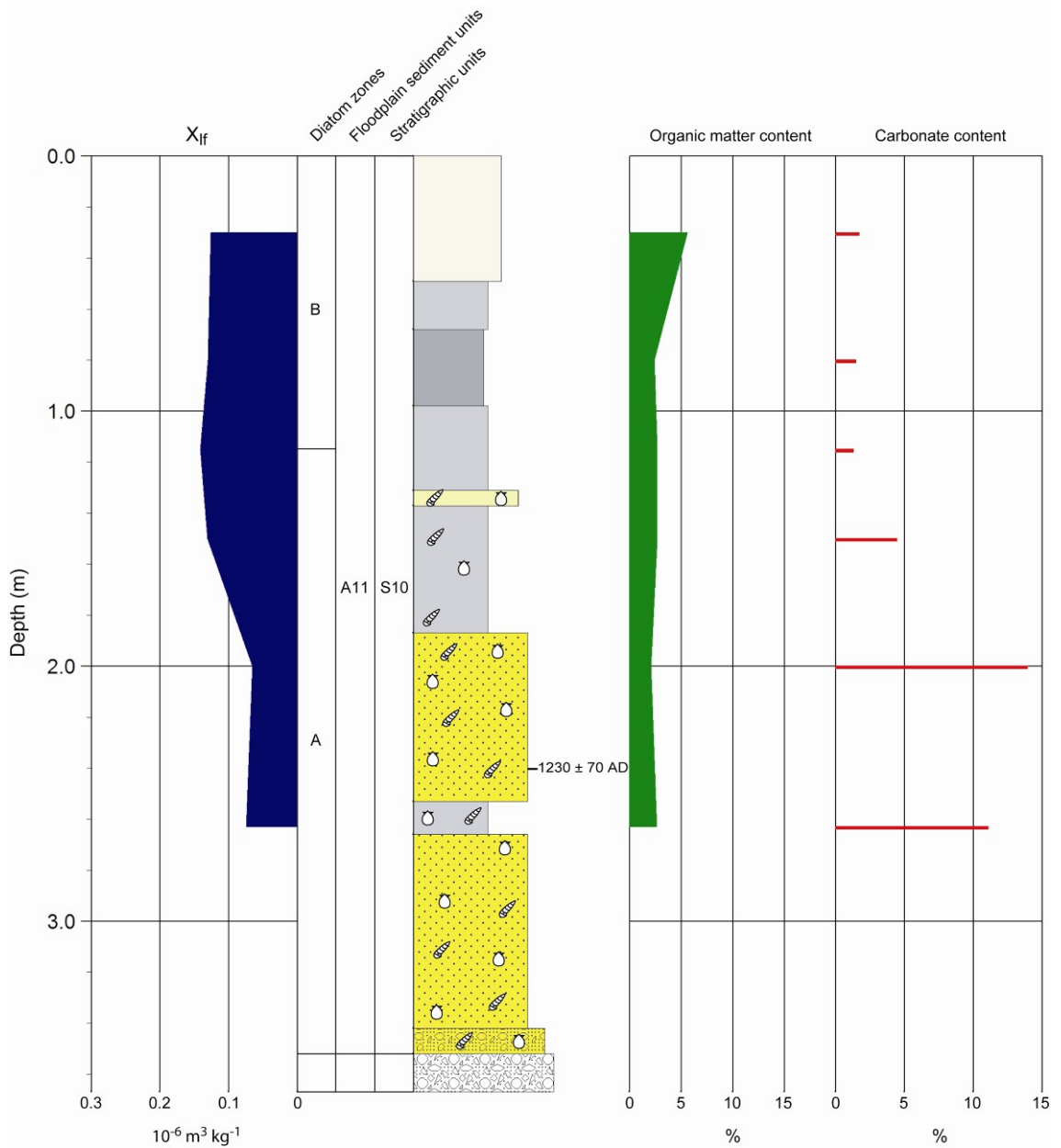


Figure 5.11 PL3 core log. See figure 5.2 for lithology legend. Diatom zones are derived from figure 5.12. Floodplain sediment units (FSUs) are discussed in section 5.2.8. Stratigraphic units are discussed in chapter 7.

The X_{lf} values remain low ($<0.1 \text{ } 10^{-6} \text{ m}^3 \text{ kg}^{-1}$) in the channel sands, then rise in the vertically accreting saltmarsh sediments above. This was observed in the Taw Estuary, where X_{lf} values increased at the base of the pioneer saltmarsh zone, before declining again in the upper high saltmarsh.

Geochronology

An OSL date from 2.38m, in the lower part of the upper fine-medium sand, gives a

depositional age of 1230 +/-70 cal.yr.AD. The stratigraphy (figure 5.4) suggests the estuarine channel migrated to the east after this date, followed by vertical accretion of saltmarsh sediments at the PL3 site.

Diatom analysis

Figure 5.12 shows a diatom diagram for PL3. All species with counts of >3%TDV are shown, along with the diatom sums. Cluster analysis resulted in 2 diatom zones (A and B). Diatom valves were found to be slightly more abundant than in PL2, but still in relatively low concentrations. Valves were also significantly fragmented at all levels (especially zone A), indicative of transportation in high velocity tidal currents.

Zone A (3.52m – 1.15m)

This zone corresponds with the channel sands and shelly silts. The DSI value in the basal sands starts at 0.11, indicating total dominance by marine taxa. This value is typical for the tidal flat zone in the Taw Estuary. In the shelly saltmarsh silts at the top of the zone, the DSI rises to 0.20, analogous to the rise seen at the start of the pioneer saltmarsh zone in the Estuary transect. This zone is dominated by a large polyhalobous group (68-76%), a small but stable mesohalobous group (5.5%), and minor rises in the rare halophilous (0 to 3%) and indifferent taxa (2 to 5%) through the zone.

The zone is dominated by marine planktonic and tycho planktonic species, especially *Paralia sulcata* (26-33%). The other dominant planktonics are *Actinocyclus senarius* (>10%TDV) and *Coscinodiscus radiatus*, *Cymatosira belgica*, *Podosira stelligera* and *Rhaphoneis amphiceros* (all at >5%TDV). In the Taw Estuary, this level of polyhalobous dominance was only seen in the low saltmarsh and below, giving support to an estuarine channel and pioneer/low saltmarsh environment.

Zone B (1.15m – 0.00m)

This zone corresponds with the non-shelly clayey silt, silty clay and sandy silt in the upper part of the core. The polyhalobous sum falls to 61%, and the mesohalobous and freshwater indifferent sums rise to 10% and 9% respectively. Zone B remains dominated by marine planktonic species, but numbers of *Podosira stelligera* are seen to rise to >10%TDV. This species had its optimum abundance in the low and mid saltmarsh zones of the Taw Estuary. The polyhalobous tycho planktonic *Odontella*

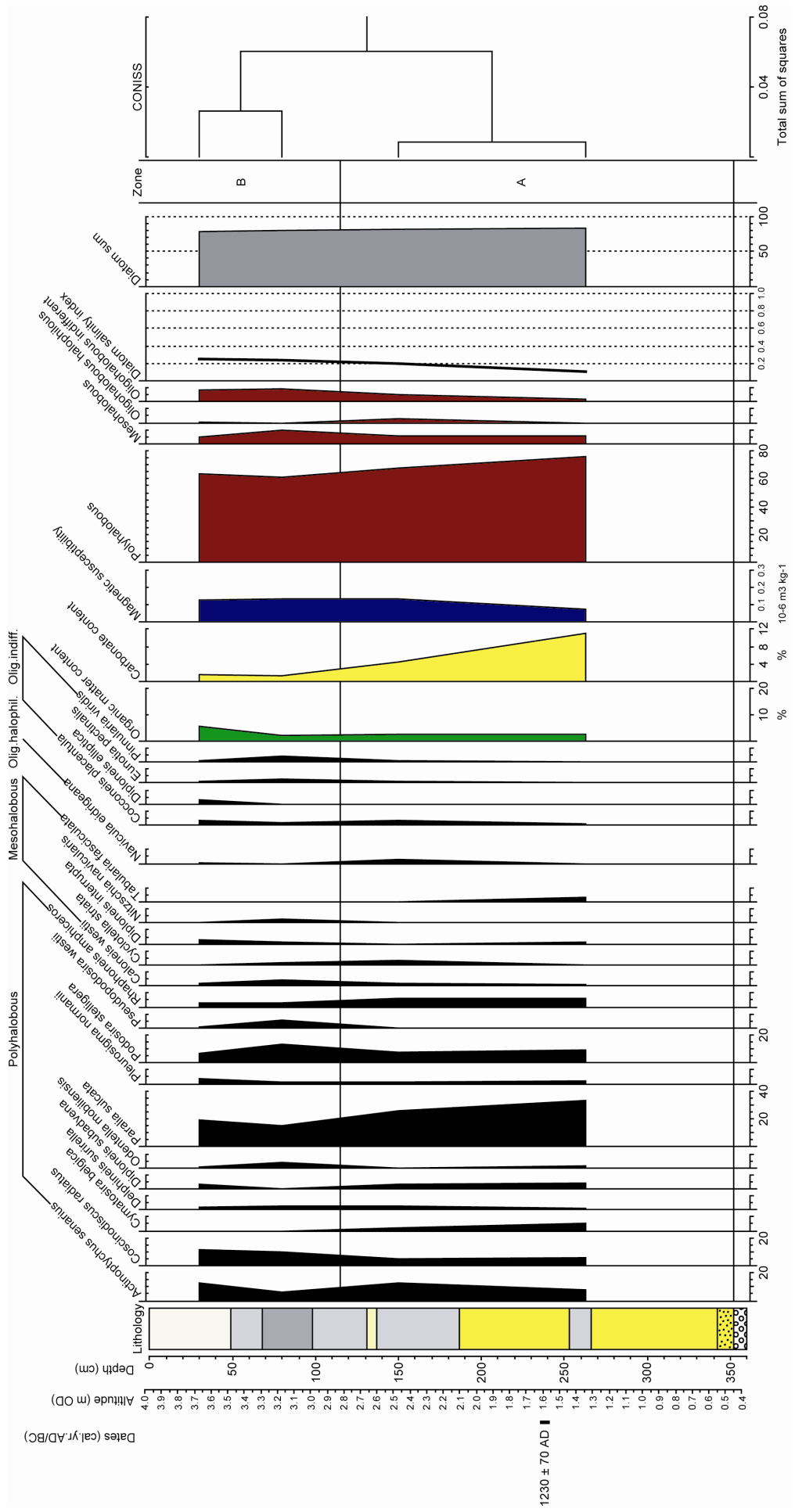


Figure 5.12 Diatom diagram for PL3 core (>3% TDV spp.). Organic matter content, carbonate content, X_{fr} and Diatom Salinity Index is also shown.

mobilis also peaks in abundance in zone B. This species had its optimum abundance at the low-mid saltmarsh boundary in the Taw Estuary. The mesohalobous group sees rises in *Caloneis westii* and *Nitzschia navicularis* to >3%TDV, indicative of a rise in tidal frame position into the mid to high saltmarsh zones (*i.e.* more proximal to MHWST; Zong and Horton, 1999; Hill *et al.*, 2007). Zone B is therefore likely to have been deposited in the mid saltmarsh zone.

5.2.6 PL4 core

Sedimentology and magnetic properties

Figure 5.13 shows the core log for PL4. This figure shows down-core changes in sediment lithology, X_{if} , organic matter and carbonate content. In addition, the FSUs (see section 5.2.8) and stratigraphic units (see chapter 7) are indicated.

The lower part of the core, from the basal gravel (3.33m) to 2.10m, consists of layers of shelly fine-medium sand and silty fine sand. Both grades of sediment show tidal lamination. This sandy unit represents estuarine channel deposits which have laterally accreted during channel migration. The 5-17% carbonate content of this unit is similar to the range seen in the Taw Estuary tidal flat zone.

Between 1.51m and 2.10m is a unit of shelly silty fine sand with lamination partings of shelly fine-medium sand. The sediment also contains occasional 3-5mm sand lenses and a 6cm layer of shelly sand at 1.68m – 1.74m. Occasional rootlets are seen throughout. The sediment indicates deposition on a pioneer saltmarsh with sparse vegetation cover and frequent/daily tidal inundation. Between 0.62m and 1.51m is a unit of grey-brown sandy silt, with some rootlets and plant fragments. The basal part, below 1.39m, is slightly shelly and contains 4-10mm lenses/laminae of shelly fine-medium sand. This unit is thought to represent low and middle saltmarsh zone deposition. This is overlain by a more organic finer grained grey-brown silt deposit with many rootlets and occasional plant fragments. Occasional shell sand grains are dispersed through the sediment. The sediment properties and low carbonate content (1.3-1.9%) suggest deposition in the middle and lower high saltmarsh zones.

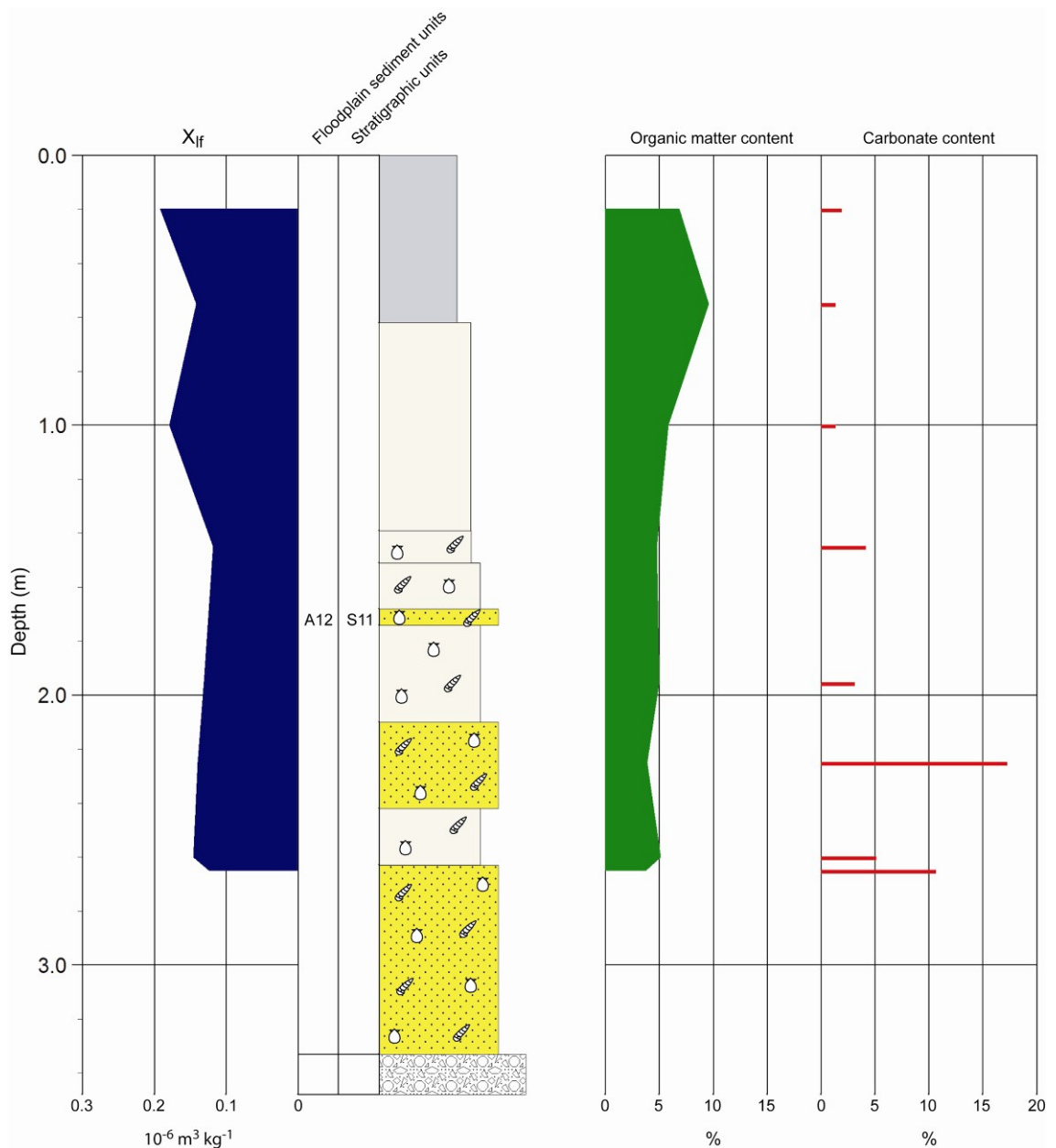


Figure 5.13 PL4 core log. See figure 5.2 for lithology legend. Floodplain sediment units (FSUs) are discussed in section 5.2.8. Stratigraphic units are discussed in chapter 7.

X_{lf} values remain quite similar throughout PL4 ($0.12\text{-}0.19 \times 10^{-6} \text{ m}^3 \text{ kg}^{-1}$), although the highest values are seen in the upper non-shelly facies, supporting the proposal that these units were deposited in a saltmarsh environment. PL4 therefore represents sandy estuarine channel facies overlain by vertically accreting saltmarsh sediment, with evidence for a gradual rise in tidal frame position as the marsh matured.

5.2.7 PL5 core

Sedimentology and magnetic properties

Figure 5.14 shows the core log for PL5. This figure shows down-core changes in sediment lithology, X_{if} , $X_{fd\%}$ organic matter and carbonate content. In addition, the FSUs (see section 5.2.8) and stratigraphic units (see chapter 7) are indicated.

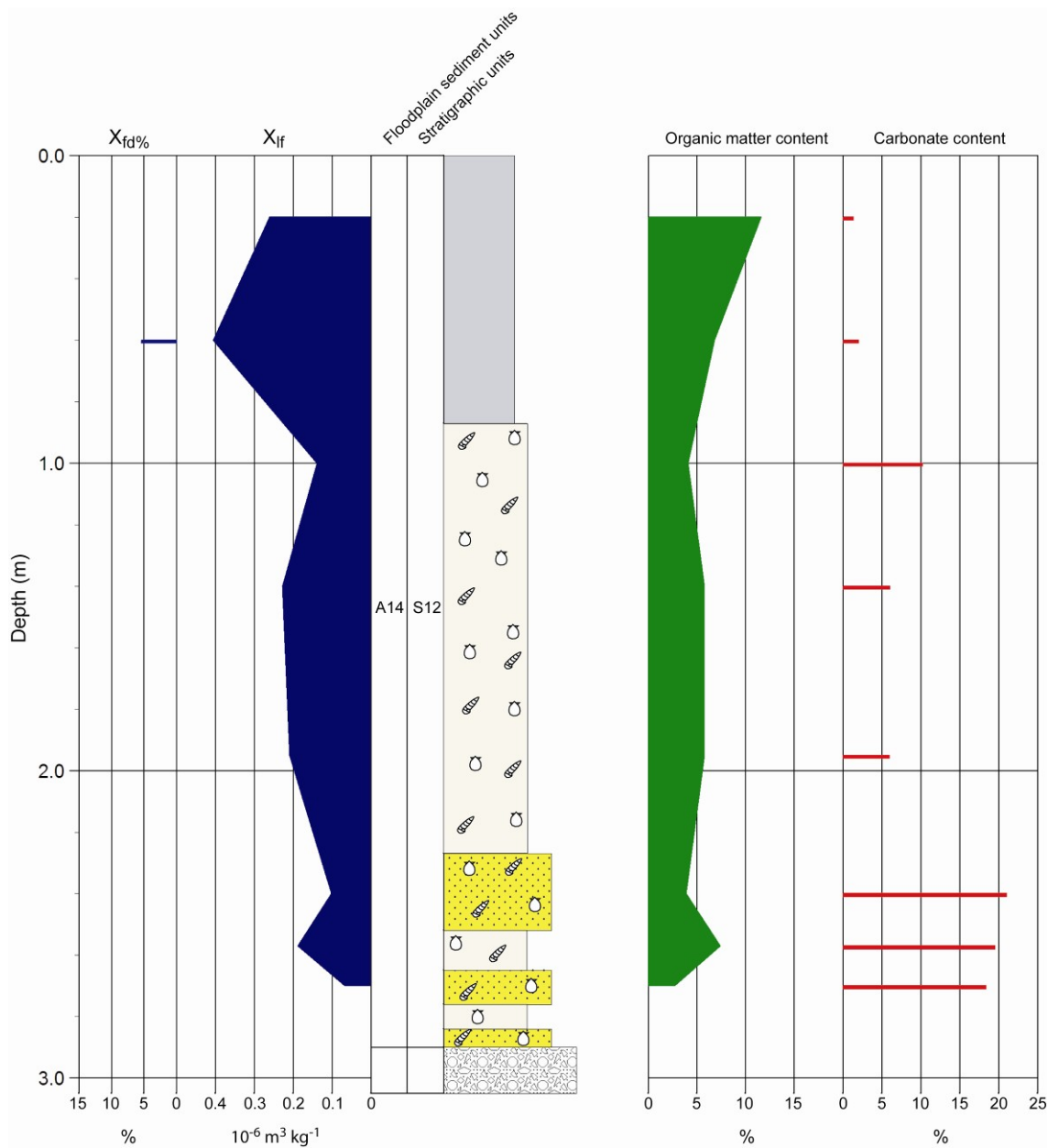


Figure 5.14 PL5 core log. See figure 5.2 for lithology legend. Floodplain sediment units (FSUs) are discussed in section 5.2.8. Stratigraphic units are discussed in chapter 7.

The lower part of the core, from the basal gravel (2.90m) to 2.52m, consists of intercalated layers of shelly fine-medium sand and shelly sandy silt. The silt layers are laminated with sandy partings. The sand layers contain thin beds (2-5cm) of laminated sandy silt. This lower unit represents estuarine channel deposits, with the intercalated beds of sand and silt typical of inner estuary mobile tidal sandbars (Allen and Posamentier, 1993), with the internal flaser lamination of the sand beds typical of an inner estuary mixed tidal flat environment (Dalrymple et al., 1990). The 18-21% carbonate content of this unit is at the top end of the range seen in the Taw Estuary tidal flat zone.

The sand is overlain between 1.21m and 2.27m by grey-brown slightly shelly sandy silt with many lenses and laminations (2-25mm) of shelly fine-medium sand. The sediment contains occasional rootlets. This deposit suggests deposition in a pioneer saltmarsh with frequent flooding and influx of the coarser sand layers during high velocity flood tides. Further deposition of slightly shelly sandy silt occurs between 0.87m and 1.21m. However, the sand laminae are not present, indicating further distance from the marsh edge and possibly a slightly high elevation. The 6-10% carbonate content values for these silt units are similar to that found in the Taw Estuary pioneer and low saltmarsh zones. The sandy silts are overlain by increasingly organic (7-12% organic matter content) grey silts with rootlets and plant fragments. Occasional shell sand grains are dispersed through the sediment. The rising organic matter content values suggest deposition in the middle and lower high saltmarsh zones.

X_{ir} values rise to $0.2 \cdot 10^{-6} \text{ m}^3 \text{ kg}^{-1}$ in the shelly silt unit, and then rise again to $0.4 \cdot 10^{-6} \text{ m}^3 \text{ kg}^{-1}$ in the upper silt, a value very similar to that found in the Taw Estuary low to high saltmarsh zones. The $X_{fd\%}$ value of 5% indicates a low concentration of fine viscous (SP/SSD boundary) magnetite, often formed during pedogenesis. The high values are probably derived from bacterial magnetite and/or greigite, produced by magnetotactic bacteria under anaerobic conditions (Blakemore, 1982; Snowball, 1994). Several studies have shown that fine grained saltmarsh sediments have high concentrations of bacterial magnetosomes (Oldfield and Yu, 1994; Wheeler *et al.*, 1999; Gibbs, 2000).

PL5 is therefore similar to PL4, and represents sandy estuarine channel facies overlain by vertically accreting saltmarsh sediment, with evidence for a gradual rise in tidal frame position as the marsh matured.

5.2.8 Phases of geomorphic and environmental change in the Pill Lane reach

Several phases of alluviation are discernable in the stratigraphy of transect A (figure 5.4). Figure 5.15 (and 5.16) shows the FSU division for transect A, with FSU A1 being the oldest. Each unit will now be summarised and interpreted in terms of geomorphic/environmental change.

FSU A1

The start of this phase records a period of estuary expansion, with saltmarsh sediment encroaching onto the pre-existing gravel surface during an up-valley transgression of marine facies during the mid-Holocene. This is followed by estuary contraction and the progradation of a brackish marsh at 4784-4555 cal.yr.BC, driven by the rise in water-table associated with sea-level rise. Continuing marsh accretion, and a fall in palaeosalinity, allows a fen wood environment to develop close to HAT with the accumulation of wood peat.

FSU A2

The organic phase comes to an end at 4454-3973 cal.yr.BC, when the continuing rise in RSL causes increased tidal inundation and the expansion of minerogenic sedimentation, with the palaeo-surface now just below MHWST at the start of FSU A2. However, instead of saltmarsh, a brackish tidal-floodplain environment is evident at PL1. This suggests a contemporaneous change to a wetter climate causes an increase in river discharge, resulting in the expansion of the freshwater tidal zone, the downstream migration of the salinity front and an increase in fluvial alluviation. Continuing RSL rise in the middle part of FSU A2, combined with a reduction in river discharge, causes estuary expansion and increasing palaeosalinity, with the increase in hydraulic duty causing the marsh surface to gradually fall in tidal frame position to a low saltmarsh elevation. Estuary expansion at this time is also evident in figure 5.5, with the erosion of an estuarine channel into the saltmarsh platform between PL1 and the valley side. The later part of FSU A2 shows gradual estuary contraction and accretion of the marsh surface to high saltmarsh levels. This may have been associated with a reduction in the rate of RSL rise at this time.

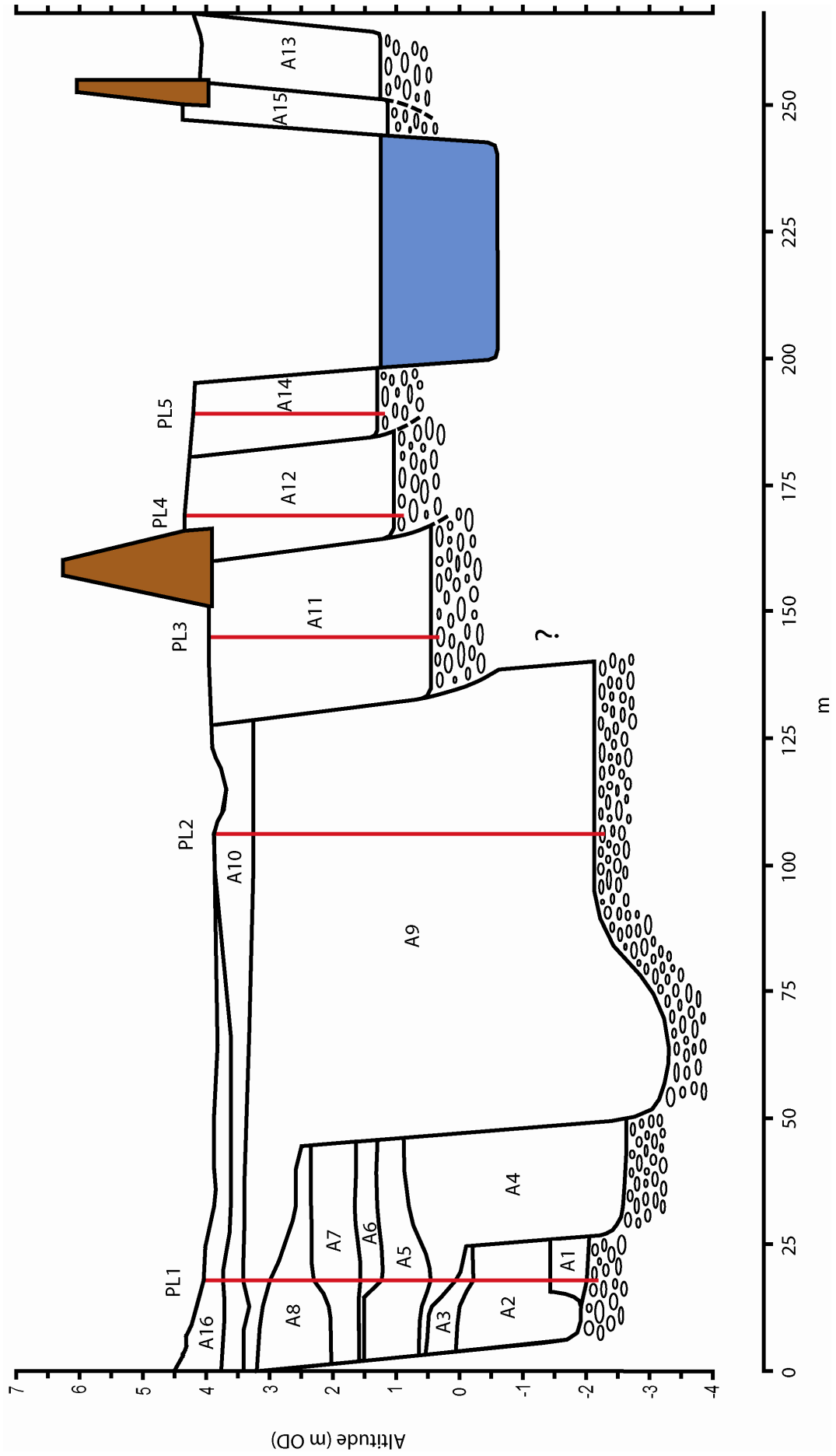


Figure 5.15 Transect A (Pill Lane transect) Floodplain Sediment Units (FSUs).

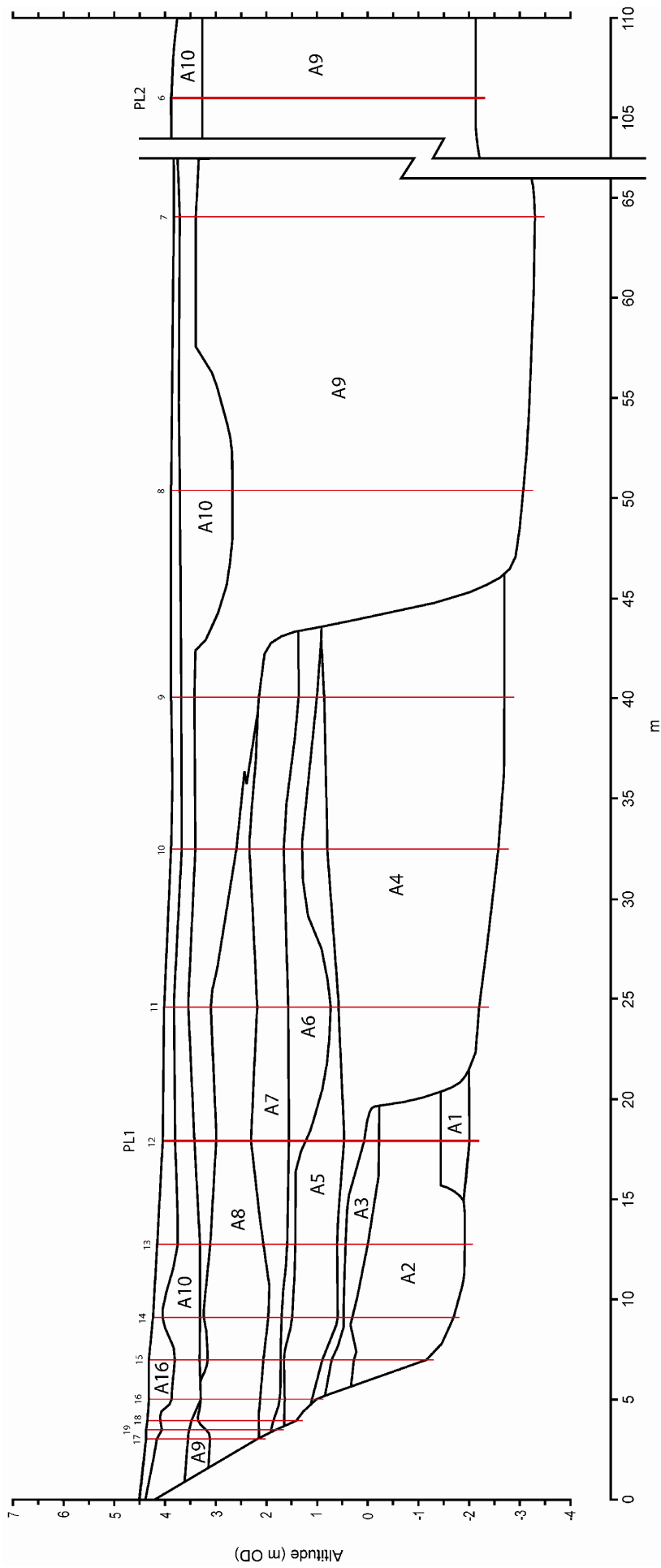


Figure 5.16 Floodplain Sediment Units (FSUs) in the vicinity of PL1 (Transect A).

FSU A3

At 3644-3382 cal.yr.BC, continuing estuary contraction causes the progradation and accretion of a brackish reedswamp at PL1, with the marsh surface at about MHWST+20cm. This environment is maintained until 3519-3137 cal.yr.BC.

FSU A4

An increase in marine influence at 3519-3137 cal.yr.BC is probably associated with an increase in the rate of RSL rise, causing estuary expansion, a rise in palaeosalinity and a return to minerogenic sedimentation, with the marsh surface falling in the tidal frame to lower high saltmarsh levels. Evidence of this phase of estuary expansion is also seen in figure 5.5, with the erosion of an estuarine channel close to the east of PL1, and deposition of tidal flat and sub-tidal shelly sand.

FSU A5

At 2900-2668 cal.yr.BC, a phase of estuary contraction and reduced marine influence causes the renewed progradation and accretion of a brackish organic marsh at PL1, with a fall in palaeosalinity and some *Phragmites* growth. The marsh surface accretes to about MHWST+20cm. A brackish marsh environment is maintained until 2279-2026 cal.yr.BC.

FSU A6

At 2279-2026 cal.yr.BC, another phase of estuary expansion is evident, with a probable increase in the rate of RSL rise. Minerogenic saltmarsh sedimentation returns, with diatom evidence suggesting the marsh surface is at mid-saltmarsh levels. To the east of PL1, saltmarsh tidal creek development (second or third order channel; Havelock, 2001) has caused the erosion of the underlying brackish marsh surface (figure 5.5).

FSU A7

At 1964-1748 cal.yr.BC, a phase of estuary contraction causes the renewed progradation and accretion of a brackish marsh peat at PL1, with a fall in palaeosalinity and some *Phragmites* growth. The palaeo-environment is very similar to that seen in FSU A5, with the marsh surface accreting to about MHWST+30cm at the end of this period. A short period of estuary expansion is recorded in the middle of this unit, where the marsh surface temporarily falls in the tidal frame to upper high saltmarsh levels.

FSU A8

This unit shows further estuary contraction and accretion of organic peat in a brackish wetland environment. The age of the start of this phase is estimated at 820 cal.yr.BC, with organic deposition abruptly ending at 385-186 cal.yr.BC. A mixed alder carr and reedswamp environment is maintained for most of this unit, at an elevation of about MHWST+40cm. The growth of Alder at this tidal frame position would suggest this unit coincided with a period of higher river discharge and reduced palaeosalinity, with down-stream expansion of the freshwater and brackish tidal zones. Higher river discharge levels may be related to the combined effects of late Bronze Age/early Iron Age woodland clearance, which would cause higher rates of surface run-off, and to a change in the climate to cooler, wetter conditions. The low humification of the peat is also indicative of a wetter (and cooler) climate (Blackford and Chambers, 1995; Anderson, 1998). Diatom evidence in the upper part of FSU A8 indicates a further rise in the marsh surface to an elevation close to HAT, with a brackish marsh maintained at the PL1 site.

FSU A9

At 385-186 cal.yr.BC, an abrupt phase of estuary expansion is seen to commence at the PL1 site, with the HAT marsh flooded and inundated by lower high saltmarsh sedimentation at increased palaeosalinities. This suggests that there was a significant increase in the rate of RSL at this time that quickly increased the frequency and hydraulic duty of overmarsh tides, due to the lowering of the marsh surface in the tidal frame. East of PL1, the increase in RSL coincides with significant geomorphic activity, with westwards migration of the inner estuarine channel causing erosion of the middle Holocene marsh sequence and incision of the subtidal channel to -3.30m OD (figures 5.4 and 5.5), with deposition of subtidal shelly sands. However, the diatom evidence in the PL1 core indicates that the sharp increase in the rate of RSL rise was only maintained for 100-200 years, with the marsh surface rising again to about MHWST after this period. This suggests a significant oscillation occurred in RSL at this time, followed by a slower rate of rise which allowed a MHWST palaeo-surface to be maintained until 668-869 cal.yr.AD. This later period of FSU A9 sees some aggradation of the inner estuarine channel bed and a gradual eastwards migration of the channel. By 70 +/-160 cal.yr.AD, the western bank of the channel has reached PL2, with channel facies sands deposited by lateral accretion.

During the *c.*1150 year period between channel deposition at PL2 and PL3 (*i.e.* 70 +/-160 cal.yr.AD to 1230 +/-70cal.yr.AD), there is a hiatus in the preserved sedimentary record of channel movement. The channel is thought to have migrated to the east of the valley and then migrated back westwards to the PL3 site during this time. This accounts for the near-vertical erosion surface between PL2 and PL3 in figures 5.4 and 5.15, caused by the westwards erosion of the channel bank during FSU A11 deposition (see below). An alternative scenario (not shown in the lithostratigraphic interpretation given in figure 5.4) would have been for the channel to only migrate the 40m distance between PL2 and PL3. This minimal amount of channel movement over a 1150 year period seems highly unlikely.

FSU A10

This unit starts at 668-869 cal.yr.AD in PL1 and has been correlated with similar changes near the top of PL2. A renewed phase of estuary expansion is seen with the organic MHWST marsh (high saltmarsh - marsh border boundary) being replaced in the west of the transect by more minerogenic sedimentation, although diatom evidence suggests only a small fall in tidal frame position (perhaps 30cm). Diatom evidence also suggests a slight fall in estuarine palaeosalinity. This correlates with up-stream geomorphic evidence of an increasingly wet climate in the 7th and 8th Centuries AD, when discharge levels would have risen, causing a general fall in estuarine salinity. The mineral magnetic results for PL1 indicate an increase in catchment-derived haematite during this unit, suggesting overbank fluvial deposition may contribute to marsh alluviation in the inner estuary during this period. As stated earlier, channel deposits are not preserved for FSU A10, indicating the tidal river had migrated to the east of the valley where the record was removed by later phases of erosion or was buried beneath gravel layers during aggradation of the channel bed.

FSU A11

This phase of sedimentation followed a period of sustained channel aggradation, with the channel bed located at 0.45m OD at PL3, a rise of 2.58m since deposition at PL2. The channel is thought to have initially migrated west from the east of the valley at the start of A11, and then after reaching the PL3 site, migrated back east. This could have been caused by downstream translation of a meander. An inner estuarine environment is maintained in A11, with deposition of shelly channel sands, dated at 1230 +/-70

cal.yr.AD. These are overlain by saltmarsh deposits, accreted after the channel had migrated to the east.

FSU A12

In FSU A12, estuarine channel shelly sands were deposited at the PL4 site. These are overlain by saltmarsh deposits, indicating lateral accretion of the channel facies during channel migration, followed by vertical accretion of marsh sediments. There are two possible scenarios for channel movement from the PL3 site (FSU A11) to PL4. There may have been a meander oscillation on the east of the valley in between deposition of PL3 and PL4, as probably occurred between PL2 and PL3. This scenario is followed in the lithostratigraphic interpretation shown in figures 5.4 and 5.15, with an erosive cutbank boundary separating A11 and A12. However, as the PL4 core was not dated, the channel may equally have simply migrated the 24m east between PL3 and PL4, over a relatively short time period. In this case, the near-vertical erosion surface would not be present.

FSU A13

The tidal channel is then thought to have migrated to FSU A13, on the eastern side of the valley, where estuarine channel sand deposition is continued. The migration of the tidal meander after PL4 deposition, and subsequent migrations indicated in FSUs A14 and A15, suggests high rates of bank erosion during the last *c.*500-600yrs. This suggests a wetter climate and associated high river discharge levels.

FSU A14

Following a migration of the tidal channel to the west, shelly channel sands are deposited at the PL5 site. This is followed by subsequent marsh accretion after the channel is seen to migrate to the east again (FSU A15).

FSU A15

This unit represents the most recent deposition, following eastward migration of the tidal meander from A14. The shelly channel facies in this unit is seen to be finer grained than previous FSU phases, suggesting a lower-energy environment.

As the deposits in FSUs A12 to A15 were not dated, the order of deposition between units, and therefore the tracking of the active channel as it migrated, was based on

sedimentary grounds. Figure 5.4 shows that the top of the shelly channel facies is seen to consistently rise in elevation between A9 and A15. The upper limit of this facies in the modern estuary (chapter 4) was seen to occur in the low saltmarsh. The change in elevation of this facies boundary in FSUs A9-A15 is thought to be related to ongoing RSL rise. This enables the order of FSU deposition to be postulated. Other evidence includes varying degrees of pollution found in the sediments of FSU A14 and A15. The sands and silts between 1.5m and 2.5m depth in A15 are stained black from tide-transported pollution, probably from Barnstaple. This supports this unit being the youngest, with deposition occurring in the 19th Century or early 20th Century. The upper saltmarsh sediments in A14, at 0.5-1.0m depth, are also stained by pollution, though not to such a degree, suggesting overbank deposition at the time of channel pollution in A15. The channel sands at A14 should then be older than A15, possibly early 19th Century. In FSU A13, there are no signs of pollution in the channel facies or the overlying marsh sediments. This suggests that accretion of the marsh had taken place prior to the 19th Century meaning that A13 is older than A14.

5.3 GEOMORPHOLOGY AND STRATIGRAPHY OF THE TAWSTOCK REACH

5.3.1 Reach geomorphology

The geomorphology of the Tawstock reach is shown in figure 5.17. The Taw valley widens in this reach to *c.*600m, with the Holocene floodplain being typically 500m wide. The location of Transect B (Tawstock transect) is shown, along with associated cores TS1, TS2, TS3, CF1, CF2, CH1 and CH2. Transect B is located directly west of Codden Hill, near the village of Bishop's Tawton. The river is tidal throughout this reach, with the active channel remaining on the west of the valley with a straight planform. The river is bounded by flood embankments to protect the enclosed fields which are mainly used for pasture.

Late Pleistocene terraces (T6 and T7) are preserved on both valley sides, with the oldest parts of Bishop's Tawton (the church and Court Farm) built on the terrace surfaces. The coalescence of the low Holocene terraces (T1 and T3) with the naturally tidal floodplain occurs in this reach just south of transect B. Some of the thinner palaeochannels shown on the T3 surface are former flood channels, formed by high-stage overbank flood waters draining back to the active channel. Despite the presence of many drainage ditches, several parts of the floodplain surface are covered in *Juncus* marsh, with some Alder carr preserved just north of TS1. These wetlands are typical of an inner estuarine setting where the proximity to the estuary maintains a high water-table. The marsh on the east of the valley near CH1 is also fed by springs which are seen to seep from the base of T7 (probably at the bedrock-terrace gravel boundary). The strips of unembanked floodplain beside the channel have a mix of high salt marsh flora and salt-tolerant brackish marsh flora (*e.g.* *Phragmites*). This suggests that prior to embanking, most of the enclosed fields would have been occupied by saltmarsh and brackish wetland, especially north of the floodplain-terrace merge zone, as floodplain altitudes south of this point start to rise.

5.3.2 Lithostratigraphy of the Tawstock transect

Figure 5.18 shows the lithostratigraphy of transect B. The floodplain surface is

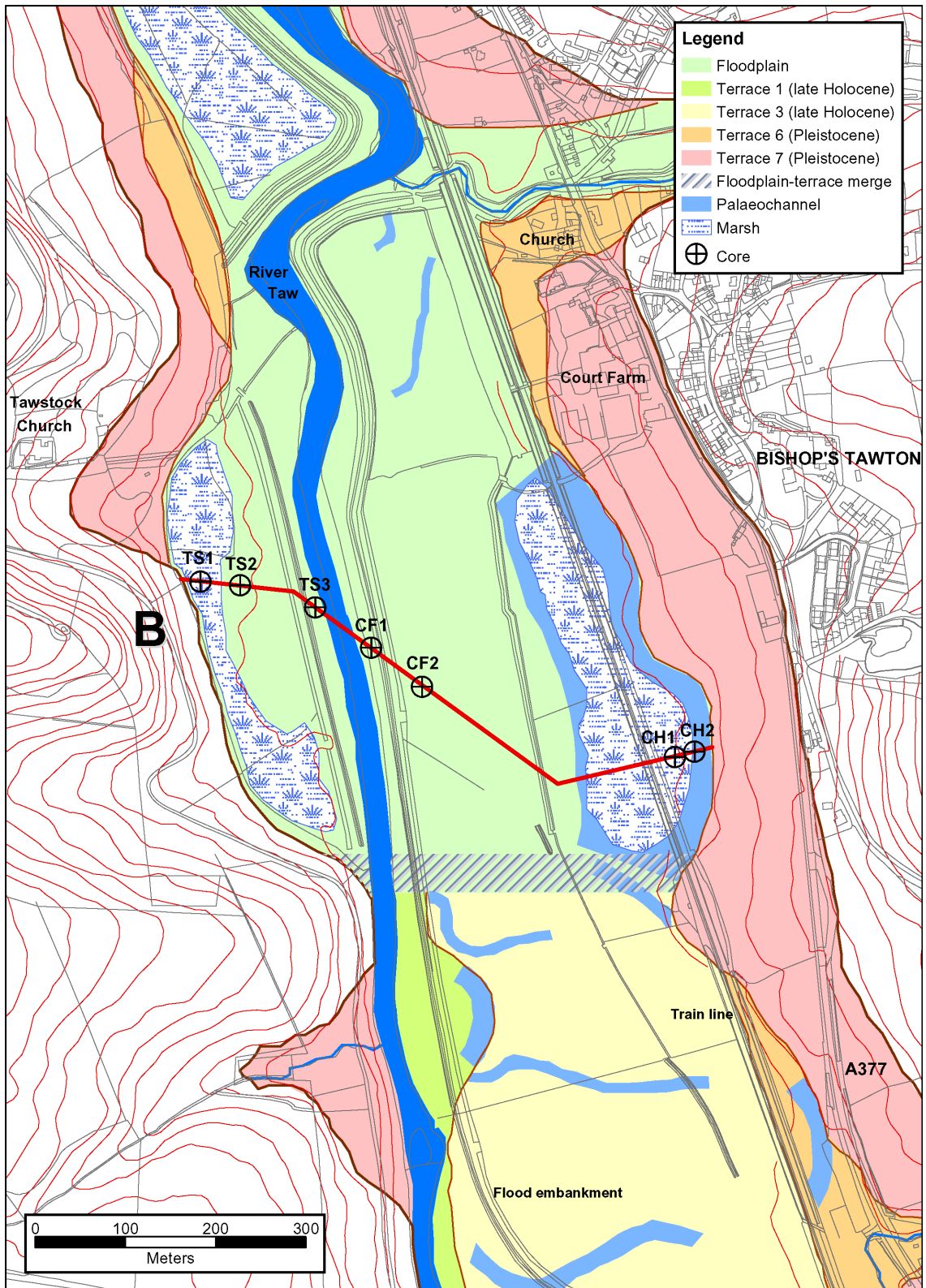


Figure 5.17 Geomorphology of the Tawstock reach. The location of transect B (Tawstock transect) and associated cores are indicated. This map was produced in a GIS and incorporates OS Landform Profile (5m contours) and OS MasterMap layers (supplied by Ordnance Survey/EDINA Digimap).

generally between 4.0 and 4.5m OD, with the mire on the east of the valley rising to 5.35m at CH2. On the east of the valley, a 125m wide *Juncus* mire is underlain by

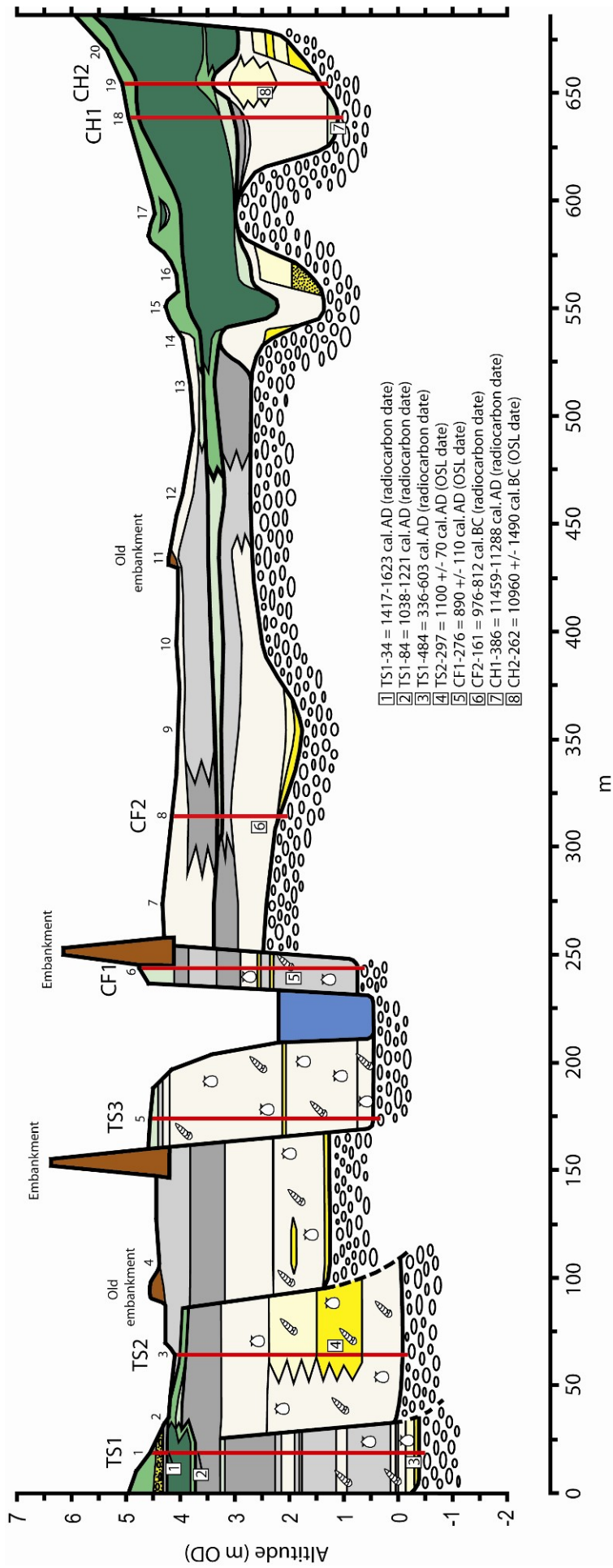


Figure 5.18 Lithostratigraphy of transect B (Tawstock transect). The location of analysed cores, stratigraphic cores (1-20) and radiocarbon/OSL samples (see tables 5.1 and 5.2) is shown. See figure 5.2 for legend.

thick peat deposits, 2.0-2.5m thick. Two wide paleochannels are revealed underneath this peat, predominantly infilled with sandy silt and silty sand. The stratified coarser sand units on the edges of the channels possibly represent relic point bars or lateral bars.

The proximity of these palaeochannels and their similar geometry (wide and shallow) suggest that they were part of the same multi-channeled braided river prior to abandonment. Wood from the gravel surface at the base of the CH1 channel has given an age of 11459-11288 cal.yr.BC, representing initial channel abandonment during the the Late glacial interstadial (Allerød stage). Following deposition of a thin peaty clay at CH1, the channel appears to have been re-occupied by a sand bed river later in the Allerød stage, with a mid-channel sand bar deposit giving an OSL age of 10960 +/-1490 cal.yr.BC for final abandonment at the start of the Younger Dryas stadial.

Between the mire and the active channel zone, the gravel surface is relatively high and is overlain by a thin sequence of overbank sediments. These consist of silty sands, silts and clays, with a laterally persistent thin peat horizon in the middle of the alluvium. Below the peat, the sediment contains many *Phragmites* fragments, suggesting a wetland environment. This marsh sediment was dated in CF2 at 976-812 cal.yr.BC.

The lithostratigraphy on the west of the valley, near the active channel, shows that this area has been the focus of sustained geomorphic change. Five late Holocene phases of incision, channel migration and aggradation have been recognised since the 5th Century AD. Reworking of the tidal floodplain has resulted in the removal of the earlier record, with the oldest deposits found on the valley side at TS1. A radiocarbon date at the base of this deposit gave an age of 336-603 cal.yr.AD. The deposits themselves consist of estuarine shelly sands and silts overlain by finer grained marsh and tidal floodplain overbank alluvium. A period of peat accumulation at the west of this zone (TS1) has been radiocarbon dated, revealing that this organic phase commenced at 1038-1221 cal.yr.AD, and ended at 1417-1623 cal.yr.AD when increased flooding by estuarine water caused the resumption of minerogenic deposition. The dated regressive and transgressive overlaps at the top and bottom of this peat have been used as SLIPs in the sea-level reconstruction presented in chapter 7. The description of the diatom biostratigraphy of PL1 will give verification of changes in marine influence at each of these SLIPs.

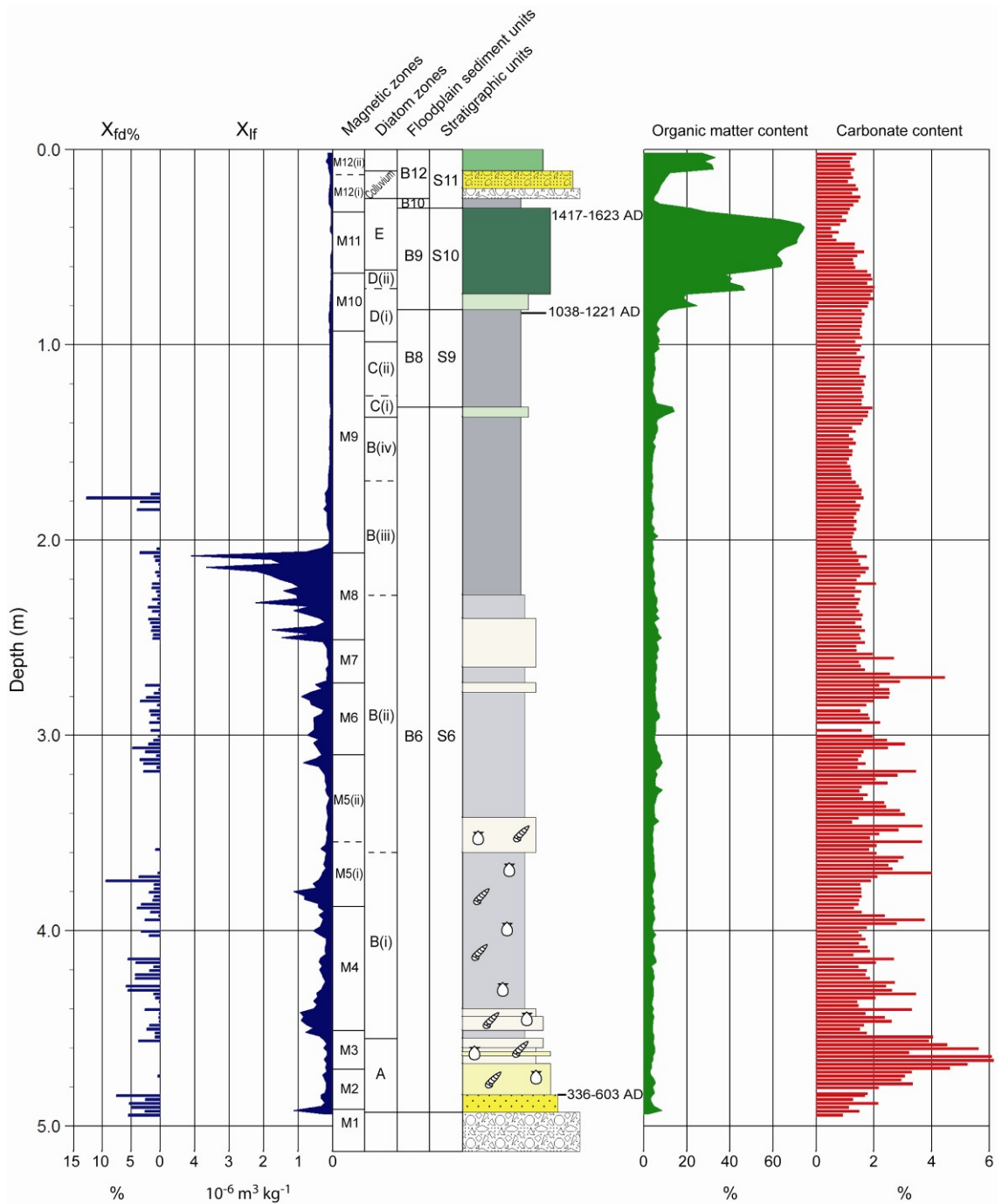


Figure 5.19 TS1 core log. See figure 5.2 for lithology legend. Magnetic zones are derived from figure 5.20, diatom zones are derived from figure 5.21. Floodplain sediment units (FSUs) are discussed in section 5.3.9. Stratigraphic units are discussed in chapter 7.

5.3.3 TS1 core

Sedimentology

Figure 5.19 shows the core log for TS1. This figure shows down-core changes in

sediment lithology, organic matter and carbonate content, X_{lf} and $X_{fd\%}$. In addition, the magnetic and diatom zones (see later), FSUs (see section 5.3.9) and stratigraphic units (see chapter 7) are indicated. The TS1 lithostratigraphy contains several overlaps which were identified for use as SLIPs in the RSL reconstruction.

The TS1 core is underlain by gravel at 4.93m (-0.38m OD). Above this contact, 9cm of well sorted medium quartz sand are deposited, containing some detrital wood (tree branches/ twigs) and leaves. The low carbonate content (c.1.2%) and sediment characteristics suggest fluvial deposition. Above an erosive contact, a fining up sequence of shelly fine sand and silt is deposited between 4.84m and 4.40m. Carbonate content reaches 6% and the deposit suggests estuarine channel deposition, followed by channel abandonment at 4.40m. This unit is overlain by a thick deposit of intercalated grey fine grained sandy silt and silty clay between 4.40m and 2.28m. Sand grade shell fragments are visible in the sediment up to 3.42m suggesting low intertidal estuarine conditions and some connection to the now relocated estuarine channel allowing rapid infilling of the partially abandoned channel. Carbonate values vary between 1.5% and 4%. Higher in this unit (above 3.42m), the sediment is often finely laminated and contains rare rootlets, suggesting relatively rapid further infilling of the channel by tidal sedimentation with occasional plant growth. Carbonate values remain at 1.5-4.0% up to 2.58m, suggesting the continued presence of organic carbonate.

Above 2.28m, fine grained grey silty clay has accreted up to 0.82m with reduced carbonate content values of 1.2-1.7%. The clay contains many fine rootlets and has typical organic matter content values of c.4%, rising to c.7% at 1.02m, where rootlets increase. Within the middle of the clay, at 1.32-1.37m, is a thin peaty clay horizon, with organic matter values temporarily rising to 14%. The clay below this horizon may represent a tidal floodplain or saltmarsh environment, while the upper clay contains *Juncus*, sedge and *Scirpus* fragments, suggesting a brackish wetland.

Between 0.82m and 0.74m, the sediment becomes more organic (organic matter content values of 18-25%) and a peaty clay accumulates. Above a sharp, undulatory contact (possible erosion or rapid change in environment) at 0.74m, a fibrous dark brown peat accumulates up to 0.30m, containing lots of wood (possibly *Alnus*) fragments suggesting an alder carr environment. Organic matter content values reach 73%. Some *Phragmites* fragments appear in the upper 7cm, suggesting a more open environment.

At 0.40m, a wedge shaped alder wood fragment was recovered with signs of being cut by an axe (it does not show the characteristic signs of being cut by a beaver and was not cut by the gouge). This suggests that the Alder carr was being actively coppiced.

The peat is overlain by a thin light grey silty clay deposit, with fine rootlets throughout. The lower peat-clay contact is sharp and undulatory, suggesting erosion. On both sides of the boundary, the sediment is heavily root bioturbated, with clay infilling root voids at the top of the peat, and small pockets of peat present in the lower 3cm of clay. This suggests very low rates of accretion in the clay, allowing time for the sediment to be bioturbated.

Above the clay, a sharp undulatory contact is located at 0.25m, with infilled dessication cracks and manganese mineralisation indicating a hiatus. Above this is a 5cm layer of heavily weathered sandstone and shale gravel (angular 2-29mm clasts) with a clay-silt matrix and rootlet fragments. The deposit appears to be colluvium from the adjacent valley side and grades up into a further 9cm of gravelly silt. The steep valley side is within 20m of this site and bedrock exposures show inter-bedded fissile shales and thin sandstones, with the strata steeply dipping and unstable.

The upper 11cm of sediment above the colluvium is a brown clayey peat, currently covered in *Juncus* marsh. The peat contains some woody tree roots and as an area of surviving Alder carr is located only 10m to the north, was probably initiated in an Alder carr environment prior to recent removal of the woodland.

Geochronology

Wood from the basal sand layer has been radiocarbon dated, giving an age of 336-603 cal.yr.AD for the latest stage of channel activity prior to channel abandonment. A seed from the top of the silty clay at 0.84m was radiocarbon dated and gave an age of 1038-1221 cal.yr.AD for the regressive overlap and transition to peat deposition. At the transgressive overlap at the top of the peat (0.34m), a wood sample gave an age of 1417-1623 AD for final peat deposition.

Magnetic properties

Figure 5.19 shows X_{if} values for TS1 (at 2cm resolution) and $X_{fd\%}$ for those samples that had a K_{if} value of $>25.0 \cdot 10^{-5} \text{ m}^3 \text{ kg}^{-1}$. A suite of mineral magnetic remanence measurements were also done on 80 samples from TS1 (c.6cm resolution). The results of these measurements and derived parameter ratios/quotients are shown in figure 5.20. Tables 3.2 and 3.3 were used in the identification of magnetic mineral components and constrained cluster analysis (CONISS) was used to divide the core into 12 magnetic zones (M1 to M12).

Zone M1 (4.91m – 5.05m)

This zone corresponds with the basal 2cm of the fluvial sand at the base of TS1 and is thought to be more associated with the underlying gravel than the sediment sequence above. The high X_{if} value indicates a significant concentration of ferrimagnetic minerals, or, if they are not present, antiferromagnetic minerals. However, the SIRM value is low, as are the X_{arm} and $X_{fd\%}$ (2.6%). Low values in these three parameters collectively indicate an MD dominated assemblage with low SSD concentration and virtually no SP grains. IRM_{soft} and IRM_{int} values are low, while IRM_{hard} and the S-ratio are high. This indicates a high concentration of antiferromagnetic minerals (haematite), supported by the very high SIRM- IRM_{300mT} /SIRM value. This would support a sedimentary link with the underlying fluvial gravels.

Zone M2 (4.71m – 4.91m)

This zone corresponds with the basal quartz sand (above 4.91m) and the bed of shelly fine sand bed above this. Carbonate values gradually rise to 5.3% in this zone. In this zone X_{if} values fall to moderate levels ($0.2\text{-}0.3 \cdot 10^{-6} \text{ m}^3 \text{ kg}^{-1}$), while other concentration-related parameters rise, suggesting an increase in ferrimagnetic minerals. X_{arm} values rise, indicating the presence of SSD magnetite. $X_{fd\%}$ values show some variation from 0.5% to 7.5%, suggesting there is some variation in the concentration of SP grains within the assemblage. Both IRM_{soft} and IRM_{hard} are relatively high, indicating a mixed ferrimagnetic-antiferromagnetic mineral assemblage. However, the low S-ratio indicates ferrimagnetic magnetite dominance. Increasingly high X_{arm} /SIRM values indicate that SSD or SP magnetite dominates the ferrimagnetic component in the shelly sand, suggesting transported estuarine bacterial magnetite may be present. A small peak in IRM_{20mT}/IRM_{300mT} also suggests fine grained magnetite of a fine viscous SD (SSD/SP

boundary) grain size. This zone therefore indicates a more fluvio-estuarine location than that seen in PL1, with magnetic minerals sourced from both the catchment and estuary.

Zone M3 (4.50m – 4.71m)

This zone corresponds with the peak in carbonate content (4-6%) in the basal channel sands. The most notable feature of this zone is the very high X_{arm} values, indicating the assemblage is dominated by SSD magnetite (there are no collective indications of SSD greigite). This is also indicated by very high X_{arm}/X values. The very high $X_{arm}/SIRM$ values suggest that this SSD magnetite has a bacterial origin. In this coarse grained sediment, it is unlikely to have formed in-situ, so is probably sourced from further out in the estuary. The overall concentration of this magnetite is not high however, shown by the moderate X_{lf} values. Ferrimagnetic dominance is also seen in the low S-ratio. Relatively high IRM_{hard} values suggest that haematite also contributes to the assemblage, indicating a continuing fluvio-estuarine location with sediment sourced from the catchment and estuary.

Zone M4 (3.88m – 4.50m)

This zone corresponds with the lower part of the shelly silt. An initial peak in X_{lf} , SIRM and IRM_{soft} , combined with lows in grain size parameters $X_{fd\%}$, X_{arm}/X and $X_{arm}/SIRM$ suggest a significant contribution by MD magnetite at this horizon. This is supported by a peak in IRM_{20mT}/X_{arm} . The rest of the zone has moderate levels in the concentration-related parameters X_{lf} , SIRM, IRM_{soft} and IRM_{hard} , combined with a low S-ratio, suggesting the assemblage is dominated by ferrimagnetic magnetite but also has a significant antiferromagnetic (haematite) contribution. The relatively high X_{arm} values suggest SSD dominance in the magnetite, with low $X_{fd\%}$ (<6%) and $X_{arm}/SIRM$ values indicating very minor amounts of fine viscous SSD/SP grains. Low IRM_{20mT}/X_{arm} values also indicate SSD dominance (in both the magnetite and haematite components), with little contribution by MD grains. This assemblage suggests the sediment was predominantly sourced from the estuary on flood tides, but the significant haematite component also indicates a fluvio-estuarine transitional environment with some sediment sourced from the catchment.

Zone M5 (3.09m – 3.88m)

Cluster analysis suggests a lot of similarity within this zone. However, there are some differences in the concentration-related parameters and zone M5 has been divided into

two subzones. Zone M5(i) largely corresponds with the top of the shelly silt, while M5(ii) corresponds with the non-shelly silt with occasional roots.

In M5(i), X_{lf} values remain similar to zone M4, but SIRM, IRM_{soft} and especially IRM_{hard} all show significant rises, indicating an increase in the concentration of both magnetite and especially haematite. However, the low S-ratio indicates that magnetite remains the dominant component. The magnetite is dominated by SSD grains, as indicated by high X_{arm} and X_{arm}/X values. The TS1 site was therefore still located in a fluvio-estuarine environment with mixing of estuarine and fluvial waters (and their respective suspended sediment loads).

In M5(ii), the concentration of magnetic minerals in the sediment falls to low levels, as indicated by low X_{lf} and SIRM values. IRM_{soft} values also become low, but IRM_{hard} values remain at moderate levels suggesting the assemblage is dominated by the antiferromagnetic mineral haematite. This is supported by a rise in the S-ratio and a corresponding rise in SIRM- IRM_{300mT} /SIRM values. This indicates high-stage overbank flooding provides the largest contribution to sedimentation. Moderate X_{arm} values and a rise in $X_{arm}/SIRM$ suggests a smaller, but significant contribution by bacterial magnetite, which unlike in the channel sands below, is now possibly formed in-situ, within an abandoned estuarine channel environment.

Zone M6 (2.74m – 3.09m)

This zone corresponds with further clayey silt deposition. X_{lf} values rise in this zone, indicating an increase in ferrimagnetic mineral concentration. A peak in SIRM at the bottom of the zone correlates with corresponding sharp rises in IRM_{soft} and IRM_{hard} , indicating a mixed ferrimagnetic-antiferromagnetic assemblage of mixed estuary-catchment provenance. The S-ratio is low, indicating magnetite dominance, but it should be remembered that ferrimagnetic minerals contribute much more to IRM than similar concentrations of antiferromagnetic minerals, so haematite may still form a significant part of the assemblage. A small rise in X_{arm} , combined with rises in SIRM/ X and IRM_{20mT}/X_{arm} suggests a mixed SSD and MD grain assemblage, with little contribution by SP grains (low $X_{fd\%}$ and $X_{arm}/SIRM$).

A second sharp rise in SIRM at the top of the zone also correlates with peaks in IRM_{soft} and IRM_{hard} , suggesting a mix of ferrimagnetic and antiferromagnetic minerals, although

ferrimagnet dominance is indicated by a low S-ratio. However, there are also large rises in IRM_{int} , $SIRM/X$ and $SIRM/X_{arm}$, indicating the presence of the ferrimagnetic mineral greigite. This is supported by a reverse field divergence (similar back field divergences further down the core did not have the other indicators for greigite). The relatively high X_{arm} and very low $X_{fd\%}$ values suggest that the greigite is dominated by SSD grains. This is likely to have formed in-situ and may be authigenic or biogenic (bacterial). The high IRM_{hard} also indicates a contribution by haematite which may have a mixed SSD-MD grain size assemblage, as shown by a small peak in IRM_{20mT}/X_{arm} . The assemblage is therefore dominated by SSD greigite, indicating an estuarine environment. However, the significant haematite contribution indicates an inner estuary fluvio-estuarine environment is maintained.

Zone M7 (2.49m – 2.74m)

This zone corresponds with further silt deposition and is very similar to zone M5(ii) in its magnetic properties. The concentration of magnetic minerals in the sediment falls to low levels again, as indicated by low X_{lf} and SIRM values. IRM_{soft} and IRM_{hard} values fall to moderate levels, indicating a mixed ferrimagnetic-antiferromagnetic assemblage of magnetite and haematite. A higher contribution by catchment haematite is indicated by a rise in the S-ratio and a corresponding rise in $SIRM-IRM_{300mT}/SIRM$ values. Moderate X_{arm} values and a significant rise in $X_{arm}/SIRM$ suggests the magnetite has a bacterial origin, which like in M5(ii), is probably formed in-situ (secondary origin).

Zone M8 (2.07m – 2.49m)

This zone corresponds with the start of reduced carbonate content values, encompassing the final phase of silt deposition and the start of silty clay marsh sedimentation. Zone M8 sees X_{lf} values rise to very high levels ($2.2 \cdot 10^{-6} \text{ m}^3 \text{ kg}^{-1}$) indicating a high concentration of magnetic minerals. The S-ratio shows a great deal of variation within the zone, indicating several phases of ferrimagnetic and antiferromagnetic dominance. SIRM values also vary, but high values are seen to correlate with the ferrimagnetic mineral dominated phases (low S-ratio and peaks in IRM_{soft}) which carry more remanence. Conversely, peaks in $SIRM-IRM_{300mT}/SIRM$ correlate with the high S-ratio phases, supporting the presence of haematite in these horizons. X_{arm} , $X_{fd\%}$, X_{arm}/X and $X_{arm}/SIRM$ values are all generally low, indicating only minor amounts of SSD or SP grains in the assemblages. This is supported by a rise in the MD indicative parameter IRM_{20mT}/X_{arm} . The lowest ferrimagnet phase in the zone correlates with peaks in IRM_{int} .

SIRM/X and SIRM/ X_{arm} , and with a reverse field divergence, all indicating the presence of greigite.

Zone M8 therefore contains several horizons where MD ferrimagnetic minerals are dominant (both magnetite and greigite) and several horizons where MD haematite is dominant. This suggests that the marsh surface was inundated by sediment derived from two separate sources. The MD magnetite is likely to have been introduced in estuarine tidal water, while the haematite was deposited in fluvial high-stage floods, with sediment derived from the catchment. The greigite may have formed authigenically in-situ or be tidally derived from re-worked sediment further out in the estuary.

Zone M9 (0.94m – 2.07m)

This zone corresponds with the silty clay marsh sediment below the upper peat (including the thin peat horizon). X_{lf} and SIRM values are very low in this zone, indicating very low concentrations of magnetic minerals in the sediment. This may indicate that the marsh surface had reached a mid-high saltmarsh tidal frame position. The only concentration-related parameter to indicate remanence carrying minerals is IRM_{hard} , which has moderate values throughout this zone. This indicates that the small magnetic assemblage present is dominated by antiferromagnetic minerals. This is supported by a significant rise in the S-ratio and consistently high SIRM- IRM_{300mT} /SIRM values, both indicating dominance by haematite. IRM_{soft} values are very low throughout the zone, as are X_{arm} values, indicating very little magnetite is present. Relatively high IRM_{20mT}/X_{arm} values suggest the haematite is predominantly MD grains, indicating a primary detrital origin (Dearing, 1999).

Zone M10 (0.63m – 0.94m)

This zone corresponds with the uppermost part of the silty clay, where organic matter rises, and the lower part of the peat, which is more minerogenic. As in zone M9, all concentration-related parameters remain low apart from a low IRM_{hard} signal, which declines through the zone. High S-ratio and IRM_{20mT}/X_{arm} values correspond with the higher IRM_{hard} values, indicating the continuing presence of haematite in the uppermost clay and overlying clayey peat layer. A rise in X_{arm} /SIRM in this zone suggests the very small IRM_{soft} signal is created by SSD or SP magnetite of a probable bacterial origin. A small magnetic assemblage, dominated by bacterial magnetite, has so far been shown to consistently occur in the organic deposits just below MHWST and above.

Zone M11 (0.33m – 0.63m)

This zone corresponds with the organic peat. X_{if} and SIRM values remain very low, indicating low concentrations of ferrimagnetic mineral. The IRM_{hard} signal disappears and is replaced by a small rise in IRM_{soft} values, indicating the presence of ferrimagnetic minerals. This is supported by a low S-ratio and low IRM_{20mT}/X_{arm} values, indicating the small assemblage is dominated by magnetite. Large rises in SIRM/X (which can be grain size dependent), X_{arm}/X and $X_{arm}/SIRM$ values indicate that the magnetite has an SSD grain size, of possible in-situ bacterial origin. High IRM_{20mT}/IRM_{300mT} values also suggest a fine grain size (fine viscous SD grains).

Zone M12 (0.00m – 0.33m)

This zone has been divided into two subzones, with M12(i) corresponding with the thin clay and overlying colluvium, and M12(ii) corresponding with the surface peat.

M12(i) sees a slight rise in X_{if} values, suggesting an increase in the magnetic mineral concentration. A significant rise in IRM_{hard} points to antiferromagnetic minerals being the main source of this X_{if} signal. This is supported by a large rise in the S-ratio (to positive values) and a large rise in SIRM- $IRM_{300mT}/SIRM$ values, both indicating the presence of antiferromagnets (haematite). The small magnetic assemblage appears to be similar to that seen below the peat in zone M9, suggesting a similar depositional environment. The colluvium IRM_{hard} values are significantly higher than the clay, suggesting a higher concentration of haematite. This is probably due to the proximal primary origin of the sediment.

M12(ii) sees similar X_{if} values but also a small rise in SIRM. IRM_{hard} values remain relatively high, but are joined by rises in IRM_{soft} and X_{arm} , indicating a mixed ferrimagnetic-antiferromagnetic assemblage. This is supported by a fall in the S-ratio and SIRM- $IRM_{300mT}/SIRM$ to mixed assemblage values. Therefore, detrital haematite remains a significant assemblage component, but a rise in X_{arm} , X_{arm}/X , $X_{arm}/SIRM$ and IRM_{20mT}/IRM_{300mT} values indicate a fine grained magnetite component is present of SSD (X_{arm} , X_{arm}/X), fine viscous SD (IRM_{20mT}/IRM_{300mT}) and possibly SP ($X_{arm}/SIRM$) grain size. This suggests secondary bacterial magnetite and soil-derived SSD/SP magnetite which were both probably formed in-situ (the soil derived component could have been confirmed if X_{if} values were high enough to allow reliable $X_{fd\%}$ measurements).

Diatom analysis

As the diatom record of TS1 is being used to validate two potential SLIPs located at transgressive and regressive overlaps, the bio-stratigraphy is especially important as it is used to verify changes in marine influence at these overlaps.

Figure 5.21 shows a diatom diagram for TS1. All species with counts of >3%TDV are shown, along with the diatom sums. Cluster analysis resulted in five diatom zones (A to E). Diatom valves were found to be well preserved and relatively abundant throughout most of TS1 apart from in the peat where they were sparse, and in the basal channel sand, where they were fragmented and present in low concentrations.

Zone A (4.55m – 4.93m)

This zone corresponds with the basal estuarine channel sands. Polyhalobous taxa dominate the zone with a sum total of 59%, with smaller sums for mesohalobous taxa (14%) and oligohalobous indifferent species (12%) being dominated by the brackish planktonic *Cyclotella striata* (>5%TDV) and various freshwater species (*Synedra ulna* being the most abundant at 4%TDV). The polyhalobous group consists of planktonic and tychoplanktonic species, with *Actinoptychus senarius*, *Coscinodiscus radiatus*, *Paralia sulcata* and *Podosira stelligera* all present at >10%TDV. This dominance by marine and brackish planktonics suggests a low intertidal/subtidal environment with high salinities due to fluvial discharge being relatively minor compared with the large tidal prism.

Zone B (1.37m – 4.55m)

This large zone corresponds with the estuarine silts (probably representing rapid infilling of the abandoned tidal channel) and the overlying marsh sediments up to the thin peat horizon at 1.37m. Cluster analysis indicates a similar diatom flora for the whole of the zone, but also shows four sub-groups that have been used to divide this zone into four subzones. These correlate well with the sedimentary divisions of shelly silt (B(i)), non-shelly silt with rare rootlets (B(ii)), and the silty marsh clay (B(iii) and B(iv)).

Polyhalobous planktonics/tychoplanktonics dominate the zone at 42-76% (mean = 60%) abundance, with *Paralia sulcata* and *Podosira stelligera* present at >10%TDV

throughout the zone. The rest of the marine assemblage remains diverse, with at least four other planktonics present at >5%TDV in subzones B(i) to B(iii). However, in subzone B(iv), *Paralia sulcata* and *Podosira stelligera* are only joined by two other polyhalobous species at >5%TDV (*Actinoptychus senarius* and *Rhaphoneis amphicerus*), indicative of the correlation between tidal frame position and marine species diversity seen in the Taw Estuary (the reduction taking place in the low saltmarsh zones).

Mesohalobous and indifferent species numbers remain at low levels (11-22% and 5-17% respectively), suggesting deposition at tidal flat and low-mid saltmarsh elevations. The epiphytes *Synedra ulna* and halophilous *Epithemia turgida* are seen to be present in highest numbers in zones B(iii) and (Biv), giving support to a vegetated low-mid saltmarsh environment in the silty clay.

Zone C (0.98m – 1.37m)

This zone has been divided into two subzones with subzone C(i) corresponding with the thin peaty clay horizon and subzone C(ii) corresponding with the bulk of the overlying silty clay deposit.

In the C(i) peaty clay layer, the DSI value of 0.56 is indicative of a mixed marine-brackish-freshwater assemblage, indicating a significant reduction in marine influence. This is seen in the diatom group sums with polyhalobous taxa falling to 30%, and the oligohalobous indifferent sum rising to 24%. A significant rise in halophilous numbers is also seen, rising to 9%. *Paralia sulcata* (>10%TDV) and *Podosira stelligera* (>5%TDV) are the only dominant marine planktonics present, and this is similar to the Taw Estuary high saltmarsh zone around MHWST. *Cyclotella striata* is replaced by *Navicula peregrina* (>10%TDV) in the mesohalobous group, suggesting a rise in tidal frame position to just below MHWST (lower high saltmarsh zone) or above. Rises in halophilous *Navicula eidrigeana* and salt-tolerant *Navicula cari* (present in the high saltmarsh Taw Estuary zone) numbers also suggest a high saltmarsh environment close to MHWST. The organic matter content value of 14% is similar to the Taw Estuary lower high saltmarsh zone (just below MHWST) and this tidal elevation is proposed for this subzone.

Subzone C(ii) shows a return to silty clay deposition and the diatom assemblages show

some similarities with zone B(iv), with polyhalobous planktonics becoming dominant again (60%), joined by the mesohalobous planktonic *Cyclotella striata* at >10%TDV. This indicates an increase in marine influence. Freshwater and halophilous species fall to low levels (5% and 2% respectively), suggesting a fall in tidal frame position. However, the mesohalobous species *Nitzschia navicularis* is seen in large numbers in this subzone (>10%TDV). As has been stated earlier, this epipelagic species was seen in relatively higher numbers in the Taw Estuary at the mid-high saltmarsh boundary and various studies (e.g. Hill *et al.*, 2007) have recorded this elevation as its optimum. A fall in tidal frame position to a mid saltmarsh environment (approximately MHWST-90cm) is therefore proposed for subzone C(ii).

The thin peat layer in subzone C(i) contains a regressive overlap at its base and a transgressive overlap at its upper boundary. Although the diatom evidence shows these overlaps relate to changes in marine influence, they were not dated, therefore cannot be used as SLIPs. However, the transgressive overlap is thought to correlate with the 684-777 cal.yr.AD (1-sigma age) transgressive overlap seen in PL1. This will be discussed further in chapter 7.

Zone D (0.59m – 0.98m)

This zone has been divided into two subzones. Subzone D(i) corresponds with the uppermost part of the silty clay (where root density increases) and the peaty clay (c.20% organic matter content) at the base of the upper peat. The silty clay and peaty clay are separated by a regressive overlap, dated at 1038-1221 cal.yr.AD. DSI values rise from 0.51 to 0.61 across this overlap, indicating a fall in marine influence. Subzone D(ii) corresponds with the lower part of the more organic peat. Figure 5.19 indicates that the D(ii) peat horizon has a larger minerogenic component (c.40% organic matter) than the zone E peat above (>60% organic matter).

At the base of subzone D(i), in the silty clay, the polyhalobous sum falls significantly to 25% from the previous 60% value in subzone C(ii), with only *Paralia sulcata* attaining >5%TDV abundance, and with *Podosira stelligera* at 4.5%TDV and *Actinoptychus senarius* at 4%TDV. This suggests a rise in tidal frame position to the zone around MHWST. The mesohalobous sum rises to 36% and is dominated by rises in *Diploneis interrupta* and *Navicula peregrina* (both to >10%TDV). The aerophilous species *Diploneis interrupta* has been recorded in optimum abundance at MHWST (Shennan *et*

al., 1995; Zong and Horton, 1998, 1999), suggesting the marsh palaeo-surface has accreted into the high saltmarsh zone. The oligohalobous indifferent sum rises to 23% and is dominated by the epipellic species *Diploneis elliptica* (>5%TDV) and the aerophilous species *Stauroneis anceps*. *Diploneis elliptica* appears to be somewhat salt-tolerant as it was found in both high saltmarsh and marsh border assemblages in PL1. Considering the reduced, but significant, marine planktonic assemblage component, and the relatively low organic matter content in the silty clay, a lower high saltmarsh elevation is proposed for the base of subzone D(i), at about MHWST-50cm.

In the peaty clay (0.74-0.82) at the top of subzone D(i), the DSI value rises to 0.61, indicating a mixed assemblage with brackish-freshwater dominance. The polyhalobous sum falls further to 18-20%, indicating decreasing marine influence, with the planktonics *Paralia sulcata* present at >5%TDV at the start of the zone, and *Podosira stelligera* present at 3%TDV throughout. The mesohalobous and oligohalobous indifferent sums remain at similar levels to the silty clay below, but there is a significant rise in halophilous species to 11%. This is mainly due to the appearance of *Navicula pusilla* at >5%TDV and *Navicula eidrigeana* at 4.5%TDV. *Navicula eidrigeana* has consistently been seen to appear in core assemblages in this study at around MHWST. *Navicula pusilla* was seen in the Taw Estuary at just below MHWST and above, and as mentioned earlier, has been recorded in various studies between MHWST and HAT (e.g. Nelson and Kashima, 1993; Shennan *et al.*, 1995). The mesohalobous group is dominated by *Navicula peregrina* at 17-23%TDV, again suggesting a tidal frame elevation of MHWST or above. The salt-tolerant freshwater taxa *Diploneis elliptica* remains the dominant freshwater species. The assemblage characteristics in the peaty clay therefore suggest an elevation just above MHWST (equivalent to the Taw Estuary marsh border). This indicates that the tidal frame position of the marsh surface continues to rise during subzone D(i) deposition.

In the subzone D(ii) peat, the polyhalobous sum falls to 6.5%, with none of the marine planktonics present at >2%TDV. The indifferent and halophilous groups remain at similar numbers to zone F, while the mesohalobous group becomes dominant at 45%. This is due to *Navicula peregrina* numbers increasing to 41%TDV, making it by far the most dominant species in the assemblage. The halophiles *Navicula pusilla* and *Navicula eidrigeana* remain in slightly reduced numbers, being partly replaced by the epiphyte *Epithemia turgida* (4%TDV). In the freshwater indifferent group, *Diploneis elliptica*

abundance falls to 3%TDV and *Pinnularia major* and *Pinnularia viridis* appear at >5%TDV and 3.5%TDV respectively. The dominance by epiphytic and aerophilous taxa in the oligohalobous groups indicates that the largely autochthonous marsh assemblage is experiencing fewer periods of tidal inundation, caused by the brackish marsh accumulating further above MHWST. The dominance by *Navicula peregrina* suggests a close proximity to a saline environment. The numbers recorded in this core and in peats in PL1, suggest its optimum is slightly higher in the Taw Estuary than that seen in some other studies (e.g. Shennan *et al.*, 1995; Zong and Horton, 1999). The assemblage in subzone D(ii) therefore represents deposition in a brackish marsh located between MHWST and HAT (possibly at 30-40cm above MHWST).

Zone E (0.25m – 0.59m)

This zone incorporates both the organic peat and overlying silty clay (deposited below the colluvium). A transgressive overlap, dated at 1417-1623 cal.yr.AD, separates the organic and minerogenic units. As noted earlier, the sedimentary and plant macro-fossil evidence suggest that most of the peat accumulated in an Alder carr environment, with a more open reedwamp developing in the later stages of peat accumulation. DSI values fall from 0.80 in the Alder carr peat to 0.76 in the reedswamp peat to 0.60 in the overlying silty clay. This indicates the peat contains a freshwater species dominated assemblage with a significant brackish component, while the silty clay contains a mixed marine-brackish-freshwater diatom assemblage.

There is a significant rise in the oligohalobous indifferent group sum to 31-42% in zone E, with a diverse group of freshwater indifferent species present. Halophilous and polyhalobous taxa remain at similar levels to subzone D(ii), while the mesohalobous group falls to 14%, mainly due to a decrease in *Navicula peregrina* to 8-10%TDV. In the halophilous group, *Navicula pusilla* and *Navicula eidrigeana* are joined by the aerophilous species *Diploneis ovalis* at 4%TDV. This species was given an optimum of MHWST in the quantitative study by Zong and Horton (1999). However, *Diploneis ovalis* is very tolerant of a wide range in salinity (Nelson and Kashima, 1993), and other studies have recorded optimum abundance above MHWST in the marsh border zone (e.g. Nelson and Kashima, 1993). Zong (1997) recorded *Diploneis ovalis* in core assemblages associated with deposition closer to HAT. The dominant species in the oligohalobous indifferent group are *Cocconeis placentula*, *Pinnularia abaujensis* and *Pinnularia major*, all at >5%TDV. These are joined by *Eunotia pectinalis*, *Pinnularia*

viridis and *Synedra ulna*, all at >4%TDV. This large freshwater flora suggests the marsh/Alder carr palaeo-surface is now close to HAT. However, the diatom assemblage does contain some marine planktonics with *Podosira stelligera* reaching 6%TDV at the start of the zone, indicating that the marsh was still occasionally inundated by high tides.

In the thin silty clay above the transgressive overlap, the polyhalobous group sum rises to 24%, with other rises in the mesohalobous group (to 24%) and halophilous group (to 11%) indicating an increase in marine influence. The oligohalobous indifferent sum falls to 24%. The assemblage at the top of zone E represents a brackish environment (DSI = 0.60), reflected in the dominant species coming from all diatom groups. The dominant polyhalobous taxa are the planktonics *Paralia sulcata* and *Podosira stelligera* (both >5%TDV), along with *Actinoptychus senarius* at 4%TDV. The mesohalobous group remains dominated by epipellic *Navicula peregrina* (>10%TDV) and the halophilous group becomes dominated by aerophilous *Navicula pusilla* (9%TDV). The oligihalobous indifferent group is dominated by the robust and wide ranging epiphyte *Cocconeis placentula* (>5%TDV), along with the epiphyte *Synedra ulna* at 3.5%TDV. The halophobe *Pinnularia subsolaris* also emerges at 4%TDV. The general dominance by marine and brackish species suggests relatively frequent inundation by tides in the upper intertidal zone. In the Taw Estuary, both *Paralia sulcata* and *Podosira stelligera* were not found in >5%TDV numbers above MHWST, and the highest recording of *Actinoptychus senarius* was the upper high saltmarsh, just below MHWST. This suggests a high saltmarsh depositional environment. This is supported by the brackish groups being dominated by *Navicula pusilla* (recorded in the Taw Estuary high saltmarsh zone) and *Navicula peregrina* (associated with just below MHWST and above). Because of the low organic matter content, a lower high saltmarsh zone environment is proposed for the silty clay layer (*i.e.* 40-60cm below MHWST), indicating a large change in tidal frame position at the end of zone E, with lower high saltmarsh silt deposition replacing the earlier organogenic deposition of an Alder carr and reedswamp environment.

5.3.4 TS2 core

Sedimentology and magnetic properties

Figure 5.22 shows the core log for TS2. This figure shows down-core changes in sediment lithology, X_{if} , organic matter and carbonate content. In addition, the diatom zones (see later), FSUs (see section 5.3.9) and stratigraphic units (see chapter 7) are indicated.

The TS2 core is underlain by gravel at 4.19m (-0.08m OD). Between 1.74m and the basal gravel is a thick deposit of shelly laminated sand. The lower part, below 3.44m, contains planar normal graded laminations (10-15mm, fine-medium sand grading to silty fine sand), indicative of the regular changing tidal and fluvial flow velocities in a tidal regime. A middle coarser unit (2.61m – 3.44m) contains a higher percentage of fine-medium sand (60%) and shows wavy lamination, indicative of both changing flow velocities and migrating ripple bedforms. The upper part of the sand (1.74m – 2.61m) is predominantly fine sand with occasional laminae/lenses (up to 15mm) of fine-medium sand. These shelly sand units represent inner estuarine (tidal river) channel deposits. Carbonate content values are generally *c.*6%, so lower than that seen in the channel deposits of Transect A.

Between 0.88m and 1.74m is a unit of grey laminated silty fine sand. The sediment contains many *Phragmites* fragments, especially above 1.19m, suggesting some in-situ growth, and is shelly below 1.30m (4.7% carbonate content). The modern flora in this area is dominated by *Phragmites* at tidal elevations equivalent to the pioneer saltmarsh zone in the Taw Estuary, indicative of the less saline environment in this inner estuarine environment. This unit is thought to represent deposition at tidal frame elevations equivalent to the pioneer and low saltmarsh zones.

Between 0.22m and 0.88m, a laminated grey silty clay with many oxidised rootlets and plant fragments (grass and sedge) has been deposited. Carbonate content is *c.*1.5%. This sediment is thought to represent a brackish sedge marsh, deposited below MHWST. Between 0.10m and 0.22m, a brown silty peat (33% organic matter content) has accumulated, suggesting organic deposition above MHWST. Above 0.10m, an organic grey-brown clayey silt has been deposited, containing many rootlets (18% organic

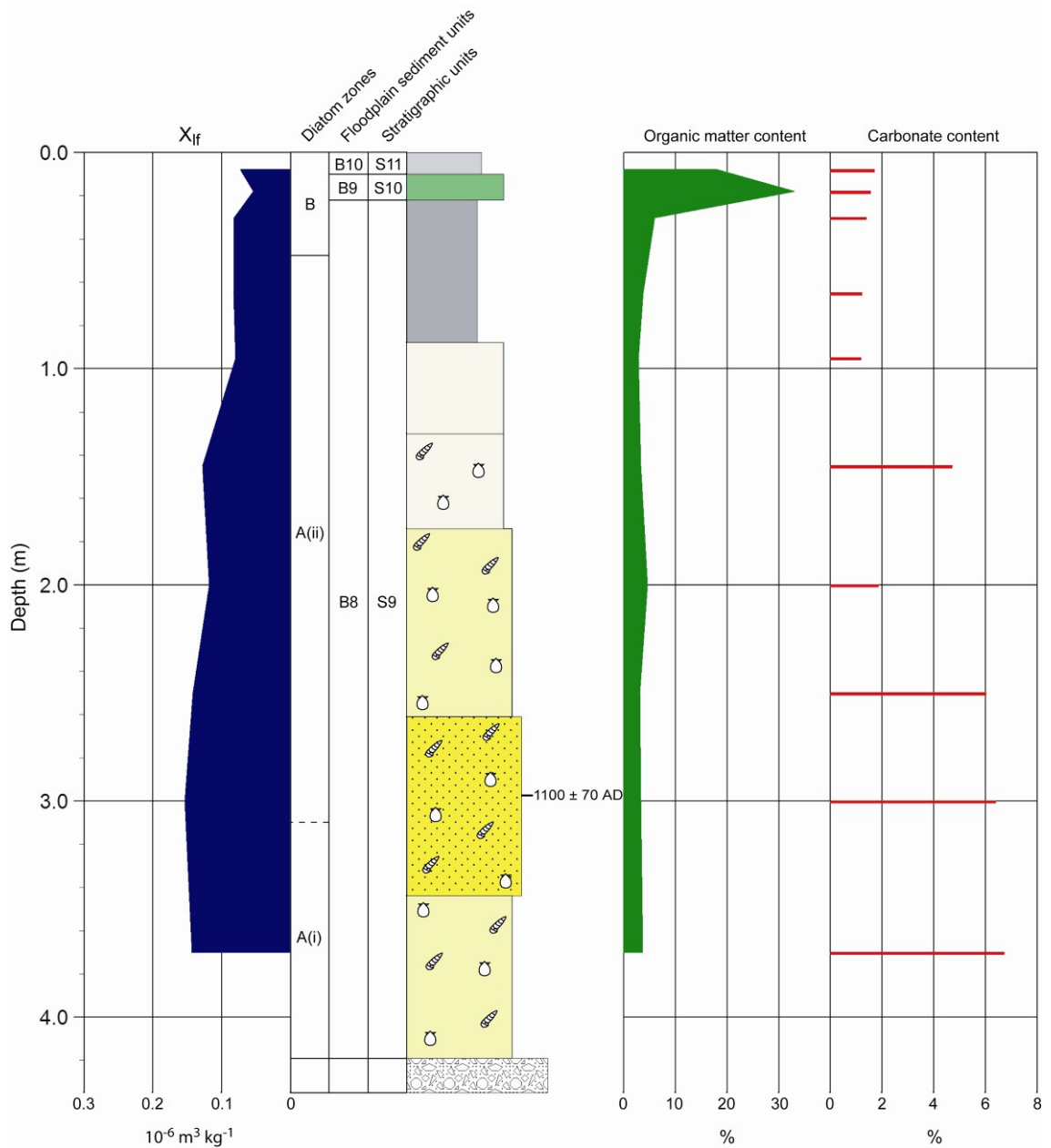


Figure 5.22 TS2 core log. See figure 5.2 for lithology legend. Diatom zones are derived from figure 5.23. Floodplain sediment units (FSUs) are discussed in section 5.3.9. Stratigraphic units are discussed in chapter 7.

matter content at its base). Magnetic mineral concentrations are low throughout this core as, with typical X_{lf} values of $0.13\text{-}0.15 \times 10^{-6} \text{ m}^3 \text{ kg}^{-1}$ in the shelly sands and silts, falling to $c.0.08 \times 10^{-6} \text{ m}^3 \text{ kg}^{-1}$ in the overlying fines.

The basal sands in this core represent estuarine channel sediments, laterally accreted during channel migration, followed by vertically accreting marsh sediments which show a gradual rise in tidal frame position, before flooding of the marsh palaeo-surface at 0.10m.

Geochronology

The middle of the lower channel sands have been OSL dated, giving an age of 1100 +/- 70 cal.yr.AD for channel activity at this location.

Diatom analysis

Figure 5.23 shows a diatom diagram for TS2. All species with counts of >3%TDV are shown, along with the diatom sums. Cluster analysis resulted in two diatom zones (A and B). Diatom valves were found to be well preserved and relatively abundant throughout most of TS2, except for the lower part of the silty clay unit, where valves were present in low concentrations.

Zone A (0.47m – 4.19m)

This large zone has been divided into two subzones with subzone A(i) corresponding with the basal part of the estuarine channel sands and subzone A(ii) corresponding with the upper part of the channel sands and the lower part of the overlying silty clay marsh sediment.

In subzone A(i), the DSI value is 0.51, indicating a very mixed assemblage of brackish marine and freshwater taxa. This is shown in the diatom group sums, with a polyhalobous sum of 35%, a mesohalobous sum of 12%, and an oligohalobous indifferent sum of 28%. The polyhalobous group is dominated by the robust tychoplanktonic *Delphineis surirella* (>5%TDV) and the planktonics *Paralia sulcata* (>5%TDV) and *Podosira stelligera* (4.5%TDV). The freshwater indifferent taxa are dominated by *Achnanthes exilis* (>10%TDV) and *Cymbella silesiaca* (>5%TDV). This mix of marine planktonics and freshwater species, dominated by the very small and transportable *Achnanthes exilis*, is similar to that seen at the base of PL2, and suggests that sedimentation in this basal part of the channel was more influenced by the residual fluvial flow during low tide conditions. The marine species would have been transported in on the flood tide, with the alternations in flow velocities evident in the pronounced tidal lamination. The mesohalobous epiphytic taxa *Ctenophora pulchella* emerges in this zone at >5%TDV, and as it was not seen in the the more saline transect A cores, is possibly derived from a more proximal source (vegetated channel banks).

In the estuarine channel sands and silty sands below 0.88m in subzone A(ii), the diatom assemblages are dominated by polyhalobous planktonic and tychoplanktonic taxa (58-69%), with the DSI value falling to 0.19. Polyhalobous species include *Actinoptychus senarius*, *Delphineis surirella* and *Paralia sulcata* all at >10%TDV, along with *Coscinodiscus radiatus*, *Podosira stelligera*, *Rhaphoneis amphiceros* and *Thalassiosira eccentrica* all at >5%TDV. This group is joined by the mesohalobous planktonic *Cyclotella striata* at >5%TDV abundance. This part of subzone A(ii) is therefore dominated by species from the Taw Estuary tidal flat zone. However, a rise in freshwater indifferent species (to 17%) occurs in the the non-shelly silty sand (0.88-1.30m), supporting the sedimentary evidence of deposition at a higher tidal frame position in a pioneer-low marsh environment.

At the top of subzone A(ii), in the lower part of the silty clay, polyhalobous planktonic taxa remain dominant (at 54%), although with reduced diversity. Four species are present at >5%TDV, with two of these (*Coscinodiscus radiatus* and *Podosira stelligera*) present at >10%TDV. The rise in *Podosira stelligera* to 20%TDV suggests it may be at its optimum elevation in the low-mid marsh zones. The oligohalobous indifferent taxa (13%) remain in numbers similar to that seen in the sandy silt below. The mesohalobous sum rises to 17%, with *Cyclotella striata* remaining dominant (>10%TDV). The mesohalobous species *Nitzschia navicularis* appears at >5%TDV, suggesting the marsh palaeo-surface is now not far below MHWST. A tidal frame position equivalent to the Taw Estuary mid-saltmarsh zone is proposed for the silty clay sample horizon at 0.65m, indicating continuing marsh accretion towards the equilibrium high marsh level close to MHWST.

Zone B (0.00m – 0.47m)

This zone incorporates the upper part of the silty clay, the thin peat layer and the overlying organic silt. DSI values rise from 0.69 in the silty clay to 0.78-0.83 in the organic deposits above, indicating a change from dominance by freshwater and brackish species to freshwater species dominance at the top of the core.

In the upper part of the silty clay, the DSI value of 0.69 indicates dominance by brackish-freshwater species. The polyhalobous sum falls significantly to 19%, with a corresponding rise in oligohalobous indifferent species to 32%, with the emergence of a halophobous species, *Pinnularia subsolaris*, at 7%TDV abundance. The mesohalobous

group (16%) remains at similar levels to the subzone A(ii) part of the silty clay, but is now dominated by *Navicula peregrina* (>10%TDV), suggesting deposition close to MHWST (high saltmarsh levels or above). This sample horizon also sees the emergence of a halophilous species, *Navicula pusilla*, at 6.5%, which also suggests a high saltmarsh or marsh border environment. *Paralia sulcata* remains the only marine planktonic at >5%TDV. A rise in *Paralia sulcata* numbers was observed in the Taw Estuary close to MHWST (also seen by Nelson and Kashima, 1993), suggesting deposition at mid or high saltmarsh elevations. With the relatively low organic matter content value of 6% (although some will have been removed by oxidation in this relatively dry transect B location), a tidal frame position equivalent to the lower high saltmarsh zone (40-60cm below MHWST) is proposed for the 0.30m sample horizon.

In the thin peat layer (0.10-0.22m), the DSI value rises to 0.83, indicating the assemblage is dominated by freshwater species. This is seen in the diatom group sums at 0.18m, with the oligohalobous indifferent sum rising to 49%, the polyhalobous sum falling to 10% and the mesohalobous sum falling to 9%. There are no marine planktonics present at >5%TDV in the peat, but *Actinocyclus senarius*, *Paralia sulcata* and *Podosira stelligera* remain at >2%TDV levels. This suggests that the marsh is only inundated during the higher spring tides, but still probably remains quite close to MHWST. The mesohalobous species *Navicula peregrina* remains at >5%TDV, indicating proximity to MHWST, with the marsh palaeo-surface now probably located above MHWST at the base of the marsh border zone. This is supported by the presence of the the halophiles *Navicula pusilla* and *Navicula mutica*, both abundant in the marsh border, just above MHWST. The diverse freshwater indifferent group is dominated by *Cocconeis placentula*, *Hantzschia amphioxys*, *Navicula joubaudii* and *Pinnularia subcapitata*, along with the halophobe *Pinnularia subsolaris* (all at >5%TDV). Both *Hantzschia amphioxys* and *Pinnularia subcapitata* were found in the Taw Estuary to become dominant species (>5%TDV) in the marsh border sampling station at MHWST+24cm. The aerophilous species *Hantzschia amphioxys* was also recorded by Zong and Horton (1998) and Hill *et al.* (2007) in the marsh border zone, with the highest numbers appearing nearer HAT, rather than MHWST. Vos and de Wolf (1993a) included this species in their brackish-freshwater aerophilous ecological group (which includes *Navicula pusilla* and *Navicula mutica*), indicating it is salt-tolerant. A marsh border zone elevation is therefore proposed for the silty peat deposition, probably 30-50cm above MHWST.

The diatom assemblage characteristics of the upper organic silt (sampled at 0.08m) is very similar to that seen in the peat below, with the main differences being an increase in diversity in the marine planktonics/tychoplanktonics, a slight rise in the mesohalobous sum (still dominated by *Navicula peregrina*) and small falls in the oligohalobous groups. This suggests a slightly lower tidal frame position of MHWST or just above.

5.3.5 TS3 core

Sedimentology and magnetic properties

Figure 5.24 shows the core log for TS3. This figure shows down-core changes in sediment lithology, X_{lf} , $X_{fd\%}$, organic matter and carbonate content. In addition, the FSUs (see section 5.3.9) and stratigraphic units (see chapter 7) are indicated.

This core lies close to the western bank of the modern tidal river, within the narrow un-embanked zone. The TS3 core is underlain by gravel at 4.11m (0.45m OD). Between 0.70m and the gravel at 4.11m (*i.e.* most of the core) the sediment consists of shelly silty fine sand showing graded tidal laminations throughout. Lenses and laminations of shelly fine-medium sand are present throughout the deposit, becoming more frequent below 2.50m. A thicker layer of fine-medium sand is present at 2.43m – 2.50m. Towards the base of the sand (3.41m – 3.80m), the coarser laminations consist of non-shelly quartz sand, indicating intercalated periods of fluvial and tidal sedimentation at the base of the channel. Carbonate content values in the sand typically range from 4% to 7% and the unit represents laterally accreted inner estuarine river channel sands.

Overlying the sand between 0.23m and 0.70m is a unit of grey-brown sandy silt containing many rootlets and rootlet traces. The silt becomes slightly shelly at its base (2.2% carbonate content) and the numbers of rootlets diminish with depth. This deposit is thought to represent vegetated bank-top and overbank sedimentation at a low-mid marsh tidal frame level. Above 0.23m is a grey-brown organic sandy silt (with many rootlets and plant fragments) which grades up into a peaty clayey silt at 0.15m. This represents lower high saltmarsh level silts, accreting up into the modern brackish marsh

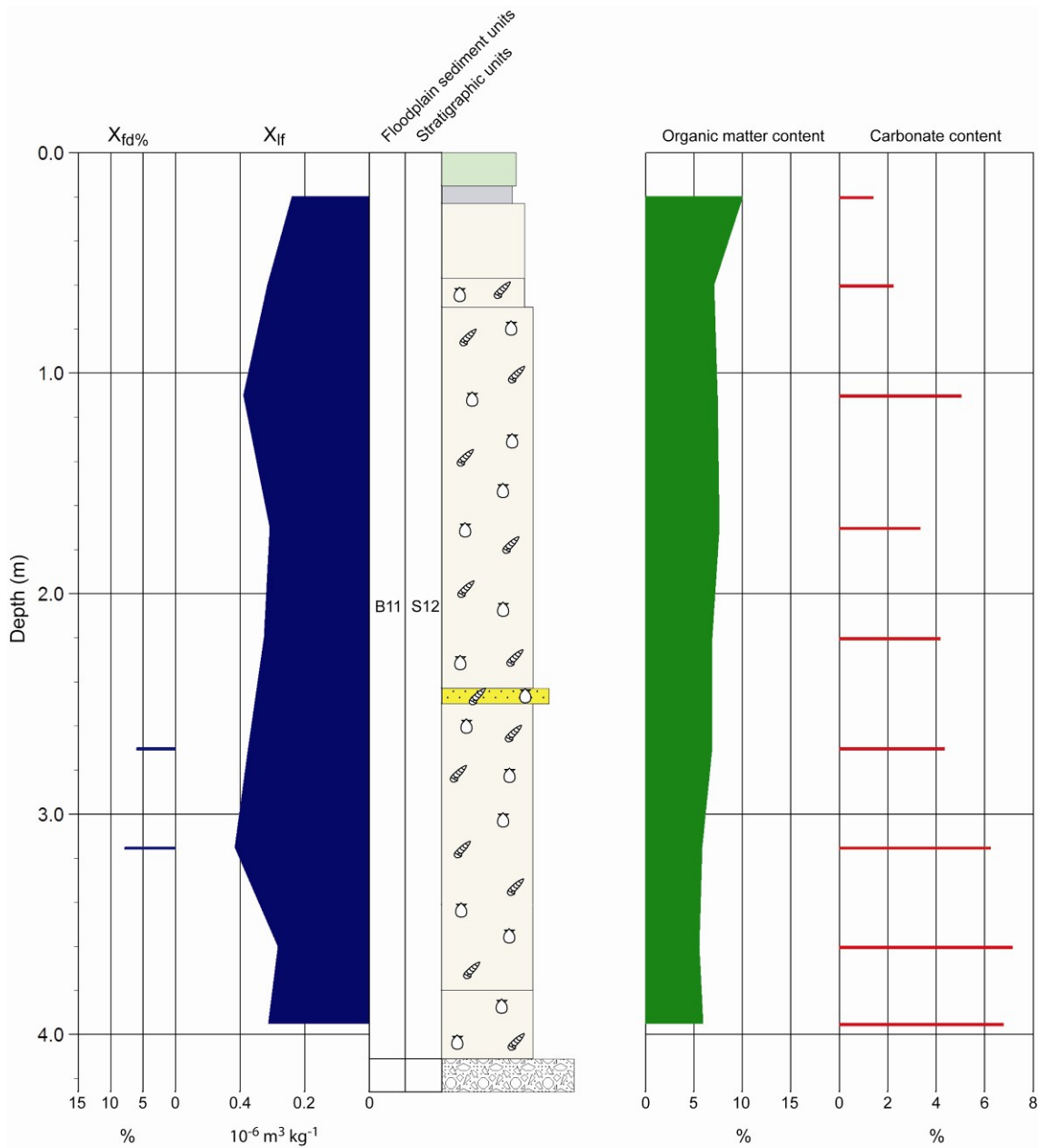


Figure 5.24 TS3 core log. See figure 5.2 for lithology legend. Floodplain sediment units (FSUs) are discussed in section 5.3.9. Stratigraphic units are discussed in chapter 7.

which is located at MHWST-14cm (equivalent to the Taw Estuary upper high saltmarsh zone).

X_{lf} values remain quite similar and at moderate levels ($0.3-0.4 \times 10^{-6} \text{ m}^3 \text{ kg}^{-1}$) throughout TS3, indicating the presence of ferrimagnetic minerals in the sediment. The $X_{fd\%}$ values within the shelly sand indicate low levels of fine viscous (SSD/SP boundary) magnetite, suggesting any contribution by authigenic soil magnetite is minor. The source of the X_{lf} signal could be detrital or bacterial in origin.

Within the channel sand deposits, between 2.30m and 2.79m, the sands are stained black. This is thought to be 19th Century and early 20th Century pollution, transported here on flood tides from the town of Barnstaple. This pollution is very similar to that seen in the channel sands east of the river in transect A (*i.e.* FSU A15) and the TS3 deposit is thought to be contemporaneous.

5.3.6 CF1 core

Sedimentology and magnetic properties

Figure 5.25 shows the core log for CF1. This figure shows down-core changes in sediment lithology, X_{lf} , organic matter and carbonate content. In addition, the diatom zones (see later), FSUs (see section 5.3.9) and stratigraphic units (see chapter 7) are indicated.

This core lies close to the eastern bank of the modern tidal river, within the narrow un-embanked zone. The CF1 core is underlain by gravel at 3.98m (0.72m OD). Below 2.38m, the sediment consists of laminated grey-brown silt (slightly shelly below 3.48m) with some lenses (<10mm) and partings of shelly fine-medium sand and an upper 8cm bed of shelly medium sand. Occasional detrital plant fragments are found in the lamination partings and carbonate content values range from 4.5% to 5.3%. The upper sand is overlain by another laminated grey silt deposit with occasional plant fragments in the partings. However, there are no shelly laminae in this silt. Above this silt, between 2.15m and 2.21m, is a layer of medium-coarse fluvial sand, followed by laminated grey-brown slightly shelly (3.1% carbonate) sandy silt, again containing detrital plant fragments. The sediments between 1.85m and the basal gravel represent relatively fine grained fluvio-estuarine channel deposits, accreted laterally during channel migration.

Between 0.63m and 1.85m, a unit of laminated grey-brown silty clay and clayey silt has accreted, with occasional rootlets throughout. Organic matter content remains low (4-5%) and carbonate values are *c.*1.3%. This unit represents bank-top and overbank fines, with deposition below MHWST. The upper 63cm consists of sandy clayey silt, with increasing root density towards the surface.

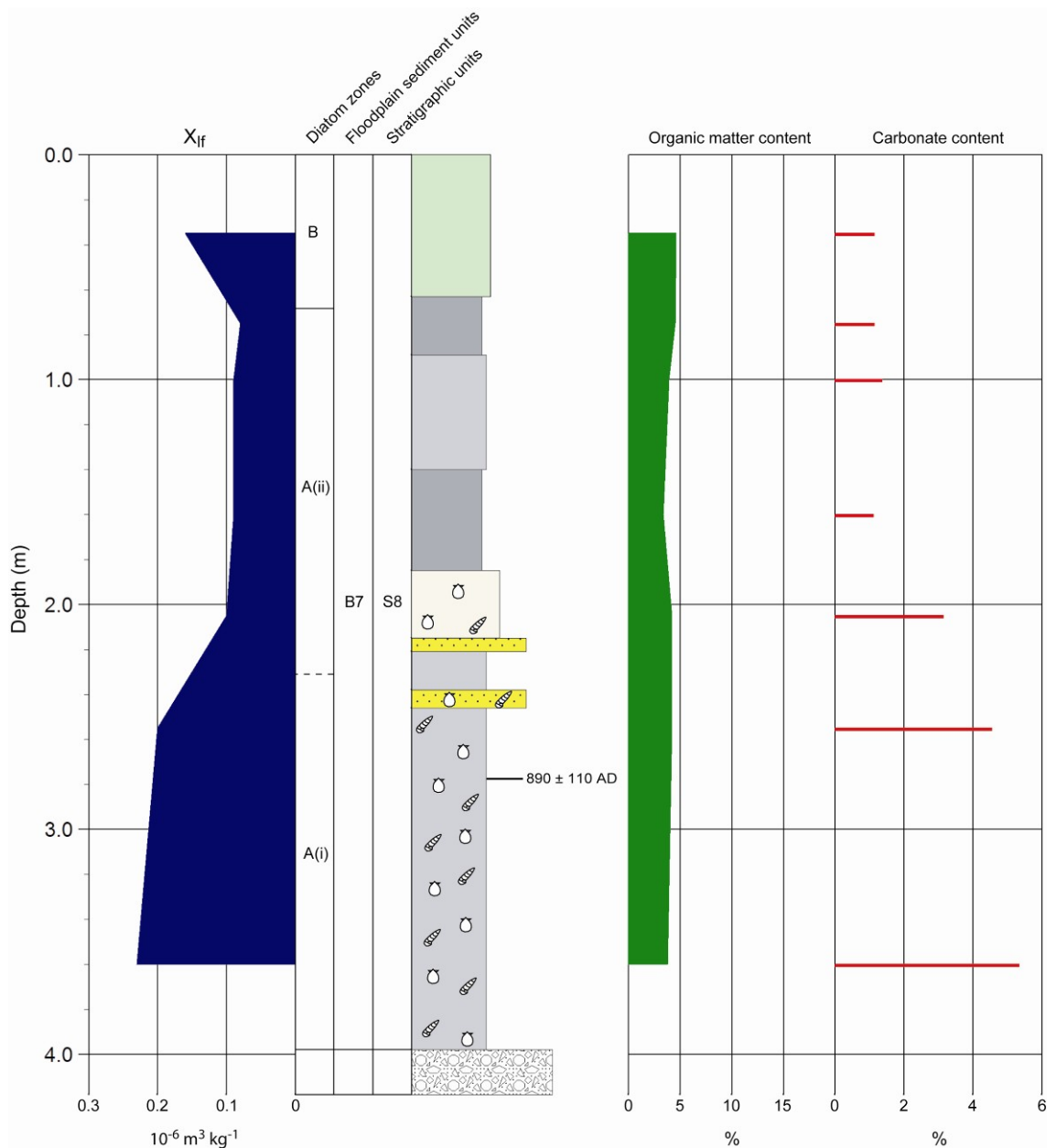


Figure 5.25 CF1 core log. See figure 5.2 for lithology legend. Diatom zones are derived from figure 5.26. Floodplain sediment units (FSUs) are discussed in section 5.3.9. Stratigraphic units are discussed in chapter 7.

Figure 5.25 shows X_{lf} values are $c.0.2 \cdot 10^{-6} \text{ m}^3 \text{ kg}^{-1}$ in the basal shelly silts, before falling to $c.0.1 \cdot 10^{-6} \text{ m}^3 \text{ kg}^{-1}$ in the overbank deposits, with a slight rise in the upper organic layer (possibly from secondary bacterial magnetite).

Geochronology

The shelly silt channel deposits were OSL dated, giving an age of $890 \pm 110 \text{ cal.yr.AD}$ for channel activity at this site.

Diatom analysis

Figure 5.26 shows a diatom diagram for CF1. All species with counts of >3%TDV are shown, along with the diatom sums. Cluster analysis resulted in two diatom zones (A and B). Diatom valves were found to be well preserved and relatively abundant throughout most of CF1, except for the lower part of the silty clay unit, where valves were present in low concentrations, and in the shelly silty sand layer, where valves were very fragmented.

Zone A (0.67m – 3.98m)

This zone corresponds with all of the channel facies and the overlying overbank fines up to 0.67m. Zone A was split into two subzones, A(i) and A(ii). Subzone A(i) corresponds with the basal shelly silt channel deposits and is dominated by polyhalobous planktonic and tychoplanktonic taxa (47-66%). *Paralia sulcata* and *Delphineis surirella* are present at >10%TDV, with *Actinoptychus senarius*, *Coscinodiscus radiatus*, *Cymatosira belgica* and *Podosira stelligera* all present at >5%TDV. These species are all dominant in the Taw Estuary tidal flat zone, indicating the sediment and environment is predominantly estuarine in nature. However, the oligohalobous group is larger (11-16%) than that seen in other transect B cores (TS1 and TS2) suggesting that fluvial sedimentation is more significant here. The smaller mesohalobous group (5-9%) is dominated by *Ctenophora pulchella* (>5%TDV).

Subzone A(ii) corresponds with the upper part of the channel facies and the overlying overbank fines. Polyhalobous planktonic-tychoplanktonic taxa continue to dominate this zone (53-61%). However, the marine group becomes dominated by the three species, *Paralia sulcata*, *Podosira stelligera* and *Actinoptychus senarius*, all at >10%TDV. These are joined by the mesohalobous planktonic *Cyclotella striata* at >10%TDV, and the epipellic *Navicula Peregrina* appears in low numbers (2%TDV). The oligohalobous indifferent sum increases slightly to 14-18% and is dominated by *Cocconeis placentula* and *Pinnularia viridis* (both >5%TDV). The increased freshwater species numbers and appearance of *Navicula peregrina* suggests that this vegetated floodplain-marsh has now accreted into the low-mid saltmarsh zone of the tidal frame.

Zone B (0.00m – 0.67m)

This zone corresponds with the upper more organic sandy silt. The polyhalobous sum

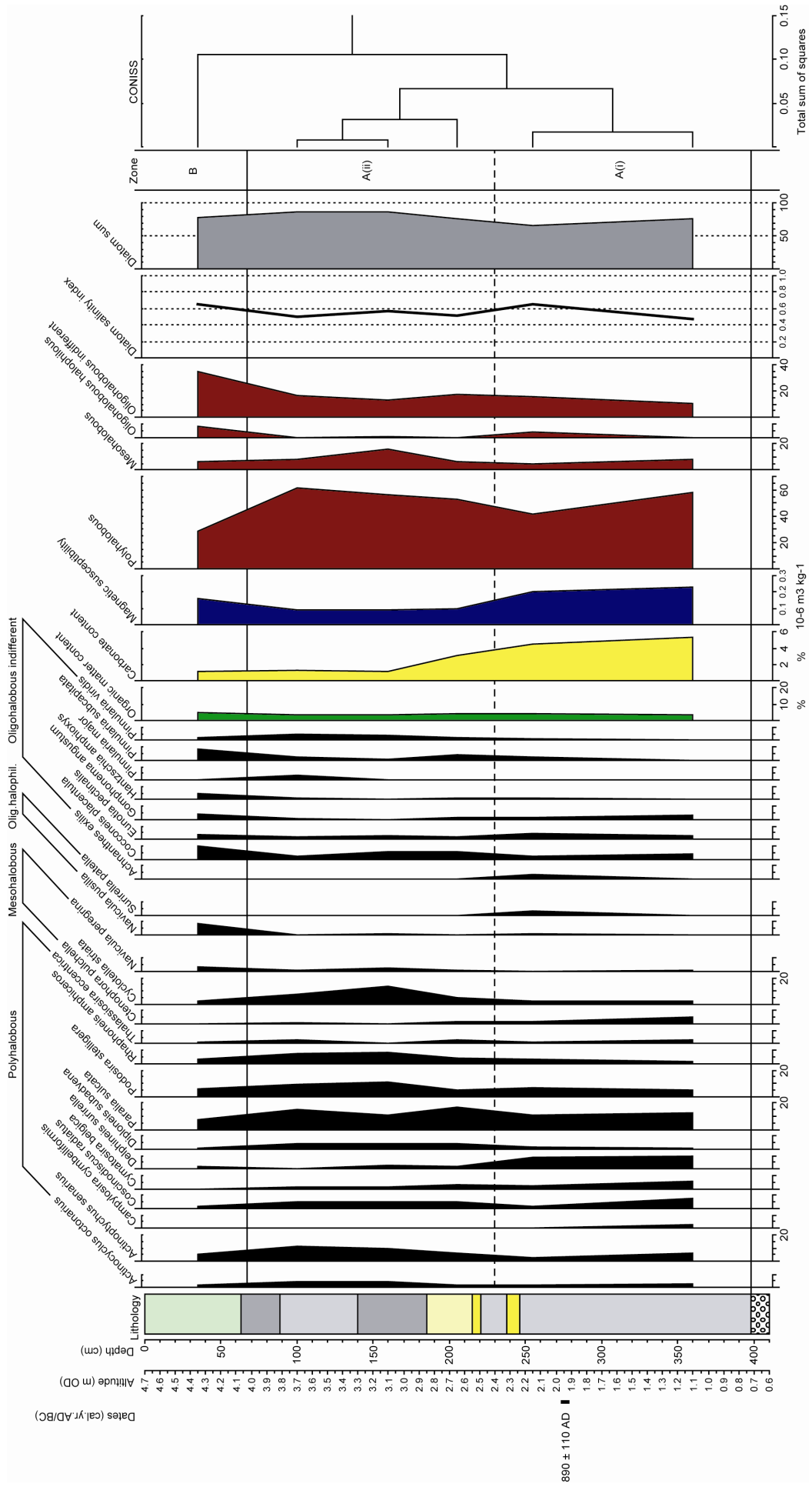


Figure 5.26 Diatom diagram for CF1 core (>3%TDV spp.). Organic matter content, carbonate content, X_r and Diatom Salinity Index is also shown.

falls significantly to 28%, with corresponding rises in the halophilous sum (to 8.5%) and freshwater indifferent sum (to 35%). The mesohalobous group declines to 6%. *Paralia sulcata*, *Podosira stelligera* and *Actinoptychus senarius* remain the dominant polyhalobous species, but now at >5%TDV. At 3.5%, *Navicula peregrina* is the most abundant mesohalobous species, indicating an upward move in tidal frame position towards its optimum. The aerophilous halophile *Navicula pusilla* becomes present at 8.5%TDV. As referred to earlier, this species is associated with the zones around MHWST, suggesting a further rise in tidal frame position to just below MHWST. The oligohalobous indifferent group is dominated by *Cocconeis placentula*, *Pinnularia subcatpitata* and *Hantzschia amphioxys*. *Pinnularia subcatpitata* and *Hantzschia amphioxys* both appeared in the Taw Estuary high saltmarsh and marsh border zones, supporting a high saltmarsh tidal frame position. Because of the relative abundance of marine planktonics, a lower high saltmarsh elevation is proposed for most of the upper silt, with surface sediment currently at MHWST (4.70m OD).

5.3.7 CF2 core

Sedimentology and magnetic properties

Figure 5.27 shows the core log for CF2. This figure shows down-core changes in sediment lithology, X_{lf} , $X_{fd\%}$, organic matter and carbonate content. In addition, the diatom zones (see below), FSUs (see section 5.3.9) and stratigraphic units (see chapter 7) are indicated.

The CF2 core is underlain by gravel at 1.97m (2.18m OD). A thin layer (4cm) of granular fine-medium sand overlies the gravel. Between 1.08m and 1.93m, a deposit of grey mottled green-brown sandy silt/silty sand has accumulated. The sediment contains long 2-5mm thick roots from possible marsh/aquatic flora and some *Phragmites* fragments. Between 0.91m and 1.08m is an organic (13.5% organic matter content) grey-brown clayey silt with increasing amounts of fibrous plant material towards the top. This is overlain by 8cm of brown peaty clayey silt with some fine roots. The deposits below the top of the peat are thought to represent a minerogenic marsh environment developing up into a more organic wetland. Above a sharp contact, a unit of laminated light grey silty clay is deposited between 0.30m and 0.83m with occasional

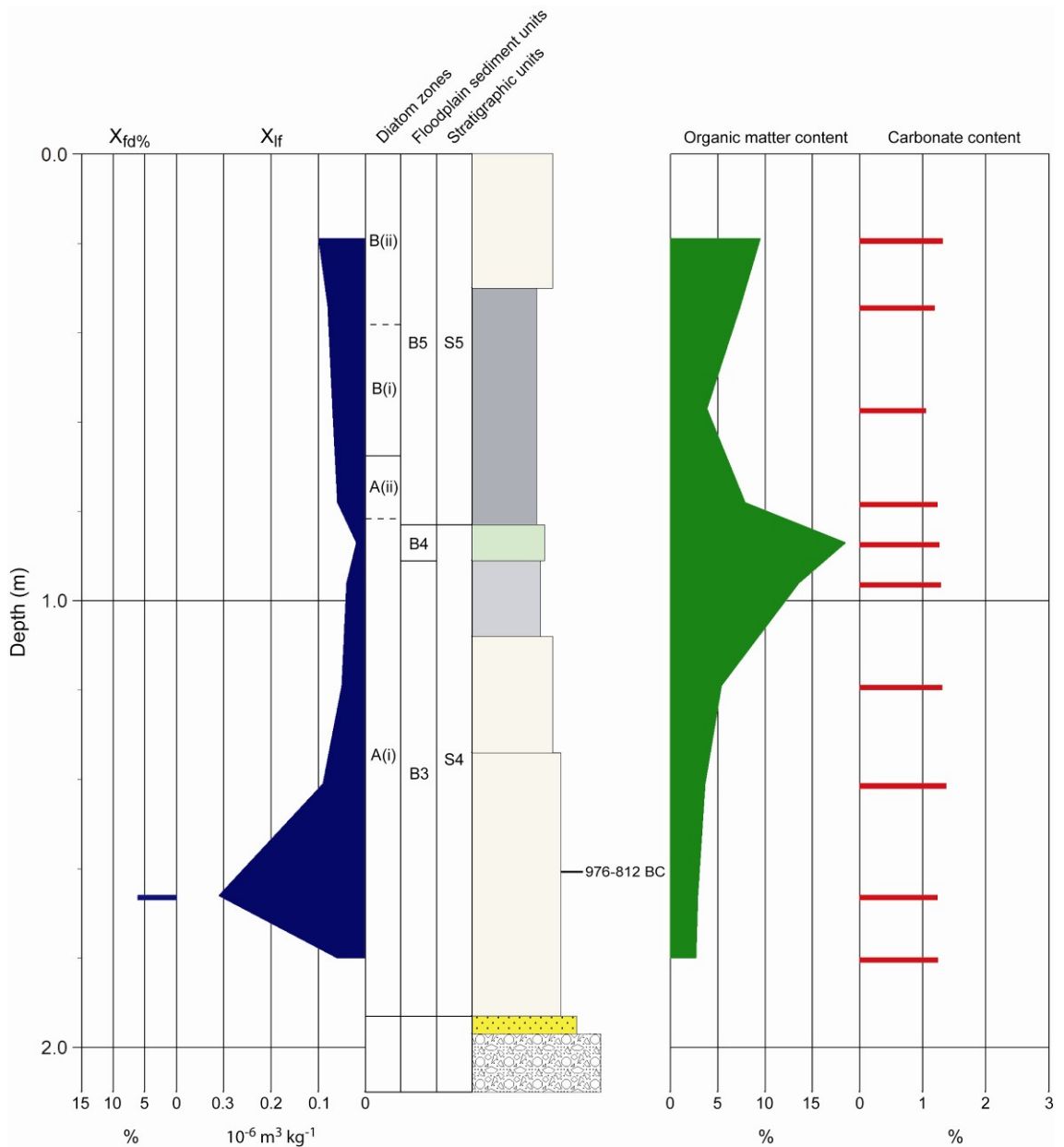


Figure 5.27 CF2 core log. See figure 5.2 for lithology legend. Diatom zones are derived from figure 5.28. Floodplain sediment units (FSUs) are discussed in section 5.3.9. Stratigraphic units are discussed in chapter 7.

plant fragments. The upper 0.30m consists of grey-brown sandy silt with rootlets. The upper clay and silt layers represent overbank floodplain sedimentation.

Carbonate content values are low throughout the core (1.0-1.4%), typical of River Taw floodplain alluvium, with the palaeoenvironment being either upstream of estuarine sedimentation or high in the tidal frame so that the palaeo-surface was unaffected by the mid-low intertidal environment where shelly sands can accumulate.

Above 1.5m, the sediments contain a very low concentration of magnetic minerals, with X_{if} values of 0.02-0.1 $10^{-6} \text{ m}^3 \text{ kg}^{-1}$. In the basal silty sands however, X_{if} values rise to 0.3 $10^{-6} \text{ m}^3 \text{ kg}^{-1}$, indicative of a significant ferrimagnetic mineral assemblage. This may have a detrital origin in this minerogenic marsh, or may be due to secondary in-situ bacterial magnetite/greigite. The low $X_{fd\%}$ value indicates fine viscous SSD/SP grains, typical of authigenic soil ferrimagnets, are not significant in the assemblage.

Geochronology

Detrital wood in the basal silty sand was radiocarbon dated and gave an age of 976-812 cal.yr.BC for minerogenic marsh accumulation.

Diatom analysis

Figure 5.28 shows a diatom diagram for CF2. All species with counts of >3%TDV are shown, along with the diatom sums. Cluster analysis indicates two diatom zones (A and B). Diatom valves were found to be well preserved and relatively abundant in the organic silt, clayey peat and overlying overbank sediments. However, in the basal minerogenic unit, diatoms become increasingly rare, with a diatom count only possible in the sandy silt. In the lower silty sands, only two valves were found at 1.41m and 15 valves at 1.80m.

Zone A (0.67m – 1.93m)

This zone has been divided into two subzones with A(i) incorporating both the basal minerogenic marsh sediments and the overlying wetland deposit of organic silt and peaty silt. A(ii) corresponds with the basal part of the silty clay deposited above the peat.

The relatively diverse sedimentary sequence within subzone A(i) contains diatom assemblages with very similar DSI values of 0.88-0.91. These values are indicative of dominance by freshwater species throughout this subzone, but with a significant brackish assemblage component. The diatom group sums and species abundance data given in figure 5.28 shows some minor but significant changes between the separate sedimentary layers of subzone A(i) that indicate a gradual lowering of the marsh palaeo-

surface in the tidal frame. The assemblages of each sedimentary unit in A(i) will therefore be described separately.

In the basal minerogenic silts and silty sands a full diatom count was only possible at 1.19m at the top of the unit. The assemblage is dominated by oligohalobous indifferent taxa (37-62%), with >10%TDV species represented by *Cocconeis placentula* and *Pinnularia viridis*. Other dominant freshwater species (>5%TDV) include *Eunotia pectinalis*, *Pinnularia major*, *Pinnularia microstauron* and *Pinnularia subcapitata*. The polyhalobous and mesohalobous groups only represent 4% of the assemblage, indicative of an environment close to HAT. However, the halophilous marsh border species *Navicula pussilla* is present at >10%TDV, suggesting the marsh surface tidal frame position is slightly lower, possibly half way between MHWST and HAT (*i.e.* MHWST+50cm). The valves identified at 1.80m, at the base of the silty sand, are dominated by freshwater taxa but also included three valves from more brackish species (*Navicula peregrina*, *Navicula pusilla* and *Navicula avenacea*). As this suggests a similar environment to the assemblage at 1.19m, subzone A(i) has been extended to the base of the core.

In the overlying organic silt, a sample from 0.87m sees the oligohalobous taxa remain the dominant group, but present in reduced numbers (37%). Marine planktonics remain present in very low numbers (2%), but the appearance of *Navicula peregrina* at >10%TDV accounts for a significant rise in the mesohalobous sum (12%). Combined with an increase in *Navicula pusilla* abundance, this suggests a fall in tidal frame position to the base of the marsh border zone (*i.e.* 20-30cm above MHWST).

In the peaty silt layer at the top of subzone A(i), the freshwater indifferent sum rising to 50%, and the oligohalobous halophobous sum rising to 12%. The halophobes are dominated by undifferentiated *Eunotia species* (9%TDV), with this rise in epiphytic *Eunotia taxa* also seen in the indifferent group, where *Eunotia pectinalis* numbers rise to 18%TDV. This may be largely influenced by the change from a minerogenic marsh to an organic marsh, with the epiphyte *Cocconeis placentula* also present at >10%TDV. The halophilous aerophilous species *Navicula pusilla* remains in similar numbers (>10%TDV) to below, with the mesohalobous species *Navicula peregrina* also present, but in reduced numbers (4%TDV). This suggests some proximity to MHWST, with the marsh palaeo-surface remaining at the base of the marsh border zone. This is supported

by a rise in marine planktonics (principally *Paralia sulcata* and *Podosira stelligera*) to 6.5%, indicative of an increase in tidal inundation frequency, with the marsh surface possibly being located at MHWST.

Above the peaty horizon, in the silty clay of subzone A(ii), a significant fall in DSI value to 0.67 indicates an increased contribution by brackish-marine species and a fall in tidal frame position. This indicates a transgressive overlap between the peat and overlying silty clay with diatom evidence of an increase in marine influence. The group sums indicate a mixed assemblage with the halophobous taxa all but disappearing, the oligohalobous indifferent sum falling to 25%, the halophilous group remaining in similar numbers (16%), the mesohalobous group rising to 14%, and the polyhalobous planktonics rising to 12%. The polyhalobous group remains dominated by the planktonics *Paralia sulcata* (5.5%TDV) and *Podosira stelligera* (4%), suggesting deposition in the high saltmarsh zone, just below MHWST. The two dominant species in the assemblage are the mesohalobous species *Navicula peregrina* and the halophilous species *Navicula pusilla* (both >10%TDV), suggesting deposition close to their optimums at just below MHWST (upper high saltmarsh zone) and above. An upper high saltmarsh zone tidal frame position is proposed for subzone A(ii) (*i.e.* MHWST to MHWST-30cm).

The transgressive overlap between the top of the D(i) peat and the D(ii) clay was not dated, so cannot be used as a SLIP. However, the CF2 overlap is thought to correlate with the transgressive overlap dated in the PL1 core at 385-186 cal.yr.BC. This will be discussed further on chapter 7.

Zone B (0.00m – 0.67m)

This zone has been divided into two subzones with subzone B(i) corresponding with the rest of the laminated silty clay unit and subzone B(ii) corresponding with the upper sandy silt.

In B(i), the DSI value falls further to 0.49, indicating increasing brackish-marine species dominance and increased marine influence. The oligohalobous indifferent sum falls slightly to 17%, the halophilous taxa largely disappear (3%), the mesohalobous sum rises to 29% and the polyhalobous sum rises to 22%. The two dominant species (>10%TDV) are the mesohalobous species *Navicula peregrina* and the marine

planktonic *Paralia sulcata*. The high numbers of *Navicula peregrina* suggest deposition remains within the high saltmarsh zone, with proximity to MHWST shown by the appearance of *Nitzschia obtusa* (>5%TDV). However, the increase in *Paralia sulcata*, along with marine planktonics *Podosira stelligera* and *Actinoptychus senarius* (both at 5%TDV), shows some similarity with the rise in certain planktonic species in the Taw Estuary mid-high saltmarsh zones (also seen by Nelson and Kashima, 1993). Deposition at a lower high saltmarsh elevation is therefore proposed for subzone B(i) (40-60cm below MHWST).

In subzone B(ii), the DSI value rises to 0.76, indicating a mixed assemblage with dominance by freshwater species. The oligohalobous indifferent group rises to 45%, with the most abundant species being *Cocconeis placentula*, *Hantzschia amphioxys* and *Pinnularia subcapitata*. All three of these species have been shown to be more salt-tolerant than most indifferent taxa, suggesting deposition near MHWST. This is supported by the presence of mesohalobous *Navicula peregrina* at >10%TDV and halophilous *Navicula pusilla* at >5%TDV, both with optimums in the zones either side of MHWST. Marine planktonic numbers fall to 10%, with *Paralia sulcata* present at >5%TDV. This suggests deposition at a high saltmarsh zone elevation. An upper high saltmarsh tidal frame position is therefore proposed (*i.e.* 10-30 cm below MHWST).

5.3.8 CH1 core

Sedimentology and magnetic properties

Figure 5.29 shows the core log for CH1. This figure shows down-core changes in sediment lithology, X_{if} , organic matter and carbonate content. In addition, the FSUs (see section 5.3.9) and stratigraphic units (see chapter 7) are indicated.

The CH1 core is underlain by gravel at 3.88m (1.08m OD). A thin 3cm layer of fine-coarse sand is draped on top of the gravel, representing the final channel deposition prior to channel abandonment. Between 3.56m and the basal sand is a layer of grey-brown peaty silt (12-18% organic matter content), grading up into a sandy silt. Both layers contain many *Phragmites* and sedge fragments, with many fine rootlets and occasional twigs in the peaty silt. A palaeochannel reedswamp environment is

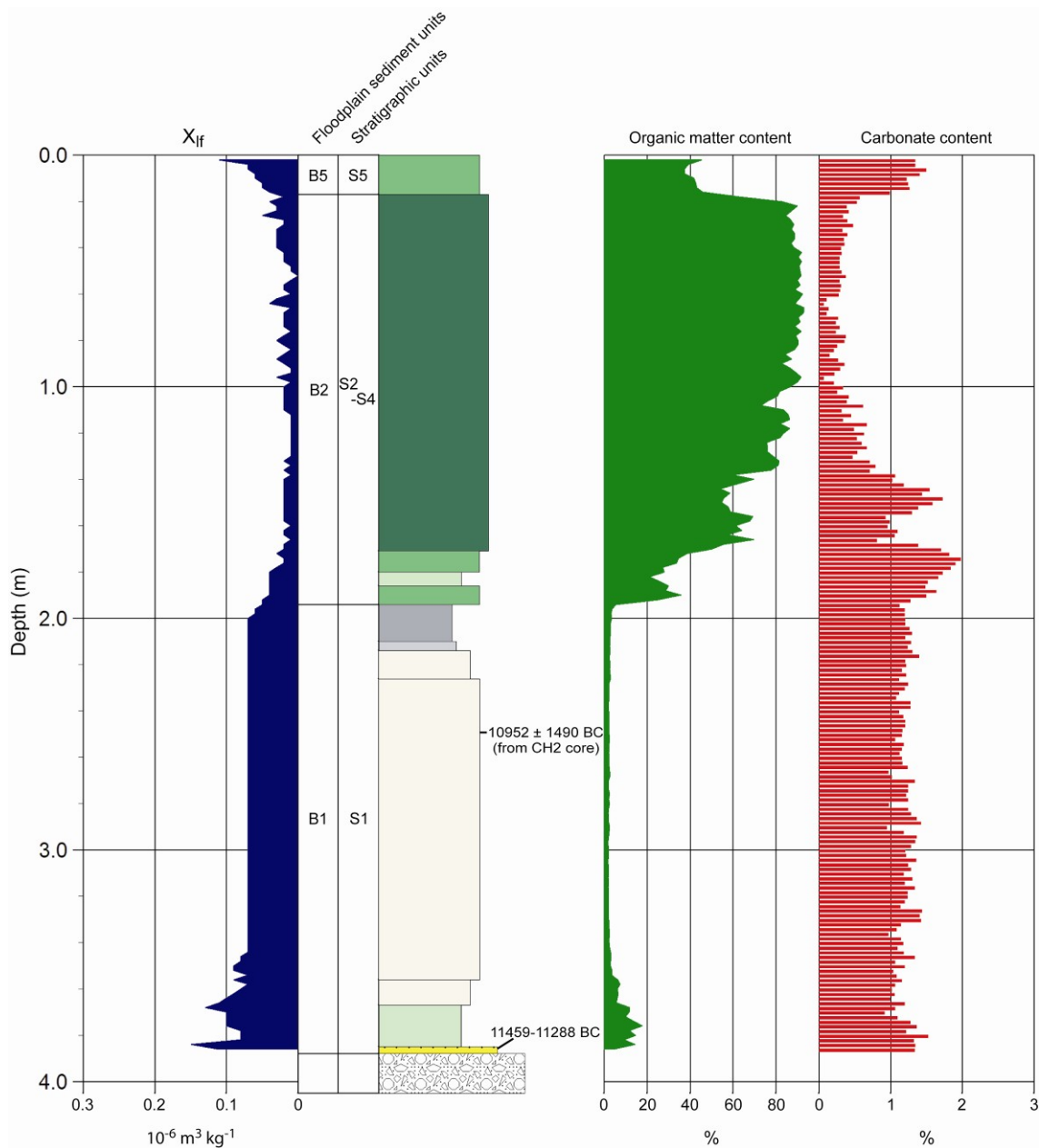


Figure 5.29 CH1 core log. See figure 5.2 for lithology legend. Floodplain sediment units (FSUs) are discussed in section 5.3.9. Stratigraphic units are discussed in chapter 7.

envisaged. Between 2.26m and 3.56m, a thick layer of grey silty fine sand has been deposited. Some lamination is seen at the top and bottom of the unit, but most of the deposit is massive, suggestive of rapid deposition. The low carbonate content (*c.*1.2%), suggests fluvial deposition, indicating the palaeochannel was briefly re-occupied during a large magnitude flood. The sand is penetrated by occasional woody roots (*c.*1cm thick) which are thought to be post-depositional, having grown down into the sand from be the wood peat above. Between 1.94m and 2.26m, a fining up laminated minerogenic sequence of grey sandy silt, clayey silt and silty clay has been deposited. This represents another quite rapid phase of channel abandonment with reduced flow velocities, before

sedimentation of clay in a palaeochannel pond/depression. The only organic matter present is woody tree roots, derived from above, indicating a largely unvegetated environment.

Between 1.80m and 1.94m, a thin layer of grey clayey peat, then peaty clay, has accumulated. The sediment contains many plant fragments, suggesting a more organic freshwater marsh/mire has developed. Between 1.69m and 1.80m, another clayey peat layer contains many wood fragments/twigs, suggesting a wooded fen environment. A rise in carbonate content to 2% is thought to be more indicative of the high clay content (with further de-watering in the clay at the higher LOI temperature) rather than any influence by estuarine carbonate. Between, 1.42m and 1.69m, a dark grey-brown peat has accumulated with many plant fragments, including sedge stems. There is little wood, and a sedge mire is envisaged. Between 0.18m and a sharp contact at 1.42m, a thick deposit of dark brown massive wood peat has accumulated. Some of the wood is identifiable as alder and birch, suggesting an alder carr environment with some birch trees. The surface 18cm consists of brown silty peat with many plant fragments and rootlets, suggestive of a grass-sedge dominated bog.

Geochronology

Detrital wood from the basal coarse sand layer has been radiocarbon dated at 11459-11288 cal.yr.BC, giving an age for initial channel abandonment in the middle of the Allerød stage of the late Glacial interstadial. The upper part of the channel fill sand has been OSL dated in the adjacent CH2 core, giving an age of 10960 +/-1490 cal.yr.BC for channel re-occupancy and abandonment at the start of the Younger Dryas stadial. The overlying minerogenic silt and clay is thought to have accumulated during the Younger Dryas stadial, with a largely barren, unvegetated ground surface. The overlying peat deposition is likely to have commenced at the start of the Holocene period, with peat accumulation continuing for the whole of the Holocene.

5.3.9 Phases of geomorphic and environmental change in the Tawstock reach

Figure 5.30 shows the FSUs for transect B (Tawstock transect).

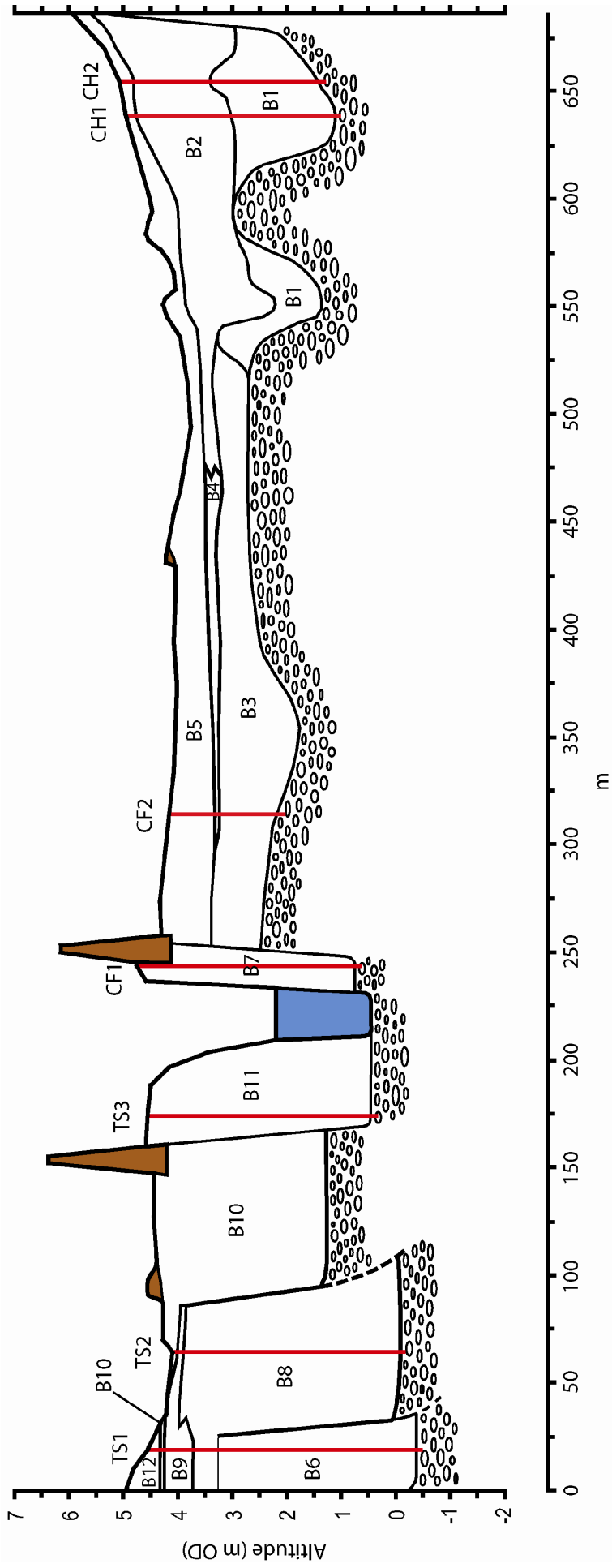


Figure 5.30 Transect B (Tawstock transect) Floodplain Sediment Units (FSUs).

FSU B1

This unit incorporates a phase of Late glacial fluvial deposition. At 11459-11288 cal.yr.BC, in the middle of the Allerød inter-stadial, a multi-channel braided gravel-bed river was abandoned. A *Phragmites* and sedge marsh developed and occupied the base of the abandoned channel for most of the remaining inter-stadial period. At the end of the Allerød stage, the channel was reoccupied by a sand-bed river, with sandy point bars developing on channel sides. At the start of the Younger Dryas stadial, at 10960 +/- 1490 cal.yr.BC, the channel was abandoned again. During the younger Dryas stadial, a thin layer of silty clay and clay accumulated within a surface depression or shallow pond. An unvegetated periglacial environment existed on the palaeochannel surface at this time.

FSU B2

This unit sees the development of a spring-fed mire and peat accumulation at the eastern valley side. It is thought to have commenced at the beginning of the Holocene with the development of a freshwater marsh. This was followed by periods of wood-fen and sedge mire during the early Holocene. An alder carr environment (with some birch) then persisted until the late Holocene. The upper minerogenic 20cm of the peat are included in FSU B5. A similar spring-mire peat was reported by Fyfe (2000) in the River Exe valley at Exebridge, where peat development also commenced at the start of the early Holocene.

FSU B3

At 976-812 cal.yr.BC, a minerogenic brackish wetland with some *Phragmites* developed across the floodplain at an elevation between MHWST and HAT. The marsh sediments are deposited on top of a high gravel surface that is thought to be part of the Late-glacial braid-plain. This would suggest that channel activity has been constrained to the western side of the valley throughout the Holocene, at this location. This also suggests that previous early-mid Holocene floodplain sediments have been removed from this site by floodplain stripping (Nanson, 1986), during a period of mega-floods (Knox, 1985, 1993, 2003; Brown *et al.*, 1999; Baker, 2003).

FSU B4

This unit sees the minerogenic marsh in B3 develop into a more organic brackish wetland, with a thin laterally persistent peat forming across the floodplain. Diatom

evidence suggests deposition occurred at MHWST or just above. The cessation of this organic wetland environment is brought about by a significant increase in marine influence, which resulted in more frequent tidal inundation and high saltmarsh minerogenic sedimentation (FSU B5). The increase in marine influence and fall in tidal frame position in transect B may be associated with the sharp rise in RSL evident above the organic peat in transect A, at the start of FSU A9. This correlation would give an age of 385-186 cal.yr.BC for the transgressive overlap at the top of the B4 peat.

FSU B5

Above the B4 peat, a more minerogenic and saline high saltmarsh environment existed. As stated above, this change in environment is thought to have been initiated by a rise in RSL that was dated at 385-186 cal.yr.BC in transect A.

FSU B5 also incorporates the upper 20cm of valley-side peat, elevated as a grass-sedge mire, 0.5-1.5m above the contemporaneous saltmarsh surface. The more minerogenic nature of this surface peat (compared with the organic wood peat in B2) and the lack of wood is thought to be related to woodland clearance that led to increased run-off and influx of minerogenic silt from the exposed terrace and valley side above. Pollen records from the wider Devon and Somerset area (Godwin, 1948; Simmons, 1964; Merryfield and Moore, 1974; Brown, 1977; Beckett and Hibbert, 1979; Moore *et al*, 1984; Fyfe, 2000; Fyfe *et al*, 2003; Hawkins, 2005) indicate that on a regional scale, the main phase of woodland clearance took place in the late Bronze Age and Iron Age. The only published lowland pollen record in the Taw catchment is in the tributary valley of the River Yeo. Casledine *et al*. (2000) provided pollen evidence that clearance at this site was extensive by about 300 cal.yr.BC (the start of their record) and may have taken place well before this date. However, in transect B, the stratigraphy (figures 5.18 and 5.30) suggests the surface minerogenic peat layer (at CH1) was initiated at around the same time as the valley floor saltmarsh development. This would indicate that woodland clearance occurred locally in the lower Taw valley, during the late Iron Age at *c.*250 BC.

FSU B6

This unit represents the earliest Holocene channel deposit found in transect B. The basal 50cm of B6 contains shelly estuarine channel sands deposited at 336-603 cal.yr.AD (415-540 cal.yr.AD 1 σ age). There is evidence for channel abandonment only 50cm

above the gravel. This indicates that the estuarine channel was abandoned by avulsion or tidal meander neck cut-off, rather than channel migration. Meander cut-off is very unlikely, given the limited space available for tight meander development between TS1 and the un-eroded Late glacial gravel, 230m to the east. Above the abandonment surface, B6 contains a channel-fill sequence of fine grained sediments (silts and clays with thin fine sands) with rootlets, deposited at increasingly higher tidal elevations. This sequence culminates in the thin peat seen in TS1 which diatom evidence suggests was deposited just below MHWST at a lower high saltmarsh altitude.

FSU B7

B7 is located 230 metres to the east of B6, on the western edge of the un-eroded Late glacial gravel. The unit contains a thick deposit of fine grained channel silts and sands with tidal laminations and lenses of shelly sand, deposited at 890 +/-110 cal.yr.AD. Compared with other channel deposits in transect B (i.e. B8, B10, B11 and the base of B6), these channel deposits are finer grained and less shelly, suggesting deposition in a transitional fluvio-estuarine environment. FSU B7 was also a somewhat aggradational phase, with the channel bed 1.1m higher than that seen in B6. The channel facies are overlain, at the top of the unit, by saltmarsh sediments deposited once the channel had migrated to the west.

FSU B8

B8 is located 160m to the west of B7. This unit contains an estuarine channel sequence of shelly sands and overlying saltmarsh/brackish marsh deposits, indicating active migration of the channel. The sands have been dated at 1100 +/-70 cal.yr.AD, which means that the channel migrated 160m from the B7 site, over 210 years. This would have required a net migration rate of 0.76m/yr, which indicates that bank erosion rates and river discharges were particularly high in the 10th and 11th Centuries AD.

FSU B9

Overlying B8, a phase of reduced salinity and estuary contraction is seen with the progradation and accretion of brackish marsh and alder carr at the valley sides between 1038-1221 cal.yr.AD (1051-1213 cal.yr.AD 1 σ age) and 1417-1623 cal.yr.AD (1433-1485 cal.yr.AD 1 σ age).

FSU B10

Following eastwards migration of the tidal channel, estuarine channel shelly sands were deposited at B10 by lateral accretion. The overlying saltmarsh/brackish marsh deposits are seen to over-run and inundate the valley side peats formed during B9, indicative of a rise in RSL and a period of estuary expansion. The transgressive overlap at the top of the B9 peat was dated at 1433-1485 cal.yr.AD (1σ age) so B10 channel deposition and migration probably commenced in the early 15th Century AD. The stratigraphy also suggests a period of channel bed aggradation between B8 and B10, with the B10 channel bed 1.4m higher than that found in B8 (see figures 5.18 and 5.30).

FSU B11

Following eastwards migration of the channel and some incision (0.9m), shelly estuarine channel sands were deposited at B11. This unit represents the youngest alluvial FSU in transect B, and signs of pollution within the tidal sands indicates it may represent estuarine deposition during the 19th and early 20th Centuries.

FSU B12

The colluvium that overlies B10 in the TS1 core has been designated as FSU B12. The exact age of this deposit is not known, but its stratigraphic relationship with B10 indicates it was probably formed at some point in the later stages of the Little Ice Age (17th to early 19th Centuries), when increased physical weathering would have made the adjacent steep valley side more unstable.

5.4 GEOMORPHOLOGY AND STRATIGRAPHY OF THE NEW BRIDGE REACH

5.4.1 Reach geomorphology

The geomorphology of the New Bridge reach is shown in figure 5.31. The Holocene alluvial floodplain remains at *c.*500m wide. The location of Transect C (Straypark Wood transect) and transect D (New Bridge transect) is shown, along with associated cores SW1 to SW4, and NB1 to NB4. This reach is located close to the tidal head of the River Taw, with mean tides reaching the downstream start of the reach (the mean tide limit is indicated on figure 5.31). With flood embankments stopping in the vicinity of MTL, the fields upstream of the embankments, and downstream of New Bridge, are prone to flooding several times a year during the higher spring tides, especially the area west of the river, crossed by transect C. The location of the HAT salinity front has been shown (chapter 4) to be located in the vicinity of transect D, with freshwater tides reaching up into the Bridgetown reach (chapter 6) during exceptionally high tides.

The late Pleistocene terrace T7 is preserved on both valley sides, elevated at *c.*8m above the Holocene alluvium. A further three late Holocene terraces (T1, T2 and T3) are present, with altitudinal differences becoming more apparent south of New Bridge. Palaeochannels are especially evident on the T1 and T2 terrace surfaces, showing evidence of late Holocene channel change. On T2, southwest of New Bridge, a 500m long palaeochannel segment is seen at the base of T7. The relatively straight nature of this palaeochannel shows that channel abandonment was brought about by channel avulsion. On the T1 surface, there are several examples of meander cut-off and rotation, illustrative of an active period of channel change and floodplain re-working. The modern floodplain occupies the insides of meanders, indicative of recent meander migration. The active channel has a sinuous meandering planform in this reach ($S = 1.57$), with tight meanders in the vicinity of transects C and D.

5.4.2 Lithostratigraphy of the Straypark Wood transect

Figure 5.32 shows the lithostratigraphy of transect C. The floodplain-terrace surfaces are between 5.0m and 5.9m OD, with the higher elevations found nearer the active

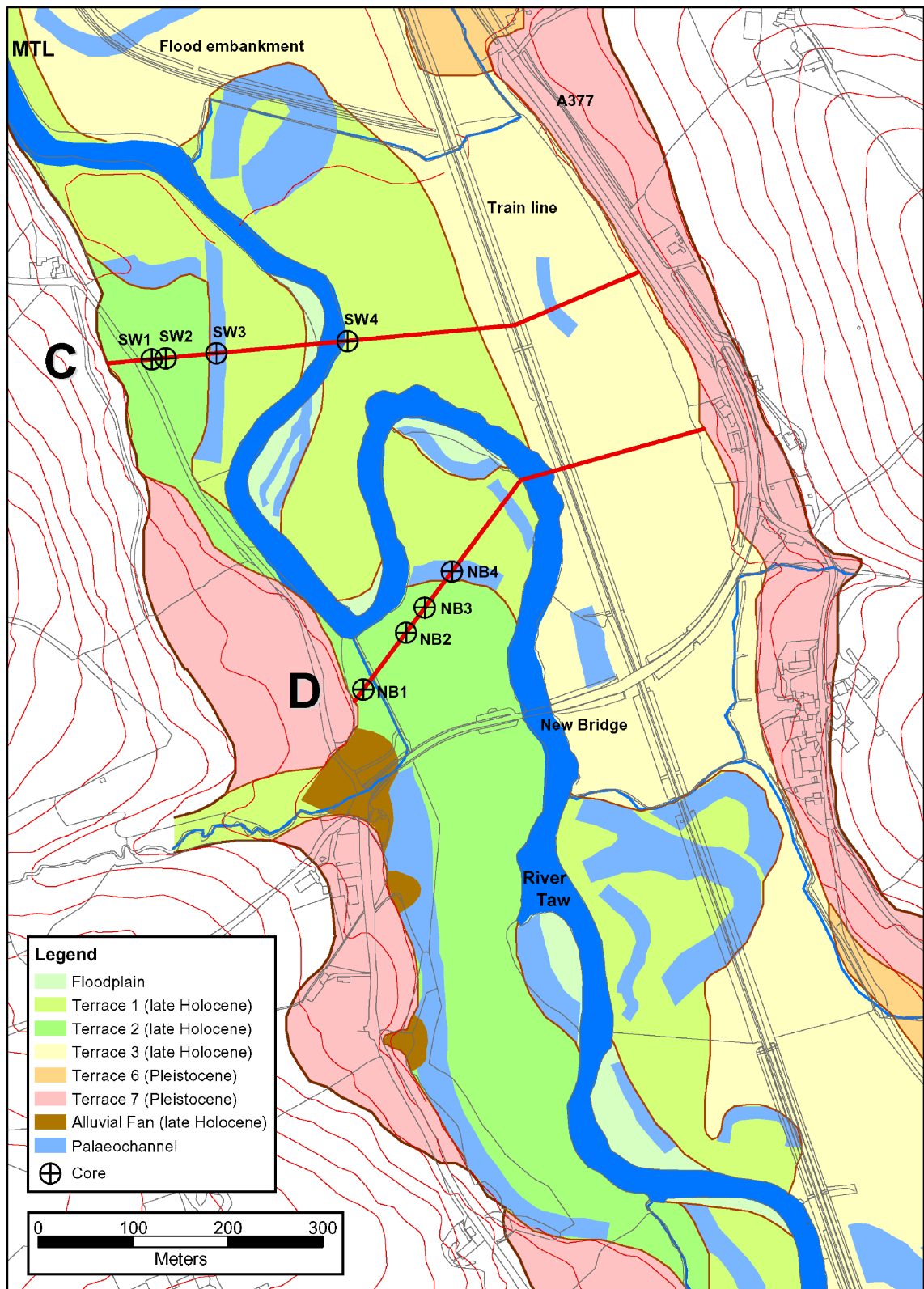


Figure 5.31 Geomorphology of the New Bridge reach. The location of transect C (Straypark Wood transect), transect D (New Bridge transect) and associated cores are indicated. The location of Mean Tidal Limit (MTL) is indicated. This map was produced in a GIS and incorporates OS Landform Profile (5m contours) and OS MasterMap layers (supplied by Ordnance Survey/EDINA Digimap).

channel. In the east of the transect, two phases of floodplain development are identified within T3 age deposits. Fine grained floodplain alluvium has been deposited on top of a

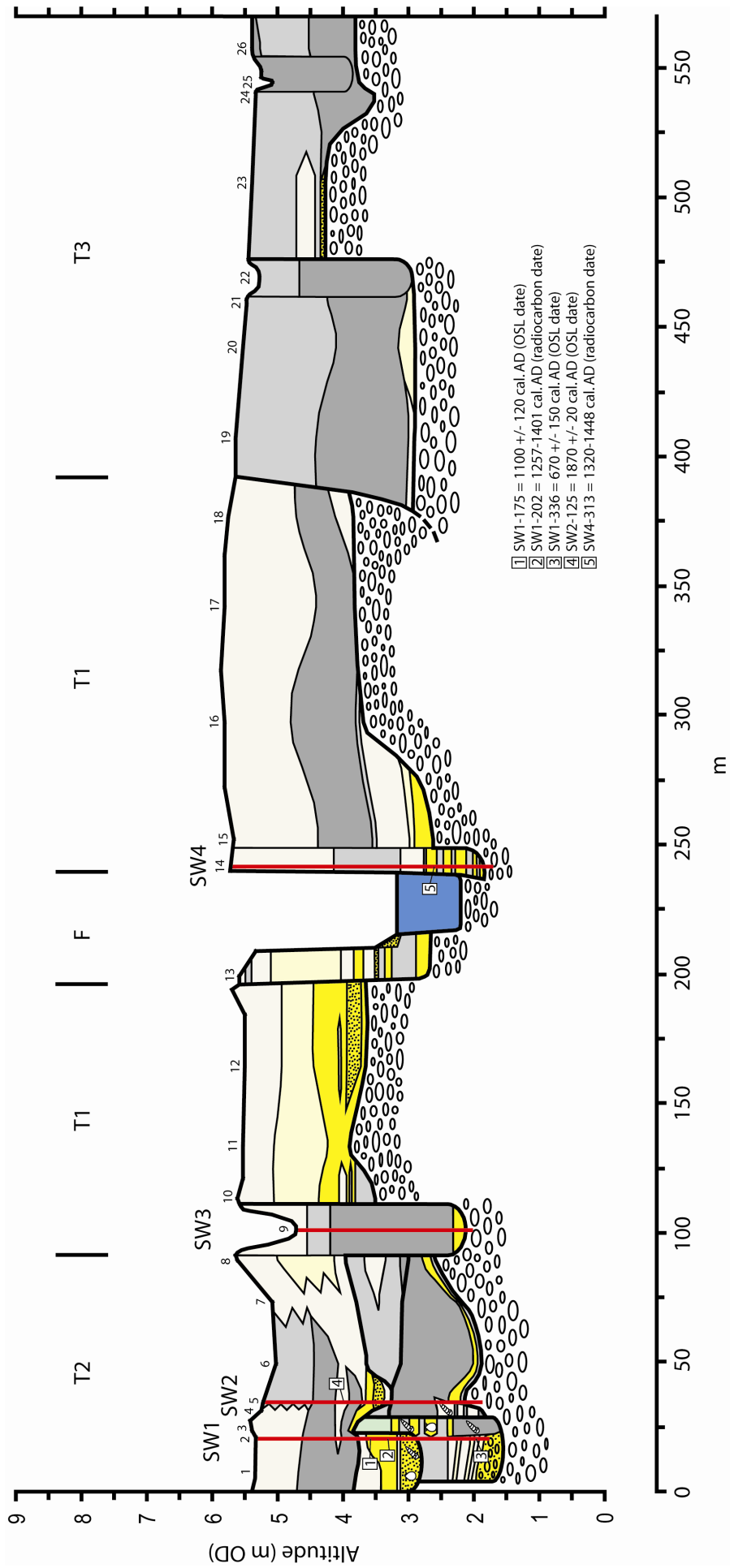


Figure 5.32 Lithostratigraphy of transect C (Straypark Wood transect). The location of analysed cores, stratigraphic cores (1-26) and radiocarbon/OSL samples (see tables 5.1 and 5.2) is shown. See figure 5.2 for legend.

gravel surface that is only 1.1-1.5m beneath the surface in the older, eastern phase of alluviation. The overbank deposits consist of grey clayey silts overlying lighter grey silty clays. The sediments are mottled orange-brown from oxidised rootlets and post-depositional manganese mineralisation. Charcoal fragments are also quite common. Thin palaeochannels (*c.*12m wide), with clay plugs, suggest a multi-thread anastomosing channel system was active at this time.

Nearer the eastern side of the active channel, T1 age floodplain alluvium has been deposited. The sediments consist of brown sandy silts and silty sands, overlying light brown silty clays. Coarser sands and silts infill depressions in the underlying gravel surface. The deeper alluvium below *c.*1.0-1.3m is mottled from manganese mineralisation. The alluvium is thought to have been deposited through floodplain over bank sedimentation. However, a palaeochannel (SW4) within this unit is exposed on the eastern bank of the River Taw, and is infilled with coarser channel facies sediments (intercalated sands and silts) before being overlain by floodplain sediment, similar to that seen to the east.

On the western bank of the modern river channel, beside a gravel point bar, a narrow unit of relatively recent sediment has been deposited on the inside of the meander. This largely consists of intercalated fine and medium sand, and sandy silt, and represents a laterally accreted channel/point bar sequence, deposited during recent channel migration.

West of this, beneath stratigraphic cores 10 to 12 (figure 5.32), another unit of T1 shows a fining up sequence of gravelly sand, medium-coarse sand, fine sand and sandy silt, overlying an elevated gravel surface. This represents channel and point bar lateral accretion deposits from a migrating gravel-sand bed river.

Beneath the western end of the transect (T2), the basal gravel is incised down to 1.8m OD. The lithostratigraphy reveals a complex sequence of nested palaeochannel deposits and marginal marsh and mudflat silts. Both of the palaeochannel fills beneath stratigraphic cores 1-3 (including SW1) contain some amounts of shelly sand/silt, indicating inner estuarine tidal sedimentation. Beneath cores 4-7, at approximately 3.0m OD (2.0-2.5m depth), the grey laminated tidal marsh and mudflat silts abruptly change into grey and brown mottled clayey silts (with manganese) typical of more fluvial

floodplain alluvium. This floodplain sediment is then overlain by a flood deposit of overbank sandy silt and silty clay, with a gravel lag in places (SW2). Coal and charcoal fragments are found dispersed throughout this upper unit (especially below stratigraphic cores 6-8), suggesting a more recent age. This flood deposit is thought to be related to the adjacent thin palaeochannel beneath stratigraphic core 9, which also contains occasional coal fragments. This channel is shown on Ordnance Survey first series maps as an active flood channel in the mid 19th Century. The stratigraphy suggests that during a high magnitude flood, flood water from this channel overtopped the banks and caused significant erosion and stripping of the previous floodplain sediment to the west (to a depth of *c.* 1.5m). This was followed by gradual infilling of the floodplain scour.

5.4.3 SW1 core

Sedimentology

Figure 5.33 shows the core log for SW1. This figure shows down-core changes in sediment lithology, X_{lf} , $X_{fd\%}$, organic matter and carbonate content. In addition, the diatom zones (see later), FSUs (see section 5.4.12) and stratigraphic units (see chapter 7) are indicated.

The SW1 core is underlain by gravel at 3.50m (1.83m OD). Between 2.93m and the basal gravel, a sequence of intercalated silty sand and fine or medium sand has been deposited. The sediments show ripple cross-lamination with some clay mud drapes (indicative of a tidal environment) and slightly shelly horizons (where carbonate content reaches 2.5-3.5%). The deposits suggest deposition within a channel bar sequence, in a transitional fluvio-estuarine environment.

Between 2.45m and 2.93m, a sequence of grey ripple cross-laminated sandy coarse silts is intercalated with occasional grey-brown layers of silty clay or fine silt. The sandy silt layers have many detrital plant fragments, leaves and small twigs aligned on cross-lamination partings. The clay/silt layers contain wavy lamination (and some low angle cross-lamination) and are thought to have been deposited during periods of slack water. This sequence represents deposition in a low-energy tidal river channel, possibly after partial abandonment.

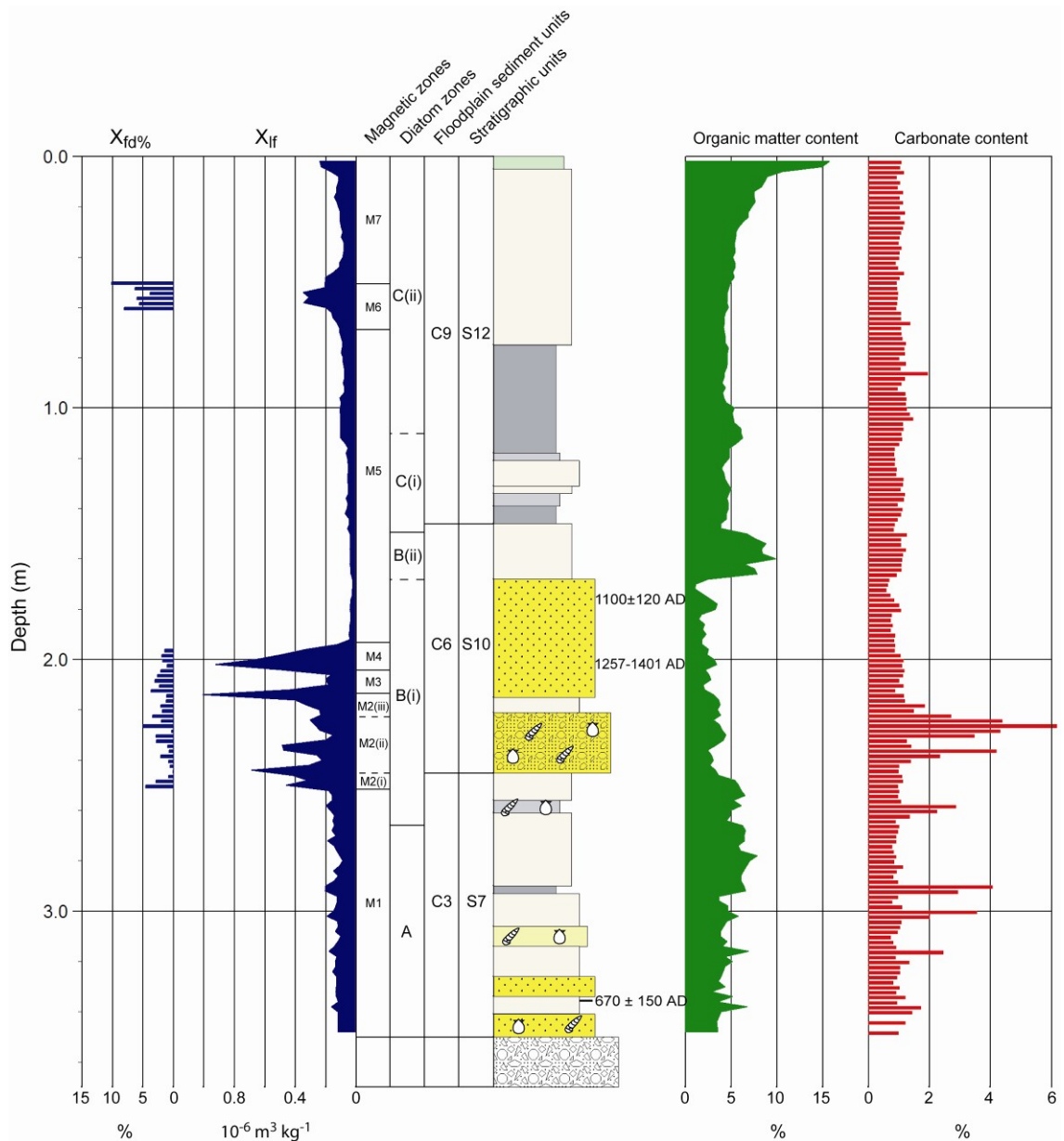


Figure 5.33 SW1 core log. See figure 5.2 for lithology legend. Magnetic zones are derived from figure 5.34, diatom zones are derived from figure 5.35. Floodplain sediment units (FSUs) are discussed in section 5.4.12. Stratigraphic units are discussed in chapter 7.

Above an undulatory erosion surface at 2.45m, a bed of gravelly shelly fine-medium sand is deposited up to 2.21m. The bed contains trough ripple cross-lamination, with some mud drapes and occasional wood detritus. The gravel clasts are mainly subangular, suggesting a relatively local source. This layer is thought to represent a basal flood channel deposit, with a possible storm-surge event transporting estuarine sediment up-river. The sediment contains many mud casts of burrows formed by estuarine crustaceans (or worms), suggesting a hiatus in deposition occurred immediately after this sediment was deposited. This supports the hypothesis of a storm-surge event. This hiatus coincides with a thin layer of silty fine sand with low angle

cross-lamination, suggesting tidal sedimentation in a largely abandoned channel with only partial connection with the active channel. Above this layer, the flood channel was again temporarily reoccupied, and a bed of well sorted fine-medium sand has been deposited between 1.68m and 2.15m. The bed contains ripple cross-lamination, with some mud drapes below 1.94m, suggestive of more tidal conditions during the early phase of deposition. Between 1.46m and 1.68m, a unit of sandy silt is deposited, containing occasional wood/seed detritus, suggesting partial channel abandonment. Wavy and planar graded lamination suggests a tidal influence on sedimentation.

Above a sharp contact at 1.68m, fine grained sediments suggestive of a floodbasin or palaeochannel marsh are deposited up to 0.75m. They consist of light grey silty clays and clayey silts with rootlets and rootlet traces throughout and some post-depositional manganese mineralisation. The unit contains a thin silty sand layer at 1.21-1.31m containing many oxidised rootlet traces. The upper 75cm of SW1 consists of grey-brown sandy silt with rootlets throughout and some manganese below 0.34m. Occasional charcoal and coal fragments are present between 0.50 and 0.60m.

Geochronology

The basal channel bar sequence was OSL dated, giving an age of 670 +/-150 cal.yr.AD for channel activity at this site, prior to possible partial abandonment. Detrital wood from the well sorted channel sand in the upper palaeochannel deposit was radiocarbon dated, giving an age of 1257-1401 cal.yr.AD for channel activity immediately after the possible storm-surge event. This sand was also OSL dated, giving an age of 1100 +/-70 cal.yr.AD. The OSL age is approximately 200 years older than the radiocarbon age. This may be due to partial bleaching of some of the sand grains (Wallinga, 2002; Duller, 2004), or the modern water content may not be representative of the water content present during most of the sediment's burial history (Bailiff and Tooley, 2000).

Magnetic properties

Figure 5.19 shows X_{if} values for SW1 (at 2cm resolution) and $X_{fd\%}$ for those samples that had a K_{if} value of $>25.0 \cdot 10^{-5} \text{ m}^3 \text{ kg}^{-1}$. A suite of mineral magnetic remanence measurements were also done on 62 samples from SW1 (c.6cm resolution). The results of these measurements and derived parameter ratios/quotients are shown in figure 5.34.

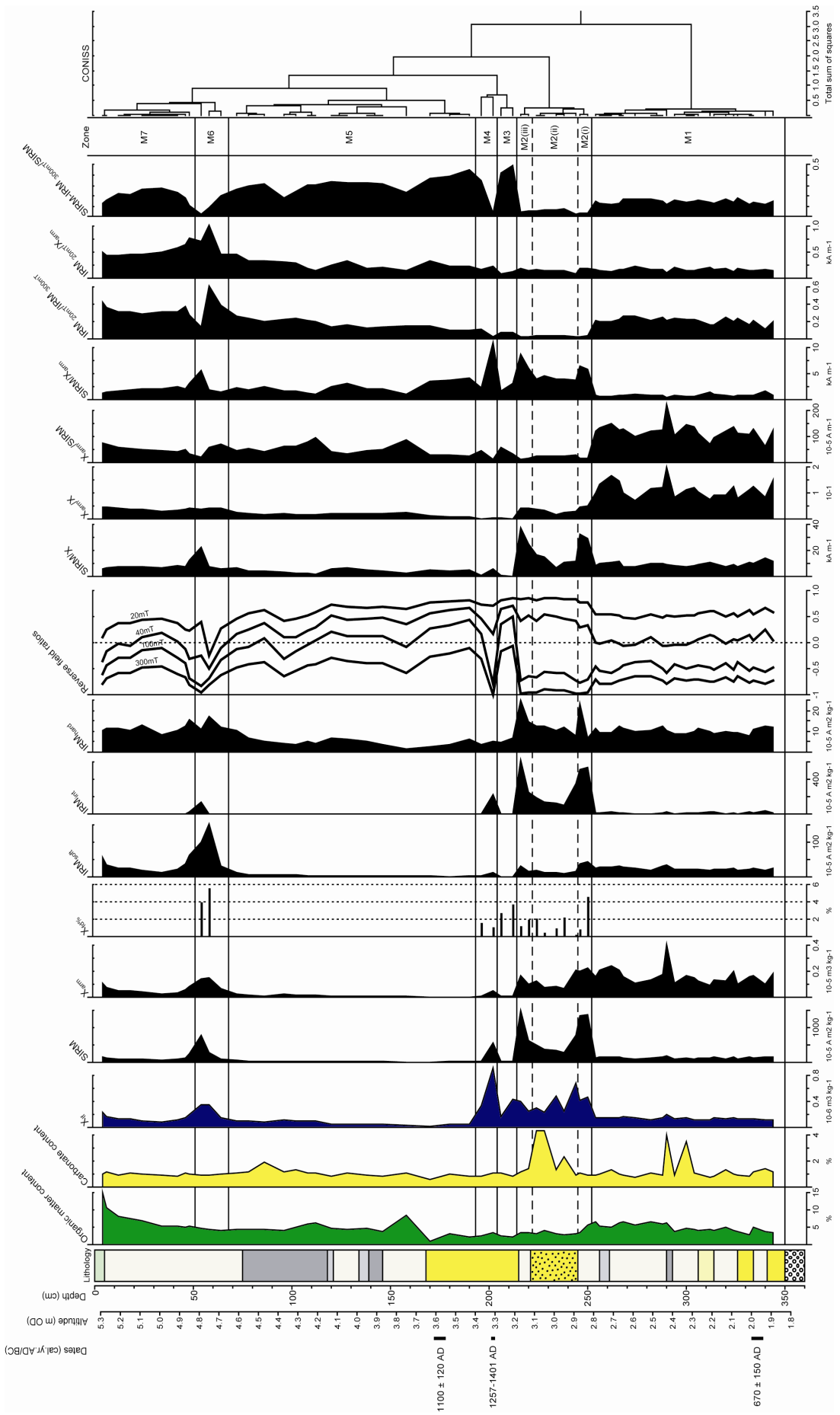


Figure 5.34 Magnetic characteristics of SW1 core and resulting magnetic zones.

Tables 3.2 and 3.3 were used in the identification of magnetic mineral components and constrained cluster analysis (CONISS) was used to divide the core into seven magnetic zones (M1 to M7).

Zone M1 (2.52m – 3.50m)

This zone corresponds with the channel sands and silts of the lower palaeochannel. Moderate X_{if} values indicate the presence of a magnetic mineral assemblage, with IRM_{soft} and IRM_{hard} values indicating a mixed ferrimagnetic-antiferromagnetic assemblage (as does the S-ratio value of *c.*-0.4). High X_{arm} values indicate the ferrimagnetic component is predominantly of an SSD grain size, which is supported by high X_{arm}/X values. High $X_{arm}/SIRM$ values indicate that the ferrimagnetic component is probably SSD bacterial magnetite (in-situ or transported from the estuary). The antiferromagnetic component is most likely to be detrital haematite, sourced from the catchment, indicating a transitional fluvio-estuarine environment.

Zone M2 (2.14m – 2.52m)

This zone corresponds with the upper 7cm of the lower palaeochannel silt, and the flood deposit and thin silty sand layer at the base of the upper palaeochannel fill. Zone M2 has been divided into three subzones that correspond with the three sedimentary divisions. The whole of zone M2 has high X_{if} and SIRM values, indicative of a high concentration of magnetic and remanence carrying minerals, with the low S-ratio indicating that the assemblage is dominated by ferrimagnetic minerals. Subzones M2(i) and M2(iii) show peaks in IRM_{int} , SIRM, SIRM/X and SIRM/ X_{arm} , indicative of the presence of greigite. These parameters are also relatively high in subzone M2(ii), and a reverse field divergence persists for the whole of zone M2. This indicates that greigite is significant throughout the zone, with higher concentrations in M2(i) and M2(iii). Relatively high X_{arm} values suggest that the greigite has an SSD grain size (supported by low IRM_{20mT}/X_{arm} values), with low $X_{fd\%}$ values (<4%) indicating few fine viscous grains. A smaller contribution by haematite is indicated by high IRM_{hard} values.

The greigite in this zone is likely to have a secondary authigenic origin (although it may be biogenic). The hiatus in sedimentation that may have occurred after deposition of the storm-surge deposit would have allowed greigite to form in the surface sediment, and may account for why the greigite has also precipitated in the top few centimetres of the

palaeochannel deposits below the erosion surface at 2.45m (*i.e.* it is associated with the upper palaeochannel palaeoenvironment).

Zone M3 (2.04m – 2.14m)

This zone corresponds with the base of the fine-medium sand bed. High X_{if} values indicate a significant magnetic mineral assemblage, with corresponding very low SIRM values suggesting that the assemblage is dominated by antiferromagnets, as these minerals contribute much less to SIRM than ferrimagnetic minerals. A haematite dominated assemblage is supported by virtually no IRM_{soft} signal, a moderate IRM_{hard} value, a high S-ratio and high SIRM- IRM_{300mT} /SIRM values. As the haematite is likely to have a catchment source, this suggests the base of this sand bed was deposited in a fluvial overbank flood, which re-occupied the channel eroded by the storm-surge.

Zone M4 (1.93m – 2.04m)

This zone corresponds with the highest part of the fine-medium sand to contain tidal mud drapes. Zone M4 shows very high X_{if} values ($0.93 \cdot 10^{-6} \text{ m}^3 \text{ kg}^{-1}$), indicating a high concentration of ferrimagnetic minerals. Ferrimagnetic dominance is shown by a very low S-ratio and high SIRM- IRM_{300mT} /SIRM values. Peaks in SIRM, IRM_{int} and SIRM/ X_{am} indicate that greigite is the dominant magnetic mineral. This is supported by some signs of a back field divergence, with the IRM_{-40mT} /SIRM ratio not tracking the decline in the S-ratio. The greigite in this channel sand is likely to have formed further out in the estuary (in the saltmarshes and mudflats) before being transported up-river on the flood tide, which gives support to the sedimentary evidence for a tidal environment at this horizon.

Zone M5 (0.68m – 1.93m)

This zone includes the rest of the upper palaeochannel sand and the overlying floodbasin silts and clays. X_{if} and SIRM values are very low throughout, indicating a low concentration of magnetic minerals. The S-ratio is high (mainly positive), indicative of an assemblage dominated by antiferromagnetic minerals (haematite). This is also indicated by almost no IRM_{soft} signal, moderate IRM_{hard} values, and high SIRM- IRM_{300mT} /SIRM values, suggesting that the rest of the sand was again deposited by fluvial flooding.

Zone M6 (0.51m – 0.68m)

This zone is located within the middle of the upper sandy silt unit. High X_{if} and SIRM values are seen in this zone, indicative of a high concentration of magnetic minerals in the sediment. High IRM_{soft} and IRM_{hard} values indicate a mixed ferrimagnetic-antiferromagnetic assemblage, with the low S-ratio and fall in $SIRM-IRM_{300mT}/SIRM$ values indicating that the ferrimagnets are dominant. High X_{arm} values indicate the ferrimagnets are predominantly SSD grains, although high IRM_{20mT}/X_{arm} also indicates some MD magnetite. An $X_{fd\%}$ value of 6% at the base of the zone indicates the presence of some fine viscous SD grains at this horizon. This is supported by a corresponding peak in IRM_{20mT}/IRM_{300mT} , suggesting there is some secondary soil-derived magnetite in the assemblage. Greigite may give a minor contribution to the assemblage near the top of the zone as there are corresponding peaks in IRM_{int} , SIRM, $SIRM/X$ and $SIRM/X_{arm}$, along with a small back field divergence.

In summary, zone M6 has a very mixed magnetic mineralogy and magnetic grain size but is dominated by SSD and MD detrital magnetite, with smaller contributions by greigite, soil-derived fine viscous SD magnetite, and detrital haematite. This suggests flooding by tidal water in a transitional fluvio-estuarine environment where the suspended sediment load is derived from both the catchment (*e.g.* haematite and soil-derived magnetite) and the outer estuary (*e.g.* greigite, SSD magnetite).

Zone M7 (0.00m – 0.51m)

This zone corresponds with the top of the upper sandy silt unit. X_{if} and SIRM values are relatively low throughout, indicating a low concentration of magnetic minerals. The S-ratio is high (though not as high as in zone M5), indicative of an assemblage dominated by antiferromagnetic minerals (haematite). This is also indicated by high IRM_{hard} and high $SIRM-IRM_{300mT}/SIRM$ values. A small contribution by SSD magnetite is shown by low-moderate IRM_{soft} and X_{arm} values. High IRM_{20mT}/IRM_{300mT} values also suggest the presence of fine viscous SD ferrimagnetic grains. This may be due to soil-derived magnetite, but further confirmation would need $X_{fd\%}$ values to be present. The assemblage in zone M7 is therefore largely sourced from the catchment (haematite and soil-derived magnetite).

Diatom analysis

Figure 5.35 shows a diatom diagram for SW1. All species with counts of >3%TDV are shown, along with the diatom sums. Cluster analysis resulted in three diatom zones (A to C). Diatom valves were found to be well preserved and relatively abundant in the basal palaeochannel fill (below 2.45m) and in the floodbasin and floodplain sediments above 1.46m. However, in the sandy upper palaeochannel fill between 1.46m and 2.45m, diatom valves were sparse and very fragmented, with signs of some dissolution.

Zone A (2.64m – 3.50m)

This zone corresponds with the basal channel bar sands and overlying cross-laminated sandy silts. DSI values range from 0.70 at the base of the zone in the channel bar sands to 0.93 in the overlying laminated silts. This indicates a fluvio-estuarine environment with diatom assemblages that are freshwater species dominated but also contain significant brackish-marine components, especially at the base of the zone. The oligohalobous indifferent group sum rises from 45% at the base of zone A (at 3.40m) to 62% higher up the zone and is dominated by *Achnanthes exilis* and *Cocconeis placentula* (>10%TDV), along with *Gomphonema angustum* and *Synedra ulna* (>5%TDV). The dominance by epiphytic species (*Cocconeis placentula*, *Gomphonema angustum* and *Synedra ulna*) in the channel sands of zone A demonstrates the assemblage is largely allochthonous. The mesohalobous group (11%) is dominated by the epiphyte *Ctenophora pulchella* at 5%TDV (the up-river appearance of this species occurred in transect B, cores TS2 and CF1). The polyhalobous sum is significant at 14% at the base of zone A (3.40m sample), but is only 1% in the rest of the zone. The dominant marine species in the basal sands are the tidal flat tycho planktonic species *Dephineis surirella* and the mid saltmarsh planktonic *Podosira stelligera*, both of which will be allochthonous in this depositional environment.

However, when the diatom sample horizons are related to the carbonate content record in zone A (see figure 5.33), the trend of increasing DSI up through zone A may be an artefact of the low sampling resolution for diatoms. Figure 5.33 indicates that the 3.40m sample horizon has a small peak in carbonate of 1.7% (in a sand, so probably not caused by clay dewatering at the higher LOI temperature) while the 2.74m and 3.10m sample horizons have typical fluvial sand values of 0.8%. The presence of marine planktonics at 3.40m may therefore be caused by sedimentation from a particularly high tide.

Several other peaks in carbonate are seen higher in zone A but these horizons were not sampled for diatoms. Therefore, there may be significant fluctuation in the marine-freshwater diatom ratio throughout zone A. This would support a transitional fluvio-estuarine environment close to the salinity front.

Zone B (1.50m – 2.64m)

This zone has been divided into two subzones. B(i) incorporates the upper 19cm of sandy silt in the lower palaeochannel fill, and the upper palaeochannel fill sands (deposited in the 13th/14th Century AD after a possible storm-surge event). B(ii) corresponds with the abandonment phase silts of the upper palaeochannel.

In the the upper unit of sandy silt in the lower palaeochannel fill, the only sample horizon is located in the 5cm layer of pale grey-brown wavy laminated silt, which shows more of a tidal influence than the surrounding sandy silts. The assemblage here is dominated by marine planktonic-tychoplanktonic species (46%) with the oligohalobous indifferent sum falling to 16%, and the mesohalobous sum remaining at 11%. The freshwater species that were dominant in zone A continue to be the dominant freshwater species in the lower part of subzone B(i), but now in <5%TDV numbers. This suggests some connection with the environment of zone A, which is apparent in the sedimentology of the sediments below the erosion surface at 2.45m. The marine planktonic taxa at this horizon are dominated by *Actinoptychus senarius*, *Coscinodiscus radiatus*, *Paralia sulcata*, *Podosira stelligera* and *Rhaphoneis amphiceros*, all at >5%TDV. This indicates that the sediment has been transported from an estuarine environment, during a phase of particularly high tides (or reduced discharge). The corresponding 2.9% peak in carbonate content supports this (figure 5.33). The channel sands and silts of the lower palaeochannel fill (zone A and the base of subzone B(i)) are therefore located in a transitional fluvio-estuarine zone with fluvial sedimentation being dominant, but intercalated with shorter periods of marine sediment influx during high spring tides, or periods of reduced river discharge.

In the coarser grained sediments of the upper palaeochannel fill (subzone B(ii)), the DSI values of 0.40-0.57 indicate a mixed assemblage with some dominance by brackish-marine species. This is seen in the group sums, with the polyhalobous sum at 28-50%, the mesohalobous sum at 14-18%, and the oligohalobous indifferent sum at 26-34%. The polyhalobous planktonic-tychoplanktonic species present are dominated by *Paralia*

sulcata and *Podosira stelligera* (both at >10%TDV), which in the Taw Estuary were the two most abundant species at high tidal frame positions. Other marine planktonics include *Actinocyclus octonarius*, *Coscinodiscus radiatus* and *Delphineis surirella*, all at >5%TDV. The mesohalobous group is dominated by *Cyclotella striata* and *Nitzschia navicularis*, both present in >5%TDV numbers within the thin sandy silt horizon that overlies the storm-surge deposit. This layer is thought to represent a temporary hiatus in channel activity, with only minor connection with the active channel. Therefore, the benthic species *Nitzschia navicularis* may be autochthonous in this layer. In transects A and B cores (PL2, PL3, TS1 and TS2), this species has been consistently associated with the mid-saltmarsh zone of the tidal frame, suggesting that this horizon was deposited at a similar tidal frame position. The sands above and below this horizon (within subzone B(i)) represent two temporary phases of channel occupancy, with a fully allochthonous assemblage seen in the sampled fine-medium sand.

In the subzone B(ii) silt, associated with channel abandonment, the DSI value rises to 0.74, indicative of a freshwater dominated assemblage, but with a significant brackish-marine species component. This is seen in the diatom group sums with the oligohalobous indifferent sum rising to 48%, the mesohalobous sum falling to 9%, and the polyhalobous sum falling significantly to 14%. The polyhalobous taxa are dominated by the planktonics *Paralia sulcata* (4%) and *Podosira stelligera* (3%), values that are typical of a high saltmarsh tidal frame position. The freshwater assemblage is dominated by *Pinnularia major*, at 16%TDV. The dominant mesohalobous species are the benthics *Navicula peregrina*, at 4%TDV, and *Nitzschia navicularis* at 2%TDV. These species are thought to be autochthonous in this fine grained sediment, and the presence of *Navicula peregrina* suggests deposition not far below MHWST. A tidal frame position of 40-60cm below MHWST is proposed for the silt palaeo-surface in this partially abandoned channel environment.

Zone C (0.00m – 1.50m)

This zone corresponds with the unit of fine grained floodbasin and floodplain sedimentation that is thought to be much younger (19th Century) than the sediments below. Two subzones are recognised.

In subzone C(i), at the base of the floodbasin sediments, the DSI value rises to 0.93-0.95, indicating dominance by freshwater species, with a minor contribution by brackish

taxa. The oligohalobous group dominates the assemblage at 53-56%. Polyhalobous taxa are virtually absent (1%), while the mesohalobous sum remains significant at 9-12%. There is a significant peak in halophilous species to 14% in C(i). The oligohalobous indifferent group is dominated by the salt-tolerant taxa *Cocconeis placentula* at >10%TDV. This species is joined by *Pinnularia major*, *Synedra ulna* and *Navicula cari* (also salt-tolerant, appearing in the high saltmarsh zone of the Taw Estuary) at >5%TDV each. The presence of the mesohalobous species *Navicula peregrina* (6-8%) and the aerophilous halophile *Navicula pusilla* (8-14%) in large numbers suggests they are autochthonous and deposition is occurring around MHWST. However, the depositional environment of subzone C(i) appears to be a brackish-freshwater tidal environment, up-river of the zone to which allochthonous marine planktonics can be transported. It is proposed that the C(i) palaeo-surface was located at a tidal frame position equivalent to either the high saltmarsh or the base of the marsh border zone, *i.e.* anywhere between 60cm below MHWST and *c.*30cm above MHWST.

Subzone C(ii) corresponds with the upper floodbasin and floodplain sediments. The DSI value remains at *c.*0.94 for most of the subzone, indicating freshwater species dominance, but drops to 0.90 at the horizon where the mineral magnetic assemblage indicated flooding by brackish tidal water, with entrained sediment sourced from both the estuary and catchment. The oligohalobous indifferent sum rises to 60-67% in C(ii), indicating an increasingly freshwater environment, with the halophobous species *Pinnularia subsolaris* reaching 5%TDV abundance. *Cocconeis placentula* remains the dominant freshwater indifferent species (18-26%TDV), along with *Eunotia pectinalis*, *Gomphonema angustatum*, *Gomphonema angustum*, *Pinnularia subcapitata* and *Synedra ulna* all at >5%TDV. The halophilous species *Navicula pusilla* almost disappears (1%TDV), suggesting a higher tidal frame position. The polyhalobous sum remains at 1% for most of the zone but rises to 4% at the horizon where the mineral magnetics suggest a partly estuarine sediment source. At this horizon, *Actinoptychus senarius* numbers increase to 2%TDV and *Podosira stelligera* numbers increase to 1.5%TDV, suggesting that these marine planktonics were transported on to the floodplain surface during a period of increasingly high tides, or there is greater connectivity between the active channel and the floodplain due to nearby channel change. The mesohalobous sum, which is at 6-8% for most of subzone C(ii), also rises to 12% at this horizon and is dominated by *Ctenophora pulchella* at 6.5%TDV. A brackish floodplain environment is envisaged for C(ii), with the depositional surface

located at approximately MHWST+30-60cm. The modern floodplain elevation of MHWST+63cm supports this.

5.4.4 SW2 core

Sedimentology and magnetic properties

Figure 5.36 shows the core log for SW2. This figure shows down-core changes in sediment lithology, X_{lf} , $X_{fd\%}$, organic matter and carbonate content. In addition, the diatom zones (see below), FSUs (see section 5.4.12) and stratigraphic units (see chapter 7) are indicated.

The SW2 core is underlain by gravel at 3.07m (2.14m OD). Above the gravel, the basal 7cm of SW2 consists of dark grey laminated silty clay. The deposit contains some comminuted shell debris (coarse sand) and this is reflected in a carbonate content of 4%. The sediment suggests a tidal flat depositional environment. Between 2.78m and an erosion surface at 3.00m, a coarser grained unit of fine sand and centre-graded sandy gravel has been deposited. The sediment has a low carbonate content (0.8-1.5%) and contains many detrital plant fragments and small leaves, and is thought to represent a single freshwater flood event. This is preceded by a unit of grey laminated sandy silt and fine sand, with carbonate content values reaching 3%, suggestive of a return to a tidal flat environment, possibly on the edge of a tidal river. Between 1.96m and 2.62m, a unit of dark grey planar laminated micaceous silty clay has been deposited, with leaf and other plant fragments found in some of the partings. Blackened rootlets (some 1-2mm wide) are dispersed throughout the sediment, as are occasional vivianite inclusions. The sediment contains occasional shell grains and the carbonate content value fluctuates between 1.3% and 2.7%. The upper 10cm shows graded lamination, suggestive of a tidal environment. The unit is thought to represent a low-lying area of brackish marsh, marginal to a tidal river within a transitional fluvio-estuarine environment. The wider stratigraphy (figure 5.32) shows that the associated river channel is probably the lower palaeochannel underlying the SW1 core. This channel may have formerly occupied the SW2 site and the area to the east (see figure 5.32, stratigraphic cores 5-7), and following quite rapid westward channel migration to the SW1 site, the eastern area was abandoned as a 50m wide low-lying vegetated

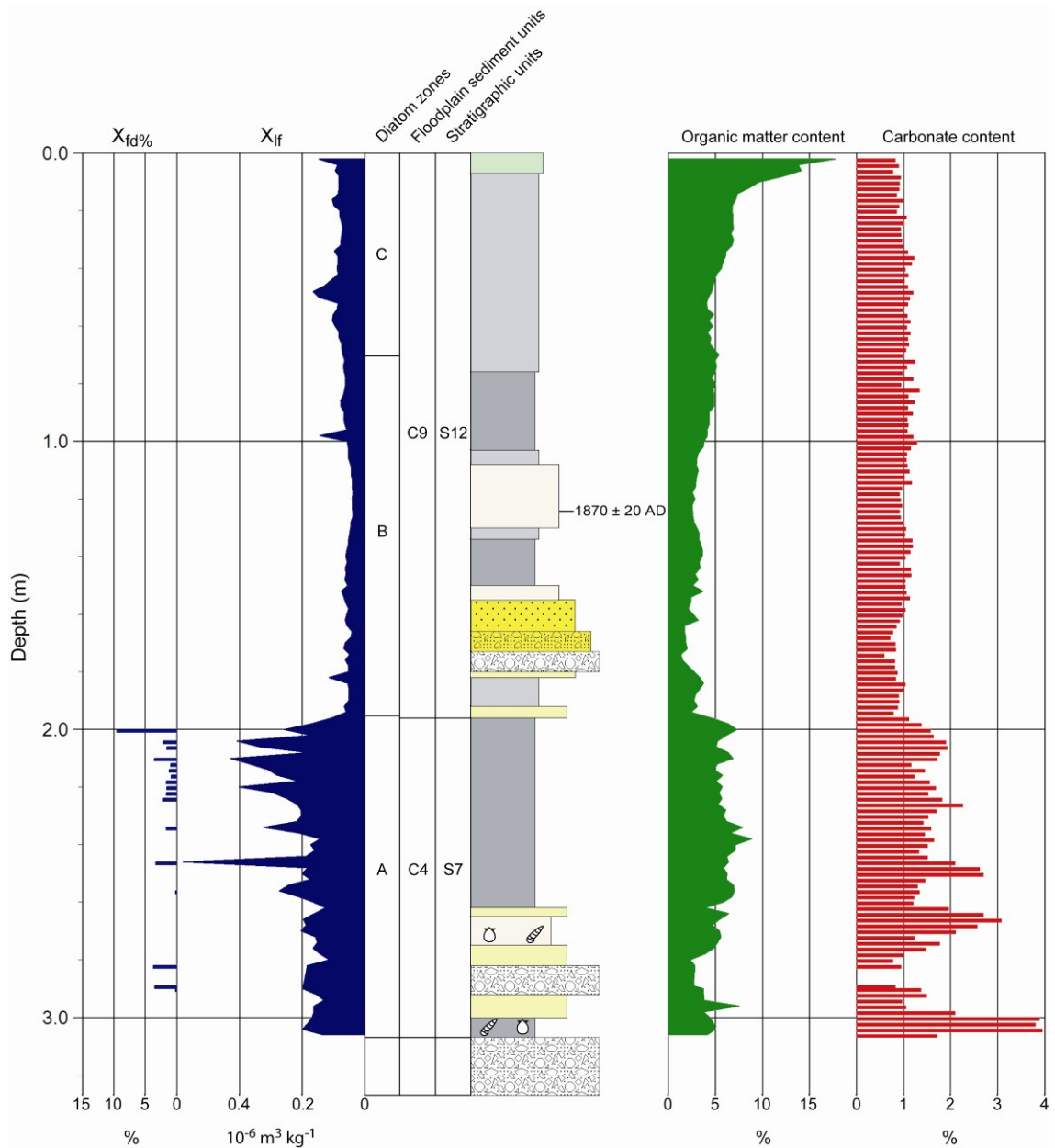


Figure 5.36 SW2 core log. See figure 5.2 for lithology legend. Diatom zones are derived from figure 5.37. Floodplain sediment units (FSUs) are discussed in section 5.4.12. Stratigraphic units are discussed in chapter 7.

bar/marginal marsh, occasionally occupied during high-stage river flow and spring tides. A similar modern analogue environment is located *c.*300m south of New Bridge (see figure 5.31), where vegetated fine grained bars, and a recently abandoned channel, are occasionally inundated by freshwater high tides and high-stage floods.

Above an erosion surface at 1.96m, the upper part of the core has been deposited in an overbank and flood-channel environment, and is known to be much younger (see below). Between 1.82m and 1.96m, a well sorted fluvial sand layer and a graded bed of sandy silt (with occasional rounded pebbles) is deposited. Above this, between 1.50m

and 1.82m, a fining-up sequence of sandy gravel (rounded clasts), gravelly coarse sand, medium sand, and silty sand has been deposited. This is thought to represent a single event flood channel deposit. Between 0.76m and 1.50m, the sediments consist of a mixture of silty clay, clayey silt, and silty sand. Rootlets are found throughout the deposit and the unit probably represents overbank deposition in the flood channel depression. Above 0.76m, grey-brown mottled red-brown floodplain silts have been deposited, with rootlets throughout and occasional coal and cinder fragments.

The X_{lf} results show a marked division between the younger sediments, above 1.96m and the older sediments below. The upper unit has very low values of 0.05-0.10 $10^{-6} \text{ m}^3 \text{ kg}^{-1}$, indicating low concentrations of magnetic minerals. Values in the lower tidal deposits generally range from 0.15 and 0.4 $10^{-6} \text{ m}^3 \text{ kg}^{-1}$, indicative of the typically high values of ferrimagnetic minerals (magnetite and greigite) found in estuarine tidal sediments.

Geochronology

The layer of sandy silt in the flood channel depression has been OSL dated, giving an age of 1870 +/-20 cal.yr.AD. The flood channel itself was probably initiated in the early 19th Century. The channel-margin marsh sediment at the base of the core is probably of a similar age to the SW1 channel, which was OSL dated at 670 +/-150 cal.yr.AD.

Diatom analysis

Figure 5.37 shows a diatom diagram for SW2. All species with counts of >3%TDV are shown, along with the diatom sums. Cluster analysis resulted in three diatom zones (A to C). Diatom valves were found to be well preserved and relatively abundant throughout SW2 (the coarse sand and gravel layers were not analysed).

Zone A (1.95m – 3.07m)

This zone corresponds with the basal fluvio-estuarine sediments. DSI values fluctuate from 0.33 in the basal clay, indicative of marine species dominance, to 0.57-0.67 in the coarser grained layer and basal part of the overlying silty clay, indicating a mixed assemblage. The DSI then falls again to 0.22 at the top of the clay, indicating a return to a marine species dominated assemblage.

This DSI fluctuation is reflected in the species composition and abundance record for zone A. The basal clay at 3.00-3.07m is dominated by polyhalobous planktonic and tychoplanktonic species (45%), with *Delphineis surirella* and *Paralia sulcata* present at >10%TDV, along with *Cymatosira belgica* and *Podosira stelligera* present at >5%TDV. This indicates an intertidal estuarine environment, with the lack of rootlets in the sediment suggesting deposition on a tidal flat that is usually submerged, on the margins of a tidal river channel. There are no mesohalobous or freshwater species present at >5%TDV in this basal clay.

In the middle of zone A, the number of marine planktonics steadily falls to 20%, while the oligohalobous indifferent sum rises to 34%, indicating a mixed fluvio-estuarine environment. The freshwater taxa are dominated by *Achnanthes exilis* and the epiphyte *Cocconeis placentula* at >10%TDV each, with the epiphyte *Synedra ulna* present at >5%TDV. *Achnanthes exilis* has been associated with brackish estuarine channel deposits in other cores (PL2, CF1, TS2), including the adjacent SW1 palaeochannel deposit. The polyhalobous group remains diverse, supporting an estuarine channel margin environment. The mesohalobous sum is 14% at the base of the laminated clay with *Ctenophora pulchella* the dominant brackish species at >5%TDV. This species has become more abundant up-estuary suggesting that this brackish epiphyte may have its ecological niche in the brackish channel margins of the inner estuary. It is an easily fragmented pennate diatom which enables it to be easily transported and incorporated into the channel facies.

At the top of zone A, where the fine grained vegetated channel bar sediments contain tidal lamination and the highest X_{if} values, the DSI value falls to 0.22, indicating dominance by marine taxa. This is seen in the group sums with the polyhalobous sum (planktonic and tychoplanktonic marine species) rising to 62%, with a corresponding fall in freshwater indifferent species numbers to 6%. The mesohalobous sum remains similar to below at 13%. The marine planktonic-tychoplanktonic assemblage is diverse and abundant, with *Paralia sulcata* present at >10%TDV, along with *Actinoptychus senarius*, *Coscinodiscus radiatus*, *Delphineis surirella*, *Podosira stelligera* and *Rhaphoneis amphiceros* all at >5%TDV. This indicates the environment is fully subaqueous for most of the tidal cycle, with sediment sourced from the estuary. However, a small rise in *Nitzschia navicularis* numbers (3.5%TDV) suggests the tidal frame position may equate to the low-mid marsh zones of the Taw Estuary, with some

periods of emergence, although this species may be allochthonous.

Zone B (0.69m – 1.95m)

This zone corresponds with the coarser grained floodchannel deposit above 1.96m and the overlying fine grained fill. Figure 5.37 shows a marked change in environment at the start of this zone, with the disappearance of marine planktonics (0% in the fluvial sand at 1.86m) and the appearance of a large diverse freshwater group (63%), reflected in the initial DSI value of 0.94 at 1.86m. The oligohalobous indifferent group is dominated in this channel sand and silt by the robust *Cocconeis placentula* species and the easily fragmented and transported *Synedra ulna* species (both >10%TDV), with *Pinnularia major* and *Gomphonema angustum* present at >5%TDV. This indicates a largely fluvial environment. The mesohalobous group (11%) is dominated by *Ctenophora pulchella* (8%TDV).

Above the fining-up sequence of bedload deposited gravel and sand, a sample from the silty clay channel fill at 1.42m shows a rise in polyhalobous planktonic-tychoplanktonic numbers to 12.5%, with species dominance by *Paralia sulcata* (6%TDV) and *Podosira stelligera* (2.5%). This indicates that following abandonment of the floodchannel, there was relatively frequent inundation by tidal water with the palaeochannel surface located below MHWST. The numbers of *Paralia sulcata* valves present suggest a tidal frame position equivalent to the Taw Estuary mid-high marsh zones. Also at this horizon (1.42m), a significant mesohalobous group (18%) is dominated by *Ctenophora pulchella* (10%TDV) and *Navicula peregrina* (4%TDV). The presence of *Navicula peregrina* suggests deposition at a high marsh tidal frame position. However, the mid marsh species *Nitzschia navicularis* is also present at 2%TDV at this horizon, suggesting that the tidal frame position may be at the top of the mid-marsh zone, especially given the less saline inner estuary location of SW2, where numbers of this species (if it is autochthonous) are unlikely to reach that seen in transects A and B. Brackish tidal conditions are also indicated by the presence of the halophile *Navicula pusilla* at 8%TDV at 1.42m. The freshwater group (41%) within the silty clay is dominated by the epiphytes *Cocconeis placentula* (>10%TDV) and *Synedra ulna* (>5%TDV).

A sample from higher in zone B at 1.20m sees the marine planktonics group fall to 2.5%, with *Paralia sulcata* present at 2%TDV, suggesting more infrequent tidal

submergence at a high saltmarsh zone elevation. The mesohalobous and halophilous groups are dominated by *Navicula peregrina* and *Navicula pusilla*, also suggesting a high saltmarsh tidal frame position, with *Nitzchia navicularis* disappearing from the assemblage. The oligohalobous indifferent group rises to 51% at this horizon, with *Gomphonema* species joining *Cocconeis placentula* and *Synedra ulna* at >5%TDV.

The most notable change at the top of zone B (at 0.90m) is the further decline in marine planktonics (1%), reduction in numbers of *Navicula peregrina* to 1.5%, and the increase in *Navicula pusilla* to 10%TDV, all suggesting deposition above MHWST.

Zone C (0.00m – 0.69m)

This zone corresponds with the upper floodplain silts. The oligohalobous indifferent group rises further to 57-64% in this zone, indicating a largely freshwater environment. This is supported by polyhalobous numbers remaining at 1%, and halophile species abundance falling to 1%. However, the mesohalobous sum of 8-12% indicates that a freshwater-brackish environment is maintained. This group is dominated by *Navicula avenacea* (10%TDV at the top of the zone) and *Ctenophora pulchella* (5%TDV). *Navicula avenacea* was recorded in low numbers in all Taw Estuary zones, from the tidal flat to the marsh border. Its optimum was actually in the low-mid saltmarsh zones, but this is not a possibility here, with a current depositional altitude of *c.*5.0m (MHWST+30cm) for the sample horizon. However, as shown in chapter 4, this brackish species was recorded in high numbers beyond the up-river tidal limit (HAT), suggesting it is equally freshwater tolerant.

5.4.5 SW3 core

Sedimentology and magnetic parameters

Figure 5.38 shows the core log for SW3. This figure shows down-core changes in sediment lithology, X_{ir} , organic matter and carbonate content. In addition, the FSUs (see section 5.4.12) and stratigraphic units (see chapter 7) are indicated.

The SW3 core is located in a recent palaeochannel and is underlain by gravel at 2.60m (2.12m OD). Between 2.40m and the gravel, interstratified planar layers of coarse

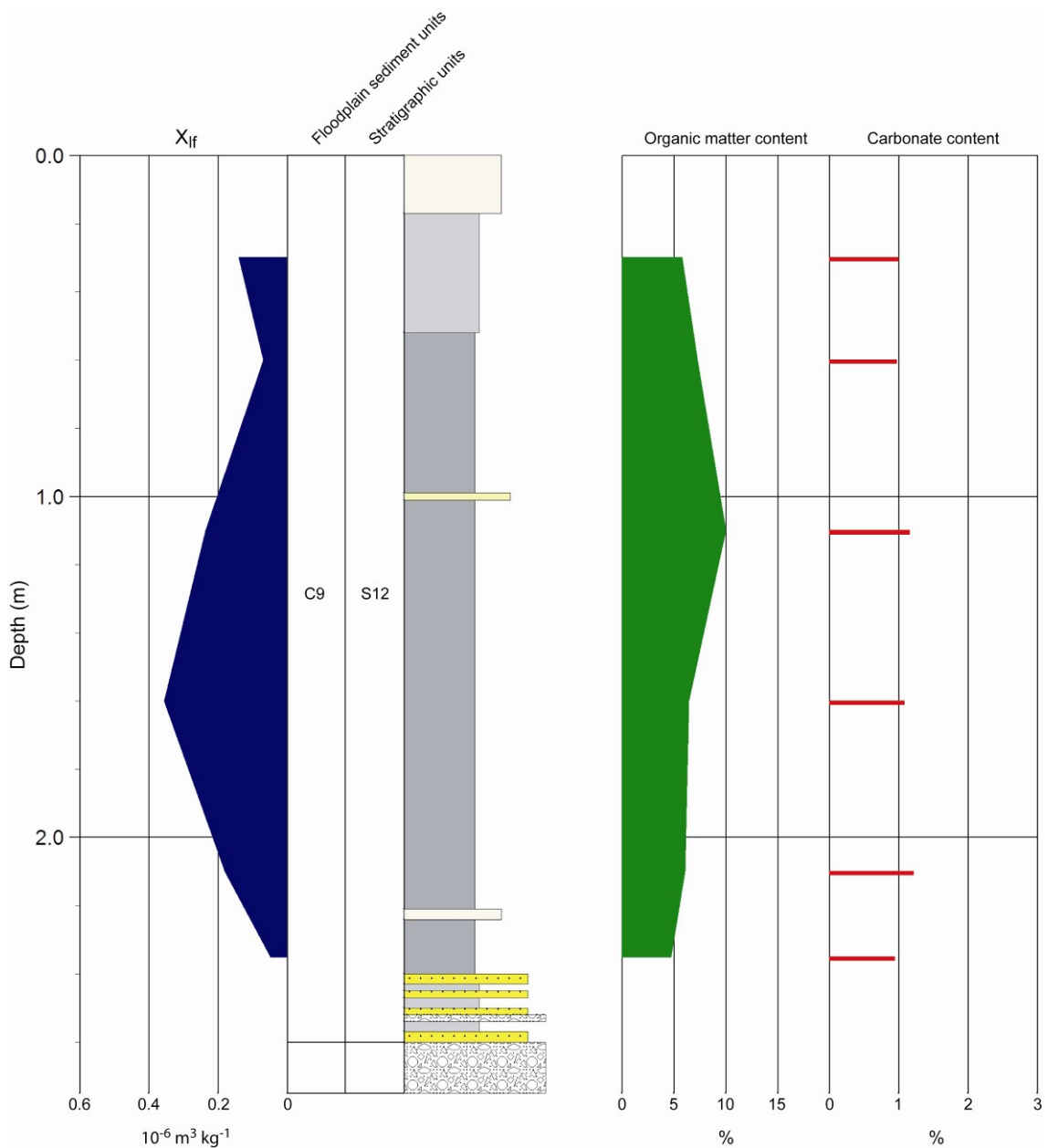


Figure 5.38 SW3 core log. See figure 5.2 for lithology legend. Floodplain sediment units (FSUs) are discussed in section 5.4.12. Stratigraphic units are discussed in chapter 7.

sand/sandy gravel (1-5cm) and clayey silt (1-3cm) have been deposited. This suggests periods of fluvial bedload deposition, intercalated with periods of reduced flow, possibly indicative of a tidal environment. The gravel layers contain subrounded sandstone gravel clasts and occasional angular coal fragments. Between 0.52m and 2.40m, dark grey silty clay has been deposited following channel abandonment. The sediment contains many plant fragments and occasional twigs. Two thin (1-2cm) layers of fine sand are located at 1.00m and 2.21m. Between the surface and 0.52m, the deposit coarsens from a clayey silt to a silty sand, with many fine rootlets.

X_{ir} values are low ($0.1 \cdot 10^{-6} \text{ m}^3 \text{ kg}^{-1}$) at the top and bottom of the clay-silt unit, but rise to $0.36 \cdot 10^{-6} \text{ m}^3 \text{ kg}^{-1}$ in the middle of the clay. This is possibly caused by bacterial magnetite in the water-logged anaerobic conditions likely to be found in a muddy paleochannel fill.

Geochronology

The channel deposits were not dated, but first series Ordnance Survey maps show that it was filled with water in the mid 19th Century. The abandonment of active flow and bedload transport may however have occurred several decades earlier, with the dark grey organic silty clay being deposited in a standing water environment in the mid-late 19th Century.

Diatom analysis

Figure 5.39 shows a diatom diagram for SW3. All species with counts of $>3\%$ TDV are shown, along with the diatom sums. Diatom zones were not justified in this core due to the low number of samples. Diatom valves were found to be well preserved and abundant throughout SW3.

A sample from the silty clay at the base of the core, deposited immediately after channel abandonment, gives a DSI value of 0.74. This is indicative of a diatom assemblage dominated by freshwater species, but also with some brackish-marine taxa. A large oligohalobous indifferent group (48%) is dominated by *Cocconeis placentula* at $>10\%$ TDV, along with *Achnanthes exilis* and *Gomphonema angustum* at $>5\%$ TDV. A small mesohalobous assemblage (5%) is joined by a larger (8%) polyhalobous group, with *Paralia sulcata* present at $>5\%$ TDV. This shows a below MHWST tidal influence, but with a lack of other evidence, a more specific tidal frame position cannot be proposed.

Diatom assemblages from the middle and upper part of the core have DSI values of 0.82-0.84. The assemblages are dominated by freshwater taxa, with the oligohalobous indifferent sum rising to 54-57%. In the middle of the core, this is largely due to an increase in *Achnanthes exilis* numbers to 20%TDV, with *Cocconeis placentula* remaining at $>10\%$ TDV and *Cymbella silesiaca* reaching $>5\%$ TDV. At the top of the

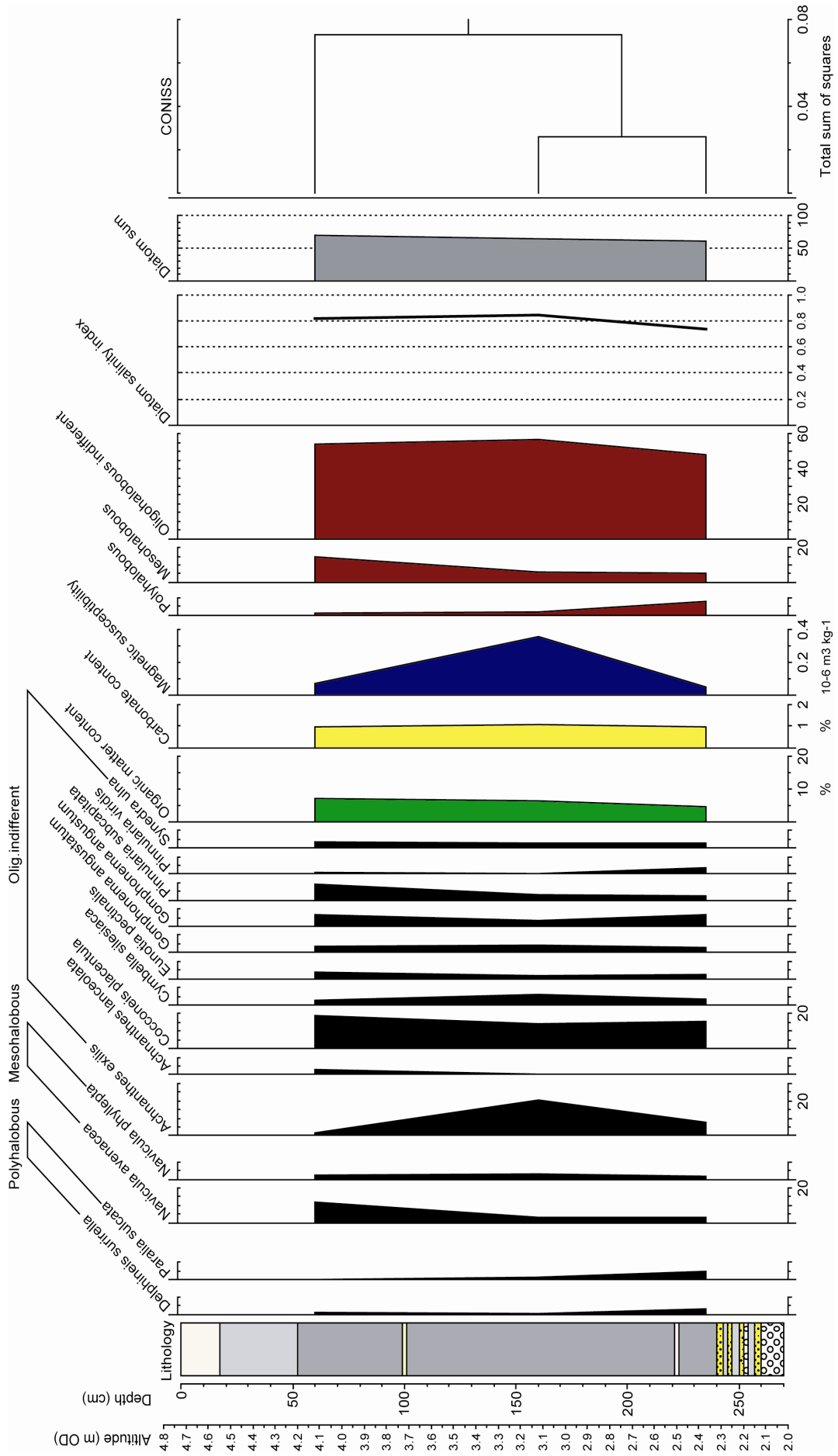


Figure 5.39 Diatom diagram for SW3 core (>3%TDV spp.). Organic matter content, carbonate content, X_{if} and Diatom Salinity Index is also shown.

core, the freshwater group is dominated by *Cocconeis placentula* at >10%TDV, along with *Gomphonema angustum* and *Pinnularia subcapitata* at >5% TDV. *Achnanthes exilis* all but disappears (1.5%TDV), suggesting an increasingly subaerial environment. In the middle and upper parts of the core the polyhalobous sum falls to just 1-2%. The small number of marine planktonics suggests there is little estuarine tidal inundation. The mesohalobous sum remains at 6% in the middle of the core and then rises to 14%, due to an increase in *Navicula avenacea* to >10%TDV, indicating that a slightly brackish environment persists. With a lack of indicator species in the silty clay of the middle and upper core, a tidal frame position cannot be given. However, the current ground surface (60cm above the highest sample horizon) is at 4.7m OD (*i.e.* MHWST). The depositional environment in this young deposit was therefore certainly beneath MHWST, with the lack of marine-brackish planktonics suggesting the palaeochannel depression had little connection with the active channel following initial abandonment.

5.4.6 SW4 core

Sedimentology and magnetic properties

Figure 5.40 shows the core log for SW4. This figure shows down-core changes in sediment lithology, X_{IF} , organic matter and carbonate content. In addition, the diatom zones (see later), FSUs (see section 5.4.12) and stratigraphic units (see chapter 7) are indicated.

The SW4 core is underlain by gravel at 3.88m (1.85m OD). An exposure on the active channel cut-bank (2m from core) reveals that the core is located within a 26m wide palaeochannel (similar width to the current river). The palaeochannel is bounded by gravel banks, with *c.*2.0m of relief between the palaeochannel bed and the top of the gravel (which is *c.*2.0m below ground surface). In the core, between 2.96m and the gravel at 3.88m, interstratified layers of fine-medium sand (5-15cm thick) and dark grey clayey silt (3-13cm thick) are deposited. This indicates mixed fluvio-estuarine channel sedimentation with the clayey silts depositing out of suspension during high tide slack water. Carbonate content values reach 2.4% at the base of this unit, suggestive of estuarine carbonate. Between 2.60m and 2.96m, grey silty sand has accumulated, with occasional detrital plant and wood, indicative of a reduced flow velocity and the start of

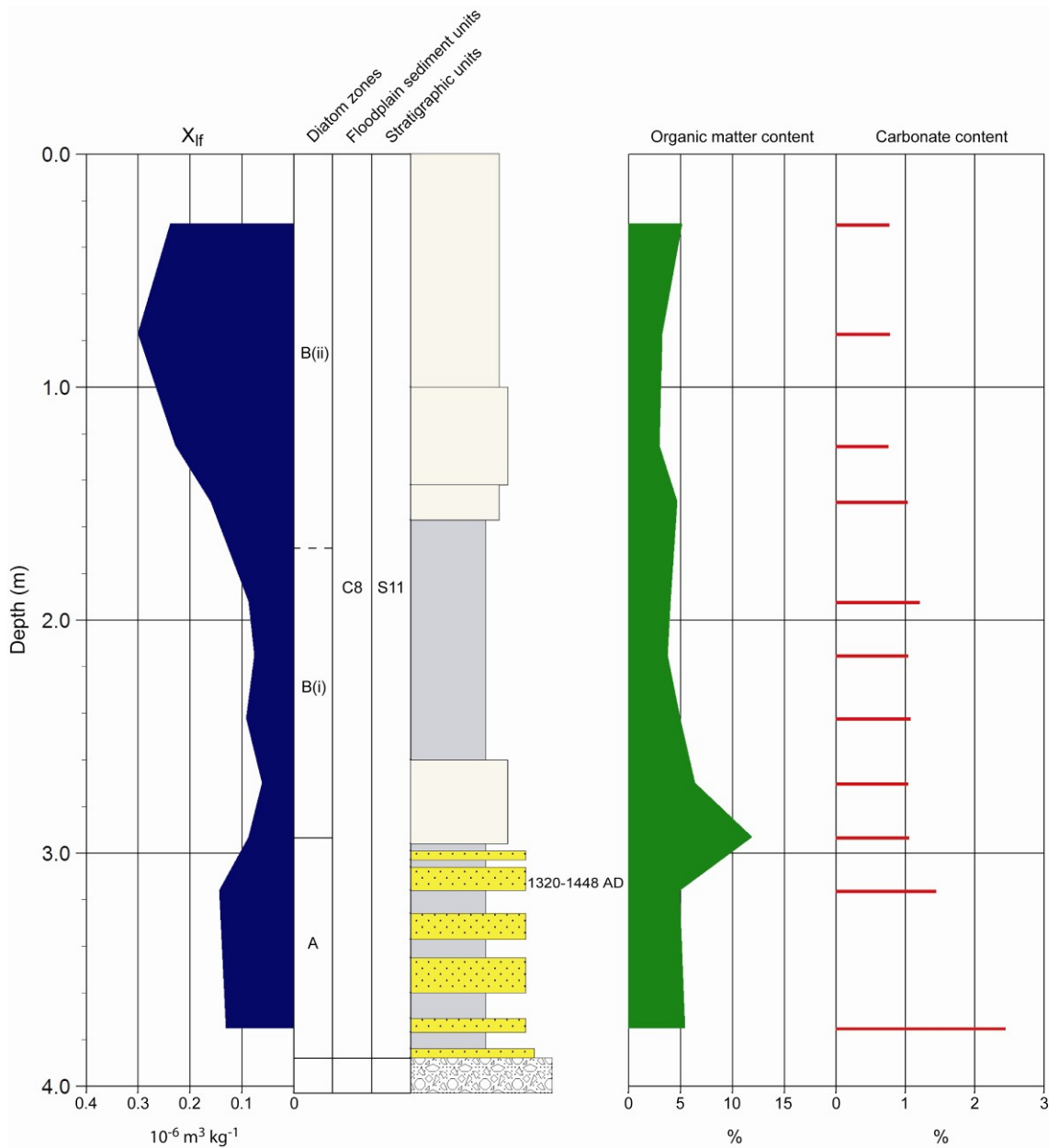


Figure 5.40 SW4 core log. See figure 5.2 for lithology legend. Diatom zones are derived from figure 5.41. Floodplain sediment units (FSUs) are discussed in section 5.4.12. Stratigraphic units are discussed in chapter 7.

channel abandonment. Between 1.57m and 2.60m, grey laminated clayey silts have been deposited, with greenish mottling and occasional plant fragments below 2.28m, and rootlets above 2.28m. These fines represent the gradual filling up of the palaeochannel by overbank sedimentation. Between the surface and 1.57m, brown floodplain sandy silts and silty fine sands have been deposited, with rootlets throughout. The high sand content suggests a levee environment.

X_{lf} values are $c.0.13 \cdot 10^{-6} \text{ m}^3 \text{ kg}^{-1}$ in the tidal channel sands, with the magnetic minerals probably composed of a mixture of detrital haematite and magnetite in this mixed-

source fluvio-estuarine environment. X_{fr} values fall to $c.0.08 \cdot 10^{-6} \text{ m}^3 \text{ kg}^{-1}$ in the palaeochannel fill fines, before rising to $0.3 \cdot 10^{-6} \text{ m}^3 \text{ kg}^{-1}$ in the floodplain sediments. These relatively high values may be due to soil-derived secondary magnetite, but in the absence of reliable $X_{fd\%}$ values, this cannot be confirmed.

Geochronology

A detrital leaf from the top of the basal channel sands and silts was radiocarbon dated, giving an age of 1320-1448 cal.yr.AD for channel abandonment.

Diatom analysis

Figure 5.41 shows a diatom diagram for SW4. All species with counts of $>3\%$ TDV are shown, along with the diatom sums. Cluster analysis resulted in two diatom zones (A and B). Diatom valves were found to be well preserved and abundant throughout SW4.

Zone A (2.93m – 3.88m)

This zone corresponds with the basal tidal channel facies (sands and silts). A DSI value of 0.23 indicates dominance by marine taxa. This is shown in the diatom group sums with the polyhalobous group dominating at 54%, with the smaller mesohalobous and oligohalobous indifferent sums being 9% and 7% respectively. The marine assemblage is composed of planktonic and tycho planktonic species, with *Paralia sulcata* being the dominant species at $>10\%$ TDV. This is joined by *Actinoptychus senarius*, *Coscinodiscus radiatus*, *Cymatosira belgica*, *Delphineis surirella* and *Podosira stelligera* all at $>5\%$ TDV. This indicates an inner estuarine channel environment (with species composition similar to the Taw Estuary tidal flat zone) with dominance by allochthonous marine planktonics. However, it should be noted that the sand layers were not sampled, so there could also be a more fluvial diatom flora intercalated with the marine assemblages.

Zone B (0.00m – 2.93m)

This zone has been divided into two subzones. B(i) corresponds with the bed of organic silty sand and overlying laminated silts associated with channel abandonment. B(ii) corresponds with the floodplain fine sands and silts at the top of the core.

At the base of B(i), in the silty fine sand bed at 2.70m, the DSI value rises to 0.78, indicating a brackish-freshwater assemblage. The numbers of polyhalobous taxa fall to 13%, with the oligohalobous indifferent sum rising to 51%. Despite the relatively small polyhalobous group, diversity in the marine planktonics remains high with four species over 2%TDV (*Paralia sulcata*, *Podosira stelligera*, *Cymatosira belgica* and *Delphineis surirella*). The collective numbers and diversity of marine planktonics would suggest a tidal environment with relative frequent inundation, at a tidal frame position equating to the mid or lower high saltmarsh zones of the Taw Estuary. This is supported by the presence of the mesohalobous species *Navicula salinarum* in the assemblage. In the Severn Estuary quantitative study by Hill *et al.* (2007), this epipelagic species was found to have a particularly small range, with regard to altitude and submergence duration. It was most abundant in the mudflat and low saltmarsh edge, which in the Taw Estuary tidal frame would equate to the mid saltmarsh zone. No counts were recorded by Hill *et al.* (2007) above MHWST. A mid-saltmarsh altitude is tentatively proposed (rather than a lower high saltmarsh altitude) for the 2.70m sample horizon. This is based on the numbers of marine planktonics present (13%) in a transitional fluvio-estuarine environment and the presence of *Navicula salinarum* (which is very tenuous given the 1% abundance value), and partly because the next sampling horizon, 28cm above (2.42m), shows evidence of deposition remaining below MHWST.

In the laminated silts at the top of subzone B(i), the DSI value gradually increases from 0.83 to 0.89, indicating a brackish-freshwater assemblage with increasing amounts of freshwater taxa. This is probably related to upward accretion of the palaeo-surface through the tidal frame during infill of the abandoned channel. The polyhalobous sum declines from 6% at 2.42m to 2% at 2.15m. The marine planktonic assemblage at the 2.42m horizon contains *Actinoptychus senarius*, *Cymatosira belgica*, *Paralia sulcata* and *Podosira stelligera*, all at >1%TDV. This indicates infrequent inundation of the palaeochannel surface by estuarine tidal water, suggesting a tidal frame position below MHWST (high saltmarsh zone) at the base of the laminated silts, rising to MHWST or above at the top of the subzone (marsh border tidal frame zone). This is supported by a decline in the mesohalobous sum from 13% at 2.42m, to 10% at 2.15m. The dominant brackish species are *Ctenophora pulchella* and *Navicula avenacea* (both >5%TDV), while the large freshwater indifferent assemblage (58-59%) is dominated by the salt-tolerant species *Cocconeis placentula* (>10%TDV).

In the upper floodplain sands and silts of subzone B(ii), the DSI rises to 0.93-0.96, indicative of freshwater species dominance. This is reflected in the mesohalobous sum fall to 6%. The large oligohalobous indifferent group (73-74%) is dominated by the salt-tolerant epiphyte *Cocconeis placentula* (22-32%TDV), along with *Achnanthes exilis*, *Cymbella silesiaca*, *Eunotia pectinalis* and *Gomphonema angustum*, all at >5%TDV. This zone sees the appearance of *Hantzschia amphioxys* at 3%TDV. This aerophilous species was recorded by Zong and Horton (1998) and Hill *et al.* (2007) in the marsh border zone, with the highest numbers appearing nearer HAT, rather than MHWST. Vos and de Wolf (1993a) included this species in their brackish-freshwater aerophilous ecological group (which includes *Navicula pusilla* and *Navicula mutica*), indicating it is salt-tolerant. A tidal frame position close to HAT is therefore proposed. Low numbers (3%) of marine planktonics are recorded in this subzone, suggestive of tidal deposition by very high spring tides, supporting an elevation close to HAT.

5.4.7 Lithostratigraphy of the New Bridge transect

Figure 5.42 shows the lithostratigraphy of transect D (New Bridge transect). The floodplain-terrace surfaces are between 5.7m and 6.6m OD, with the higher elevations found in the T1 age deposits within the meander core. The T1 surface is located between 5.90m and 6.59m OD, so above the 5 year HAT of 5.7m OD. However, the NB4 depression, within T1, has a 5.56m OD elevation and was observed to flood during the HAT tide. The T2 surface ranges from 5.69m to 5.98m OD, and a few centimetres of tidal water were observed to flood the lowest depression at NB2 during the HAT tide. The T3 surface is located above the level of HAT, at 5.84m - 6.02m OD.

To the east of the river Taw, fine grained T3 floodplain alluvium has been deposited on top of a shallow gravel surface at 1.6m – 1.9m depth. The overbank deposits consist of grey-brown clayey silts overlying grey mottled grey-brown silty clays. The sediments are mottled orange-brown from oxidised rootlets and post-depositional manganese mineralisation (especially below *c.*80cm). Charcoal fragments are also quite common. Thin palaeochannels (8-15m wide), with clay plugs, suggest a multi-thread anastomosing channel system was active at this time. These deposits and palaeochannel characteristics are very similar to the T3 deposits seen in transect C.

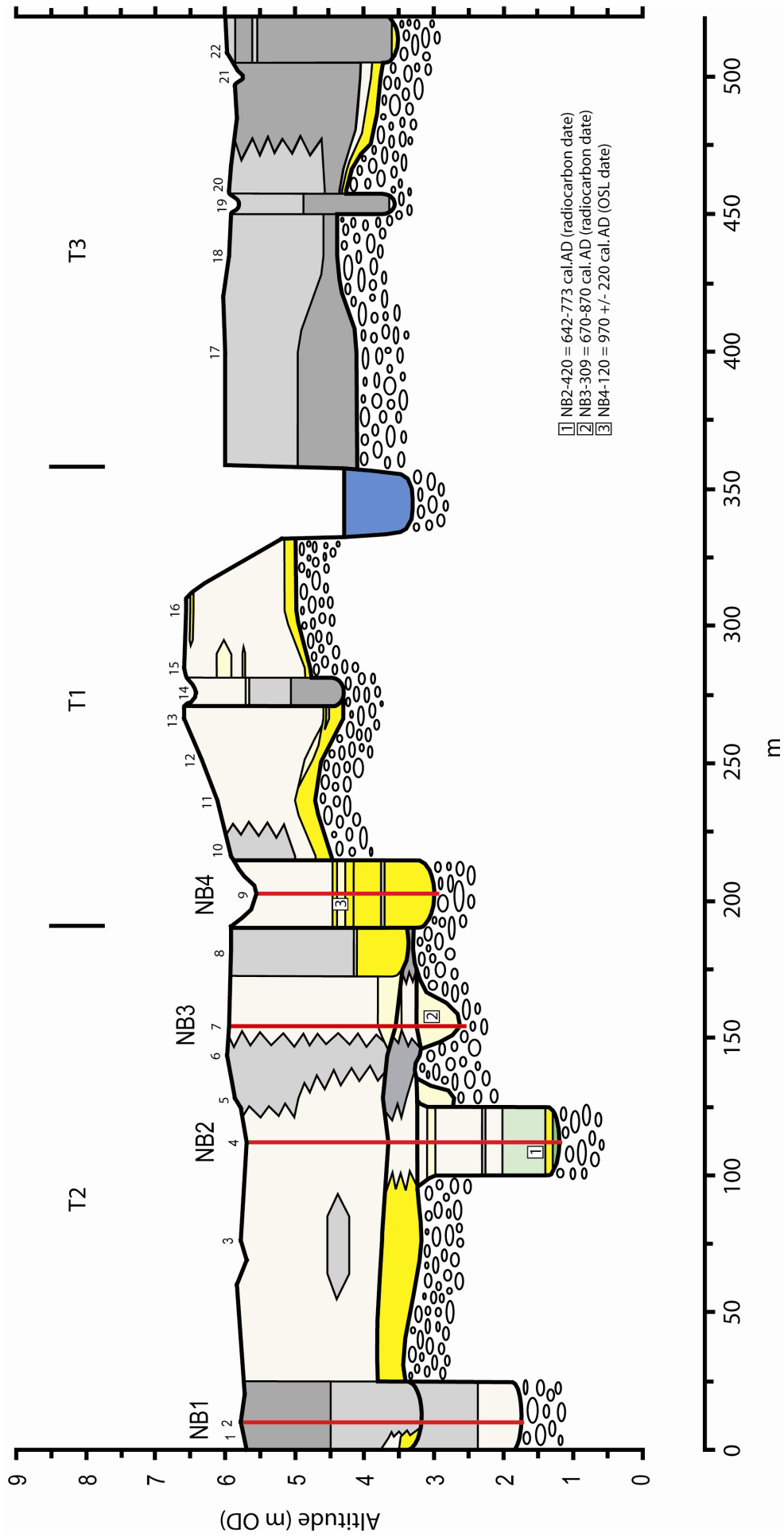


Figure 5.42 Lithostratigraphy of transect D (New Bridge transect). The location of analysed cores, stratigraphic cores (1-22) and radiocarbon/OSL samples (see tables 5.1 and 5.2) is shown. See figure 5.2 for legend.

To the west of the river, within the current meander core, T1 age coarser grained sediments have been deposited during meander migration. Basal point bar gravels are elevated *c.*1.0m above the surrounding T2 and T3 gravel surfaces. These are overlain by bar top medium sands and floodplain sandy silts. A possible chute channel beneath stratigraphic core 14 has been abandoned and infilled with overbank clay and silt. The T1 palaeochannel beneath NB4 was OSL dated at 970 +/-220 cal.yr.AD.

T2 age deposits can be split into two parts. The upper *c.*2.2m consists of sandy silts and silty fine sands. This unit is thought to represent relatively coarse grained overbank alluvium, which has been vertically accreted within a levee environment, with proximity to an active channel. Two paleochannel fills are located within this upper unit (including NB1), containing fine grained silt and clay. The stratigraphy suggests that they were abandoned in avulsion events. A marked change in depositional environment occurs below *c.*2.2m in T2, with the boundary often showing intense manganese mineralisation, suggesting a hiatus in accretion and water-table movement. A 30-40cm layer of grey-green silty sand and organic grey-green silty clay has accumulated over the gravel surface and buried palaeochannel fills (see below). *Phragmites* fragments are found in the silty clay units, indicating a reedswamp environment which extends laterally into the coarser silts which show pronounced greenish staining (the silts tend to overlie deeper palaeochannel fills; *e.g.* NB2 and NB3). Beneath this layer, several palaeochannels are incised into the surrounding gravel (NB1, NB2), with undulating overbank scour occurring in other areas (NB3). The eastern channels and depressions (NB2, NB3) are infilled with organic sandy silts/silty sands (with lots of detrital leaf and plant fragments) and detrital wood peats. The western channel (NB2, lower palaeochannel) contains a finer grained organic silt and silty fine sand fill.

5.4.8 NB1 core

Sedimentology and magnetic properties

Figure 5.43 shows the core log for NB1. This figure shows down-core changes in sediment lithology, X_{lf} , organic matter and carbonate content. In addition, the diatom zones (see later), FSUs (see section 5.4.12) and stratigraphic units (see chapter 7) are indicated.

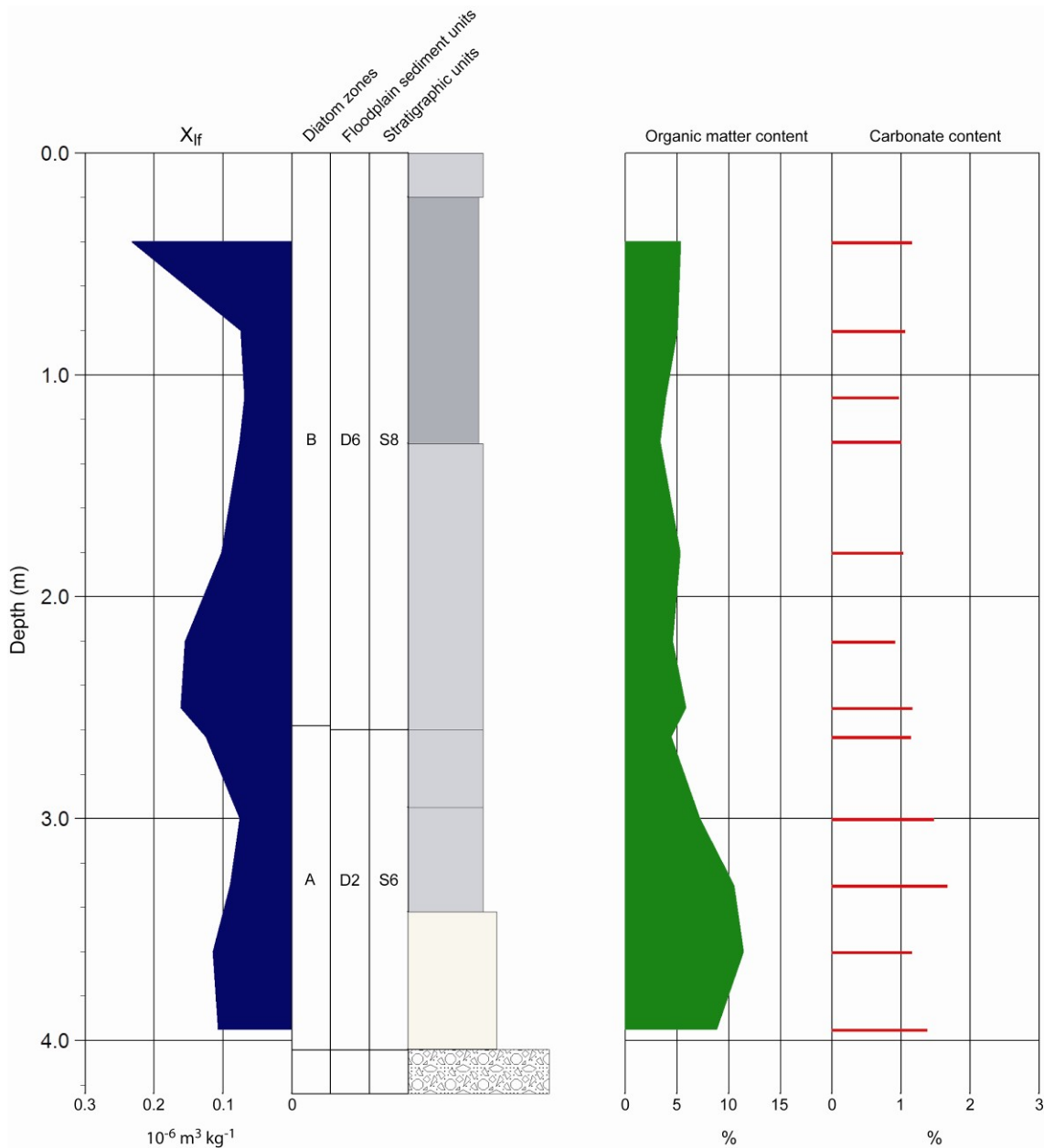


Figure 5.43 NB1 core log. See figure 5.2 for lithology legend. Diatom zones are derived from figure 5.44. Floodplain sediment units (FSUs) are discussed in section 5.4.12. Stratigraphic units are discussed in chapter 7.

The NB1 core is underlain by gravel at 4.04m (1.74m OD). Between 3.42m and the gravel, a brown-purple organic silty sand has been deposited. The sand is laminated, with leaf/plant fragments in the partings. This unit was deposited during the initial stage of channel abandonment, with some connection with the active channel likely. Between 2.60m and 3.42m, a layer of laminated organic clayey silt (with occasional wood/nut/plant fragments) is overlain by a more minerogenic laminated clayey silt. The lack of roots suggests this unit was deposited in a palaeochannel pond.

Above a sharp contact at 2.60m, a unit of grey clayey silt has been deposited up to

1.31m, with greenish staining and some *Phragmites* fragments suggesting a palaeochannel reedswamp. An adjacent core found a thin sandy gravel at the basal boundary, suggesting this upper unit belongs to a separate younger palaeochannel. This nesting of palaeochannels at the valley side was also seen in transect C. Between 0.20m and 1.31m, a gleyed grey mottled brown silty clay has been deposited, suggesting deposition in a waterlogged palaeochannel depression. The sediment contains rootlets/rootlet traces throughout and occasional manganese mineralisation. Above 0.20m, is a grey-brown clayey silt with rootlets.

X_{ir} values range from 0.07 to 0.23 $10^{-6} \text{ m}^3 \text{ kg}^{-1}$, with higher values corresponding with the basal part of each palaeochannel and the surface floodplain sediment. The higher values at the base of each channel are probably due to higher amounts of detrital magnetite or haematite. This gives support for two separate palaeochannel deposits.

Diatom analysis

Figure 5.44 shows a diatom diagram for NB1. All species with counts of $>3\%$ TDV are shown, along with the diatom sums. This figure also indicates the presence of rare species (1-2%TDV) in the polyhalobous, mesohalobous and halophilous groups. These species are not included in the diatom sums and $<1\%$ TDV species are not shown. Cluster analysis resulted in two diatom zones (A and B). Diatom valves were found to be well preserved and abundant in the lower palaeochannel fill, but were very sparse and poorly preserved in the upper palaeochannel.

Zone A (2.57m – 4.04m)

This zone corresponds with the lower palaeochannel fill. DSI values range from 0.93 to 0.96, indicative of a freshwater species assemblage with a small brackish component. Dominant species ($>10\%$ TDV) in the diverse freshwater indifferent group (64-78%) are *Cocconeis placentula* and *Achnanthes exilis*. Significant numbers of halophobous taxa are present in the upper part of the zone (7-8%) where the tychoplanktonic species *Tabellaria flocculosa* reaches 7.5%TDV, giving support to a palaeochannel pond environment. The mesohalobous group remains at 6% with *Navicula avenacea* being the dominant species ($>5\%$ TDV). None of the polyhalobous, mesohalobous or halophilous species that can be used to indicate tidal frame position are present at $>3\%$ TDV. This makes it impossible to classify tidal frame position and suggests that

deposition occurred upstream of the salinity front in the freshwater tidal zone. However, the rare presence of *Paralia sulcata* (1%TDV), *Podosira stelligera* (1%TDV), *Cyclotella meneghiniana* (1%TDV), *Nitzschia sigma* (2%TDV), *Navicula mutica* (2%TDV) and *Diploneis ovalis* (1%TDV) suggests a tidal frame position close to MHWST and suggests some brackish-marine planktonics do become mixed into the freshwater tidal zone. However, they could also be sourced from reworking of channel banks during freshwater back-up.

Zone B (0.00m – 2.57m)

This zone corresponds with the upper palaeochannel fill. In the lower reedswamp silt part of zone B, DSI values range from 0.89-0.94, indicating that the upper palaeochannel is freshwater dominated like in zone A, but with a larger brackish species component. This is seen in the group sums with the mesohalobous sum reaching 13%, with dominant brackish species being *Ctenophora pulchella* and *Navicula avenacea* (both >5%TDV). A small polyhalobous component is also present in the lower part of zone B. The robust tycho planktonic *Delphineis surirella* is present at 3%TDV at the base of the zone (2.50m). This is joined by *Cocconeis scutellum* (2%TDV) and *Podosira stelligera* (1%TDV) at the same horizon, suggesting a tidal environment just down-river of the salinity front, and probably just below MHWST. In the silty clay at the top of zone B the DSI falls to 0.98, indicating an almost total freshwater assemblage. This is reflected in the group sums with the mesohalobous sum falling to 4% and the oligohalobous indifferent sum rising from 69-85% at the bottom of zone B to 90% at the top of the zone.

The freshwater assemblage in zone B is very diverse, but also shows some significant differences in assemblage composition from zone A. Some species disappear (e.g. *Achnanthes exilis*, *Cymbella silesiaca*, *Fragilaria capucina*, *Tabellaria flocculosa*), while others emerge in this zone (e.g. *Pinnularia major*, *Gomphonema acuminatum*, *Hantzschia amphioxys*), signifying a change in the freshwater environment between the two palaeochannel deposits.

5.4.9 NB2 core

Sedimentology

Figure 5.45 shows the core log for NB2. This figure shows down-core changes in sediment lithology, X_{lf} , organic matter and carbonate content. In addition, the diatom zones (see later), FSUs (see section 5.4.12) and stratigraphic units (see chapter 7) are indicated.

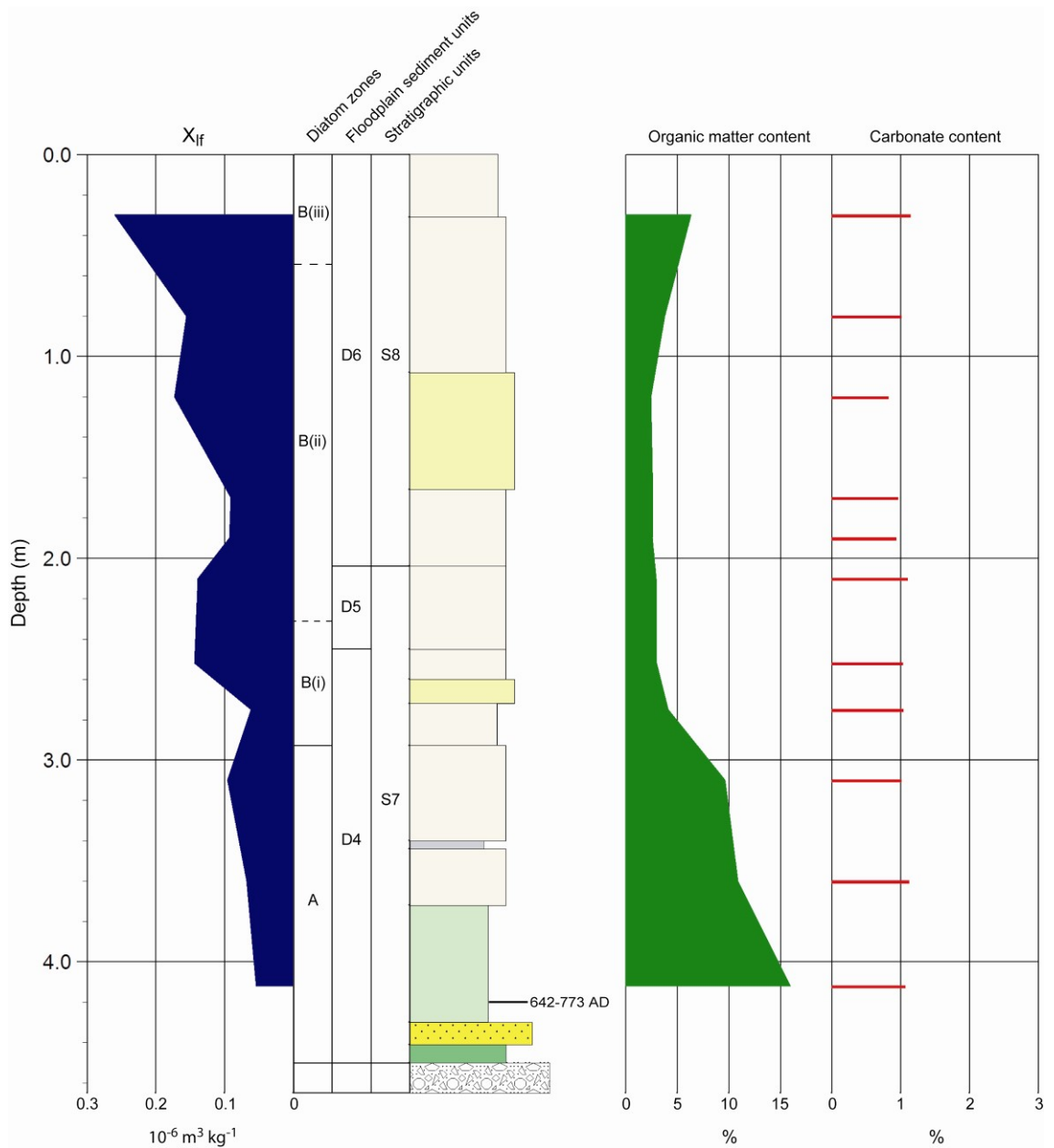


Figure 5.45 NB2 core log. See figure 5.2 for lithology legend. Diatom zones are derived from figure 5.46. Floodplain sediment units (FSUs) are discussed in section 5.4.12. Stratigraphic units are discussed in chapter 7.

The NB2 core is underlain by gravel at 4.50m (1.19m OD). A thin layer of wood detritus and medium-very coarse sand is located at the base of the core, deposited during quite rapid channel abandonment. Above this, between 2.93m and 4.30m, is a unit of organic silty fine sand (10-15% organic matter content). The deposit contains an abundance of organic detritus, including wood, leaves, grass and sedge stems. This suggests deposition within an abandoned channel, possibly ponded, and bounded by tree cover. This deposit grades into a similar but finer grained sandy silt between 2.72m and 2.93m. Between 2.45m and 2.72m, a thin layer of grey fine sand and silty fine sand is deposited, probably deposited during a brief flood through the abandoned channel. Above a sharp contact with much manganese mineralisation at 2.45m is a layer of grey silty fine sand with pronounced greenish staining, suggesting deposition in a minerogenic marsh. Above another sharp contact at 2.04m, again with much manganese mineralisation, the sediments in the upper part of the core consist of minerogenic grey-brown sandy silts, silty sands and fine sands, with occasional manganese concretions and rootlets throughout. This unit suggests overbank floodplain deposition, with proximity to an active channel suggested by the high sand content.

X_{ir} values are relatively low ($0.05-0.14 \times 10^{-6} \text{ m}^3 \text{ kg}^{-1}$) below 1.50m, indicating a small magnetic assemblage. Above 1.50m, the upper floodplain sediment show higher X_{ir} values ($0.16-0.26 \times 10^{-6} \text{ m}^3 \text{ kg}^{-1}$), possibly caused by some soil-derived secondary magnetite.

Geochronology

A detrital tree branch from the base of the lower palaeochannel was radiocarbon dated, giving an age of 642-773 cal.yr.AD for channel abandonment.

Diatom analysis

Figure 5.46 shows a diatom diagram for NB2. All species with counts of $>3\%$ TDV are shown, along with the diatom sums. Rare (1-2%TDV) species from the polyhalobous, mesohalobous and halophilous groups are also shown. Cluster analysis resulted in two diatom zones (A and B). Diatom valves were found to be well preserved and relatively abundant below 1.6m, but sparse and fragmented in the upper floodplain deposits.

Zone A (2.93m – 4.50m)

This zone corresponds with the lower organic palaeochannel fill. A largely freshwater assemblage is shown by DSI values of 0.94-0.95. The large diverse oligohalobous indifferent group (73-80%) is dominated by *Achnanthes exilis* and the epiphyte *Gomphonema angustum* (both >10%TDV). The small diatom *Achnanthes exilis* has consistently been associated with channel and ponded palaeochannel environments in transects B, C and D, suggesting that this epontic diatom (Denys, 1991) may also have a tychoplanktonic life form. The small mesohalobous group (8-10.5%) is dominated by *Navicula avenacea* (>10%TDV), which has been seen in chapter 4 to have very wide tolerance of both freshwater and brackish salinities. There are no indicator species present at >3%TDV that would justify a tidal frame position being proposed (*i.e.* largely salt-tolerant species found in the Taw Estuary transect, or in other other studies, that have been shown to have an altitudinal range and optimum relating to tidal submergence duration). This suggests deposition occurred upstream of the salinity front within the freshwater tidal zone where saline ground water intrusion can still maintain a slightly brackish environment.

Zone B (0.00m – 2.93m)

This zone has been divided into three subzones. B(i) corresponds with the sandy silt and fine sand immediately above the organic palaeochannel deposit and below the greenish sands. B(ii) corresponds with both the greenish sands and the bulk of the floodplain sands and silts above. B(iii) corresponds with the top of the floodplain sediments above 0.55m.

In B(i), the DSI values remain similar to zone A at 0.93-0.95, indicating a largely freshwater assemblage. The diverse oligohalobous indifferent group (65-76%) is dominated by the epiphyte *Cocconeis placentula* (>10%TDV), with *Achnanthes exilis* numbers falling significantly to 4% at the base of the subzone and disappearing at the top of the zone, suggesting the pond has now been filled up with sediment. Tychoplanktonic *Fragilaria* species also disappear. *Navicula avenacea* remains the dominant brackish species (>5%TDV) in the small mesohalobous group (9-11%). A tidal frame position cannot be proposed due to a lack of indicator species.

Above the mineralised sharp contact at 2.45m, the DSI falls to 0.88-0.90 in the lower part of subzone B(ii). This indicates an increase in the abundance of brackish species

and this is reflected in the mesohalobous sum which rises to 21%. This is largely due to the increase in numbers of the brackish epiphyte *Ctenophora pulchella* (to 20%TDV). This species lives in aquatic and moist subaerial conditions (Denys, 1991), suggesting a brackish waterlogged marsh environment. Although a tidal frame position cannot be proposed for this part of the core, the increase in brackish species numbers suggests the location of this site is now more proximal to the salinity front. The oligohalobous indifferent group falls to 59% at the base of B(ii) and is dominated by the epiphytes *Cocconeis placentula* and *Synedra ulna* (both >10%TDV). The top of the subzone B(ii), sees a rise in oligohalobous indifferent taxa (69%) and a fall in the mesohalobous group (11%), reflected in a rise in the DSI value to 0.94. This suggests a higher depositional elevation.

At the top of the core in subzone B(iii), the DSI value rises to 1.00, indicating a total freshwater assemblage. The freshwater assemblage is dominated by *Cocconeis placentula*, *Hantzschia amphioxys* and *Pinnularia subcapitata* (all >10%TDV). The only mesohalobous or halophilous species present is *Ctenophora pulchella*, at 1%TDV. This suggests the high elevation of the floodplain is now above the level of HAT (which is confirmed by a current elevation of HAT+39cm for the sample horizon).

5.4.10 NB3 core

Sedimentology and magnetic properties

Figure 5.47 shows the core log for NB3. This figure shows down-core changes in sediment lithology, X_{lf} , $X_{fd\%}$, organic matter and carbonate content. In addition, the diatom zones (see below), FSUs (see section 5.4.12) and stratigraphic units (see chapter 7) are indicated.

The NB3 core is underlain by gravel at 3.34m (2.61m OD). Between 2.93m and the gravel, a unit of grey mottled green laminated sandy silt has been deposited. The silt is interlaminated with thinner layers of fine sand (2-6cm), indicating some fluvial deposition in this floodplain scour (figure 5.42). Some detrital grass and leaf fragments are seen in the lamination partings. Between 2.41m and 2.93m, a unit of interbedded fine sand and silty sand indicates some bedload transport within a possible depression

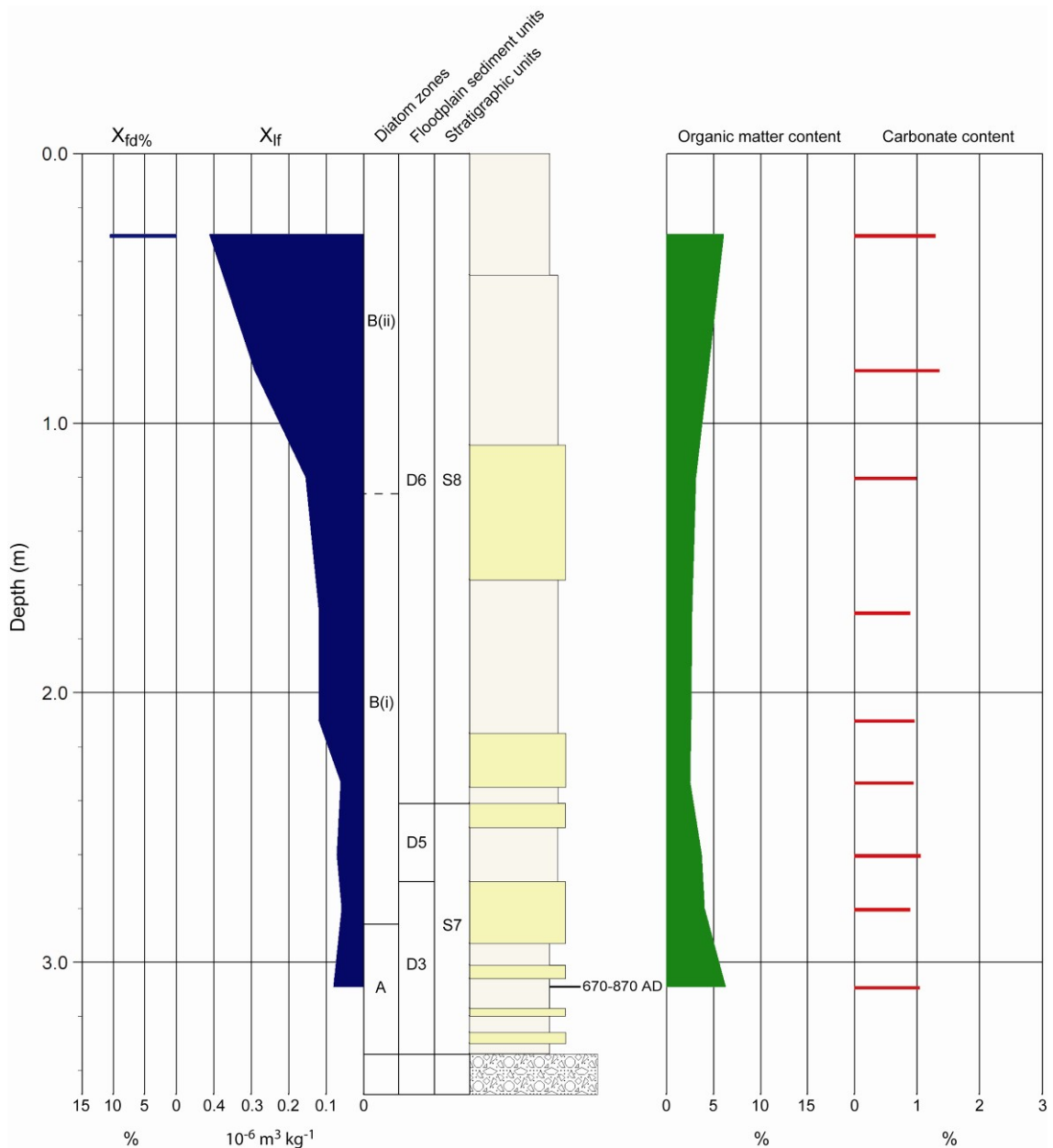


Figure 5.47 NB3 core log. See figure 5.2 for lithology legend. Diatom zones are derived from figure 5.48. Floodplain sediment units (FSUs) are discussed in section 5.4.12. Stratigraphic units are discussed in chapter 7.

above the more active fluvial scour deposits. This may have been inundated during high-stage floods. However there is also pronounced greenish staining and occasional *Phragmites* fragments, suggesting the depression was also vegetated by reedswamp.

Above a sharp contact, with much manganese mineralisation, a unit of grey fine sand and grey-brown silty fine sand has been deposited up to 1.58m, with occasional manganese concretions and another horizon of intense manganese mineralisation at 2.15m. These sands may have been deposited laterally and be associated with lateral migration of an adjacent palaeochannel deposit (see stratigraphic core 8, figure 5.42).

The surface sediments above 1.58m consist of a fining-up sequence of brown fine sand, brown silty fine sand, and grey-brown sandy silt, with occasional rootlets throughout. These sediments have probably been accreted vertically within a floodplain levee environment.

X_{if} values are very low throughout most of the core ($0.06-0.15 \cdot 10^{-6} \text{ m}^3 \text{ kg}^{-1}$), before rising to $0.29-0.41 \cdot 10^{-6} \text{ m}^3 \text{ kg}^{-1}$ in the surface 1m of the floodplain sediments. An $X_{fd\%}$ value of 10.6% indicates the magnetic assemblage is dominated fine viscous SSD/SP grains, which are often associated with soil-derived secondary magnetite.

Geochronology

A leaf from the basal interlaminated silt and sand unit was radiocarbon dated, giving an age of 670-870 cal.yr.AD for abandonment of the basal flood deposit, and the start of a sandy reedswamp marsh environment. This date is very similar to the abandonment age of the adjacent NB2 palaeochannel, suggesting that the two environments were contemporaneous, with the NB2 scour infill deposit representing a chute or slough channel environment at the back of a wide pont bar (Harms *et al.*, 1963). Both the river and the bar top/chute facies were then abandoned, to be replaced by a reedswamp over the former channel zone. This is very similar to what was seen in transect C, beneath SW1 and SW2. The SW1 basal palaeochannel also had a similar 7th/8th Century AD age, suggesting that the deposits beneath NB2 and NB3 are an upstream continuation of the same river channel zone.

Diatom analysis

Figure 5.48 shows a diatom diagram for NB3. All species with counts of $>3\%$ TDV are shown, along with the diatom sums. Rare (1-2%TDV) species from the polyhalobous, mesohalobous and halophilous groups are also shown. Cluster analysis resulted in two diatom zones (A and B). Diatom valves were found to be well preserved and relatively abundant throughout NB3, although valves above 2.40m were slightly more fragmented.

Zone A (2.85m – 3.34m)

This zone corresponds with the basal interstratified sands and silts (possible chute

environment). A DSI value of 0.94 indicates a largely freshwater assemblage. The large oligohalobous indifferent group (76%) is dominated by *Achnanthes exilis* (which has been associated with flowing or standing water) and the epiphyte *Cocconeis placentula* (both >10%TDV). The small mesohalobous group (9%) is dominated by *Ctenophora pulchella* (4%TDV). The brackish epipellic species *Navicula phyllepta* is present at 3%TDV in zone A. This species was observed in the Taw Estuary to have a wide range from the tidal mudflat up to MHWST. However, its optimum was in the high saltmarsh zone, just below MHWST, where levels reached 12.5%TDV. This may suggest a similar tidal frame position, but any inference would be very tentative as this species was also found in the river Taw samples to be freshwater-tolerant.

Zone B (0.00m – 2.85m)

This zone has been divided into two subzones. B(i) corresponds with both the greenish silts and sands (possible marsh environment) at 2.41-2.93m and the overlying channel deposit of laterally accreted fine sand and silty fine sand. B(ii) corresponds with the fining-up sequence of brown floodplain sands and silts.

In the green sands at the base of B(i) the DSI value of 0.95 is very similar to zone A and indicates a similarly largely freshwater assemblage. The large oligohalobous indifferent group (69%) is dominated by the epiphytes *Cocconeis placentula* (>10%TDV), *Eunotia pectinalis* and *Gomphonema angustum* (both >5%TDV), with the dominance by epiphytes supporting a marsh depositional environment. *Ctenophora pulchella* remains the dominant mesohalobous species (6%TDV). A lack of tidal frame indicator species means a tidal frame position cannot be proposed. This probably means that the site is non-tidal or only reached by occasional freshwater tides.

Above the sharp contact with manganese mineralisation at 2.41m, the DSI in the laterally accreted channel sands falls to 0.90-0.92. This suggests a freshwater species dominated assemblage with a significant brackish component. The oligohalobous indifferent sum falls to 57%, with the dominant species being *Cocconeis placentula* (>10%TDV). A rise in the halophobous sum at the top of subzone B(i) is due to the presence of *Pinnularia subsolaris* at 11%TDV. The mesohalobous group rises to 16-17% (from 9% at the base of subzone B(i)), indicating an increasingly mixed freshwater-brackish environment, with probable proximity to the salinity front. This

group is dominated by *Ctenophora pulchella* at >10%TDV. A lack of indicator species means a tidal frame position cannot be proposed.

In the the floodplain sands and silts of subzone B(ii) the DSI value rises to 0.99, indicating an almost exclusively freshwater assemblage. The large oligohalobous indifferent group (69-81%) is dominated by the epiphytes *Cocconeis placentula* and *Gomphonema angustum* (both >10%TDV). *Ctenophora pulchella* is the only mesohalobous species at the top of the subzone (1.5%TDV). The increasingly freshwater assemblage in this subzone suggests floodplain accretion above HAT.

5.4.11 NB4 core

Sedimentology and magnetic properties

Figure 5.49 shows the core log for NB4. This figure shows down-core changes in sediment lithology, X_{lf} , $X_{fd\%}$, organic matter and carbonate content. In addition, FSUs (see section 5.4.12) and stratigraphic units (see chapter 7) are indicated.

The NB4 core is underlain by gravel at 2.55m (3.01m OD). Between 1.39m and the gravel at 2.55m, a thick unit of gravelly medium-very coarse sand is deposited, indicating a high-energy fluvial channel environment. This unit may represent an abandoned bar deposit or an aggrading channel bed. A thin lense (5cm) of grey minerogenic clayey silt in the middle of the deposit may indicate slack water deposition during a particularly high freshwater tide. Between 1.12m and 1.39m, interstratified layers of fine and medium sand may represent finer bar top sediment (Cant and Walker, 1978) or lower flow velocities associated with the start of channel abandonment. The upper part of the core, above 1.12m, consists of brown silty fine sand (0.38m – 1.12m), overlain by grey-brown sandy silt (0.00m – 0.38m). A lack of rootlets in the silty sand suggests deposition by lateral accretion during migration of a sandy point bar, with meander migration being the cause of channel change rather than cut-off or avulsion. The upper silts do contain rootlets, and represent vertical floodplain accretion following channel migration.

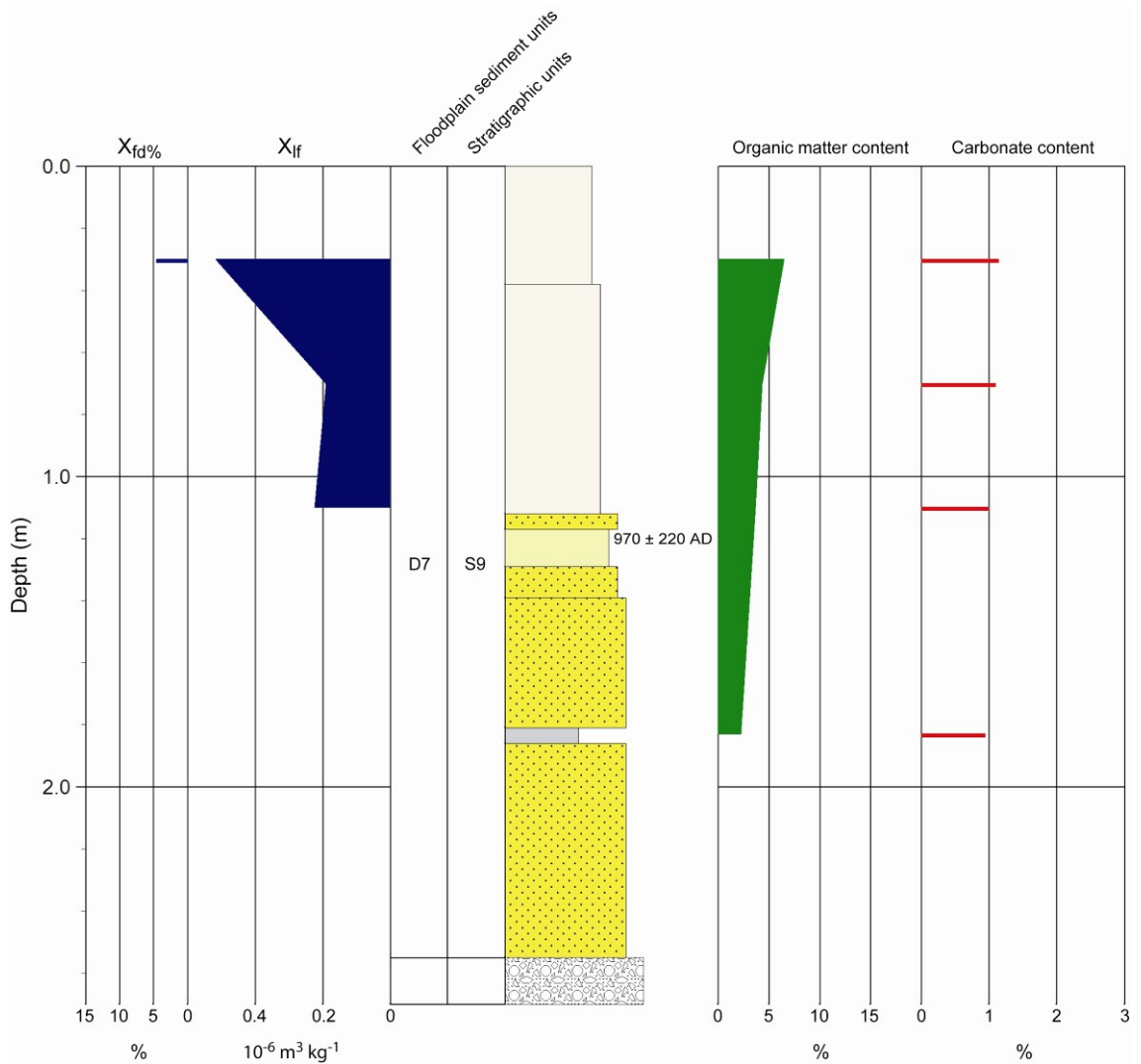


Figure 5.49 NB4 core log. See figure 5.2 for lithology legend. Floodplain sediment units (FSUs) are discussed in section 5.4.12. Stratigraphic units are discussed in chapter 7.

X_{if} values show moderate values in the silty sand bar top sediments ($0.19\text{-}0.22 \cdot 10^{-6} \text{ m}^3 \text{ kg}^{-1}$) and is probably mainly derived from catchment sourced haematite. A high concentration of magnetic minerals is seen in the upper floodplain silt, where X_{if} values rise to $0.52 \cdot 10^{-6} \text{ m}^3 \text{ kg}^{-1}$. The $X_{fd\%}$ value is 4.5%, indicating only minor amounts of fine viscous SSD/SP grains, suggesting that most of the magnetic grains are SSD or MD and detrital (primary) in origin. There was insufficient sample recovered from the silt lense to make a reliable magnetic susceptibility measurement.

Geochronology

The bar top medium/fine sands were OSL dated, giving an age of $970 \pm 220 \text{ cal.yr.AD}$

for channel migration away from this site. The wider stratigraphy (figure 5.42) suggests migration to the north-east.

Diatom analysis

Figure 5.50 shows a diatom diagram for NB4. All species with counts of >3%TDV are shown, along with the diatom sums. Rare (1-2%TDV) species from the polyhalobous, mesohalobous and halophilous groups are also shown. Diatom zones were not justified in this core due to the low number of samples. Diatom valves were found to be moderately preserved (some fragmentation) and relatively abundant throughout NB4 (the coarse sands were not sampled).

Within the basal coarse channel bar sands, only the silt lense was sampled, so the assemblage may not be representative of the coarser sediment facies. A DSI value of 0.90 indicates dominance by freshwater species, but with a significant brackish component. This is shown in the group sums with the oligohalobous indifferent sum being 57%, and the mesohalobous sum being 20%. Dominant freshwater species are *Cocconeis placentula* and *Synedra ulna* (both >10%TDV). The mesohalobous group is dominated by *Ctenophora pulchella* (12%TDV) and *Navicula avenacea* (8%TDV). The numbers of these species suggest a brackish environment but the total lack of any marine or brackish planktonics indicates a location upstream of the salinity front, with deposition of the silt by a freshwater high tide. These mesohalobous species will therefore be allochthonous, having been sourced from the adjacent channel banks/floodplain which will be slightly brackish because of saline groundwater intrusion.

In the silty fine sands and floodplain silts above 1.12m, the DSI values fall to 0.95-0.97, indicating a freshwater assemblage, with a minor contribution by brackish species. The oligohalobous indifferent sum rises to 69-73%, with the dominant freshwater species being *Cocconeis placentula*, *Pinnularia subcapitata* and *Synedra ulna* (all >10%TDV). The aerophilous species *Hantzschia amphioxys* also reaches >10%TDV abundance in the surface floodplain silts. The mesohalobous group falls to 4-8% and is dominated by *Ctenophora pulchella* (8%TDV at the base of the fine sands; 2.5%TDV at the top of the core). The assemblage indicates deposition upstream of the salinity front and if the environment is still tidal (freshwater) there are no tidal frame indicator species present

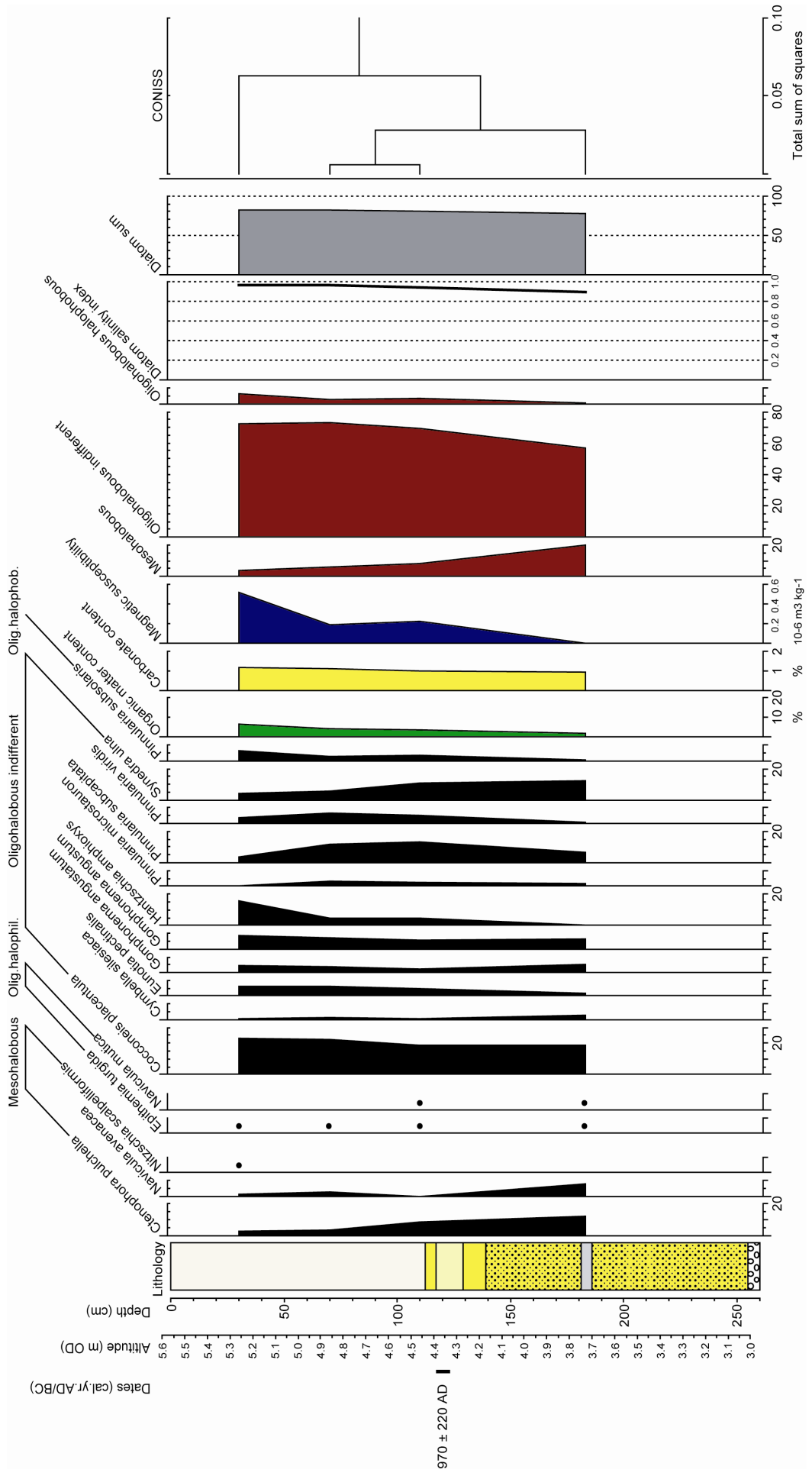


Figure 5.50 Diatom diagram for NB4 core (>3%TDV spp.). Organic matter content, carbonate content, X_r and Diatom Salinity Index is also shown.

to propose a tidal elevation. However, as the modern floodplain surface at NB4 is at 5.56m OD (*i.e.* HAT + 26cm), the upper part of the core is likely to have accreted above HAT.

5.4.12 Phases of geomorphic and environmental change in the New Bridge reach

Straypark Wood Transect

Figure 5.51 shows the FSUs for transect C (Straypark Wood transect).

FSU C1

This unit represents a phase of fine grained (silt and clay) floodplain alluviation over a shallow gravel surface. Palaeochannel dimensions, which are too small individually to contain a bank-full discharge, suggest an anastomosing multi-thread channel system.

FSU C2

This unit is very similar to C1 with a combination of fine grained vertically accreted floodplain sediments and thin palaeochannels suggesting an anastomosing channel system (Smith and Smith, 1980; Makaske, 2001).

FSU C3 and FSU C4

FSU C3 represents deposition in a meandering sand bed river, with stratified bank-attached sand bars and minor amounts of estuarine shelly sand. The site is located not far downstream from the salinity front, within a tidal fluvio-estuarine environment. The channel was abandoned at 670 +/-150 cal.yr.AD. The adjacent FSU C4 represents a wide vegetated sand and silt bar complex, which was initially the site of the C3 river before it migrated 50m to the west. Much of it is thought to have been deposited contemporaneously with the C3 channel deposits within a marginal channel environment that is tidal and frequently submerged during high-stage floods and high tides. The channel system appears to have been abandoned during an avulsion event, with the new river course now removed from the record during later FSU C7 channel activity (figure 5.51). The geomorphic change evident in the C3-C4 channel complex shows that the 7th Century AD was a time of significant instability in the fluvio-estuarine system.

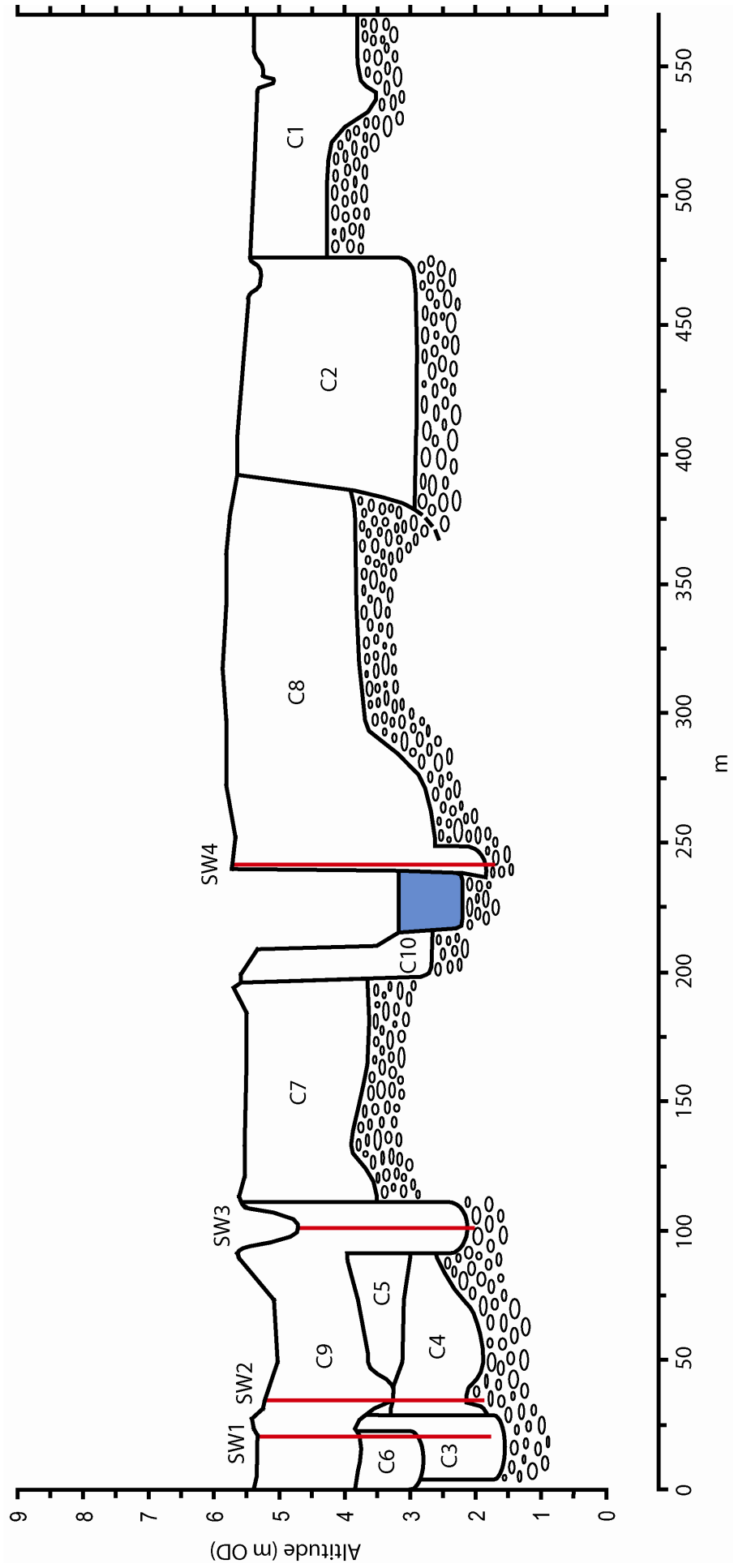


Figure 5.51 Transect C (Straypark Wood transect) Floodplain Sediment Units (FSUs).

FSU C5

Overlying the C4 vegetated bar sediments is FSU C5. This unit shows that following abandonment of the channel environment below, vertically accreted floodplain sediments were deposited over the site. These consist of mottled grey-brown clayey silts (with some manganese mineralisation), typical of more fluvial overbank floodplain alluviation.

FSU C6

This unit represents a buried palaeochannel deposit on the western edge of the valley floor. It is thought to be a flood channel deposit, that has re-occupied the site of the former C3 river. There is evidence that the basal estuarine channel fill was deposited during a storm surge at *c.*1300 AD. This date is based on a 1257-1401 cal.yr.AD radiocarbon date from wood in a sand bed 40cm above the basal erosion surface. The probability curve for this date shows two discrete peaks (see chapter 7, figure 7.3). The earlier, and larger, peak is thought to be the most likely and this has a 1σ age of 1274-1311 cal.yr.AD.

The storm surge deposit consists of poorly sorted gravelly shelly fine-medium sand, containing many mud casts created by crustaceans (or worms). These organisms must have been transported from the mid/outer estuary mudflats in a high velocity, turbulent tidal surge. The deposit shows immediate abandonment, with a phase of low-energy silt deposition prior to being briefly re-occupied, with fluvio-estuarine sand deposition.

FSU C7

An aggradational phase of sedimentation is seen to the west of the River Taw. This unit contains a fining-up sequence of gravelly sand, medium-coarse sand, fine sand and sandy silt, overlying an elevated gravel surface. This represents channel and point bar lateral accretion deposits from a migrating gravel-sand bed river, indicating a high-energy fluvial regime (high discharge and bed shear stress) with significant levels of coarse grained sediment influx.

FSU C8

On the east bank of the river, a 240m wide unit of floodplain alluvium has been deposited. The gravel surface is generally at the same elevation as that seen in C7 (figures 5.32 and 5.51), suggesting a continuation of the aggradational phase of

floodplain development. The basal gravel reflects gravel point bar migration, with the overlying finer grained sediments (silty clays and silty sands, with some coarse sands on the bar top) accreted both laterally and vertically during active channel migration. A palaeochannel deposit within this unit (SW4) shows a mixed fluvio-estuarine tidal environment, with intercalated channel deposits of tidal silt and fluvial sand. Diatom evidence indicates a brackish environment (in both the channel and channel margins), with tidal silt layers containing assemblages dominated by marine planktonic-tychoplanktonic taxa, indicating an estuarine provenance. The significant phase of channel migration that takes place in this unit suggests a period of high discharge and sustained channel-bank erosion.

FSU C9

This unit includes the SW3 palaeochannel and the upper *c.*1.5m of floodplain sediment to the west. SW3 is thought to be a flood channel that was initiated in the early 19th Century AD, and was later infilled by fine grained sediments, deposited within a brackish palaeochannel pond. The alluvium to the west of this channel was deposited in a high-magnitude flood, also in the early 19th Century (possibly in the same event that created the SW3 channel), which caused the erosion and stripping of the previous floodplain sediment down to a maximum of 1.96m, and left a gravel lag within the flood scour, before being gradually filled in by later high tides and high-stage overbank floods.

FSU C10

This unit is located on the inner bend of a currently active meander, beside a gravel point bar, and is thought to have been deposited during the 20th Century AD. It consists of intercalated sands and sandy silts, representing a laterally accreted channel/point bar sequence deposited during recent channel migration. The gravel bar surface is *c.*1.0m deeper than the gravel bars of C7 and C8, suggesting a reduction in sediment supply and/or discharge.

New Bridge Transect

Figure 5.52 shows the FSUs for transect D (New Bridge transect).

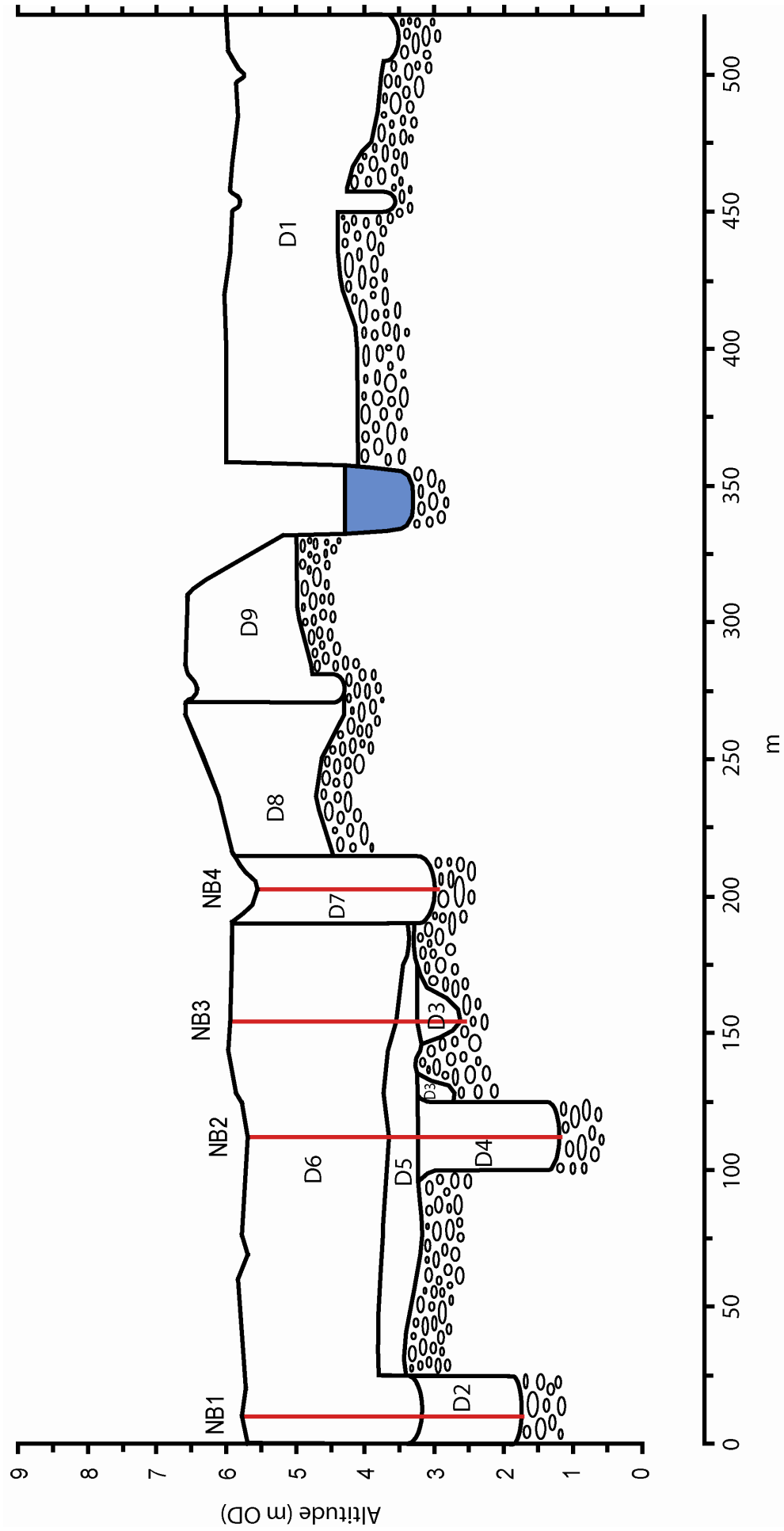


Figure 5.52 Transect D (New Bridge transect) Floodplain Sediment Units (FSUs).

FSU D1

This unit represents a phase of fine grained (silt and clay) vertically accreted floodplain alluviation over a shallow gravel surface, very similar to that seen in C1 and C2. Thin palaeochannels (with clay plugs) suggest an anastomosing multi-thread channel system.

FSU D2

This unit is based on the lower NB1 palaeochannel which contains a fine-grained abandoned channel fill, deposited within a slightly brackish environment, upstream of the salinity front.

FSU D3 and FSU D4

FSU D3 represents deposition in a slightly brackish ponded abandoned channel (just upstream of the salinity front), with a fill of organic sand and silt with much wood and leaf detritus. The channel was abandoned at 642-773 cal.yr.AD. The adjacent FSU D4 represents deposition of laminated sandy silts within a bar-top chute environment. It is thought to represent deposition on top of a bank-attached gravel bar that was contemporaneous with the D3 channel. The chute fill was dated at 670-870 cal.yr.AD (683-779 cal.yr.AD 1σ age). The channel is thought to be the up-river continuation of the channel in FSUs C3 and C4 (transect C). This again shows that the 7th/8th Century AD was a time of significant instability in the fluvio-estuarine system. The channel was either abandoned through avulsion or meander cut-off.

FSU D5

This unit represents a slightly brackish reedswamp environment that accumulated up over the site of the former abandoned D3-D4 channel zone.

FSU D6

This unit occupies the surface 2.0-2.5m of alluvium west of the NB4 channel. Floodplain deposits consist of relatively coarse grained (sandy silts and fine sands) vertically accreted overbank alluvium. Two paleochannel fills contain fine grained silt and clay, with diatom evidence (NB1) suggesting deposition in a tidal environment just down-river of the salinity front, and probably just below MHWST. The stratigraphy suggests that these channels were abandoned in avulsion events. This unit is thought to have been deposited in the 9th and 10th Centuries AD, during a phase of active floodplain and channel aggradation. This could account for the coarse grained texture of the

floodplain sediments, with frequent over-bank floods transporting sand and silt onto the floodplain surface.

FSU D7

This unit occupies the curved NB4 palaeochannel meander. A channel bar unit of gravelly coarse sand at the base of the channel is overlain by a fining-up sequence of bar-top sands, representing point bar lateral accretion and the migration of a sand-bed river to the north-east. Diatoms in a silt lense/horizon suggest tidal deposition within a slightly brackish environment.

FSU D8

This unit corresponds with deposition within the core of a current River Taw meander. Active channel migration to the north-east is seen to continue in this unit, but here the coarse sand bar present in D7 is replaced by a gravel bar. This suggests a phase of channel bed aggradation and gravel bedload transport within a high-energy regime of increased discharge and greater coarse grained sediment influx. Above the gravel, bar-top medium sands and floodplain sandy silts have been deposited during active lateral migration of the point bar sequence. The D8 floodplain surface also rises in elevation, possibly due to channel-bed aggradation causing more frequent over-bank floods, due to a decreased bank-full volume.

FSU D9

This unit occupies the inside of the modern River Taw meander, and is similar to D9 with lateral migration of a gravel point sequence. Channel aggradation continues, with the gravel surface increasing in elevation. A thin chute channel (with a clay and silt fill) is preserved within D9, on the outside of a scroll bar. The fluvial system remains geomorphically active within this unit, with high discharge levels causing active channel migration.

6 LITHO- AND BIO-STRATIGRAPHY OF THE NON-TIDAL TAW VALLEY: A HOLOCENE RECORD OF GEOMORPHIC AND ENVIRONMENTAL CHANGE UPSTREAM OF THE TIDAL HEAD

6.1 INTRODUCTION

6.1.1 Chapter objectives

This chapter will describe the geomorphology, litho- and bio-stratigraphy of a reach of the non-tidal River Taw valley, immediately upstream of the modern tidal head. The study area extends for 4km upstream of HAT and incorporates the zone affected by brackish groundwater intrusion.

The aims of this chapter are as follows:

- (1) To investigate Holocene geomorphic change in the fluvial zone upstream of HAT, and to identify (and date) phases of active channel change during the late Holocene (*e.g.* Knox, 1985, 1993, 2003; Macklin & Lewin, 1993, 2003; Rumsby & Macklin, 1996; Brown, 1998; Taylor *et al.*, 2000; Maddy *et al.*, 2003; Starkel, 2003; Lewin *et al.*, 2005; Macklin *et al.*, 2005, 2006).
- (2) To determine if any marine incursions of the tidal environment have extended into this zone during the late Holocene. This will be ascertained using sedimentological and diatom evidence.
- (3) To determine the spatial extent of marine groundwater intrusion into this zone during the late Holocene. This will be based on diatom evidence of slightly brackish conditions (see chapter 4).

The non-tidal fluvial zone is divided into three reaches, centred around one or two cross-valley auger transects. The geomorphology of each reach will be introduced and described. The location of transects and analysed cores will be shown and valley-wide 2-D lithostratigraphic sections will be constructed to reveal the Holocene alluvial fill. The geochronology of the deposits will be determined through radiocarbon and OSL

dating. For each transect, the lithostratigraphy will be analysed for sedimentary and stratigraphic evidence of geomorphic change. Individual cores will be analysed for diatom evidence of brackish conditions. At the end of each reach description evidence of brackish groundwater intrusion will be summarised, and based on comparisons with the contemporary zonation of the non-tidal reach (chapter 4), inferences will be made on palaeo-discharge.

6.1.2 Geomorphology of the non-tidal River Taw and location of transects

The geomorphology of the fluvial zone is presented in figure 6.1, along with the location of auger transects E to I and the location of analysed cores. The approximate upstream limit for the latest 20yr HAT (predicted at 5.9m OD) is indicated in the vicinity of transect E (figure 6.1). This location is based on the field observation of a 5.7m OD (2007 HAT tide), which was tracked upstream during the flood tide to its tidal head location. The River Taw is seen to be a single-thread meandering river throughout this reach.

Seven late Quaternary river terraces (T1 to T7) were identified within the non-tidal fluvial zone. The most recent valley floor deposits are labelled 'floodplain' in figure 6.1 and mainly occupy the inside of meander bends, being formed by relatively recent channel migration. T1 to T5 are Holocene in age, while T6 and T7 are of late Pleistocene (Devensian) origin (Edmonds *et al.*, 1979). T7 is preserved extensively on the western side of the valley where the terrace width can be up to 600m wide. T7 is typically elevated *c.*8.0-10.0m above the highest Holocene alluvium and occasional exposures of this terrace reveal rounded framework river gravels capped by thin (0.50-0.75m) fine grained sands and silts, typical of braided-river deposits (Collinson, 1996).

Altitudinal changes between each of the Holocene terraces are typically only 30-70cm. However, in the north of the zone, very minor elevational difference is seen, with the mapping of these terraces partly based on the surface micro-topography and geomorphology, and on the alluvial stratigraphy. Palaeochannels are preserved on all of the Holocene terrace surfaces, with evidence for differing channel planforms between some terraces. For example, T5 shows an anastomosing planform south of transect G, and evidence of some multi-thread channel braiding is seen in the T1 deposits near the

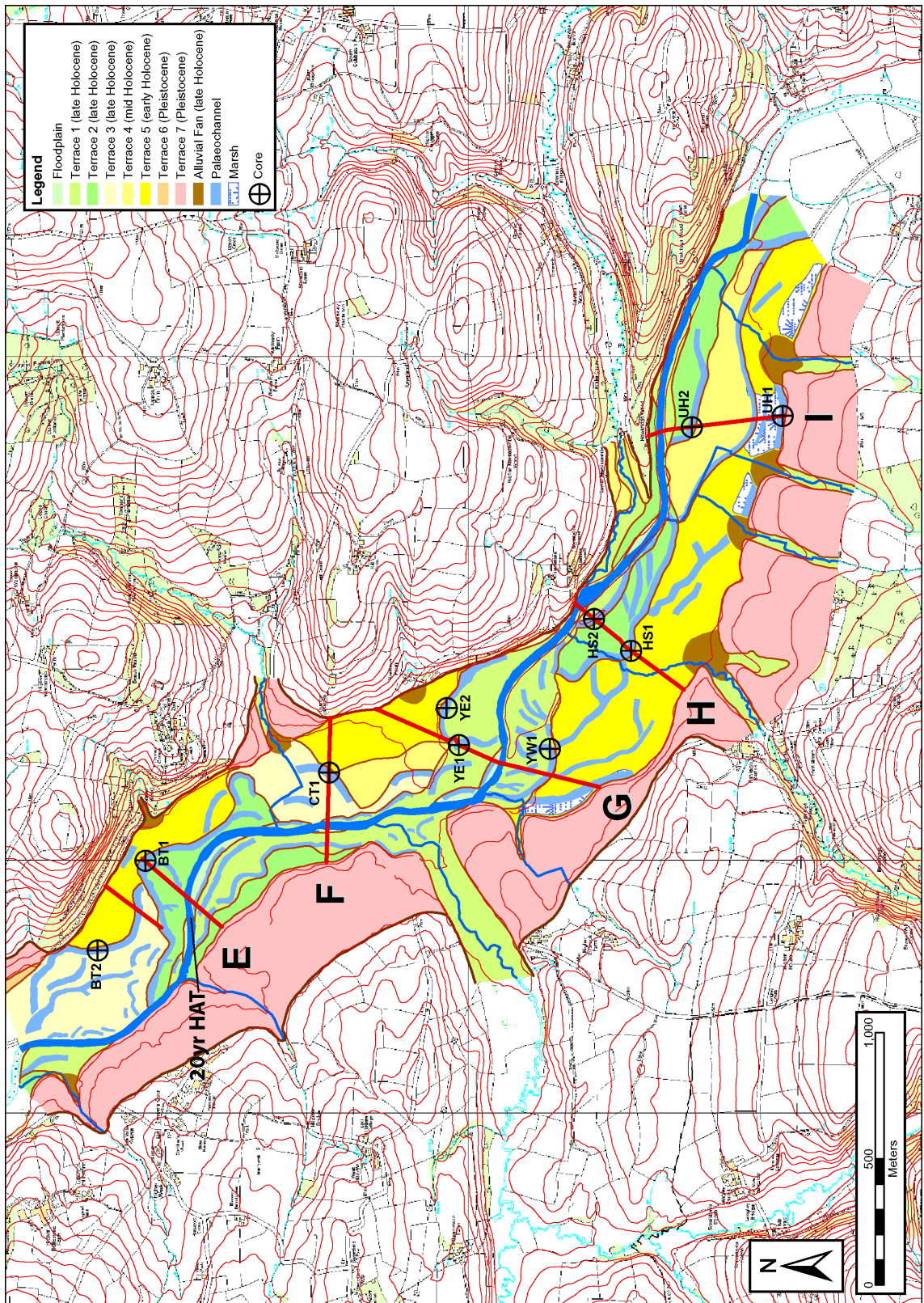


Figure 6.1 Geomorphology of the non-tidal River Taw zone. The location of transects E to I and all cores are indicated. HAT (highest astronomical tide) is located near the start of the reach. This map was produced in a GIS and incorporates OS Landform Profile (5m contours) and OS 10,000 colour raster layers (supplied by Ordnance Survey/EDINA Digimap).

YW1 core (transect G). The fluvial zone was divided into three reaches with the Bridgetown reach centred around transects E and F, the Yeotown reach centred around transect G, and the Umberleigh House reach centred around transects H and I. The geomorphology will be described in more detail, in relation to each of these reaches, in sections 6.2, 6.3 and 6.4

6.1.3 Legend for sedimentary sections

For each of the core transects, the alluvial lithostratigraphy has been divided into four sediment types. These are shown in the key presented in figure 6.2. The medium to coarse sand category generally represents channel bedload and channel bar deposits and can be inter-stratified with finer sands/silts. The silty sand to fine sand deposits can represent either bar top deposits, open abandoned channel fills, or coarse grained overbank alluvium. The clay to sandy silt deposits can represent closed abandoned channel fills or overbank floodplain alluvium. The organic peats are located either at the base of abandoned channels where they consist of detrital peaty silts/sands, or at the top of abandoned channel fills where they represent palaeochannel marsh deposits.

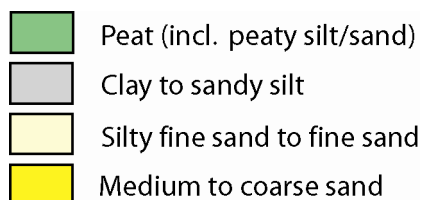


Figure 6.2 Legend for lithostratigraphic transect sections in chapter 6.

6.1.4 Radiocarbon and luminescence dates

The age results for all radiocarbon samples taken from cores in the non-tidal fluvial zone (transects E to I) are presented in table 6.1. A variety of terrestrial plant macrofossils were submitted for AMS radiocarbon dating. These included seeds, an acorn (*Quercus* sp.) and sub-aerial wood. A larger section of tree branch (sample F5) was submitted for conventional radiometric dating. Table 6.1 includes the sample $\delta^{13}\text{C}$ ‰ values. The results show values typical for wood and terrestrial C_3 plants,

Non-tidal River Taw Radiocarbon Dates

Thesis code	Sample code	Laboratory code	Dating method	Sample material	¹⁴ C enrichment (% Modern +/-1)	Carbon content (% by wt.)	$\delta^{13}\text{C}_{\text{VPDB}}\text{‰}$ +/-0.1	Conventional ¹⁴ C Age (years BP +/-1)	2 σ Calibrated Age (Cal.yr.BP)	1 σ Calibrated Age (Cal.yr.AD/BC)	2 σ Calibrated Age (Cal.yr.AD/BC)
Transect E											
E2	BT1-244	SUERC-15769	AMS	Fruit/seed	85.01 +/- 0.40	43.0	-29.0	1304 +/- 37	1297-1174	664-767 AD	654-777 AD
Transect F											
F4	CT1-230	SUERC-15755	AMS	Seed	73.56 +/- 0.34	54.0	-25.0	2466 +/- 37	2711-2363	753-514 BC	762-414 BC
F5	CT1-274	Beta-216112	Radiometric	Wood (branch)	na	na	-28.8	2540 +/-50	2758-2377	796-553 BC	809-428 BC
Transect G											
G1	YW1-116	SUERC-15770	AMS	Wood (twig)	90.18 +/- 0.39	54.0	-28.1	830 +/- 35	892-678	1185-1255 AD	1058-1272 AD
G2	YE1-255	SUERC-15773	AMS	Wood (twig)	94.37 +/- 0.42	60.0	-29.0	466 +/- 35	545-470	1420-1449 AD	1405-1480 AD
G3	YE2-126	SUERC-15756	AMS	Seed	92.87 +/- 0.43	30.9	-26.2	594 +/- 37	655-537	1309-1403 AD	1296-1414 AD
Transect H											
H2	HS2-135	SUERC-15757	AMS	Acorn shell	95.65 +/- 0.42	50.7	-24.4	357 +/- 35	499-315	1469-1627 AD	1452-1635 AD

Table 6.1 Radiocarbon dates for transects E to I, the non-tidal River Taw (na = data not available).

Non-tidal River Taw OSL Dates

Thesis code	Sample code	Oxford Lab code	Depth (m)	Altitude (m OD)	Grain size (μm)	H ₂ O content (%)	U (ppm)	Th (ppm)	K (wt.%)	External gamma-dose (Gy/ka)	Total dose rate (Gy/ka)	D ₀ (Gy)	OSL age (yrs)	OSL age (yr.AD/BC)
Transect E														
E1	BT1-133	X2913	1.33	5.88	90-125	37.92	3.8	12.2	2	not available	2.39 +/-0.17	1.99 +/-0.05	830 +/-60	1170 +/-60 AD
Transect F														
F1	CT1-48	X2914	0.48	8.41	90-125	33.17	3.8	10.6	1.7	not available	2.35 +/-0.26	3.73 +/-0.10	1590 +/-180	410 +/-180 AD
F2	CT1-134	X2915	1.34	7.55	90-125	39.31	3.8	10.8	1.7	not available	2.14 +/-0.16	3.78 +/-0.13	1760 +/-140	240 +/-140 AD
F3	CT1-196	X2916	1.96	6.93	90-125	25.37	3.2	9.6	1.4	not available	2.24 +/-0.16	7.44 +/-0.63	3320 +/-360	1320 +/-360 BC
Transect H														
H1	HS1-128	X3251	1.28	9.40	125-180	27.40	3.6	9.9	1.5	not available	2.29 +/-0.17	2.99 +/-0.29	1300 +/-160	700 +/-160 AD
Transect I														
I1	UH1-65	X2912	0.65	13.07	90-125	52.33	3.7	12.3	2.6	0.87 +/-0.01	2.21 +/-0.21	19.94 +/-1.19	9040 +/-1010	7040 +/-1010 BC
I2	UH1-116	X2911	1.16	12.56	90-125	22.48	3.1	10.5	2.0	1.06 +/-0.01	2.83 +/-0.16	36.12 +/-1.60	12740 +/-910	10740 +/-910 BC

Table 6.2 OSL dates for transects E to I, the non-tidal River Taw.

though most samples do show some depletion in the $^{14}\text{C}:$ ^{13}C ratio caused by isotopic fractionation. A correction will have been made to the measured ^{14}C activity because of this.

The age results for all OSL samples taken from cores in the non-tidal fluvial zone are presented in table 6.2. As with the inner estuary samples, the total annual dose rate was calculated from sediment radionuclide concentration (U, Th and K), water content and estimated cosmic ray contribution (based on sample depth, elevation and assumed burial history) using the methods of Aitken (1998) and Prescott and Hutton (1994). The depth related necessity for most samples in the fluvial zone to be recovered by coring precluded the use of a field gamma detector. However, in the UH1 core, the shallow depth to the basal gravel permitted a pit to be dug for in-situ access to the identified sample horizons (see the methods of Aitken (1998) and Prescott and Hutton (1994). The depth related necessity for most samples in the fluvial zone to be recovered by coring precluded the use of a field gamma detector. However, in the UH1 core, the shallow depth to the basal gravel permitted a pit to be dug for in-situ access to the identified sample horizons (see figures 3.3 and 3.4, chapter 3). A field gamma detector was used here to measure the in-situ external gamma-dose. In the core samples, the gamma-dose was determined from radionuclide concentrations (Aitken, 1998). It was assumed that the light-sensitive trapped charge of each grain in the sample was zeroed prior to deposition. All OSL ages (table 6.2) were initially expressed as years before 2000 AD, rounded to the nearest 10 years. A 2σ uncertainty is attached to all dates. This value is based on random and systematic errors from beta-source calibration, dose rate determination, subsampling for chemical data, and optical measurement errors following methods in Aitken and Alldred (1972) and Aitken (1976, 1985). OSL ages are also expressed in calendar years AD/BC (table 6.2) for easier comparison with radiocarbon age results.

6.2 GEOMORPHOLOGY AND STRATIGRAPHY OF THE BRIDGETOWN REACH

6.2.1 Reach geomorphology

The geomorphology of the Bridgetown reach is shown in figure 6.3. The Holocene

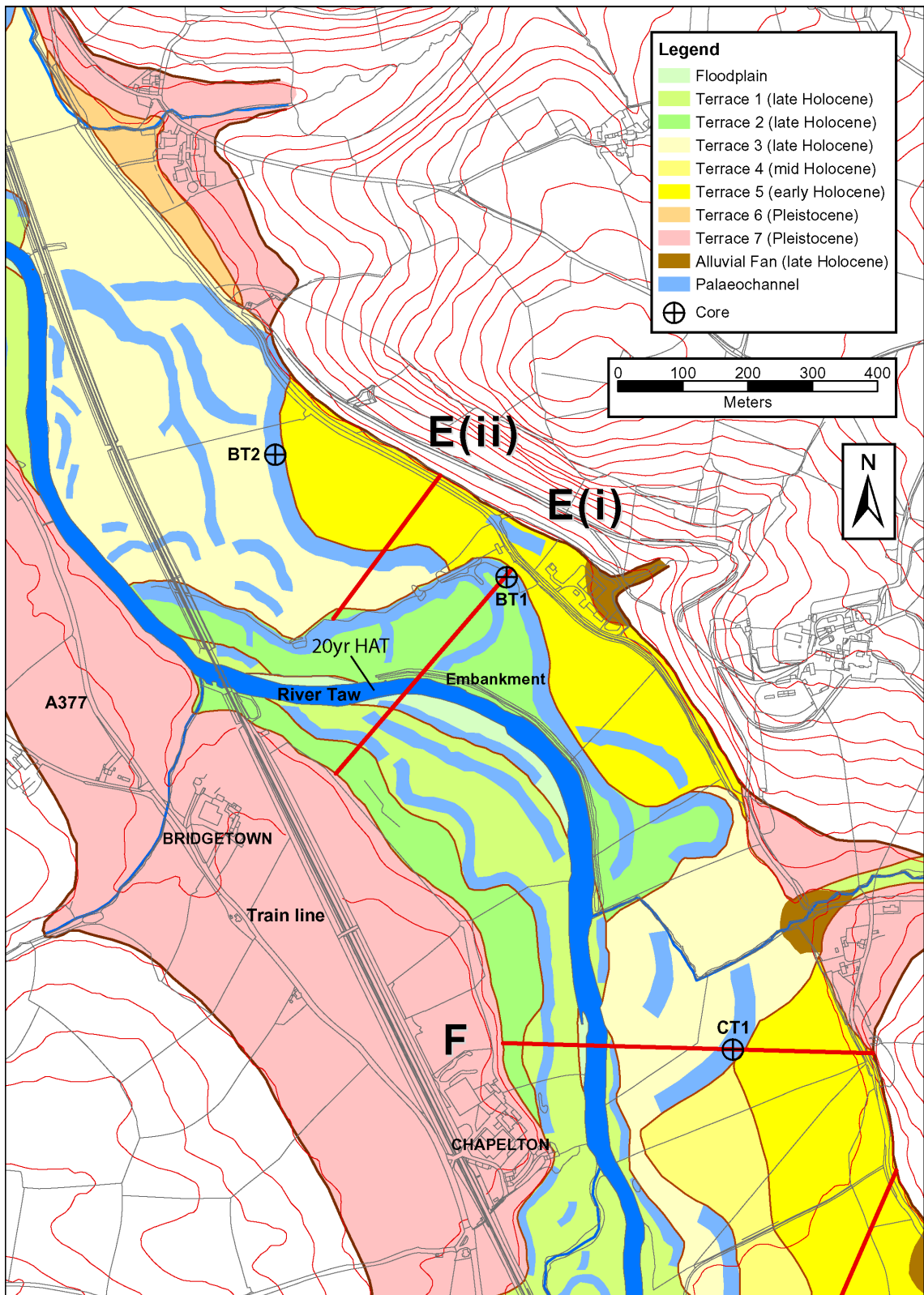


Figure 6.3 Geomorphology of the Bridgetown reach. The location of transects E (Bridgetown transect) and F (Chapelton transect) and associated cores are indicated. This map was produced in a GIS and incorporates OS Landform Profile (5m contours) and OS MasterMap layers (supplied by Ordnance Survey/EDINA Digimap).

alluvial floodplain is *c.*500m wide, which is similar to the New Bridge Reach. The location of transect E (Bridgetown transect) and transect F (Chapelton transect) is shown, along with associated cores BT1, BT2, and CT1. In order to cover a wider diversity of terrace deposits, transect E is split into auger transects, E(i) and E(ii). This reach includes the HAT tidal head of the River Taw, with the 20yr HAT located at a riffle beside transect E (figure 6.3). The 2007 5.7m OD HAT was observed to reach the train bridge, 200m downstream of the 20yr HAT. All HAT tides that penetrate this reach are freshwater, caused by tidal back-up. The active channel has a sinuous meandering planform in this reach ($S = 1.22$).

Extensive Pleistocene (Devensian) T7 deposits are preserved on the western side of the valley, with the Bridgetown and Chapelton farms located on the terrace surface. A further four Holocene Terraces (T1, T2, T3 and T5) are present, with altitudinal differences most apparent between T3 and T5 (60cm in transect F). The lower T1 and T2 terraces are occasionally inundated during high-stage floods, and because of little elevational difference, behave as a single floodplain.

Numerous palaeochannels are evident on the T1, T2 and T3 terrace surfaces, showing evidence of late Holocene channel change. Very few palaeochannels are present on the T5 terrace in this reach. This terrace is dated as early Holocene in the upstream UMBERLEIGH HOUSE reach (6.4.6). The T1 terrace, west of the river in transect E, shows evidence of gradual channel migration to the east, with T1 merging into the modern floodplain on the inside of the meander bend. A series of scroll bars are located across this floodplain-T1 surface. Palaeochannel evidence from T2 indicates a period of particularly intense geomorphic activity and floodplain reworking, with the formation of tight meanders and examples of channel abandonment through meander neck cut-off and avulsion. North-west of transect E, the T3 terrace surface contains several long palaeochannels showing a period of channel change with some localised evidence of a multi-thread channel system, possibly anastomosed. The palaeochannel containing the BT2 core is *c.*800m long and contains a complete meander wavelength. The preservation of this extensive channel segment suggests it was abandoned during an avulsion event. The T3 terrace edge contains several small flood channels caused by drainage of overbank water and localised scour.

6.2.2 Lithostratigraphy of the Bridgetown transect

Figure 6.4 shows the lithostratigraphy of transect E. The floodplain-terrace surfaces are located at 7.8-8.7m OD, with the higher elevations found on T5 and proximal to the active channel. The rise in T2 between stratigraphic cores 1 and 3 is partly due to the transect line coinciding with an old levee associated with the adjacent palaeochannel. The area to the south-west of the river was not cored.

The T2 deposits (figure 6.4) contain a coarse grained fining-up sequence of gravel or coarse sand, overlain by fine sand. This represents a point bar sequence, deposited during active channel migration of a sand-gravel bed river. Deposition of this sediment culminated in the BT1 channel abandonment via avulsion at 654-777 cal.yr.AD, with subsequent infilling of the channel by fine grained sediments. However, an erosive layer of sand within the BT1 fill suggests that this channel was re-occupied in the 12th Century with an OSL date giving an age of 1170 +/-60 cal.yr.AD for subsequent abandonment.

The T3 deposit contains the BT2 palaeochannel and a relatively thick vertically accreted floodplain unit of mottled grey-brown silty sand-fine sand. The coarse nature of these overbank alluvial deposits suggests a high palaeo-discharge with frequent high-stage floods.

The early Holocene T5 deposit contains a relatively thin (1.0-1.4m) finer grained overbank deposit of sandy silt overlying an elevated gravel surface. A palaeochannel within this unit contains a fill of light grey clay, overlain by clayey silt, suggesting fluvio-lacustrine deposition within a palaeochannel pond. The palaeochannel is relatively shallow, suggesting a low bankfull discharge or that it is part of a multi-thread, possibly anastomosed system. There is very minor surface expression to this channel (not shown on figure 6.4) but a slight depression trends north-east – south-west. This results in the channel crossing the transect line at an acute angle, giving the impression it is much wider in figure 6.4 than it actually is.

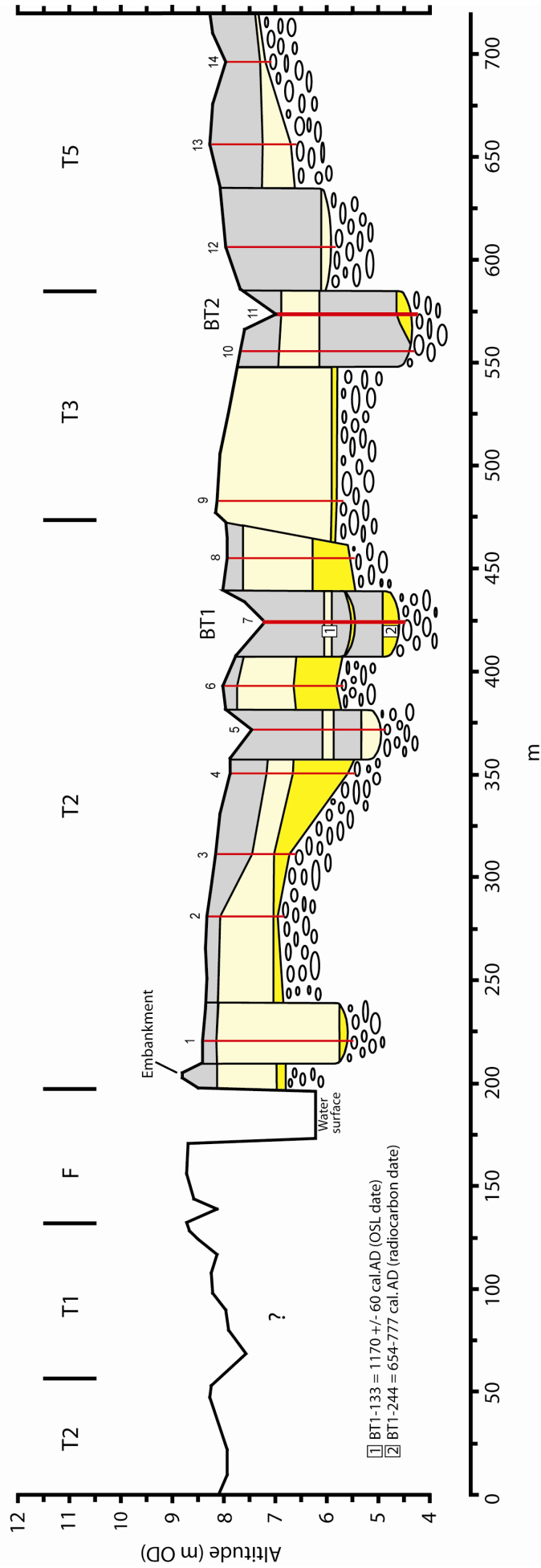


Figure 6.4 Lithostratigraphy of the Bridgetown transect. The location of analysed cores and stratigraphic cores (1-14) are indicated. See figure 6.2 for legend.

6.2.3 BT1 core

Sedimentology and magnetic properties

Figure 6.5 shows the core log for BT1. This figure shows down-core changes in sediment lithology, X_{lf} , $X_{fd\%}$, organic matter and carbonate content. In addition, the diatom zones (see later) and stratigraphic units (see chapter 7) are indicated.

The BT1 core is underlain by gravel at 2.62m (7.21m OD). Between 2.29m and the gravel, a unit of medium and coarse grained sand suggest channel deposition within a sand-bed river. This is overlain (up to 1.75m) by a deposit of peaty sandy silt with many wood and plant fragments (dominated by *Salix caprea* leaves), indicative of channel abandonment. At 1.75m, an erosion surface is overlain by a 6cm layer of fluvial medium sand, which is in turn overlain by a unit of laminated clay and subsequent sandy silt and silty sand deposition up to 1.6m. This suggests the channel was briefly re-occupied, and used as an occasional flood channel (with sand deposition). Between 0.35m and 1.06m, a unit of silty clay, with no rootlets, suggests full abandonment and deposition within a palaeochannel pond environment. This unit is overlain by organic silts deposited in a palaeochannel depression marsh.

X_{lf} values are low ($0.1 \cdot 10^{-6} \text{ m}^3 \text{ kg}^{-1}$) throughout most of the core indicative of low concentrations of magnetic minerals. However, in the upper palaeochannel pond clay, X_{lf} values rise to $0.2\text{-}0.3 \cdot 10^{-6} \text{ m}^3 \text{ kg}^{-1}$. $X_{fd\%}$ values of 5-10% indicate that the rise in X_{lf} is partly due to the presence of some soil-derived fine viscous grains, possibly washed into the pond. Within a fluvio-lacustrine environment, secondary bacterial magnetite may also be a possible source of ferrimagnetic minerals.

Geochronology

A seed from the basal sand was radiocarbon dated, giving an age of 654-777 cal.yr.AD for initial channel abandonment. The layer of silty sand in the overlying flood channel deposit has been OSL dated, giving an age of 1170 +/-60 cal.yr.AD for channel re-occupation.

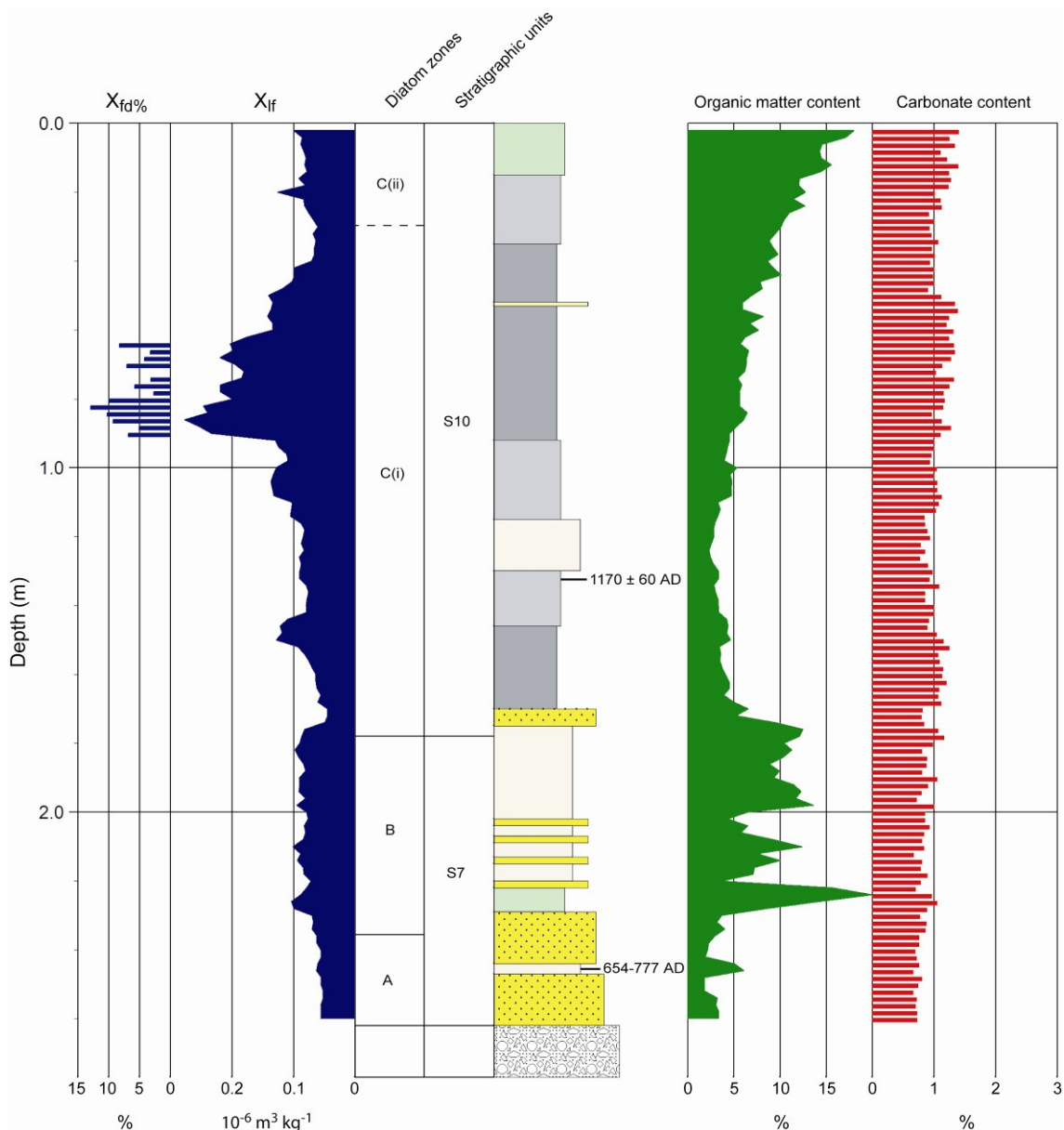


Figure 6.5 BT1 core log. See figure 5.2 for lithology legend. Diatom zones are derived from figure 6.6. Stratigraphic units are discussed in chapter 7.

Diatom analysis

Figure 6.6 shows a diatom diagram for BT1. All species with counts of $>3\%$ TDV are shown (plus rare brackish species $>1\%$ TDV), along with the diatom sums. Cluster analysis resulted in three diatom zones (A to C).

DSI value range from 0.86 to 0.92, indicating a freshwater assemblage with a significant contribution by brackish species. This is also seen in the diatom group sums with the mesohalobous sum peaking at 22% in the basal peaty silt (zone B), following channel abandonment, and at 17% in the silty clay (at 1.34m in zone C(i)) that is

deposited after channel re-occupancy and subsequent abandonment. The mesohalobous assemblage in zones B and C(i) is dominated by the epiphyte *Ctenophora pulchella* (>10%TDV) and *Navicula avenacea* (>5%TDV). The occurrence of these species in this abundance indicates that brackish conditions existed within the closed abandoned channel environment, suggesting proximity to the estuarine environment and HAT during both phases of palaeochannel deposition, with brackish groundwater migrating upstream ahead of the tidal head.

Within the basal palaeochannel deposit (zones A and B), the dominant freshwater species are *Cocconeis placentula*, *Achnanthes exilis* and *Fragilaria vaucheriae* (all >10%TDV). The upper flood channel deposit and subsequent pond environment (zone C) is dominated by the epiphytes *Cocconeis placentula* and *Synedra ulna* (both >10%TDV).

6.2.4 BT2 core

Sedimentology and magnetic properties

Figure 6.7 shows the core log for BT2. This figure shows down-core changes in sediment lithology, X_{lf} , $X_{fd}\%$, organic matter and carbonate content. The stratigraphic unit (see chapter 7) is also indicated.

The BT2 core is underlain by gravel at 2.64m (6.98m OD). Between 2.33m and the gravel, a poorly sorted fine-coarse sand with ripple-cross lamination has been deposited, representing channel deposition within a sand-bed river. An 8cm thick detrital branch was penetrated above the gravel contact. Between 1.98m and 2.33m, a massive blue-grey clay (with some greenish staining) has been deposited, representing fluvio-lacustrine deposition. This clay grades into a grey silty clay between 1.26m and 1.98m indicating a continuation of a sub-aqueous environment. Between 0.82m and 1.26m, a unit of grey-brown mottled brown clayey silt grades up into a sandy silt, suggesting the gradual infilling of the palaeochannel pond. Post-depositional manganese mineralisation is prominent throughout this unit. The upper 0.82m of the core consists of sandy silt and silty sand with many grass rootlets throughout, representing overbank floodplain deposition.

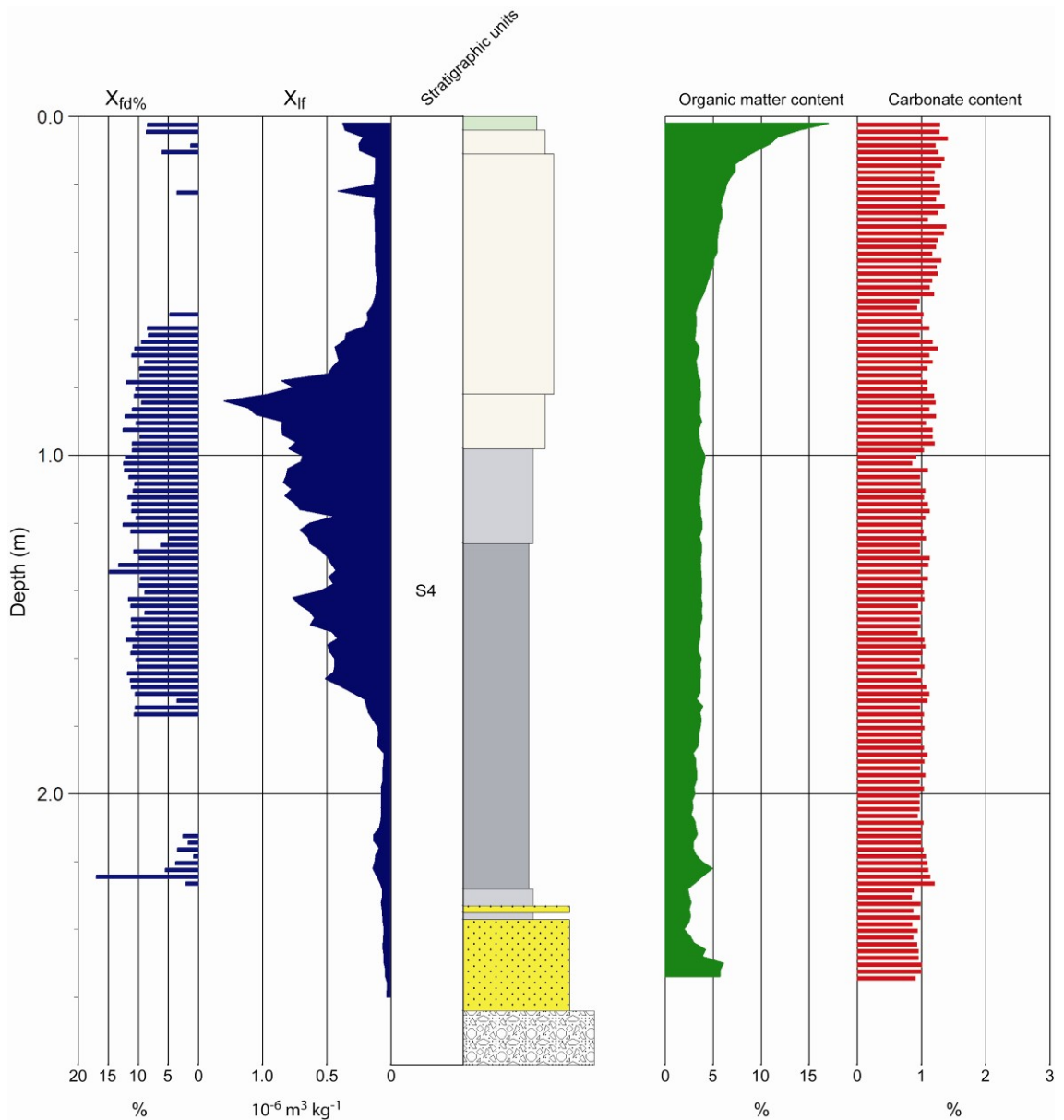


Figure 6.7 BT2 core log. See figure 5.2 for lithology legend. Stratigraphic units are discussed in chapter 7.

X_{if} values are generally very low ($<0.1 \cdot 10^{-6} \text{ m}^3 \text{ kg}^{-1}$) at the base and top end of the BT2 core. However, in the middle part of the core, between 0.7m and 1.7m, X_{if} values are very high, at $0.5\text{-}1.2 \cdot 10^{-6} \text{ m}^3 \text{ kg}^{-1}$. Corresponding $X_{fd\%}$ values of $>10\%$ indicate the magnetic assemblage is dominated by fine viscous grains. This suggests significant in-wash from the surrounding terrace of soil-derived sediment (a source of secondary fine viscous magnetite; Oldfield *et al.*, 1983; Maher, 1986).

6.2.5 Lithostratigraphy of the Chapelton transect

Figure 6.8 shows the lithostratigraphy of transect F. The T1-T2 terrace surface is

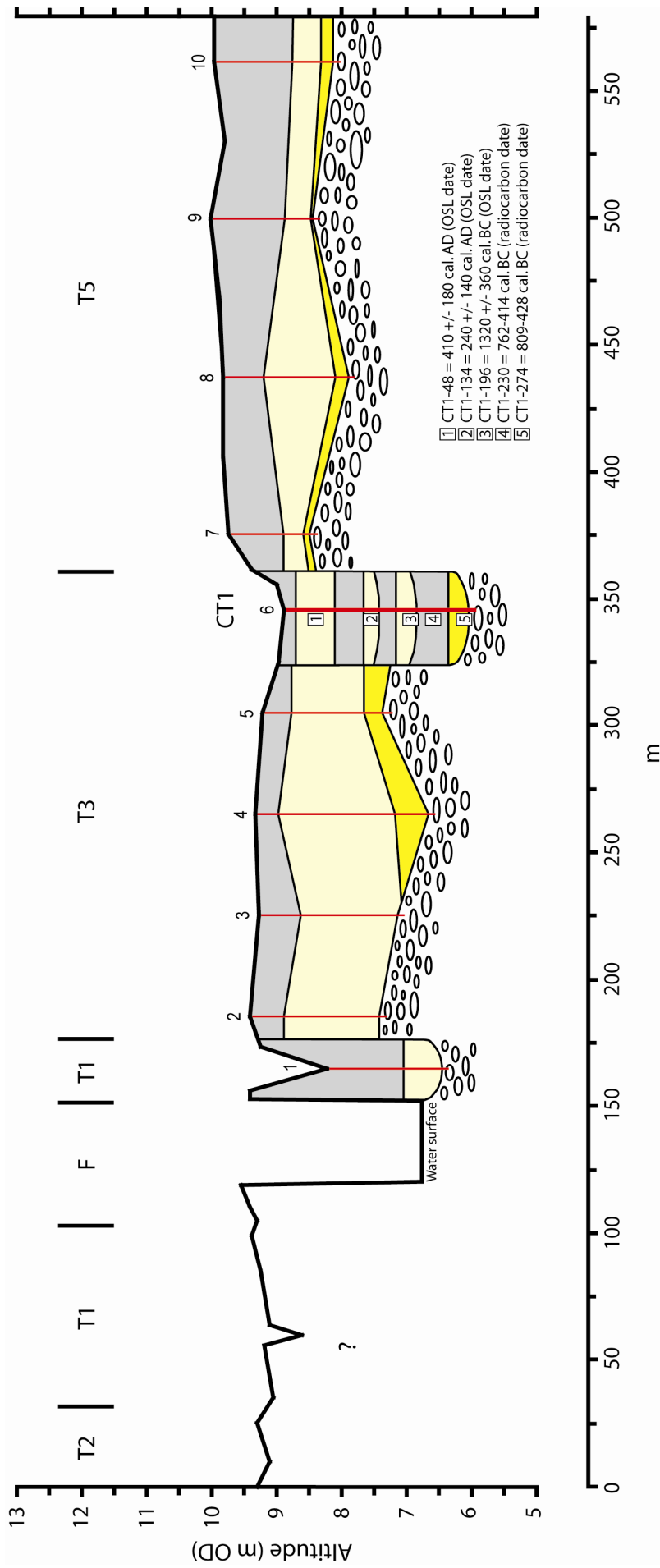


Figure 6.8 Lithostratigraphy of the Chapelton transect. The location of analysed cores and stratigraphic cores (1-10) are indicated. See figure 6.2 for legend.

located at *c.*9.10m OD, the T3 surface is located at *c.*9.35m OD, and the T5 surface is located at *c.*10.0m OD. The area to the west of the river was not cored.

The T5 deposits contain a 1.2-1.9m fining-up sequence of overbank floodplain alluvium, consisting of silty sand and sandy silt. Manganese concretions were found throughout the sediments. No channel deposits were preserved in the 200m wide terrace fragment. The T3 terrace contains a thicker (1.9-2.7m) fining-up alluvial sequence. An undulating gravel surface is overlain by a layer of gravelly fine-coarse sand and medium sand, which grades into a fine sand. This basal unit is thought to represent laterally accreted gravel/gravelly sand point bar deposition overlain by bar top sands. The upper part of the terrace alluvium (above *c.*1.3m) consists of overbank silty sand and sandy silt, which was vertically and laterally accreted during channel migration. The CT1 palaeochannel is located within T3 and contains an alternating sequence of coarse and fine grained units, with initial channel abandonment taking place at 809-428 cal.yr.BC. There is sedimentary and dating evidence (see 6.2.6) of the channel being re-occupied and abandoned in the 3rd Century AD.

6.2.6 CT1 core

Sedimentology and magnetic properties

Figure 6.9 shows the core log for CT1. This figure shows down-core changes in sediment lithology, X_{lf} , $X_{fd\%}$, organic matter and carbonate content. In addition, the diatom zones (see later) and stratigraphic units (see chapter 7) are indicated.

The CT1 core is underlain by gravel at 2.84m (8.89m OD). Between 2.42m and the basal gravel, a fining-up unit of fine-coarse sand contains large woody debris at the base and many leaf/plant fragments within ripple-cross laminae partings at the top. This unit indicates channel abandonment within a sand-bed river. Between 2.06m and 2.42m, a unit of organic (detrital plant fragments) clayey silt is deposited with wavy and ripple-cross lamination and lenses (2-20mm) of medium sand. This suggests partial abandonment, with some connection with the active channel. Between 2.06m and 1.72m, evidence of more active fluvial flow within the CT1 channel is seen by the deposition of a unit of well sorted ripple cross-laminated fine sand. Final abandonment

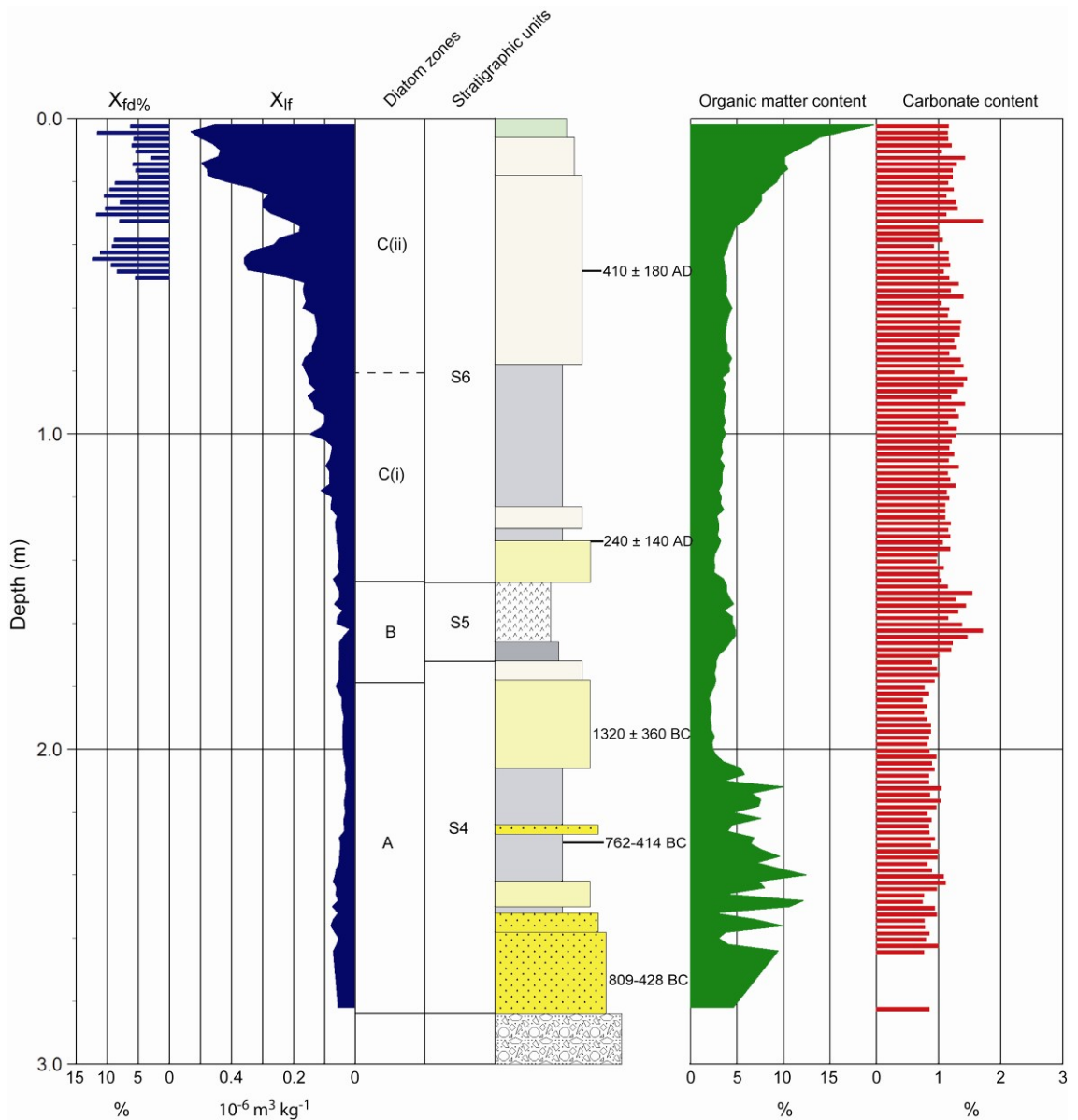


Figure 6.9 CT1 core log. See figure 5.2 for lithology legend. Diatom zones are derived from figure 6.10. Stratigraphic units are discussed in chapter 7.

the channel is seen at 1.72m with the deposition of a light grey silty clay up to 1.47m. The boundary between the sand and clay shows pronounced manganese mineralisation, indicative of a hiatus in deposition. Above the clay, an erosion surface at 1.47m is overlain by a fining-up unit of fine sand and silty fine sand, suggesting the channel site was briefly re-occupied during a high-stage flood. The upper part of the core consists of grey-brown mottled brown overbank clayey silts and sandy silts.

Magnetic mineral concentrations only become significant above *c.*0.9m, where X_{lf} values gradually rise to $0.5 \cdot 10^{-1} \text{ m}^3 \text{ kg}^{-1}$. Corresponding $X_{fd\%}$ values are high at 6-12%, indicating the magnetic assemblage is dominated by soil-derived fine viscous grains.

Geochronology

Wood the basal sand was radiocarbon dated, giving an age of 809-428 cal.yr.BC for initial channel abandonment. A seed from the overlying organic silt was also radiocarbon dated, giving a similar age of 762-414 cal.yr.BC. The overlying unit of fine sand (below the clay) was OSL dated, giving an age of 1320 +/-360 cal.yr.BC. This date is thought to be erroneous as it is *c.*600 years older than the underlying radiocarbon dated sediments. This may be due to partial bleaching of some of the sand grains (Wallinga, 2002; Duller, 2004), or the modern water content may not be representative of the water content present during most of the sediment's burial history (Bailiff and Tooley, 2000). The date will therefore not be used in discussion of environmental change. The flood-channel sand that overlies the clay was OSL dated (at 1.34m), giving an age of 240 +/-140 cal.yr.AD for brief channel re-occupancy. The upper sandy silt floodplain sediment at 0.48m was also OSL dated, giving an age of 410 +/-180 cal.yr.AD.

Diatom analysis

Figure 6.10 shows a diatom diagram for CT1. All species with counts of >3%TDV are shown (plus rare brackish species >1%TDV), along with the diatom sums. Cluster analysis resulted in three diatom zones (A to C).

DSI value range from 0.94-0.96 in zone A, indicating a freshwater assemblage with a minor contribution by brackish species in the basal palaeochannel deposits. The brackish contribution is dominated by the mesohalobous species *Navicula avenacea* at >5%TDV. The freshwater assemblage in zone A is dominated by *Cocconeis placentula*, *Achnanthes exilis* and *Synedra ulna*.

The Zone B clay has a DSI value of 1.00, indicating a pure freshwater assemblage. The assemblage is dominated by *Eunotia pectinalis* at 60%TDV. This indicates an algal bloom of this species within a fluvio-lacustrine environment, indicative of eutrophic conditions. Diatom valves are present in very high concentrations, contributing to >90% of the sediment silica content, with subordinate quartz silica. This indicates that the clay can be classified as a diatomite. Although diatomites are often associated with lake

deposits, they have also been found in several river valleys, e.g. Ripple Brook in the Seven Valley (Brown and Barber, 1985) and several sites in Ireland (Brown *et al.*, 2007).

DSI values of 0.98 are found in most of zone C, indicating a freshwater assemblage. Dominant oligohalobous indifferent species are *Cocconeis placentula*, *Pinnularia viridis*, *Pinniularia major*, *Pinnularia subcapitata*, *Synedra ulna* and *Hantzschia amphioxys*, along with the halophobe *Pinnularia subsolaris* (all at >10%TDV). However, in the clayey silt overbank sediment found in the middle of zone C, the DSI value falls to 0.93 (at 1.02m), indicating a brackish component. Figure 6.10 shows that this fall in DSI is actually caused by the occurrence of rare polyhalobous species. The marine planktonic *Coscinodiscus radiatus* and the marine tycho planktonic *Cymatosira belgica* both occur at 1%TDV. In addition to these two species, single counts (0.5%TDV) of eight other marine planktonic and tycho planktonic species were identified at this horizon, giving a total polyhalobous sum of 6%. Given the current location of the CT1 core in the salinity gradient, this is quite remarkable and a possible cause is proposed in 6.2.7.

6.2.7 Brackish groundwater intrusion in the Bridgetown reach

BT1

The BT1 palaeochannel core is located in the middle of the modern Riv 3(ii) zone (0.83 DSI). Two phases of palaeochannel deposition are recognised and these have been dated at 654-777 cal.yr.AD and 1170 +/-60 cal.yr.AD, relating to diatom zones A and B. DSI values range from 0.86 to 0.92 in both core zones suggesting groundwater salinity was either similar to modern conditions or slightly less saline during both the early 8th Century and 12th Century AD. The range of DSI values suggest that BT1 may have been located 1.3 km upstream at the boundary of contemporary zones Riv 3(ii) and Riv 4(i). The mesohalobous sum peaks of 22% (zone A) and 17% (zone B) also suggest this, being the same or slightly less than the Riv 3(ii) zone values of 22-27%. The small difference in DSI at BT1 makes it difficult to draw any conclusions on palaeo-discharge in the 8th and 12th Centuries. The core DSI values could either suggest a slightly higher discharge during these centuries, or that river discharge was similar to today, and the

slightly less saline conditions at BT1 were caused by a lower RSL, with the tidal head located further downstream.

CT1

The CT1 palaeochannel core is located at the upstream end of the modern Riv 3(ii) zone (0.83 DSI). Three phases of deposition are recognised, relating to diatom zones A and B and C. The basal zone A has been dated at 809-428 cal.yr.BC to 762-414 cal.yr.BC. The age of the zone B diatomite has not been determined, but its location in the core stratigraphy suggests it was deposited at some point between 400 cal.yr.BC and 100 cal.yr.AD. Zone C has been dated at 240 +/-140 cal.yr.AD to 410 +/-180 cal.yr.AD.

During the 5th to 8th Century BC, the DSI values of 0.94 to 0.96 (zone A) are typical of the less saline Riv 4(i) zone (0.94-0.96 DSI) which starts just 0.5 km upstream. This suggests that river discharge was higher at this time, with the salinity front located further downstream. However, since this deposit is over 2400 years old, the lower groundwater salinity was probably caused by a lower RSL at this time. No conclusions can therefore be made on palaeo-discharge.

The Zone B diatomite has a DSI value of 1.00, indicating a pure freshwater assemblage. As this was not found in the modern analogue survey, it suggests the location of CT1 in the salinity gradient at this time was upstream of the Riv 4(ii) zone, therefore at least 3.5 km upstream of its current location in the gradient. Even accounting for RSL rise over the last 2000 years, this suggests that river discharge in the 1st to 2nd Century BC was higher than today.

In the overbank sediments found in the middle of zone C, the DSI value falls to 0.93. As noted earlier, this fall in DSI is caused by the presence of rare polyhalobous planktonics and tychplanktonics, which given the location of the CT1 core, is quite remarkable. Based on the modern analogue results, the presence of this polyhalobous component would suggest a location just upstream of the salinity front at the start of the freshwater tidal zone. The current location of this environment (at R9 in the river survey) is currently located 3 km downstream of the CT1 site. As indicated in chapter 4, a storm surge of the magnitude seen in 1607 AD (Haslett and Bryant, 2004) would place the freshwater tidal head in the vicinity of the CT1 core. However, it would have to raise tidal levels even higher to transport marine planktonics as far as CT1. The presence of

the polyhalobous planktonics does suggest an extreme storm surge, with the OSL dates either side of this horizon placing it in the 4th Century AD.

6.3 GEOMORPHOLOGY AND STRATIGRAPHY OF THE YEOTOWN REACH

6.3.1 Reach geomorphology

The geomorphology of the Yeotown reach is shown in figure 6.11. The Holocene alluvial floodplain widens in this reach to *c.*700m wide. The location of transect G (Yeotown transect) is shown, along with associated cores YW1, YE1 and YE2. The active channel continues to have a sinuous meandering planform in this reach ($S = 1.15$).

Extensive Pleistocene (Devensian) T7 deposits are preserved on the western side of the valley, elevated *c.*10m above the Holocene alluvium. A further five Holocene Terraces (T1, T2, T3, T4 and T5) are present, with altitudinal differences now apparent between all terrace surfaces. Areas of modern floodplain are located on the inside of the meander, south-west of the YE1 core. The active channel and floodplain fragments are bounded by natural levees on both banks, but during high-stage floods the lower T1 terrace is occasionally inundated, with floodwater following the palaeochannels at the back of the terrace.

The T1 terrace is particularly extensive in this reach and contains numerous palaeochannels that show evidence of extensive fluvial geomorphic activity, with active floodplain reworking and channel change. To the north-east of the River Taw, palaeochannels show evidence of meander migration and floodplain reworking, with the low sinuosity meander segment preserved in the east of the valley (containing the YE2 core) suggesting abandonment by avulsion. South-west of the River Taw, in the vicinity of the YW1 core, a palaeochannel shows a tortuous (Kellerhals *et al.*, 1976) asymmetrical meander with evidence of meander rotation and channel abandonment by neck cut-off. This area of the T1 floodplain also contains evidence of localised multi-channel braiding and mid-channel bar formation, indicating deposition during a period of increased bedload sediment supply (often associated with a highly variable

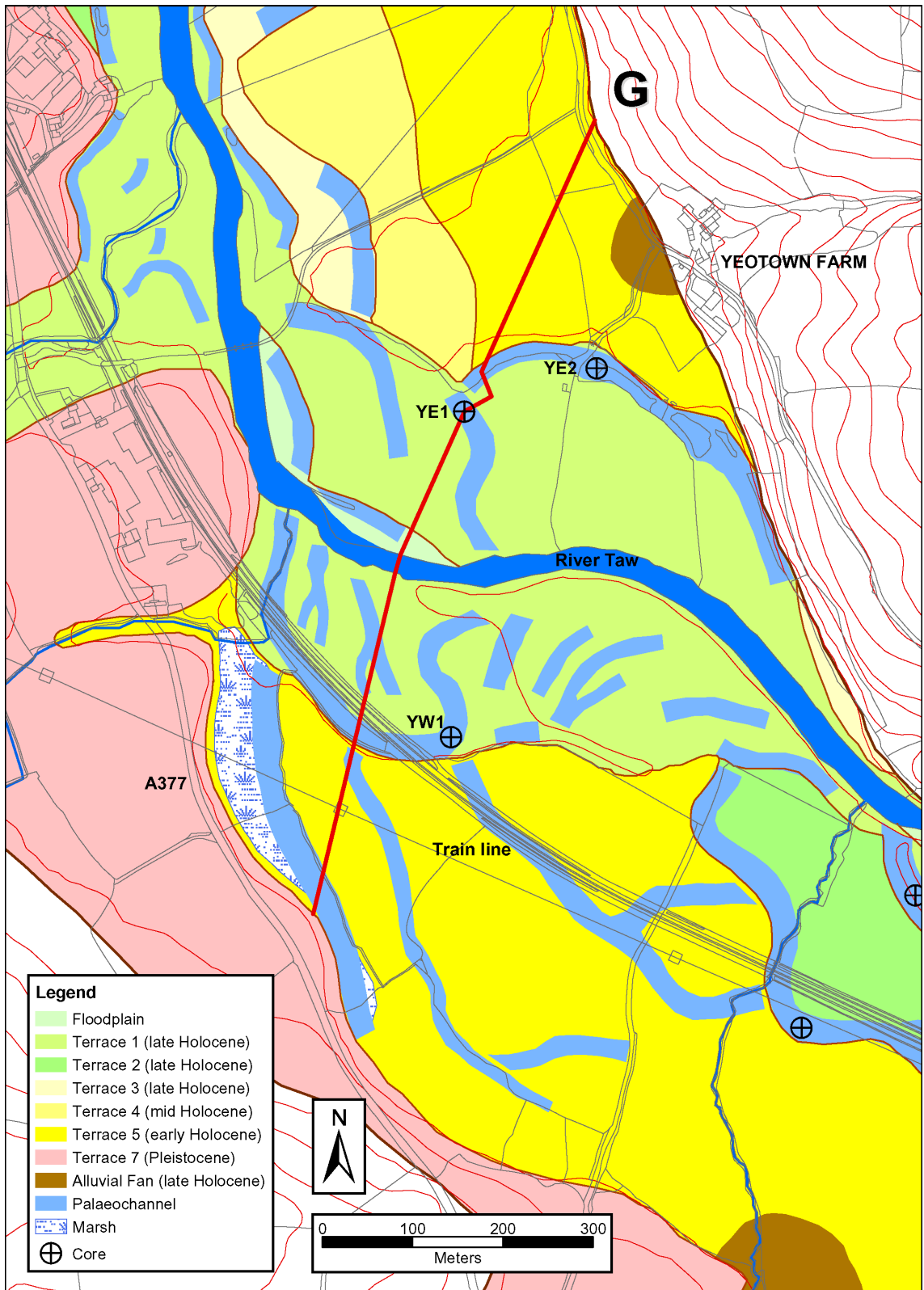


Figure 6.11 Geomorphology of the Yeotown reach. The location of transect G (Yeotown transect) and associated cores are indicated. This map was produced in a GIS and incorporates OS Landform Profile (5m contours) and OS MasterMap layers (supplied by Ordnance Survey/EDINA Digimap).

discharge), and suggesting the underlying sediments are readily mobilised in this reach (Knighton, 1998).

The T2 terrace is preserved in the south-east of the reach. However, this is more associated with the upstream Umberleigh House reach and will be described in section 6.4. Only a small fragment of T3 terrace is preserved in the north of the reach and this contains a relatively short palaeochannel meander fragment. This reach contains one of the few examples of T4 terrace. This is preserved within a T3, T4, T5 terrace staircase north of transect G. No palaeochannels are evident on the surface of this terrace and the alluvium was not investigated through coring (T4 is cored in the Umberleigh House reach). T5 is preserved at the north end of transect G, and extensively preserved in the south of the reach (including the southern end of transect G). The northern terrace fragment shows no evidence of palaeochannels, but the occurrence of many rounded river pebbles on a cultivated field surface near the valley side suggests the underlying gravel is overlain by a relatively thin cover of alluvium. The T5 surface in the south of the reach contains examples of a low sinuosity anastomosing palaeochannel planform, suggesting a stable river system with a relatively small sediment load that is dominated by suspended load (Schumm, 1981, 1985).

6.3.2 Lithostratigraphy of the Yeotown transect

Figure 6.12 shows the lithostratigraphy of transect G. The T1 terrace surface is generally located at *c.*10.0m OD. However, it rises to *c.*10.6m OD in the levee environment near the active channel. A sub-terrace T1 unit to the east of the YE1 palaeochannel (figure 6.11) is also elevated slightly higher at *c.*10.4m OD. T5 is located at 11.0-11.5m OD.

In the north of transect G, T5 deposits consist of relatively fine grained alluvium overlying a sloping gravel surface. The stratigraphy of the alluvium shows a basal fine-medium sand layer that thins and wedges out towards the valley side, overlain by overbank silty sand and sandy silt. The entire alluvial sequence thins towards the valley side where it is only 0.62m thick (stratigraphic core 17). The sequence thickens towards the outer terrace edge where it is 2.52m thick (stratigraphic core 15), with a 0.5m thick basal sand layer. There are no palaeochannel deposits. The alluvium is thought to represent overbank floodplain deposition on top of an inherited Late glacial or

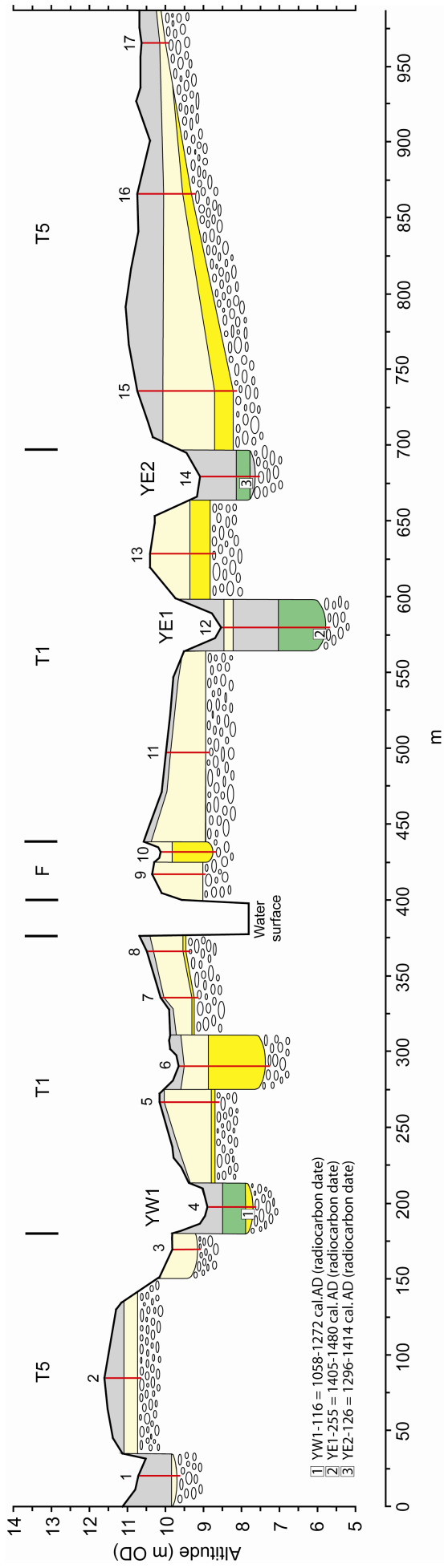


Figure 6.12 Lithostratigraphy of the Yeotown transect. The location of analysed cores and stratigraphic cores (1-17) are indicated. See figure 6.2 for legend.

Pleistocene (Devensian) gravel surface topography. The sediment texture and lack of palaeochannels suggests relative stability in the fluvial system, with dominance by suspended load overbank deposition. The T5 deposits in the south of the transect consist of a thin (0.86m) layer of fine grained (silty sand grading to sandy silt) overbank floodplain alluvium overlying an elevated gravel surface. The transect includes two T5 palaeochannels. These channels are relatively shallow with their bases 1.5m to 2.0m below the surrounding terrace surface, suggesting a low contemporaneous bankfull discharge or a multi-thread anastomosed (anabranching) channel system. The surface palaeochannel planform supports the latter option. The southern palaeochannel fill contains a light grey silty clay plug with occasional long thin rootlets suggesting marsh/aquatic vegetation. The northern palaeochannel fill has been largely removed by later overbank flood scour.

The T1 terrace south-west of the river is underlain by a thin 0.9-1.5m layer of sandy alluvium on top of an undulatory gravel surface. The alluvium consists of medium-coarse sand grading into fine sand and silty sand, with a very thin (0.15m) upper unit overbank sandy silt. The transect crosses two palaeochannels. The northern one is largely infilled with coarse sand, indicating abandonment of a bedload dominated river. This channel forms part of the braided channel network and the surrounding elevated gravel surface and sandy alluvium suggest a mobile channel system dominated by gravel bars with bar top sands. The elevated and easily erodible gravel surface within a bed-load dominated high-discharge system would facilitate channel braiding in this area. The southern palaeochannel (YW1) is part of the asymmetrical meander seen in figure 6.11, and contains a detrital silty peat which grades up into a silt. The channel was abandoned in 1185-1255 cal.yr.AD (1σ age).

North-east of the river, the T1 deposits contain two palaeochannel fills (YE1 and YE2). YE1 is incised c.4m below the surrounding terrace surface, suggesting a locally deep thalweg at the core site, and is infilled with a detrital peat and silt which accumulated after channel abandonment in 1420-1449 cal.yr.AD (1σ age). The T1 alluvium to the west of this channel is largely composed of a relatively thin layer of silty sand with little finer grained silt present. This is thought to represent laterally accreted bar top and sandy floodplain alluvium, deposited on top of a gravel point bar during lateral migration of the YE1 channel. The T1 floodplain alluvium east of the YE1 palaeochannel consists of a laterally accreted fining-up point bar sequence of gravelly

sand, fine-medium sand, fine sand and silty sand, indicating a high discharge/stream power and active channel migration. The YE2 palaeochannel was abandoned in 1309-1403 cal.yr.AD (1σ age), with subsequent deposition of a closed abandoned channel fill of peaty silt and overlying clay.

On the northern bank of the river Taw a recent point bar complex has been abandoned during channel migration. This consists of a gravel bar and fine sand bar top unit, with an abandoned chute channel fill of medium sand.

6.3.3 YW1 core

Sedimentology and magnetic properties

Figure 6.13 shows the core log for YW1. This figure shows down-core changes in sediment lithology, X_{if} , organic matter and carbonate content. Stratigraphic units (see chapter 7) are also indicated.

The YW1 core is underlain by gravel at 1.25m (8.95m OD). Between 0.46m and the basal gravel, a detrital (leaf and twig) peaty silt grades up into a peaty silt with rootlets (with occasional twig detritus). This organic unit is thought to represent sub-aqueous deposition in an abandoned channel pond, followed by infilling and palaeochannel marsh deposition. Above 0.46m, grey silt (with rootlets) has been deposited during further abandoned channel infilling.

Magnetic mineral concentrations are minimal throughout the YW1 core ($<0.1 \cdot 10^{-6} \text{ m}^3 \text{ kg}^{-1}$).

Geochronology

Wood from the basal part of the peat was radiocarbon dated, giving an age of 1058-1272 cal.yr.AD (1185-1255 cal.yr.AD, 1σ age) for channel abandonment.

Diatom analysis

Figure 6.14 shows a diatom diagram for YW1. All species with counts of $>3\%$ TDV are

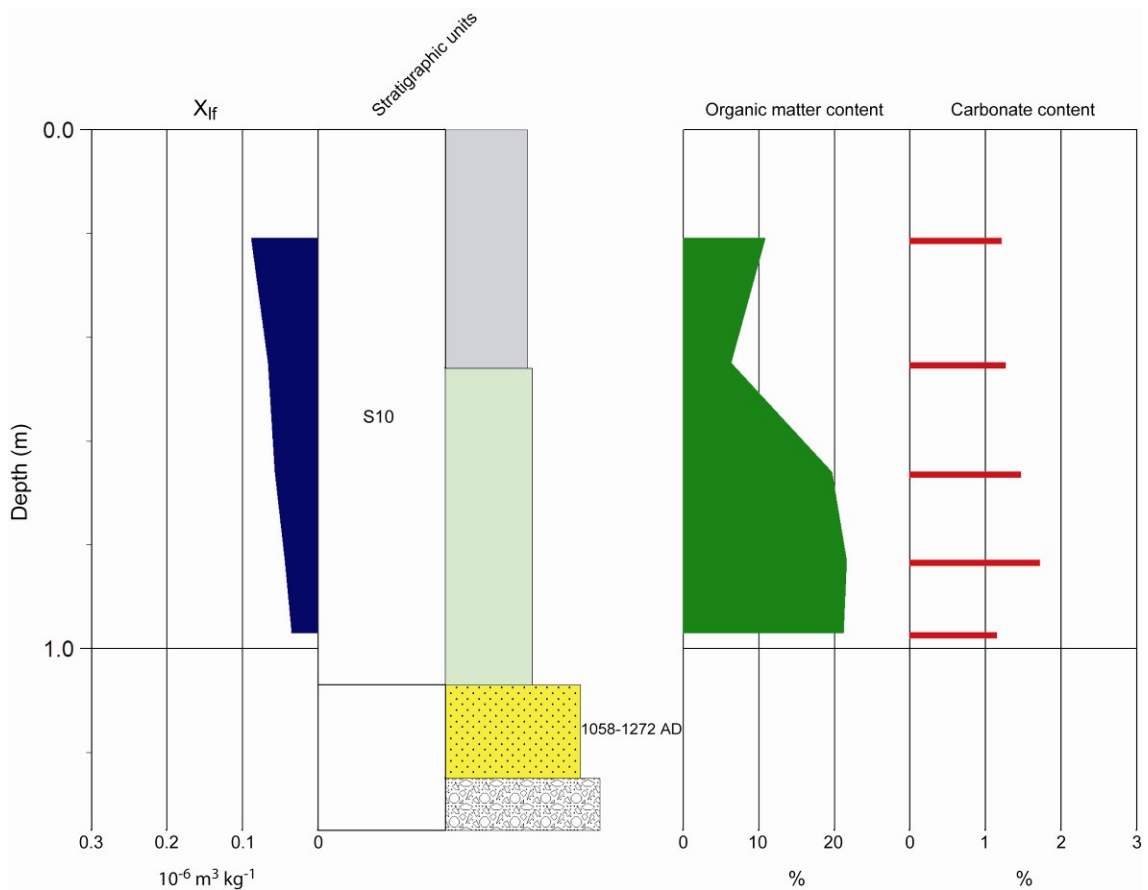


Figure 6.13 YW1 core log. See figure 5.2 for lithology legend. Stratigraphic units are discussed in chapter 7.

shown (plus rare brackish species >1%TDV), along with the diatom sums. Diatom zones were not justified in this core due to the low number of samples.

DSI values at the base and top of the core are at 0.98-0.99, indicating an almost exclusively freshwater assemblage. However, at the top of the peaty silt unit, the DSI falls to 0.96, indicating a minor contribution by brackish species in the middle of the core. This is largely accounted for by the presence of the mesohalobous species *Navicula phyllepta* at 3.5%TDV. Other rare brackish species include *Ctenophora pulchella* which reaches 2%TDV at the base of peaty silt, and *Navicula avenacea* which reaches 2%TDV in the upper grey silt. This small brackish assemblage component suggests very minor saline groundwater intrusion.

The freshwater assemblage in YW1 is dominated throughout the core by the oligohalobous indifferent species *Achnanthes exilis*, *Eunotia pectinalis* and *Eunotia curvata* (all at 10%TDV), with *Fragilaria capucina* also reaching >10%TDV in the upper grey silt.

6.3.4 YE1 core

Sedimentology and magnetic properties

Figure 6.15 shows the core log for YE1. This figure shows down-core changes in sediment lithology, X_{if} , organic matter and carbonate content. In addition, the diatom zones (see later) and stratigraphic units (see chapter 7) are indicated.

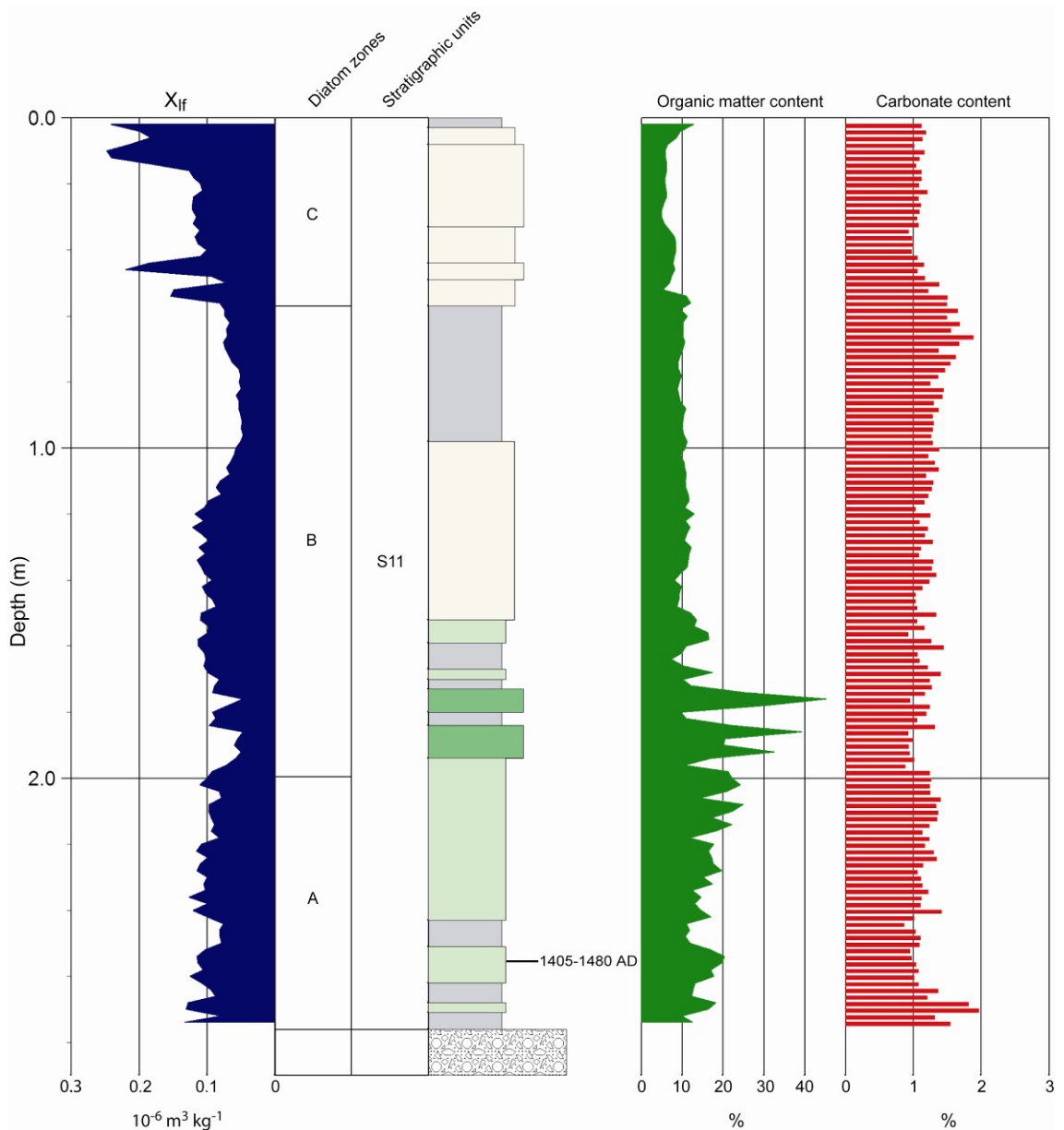


Figure 6.15 YE1 core log. See figure 5.2 for lithology legend. Diatom zones are derived from figure 6.16. Stratigraphic units are discussed in chapter 7.

The YE1 core is underlain by gravel at 2.76m (8.55m OD). Between 1.94m and the basal gravel, a silty detrital peat with organic silt horizons has been deposited, with the

organic component consisting of willow leaves and reed stems. This suggests deposition in a muddy abandoned palaeochannel pond, choked with leaf detritus from surrounding tree cover. Between 1.52m and 1.94m, intercalated layers of silty peat, peaty silt and organic silt contain abundant sedge and reed (*Phragmites*) fragments, suggesting deposition in an abandoned channel reed-sedge swamp. Between 0.98m and 1.52m, an organic sandy silt with sporadic twig, sedge and leaf fragments suggest deposition in a palaeochannel marsh which is occasionally inundated during high-stage floods. Between 0.98m and the ground surface, a coarsening-up sequence of clayey silt, sandy silt and silty fine sand (with rootlets) suggest overbank floodplain deposition within the palaeochannel depression and increasingly dry conditions.

X_{if} values are generally $0.1 \cdot 10^{-6} \text{ m}^3 \text{ kg}^{-1}$ for most of the core, suggesting a very minor magnetic mineral assemblage. However, the upper floodplain sandy silt – silty sand sees X_{if} values reach $0.25 \cdot 10^{-6} \text{ m}^3 \text{ kg}^{-1}$, possibly caused by soil-derived fine viscous magnetite (K_{if} values were not high enough to get reliable $X_{fd\%}$ values, so this cannot be confirmed).

Geochronology

Wood from the basal part of the peat was radiocarbon dated, giving an age of 1405-1480 cal.yr.AD (1420-1449 cal.yr.AD, 1σ age) for channel abandonment.

Diatom analysis

Figure 6.16 shows a diatom diagram for YE1. All species with counts of $>3\%$ TDV are shown (plus rare brackish species $>1\%$ TDV), along with the diatom sums. Cluster analysis resulted in three zones (A to C).

DSI values typically range from 0.97 to 0.99 in all zones, indicating an almost pure freshwater assemblage in these zones. However, in the organic reed-sedge swamp sediments at the base of zone B, the DSI value falls to 0.95, indicating a brackish component in the assemblage. This is largely accounted for by the presence of the mesohalobous species *Navicula phyllepta* at 4.5%TDV. Other rare brackish species include *Ctenophora pulchella* which reaches 2%TDV in zone B, and *Navicula avenacea* which reaches 2.5%TDV in zone A. This minor brackish assemblage

component, which peaks at the base of zone B, suggests some saline groundwater intrusion at this site during YE1 deposition.

The freshwater assemblage in YE1 is dominated by the oligohalobous indifferent species *Achnanthes exilis*, *Cocconeis placentula*, *Eunotia pectinalis* and *Eunotia curvata* (all at 10%TDV) in zones A and B, with *Cocconeis placentula*, *Hantzschia amphioxys* and *Pinnularia subcapitata* dominant (>10%TDV) in zone C.

6.3.5 YE2 core

Sedimentology and magnetic properties

Figure 6.17 shows the core log for YE2. This figure shows down-core changes in sediment lithology, X_{lf} , organic matter and carbonate content. In addition, the diatom zones (see later) and stratigraphic units (see chapter 7) are indicated.

The YE2 core is underlain by gravel at 1.45m (9.08m OD). Between 1.09m and the basal gravel, a unit of peaty silt (with a basal layer of organic silt) has been deposited. The sediment contains many detrital leaf, sedge stem and twig fragments suggesting subaqueous deposition in an abandoned channel pond. Between 0.97m and 1.09m, a unit of organic/peaty silt contains many rootlets and occasional wood fragments, suggesting that the abandoned channel pond has been infilled and replaced by a palaeochannel marsh. Between 0.97m and the surface, a unit of light grey clay, with oxidised rootlets (0.30-0.97m) grades into a grey silt with rootlets. This unit is thought to represent the resumption of subaqueous conditions within a shallow pond, with clay deposition from suspension, and some aquatic vegetation. This is similar to current conditions at this site.

Geochronology

A seed from the basal part of the peat was radiocarbon dated, giving an age of 1296-1414 cal.yr.AD (1309-1403 cal.yr.AD, 1σ age) for channel abandonment.

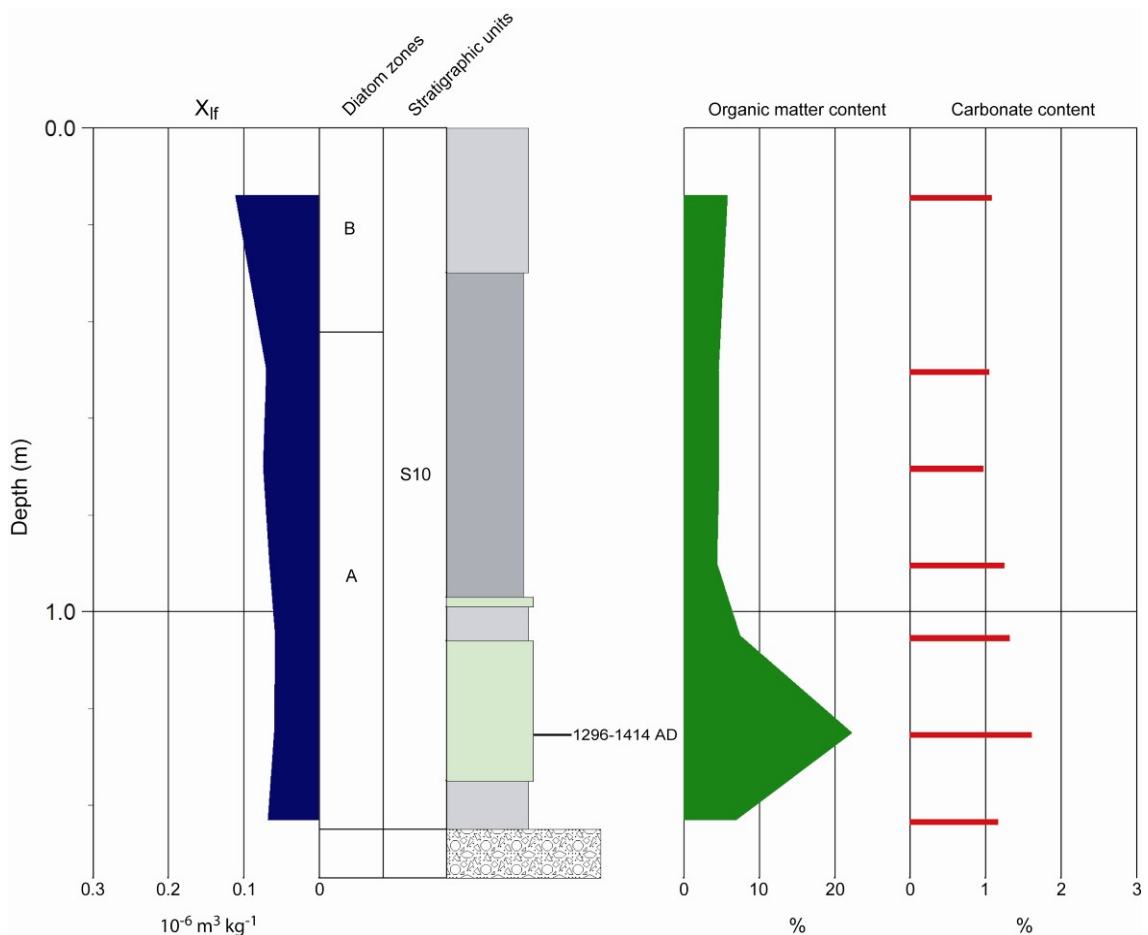


Figure 6.17 YE2 core log. See figure 5.2 for lithology legend. Diatom zones are derived from figure 6.18. Stratigraphic units are discussed in chapter 7.

Diatom analysis

Figure 6.18 shows a diatom diagram for YE2. All species with counts of >3%TDV are shown (plus rare brackish species >1%TDV), along with the diatom sums. Cluster analysis resulted in two zones (A and B).

DSI values range from 0.98-0.99, indicating an almost pure freshwater assemblage. The rare brackish (mesohalobous) component is mainly derived from the 1.0-1.5% presence of *Navicula phyllepta* (zones A and B) and a 0.5-1.0% occurrence of *Navicula avenacea* (zones A and B). The halophile *Navicula cincta* also reaches 3.5%TDV in zone A, at the top of the peaty silt. This rare brackish assemblage component suggests very minor saline groundwater intrusion.

The freshwater assemblage in YE2 is dominated by the oligohalobous indifferent species *Achnanthes exilis* and the halophobe *Tabellaria flocculosa* (both at >10%TDV)

in the organic sediment at the base of zones A, with *Eunotia curvata* and *Synedra ulna* dominant (>10%TDV) in the upper part of zone A. In zone B, *Eunotia pectinalis* and *Fragilaria capucina* are dominant (>10%TDV).

6.3.6 Brackish groundwater intrusion in the Yeotown reach

YW1

The YW1 palaeochannel core is located at the downstream end of the modern Riv 4(i) zone (0.94-0.96 DSI) and has been dated at 1185-1255 cal.yr.AD (1 σ age). The DSI values fall to 0.96, suggesting that groundwater salinity was similar to modern conditions during the early 13th Century. This would indicate that the salinity front location and river discharge during the early 13th Century was also similar to modern conditions.

YE1

The YE1 palaeochannel core is located at the downstream end of the modern Riv 4(i) zone (0.94-0.96 DSI) and has been dated at 1420-1449 cal.yr.AD (1 σ age). The DSI values fall to 0.95 in the reed-sedge swamp sediments of this core, suggesting that groundwater salinity was similar to modern conditions during the early 15th Century. This would indicate that the salinity front location and river discharge during the early 15th Century was also similar to modern conditions.

YE2

The YE2 palaeochannel core is located at the downstream end of the modern Riv 4(i) zone (0.94-0.96 DSI) and has been dated at 1309-1403 cal.yr.AD (1 σ age). However, the almost pure freshwater YE2 DSI values of 0.98-0.99 are typical of the less saline Riv 4(ii) zone (0.98 DSI) which is located 2.7 km upstream of the YE2 site (at R17). This suggests that river discharge was higher during the 14th Century AD with the salinity front located further downstream. A less saline environment in the 14th Century could also be inferred to be a result of lower RSL at this time with the tidal head located further down-river. However, this would require a significant rise in RSL over the last 600-700 years to cause the observed 2.7 km shift in groundwater zones.

The conclusions drawn about relative palaeo-discharges in the Yeotown reach can only

be seen as very tentative as the inferences are based on very small (but possibly significant) differences in DSI between the contemporary and fossil core assemblages.

6.4 GEOMORPHOLOGY AND STRATIGRAPHY OF THE UMBERLEIGH HOUSE REACH

6.4.1 Reach geomorphology

The geomorphology of the Umberleigh House reach is shown in figure 6.19. Although the valley widens in this reach, the Holocene alluvial floodplain narrows to *c.*550m. Another *c.*400m of the valley width is occupied by the Pleistocene (Devensian) T7 terrace. The location of transects H (Horestone transect) and I (Umberleigh House transect) is shown, along with associated cores HS1, HS2, UH1 and UH2. The active channel is located on the north side of the valley, where its planform straightens into a low sinuosity ($S = 1.06$) single-thread river, suggesting the valley slope is less in this reach, upstream of the Hawkrigde Brook confluence. A reduced valley slope would result in a decline in stream power, which can cause a reduction in sinuosity and promote channel change from a meandering to a straight planform (Schumm and Khan, 1972; Edgar, 1984). A possible reason for a reduction in valley slope is seen in the vicinity of transect I, where the entrenched channel (figure 6.25) has a bedrock bed, which would require a greater stream power to erode, compared with a gravel-sand bed. The low width/depth ratio of this entrenched channel reach would also reduce sinuosity (Schumm, 1963).

Extensive Pleistocene (Devensian) T7 deposits are preserved on the southern side of the valley, elevated *c.*10m above the Holocene alluvium. A further four Holocene Terraces (T1, T2, T4 and T5) are present, with altitudinal differences apparent between all terrace surfaces (see figures 6.20 and 6.25). Figure 6.19 shows that the terraces form a north-south terrace staircase, indicating the river has become more restricted to the northern valley side during the Holocene. The few fragments of modern floodplain indicate that the river is currently relatively stable.

T1 is also restricted to narrow zones near the active channel where it contains a low sinuosity palaeochannel at transect H. T2 contains higher sinuosity meandering

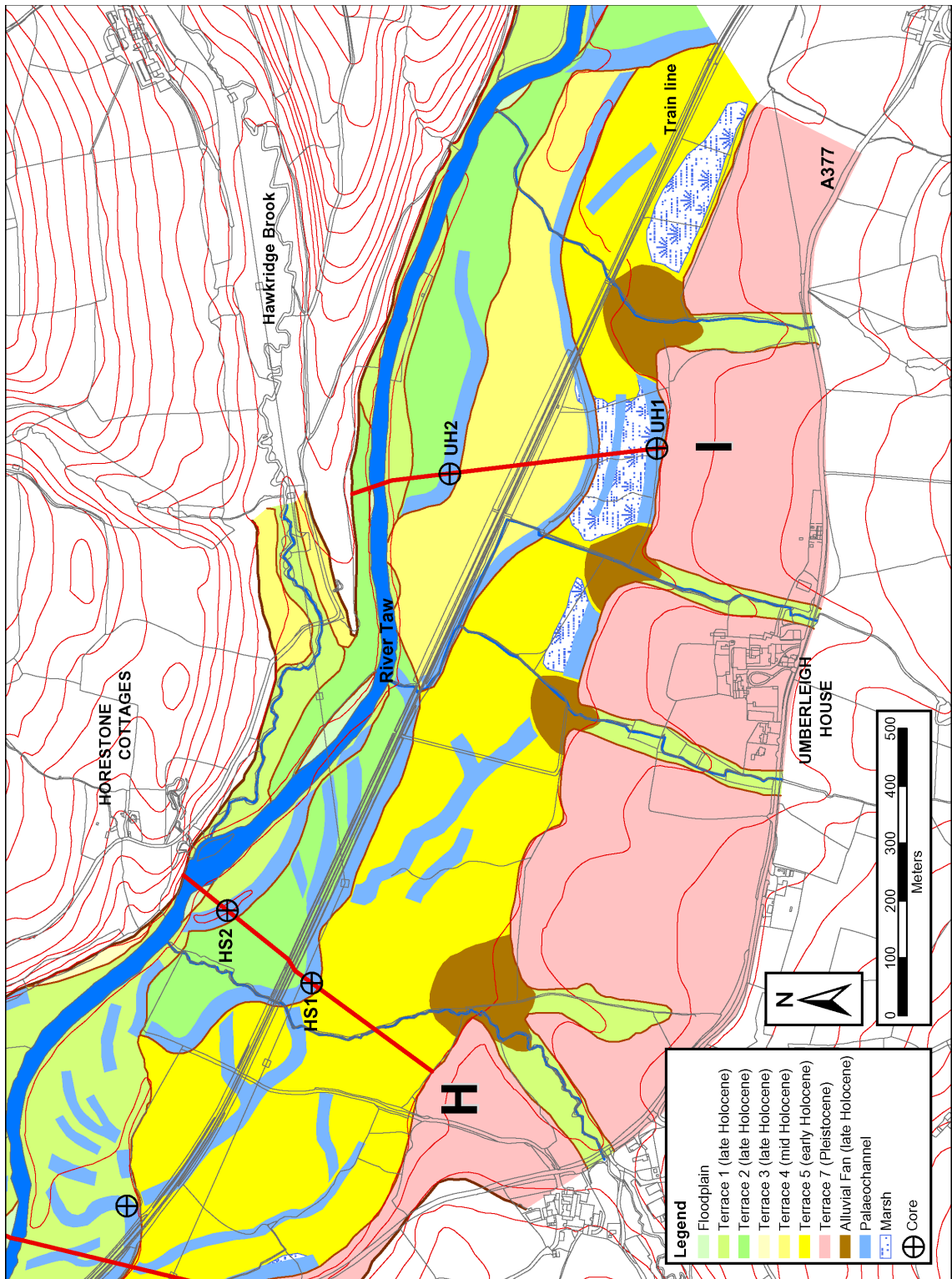


Figure 6.19 Geomorphology of the Umberleigh House reach. The location of transects H (Horestone transect) and I (Umberleigh House transect) and associated cores are indicated. This map was produced in a GIS and incorporates OS Landform Profile (5m contours) and OS MasterMap layers (supplied by Ordnance Survey/EDINA Digimap).

palaeochannels, suggesting the channels were less entrenched, with a higher width/depth ratio, and that discharge (and therefore stream power) was greater during

T2 formation. A relatively large area of T4 is preserved in the vicinity of transect I. This contains a single 1.28 km long palaeochannel segment that includes a whole meander wavelength. The sinuosity of this channel is relatively low ($S = 1.07$), suggesting a relatively stable channel active during a period of low discharge and/or relatively low rates of bedload transport with dominance by suspended load (Schumm and Khan, 1972; Schumm, 1981, 1985; Edgar, 1984; Van den Berg, 1995). The preservation of this channel suggests it was abandoned by avulsion. The wide (200-400m) T5 terrace shows a continuation from the Yeotown reach and is extensive throughout the southern side of the valley. The anabranching anastomosed channel planform is seen to continue through the Umberleigh House reach. One palaeochannel segment is 1.1 km long and if it is contemporaneous with a segment west of transect H, this would make a 1.88 km long early Holocene palaeochannel. The low sinuosity anastomosed planform suggests a low stream power with dominance by suspended load, although anastomosing channels carrying a relatively large bed load are not unknown (Knighton and Nanson, 1993).

Figure 6.19 shows several low-angle alluvial fans on the back of the T5 terrace surface. These are sourced from gullies and small tributaries that dissect the Pleistocene (Devensian) T7 terrace to the south. Coring in the fan east of the UH1 core site revealed that they are composed of fine sand and that they overlie (and post-date) the peat that is found at the top of the UH1 palaeochannel. This peat commenced in the early Holocene and is thought to have accumulated through the middle Holocene. This would give a late Holocene age for fan creation. Elsewhere, similar fans overlie T3 (Bridgetown reach) and T2 (New Bridge reach) terrace surfaces. This suggests that they were largely formed during T2 and T1 formation.

6.4.2 Lithostratigraphy of the Horestone transect

Figure 6.19 shows the lithostratigraphy of transect H. The T1 terrace surface is located at *c.*11.0m OD, the T2 surface is located at *c.*11.8m OD and the T5 surface is located at *c.*12.45m OD.

The T5 terrace deposits consist of a 1.19-1.46m layer of relatively fine-grained alluvium that overlies a gravel surface. The alluvium consists of silty fine sand, grading up into sandy silt, and is thought to represent vertically accreted overbank floodplain

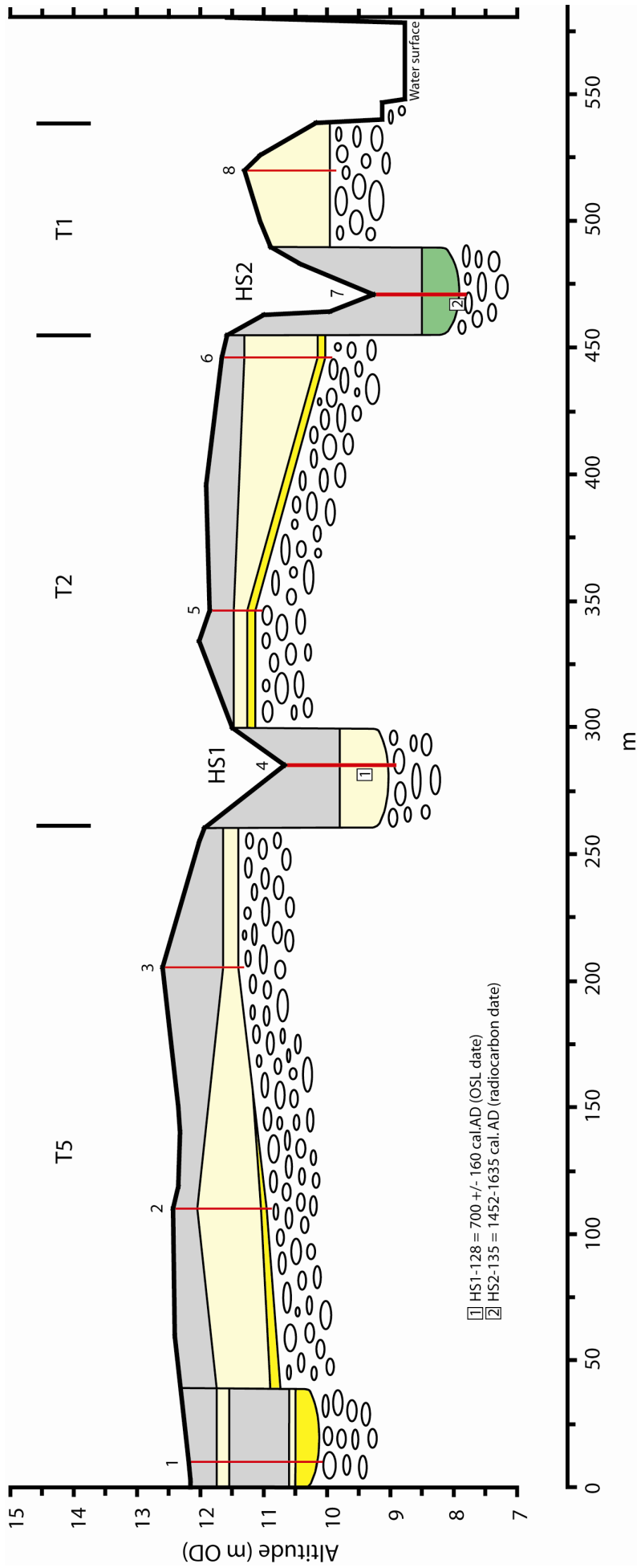


Figure 6.20 Lithostratigraphy of the Horestone transect. The location of analysed cores and stratigraphic cores (1-8) are indicated. See figure 6.2 for legend.

sedimentation. A thin (7cm) basal layer of fine-medium sand is located below stratigraphic core 2. At the back of the T5 terrace, a relatively shallow (2.03m) palaeochannel contains a basal fill of laminated fine-medium sand with some silt laminae. This is overlain by a fining-up sequence of green-grey fine sand, light grey clayey silt and light grey silty clay up to 0.65m depth. This sequence suggests abandonment of a sand-bed river, followed by deposition of clay within a subaqueous palaeochannel pond environment. The upper part of the palaeochannel fill consists of silty sand and sandy silt, similar to the adjacent floodplain sediment. The fine sand bed-load of this palaeochannel, the predominance of a clay fill, and the relatively small dimensions support the geomorphological evidence of an anastomosing river system during T5 deposition. This is further supported by the extensive vertically accreted floodplain deposits, indicating channel stability.

The T2 terrace contains a slightly coarser grained sequence that overlies an undulating gravel surface. To the north, beneath stratigraphic core 6, a thin layer of medium sand is overlain by a thick unit of interstratified fine and silty fine sand, with occasional coarse sand horizons. This is overlain by a thinner unit of overbank sandy silt. This sequence suggests lateral accretion during migration of a sand-bed river. In the south of the terrace, on the inside of a T2 palaeochannel meander, the gravel surface is significantly higher at 0.70m and is overlain by a fining-up sequence of gravelly medium-coarse sand, silty sand and sandy silt. This is thought to represent a laterally accreted gravel point bar sequence, associated with the adjacent palaeochannel. This palaeochannel (HS1) contains a minerogenic fill of fine and silty fine sand, overlain by sandy silt, with channel abandonment (probably by avulsion) at 700 +/-160 cal.yr.AD.

The T1 terrace contains the HS2 palaeochannel and a laterally accreted floodplain unit of bimodal fine sand with many medium-coarse grains and occasional sub-rounded pebbles. The HS2 channel is incised *c.*3.1m below the T1 floodplain surface and contains a basal unit of peaty silt with many plant/wood fragments and some seeds and acorn shells. This is overlain by a clayey silt with rootlets. This sequence suggests deposition within a closed abandoned channel. The channel was abandoned in 1452-1635 cal.yr.AD.

6.4.3 HS1 core

Sedimentology and magnetic properties

Figure 6.21 shows the core log for HS1. This figure shows down-core changes in sediment lithology, X_{lf} , $X_{fd\%}$, organic matter and carbonate content. In addition, the diatom zones (see later) and stratigraphic units (see chapter 7) are indicated.

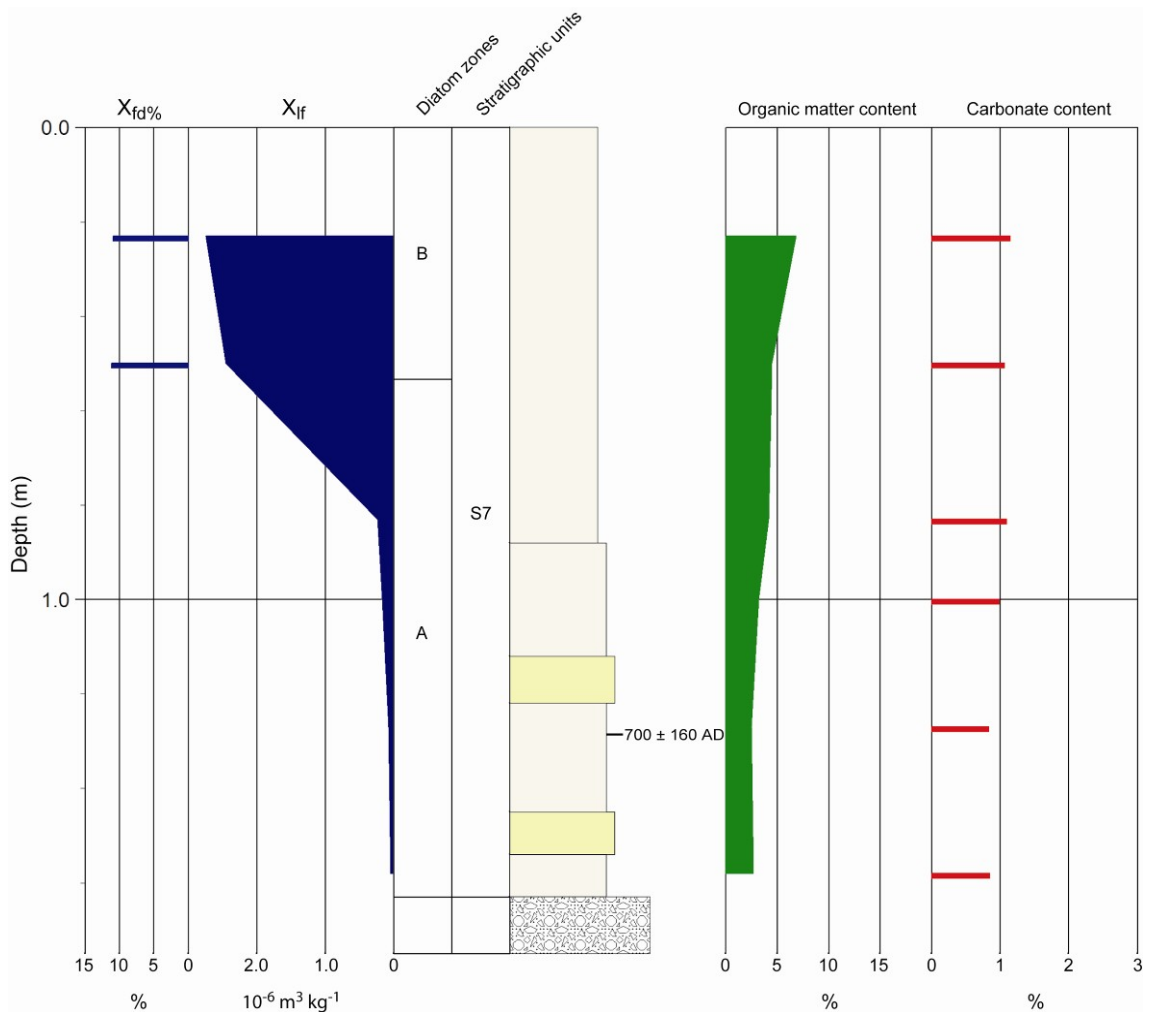


Figure 6.21 HS1 core log. See figure 5.2 for lithology legend. Diatom zones are derived from figure 6.22. Stratigraphic units are discussed in chapter 7.

The HS1 core is underlain by gravel at 1.63m (10.68m OD). Between 0.88m and the basal gravel, a sequence of interstratified fine sand and silty fine sand layers (10-20cm thick) has been deposited and is thought to represent sand bar migration within a sand-bed river. Above 0.88m, a unit of sandy silt with rootlets has been deposited following channel abandonment, and is more typical of overbank floodplain deposition.

X_{fr} values are very low in the basal channel sands ($<0.1 \cdot 10^{-6} \text{ m}^3 \text{ kg}^{-1}$), indicating a minimal magnetic mineral assemblage. However, in the upper sandy silt, X_{fr} values rise to $c.2.7 \cdot 10^{-6} \text{ m}^3 \text{ kg}^{-1}$, indicating a very high concentration of ferrimagnetic minerals. Corresponding $X_{\text{fd}\%}$ values of $>10\%$ indicate the magnetic assemblage is dominated by fine viscous ferrimagnetic grains, suggesting that the surrounding terrace surface was being actively cultivated during the 8th Century AD (date below), with soil erosion providing an influx of fine viscous magnetite.

Geochronology

The basal channel sand was OSL dated, giving an age of 700 \pm 160 cal.yr.AD for final channel activity prior to abandonment.

Diatom analysis

Figure 6.22 shows a diatom diagram for HS1. All species with counts of $>3\%$ TDV are shown (plus rare brackish species $>1\%$ TDV), along with the diatom sums. Cluster analysis resulted in two zones (A and B).

DSI values range from 0.97 to 1.00, indicating an almost pure freshwater assemblage. The minor brackish component is mainly derived from the presence of the mesohalobous species *Navicula avenacea* and *Ctenophora pulchella*, which are both present at 4%TDV in zone A. The mesohalobous group sum peaks at 6% at the base of the sandy silt unit, just above the abandonment surface. This small brackish assemblage component suggests only minor saline groundwater intrusion.

The freshwater assemblage is dominated in zone A by the oligohalobous indifferent species *Cocconeis placentula*, *Eunotia pectinalis* and *Synedra ulna* (all $>10\%$ TDV), with zone B dominated by *Eunotia pectinalis*, *Hantzschia amphioxys* and *Pinnularia subcapitata*.

6.4.4 HS2 core

Sedimentology and magnetic properties

Figure 6.23 shows the core log for HS2. This figure shows down-core changes in sediment lithology, X_{if} , organic matter and carbonate content. Stratigraphic units (see chapter 7) are also indicated.

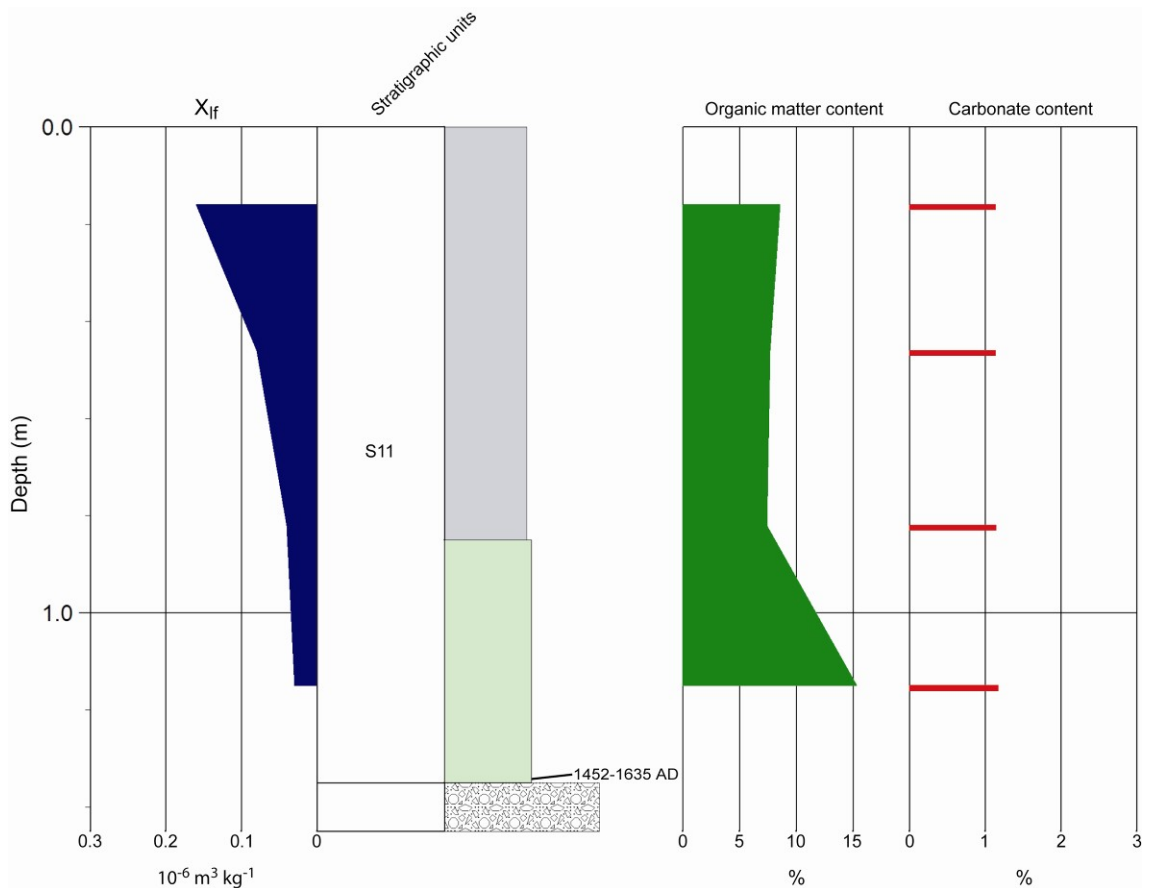


Figure 6.23 HS2 core log. See figure 5.2 for lithology legend. Stratigraphic units are discussed in chapter 7.

The HS2 core is underlain by gravel at 1.35m (9.27m OD). Between 0.85m and the basal gravel, a unit of peaty clayey silt has been deposited, with many detrital twigs and leaves, plus occasional seeds and acorn shells. This unit represents organic deposition within a closed abandoned channel, possibly within a palaeochannel pond, that was subject to occasional overbank flooding from the active channel. Above 0.85m, the sediment grades into a grey organic clayey silt with rootlets, suggesting deposition in a waterlogged palaeochannel depression. The HS2 site is currently occasionally inundated during high-stage floods from the nearby active channel. This has resulted in significant

scour with the channel depression situated *c.* 1.8m below the adjacent T1 terrace surface.

X_{f} values reach a maximum of $0.16 \cdot 10^{-6} \text{ m}^3 \text{ kg}^{-1}$ in the upper clayey silt, indicating a small magnetic mineral assemblage. The most likely contributors to this assemblage are detrital haematite (which has a low susceptibility) or a minor influx of soil derived magnetite.

Geochronology

An acorn shell from the base of the peaty silt was radiocarbon dated, giving an age of 1452-1635 cal.yr.AD (1469-1627 cal.yr.AD 1σ age) for channel abandonment.

Diatom analysis

Figure 6.24 shows a diatom diagram for HS2. All species with counts of $>3\%$ TDV are shown (plus rare brackish species $>1\%$ TDV), along with the diatom sums. Diatom zones were not justified in this core due to the low number of samples.

DSI values range from 0.97 to 0.99, indicating an almost pure freshwater assemblage. The rare brackish component is mainly derived from the presence of the mesohalobous species *Navicula avenacea* (2%TDV) and *Navicula phyllepta* (2%TDV) at the base of the organic silt. This rare brackish assemblage component suggests very minor saline groundwater intrusion.

The freshwater assemblage is dominated in the basal peaty silt by the oligohalobous indifferent species *Eunotia pectinalis* and *Eunotia curvata*, and the halophobous tychoplanktonic *Tabellaria flocculosa* (all at $>10\%$ TDV). This latter species supports deposition within an abandoned channel pond. The more minerogenic upper silt is dominated by the oligohalobous indifferent species *Cocconeis placentula*, *Eunotia pectinalis*, *Gomphonema angustum* and *Pinnularia subcapitata*.

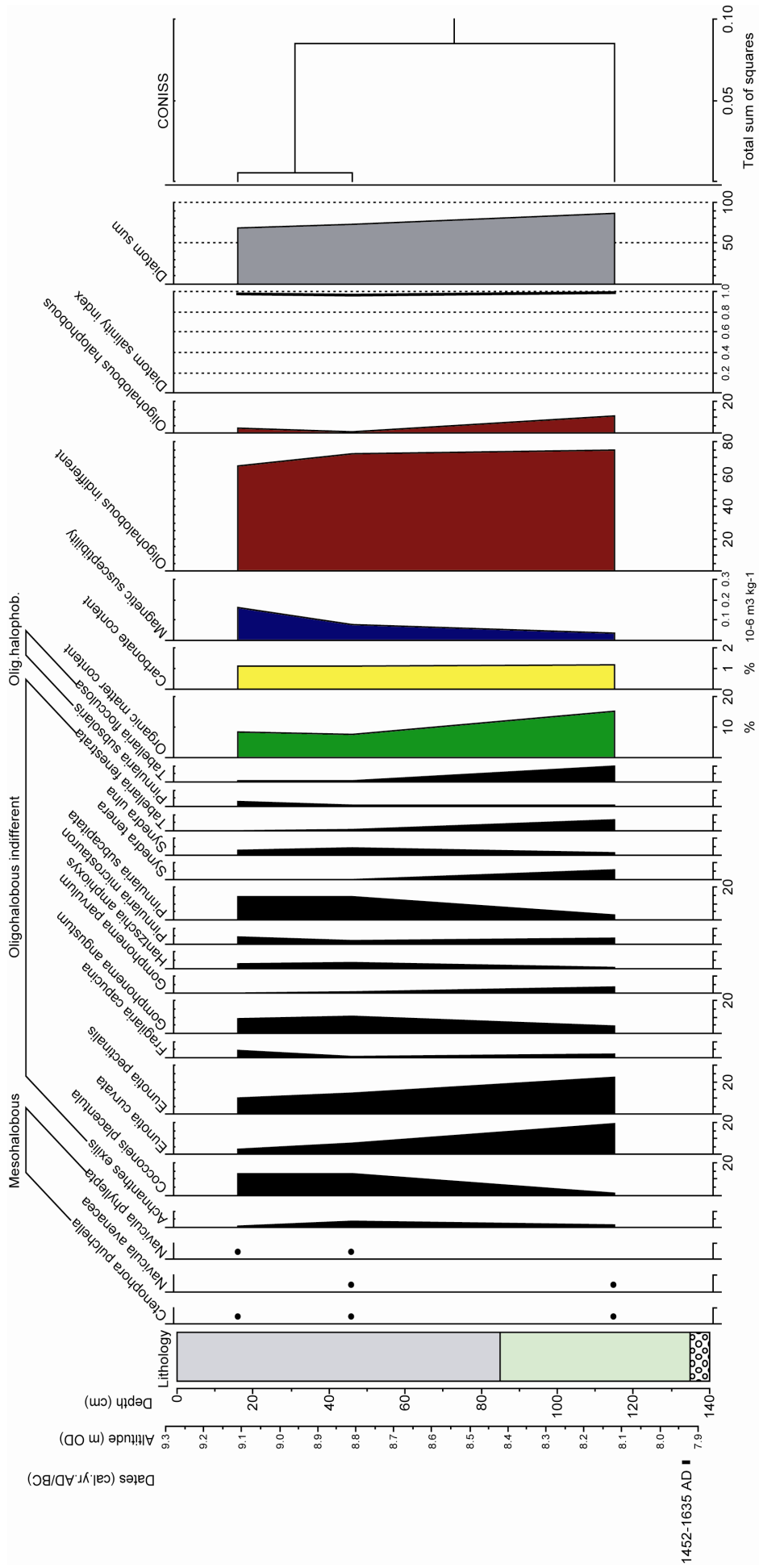


Figure 6.24 Diatom diagram for HS2 core (>3% TDV spp.). Organic matter content, carbonate content, X_{II} and Diatom Salinity Index is also shown.

6.4.5 Lithostratigraphy of the UMBERLEIGH HOUSE TRANSECT

Figure 6.25 shows the lithostratigraphy of transect I. The T1 terrace surface is located at *c.*13.3m OD, the T2 surface is located at *c.*13.5m OD, the T4 surface is located at *c.*13.8m OD and the T5 surface is located at *c.*14.25m OD.

The T5 terrace deposits consist of two palaeochannels and an intervening area of floodplain. The floodplain unit consists of a thin (0.56m) layer of relatively fine grained alluvium on top of an elevated gravel surface with a fining-up sequence of fine sand, silty fine sand and sandy silt, with rootlets throughout. This unit represents vertically accreted overbank sedimentation, probably deposited on top of a pre-existing Late glacial gravel surface. The southern palaeochannel (UH1) is relatively shallow (1.36m) and contains a basal silty fine channel sand deposited in the Late glacial interstadial (see 6.4.6). Above an erosion surface, silty clay and peat is deposited with organic deposition starting at approximately 7040 +/-1010 cal.yr.BC (see 6.4.6). This palaeochannel is part of the anastomosing T5 channel system. The erosion surface suggests the Late glacial interstadial channel site was re-occupied at the start of the early Holocene (*c.*9500 cal.yr.BC), suggesting that the T5 floodplain alluvium was predominantly accreted during the early Holocene, with the channel network partly inherited from the Late glacial. The terrace edge T5 palaeochannel (stratigraphic cores 3 and 4) contains a fine grained silty clay plug, which is typical for an anastomosing river system, dominated by suspended sediment load (Smith and Smith, 1980; Makaske, 2001).

The T4 terrace contains a single palaeochannel at the back of the terrace and a thin (0.46-0.73m) layer of fine grained clayey silt and sandy silt alluvium, on top of a gravel surface. This layer represents vertically accreted overbank alluvium and its wide extent (250m) suggests a high degree of channel stability. The palaeochannel contains a thin basal layer of fine-medium channel sand, which is overlain by a channel abandonment sequence of silty sand and sandy silt. The channel is relatively narrow, with a low width/depth ratio, which would promote channel stability and the low sinuosity seen in the surface geomorphology (Schumm, 1963). The narrow dimensions also suggest that this channel may not have been able to contain a bankfull discharge, suggesting it was part of an anastomosed multi-thread channel system (Smith and Smith, 1980; Makaske, 2001), with the other channels now eroded by later incision and floodplain reworking in

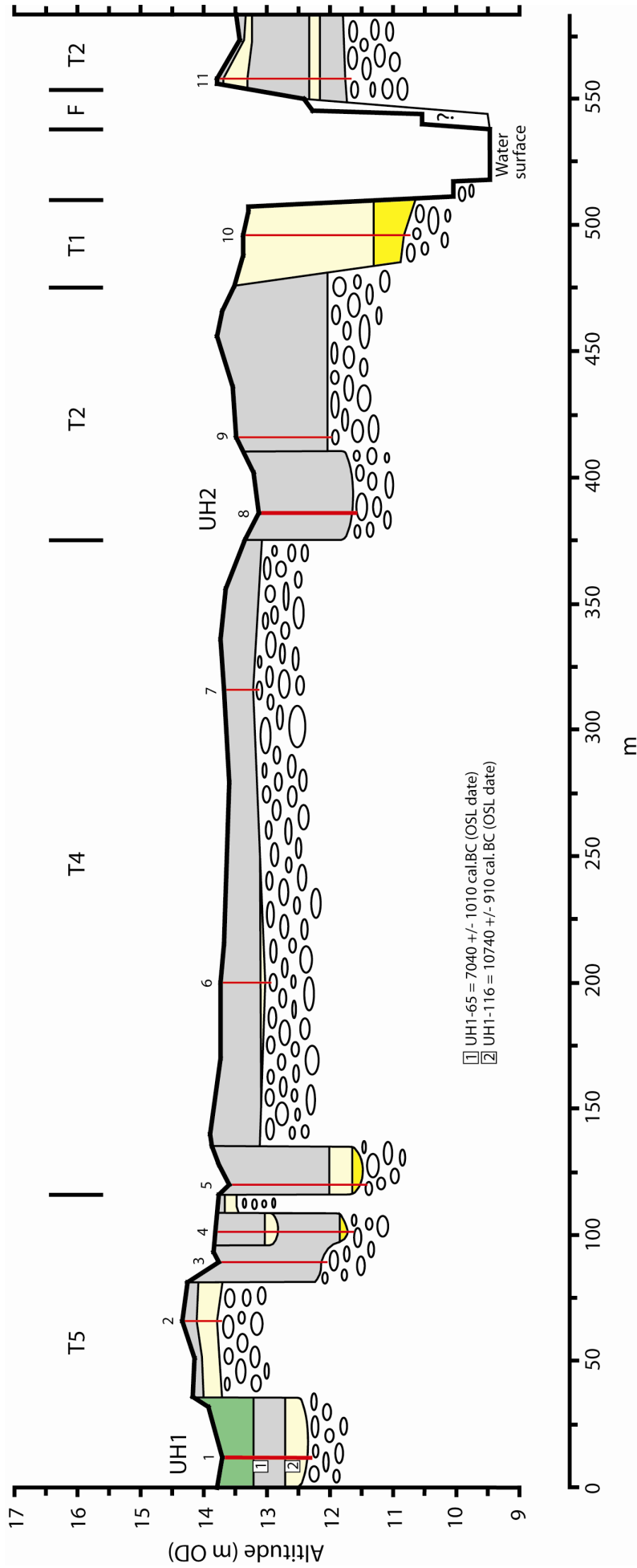


Figure 6.25 Lithostratigraphy of the Umberleigh House transect. The location of analysed cores and stratigraphic cores (1-11) are indicated. See figure 6.2 for legend.

the north of the transect. The relationship of this terrace with the higher T5 terrace, and with the lower T3 terrace in the Yeotown reach, suggests it was formed during the later early Holocene or middle Holocene.

The T2 terrace deposits are found on both sides of the contemporary River Taw and contain a palaeochannel fill (UH2) and areas of floodplain sedimentation. The floodplain alluvium beneath stratigraphic core 9 contains 1.44m of sandy silt, with rootlets throughout and some post depositional manganese mineralisation. This unit, which rests on a gravel surface, represents vertically accreted overbank sedimentation, suggesting that the UH2 channel was both initiated and abandoned during avulsion events. The T2 floodplain unit on the north bank of the River Taw contains a sequence of intercalated silty fine sand and laminated sandy silt, with no rootlets/rootlet traces. This unit, which overlies a gravel surface at 2.02m, is thought to represent lateral accretion deposition formed during active channel migration. The T2 palaeochannel (UH2) contains an abandoned channel coarsening-up sequence of silty clay, clayey silt and sandy silt.

The narrow (30m) T1 terrace on the south bank of the River Taw contains a thick 2.55m lateral accretion fining-up sequence of coarse sand, medium sand, fine sand and silty fine sand, overlying a gravel surface. This unit represents lateral accretion of a bank-attached gravel bar and bar-top sands, suggesting a period of increased coarse grained bedload supply during a phase of relatively high discharge.

6.4.6 UH1 core

Sedimentology and magnetic properties

Figure 6.26 shows the core log for UH1. This figure shows down-core changes in sediment lithology, X_{lf} , organic matter and carbonate content. In addition, the stratigraphic units (see chapter 7) are indicated. This sequence was also investigated after excavation of a pit for OSL sampling.

The UH1 core (and pit) is underlain by gravel at 1.36m (13.72m OD). Between 1.01m and the basal gravel, a unit of grey silty fine channel sand has been deposited. The

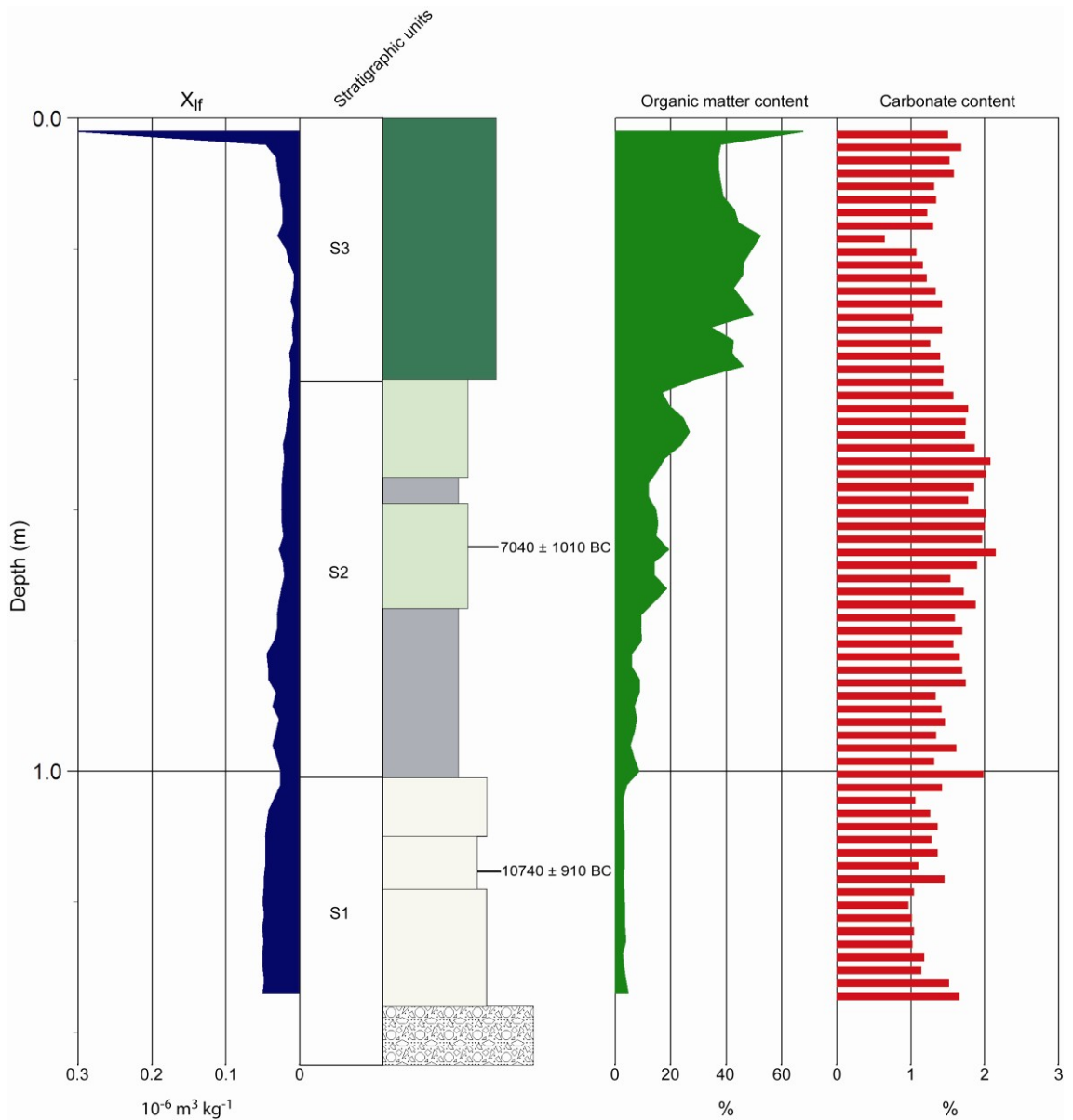


Figure 6.26 UH1 core log. See figure 5.2 for lithology legend. Stratigraphic units are discussed in chapter 7.

sediment contains trough ripple cross-lamination with laminae of coarse sand at the base of trough lamination sets. This indicates migration of undulatory asymmetrical current ripples with coarse sand collecting in ripple troughs. At 1.01m, a sharp undulatory erosion surface separates the sand from an overlying unit of light grey silty clay. (This boundary is also stained black from post-depositional influx of organic groundwater (humins/humic acid) related to the peat deposition higher in the sequence.) The erosion surface suggests the channel was re-occupied and then abandoned within a river system that was dominated by fine grained suspended sediment load. The silty clay unit is found between 0.41m and 1.01m and becomes organic/peaty at 0.75m and contains an increasing amount of long aquatic/marsh plant roots. The fine grained

texture of this deposit suggests sub-aqueous deposition. Woody tree roots, which penetrate down from the overlying peat, are also present. The upper 10cm of the clay contains grass/sedge rootlets, suggesting the establishment of a marsh after the infilling of the earlier pond. Between 0.41m and the surface, a unit of brown clayey peat has accumulated. The peat contains lots of fibrous root matter, with some humified wood and tree bark fragments below 0.20m.

Geochronology

The basal channel sand was OSL dated, giving a Late glacial interstadial (Allerød) age of 10740 +/-910 cal.yr.BC for final channel activity prior to abandonment. A sediment sample from the organic silty clay (at 0.65m) was OSL dated, giving an age of 7040 +/- 1010 cal.yr.BC for infilling after later channel abandonment.

6.4.7 UH2 core

Sedimentology and magnetic properties

Figure 6.27 shows the core log for UH2. This figure shows down-core changes in sediment lithology, X_{if} , $X_{fd\%}$, organic matter and carbonate content. Stratigraphic units (see chapter 7) are also indicated.

The UH2 core is underlain by gravel at 1.46m (13.13m OD). Between 0.93m and the basal gravel, a grey silty clay has been deposited after channel abandonment. This is overlain by a coarsening-up sequence of grey-brown clayey silt and brown sandy silt with rootlet traces and substantial post-depositional manganese mineralisation.

X_{if} values are low in the basal part of the sequence ($c.0.1 \cdot 10^{-6} \text{ m}^3 \text{ kg}^{-1}$), but rise sharply to $2.52 \cdot 10^{-6} \text{ m}^3 \text{ kg}^{-1}$ in the upper sandy silt. A corresponding $X_{fd\%}$ value of 9.5% in the sandy silt indicates that the magnetic assemblage is dominated by fine viscous magnetite, probably derived from nearby soil erosion.

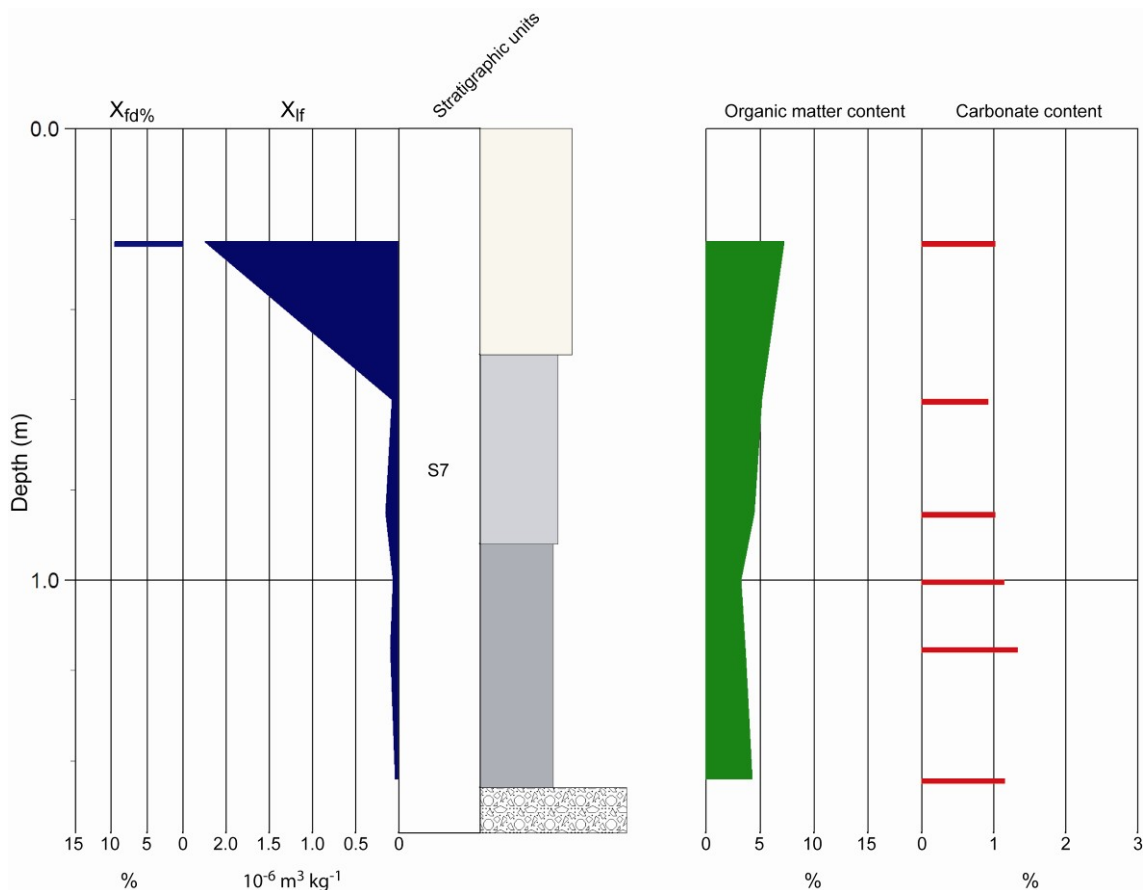


Figure 6.27 UH2 core log. See figure 5.2 for lithology legend. Stratigraphic units are discussed in chapter 7.

Diatom analysis

Figure 6.28 shows a diatom diagram for UH2. Diatom valves were not present (or were very rare) in most of this core, with the only count possible at the upper sample horizon at 0.25m. All species with counts of >3%TDV are shown (plus rare brackish species >1%TDV) are shown for this horizon, along with the diatom sums.

The DSI value of 0.995 indicates an essentially pure freshwater assemblage. Single counts of the mesohalobous species *Navicula avenacea* and *Nitzschia subcapitellata* (totalling 1%TDV) were made. The halophile *Navicula mutica* is also present at 2%TDV. The assemblage suggests that saline groundwater either did not reach the UH2 site or was very diluted and at the limit of estuarine groundwater intrusion. The freshwater assemblage is dominated by the oligohalobous indifferent species *Gomphonema angustum*, *Hantzschia amphioxys* and *Pinnularia subcapitata*.

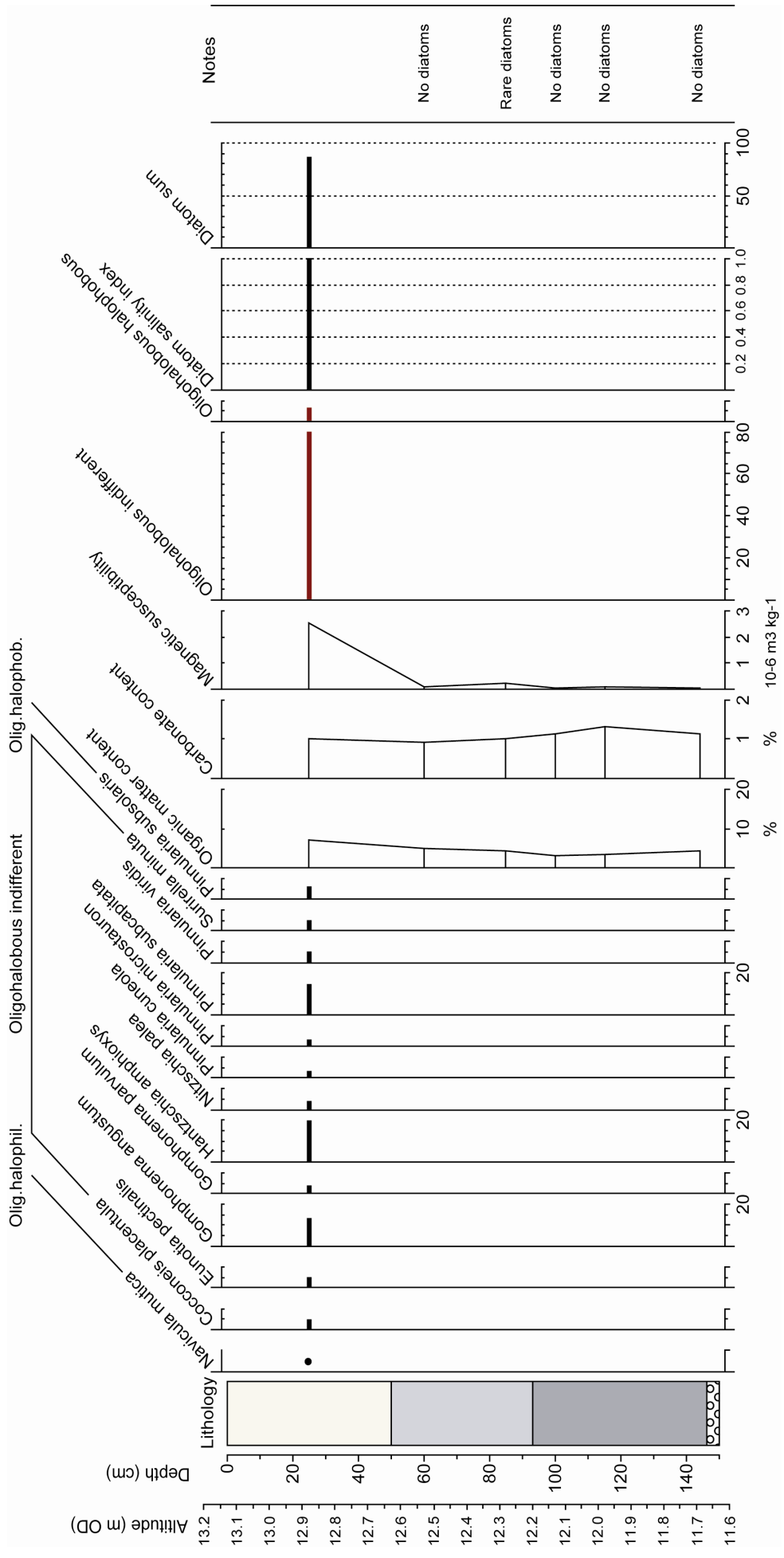


Figure 6.28 Diatom diagram for UH2 core (>3% TDV spp.). Organic matter content, carbonate content, X_p and Diatom Salinity Index is also shown.

6.4.5 Brackish groundwater intrusion in the Umberleigh House reach

HS1

The HS1 palaeochannel core is located in the modern Riv 4(i) zone (0.94-0.96 DSI) and has been dated at 700 +/-160 cal.yr.AD. However, the HS1 DSI values of 0.97 to 1.00 are typical of the less saline Riv 4(ii) zone (0.98 DSI) which is located 1.8 km upstream of the HS1 site (at R17), suggesting that river discharge was higher during the 7th or 8th Century AD with the salinity front located further downstream. However, the less saline environment in the 7th/8th Century could also be a result of lower RSL at this time with tidal head located further down-river.

HS2

HS2 is located in the modern Riv 4(i) zone (0.94-0.96 DSI) and has been dated at 1469-1627 cal.yr.AD (1 σ age). However, as in HS1, the HS2 DSI values of 0.97 to 0.99 are typical of the less saline Riv 4(ii) zone (0.98 DSI) which is located 1.8 km upstream of the HS2 site (at R17), suggesting that river discharge was higher in the 16th Century AD. Given the relatively young age of this deposit, the case for post 16th Century sea-level rise being a contributing factor in salinity gradient location is less credible.

UH2

In the UH2 core in transect I, a DSI of 0.995 places the almost pure freshwater assemblage either in the modern Riv 4(ii) zone (0.98 DSI), which is located within a few hundred metres of the UH2 site, or at an un-sampled location upstream of the Riv 4(ii) sampling station. However, the only countable sample was from the top of the core and the peak in DSI values in previous palaeochannel cores is often located lower down an abandoned channel sequence, so values may have been slightly higher if counts were possible in the underlying sediments. Therefore, the only tentative conclusion is that the UH2 site may be at the far limits of possible brackish water intrusion. This core was not dated.

As with other reaches, the conclusions drawn about relative palaeo-discharges can only be seen as very tentative as the inferences are based on very small differences in DSI between the contemporary and fossil core assemblages.

7 RESULTS SYNTHESIS: STRATIGRAPHY, CHANNEL CHANGE HISTORY, RELATIVE SEA-LEVEL CHANGE AND PALAEO-SALINITY CHANGE

7.1 STRATIGRAPHIC ARCHITECTURE

The litho-stratigraphy of core transects A to I have been divided into 13 stratigraphic units. These were based on the geochronology of the deposits (determined through radiocarbon and OSL dating), the FSUs presented in chapter 5, the geomorphology and terrace sequence, and the sedimentary and litho-stratigraphic characteristics. Figure 7.1 presents a legend for the stratigraphic sections to follow, and gives the age bracket for each unit, the relationship with the river terrace sequence, and the unit codes S1 to S13 (S1 being the oldest). It also correlates the age of these units with the main chronostratigraphic Holocene periods, with archaeological periods, with periods of known Holocene climate change (UK), and with the Blytt-Sernander model of European climatic history. Figure 7.2 indicates the occurrence of stratigraphic units in each transect, and correlates the FSUs (which are transect specific) into the overall stratigraphic framework of the inner estuary (transects A to D). Figure 7.3 shows the distribution of late Holocene radiocarbon and OSL dates. The calibrated age of each sample was plotted as a 2σ range and as a probability distribution using the program OxCal (Bronk-Ramsey, 2001). Samples are placed in date-order and their position in the stratigraphy is indicated. This new stratigraphic architecture for the lower Taw valley is presented in figures 7.4 to 7.6 and illustrates how the sedimentary units of the fluvial zone are now correlated with the sedimentary fill of the inner Taw Estuary.

The two OSL samples suspected to have undergone partial bleaching (C1 and F3) are not shown in figure 7.3. In date C1 (1100 +/-120 yrs cal.yr.AD, SW1 core), a radiocarbon date on wood from the same sand layer gave an age of 1257-1401 cal.yr.AD. This suggests a possible 200 yr over estimation of age in the OSL date. However, the gap between the 2σ age ranges is much less at only 37 yrs. In date F3 (1320 +/- 360 cal.yr.BC, CT1 core), the OSL dated sand layer was above a finer grained fluvial unit that was radiocarbon dated at 762-414 cal.yr.BC. It is thought that the overestimate on the OSL age may be 700-1000 yrs. However, because of the large uncertainty attached to both the OSL and radiocarbon age, the gap between the 2σ age

River Terrace	Strat. Unit	Age (Cal.yr.AD/BC)	Holocene & Late-glacial periods	Archaeology	Climate	Blytt-Sernander
F	S13	1900-2000 AD	Late Holocene	Modern	Little Ice Age (LIA)	Sub-atlantic
	S12	1800-1900 AD		Late & Post-Medieval		
	S11	1400-1800 AD		High Medieval	MWP deterioration	
T1	S10	1170-1400 AD		Late Anglo-Saxon	Medieval Warm Period (MWP)	
	S9	1000-1170 AD				
T2	S8	800-1000 AD		Middle Anglo-Saxon	Dark Ages deterioration	
	S7	600-800 AD				
	S6	200-600 AD				
T3	S5	300 BC - 200 AD		Late Roman - Early Anglo-Saxon	Romano-British Warm Period	
	S4	1000-300 BC				
T4	S3	6000-1000 BC	Late Bronze Age - Early Iron Age	LBA-EIA deterioration		
	S2	9500-6000 BC				
T5	S2-S4	9500-300 BC	Late Mesolithic, Neolithic, Early/Middle BA	Climatic Optimum (7000-3500 BC)		
	S1	11500-9500 BC			Pre-boreal & Boreal	
		Late-glacial (Allerod/Younger Dryas)				Late Upper Palaeolithic

Figure 7.1 Stratigraphic units for the lower Taw valley and inner Taw Estuary. The age bracket for each unit is shown. Correlations with the Taw river terrace sequence, the main chrono-stratigraphic Holocene periods, archaeological periods, periods of Holocene climate change (UK), and the Blytt-Sernander model of European climatic history are indicated.

River Terrace	Strat. Unit	Age Cal.yr.BC/AD	A	B	C	D	E	F	G	H	I
F	S13	1900-2000 AD	A15,A16		C10						✓
	S12	1800-1900 AD	A14	B11	C9				✓		
	S11	1400-1800 AD	A12,A13	B10,B12	C8	D9	✓	✓	✓	✓	
T1	S10	1170-1400 AD	A11	B9	C6,C7	D8	✓		✓		
	S9	1000-1170 AD		B8		D7					
	S8	800-1000 AD		B7	C5	D6					
T2	S7	600-800 AD	A10		C3,C4	D3,D4,D5	✓			✓	✓
	S6	200-600 AD		B6		D2		✓			
T3	S5	300 BC - 200 AD	A9	B5				✓			
	S4	1000-300 BC	A8	B3,B4	C1,C2	D1	✓	✓			
T4	S3	6000-1000 BC	A1 - A7								✓
	S2	9500-6000 BC					✓	✓	✓	✓	
T5	S2-S4	9500-300 BC		B2							
	S1	11500-9500 BC		B1							✓

Figure 7.2 Presence of stratigraphic units in each of the nine litho-stratigraphic valley sections (transects A to I). For transects A to D, stratigraphic correlation of FSUs is indicated; for transects E to I, the presence or absence of each stratigraphic unit is indicated.

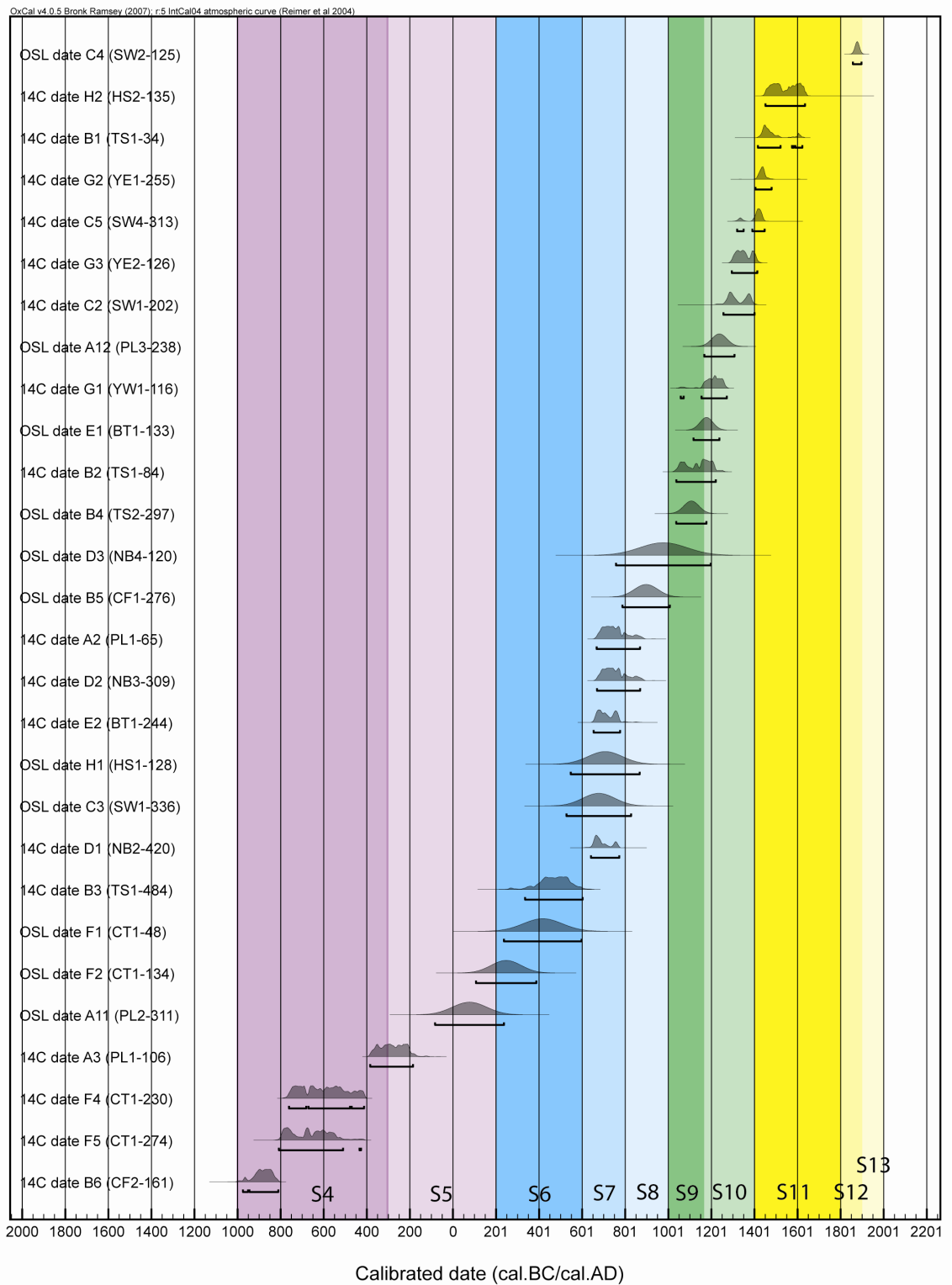


Figure 7.3 Chrono-stratigraphic distribution of late Holocene radiocarbon and OSL dates. The 2σ range for each date (cal.yr.AD/BC) is shown as a probability distribution. The correlation with the Taw stratigraphic units (S4 to S13) is indicated. Diagram based on date plot using the OxCal (v.4.0.5) program (Bronk-Ramsey, 2001).

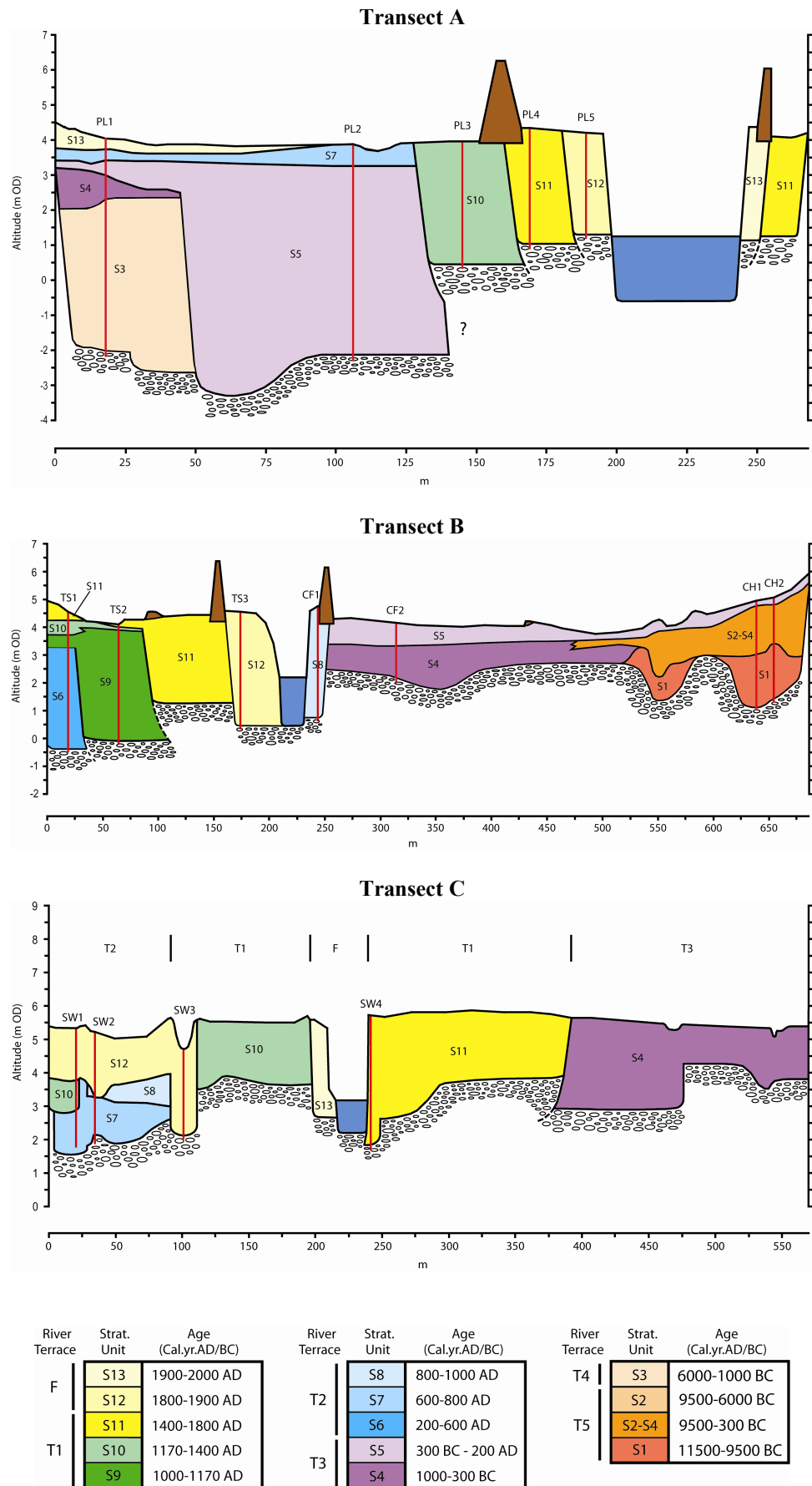
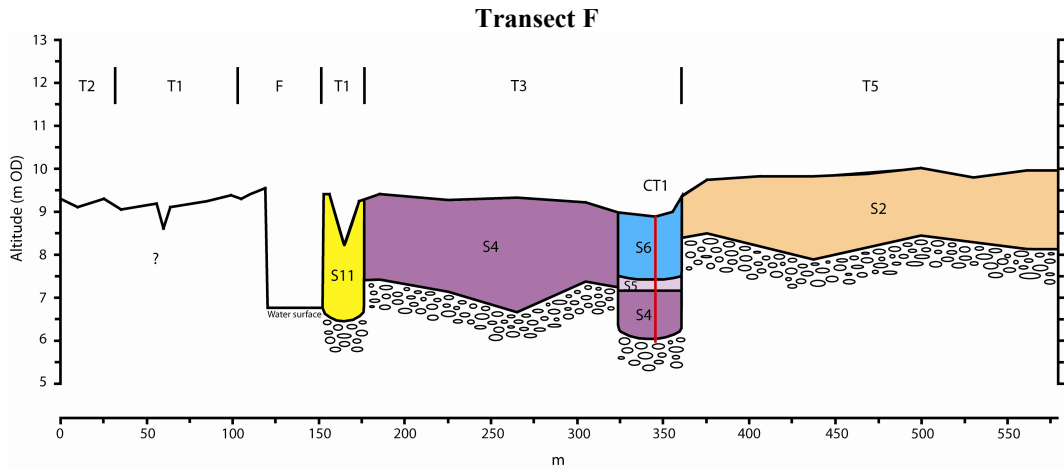
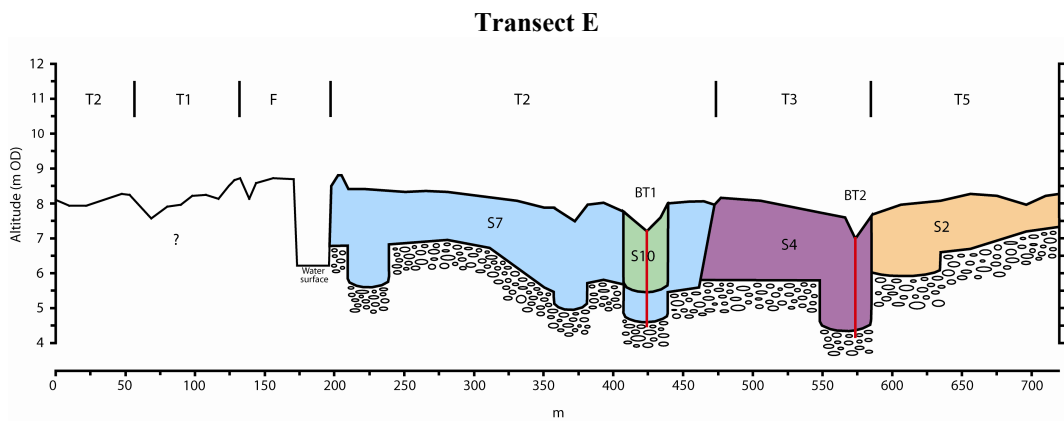
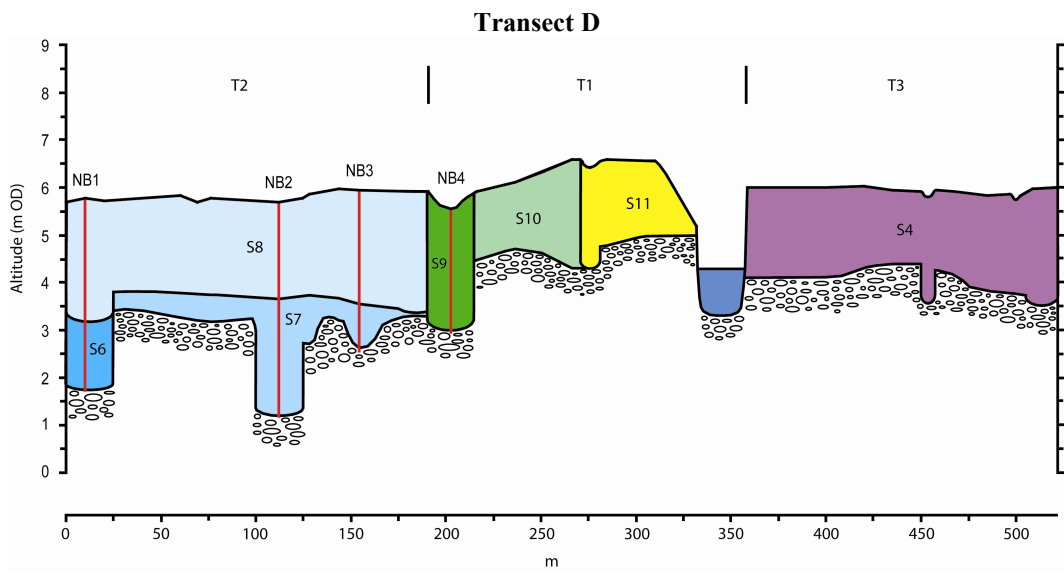
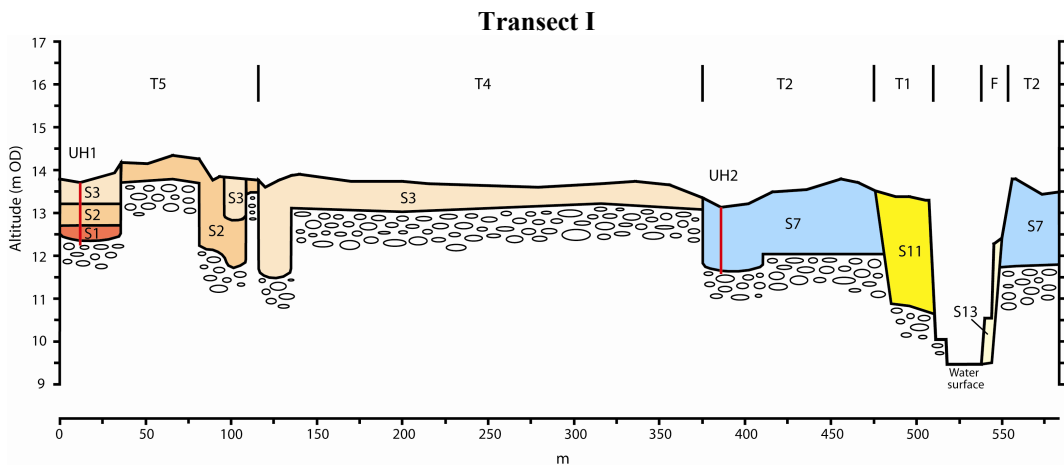
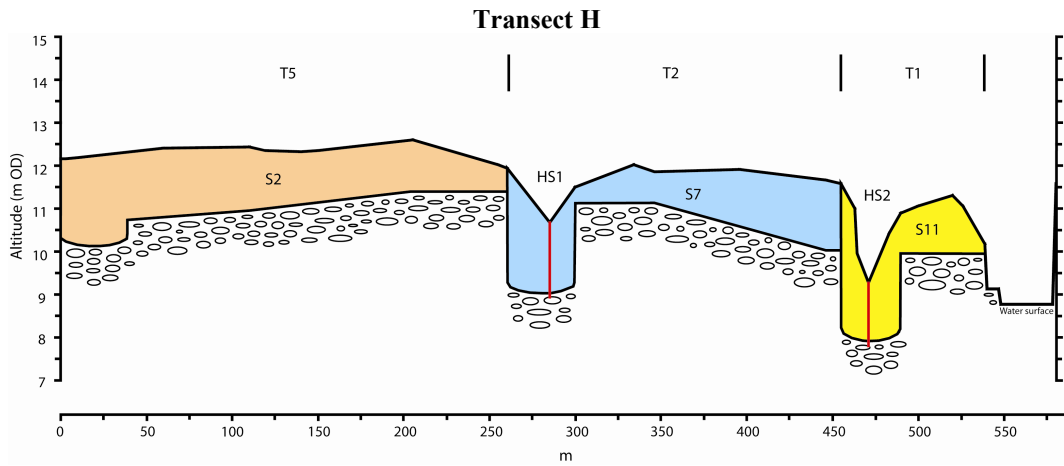
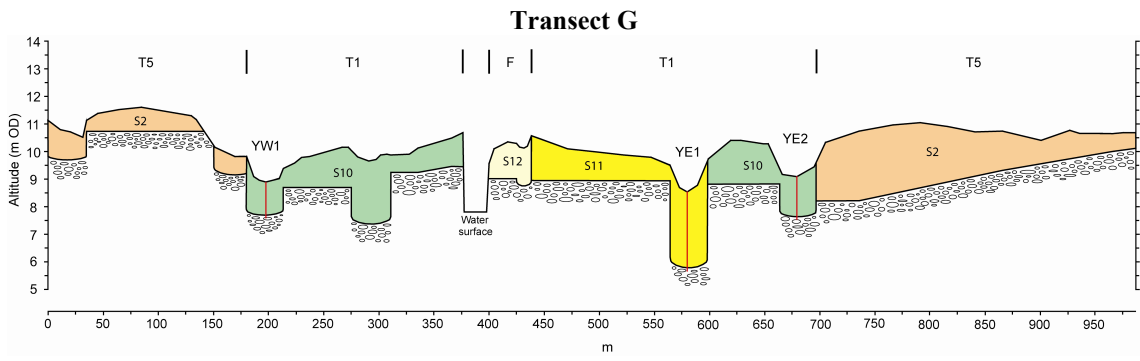


Figure 7.4 Stratigraphy of transects A, B and C. The age of each stratigraphic unit is given in the legend.



River Terrace	Strat. Unit	Age (Cal.yr.AD/BC)	River Terrace	Strat. Unit	Age (Cal.yr.AD/BC)	River Terrace	Strat. Unit	Age (Cal.yr.AD/BC)
F	S13	1900-2000 AD	T2	S8	800-1000 AD	T4	S3	6000-1000 BC
	S12	1800-1900 AD		S7	600-800 AD		S2	9500-6000 BC
	S11	1400-1800 AD		S6	200-600 AD	T5	S2-S4	9500-300 BC
T1	S10	1170-1400 AD	T3	S5	300 BC - 200 AD		S1	11500-9500 BC
	S9	1000-1170 AD		S4	1000-300 BC			

Figure 7.5 Stratigraphy of transects D, E and F. The age of each stratigraphic unit is given in the legend.



River Terrace	Strat. Unit	Age (Cal.yr.AD/BC)	River Terrace	Strat. Unit	Age (Cal.yr.AD/BC)	River Terrace	Strat. Unit	Age (Cal.yr.AD/BC)
F	S13	1900-2000 AD	T2	S8	800-1000 AD	T4	S3	6000-1000 BC
	S12	1800-1900 AD		S7	600-800 AD		S2	9500-6000 BC
	S11	1400-1800 AD		S6	200-600 AD		S2-S4	9500-300 BC
T1	S10	1170-1400 AD	T3	S5	300 BC - 200 AD	T5	S1	11500-9500 BC
	S9	1000-1170 AD		S4	1000-300 BC			

Figure 7.6 Stratigraphy of transects G, H and I. The age of each stratigraphic unit is given in the legend.

ranges is much less at only 198 yrs. Although there is some concern about the potential of partial bleaching in the other OSL dates, the majority of OSL samples are located in sedimentary units that can be correlated with radiocarbon dated units (therefore validated), usually by a combination of palaeo-environmental, sedimentary, stratigraphic and geomorphological (including river terrace division) deduction.

A brief description of each stratigraphic unit follows.

S1 (11500-9500 cal.yr.BC)

This Late glacial unit is found in transects B and I. Palaeochannel sediments at both sites are contained within relatively shallow channels (with a high width/depth ratio) and both are constrained by elevated gravel surfaces suggesting a braided river system. However, both channels also contain a fill of fine sand (largely removed by later erosion in the transect I channel), suggesting deposition in a sand-bed river. These fluvial sands have been OSL dated as late Allerød age (end of the Late glacial interstadial), indicating that sand-bed rivers were active in the Taw valley prior to the Younger Dryas stadial. They appear to have partly occupied a pre-existing braided channel network that was inherited from the Bolling (early Late glacial interstadial) or earlier Pleistocene (Devensian). A thin layer of silt and clay that overlies the abandoned Allerød channel at the transect B site is also of S1 age and is thought to represent Younger Dryas deposition.

S2-S4 (9500-300 cal.yr.BC)

This unit is thought to incorporate the whole of the early and middle Holocene up to 300 cal.yr.BC and has been assigned to the spring-mire peat in transect B. This peat has not been dated but is thought to represent continual organic accumulation since the early Holocene, during which time it was largely vegetated by alder. A similar spring-mire peat was described by Fyfe (2000) in the lower Exe valley.

S2 (9500-6000 cal.yr.BC)

S2 is represented by T5 deposits of relatively fine grained vertically accreted floodplain alluvium and palaeochannels with fine grained (clay/silt) fills. These sediments were deposited in an anastomosing river system (seen in the geomorphology) during the early Holocene.

S3 (6000-1000 cal.yr.BC)

This middle Holocene unit is only located in transects A and I. In transect A, much of the sequence of intercalated PL1 peats and silts is of this age. In transect I, the T4 deposits have been assigned an S3 age (though they were not dated), and consist of a thin layer of fine grained floodplain alluvium and a low sinuosity palaeochannel with a relatively small bankfull volume.

S4 (1000-300 cal.yr.BC)

This unit represents a phase of significant floodplain formation in transects B, C, D, E and F. In transect A, the more organic phase of peat IV accumulation at the top of the PL1 core is included in this unit, and in transect B, additional wetland deposition occurs on top of an elevated, possibly Late glacial, gravel surface. In transects C and D, S4 deposits consist of vertically accreted fine-grained floodplain alluvium with clay plugs infilling narrow palaeochannels (possibly anastomosed). In transects E and F, S4 floodplain deposits are more sandy, with larger palaeochannels and evidence of channel (and point bar) lateral migration.

S5 (300 cal.yr.BC – 200 cal.yr.AD)

S5 is also relatively rare in the fluvio-estuarine and fluvial stratigraphy, with the only possible example being the formation of a diatomite deposit in the CT1 palaeochannel fill. This may be of an older S4 age. In the estuarine transects A and B however, S5 is an important part of the stratigraphy. In transect B, it is represented by fine grained brackish floodplain/marsh deposition at FSU B5, and by silty peat deposition on the elevated spring mire top. In transect A, S5 is represented by a thick unit of estuarine channel sand that was deposited during a phase of marine incision.

S6 (200-600 cal.yr.AD)

This unit is relatively rare in the fluvio-estuarine and fluvial stratigraphy (transects C to I), with the only example being a flood channel deposit, located in the previously abandoned CT1 channel. In the estuarine transect B, the abandoned tidal channel at TS1 is dated as S6 age.

S7 (600-800 cal.yr.AD)

S7 is relatively common in the stratigraphy. In transects C and D, this unit contains fluvio-estuarine abandoned channel and associated channel bar complexes. In transects

E, H and I, S7 represents large areas of T2 deposition, instigated through channel meander migration and lateral accretion of sandy bar top sequences, with many examples of abandoned channel fills.

S8 (800-1000 cal.yr.AD)

S8 is found in transects B, C, and D and contains both units of floodplain vertical accretion (transect D) and estuarine channel migration (transect B).

S9 (1000-1170 cal.yr.AD)

S9 is relatively rare in the stratigraphy, being only found in transects B and D. It is not represented in the non-tidal fluvial reach, but in the estuarine transect B, and represents significant estuarine channel migration.

S10 (1170-1400 cal.yr.AD)

S10 is also relatively ubiquitous in the stratigraphy, and represents another phase of significant channel migration, with significant channel aggradation seen in transects A, C and D. Deposits are dominated by lateral accretion of point bar sequences, and in transect E a localised phase of channel braiding is evident. In transect C, S10 includes the storm surge deposit that occurred at *c.*1300 cal.yr.AD. In transect B, this period includes a phase of peat formation and progradation, with alder carr developing on the valley side.

S11 (1400-1800 cal.yr.AD)

S11 is widespread in the stratigraphy, and is found in all transects apart from E. In the inner estuary, it represents a prolonged phase of channel migration, floodplain reworking and aggradation, with deposition of coarse grained estuarine and fluvial sediment. In transect C, it includes flood channel/scour deposits beneath SW2. In the fluvial transects G, H, and I, S11 sediments also consist of relatively coarse grained lateral accretion deposits, having been deposited during channel migration.

S12 (1800-1900 cal.yr.AD)

S12 is found in transects A, B, C and G. In transects A and B it is composed of shelly channel sands, deposited during lateral migration of tidal meanders, overlain by

vertically accreted marsh sediment. In transect G, it includes a relatively recent laterally accreted point bar sequence.

S13 (1900-2000 cal.yr.AD)

This is the youngest unit and represents the most recent floodplain deposition. It is found in transects A, C and I where it usually represents relatively coarse grained lateral accretion deposits from recent meander migration. In transect A, it also represents surface marsh accumulation in the west of the transect.

7.2 LATE HOLOCENE PERIODS OF FLUVIAL FLOODING AND CHANNEL CHANGE

Figure 7.7 shows the late Holocene flood record for the Taw valley, based on dated channel abandonment (by avulsion or cut-off) and channel re-occupation events since 1000 cal.yr.BC. This shows that channel change events, related to major floods, are clustered in two principal periods. The first was between 600 and 800 AD and correlates with stratigraphic unit S7. The second was a prolonged period of geomorphic instability between 1000 and 1600 AD and correlates with stratigraphic units S9-S11. A peak in this cluster lies between 1200 and 1500 cal.yr.AD and correlates with stratigraphic unit S10 and the start of S11.

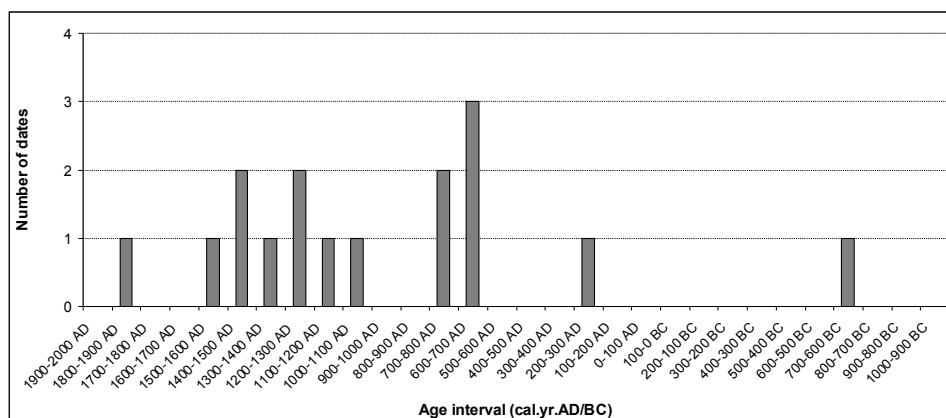


Figure 7.7 Late Holocene flood record for the Taw valley, based on dated channel abandonment and flood channel re-occupation events since 1000 cal.yr.BC.

7.3 RELATIVE SEA-LEVEL CHANGE IN THE TAW ESTUARY DURING THE MID-LATE HOLOCENE

Holocene RSL changes in the Taw Estuary were reconstructed using the traditional qualitative litho-stratigraphic approach (Shennan, 1982, 1986; Tooley, 1982; Shennan *et al.*, 1983). Diatom bio-stratigraphy (chapter 5) provided confirmation of changes in marine influence at transgressive and regressive overlaps (Shennan, 1982; Tooley, 1982; Palmer and Abbott, 1986; Vos and de Wolf, 1988). The biostratigraphy was interpreted qualitatively for evidence of changes in the location of the palaeo-marsh surface in the tidal frame. This interpretation was partly based on a local contemporary analogue of diatom distribution, located in the middle Taw Estuary (chapter 4), and partly based on previous studies that have investigated the relationship between diatom distribution and elevation in the tidal frame (UK examples used include: Shennan *et al.*, 1995; Zong, 1997; Zong and Horton, 1998, 1999; Gehrels *et al.*, 2001; Hill *et al.*, 2007). A series of eleven SLIPs were validated at transgressive or regressive overlaps in the PL1 (transect A) and TS1 (transect B) core stratigraphy, with each SLIP having an age, altitude and indicative meaning (details of each SLIP are given in table 7.1). As outlined in chapter 3.6, the indicative meaning is the height of deposition of the sample on the palaeo-marsh surface relative to a reference tide level (Van de Plassche, 1977, 1986; Shennan, 1986; Gehrels 1999). The reference tide level used in this study is MHWST, which is 4.70m OD at Barnstaple (Admiralty Tide Tables, 2008). The indicative meanings of overlap types encountered in the PL1 and TS1 stratigraphy are shown in table 7.2. These are adapted from the indicative meanings shown in table 3.4, which are from Shennan (1982, 1986), with the indicative meaning of the transgressive monocot peat – saltmarsh silt boundary taken from the modern analogue found in the middle Taw Estuary (*i.e.* MHWST – 0.27m). Table 7.1 gives both the vertical position of each SLIP, relative to modern MHWST (calculated using eq.3.2 in chapter 3.6), and the altitude of each slip in ‘m OD’.

The errors associated with determining elevation and indicative meaning for each SLIP are given in table 7.3. The stratigraphic investigation of autocompaction at the PL1 site was inconclusive; with the relatively flat upper surfaces to the peat layers (figure 5.5) suggesting minimal compaction has taken place in the sediments. However, unlike the relatively gentle basement slope seen by Haslett *et al.* (1998) at their Nyland Hill site in Somerset, the basement slopes very steeply at the edge of transect A, dropping 6.5m in

Sample	Dated material	Age cal.yr.BP (2 σ)	Ref. tide MHWST (m OD)	H (m MHWST)	D (m)	I (m MHWST)	I _{range} (m)	SLIP (m MHWST)	SLIP (m OD)	Overlap	SLIP No.
TS1-34	Wood	534-328	4.70	- 0.15	0.34	= MHWST	+/- 0.20	- 0.49	4.21	Transgressive	1
TS1-84	Seed	912-729	4.70	- 0.15	0.84	+ 0.10	+/- 0.20	- 1.09	3.61	Regressive	2
PL1-65	<i>Poaceae</i>	1283-1081	4.70	- 0.65	0.65	- 0.27	+/- 0.20	- 1.03	3.67	Transgressive	3
PL1-106	<i>Phragmites</i>	2334-2135	4.70	- 0.65	1.06	- 0.27	+/- 0.20	- 1.44	3.26	Transgressive	4
PL1-250	<i>Phragmites</i>	3913-3697	4.70	- 0.65	2.50	+ 0.10	+/- 0.20	- 3.25	1.45	Regressive	5
PL1-279	Wood	4228-3975	4.70	- 0.65	2.79	- 0.27	+/- 0.20	- 3.17	1.53	Transgressive	6
PL1-358	Wood	4849-4617	4.70	- 0.65	3.58	+ 0.10	+/- 0.20	- 4.33	0.37	Regressive	7
PL1-398	Wood	5468-5086	4.70	- 0.65	3.98	- 0.27	+/- 0.20	- 4.36	0.34	Transgressive	8
PL1-422	Wood	5593-5331	4.70	- 0.65	4.22	+ 0.10	+/- 0.20	- 4.97	- 0.27	Regressive	9
PL1-557	Wood	6403-5922	4.70	- 0.65	5.57	- 0.27	+/- 0.20	- 5.95	- 1.25	Transgressive	10
PL1-594	Wood	6733-6504	4.70	- 0.65	5.94	+ 0.10	+/- 0.20	- 6.69	- 1.99	Regressive	11

Table 7.1 Sea-level index points (SLIPs) for the inner Taw Estuary. Reference tide level = MHWST (= 4.70m at Barnstaple, Admiralty tide tables, 2008); H = height of marsh surface at core site relative to MHWST; D = Depth of dated sample in the core; I = indicative meaning, relative to MHWST (see text); I_{range} = indicative range; SLIP (m MHWST) = H - D - I

Stratigraphic boundary	Overlap type	Indicative meaning	Indicative range
<i>Phragmites</i> /monocot peat above saltmarsh silt	Regressive	MHWST + 0.10 m	+/- 0.20 m
<i>Phragmites</i> /monocot peat below saltmarsh silt	Transgressive	MHWST – 0.27 m	+/- 0.20 m
Fen-wood peat below Saltmarsh silt	Transgressive	MHWST	+/- 0.20 m

Table 7.2 Indicative meaning and indicative range of SLIP overlaps encountered in Taw Estuary stratigraphy (adapted from table 3.4, with indicative meaning of transgressive monocot peat – saltmarsh silt transition taken from modern analogue in middle Taw Estuary).

Source of error	Estimated error (m)
Identification of boundary	+/- 0.01
Measurement of depth	+/- 0.01
Angle of borehole	+/- 0.02
GPS survey	+/- 0.02
Accuracy of benchmark to OD	+/- 0.10
Indicative range (for all SLIPS in this study)	+/- 0.20
Total altitudinal error (total error = $\sqrt{a^2 + b^2 + c^2 \dots}$)	+/- 0.23

Table 7.3 Errors associated with determining altitude and indicative meaning of SLIPS in this study

only 7m. It then becomes relatively flat beneath the rest of the Holocene deposits, so if any compaction has occurred, it will be difficult to see using the method of Haslett *et al.* (1998). No compaction error has therefore been applied to the elevation of the SLIPs. Nine SLIPs were located in the PL1 core, with the oldest being dated at 6733-6504 cal.yr.BP and the youngest dated at 1283-1081 cal.yr.BP. Two more SLIPs were located in the TS1 core, with ages of 912-729 cal.yr.BP and 534-328 cal.yr.BP.

Figure 7.8 shows the reconstructed RSL curve for the Taw Estuary, with age plotted against MHWST. SLIPs are contained in error boxes associated with 2σ age uncertainty and the elevational errors given in table 7.3. An error envelope has also been applied to indicate the RSL curve for the mid-late Holocene.

Six transgressive overlaps are recorded in figure 7.8. These occur at:

6403-5922 cal.yr.BP (4342-4055 cal.yr.BC 1σ age)

5468-5086 cal.yr.BP (3498-3353 cal.yr.BC 1σ age)

4228-3975 cal.yr.BP (2199-2043 cal.yr.BC 1 σ age)

2334-2135 cal.yr.BP (360-206 cal.yr.BC 1 σ age)

1283-1081 cal.yr.BP (684-777 cal.yr.AD 1 σ age)

534-328 cal.yr.BP (1433-1485 cal.yr.AD 1 σ age)

Five regressive overlaps are recorded in figures 7.8. These occur at:

6733-6504 cal.yr.BP (4726-4611 cal.yr.BC 1 σ age)

5593-5331 cal.yr.BP (3636-3525 cal.yr.BC 1 σ age)

4849-4617 cal.yr.BP (2890-2702 cal.yr.BC 1 σ age)

3913-3697 cal.yr.BP (1927-1776 cal.yr.BC 1 σ age)

912-729 cal.yr.BP (1051-1213 cal.yr.AD 1 σ age)

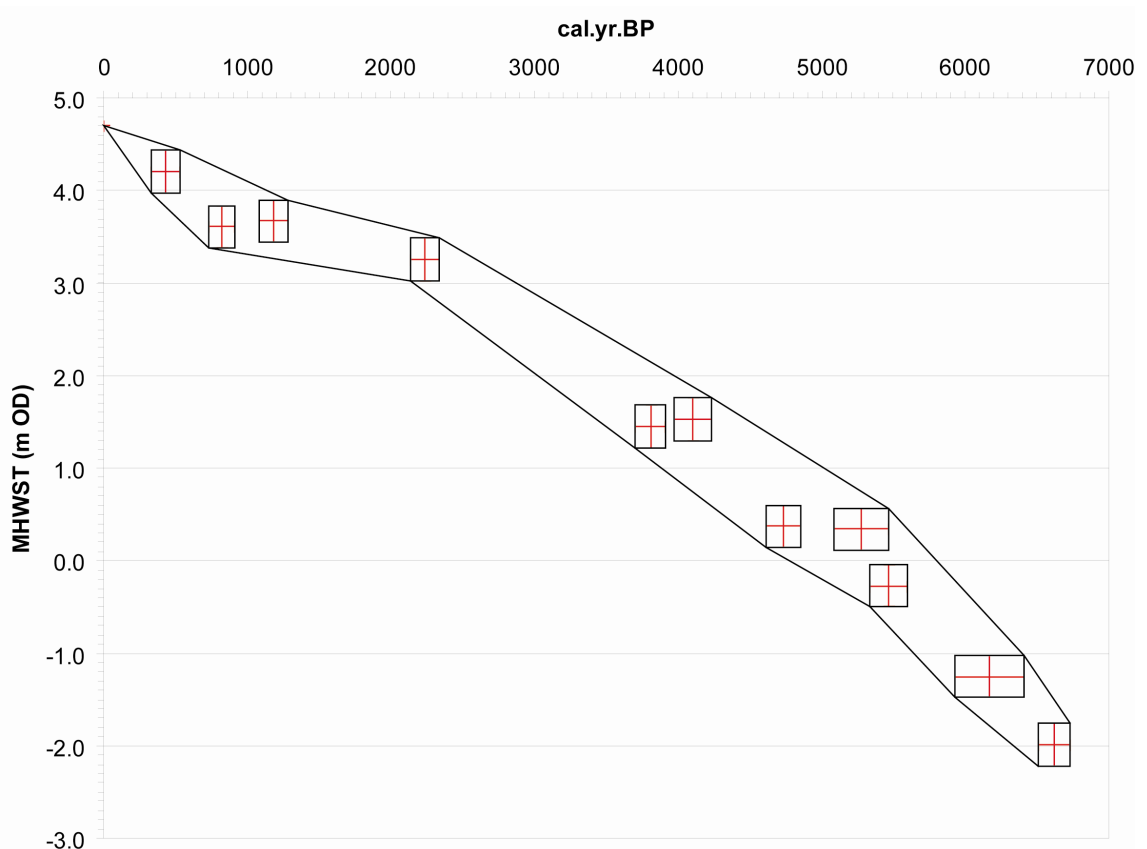


Figure 7.8 Relative sea-level curve for the Taw Estuary showing changes in the altitude of MHWST. Error boxes are indicated for each SLIP.

The RSL curve for the Taw Estuary (figure 7.8) indicates MHWST has risen 6.69m since 6733-6504 cal.yr.BP. This figure also indicates a progressive slowing down in the rate of RSL rise over the last 6500 years, with the most significant falls in the rate of

rise occurring at 5593-5331 cal.yr.BP and 2334-2135 cal.yr.BP. Between 6733-6504 and 5593-5331 cal.yr.BP, the mean rate of RSL rise was 1.49 mm yr⁻¹. Between 5593-5331 and 2334-2135 cal.yr.BP, the mean rate of RSL rise was 1.09 mm yr⁻¹. Since 2334-2135 cal.yr.BP, the mean rate of RSL rise has been 0.64 mm yr⁻¹.

7.4 ESTUARINE PALAEO-SALINITY CHANGE DURING THE LATE HOLOCENE

Late Holocene palaeosalinity change was reconstructed for the inner Taw Estuary using DSI as a proxy for salinity (Bryne *et al.*, 2001). Samples were chosen from the biostratigraphy of dated cores located in transects A, B and C. In transect D, after evaluation of the core diatom assemblages, it was decided that these could not be used in the palaeosalinity reconstruction. This was because all assemblages in this transect are freshwater dominated with only very minor contributions by brackish and marine taxa. This was due to proximity to the palaeo-salinity front. The dominance by freshwater taxa in these assemblages led to designations of former tidal frame position being somewhat problematical using qualitative methods. The DSI records from transect D were therefore not used in the estuarine palaeosalinity reconstruction. As explained earlier, three palaeo-elevation zones within the tidal frame were to be analysed separately in the core records, in order for salinity to be the main control on differences in assemblage composition, and therefore DSI. The tidal frame sub-environments used for inter-core comparisons and palaeosalinity reconstruction were lower high saltmarsh, mid saltmarsh and upper sandflat (or unvegetated estuarine channel deposits). Each of these environments relate to specific durations and frequency of tidal submergence. The modern elevations of these zones were identified in chapter 4 (figure 4.9), with each one showing relatively little internal variation in DSI. In chapter 5, these three elevational zones were identified in the core stratigraphy of the inner estuary, with diatom assemblages relating to each of the environments selected for use in the analysis. This resulted in 7-11 samples in each of the transects A, B and C that could be used in spatial and temporal comparisons of salinity (DSI). Three contemporary samples, taken adjacent to each transect during the river survey (chapter 4), were also used for their DSI values.

The details relating to each of these samples is given in table 7.4. For each sample, details of sample number, location, DSI and age are given, and the diatom inferred palaeo-elevation (tidal frame zone) is indicated. Uncertainties are attached to each DSI value, and are derived from the contemporary DSI range seen in each tidal frame zone (figure 4.9). Age uncertainties are attached to each sample, and are derived from the 1σ age (cal.yr.AD/BC) of a dated 'control' radiocarbon/OSL sample. The dated control sample is usually located below the DSI sample in the core stratigraphy (as the bases of cores were usually dated), but can also be located above the DSI sample. The age of each DSI sample horizon was therefore estimated from its position above (or below) a radiocarbon/OSL date. This was based on the marsh accretion curves of Pethick (1981) and French (1993). As a general rule, if the dated sample was within a unit of estuarine channel/tidal flat sediment, the time taken for accretion to a mid saltmarsh elevation would be 100-150 yrs, and from a tidal flat to a high saltmarsh elevation would be 200-250 yrs. Accretion from a mid to a high saltmarsh was taken as *c.*70 yrs. Details of the relationship between the dated horizon and the DSI sample horizon are given in the right-hand column of table 7.4, with an indication of the age difference. Some samples were dated by their vertical accretion relationship with a transgressive or regressive overlap, that was not dated in that core, but could be correlated with a dated overlap in another core (DSI samples 8, 9 and 13; table 7.4). All overlaps used in core correlations were validated for changes in marine influence. DSI samples 9 and 13 were taken from the TS1 core and were related to the overlap above the thin peat at *c.*1.3 m, that was correlated with the dated 684-777 cal.yr.AD (1σ age) transgressive overlap in the PL1 core. This correlation was supported by the age relationship of the thin peat to the basal TS1 date and the dated sample at the base of the upper TS1 peat. For DSI sample 8, the overlap at the top of the thin peat in the CF2 core was correlated with the 360-206

Table 7.4 (Next page) Samples used in palaeosalinity reconstruction. For each sample, details of sample number, location, DSI and age are given, and the diatom inferred palaeo-elevation (tidal frame zone) is indicated. Uncertainties are attached to each DSI value, and are derived from the contemporary DSI range seen in each tidal frame zone (figure 4.9). Age uncertainties are attached to each sample, and are derived from the 1σ age (cal.yr.AD/BC) of the control radiocarbon/OSL sample (see text). Control date codes (e.g. A3) are those listed in tables 5.1 and 5.2. The relationship between the control date age and the estimated DSI sample age is given (see text). Abbreviations used: HSM = high saltmarsh; MSM = mid saltmarsh; Upr Sandflat = upper sandflat; Ch = tidal channel; Flood Ch = overbank flood channel; correl. = correlation.

DSI sample no.	Transect	Sample	Core diatom zone	Sample altitude (m OD)	DSI	DSI uncertainty (+/-)	Palaeo-tidal frame zone	Modern zone altitude (m OD)	14C/OSL control date	Control date 1 σ median age (cal.yr.)	Age uncertainty (1 σ +/- yr)	DSI spl. age (cal.yr.)	Control date - DSI sample relationship
1	A	PL1-102	N	3.03	0.53	0.07	Lwr HSM	4.02-4.34	A3	283 BC	77	183 BC	MHWST-HSM, 100yr
2	A	PL1-54	O	3.51	0.69	0.07	Lwr HSM	4.02-4.34	A2	730 AD	46	770 AD	MHWST-HSM, 40yr
3	A	PL2-40	B	3.47	0.46	0.07	Lwr HSM	4.02-4.34	A2	730 AD	46	830 AD	Overlap correl., 100yr
4	A	PL2-75	B	3.12	0.41	0.05	MSM	3.60-4.02	A2	730 AD	46	630 AD	Overlap correl., 100yr
5	A	PL3-80	B	3.17	0.24	0.05	MSM	3.60-4.02	A12	1230 AD	35	1380 AD	Ch-MSM, 150yr
6	A	PL2-220	A(ii)	1.67	0.14	0.05	Upr Sandflat	0.90-2.25	A11	70 AD	80	90 AD	Ch-Ch, 20yr
7	A	PL3-263	A	1.34	0.11	0.05	Upr Sandflat	0.90-2.25	A12	1230 AD	35	1230 AD	Ch-Ch, 0yr
8	B	CF2-57	B(i)	3.58	0.49	0.07	Lwr HSM	4.02-4.34	A3	283 BC	77	17 AD	Overlap correl., 300yr
9	B	TS1-132	C(i)	3.23	0.56	0.07	Lwr HSM	4.02-4.34	A2	730 AD	46	720 AD	Overlap correl., -10yr
10	B	TS1-90	D(i)	3.65	0.51	0.07	Lwr HSM	4.02-4.34	B4	1100 AD	35	1100 AD	Core correl., 0yr
11	B	TS2-30	B	3.81	0.69	0.07	Lwr HSM	4.02-4.34	B4	1100 AD	35	1300 AD	Ch-HSM, 200yr
12	B	TS1-28	E	4.27	0.60	0.07	Lwr HSM	4.02-4.34	B1	1459	26	1469 AD	MHWST-HSM, 10yr
13	B	TS1-120	C(ii)	3.35	0.25	0.05	MSM	3.60-4.02	A2	730 AD	46	800 AD	Overlap correl., 70yr
14	B	CF1-160	A(ii)	3.10	0.57	0.05	MSM	3.60-4.02	B5	890 AD	55	990 AD	Ch-MSM, 100yr
15	B	TS2-65	A(ii)	3.46	0.31	0.05	MSM	3.60-4.02	B4	1100 AD	35	1200 AD	Ch-MSM, 100yr
16	B	TS1-466	A	-0.11	0.22	0.05	Upr Sandflat	0.90-2.25	B3	477 AD	62	477 AD	Ch-Ch, 0yr
17	B	CF1-360	A(i)	1.10	0.48	0.05	Upr Sandflat	0.90-2.25	B5	890 AD	55	870 AD	Ch-Ch, -20yr
18	B	TS2-145	A(ii)	2.66	0.19	0.05	Upr Sandflat	0.90-2.25	B4	1100 AD	35	1130 AD	Ch-Ch, 30yr
19	C	SW1-156	B(ii)	3.77	0.74	0.07	Lwr HSM	4.02-4.34	C2	1330 AD	56	1350 AD	Flood Ch-HSM, 20yr
20	C	SW4-242	B(i)	3.31	0.83	0.07	Lwr HSM	4.02-4.34	C5	1420	17	1490 AD	Ch-HSM, 70yr
21	C	SW1-144	C(i)	3.89	0.95	0.07	Lwr HSM	4.02-4.34	C4	1870	10	1850 AD	Core correl., -20yr
22	C	SW2-120	B	4.01	0.90	0.07	Lwr HSM	4.02-4.34	C4	1870	10	1870 AD	HSM-HSM, 0yr
23	C	SW1-218	B(i)	3.15	0.57	0.05	MSM	3.60-4.02	C2	1330 AD	56	1330 AD	MSM-Flood Ch, 0yr
24	C	SW4-270	B(i)	3.03	0.78	0.05	MSM	3.60-4.02	C5	1420	17	1440 AD	Ch-MSM, 20yr
25	C	SW2-142	B	3.79	0.75	0.05	MSM	3.60-4.02	C4	1870	10	1850 AD	HSM-MSM, -20yr
26	C	SW1-340	A	1.93	0.33	0.05	Upr Sandflat	0.90-2.25	C3	670	75	670 AD	Ch-Ch, 0yr
27	C	SW2-302	A	2.19	0.30	0.05	Upr Sandflat	0.90-2.25	C3	670	75	670 AD	Core correl., 0yr
28	C	SW4-316	A	2.57	0.23	0.05	Upr Sandflat	0.90-2.25	C5	1420	17	1420 AD	Ch-Ch, 0yr
29	A	R3	na	4.18	0.36	0.07	Lwr HSM	4.02-4.34	na	na	na	modern	na
30	B	R5	na	3.59	0.46	0.05	MSM	3.60-4.02	na	na	na	modern	na
31	C	R8	na	4.33	0.56	0.07	Lwr HSM	4.02-4.34	na	na	na	modern	na

Table 7.4 See previous page for caption.

cal.yr.BC (1σ age) transgressive overlap in PL1. This correlation was supported by the relationship of the thin peat to the basal CF2 date. Also, the overlaps in CF1 and PL1 are at very similar current altitudes (3.3 and 3.0 m OD), and it has already been established (in chapter 4) that there is not any up-valley slope in the MHWST level. The small altitude difference may therefore relate to differential compaction between the two cores. The age of other DSI samples (samples 3, 4, 10, 21, 27) was based on more straight forward stratigraphic core correlation of an unambiguous sedimentary marker horizon with a dated horizon (which was sometimes an overlap) in an adjacent core, usually a few metres away. In transect C, some samples were located in abandoned flood channel units, e.g. DSI sample 19 in the middle of the SW1 core. The vertical accretion rules of channel to high saltmarsh do not apply here as the coarse grained flood channel base (which was dated) is already at a mid or high saltmarsh elevation, as it was created in an overbank environment. The c.10cm of high saltmarsh sedimentation that occurs above the abandonment surface of this flood channel was taken as 20 yrs. Another example of an exception to the typical rate of accretion rule stated above are

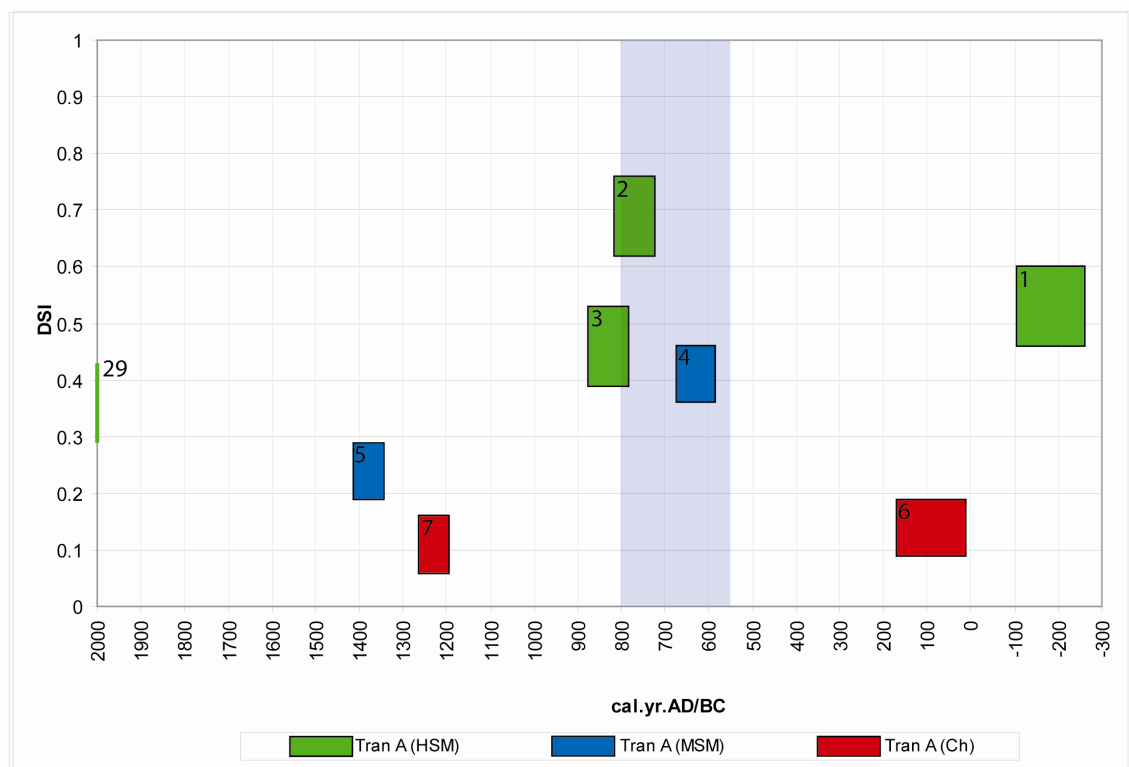


Figure 7.9 Late Holocene DSI-based palaeosalinity change in transect A. DSI trends in three separate tidal frame environments are analysed. These are the lower high saltmarsh (HSM), the mid saltmarsh (MSM); and the unvegetated tidal river channel (Ch, correlating with the upper sandflat estuary zone). High DSI indicates low salinity and periods of DSI-inferred low estuarine palaeosalinity are shaded grey. Each sample is indicated as an error box, with vertical (DSI) and horizontal (age) uncertainties given in table 7.4. Sample numbers are also indicated (table 7.4).

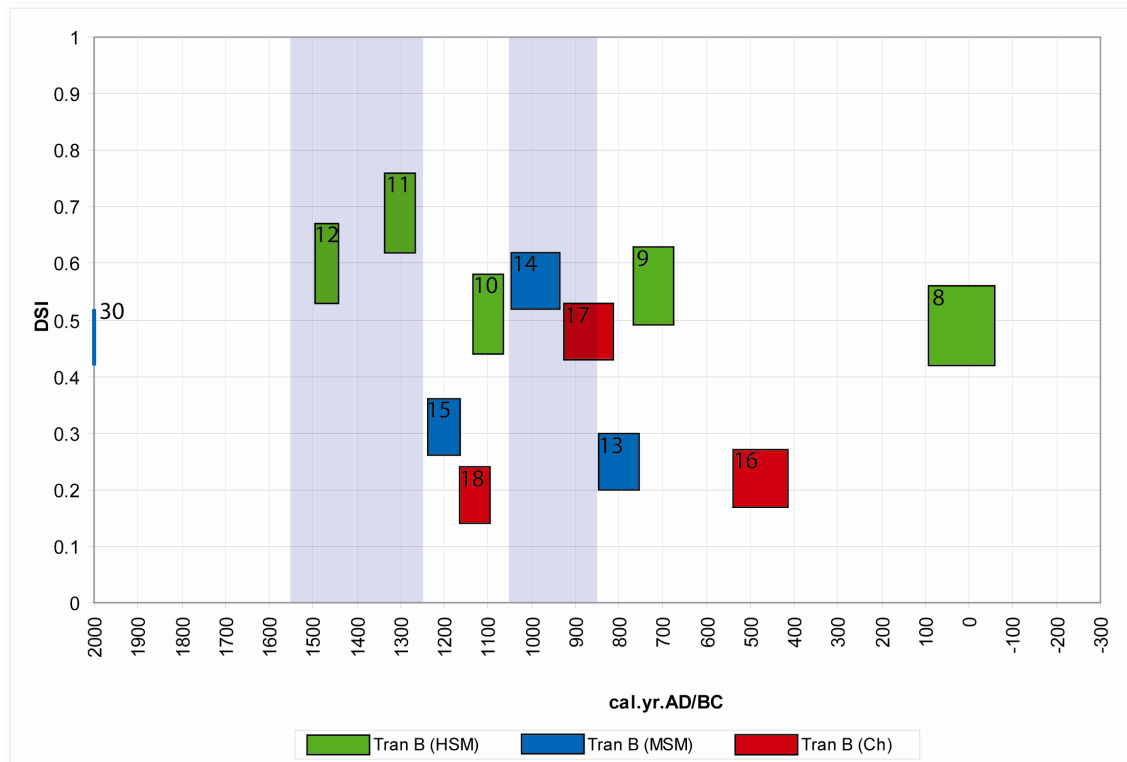


Figure 7.10 Late Holocene DSI-based palaeosalinity change in transect B. DSI trends in three separate tidal frame environments are analysed. These are the lower high saltmarsh (HSM), the mid saltmarsh (MSM); and the unvegetated tidal river channel (Ch, correlating with the upper sandflat estuary zone). High DSI indicates low salinity and periods of DSI-inferred low estuarine palaeosalinity are shaded grey. Each sample is indicated as an error box, with vertical (DSI) and horizontal (age) uncertainties given in table 7.4. Sample numbers are also indicated (table 7.4).

DSI samples 20 and 24. These are located in the SW4 core (transect C) and the dated control sample was located at the top of channel facies sediment. However, the stratigraphy suggests the unvegetated channel sediment was deposited at an elevated position on the channel bank. In the modern estuary, steep areas of channel bank are not vegetated and typical channel facies sediment can be deposited right up to the normal low-mid saltmarsh boundary (*i.e.* the pioneer and low saltmarsh are missing). This appears to be the case for the SW4 dated sample (this interpretation was aided by the palaeochannel geometry and fill visible as a section on the river bank). Therefore, the given accretion ages given in table 7.4 are typical (Pethick, 1981, French, 1993) of accretion taking place at a mid-high saltmarsh elevation.

Figures 7.9, 7.10 and 7.11 show plots of DSI against age for each of the transects A, B and C. In each transect figure, error boxes are given for samples from the three different elevation zones (*i.e.* lower high saltmarsh, mid saltmarsh and channel/tidal flat). When viewing these figures, it is important to remember that changes in DSI with age should

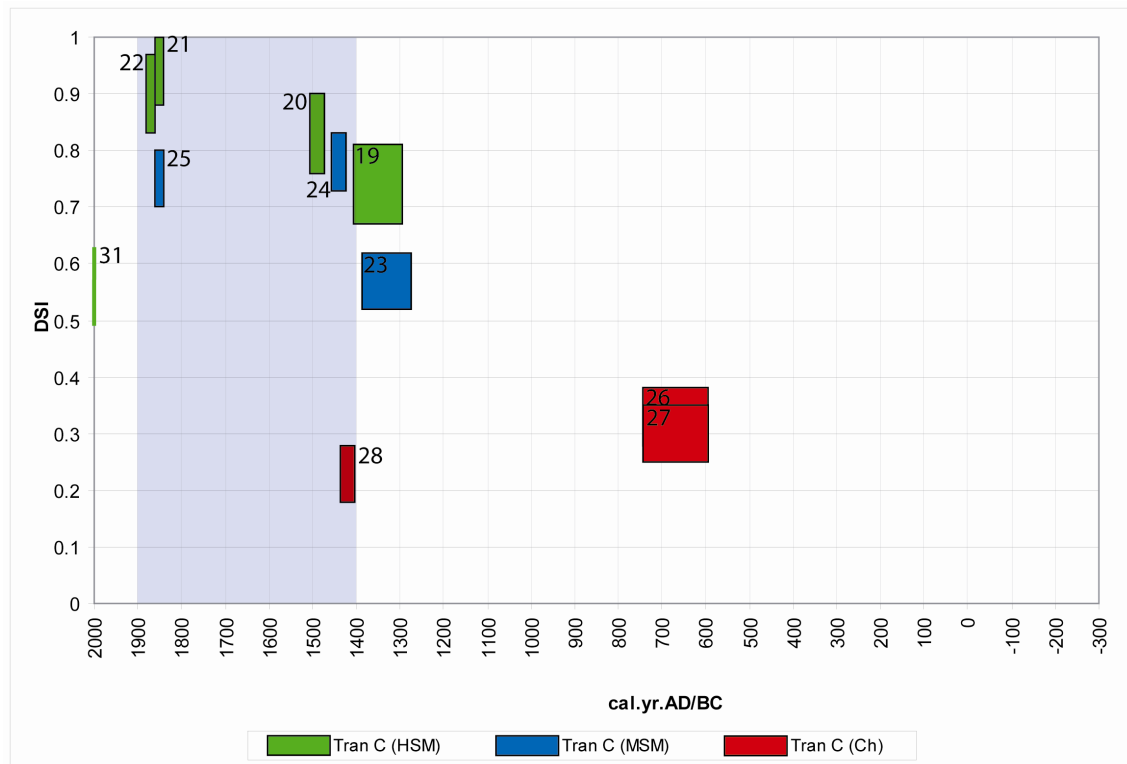


Figure 7.11 Late Holocene DSI-based palaeosalinity change in transect C. DSI trends in three separate tidal frame environments are analysed. These are the lower high saltmarsh (HSM), the mid saltmarsh (MSM); and the unvegetated tidal river channel (Ch, correlating with the upper sandflat estuary zone). High DSI indicates low salinity and periods of DSI-inferred low estuarine palaeosalinity are shaded grey. Each sample is indicated as an error box, with vertical (DSI) and horizontal (age) uncertainties given in table 7.4. Sample numbers are also indicated (table 7.4).

only be compared between samples from the same environment. It is however interesting to note that elevation does influence DSI, with a general trend of higher (fresher) DSI values between channel, mid saltmarsh and high saltmarsh samples. This immediately shows the value of first identifying, then segregating samples by elevation-related environment.

Changes in palaeosalinity in each transect can be seen by changes in DSI with time. Changes in transect A (figure 7.9) were seen to be the least useful in the interpretation. This is because some samples, such as number 6 and 7 were separated by over 1000 yrs and show very little difference in DSI. This highlights a problem that occurs several times in the age-DSI plots. When low numbers of samples are compared in a given transect, from a given environment, they have the potential to show little DSI change and therefore no context of changing palaeosalinity can be given. This is because there may have been fluctuations occurring in the *e.g.* 600 yrs between analysed samples but this is not seen. Figure 7.9 does however illustrate, in samples 2 and 3, how samples

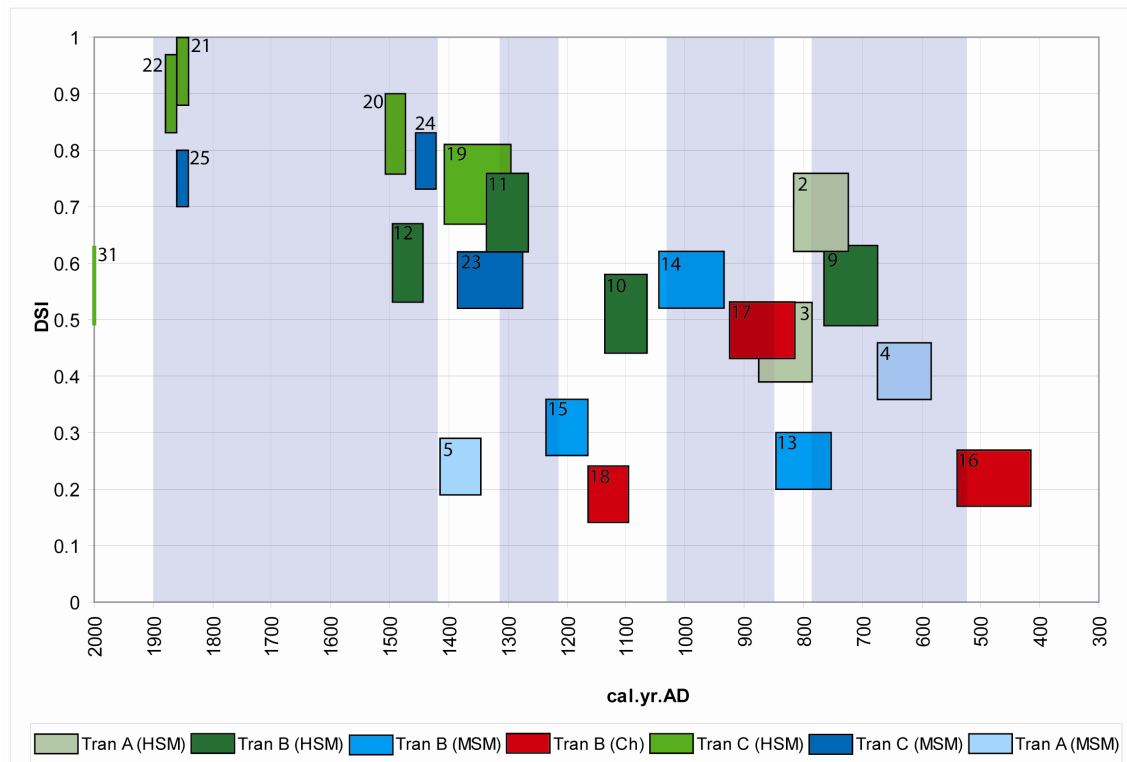


Figure 7.12 DSI-based palaeosalinity change in the Taw Estuary during the Late Holocene (transects A, B and C). DSI trends in three separate tidal frame environments are analysed. These are the lower high saltmarsh (HSM), the mid saltmarsh (MSM); and the unvegetated tidal river channel (Ch, correlating with the upper sandflat estuary zone). High DSI indicates low palaeosalinity and periods of DSI-inferred low estuarine palaeosalinity (P2, P4, P6 and P8) are shaded grey (see figure 7.13). Periods of high estuarine palaeosalinity (P1, P3, P5, P7 and P9) are unshaded. Each sample is indicated as an error box, with vertical (DSI) and horizontal (age) uncertainties given in table 7.4. Sample numbers are also indicated (table 7.4).

that are separated by smaller time intervals have a higher potential of showing centennial-scale fluctuations in palaeosalinity (DSI). Higher DSI values (*i.e.* lower salinity) are seen in the high saltmarsh and possibly mid saltmarsh data during the 7th and 8th Century AD (*c.*550-800 cal.yr.AD). A grey band highlights this identified period of below average salinity, when there was an increase in the numbers of freshwater diatom species in transect A.

The results of transects B (figure 7.10) and C (figure 7.11) have been interpreted in a similar fashion. In transect B (figure 7.10), a peak in high saltmarsh DSI values from *c.*1250-1550 cal.yr.AD is seen and a peak in estuarine channel and mid saltmarsh DSI values is seen at *c.*850-1050 cal.yr.AD. These two phases of relatively low palaeosalinity are separated by a period of higher salinity (*c.*1050 and 1250 cal.yr.AD), with low DSI values seen in the high saltmarsh, mid saltmarsh and estuarine channel data. In transect C (figure 7.11), a peak in high saltmarsh and mid saltmarsh DSI values

Palaeosalinity period	Age (cal.yr.AD/BC)	Estuarine palaeosalinity
P9	1900 – 2000 AD	High
P8	1420 – 1900 AD	Low
P7	1315 – 1420 AD	High
P6	1215 – 1315 AD	Low
P5	1030 – 1215 AD	High
P4	850 – 1030 AD	Low
P3	780 – 850 AD	High
P2	520 – 780 AD	Low
P1	300 – 520 AD	High

Figure 7.13 Late Holocene periods of high (more marine) and low (less marine) palaeosalinity in the Taw Estuary. Five periods of relatively high palaeosalinity (P1, P3, P5, P7 and P9) and four periods of relatively low palaeosalinity (P2, P4, P6 and P8) are identified since 300 AD.

at c.1400-1900 cal.yr.AD indicates a period of reduced estuarine salinity. This phase is bounded by low DSI values, suggesting above-average salinity.

Figure 7.12 shows the combined plot of transects A, B and C. Samples that had little context (*e.g.* 2 similar DSI values separated by 500 yrs or more) have been omitted. This final plot indicates four late Holocene periods after 300 cal.yr.AD when DSI values were relatively high (shaded grey), and five periods when DSI values were low (unshaded). These changes reflect alternating centennial-scale fluctuations in estuarine

palaeosalinity (Bryne *et al.*, 2001) since 300 cal.yr.AD. occurring throughout the late Holocene in the Taw Estuary. The ages of these periods are given in figure 7.13. The implications of these palaeosalinity changes, in terms of river discharge and climate, will be discussed in chapter 8.

8 DISCUSSION

8.1 MID-LATE HOLOCENE RELATIVE SEA-LEVEL CHANGE IN THE TAW ESTUARY

Figure 8.1 shows the validated SLIPs from the Taw Estuary cores (red error boxes) plotted against MSL (taken as MTL, mean tide level), with an error envelope added to show the trend of RSL rise since *c.*6600 cal.yr.BP. By referencing the SLIPs to MSL, rather than MHWST (figure 7.8), the Taw RSL curve can be compared with RSL curves from other regions. The altitude of MSL in the Taw Estuary was taken from the tide gauge predictions for Appledore, in the outer Taw Estuary, where deeper water accommodates a complete tidal range. MSL at Appledore is 0.44m OD (Admiralty Tide Tables, 2008). Existing SLIPs for the Bristol Channel, Severn Estuary and Somerset Levels are also plotted on figure 8.1. The grey SLIPs in this figure are those deemed reliable by Edwards (2006) in the sense that they all possess an indicative meaning. The blue SLIPs are the new ones identified by Edwards (2006) which had their indicative meaning's quantified using the foraminiferal transfer function for tide level established by Horton *et al.* (1999, 2000). The orange SLIPs are the ones recently established by Hill *et al.* (2007) for the Gordano valley, with indicative meanings also quantified quantitatively via a diatom-based transfer function.

None of the Taw Estuary SLIPs, or any of the other SLIPs shown in figure 8.1, have been corrected for autocompaction. This factor is known to influence reconstructions of MSL as the vertical lowering of organic-rich sediments over time will lead to an under-estimation of former MSL height and an over-estimation of the long-term rate of RSL rise (Tooley, 1978; Heyworth and Kidson, 1982; Shennan, 1986; Allen, 1996, 1999, 2000; Haslett *et al.*, 1998; Shennan *et al.*, 2000b; Edwards, 2006; Massey *et al.*, 2006). As outlined earlier, an attempt to quantify autocompaction was made with the Taw Estuary SLIPs using the stratigraphic method of Haslett *et al.* (1998), but proved inconclusive. Many studies have shown that the most reliable method for overcoming autocompaction errors is to only use SLIPs from thin basal peats as they are relatively compaction-free (*e.g.* Gehrels *et al.*, 1996; Gehrels, 1999; Donnelly *et al.*, 2004; Tornqvist *et al.*, 2004). A basal peat sequence was not found in the inner Taw Estuary so this approach could not be followed. Many of the figure 8.1 SLIPs identified in earlier studies (Godwin and Willis, 1961; Heyworth and Kidson, 1982; Housley, 1988; Smith and Morgan, 1989; Haslett *et al.*, 1998, 2001) show a large degree of scatter

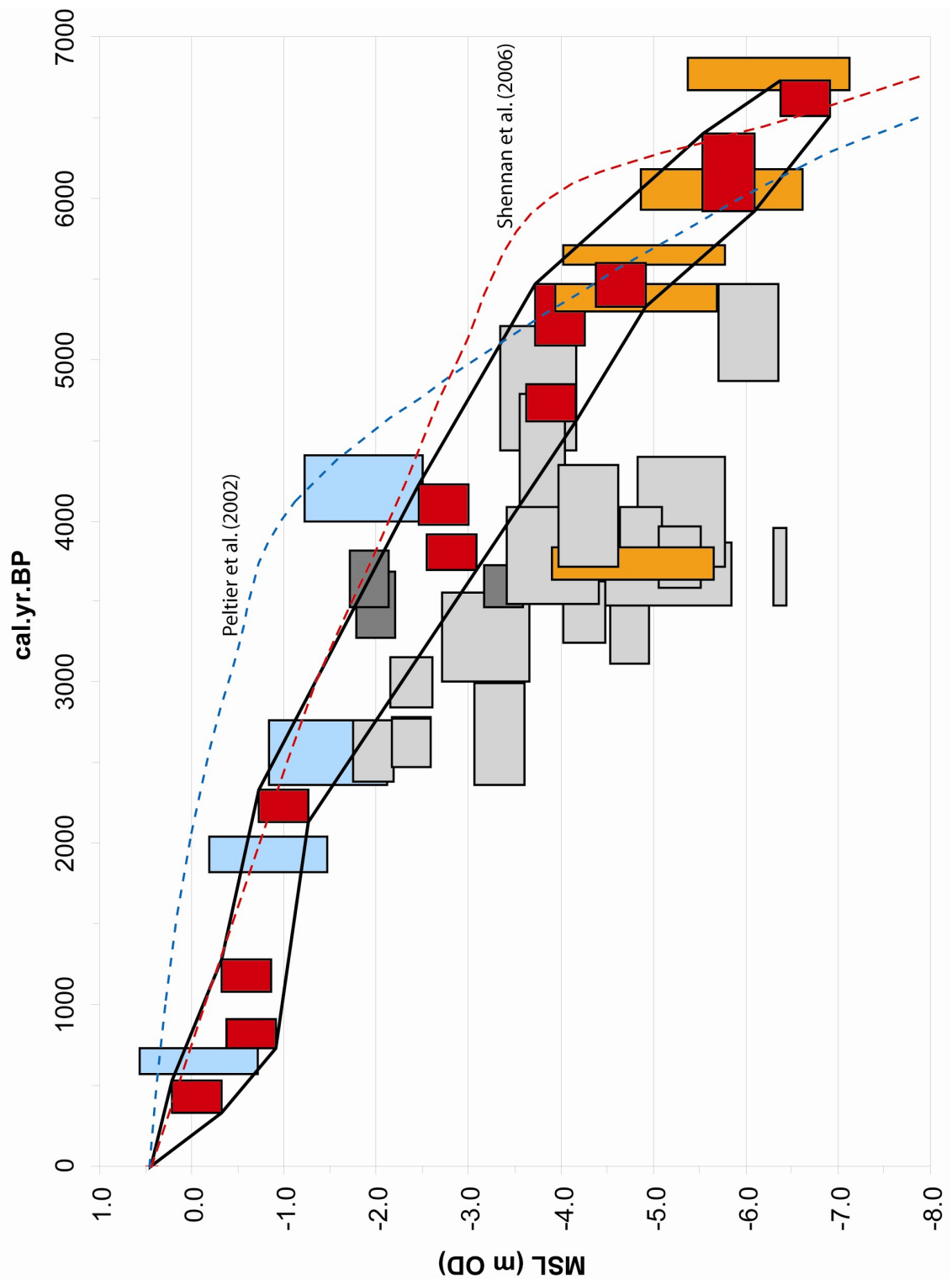


Figure 8.1 Sea-level index points for the Taw Estuary and Bristol Channel/Severn Estuary plotted against mean sea-level (MSL). Details of the SLIPs for the Bristol Channel, Severn Estuary and Somerset levels are presented in Edwards (2006). In addition, the SLIPs of Hill *et al.* (2007) have been added. None of the SLIPs have been corrected for compaction or tidal range changes. Key to colours: red = Taw Estuary (this study); blue = Edwards (2006); orange = Hill *et al.*, (2007); dark grey = Haslett *et al.* (1998) (a compaction correction was applied by this author but has not been applied in this figure); light grey = other reliable Bristol Channel/Severn Estuary SLIPs (compiled in Edwards, 2006). Also plotted are the profiles of RSL rise, as predicted by the Peltier *et al.* (2002) and Shennan *et al.* (2006) geophysical models of isostatic adjustment.

between 2500 and 5000 cal.yr.BP (and one of the Hill *et al.* (2007) SLIPs). This is thought to be partly due to variations in post-depositional sediment compaction in the organic peats common in this time period.

Variations in palaeotidal range during the Holocene can lead to an overestimation or underestimation of MSL rise. The RSL curve in figure 7.8 depicts change in MHWST through time in the Taw Estuary, based on litho-stratigraphic and bio-stratigraphic indicators of this tide level. However, if tidal range were to have increased during the mid-late Holocene, the curve of MHWST will be different from the 'true' MTL (or MSL) curve and this will have led to an overestimation of MSL rise in figure 8.1. Changes in tidal range occur because of changes in coastline shape and bathymetry and these changes have been modelled in a number of studies (in the Bay of Fundy/Gulf of Maine by Scott and Greenberg, 1983; Gehrels *et al.*, 1995; in the North Sea by Austin, 1991; Hinton, 1992, 1995; throughout the northwest European shelf seas by Hinton, 1996; Uehara *et al.*, 2006). These studies have indicated that the major changes in tidal range occurred in the early to middle Holocene when the continental shelf was transgressed, causing large-scale changes in palaeogeography. However, on the local scale, in semi-enclosed estuarine environments, changes in estuarine geomorphology, such as spit or barrier development, will also cause noticeable changes in tidal range, including during the late Holocene (Shennan and Horton, 2002). The models cited above do not incorporate such local factors. An example of regional-scale changes in tidal range comes from Gehrels *et al.* (1995), who used a modelling approach to reconstruct tidal range changes in the macro-tidal Gulf of Maine and Bay of Fundy, North America. Their results showed a progressive increase in tidal range over time with the average tidal range at 7000 BP amounting to only 54-59% of the present range and by 2000 BP, amounting to 93% of the present range. In the Bristol Channel, the modern tidal range is 8m in Barnstaple Bay and rises to 15.1m at Avonmouth in the Severn Estuary, at the head of the Bristol Channel. Hill (2007) suggests that the tidal range in the Severn Estuary will have increased during the Holocene as the width and depth of the estuary increased (Allen, 2002).

The recent European Tidal Model of Uehara *et al.* (2006) is the first to model Holocene tidal range and palaeogeography changes in the southwest of Britain. The results of this model show that most of the contemporary Bristol Channel and Severn Estuary was flooded at 9000 to 7000 cal.yr.BP during the early Holocene transgression. As the

palaeo-estuary expanded eastwards during this time, the inner estuary zone of maximum tidal range also migrated east, following the extension of the Bristol Channel. On the southern margin of the Bristol Channel, the palaeo-coastline reached the mouth of the Taw Estuary at 7000 cal.yr.BP. This is supported by the first record of brackish-marine deposition occurring in the inner Taw Estuary at *c.*6600 cal.yr.BP. At 7000 cal.yr.BP, the tidal range of Barnstaple Bay was *c.*1.0 m higher (or 0.5 m higher tidal amplitude) than the modern range. Tidal range in Barnstaple Bay then falls between 7000 and 5000 cal.yr.BP, reaching amplitudes equivalent to modern conditions at 5000 cal.yr.BP. This fall was caused by the continuing eastward extension of the Bristol channel and its associated tidal range high. The model predicts that since 5000 cal.yr.BP, the tidal range in Barnstaple Bay has remained at a similar amplitude. The Uehara *et al.* (2006) predictions would therefore indicate that for the last 5000 yrs, no corrections for tidal range need to be applied to the Taw Estuary SLIPs. Prior to 5000 cal.yr.BP, corrections for tidal range changes are required. These are given in table 8.1 for SLIPs 8 to 11 and have been applied to the basal SLIPs in the MSL reconstruction (figure 8.1). Corrections to SLIP MSL heights are based on the model prediction of tidal amplitude being *c.*0.5 m higher than present at 7000 cal.yr.BP, followed by a linear decrease in tidal amplitude and MHWST to present tidal range conditions at 5000 cal.yr.BP.

SLIP No.	Age (2 σ) (cal.yr.BP)	SLIP (m MSL)	MSL tidal range correction (m)	Corrected SLIP (m MSL)	SLIP (MSL) (m OD)
1	534-328	- 0.49	0	- 0.49	- 0.05
2	912-729	- 1.09	0	- 1.09	- 0.65
3	1283-1081	- 1.03	0	- 1.03	- 0.59
4	2334-2135	- 1.44	0	- 1.44	- 1.00
5	3913-3697	- 3.25	0	- 3.25	- 2.81
6	4228-3975	- 3.17	0	- 3.17	- 2.73
7	4849-4617	- 4.33	0	- 4.33	- 3.89
8	5468-5086	- 4.36	- 0.07	- 4.43	- 3.99
9	5593-5331	- 4.97	- 0.12	- 5.09	- 4.65
10	6403-5922	- 5.95	- 0.29	- 6.24	- 5.80
11	6733-6504	- 6.69	- 0.40	- 7.09	- 6.65

Table 8.1 Taw Estuary SLIPs (MSL) with tidal range corrections. Reference tide level = MSL (MSL = 0.44m at Appledore, Admiralty tide tables, 2008). Tidal range corrections based on European Tidal Model (Uehara *et al.*, 2006) predictions for Barnstaple Bay.

However, the Uehara *et al.* (2006) model does not show changes within the Taw Estuary itself, where the formation and development of the Braunton Burrows barrier may have had a significant influence on tidal range, with the tidal range falling as the barrier prograded across the estuary mouth. As stated in chapter 1, Braunton Burrows is

thought be at least 2000 years old (Packham and Willis, 2001), and based on cartographic evidence, there has been very little change in its dimensions during the last 150 years (May and Hansom, 2003). This lack of geomorphic change in recent centuries suggests that it may be a particularly resilient landform that has had somewhat similar dimensions throughout the last 2000 years, and that it was probably formed during the early-middle Holocene during a time of more rapid RSL rise. This suggests that the width of the estuary mouth has not changed significantly since 0 AD and that tidal range changes during this period may therefore have been minimal, with a background of low rates of RSL rise. Recent high-resolution models of tidal range in an area of the east coast of England (Shennan *et al.*, 2000c, 2002, 2003; Shennan and Horton, 2002) have incorporated local-scale geomorphological changes in coastline configuration and bathymetry. These models were based on extensive litho-stratigraphic and chrono-stratigraphic data from the region around The Wash embayment, the Humber estuary and the north Norfolk coast. A similar modelling approach for the Taw Estuary is beyond the scope of this study, as it would also require a detailed knowledge of the litho-stratigraphy of the middle and outer estuary, and the date-constrained development of Braunton Burrows would need to be known. Therefore, the only palaeotidal range corrections that can be made are those based on the Holocene evolution of the Bristol Channel (given in table 8.1 and applied to the MSL reconstruction in figure 8.1).

The RSL reconstruction for the Taw Estuary provides eleven new mid-late Holocene SLIPs in south-west England. There was previously a lack of RSL data from the 120 mile long north Devon and Cornwall coastline (Shennan and Horton, 2002; Shennan *et al.*, 2006), with the closest reliable SLIPs (with quantified indicative meaning) located in Somerset in the inner Bristol Channel (*e.g.* Heyworth and Kidson, 1982; Housley, 1988; Haslett *et al.*, 1998; 2001; Jennings *et al.*, 1998), and at the end of the Cornwall Peninsula, at Penzance (Healy, 1995). Other reliable RSL data from the south-west peninsula comes from the south Devon coast (Devoy, 1982; Massey *et al.*, 2008) and the Isles of Scilly (Ratcliffe and Straker, 1996).

The Taw Estuary RSL curve is significant in that it includes four SLIPs from the last

2500 yrs, three of which are from the last 1300 yrs. SLIPs from this period are relatively uncommon in southern Britain (Shennan and Horton, 2002; Waller and Long, 2003) because of a general switch from organic to minerogenic deposition at 2000-3000 cal.yr.BP (Long *et al.*, 2000). SLIPS younger than 1300 cal.yr.BP are rare, with only one previous SLIP of this age located in the Bristol Channel, Severn Estuary, South Wales region (Shennan and Horton, 2002; Waller and Long, 2003; Edwards, 2006; Hill, 2007). Nine reliable SLIPS younger than 1300 cal.yr.BP have been recorded from the southern coast of England (Edwards, 2001; Shennan and Horton, 2002; Waller and Long, 2003; Massey *et al.*, 2008). Five of these are from Poole Harbour in Dorset (Edwards and Horton, 2000; Edwards, 2001), of which the youngest two used the historically dated rise in *Spartina* and *Pinus* pollen to provide age estimates (Edwards and Horton, 2000). The resolution of the Taw Estuary RSL curve therefore represents the most complete single site record of RSL movement during the late Holocene in southwest England to date, with the study by Edwards (2001) in Poole Harbour being the only other study with a comparable resolution in southern England and Wales.

The error envelope in figure 8.1 shows the trend of MSL rise in the Taw Estuary since *c.*6600 cal.yr.BP. With the tidal range corrections applied, the 'true' rise in RSL over this period increases to 7.09 m, and the rate of rise prior to *c.*5500 cal.yr.BP also increases to 1.83 mm yr⁻¹. As noted in chapter 7, there is a progressive fall in the rate of RSL rise in the Taw Estuary during the mid-late Holocene, with significant falls in the rate of rise occurring at *c.*5500 cal.yr.BP (changing from 1.83 to 1.09 mm yr⁻¹) and at *c.*2250 cal.yr.BP (changing from 1.09 to 0.64 mm yr⁻¹). A similar slowdown in RSL rise is seen across parts of southern England at 6000-5500 cal.yr.BP, most noticeably in the RSL record of the Bristol Channel, and from the Hampshire (Solent Estuary) and Sussex region of the south coast (Shennan and Horton, 2002; Waller and Long, 2003). The 2250 cal.yr.BP slowdown RSL is less easy to compare with other southern England records because of the decline in SLIP numbers at this time. However, similarities can again be made with the Bristol Channel record, once the South Wales SLIPs of Edwards (2006) are added (see figure 8.1), and with the central region of the south coast, with a minor slowdown discernable in the Poole Harbour record of Edwards (2001).

The RSL record of north Devon can also be compared with other RSL records from the south-west and south coast of England to evaluate differential isostatic movements. The Taw Estuary SLIP altitudes (figure 8.1) show the most similarity with those from the

Solent (Edwards, 2001; Waller and Long, 2003) and from the Bristol Channel/South Wales region (see figure 8.1). However, this latter similarity is only obvious when the Taw record is only directly compared with the South Wales SLIPs of Edwards (2006) and the Severn Estuary record of Hill *et al.* (2007). As indicated earlier, the SLIPs from 2500-4500 cal.yr.BP (figure 8.1) show a great deal of scatter that may be related to differential compaction at and between sites (Edwards, 2006). Edwards (2006) showed that most of the SLIPs from the base of this cluster had both thicker units of overburden (*e.g.* many of the deep samples of Haslett *et al.*, 2001 and Hayworth and Kidson, 1982) and thicker units of compactable sediment below. This would preferentially result in higher rates of compaction in these SLIPs, while SLIPs from thinner sequences with smaller overburdens (*e.g.* SLIPs of Haslett *et al.*, 1998; see figure 8.1) would show less compaction error. Therefore, by comparing the Taw Estuary SLIP altitudes with the combined data of Haslett *et al.* (1998), Edwards (2006) and Hill (2007), a very good match can be seen in figure 8.1. This similarity indicates similar isostatic subsidence and RSL rise rates in these regions.

If the Taw RSL record is compared with the MSL reconstruction for south Devon (Massey *et al.*, 2008) during the period 6600-4000 cal.yr BP (there are no reliable SLIPs younger than 4000 cal.yr.BP in south Devon) the Taw SLIPs generally plot *c.*2.0m above similar intercalated south Devon SLIPs. This indicates a faster rate of RSL rise in south Devon, caused by a higher rate of crustal subsidence. In addition the intercalated south Devon SLIPs have had a geotechnical correction for autocompaction applied (by up to 0.49m) so would plot even lower if uncorrected. When compared with the west Cornwall and Scilly Isles RSL reconstruction (Healy, 1995; Ratcliffe and Straker, 1996; Massey *et al.*, 2008), the Taw SLIPs again plot higher, indicating higher rates of mid-late Holocene subsidence in the west Cornwall/Scilly Isles region. The regional comparisons indicate that a NNW-SSE trending geographic band, stretching from the outer Bristol Channel (including both the South Wales and North Devon coasts), through to the inner Severn Estuary and Somerset Levels, through to the central south coast, near the Solent, has experienced a similar isostatic history during the mid-late Holocene, with similar subsidence rates and RSL movement. In the far south-west, south Devon, Cornwall and the Scilly Isles have undergone higher rates of subsidence and faster rates of RSL rise during the same mid-late Holocene period.

Shennan and Horton (2002) calculated regional rates of subsidence in Britain since

4000 cal.yr.BP, based on the database of reliable SLIPs for the UK. They based their calculations on the assumption that the long-term eustatic contribution by melting ice-sheets has been zero since 4000-5000 cal.yr.BP and that any RSL movement since then has been caused by isostatic crustal movement. In calculating subsidence (or uplift) they also attempted to make a correction for sediment compaction, based on the vertical spread of SLIPs in the age-altitude graphs for each region (*i.e.* they used altitudes from the top end of the error envelopes). Their uncorrected subsidence rates can be directly compared with the Taw Estuary mean subsidence rate since 4000 cal.yr.BP, which has been 0.82 mm yr^{-1} . This compares relatively well with the Solent (Hampshire) subsidence rate of 0.71 mm yr^{-1} , which has been identified above as having a similar RSL record as that of the Taw Estuary. Shennan and Horton (2002) give a 1.06 mm yr^{-1} rate of subsidence for the Bristol Channel. This figure does not include the new SLIPs of Edwards (2006) or Hill *et al.* (2007). However, as discussed above, the similarity between the Taw and Bristol Channel records was based on a comparison that plotted at the top of the vertical spread in SLIPs. This is equivalent to the ‘corrected’ subsidence rate value of Shennan and Horton (2002) which is 0.76 mm yr^{-1} , a rate which is very similar to the Taw Estuary rate (0.82 mm yr^{-1}), giving support to a similar isostatic history. Shennan and Horton (2002) did not have any RSL data for North Devon and therefore did not propose a subsidence rate for this region. The new set of validated SLIPs from the Taw Estuary therefore represents a valuable new dataset that can be used to advance current knowledge on post-glacial crustal movement in south-west England. This region is important as it was not glaciated during the Last Glacial Maximum (LGM) and is in the area affected by pro-glacial forebulge collapse. RSL reconstructions can be used to help decipher the dynamics of this crustal process.

Unlike previous RSL reconstructions in the south-west (*e.g.* Massey *et al.*, 2008), the Taw Estuary RSL reconstruction includes validated SLIPs from throughout the mid and late Holocene. This enables the Taw data to be directly compared with geophysical earth models of GIA (glacial isostatic adjustment), such as the recent ones by Peltier *et al.* (2002) and Shennan *et al.* (2006), over the whole mid-late Holocene period. This is important as these two models give somewhat different predictions of isostatic adjustment in Britain since the LGM, resulting in different predictions of RSL movement in regions such as south-west England. The two different predictions that the Peltier *et al.* (2002) and Shennan *et al.* (2006) models give for RSL rise in Devon, are plotted on figure 8.1. This shows that the Peltier *et al.* (2002) model of RSL rise is more

curvilinear in trend, but with a significant fall in the rate of RSL rise at 4000 cal.yr.BP. The Shennan *et al.* (2006) model of RSL rise is more rectangular in shape, with a marked inflection point at 6000 cal.yr.BP when the rate of RSL rise slows. The complete coverage of the mid-late Holocene by the Taw Estuary SLIPs allows the different models to be tested. Figure 8.1 indicates that the Taw Estuary RSL envelope shows good agreement with the trend of the Shennan *et al.* (2006) model. The Taw envelope overlaps the Shennan model between 0 and 3000 cal.yr.BP (SLIPs 1 to 4), and then diverts slightly below the trend of the model between 3000 and 5500 cal.yr.BP (SLIPs 5 to 9). This may be related to the youngest SLIPs 1-4 having sustained only minimal autocompaction, with all of them having *c.*1 m or less overburden. The linear divergence away from the Shennan model between 3000 and 5500 cal.yr.BP may be related to increasing sediment compaction with depth in the PL1 core, with SLIP 9 located beneath *c.*4.2 m of overburden. Prior to 5500 cal.yr.BP, the Taw Estuary RSL envelope shows a steeper rate of RSL rise. This is mirrored in the predicted Shennan model curve which shows a significantly higher rate of rise prior to 6000 cal.yr.BP. Significantly, the Taw and model curves converge at the compaction-free basal SLIP 11. If compaction corrections had been applied to SLIP 10, and the overlying SLIPs (SLIP 10 is located beneath *c.*5.6 m of overburden at the top of the basal PL1 wood peat,), the rate of RSL rise in the Taw Estuary envelope prior to 5500 cal.yr.BP would have been higher, resulting in a closer match with the Shennan model predictions before 6000 cal.yr.BP. It is worth noting that if the above trends in sediment compaction occurred in the PL1 core, the slowdown in RSL rate seen in the Taw Estuary RSL envelope at *c.*2250 cal.yr.BP would have been less or non-existent, and therefore, this apparent slowdown may be entirely caused by differential compaction.

The Taw RSL envelope shows much less agreement with the Peltier *et al.* (2002) model predictions. The inflection and slowdown at 4000 cal.yr.BP is not seen in the Taw reconstruction and between 4000 and 6000 cal.yr.BP, the Peltier model predicts a significantly higher rate of RSL rise. This results in the compaction-free basal SLIP located >1.0 m above the Peltier model prediction at 6600 cal.yr.BP. The two geophysical models show a significant divergence between 4000 and 2000 cal.yr.BP, with the Peltier model predicting higher RSL heights and lower rates of subsidence. The Taw Estuary RSL reconstruction does not agree with this prediction.

The comparison of the north Devon RSL envelope with various geophysical model

predictions for the region appears to validate the Shennan *et al.* (2006) model. This suggests that this model may offer a closer reflection of crustal isostatic adjustments in the south of England.

8.2 LATE HOLOCENE PALAEO-SALINITY CHANGE: IMPLICATIONS FOR RIVER DISCHARGE AND CLIMATE CHANGE

Micropalaeontological and geochemical records of Holocene variations in estuarine palaeosalinity have been recently used in several, mainly US, estuary studies as a proxy for changes in freshwater influx from the catchment (*e.g.* Ingram *et al.*, 1996; Cronin *et al.*, 2000, 2005; Bryne *et al.*, 2001; Willard *et al.*, 2003; Malamud-Roam & Ingram, 2004; Zong *et al.*, 2006). The multidecadal-centennial scale variations in river discharge that these studies have recorded have been used to infer changes in effective precipitation and regional climate over the mid-late Holocene both on the Pacific coast of the US in San Francisco Bay (Bryne *et al.*, 2001; Malamud-Roam & Ingram, 2004; Malamud-Roam *et al.*, 2006), and on the Atlantic coast in Chesapeake Bay (Cronin *et al.*, 2000, 2005; Willard *et al.*, 2003). In addition, Zong *et al.* (2006) has recently used a diatom and carbon isotope based palaeosalinity record of the Pearl River Estuary in southern China to reconstruct the Holocene monsoon history. No study in Europe has yet taken this palaeosalinity-based approach to palaeo-climate reconstruction, but there are indications that this is about to change, with a recent study by Leorri and Cerrata (2009) in northern Spain on the potential of foraminifera in salinity reconstruction, indicative of the growing interest in this field.

The palaeosalinity record of the inner Taw Estuary is re-presented in figure 8.2, with diatom salinity index used as a proxy for palaeosalinity. The fluctuation in estuarine salinity that this record portrays indicates that the main driving-force behind these changes has a centennial to multi-centennial cyclicity. Various studies have indicated that on an annual to decadal timescale, freshwater inflow is the main control on estuarine salinity, (Peterson *et al.*, 1995; Najjar, 1999; Gibson and Najjar, 2000). On a multi-decadal to centennial timescale, changes in estuarine palaeosalinity have been correlated in other studies with proxy and instrumental records of regional climate change (Malamud-Roam and Ingram, 2004; Willard *et al.*, 2005; Malamud-Roam *et al.*, 2006), with Cronin *et al.* (2000, 2005) indicating that palaeosalinity cyclicity in the

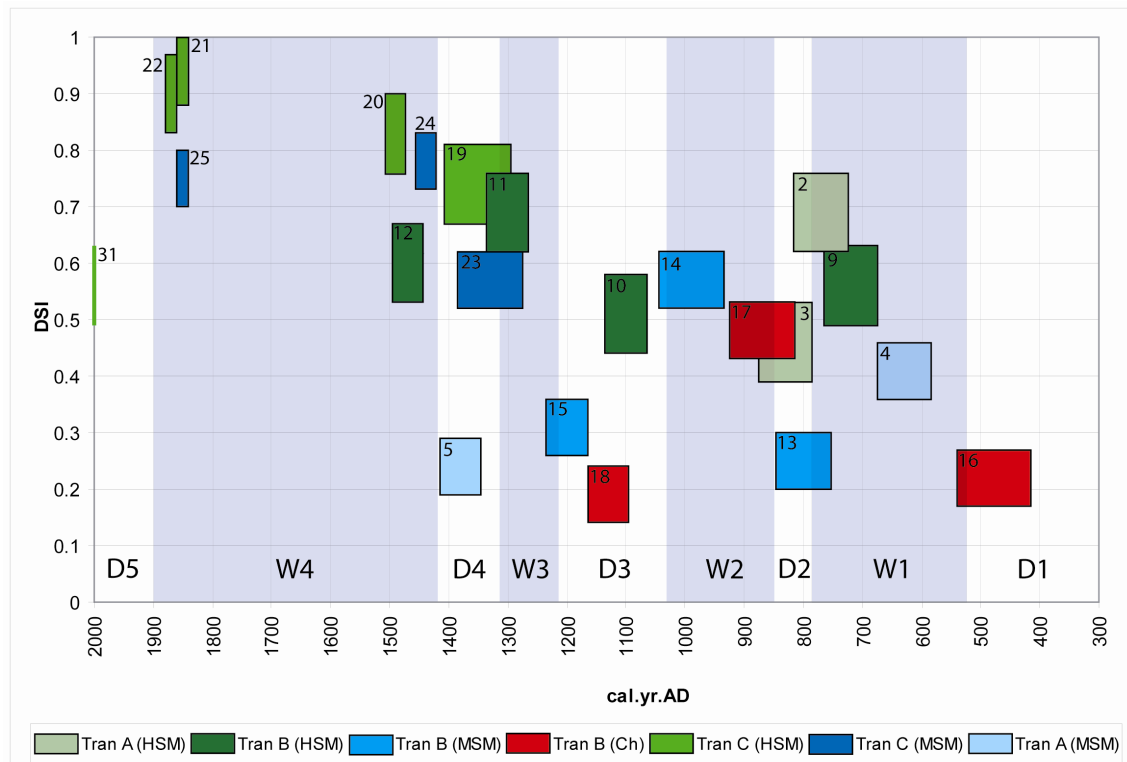


Figure 8.2 DSI-based palaeosalinity change in the Taw Estuary during the Late Holocene (transects A, B and C) and inferred palaeo-climate periods. DSI trends in three separate tidal frame environments are analysed. These are the lower high saltmarsh (HSM), the mid saltmarsh (MSM); and the unvegetated tidal river channel (Ch). Periods of low palaeosalinity are shaded grey and labelled W1 to W4 with inferred high river discharges and relatively wet climatic conditions. Periods D1 to D5 correspond to periods of high palaeosalinity, with inferred low river discharges and relatively dry climatic conditions.

eastern US can be linked to NAO-type climate change cycles. The centennial-scale palaeosalinity cyclicity evident in the Taw Estuary record suggests that these are also controlled by precipitation-driven changes in river discharge. In figure 8.2, periods of low palaeosalinity (high DSI) are interpreted as late Holocene periods of high freshwater river discharge into the estuary, while phases of high estuarine palaeosalinity (low DSI) are indicative of periods of reduced freshwater inflow. These changes can therefore be used to reconstruct precipitation-related climate change in the region over the last 1700 yrs as centennial-scale periods of high river discharge indicate wet climatic conditions with high regional precipitation, while periods of low river discharge suggest phases of below-average precipitation and relatively dry climatic conditions. The palaeosalinity periods highlighted in figure 8.2 have been labelled W1 to W4 for relatively wet climatic intervals and D1 to D5 for relatively dry climatic stages. The ages of these periods are given in table 8.2. Four intervals of above-average precipitation and low estuarine palaeosalinity are identified at 520-780, 850-1030,

1215-1315, and 1420-1900 cal.yr.AD. Five intervals of below-average precipitation and high estuarine palaeosalinity are identified at 300-550, 780-850, 1030-1215, 1315-1420, and 1900-2000 cal.yr.AD. This shows that there has been significant climatic variation in southern Britain since *c.*300 cal.yr.AD, with climatic shifts evident in the estuarine palaeosalinity record.

Palaeosalinity period	Age (cal.yr.AD/BC)	Relative discharge	Climate
D5	1900 – 2000 AD	Low	Dry
W4	1420 – 1900 AD	High	Wet
D4	1315 – 1420 AD	Low	Dry
W3	1215 – 1315 AD	High	Wet
D3	1030 – 1215 AD	Low	Dry
W2	850 – 1030 AD	High	Wet
D2	780 – 850 AD	Low	Dry
W1	520 – 780 AD	High	Wet
D1	300 – 520 AD	Low	Dry

Table 8.2 Late Holocene river discharge levels and associated climatic periods inferred from the DSI palaeosalinity record. Five relatively dry periods (D1 to D5) and four relatively wet periods (W1 to W4) are identified since 300 AD.

It was expected that estuarine palaeosalinity would also be influenced by late Holocene RSL rise in the Taw Estuary. This study has shown that locally, there has been a *c.*1.3 m rise in RSL since *c.*300 cal.yr.AD (figure 8.1) with the mean rate of rise identified at 0.64 mm yr⁻¹ during the last 2300 yrs. This rise was predicted to be shown as a long-term trend of increasing marine influence and salinity (*i.e.* reduced DSI), that would be superimposed on the cyclicity caused by centennial-scale fluctuations in discharge. However, the palaeosalinity record for the Taw Estuary (figure 8.2), does not show a background trend of increasing palaeosalinity. The longest individual record of palaeosalinity change is for the high saltmarsh in Transect B (figure 7.10). This shows that between, *c.*0 cal.yr.AD and *c.*1450 cal.yr.AD, there was no discernable trend of decreasing DSI, despite a *c.*0.9 m rise in RSL (figure 8.1). Therefore, if this magnitude of long-term RSL rise is not registered in the DSI record, it is very unlikely that smaller magnitude centennial-scale fluctuations (oscillations) in RSL have had a significant effect on estuarine palaeosalinity during the late-Holocene. This supports the argument that the fluctuations seen in palaeosalinity during the last 1700 yrs (figure 8.2) are

primarily driven by climate-related changes in river discharge, and not by fluctuations in RSL. This finding was replicated in the study by Malamud-Roam and Ingram (2004) in the San Francisco Bay Estuary, where they found evidence of palaeosalinity changes in the opposite direction, with a late Holocene trend of decreasing salinity. The Taw Estuary record therefore indicates that during periods of relatively low RSL rise, multidecadal to centennial-scale changes in regional precipitation will be the principal driver of estuarine palaeosalinity change. This may not be the case in the early-mid Holocene, when higher rates of RSL rise would have had a more direct influence on estuarine palaeosalinity. In south-west England, the significant slowdown in RSL at 6000-5500 cal.yr.BP (as shown by SLIP records and geophysical predictions), may have been the point when climate replaced RSL as the dominant driver of estuarine palaeosalinity.

If the Taw Estuary record of palaeosalinity is ultimately caused by changes in river discharge and regional precipitation (as indicated in figure 8.2 and table 8.2), validation of this may be provided via evidence of geomorphic change and fluvial instability in the Taw valley record, and by correlations with regional proxy palaeo-climate records. Therefore, each of the palaeosalinity-derived climatic periods given in table 8.2 will now be discussed with reference to the geomorphic record of the Taw estuary and river valley, and with reference to various UK and European proxy climate records (e.g. peatland water-table fluctuations, lake-level fluctuations and nationwide records of fluvial instability). In addition, documented historical accounts of climate change will be appraised. The possible geomorphic effects of late Holocene RSL fluctuations will also be discussed.

D1 (300-520 cal.yr.AD)

D1 relates to a relatively dry climatic period with high estuarine palaeosalinity and low river discharge. This period corresponds with stratigraphic unit S6. Very little fluvial activity is recorded in the Taw valley (transects E to I) or fluvio-estuarine zone (transects C and D) during this period. This suggests that the contemporaneous river system was relatively stable with little significant floodplain alluviation or channel change and a period of minimal channel or floodplain aggradation. This would indicate a regime of low river discharge and low stream power with high-stage floods rarely able to cause significant overbank flooding. The only fluvial geomorphic activity recorded is the temporary re-occupation of the CT1 palaeochannel site at 240 +/-140 cal.yr.AD.

The period just prior to D1 (corresponding stratigraphic unit S5, which started at *c.*300 cal.yr.BC) is worth mentioning at this point as it is a time of significant marine influence in the estuarine zone. In transect A, significant estuarine channel incision and lateral migration occurs, with large volumes of estuarine sediment deposited during active tidal meander migration. This S5 period commences with the transgressive overlap at 360-206 cal.yr.BC (1σ age), suggesting that the marine incursion and resulting tidal incision may have instigated the estuarine channel change (Blum and Tornqvist, 2000). Increasing marine influence after the second century BC is also seen in transect B, with brackish wetland sediments being deposited on top of a freshwater-brackish peat.

Other significant environmental change is evident in the few centuries prior to D1 (*i.e.* 300 cal.yr.BC to 300 cal.yr.AD). In transect B, evidence exists for local woodland clearance occurring at the start of this period, with the disappearance of alder and birch wood from the spring-mire peat and an increase in the peat's minerogenic content, suggestive of increased soil erosion. Phases of significant woodland clearance elsewhere in Britain have been linked with periods of increased run-off and river discharge resulting in downstream channel change and floodplain alluviation (*e.g.* Robinson and Lambrick, 1984; Brown and Barber, 1985; Brown, 1987; Tipping, 1992). This is not apparent in the Taw valley at this time, suggesting that the clearance appears to have been localised in parts of the valley, with most clearance occurring earlier in the late Bronze age or early Iron age, which is supported by the pollen evidence of Caseldine *et al.* (2000) in the River Yeo tributary. However, it has become increasingly clear that although prehistoric and historic forest clearance were important for initiating soil erosion, significant redistribution of sediment may have occurred only during periods of abrupt climatic change characterised by increases in flood frequency and magnitude (Macklin and Lewin, 1993; Coulthard and Macklin, 2001).

Returning to a discussion of the D1 period, a significant hydrological event caused the avulsion of the TS1 tidal river at 415-540 cal.yr.AD. This may have heralded the start of a deterioration in the climate at this time with a propensity for an increasing frequency of high magnitude fluvial floods. However it also may have been linked to the diatom evidence in transect F of a major storm surge occurring at this time. This was dated in the CT1 core to have occurred between 240 +/-140 cal.yr.AD and 410 +/-180 cal.yr.AD, which overlaps with the TS1 avulsion event.

From the 1st to 5th Centuries AD, historical Roman accounts document a climatic period of increasing dryness and warmer temperature (sometimes termed the Romano-British warm period or Roman Optimum) with vine cultivation possible further north in Italy and a reduction in reported river floods (Lamb,1982). Historical reports from northern Europe and Britain are too sparse to be reliable, but various peatland climate records portray a similar dry climate in Britain. For example, the surface wetness curve of Barber (1981) for Bolton Fell Moss in northern England shows a prolonged dry period up to *c.*600 cal.yr.AD that corresponds well with the D1 interval. Charman *et al.*, (2006) produced a composite record of water table variability for Northern Britain (figure 8.3), based on the stacking of peatland records from northern England and Scotland (regional composite records were also produced). His composite record indicates a period of low water table levels between *c.*200 and 450 cal.yr.AD. This period coincides with most of D1, but suggests the dry climate in southern England persisted until the end of the 5th Century AD. Individual peatland records that support this dry period include the work of Blundell & Barber (2005). Recorded flood episodes in UK fluvial sequences are also relatively uncommon during D1, with Macklin *et al.* (2005) reporting no nationwide UK-wide flood episodes in the British fluvial archive between 0 and 660 cal.yr.AD (table 8.3).

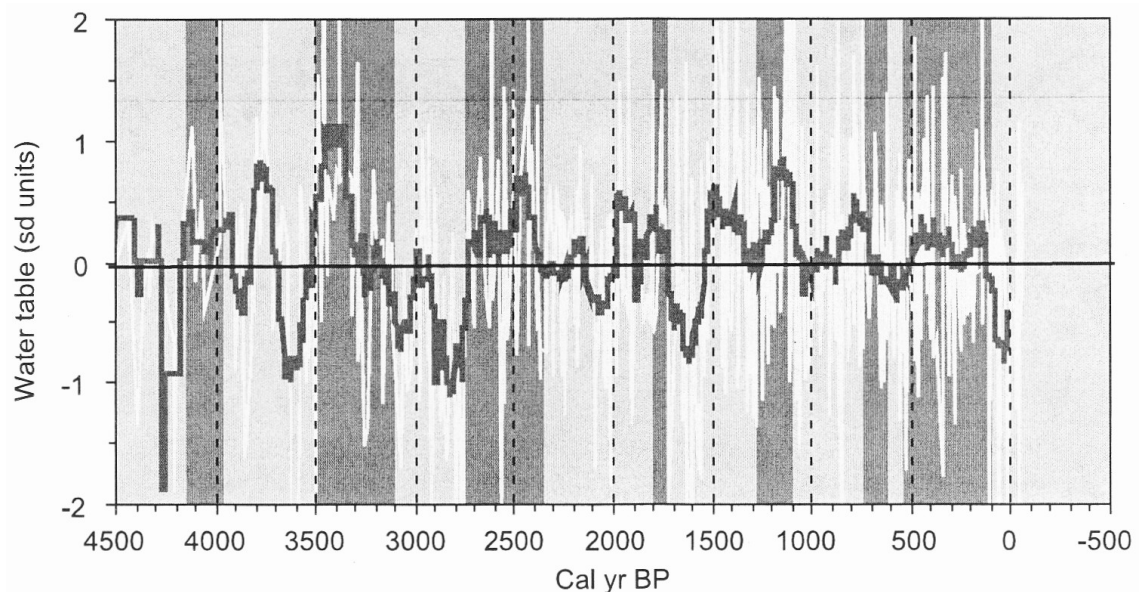


Figure 8.3 Regional composite water table record for northern Britain during the last 4500 yrs (Charman *et al.*, 2006). Positive values infer higher water tables and wetter climate. The black line is the 100 yr moving average of 12 individual records from Northern England and Scotland. Phases of high lake level in mid-Europe (Magny, 2004) are shaded grey (from Charman *et al.*, 2006).

River instability and flooding episodes (cal.yr,AD/BC)	British regions affected
330 BC	Nationwide
0 AD	Nationwide
300 AD	England
660 AD	Nationwide
1090 AD	Scotland and northern England
1290 AD	Nationwide
1380 AD	Nationwide

Table 8.3 Holocene river flooding episodes in Great Britain since 500 cal.yr.BC (from Macklin *et al.*, 2005).

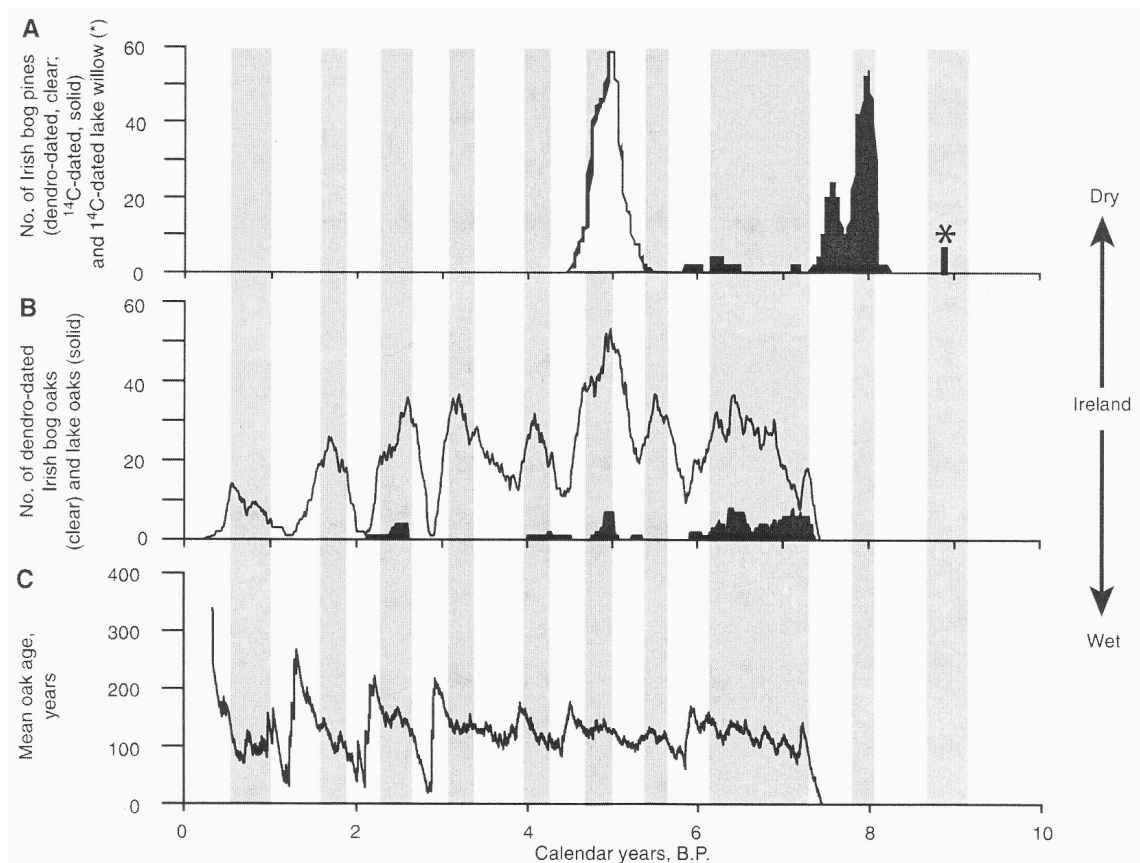


Figure 8.4 Comparison between the number of Irish (A) Scots pine, (B) bog and lake oak tree populations and (C) mean bog oak ages (Leuschner *et al.*, 2002). Grey zonation denotes inferred dry phases in Ireland (from Turney *et al.*, 2005).

D1 corresponds with a dry climatic period identified by Turney *et al.* (2005), when there was a sharp increase in the number of dated Irish lake oaks located below current

lake levels in Northern Ireland, providing unambiguous evidence for drier conditions (figure 8.4).

W1 (520-780 cal.yr.AD)

W1 relates to a relatively wet climatic period with low estuarine palaeosalinity and high river discharge. This period corresponds with stratigraphic unit S7. Significant amounts of floodplain alluviation and aggradation (T2) occur at this time in both the non-tidal fluvial reach and the fluvio-estuarine zone (transects C and D). This is associated with a period of sustained channel migration and floodplain reworking, suggestive of a regime of high discharge and high stream power. The Taw flood record (figure 7.7) indicates a peak in dated channel abandonments (*e.g.* at BT1 and HS1) occurring at this time, with the surface geomorphology indicating that abandonment occurred by meander neck cut-off and avulsion. Channel sinuosity is relatively high during this period, giving support to a high stream power and discharge (Schumm and Khan, 1972; Edgar, 1984). In the fluvio-estuarine zone at transects C and D, buried palaeochannel deposits indicate that a sand-gravel bed river underwent a phase of significant lateral bar formation, before being abandoned by avulsion, again indicative of fluvial instability and high discharge.

In transect A at PL1, a transgressive overlap occurs at the end of the W1 period at 684-777 cal.yr.AD (1σ age). Unlike the previous transgressive overlap, this phase of estuary expansion does not appear to have promoted significant tidal channel migration. However, there is a gap in the dating of transect A estuarine channel sediments between *c.*70 cal.yr.AD (PL2) and *c.*1230 cal.yr.AD (PL3). The transect A stratigraphy suggests that the intervening period included a sustained phase of channel bed aggradation and continuing tidal meander migration. This is probably partly related to the increased discharge and mobilisation of sediment seen in the upstream transects during both W1 and W2 being translocated to the inner estuary with the large influx of catchment derived sediment causing estuary infilling and aggradation. Any possible geomorphic effects of a marine incursion at 684-777 cal.yr.AD would therefore have been masked by the climate-driven aggradational phase that occurred during periods of high river discharge (W1 and W2). Following the transgressive overlap at 360-206 cal.yr.BC (1σ age) and the marine incision that followed, the RSL reconstruction (figures 7.8 and 8.1) shows a slowdown in the rate of RSL rise. This may have also promoted estuary infilling and aggradation, leading to a decline in the amount of accommodation space

available for sediment storage (Allen, 1990; Dalrymple *et al.*, 1992; Allen and Posamentier, 1993; Long *et al.*, 2000; Rees, *et al.*, 2000).

Macklin *et al.* (2005) identified sixteen episodes of major flooding and river instability in the UK since 11,160 cal.yr.BP (late Holocene ones shown in table 8.3), with a strong correspondence between flood episodes and climatic deteriorations inferred from proxy climate records (*e.g.* mire wet shifts). This was based on an analysis of 506 ¹⁴C dated fluvial units. The W1 interval coincides with a flooding episode at 660 cal.yr.AD that affected most parts of Britain. The five channel abandonment dates for W1 show a strong agreement with this episode, with figure 7.3 showing that the radiocarbon/OSL probability curve peaks all lie between 650 and 750 cal.yr.AD. This flooding episode is also recognised in the Polish fluvial archive in continental Europe (Macklin *et al.*, 2006), suggesting that it is associated with a climatic deterioration that affected most of northern Europe. W1 also corresponds with a phase of high lake levels in mid-Europe (figure 8.3 and 8.5; Magny *et al.*, 2003; Magny, 2004), which supports a period of high effective precipitation, and corresponds with a period of high winter precipitation in western Norway (figure 8.5; Nesje *et al.*, 2000). Other evidence of a wet climate comes from historical reports of wet and dry summers in Britain (Lamb, 1982) that indicate a high frequency of wet summers in the 7th Century. The composite record of water table variability (figure 8.3) given by Charman *et al.* (2006) shows a shift to wet conditions, with average to high water tables in northern Britain between 450 and 800 cal.yr.AD. The W1 wet interval is contained within this period. Other individual peatland proxy climate records that support a wet phase at this time include those of Blackford and Chambers (1991), Mauquoy and Barber (1999), Barber *et al.* (1999), Chiverrell (2001), Langdon *et al.* (2003), Blundell & Barber (2005) and Blundell *et al.* (2008). An abrupt decrease in the annual mean age of Irish bog oaks is also seen in the 7th Century (figure 8.4), reflecting a shift to wetter conditions (Leuschner *et al.*, 2002).

D2 (780-850 cal.yr.AD)

D2 relates to a relatively dry climatic period with high estuarine palaeosalinity and low river discharge. This period corresponds with the final 20yrs of stratigraphic unit S7 and the first 50yrs of stratigraphic unit S8. However, this period is thought to be largely unrepresented in the stratigraphic record, with figure 7.3 indicating a small gap in the distribution of radiocarbon and OSL dated alluvial units. This suggests a temporary

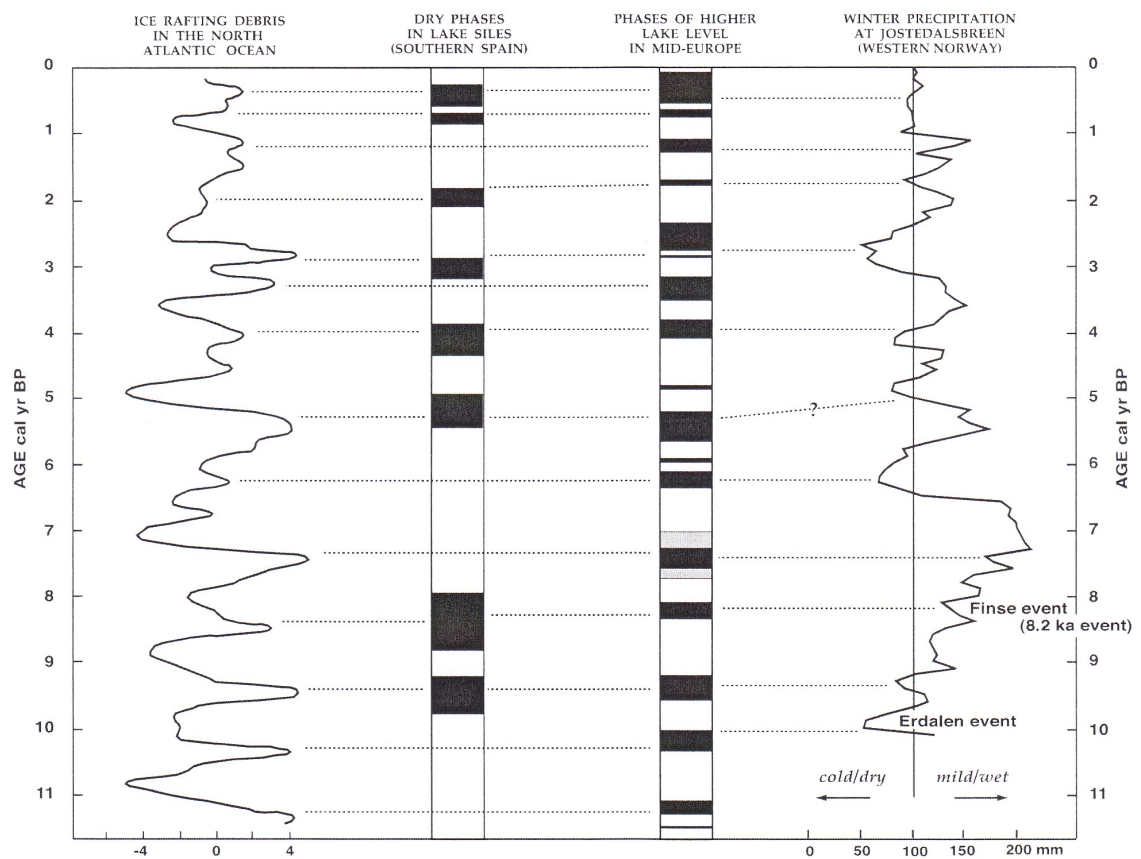


Figure 8.5 Holocene proxy climate records from the North Atlantic and Europe. Comparison of the North Atlantic IRD (ice rafted debris) record (Bond *et al.*, 2001) with hydrological records from lake Siles, southeastern Spain (Carrión, 2002), from lakes in mid-Europe (Magny, 1998; Magny, 2004), and from from the Jostedalsbreen region, western Norway (Nesje *et al.*, 2000) (from Magny *et al.*, 2003).

hiatus in fluvial and fluvio-estuarine geomorphic activity (in sharp contrast with the preceding W1 phase) when the contemporaneous river system was relatively stable with minimal channel change or floodplain formation occurring. As with D1, this would indicate a regime of low river discharge and low stream power. Within the saltmarsh/brackish marsh wetlands of the inner estuary, gradual marsh accretion continued to occur, with the DSI samples for this period located in the PL2 and TS1 cores.

The peat surface wetness curve of Barber (1981) shows a short, but distinct dry shift that corresponds well with the D2 period. Historical documents compiled by Lamb (1982) reveal a distinct drop in reported wet summers in Britain during the 8th Century that persisted to *c.*800 AD (*i.e.* D2). A short dry climatic period is also reported in Europe with a corresponding fall in river floods in Italy and a severe drought documented in the Mediterranean and the Caspian Sea area at *c.*800 AD.

W2 (850-1030 cal.yr.AD)

W2 relates to a relatively wet climatic period with low estuarine palaeosalinity and high river discharge. This period corresponds with stratigraphic unit S8 (and the start of S9). A phase of significant fine grained floodplain aggradation is preserved in the fluvio-estuarine zone with vertical floodplain accretion occurring on top of former S7 deposits that were active during W1 in transects C and D (although this W2 phase has been largely reworked by later flood channel activity in transect C). In transect D, there is evidence of some channel migration and channel abandonment by avulsion (*e.g.* the upper abandoned channel in NB1). In the more estuarine zone of transect B, lateral migration of the tidal river is evident in the CF1 core. In the CF1 core, transect B, there was a significant rise in freshwater influx during the W2 interval, with the transitional fluvio-estuarine zone extending downstream into transect B. The W2 record indicates that a fluvial regime of high discharge and high stream power was active, with frequent high-stage overbank floods that were capable of initiating channel avulsion events. The relatively fine-grained nature of the floodplain sediments and abandoned channel fills indicates that this period was dominated by high suspended sediment loads, possibly caused by an expansion of arable farming in the catchment during the 10th Century, which would result in increased soil erosion rates (Brown and Barber, 1985). Buckland and Sadler (1985) proposed that the delivery of large volumes of fine grained sediment to the lower Humber valley and Humberhead Levels was due to an increase in agricultural cultivation (and switch to winter wheat) that led to a massive influx of weathered sediment due to soil erosion in the Roman and early post-Roman period.

The compilation of Holocene river flood episodes in Britain, Spain and Poland, presented by Macklin *et al.* (2006), shows a major episode of river instability and flooding in Poland and Spain at 910 cal.yr.AD. The British fluvial record also shows a high frequency of fluvial flood events with the flood probability record of Macklin *et al.* (2005) showing a peak in fluvial instability that started at 660 cal.yr.AD (*i.e.* in W1) and lasted until the 10th Century AD (*i.e.* W2). The composite record of water table variability for northern Britain (Charman *et al.*, 2006) indicates average water table levels in northern Britain (figure 8.3), so gives inconclusive support. However, individual peatland records from northern England and the Scottish borders do show prominent wet shifts between 850 and 950 cal.yr.AD (*e.g.* Barber, 1981, 1994; Wimble, 1986; Chambers *et al.*, 1997), with the duration of a peak in the surface wetness curve of Barber (1981) showing strong agreement with the W2 age bracket. The historical

reports compiled by Lamb (1982) reveal a high frequency of reported wet summers in Britain and central Europe at the start of W2 (up to *c.*950 AD) with contemporaneous accounts of cold winters up to 1000 AD. The Irish lake oak and bog oak records of Turney *et al.* (2005) and Leuschner *et al.* (2002) show a relatively wet period that lasted from *c.*500 cal.yr.AD to *c.*1000 cal.yr.AD (figure 8.4). This corresponds with both W1 and W2, and the intervening short dry period D2.

D3 (1030-1215 cal.yr.AD)

D3 relates to a relatively dry climatic period with high estuarine palaeosalinity and low river discharge. This period corresponds with stratigraphic unit S9 and the start of S10. Very little fluvial activity is recorded in the non-tidal Taw valley (transects E to I) during this period, indicating that the contemporaneous river system was relatively stable with little significant floodplain alluviation, channel aggradation or channel change occurring. This would indicate a regime of low river discharge and low stream power with high-stage floods remaining constrained within the bankfull channel dimensions. However, towards the end of the 12th Century at the end of this period, there is evidence of increasing fluvial instability. In the fluvial zone, the BT1 palaeochannel is re-occupied and within the transitional fluvio-estuarine zone at transect D, the NB4 palaeochannel is thought to have been abandoned towards the end of D3. The associated NB4 OSL age of 970 +/-220 cal.yr.AD has a large degree of uncertainty attached, and as the coarse grained nature of the fill has similarities with the younger S10 sediments (and not with the older fine grained S8 deposits), channel abandonment is thought to have occurred at the end of the 12th Century AD, near the younger limits of the 2 σ age uncertainty. This would suggest increased climatic instability towards the end of the D3 period, with the occurrence of occasional large magnitude floods. The NB4 sediments also suggest an increase in stream power at the end of D3, enabling coarse bed load (gravelly coarse sand) to be entrained. In the estuarine zone (transect B) during the early and middle part of D3, a phase of tidal meander migration occurred in the vicinity of TS2. This suggests that during periods of low fluvial discharge, significant tidal meander migration may still occur in the inner estuary, due to the action of high energy tidal currents (especially the higher velocity flood tides). Evidence of decreasing marine influence towards the end of D3 is evident across the regressive overlap in the TS1 core, dated at 1051-1213 cal.yr.AD (1 σ age). This is followed by the progradation of alder carr peats from the transect B valley side, indicating a phase of estuary contraction.

The D3 interval coincides with the peak of the Medieval Warm Period (Hughes and Diaz, 1994). Lamb (1982) suggests that Europe experienced the warmest temperatures since post-glacial times in the 11th and 12th Centuries and associated the establishment of Norse colonies in Greenland and Newfoundland to this warm period. Lamb (1982) also reports that dry summers were documented for Britain and central Europe during this time. In their analysis of records of expansion and retreat of montane glaciers, Grove and Switsur (1994) concluded that the Medieval Warm Period (or Epoch) was a global event occurring between *c.*900 and 1250 cal.yr.AD, with the period being bracketed by glacial advances in the 7th - 9th Centuries and the late 13th Century. Macklin *et al.* (2005) reported no major UK-wide flood episodes in the British fluvial archive during D3, although a significant flood episode did occur in Scotland and northern England at 1090 cal.yr.AD (table 8.3). The composite record of water table variability for northern Britain presented by Charman *et al.* (2006) shows inconclusive support with average water table levels for most of D3, and does not support a dry climate at the end of D3, as his record shows a rise in water table levels after 1150 cal.yr.AD. This shows agreement with the geomorphic evidence in the Taw valley for a possible trend of climatic instability towards the end of the 12th Century. The Irish lake oak record of Turney *et al.* (2005) indicates that D3 coincides with the start of a relatively dry climate phase (figure 8.4). However, this oak record also shows that the dry phase in Ireland lasted until *c.*1400 cal.yr.BP, encompassing W3 and D4 as well.

W3 (1215-1315 cal.yr.AD)

W3 relates to a relatively wet climatic period with low estuarine palaeosalinity and high river discharge. This period corresponds with the early and middle part of stratigraphic unit S10. Significant amounts of floodplain alluviation and aggradation (older parts of T1 terrace) occur at this time in both the fluvial non-tidal reach and the fluvio-estuarine zone (transects C and D) with the Taw flood record (figure 7.7) indicating a peak in dated channel abandonments.

In the Yeotown reach, a localised phase of multi-thread channel braiding is evident during W3 with elevated gravel surfaces and sandy alluvium suggesting a mobile channel system dominated by gravel bars with bar top sands. This is indicative of deposition during a period of increased bedload sediment supply (often associated with a highly variable discharge), with readily mobilised alluvial sediments (Schumm, 1981, 1985; Knighton, 1998). Within the same area of floodplain, the YW1 palaeochannel

shows a tortuous asymmetrical meander with evidence of meander rotation and channel abandonment by neck cut-off. The high sinuosity indicates a high stream power and discharge (Schumm and Khan, 1972; Edgar, 1984) and the proximal association with the braided channels suggests a climatically unstable period when fluctuating discharge promoted channel metamorphosis.

In the fluvio-estuarine transects zone, the stratigraphy of transects C and D both show phases of coarse grained channel aggradation with meander migration and lateral accretion of point bar deposits suggestive of a bed-load dominated regime with high discharge and high stream power. A possible storm surge deposit is also located in transect C (SW1) with an age of *c.*1300 cal.yr.AD, placing it at the W3-D4 boundary. This age corresponds with a period in Britain that is known to have been particularly prone to storms and exceptionally high tides caused by storm set-up (*e.g.* Robinson, 1970; Lamb, 1982; Gross and Butcher, 1995; Long and Hughes, 1995; Long *et al.*, 1998). At transect A there is evidence of enhanced tidal channel migration during the W3 interval which could indicate that the high discharge levels were contributing to geomorphic change in the fully estuarine zone.

The records of Holocene flood episodes for Britain (table 8.3) and Europe (Macklin *et al.*, 2005, 2006) show that a Europe-wide episode of fluvial instability occurred in W3 at 1290 cal.yr.AD. An example of fluvial instability in the English midlands is given by Brown, *et al.* (2001), where increased flood frequency and magnitude in the River Trent between the late 12th and early 15th centuries caused floodplain instability and channel metamorphosis, from a braided system, to an anastomosing state, through to a single channel meandering system. Similar channel instability and metamorphosis occurred in the Yeotown reach of the Taw during the 13th Century. This phase of fluvial instability in the UK has been associated with a significant climatic deterioration at the end of the Medieval Warm Period and beginning of the Little Ice Age (Rumsby & Macklin, 1996; Brown, 1998).

The W3 interval corresponds with a phase of high lake levels in mid-Europe during the 13th Century (Magny *et al.*, 2003), indicative of higher precipitation. The composite record of water table variability for northern Britain given by Charman *et al.* (2006) shows high water table levels prior to 1250 cal.yr.AD, while the end of the 13th Century sees a fall to average levels (figure 8.3).

D4 (1315-1420 cal.yr.AD)

D4 relates to a relatively dry climatic period with high estuarine palaeosalinity and low river discharge. This period corresponds with the later part of stratigraphic unit S4. This period is very sparsely represented by dated alluvial units (see figure 7.3) suggesting some channel stability with relatively low levels of fluvial discharge and stream power. The only unit which can be assigned to the D4 period with any certainty in the non-tidal fluvial reach is the low sinuosity YE2 abandoned channel in the fluvial Yeotown reach. This channel is infilled with organic detritus deposited within a closed abandoned channel pond, followed by clay deposition, indicating a period following abandonment of little overbank flooding, with gradual siltation of the pond by fine grained clay sediment that was possibly sourced from inwash from the surrounding terrace surface. The surrounding terrace alluvium suggests channel migration and lateral accretion of a sandy point bar prior to channel abandonment by avulsion. The YE2 site tends to support a D4 period in the 14th Century when river discharge levels were generally low, but also showed some fluctuation with occasional high magnitude high-stage floods. In the inner estuarine reach, the flood channel created by the *c.*1300 cal.yr.AD storm surge was subsequently occupied as a temporary fluvial flood channel, with later abandonment and infilling within a brackish tidal environment. Like the YE2 site, this suggests occasional high magnitude overbank flooding.

A drier climate is indicated during this period in the composite record of water table variability of Charman *et al.* (2006), with below-average water table levels between 1300 and 1420 cal.yr.AD (figure 8.3). Lower lake levels are also seen in mid-Europe between 1330 and 1420 cal.yr.AD (figure 8.3 and 8.5; Magny *et al.*, 2003; Magny, 2004). However, an episode of river instability and flooding is seen throughout Britain (table 8.3) and in Europe towards the end of D4 at 1380 cal.yr.AD (Macklin *et al.*, 2005, 2006). This suggests a period of fluctuating discharge (as seen in the Taw geomorphic record) with occasional high magnitude floods. The peak in numbers of Irish lake oaks that began at the start of D3 lasts through to *c.*1400 cal.yr.BP (figure 8.4; Turney *et al.*, 2005). This is indicative of a dry climate and low lake levels in Ireland during D4.

W4 (1420-1900 cal.yr.AD)

W4 relates to a relatively wet climatic period with low estuarine palaeosalinity and high river discharge. This period corresponds with stratigraphic units S11 and S12.

Significant amounts of floodplain alluviation and aggradation (T2) occur at this time throughout the inner estuarine and non-tidal fluvial reaches of the Taw valley. This is associated with a prolonged period of channel migration, aggradation and floodplain reworking with large areas of floodplain creation occurring through lateral accretion of relatively coarse grained estuarine and fluvial channel sediment. This suggests a regime of high discharge and high stream power throughout much of W4 (Schumm and Khan, 1972; Edgar, 1984; Blum and Tornqvist, 2000). Active channel migration was also evident in the tidal meanders of transect A. This may have been accentuated by a period of increased marine influence, with a transgressive overlap recorded in the 15th Century at 1433-1485 cal.yr.AD (1 σ age). The Taw flood record (figure 7.7) indicates a peak in dated channel abandonments (*e.g.* at SW4 and YE1) occurring at the start of this period in the 15th Century, with the surface geomorphology indicating that abandonment usually occurred by avulsion after sustained periods of lateral channel migration. The regime of high discharge and high stream power is seen to continue into the early 19th Century, when large-scale incision and continuing channel migration initiated the creation of the modern floodplain. A 19th Century large magnitude flood caused significant overbank floodplain scour at the SW2 site.

This period corresponds with the climatic deterioration that is associated with the Little Ice Age. A major flooding episode has been identified in the British fluvial archive at 1550 cal.yr.AD (Macklin and Lewin, 2003). A shift to a wet climate with high precipitation is also seen by a prolonged phase of high lake levels in mid-Europe (Magny *et al.*, 2003; Magny, 2004). A similar pattern is seen in peatland climate records, with the composite record of Charman *et al.* (2006) showing a prolonged period of high water tables in northern Britain between 1450 and 1880 cal.yr.AD. In the Brecon Beacons of south Wales (which is relatively close to south-west England), a mire wet shift at the start of W4 at 1460 cal.yr.AD indicates a climatic deterioration to wetter conditions (Blackford and Chambers, 1991). Lamb (1982) reports a large increase in documented reports of severe weather in the early 15th Century, with the 1430's being particularly prone to prolonged cold winters and wet summers. In the beginning of the 15th Century, wheat growing appears to have been generally abandoned in northern Europe (Lamb, 1984) due to the change in weather conditions. A decline in Irish lake oaks is seen in W4 (Turney *et al.*, 2005), giving support to a wet climatic period with high lake levels.

D5 (1900-2000 cal.yr.AD)

D5 relates to the relatively dry modern period after *c.*1870 cal.yr.AD when there was an increase in estuarine palaeosalinity caused by a general reduction in river discharge. Relatively minor amounts of meander migration of floodplain creation have occurred, although the coarse grained nature of the S13 lateral accretion deposits indicates a continuance of a bed-load dominated system.

The stacked peatland record of water table variability in northern Britain (Charman *et al.*, 2006) shows a substantial dry-shift after *c.*1880 cal.yr AD with water tables falling to levels not seen since the Roman Optimum (3rd and 4th Centuries AD). This switch to a drier climate is replicated by a reduction in mid-European lake levels (Magny *et al.*, 2003; Magny, 2004).

In summary, there is generally good agreement between the late Holocene Taw Estuary palaeosalinity-based record and other proxy climate records, historical accounts, and the local geomorphic record. Exceptions include evidence of a slightly more prolonged dry phase (D1, 520-780 cal.yr.AD) in south-west England during the 5th Century AD. The short D2 (780-850 cal.yr.AD) dry period is not seen in the composite water table record of northern Britain (Charman *et al.*, 2006) or in the Irish lake oak record (Turney *et al.*, 2005). However, there is evidence of a short dry phase in some individual peatland records (*e.g.* Barber, 1981) and there is some historical support for a dry period in Britain and Europe at this time (Lamb, 1982). There is general agreement for a wet climate during the W2 period (850-1030 cal.yr.AD), but most historical and peatland records suggest that this wet phase ended at *c.*950 cal.yr.AD. The dry D3 (1030-1215 cal.yr.AD) phase coincides with the peak of the Medieval Warm Period (Hughes and Diaz, 1994), and a dry climate is given support in the Irish lake oak record (Turney *et al.*, 2005) and historical documents (Lamb, 1982). However, the composite water table record of northern Britain (Charman *et al.*, 2006) indicates a rise in water tables at the end of this phase in the late 11th Century and this is given support by some evidence of geomorphic instability in the local Taw valley fluvial record at this time. During the wet W3 period (1215-1315 cal.yr.AD), there is general support for a wet climatic phase, with the exception of the Irish lake oak record (Turney *et al.*, 2005), which suggests a continuation of a dry phase. During D4 (1315-1420 cal.yr.AD), a dry climate is supported by proxy climate records, including the composite water table record, but some climatic instability is indicated at the end of the 14th Century by a Europe wide

flood episode at 1380 cal.yr.AD (Macklin *et al.*, 2005, 2006). The timing of the W4 wet period (1420-1900) gets all-round support from climate and historical records, and largely coincides with the 'Little Ice Age' cold phase. The composite water table record of northern Britain (Charman *et al.*, 2006) and the mid-European lake level record (Magny, 2004) both support a significant switch to a dry climate in the 20th Century (D5).

The above account indicates that there is generally good agreement between the identified Taw Estuary palaeo-climatic periods and with other late Holocene proxy climate records in Britain and Europe. This correlation is also supported by historical documentation of climate change and with local geomorphic evidence for periods of fluvial instability. This shows that records of changes in estuarine palaeosalinity allow new regional precipitation-based climate records to be reconstructed. These can be used on the UK and elsewhere to supplement existing proxy climate records. Unlike peatland climate records, which are based in northern Britain and Ireland, or lake-level records, that mainly come from mid and southern Europe, the estuaries of southern Britain offer the opportunity to reconstruct palaeosalinity-based climate records that are more specific to southern England. In areas of the world that are effected by recent late 20th Century trends of increasing aridity and/or increased storminess, late Holocene reconstructions of palaeo-climate are becoming increasingly important, in order for the recent, possibly human-induced climate change to be put into context. New palaeosalinity-based reconstructions of palaeo-river discharge can therefore provide an important contribution to this endeavour.

9 CONCLUSIONS

The conclusions of this research will now be referenced to the original aims and objectives (section 1.2).

1. **Contemporary zonation of diatoms and environmental variables in the tidal frame**

This contemporary distribution of diatoms in middle Taw estuary was seen to show a zonation that could be related to elevation in the tidal frame. Four diatom zones were identified and these showed a strong correspondence with the vertical vegetation zones. Diatom zones related to tidal flat, pioneer – mid saltmarsh, high saltmarsh and marsh border sub-environments. MHWST was located at the high saltmarsh and marsh border zone boundary. This zonation of species can be used as a local qualitative modern analogue of diatom distribution in a macro-tidal environment, that can be used to help define palaeo-marsh surface elevation in Holocene sediment cores.

Various sedimentological characteristics, such as carbonate content, organic matter content and magnetic mineral concentration also showed changes that related to elevation and frequency of tidal inundation. These can therefore be used as additional indicators of palaeo-environment. Variation in pore-water salinity was seen to be relatively minor when measured along an elevation-related tidal flat - saltmarsh gradient. However, as seen in other studies, significant variations in salinity do occur between tides.

2. **Relative sea-level reconstruction**

RSL change since *c.*6600 cal.yr.BP was successfully reconstructed in the Taw Estuary, with eleven new SLIPs providing evidence of former MSL. Three of these SLIPs are from the last 1300 yrs (a rarity in southern England RSL records), enabling trends in RSL rise to be analysed for the entire mid-late Holocene. A slowdown in RSL rise is evident at *c.*5500 cal.yr.BP, and another minor slowdown is seen at *c.*2250 cal.yr.BP (although this may be related to differential core compaction). The magnitude and rates of RSL rise in north Devon were compared with other RSL records in southern Britain.

These regional comparisons indicate that a NNW-SSE trending geographic band, stretching from the outer Bristol Channel (including both the South Wales and North Devon coasts), through to the inner Severn Estuary and Somerset Levels, through to the central south coast, near the Solent, has experienced a similar postglacial isostatic history of crustal subsidence during the mid-late Holocene. The resolution of the Taw Estuary RSL record allowed it to be used to test two slightly differing geophysical models of GIA change in Devon (models by Peltier *et al.*, 2002 and Shennan *et al.*, 2006). The error envelope of the Taw Estuary reconstruction was found to be very similar to the RSL changes predicted by the Shennan *et al.* (2006) model, suggesting that this model may offer a closer reflection of crustal isostatic adjustments in the south of England.

3. The contemporary salinity gradient and diatom distribution

This study has provided a new record of contemporary diatom distribution along the salinity gradient of a tidal river, from the inner estuary to the freshwater fluvial zone. Two diatom zones were identified downstream of the salinity front, with mixed assemblages of marine, brackish and freshwater species. Upstream of the salinity front, two more diatom zones were identified, with the first subzone, associated with the freshwater tidal reach, indicating that small numbers of polyhalobous valves can be transported into the freshwater tidal zone (possibly reworked during the process of freshwater back-up). Evidence of slightly brackish conditions upstream of the tidal head was indicated by several subzones with minor brackish assemblage components (dominated by *Navicula avenacea* and *Navicula phyllepta*). An essentially pure freshwater environment was found 4 km upstream of the HAT tidal head, indicating the maximum distance of saline groundwater intrusion. The presence of these minor brackish components (dominated by specific species) upstream of the salinity front and tidal head can be used as an important indication of former proximity to the estuarine environment in the palaeo-records of lowland Holocene valley-fills.

The relationship between location in the salinity gradient and a range of sedimentary variables was investigated. Estuarine levels of carbonate were found right up to the start of the freshwater tidal zone, with a significant peak in carbonate occurring 2-3 km downstream of the salinity front. This coincided with a peak in planktonic and

tychoplanktonic diatoms, suggesting that this was the location of the turbidity maximum.

4. Palaeosalinity reconstruction

An investigation of mineral magnetic parameters in cores located along the salinity gradient (and through χ_{fr} and $\chi_{fd\%}$ measurements of surface sediments) reveal that remanence measurements in particular can be used to determine sediment source and the degree of marine or freshwater influence, and therefore location in the salinity gradient. This is based on the identification of minerals associated with the estuarine environment (*e.g.* biogenic magnetite and authigenic greigite), or the catchment environment (*e.g.* soil-derived magnetite).

The late Holocene palaeosalinity record of the inner Taw Estuary was reconstructed from multiple cores using diatom salinity index as a proxy for salinity. The results show that this is only possible if former tidal frame zones are identified first, in order for similar tidal elevations (*e.g.* high saltmarsh or mid saltmarsh) to be analysed for spatial and temporal changes separately. This separation is needed because diatom assemblage composition is controlled by both elevation (frequency of tidal inundation) and mean water salinity.

Nine centennial to multi-centennial periods of below-average or above-average palaeosalinity have been recognised in the Taw Estuary since 300 cal.yr.AD. These fluctuations in salinity are used to infer changes in climate-driven freshwater influx into the estuarine environment. This allowed the creation of a new palaeo-climatic record for southern Britain during the late Holocene. Four intervals of high river discharge and above-average precipitation are identified at 520-780, 850-1030, 1215-1315, and 1420-1900 cal.yr.AD. Five intervals of low river discharge and below-average precipitation are identified at 300-520, 780-850, 1030-1215, 1315-1420, and 1900-2000 cal.yr.AD. This shows that there has been significant climatic variation in southern Britain since *c.*300 cal.yr.AD, with climatic shifts evident in the inner estuarine record.

There has been no background trend of increasing salinity in the Taw Estuary during the last 1700 yrs, despite continuing RSL rise. This gives support to the argument that the

recorded fluctuations in palaeosalinity relate to climate-driven river discharge changes and not fluctuations (oscillations) in late Holocene RSL rise.

The inferred changes in precipitation-driven river discharge were validated by comparing the identified dry and wet climatic periods with local geomorphic evidence of fluvial instability and with other proxy climate records from the UK and Europe. A strong correspondence was found between the identified climatic periods and the local geomorphic fluvial history and flood record of the lower Taw valley (reconstructed in aim 5, see below). Periods of fluvial instability and geomorphic change are seen to correlate with periods of low estuarine palaeosalinity and periods of fluvial stability are seen to correlate with periods of high estuarine palaeosalinity (low river discharge). Comparisons with other proxy climate records and historical accounts of late Holocene climate change also show a high degree of correspondence with the Taw Estuary climate record.

5. Geomorphic evolution and fluvial flood record

In order to provide validation of the palaeosalinity-based record of changes in fluvial discharge, the local geomorphic fluvial history and flood record of the lower Taw valley was reconstructed. The entire fluvial and estuarine zone study area was split into a series of 13 stratigraphic units, covering the late glacial and Holocene. This stratigraphic division was based on the geomorphology, geochronology and lithostratigraphy of the Holocene valley-fill. Dated phases of active channel change and fluvial instability were identified. This indicated several periods of significant geomorphic change, with evidence of floodplain creation and reworking, and channel abandonment and avulsion events. These periods were also often associated with coarser grained bedload and overbank sedimentation and periods of channel aggradation. The main periods of increased geomorphic activity occurred in the late Holocene at *c.*600-750, *c.*1170-1270 and *c.*1400-1600 cal.yr.AD. This last period is thought to have extended until 1850 cal.yr.AD. Another period of finer grained floodplain creation occurred at *c.*850-950 cal.yr.AD, but this was poorly dated. There is also evidence of possible intermittent instability during the mid-late 14th Century.

Fluvial instability was usually found to translate down river into the inner estuarine system with corresponding periods of enhanced tidal channel migration and estuarine

channel-bed aggradation. A period of enhanced estuarine incision between 200 cal.yr.BC and 100 cal.yr.AD is thought to have been related to a phase of increased marine influence and estuary expansion. There is diatom and sedimentary evidence of two possible storm surges in the late Holocene. The largest is thought to have occurred in the 3rd Century AD, with marine planktonic diatoms swept several km upstream of the current tidal head. This event may have even been associated with the avulsion of the estuarine channel at the TS1 core. There is evidence of another significant storm surge at *c.*1300 cal.yr.AD, a period known for large coastal storms and exceptionally high tides, especially on the North Sea coast. Geomorphic change in the inner estuarine zone therefore appears to be mainly influenced by phases of increased river discharge and catchment precipitation, even though most of the sediment is sourced from the estuary on tidal currents. However, more extreme changes in the marine realm do result in inner estuarine geomorphic change. Examples of these in the Taw Estuary are the short, but significant transgressive phase after *c.*200 cal.yr BC, possibly caused by a significant RSL oscillation, and evidence of two possible storm surges in the 3rd and early 14th Centuries AD.

APPENDIX

The Appendix is saved as a Microsoft Excel file and can be found in the CD attached to the back cover of this Thesis.

This appendix contains the raw diatom count data for all core samples and modern surface samples. This file also contains a complete diatom species list for the Taw Estuary and lower Taw valley.

BIBLIOGRAPHY

- Aaby, B. and Berglund, B.E. (1986) Characterization of peat and lake sediments. In: Berglund, B.J. (ed), *Handbook of Holocene Palaeoecology and Palaeohydrology*, 231-246. John Wiley and Sons, Chichester.
- Admiralty Tide Tables (2007) European Waters including the Mediterranean Sea, Vol.1. Hydrographer to the Navy, Admiralty Hydrography Department, Taunton.
- Admiralty Tide Tables (2008) European Waters including the Mediterranean Sea. Vol. 1. Hydrographer to the Navy, Admiralty Hydrography Department, Taunton.
- Aitken, M.J. (1976) Thermoluminescent age evaluation and assessment of error limits: revised system. *Archaeometry*, **18**, 233-238.
- Aitken, M.J. (1985) *Thermoluminescence Dating*. Academic Press, London (359 pp).
- Aitken, M.J. (1998) *An Introduction to optical dating: the dating of Quaternary sediments by the use of photon-stimulated luminescence*. Oxford University Press.
- Aitken, M.J. and Alldred, J.C. (1972) The assessment of error limits in thermoluminescent dating. *Archaeometry*, **14**, 257-267.
- Allen, G.P. (1996) The sequence of early land-claims on the Walland and Romney Marshes, southern Britain: a preliminary hypothesis and some implications. *Proceedings of the Geologists' Association*, **107**, 271-280.
- Allen, G.P. and Posamentier, H.W. (1993) Sequence stratigraphy and facies model of an incised valley fill: the Gironde Estuary, France. *Journal of Sedimentary Petrology*, **63**, 378-391.
- Allen, J.R.L. (1990) Salt-marsh growth and stratification: a numerical model with special reference to the Severn Estuary, southwest Britain. *Marine Geology*, **95**, 77-96.
- Allen, J.R.L. (1999) Geological impacts on coastal wetland landscapes: some general effects of sediment autocompaction in the Holocene of northwest Europe. *Holocene*, **9**, 1-12.
- Allen, J.R.L. (2000) Morphodynamics of Holocene salt marshes: a review sketch from the Atlantic and Southern North Sea coasts of Europe. *Quaternary Science Reviews*, **19**, 1155-1231.

- Allen, J.R.L. (2003) An eclectic morphostratigraphic model for the sedimentary response to Holocene sea-level rise in northwest Europe. *Sedimentary Geology*, **161**, 31-54.
- Anderson, D.E. (1998) A reconstruction of Holocene climatic changes from peat bogs in north-west Scotland. *Boreas*, **27**, 208-224.
- Austin, R.M. (1991) Modelling Holocene tides on the NW European continental shelf. *Terra Nova*, **3**, 276-288.
- Bailiff, I.K. and Tooley, M.J. (2000) Luminescence dating of fine-grain Holocene sediments from a coastal setting. In: Shennan, I. and Andrews, J. (eds), *Holocene Land-Ocean Interaction and Environmental Change around the North Sea*. Geological Society, London, Special Publications, **166**, 55-67.
- Baker, V.R. (2003) Palaeofloods and Extended Discharge Records, In: Gregory, K.J. and Benito, G. (eds) *Palaeohydrology: Understanding Global Change*. Wiley.
- Barber, H.G. and Haworth, E.Y. (1981) *A guide to the morphology of the diatom frustule*. Freshwater Biological Association Paper, 44.
- Barber, K.E. (1981) *Peat stratigraphy and climatic change: a palaeoecological test of the theory of cyclic peat bog regeneration*. Balkema, Rotterdam.
- Barber, K.E. (1994) Deriving Holocene paleoclimates from peat stratigraphy: some misconceptions regarding the sensitivity and continuity of the record. *Quaternary Newsletter*, **72**, 1-9.
- Barber, K.E., Battarbee, R.W., Brooks, S.J., Eglinton, G., Haworth, E.Y., Oldfield, F., Stevenson, A.C., Thompson, R., Appleby, P.G., Austin, W.E.N., Cameron, N.G., Ficken, K.J., Golding, P., Harkness, D.D., Holmes, J.A., Hutchinson, R., Lishman, J.P., Maddy, D., Pinder, L.C.V., Rose, N.L. and Stoneman, R.E. (1999) Proxy records of climate change in the UK over the last two millennia: documented change and sedimentary records from lakes and bogs. *Journal of the Geological Society, London*, **156**, 369-380.
- Bayliss-Smith, T.P., Healey, R., Lailey, R., Spencer, T. and Stoddart, D.R. (1979) Tidal flow in salt marsh creeks. *Estuarine, Coastal and Marine Science*, **9**, 235-255.
- Battarbee, R.W. (1986) Diatom Analysis. In: Berglund, B.J. (ed), *Handbook of Holocene Palaeoecology and Palaeohydrology*, 527-570. John Wiley and Sons, Chichester.
- Beckett, S.C. and Hibbert, F.A. (1979) Vegetational change and the influence of prehistoric man in the Somerset Levels. *New Phytologist*, **83**, 577-600.

- Berger, G.W. (1990) Effectiveness of natural zeroing in of the thermoluminescence in sediments. *Journal of Geophysical Research*, **95**, 12375-12397.
- Bird, M.I., Fifield, L.K., Chua, S. and Goh, B. (2004) Calculating sediment compaction for radiocarbon dating of intertidal sediments. *Radiocarbon*, **46**, 421-435.
- Birks, H.J.B. (1986) Numerical zonation, comparison and correlation of Quaternary pollen-stratigraphical data. In: Berglund, B.E. (ed) *Handbook of Holocene Palaeoecology and Palaeohydrology*, 743-773. Wiley, London.
- Birks, H.J.B. and Birks, H.H. (1980) *Quaternary Palaeoecology*. Edward Arnold, London.
- Bjorck, S. and Wohlfarth, B. (2001) ^{14}C chronostratigraphic techniques in paleolimnology. In: Last, W.M. and Smol, J.P. (eds) *Tracking environmental change using lake sediments. Vol 1: Basin analysis, coring and chronological techniques*, 205-245. Kluwer Academic Publishers, Dordrecht, The Netherlands.
- Blackford, J.J. and Chambers, F.M. (1991) Proxy records of climate from blanket mires: evidence for a Dark Age (1400 BP) climatic deterioration in the British Isles. *The Holocene*, **1**, 63-67.
- Blackford, J.J. and Chambers, F.M. (1995) Proxy climate record for the last 1000 years from Irish blanket peat and a possible link to solar variability. *Earth and Planetary Science Letters*, **133**, 145-150.
- Blakemore, R.P. (1982) Magnetotactic bacteria. *Annual Review of Microbiology*, **36**, 217-238.
- Blong, R.J. and Gillespie, R. (1978) Fluvially transported charcoal gives erroneous ^{14}C ages for recent deposits. *Nature*, **271**, 739-741.
- Bloom, A.L. (1964) Peat accumulation and compaction in a Connecticut coastal marsh. *Journal of Sedimentary Petrology*, **34**, 599-603.
- Blum, M.D. and Tornqvist, T.E. (2000) Fluvial responses to climate and sea-level change: a review and look forward. *Sedimentology*, **47** (suppl.1), 2-48.
- Blundell, A.C. and Barber, K.E. (2005) A 2800-year palaeoclimatic record from Tore Hill Moss, Speyside, Scotland: the need for a multi-proxy approach to peat based climate reconstructions. *Quaternary Science Reviews*, **24**, 1261-1277.
- Blundell, A.C., Charman, D.J. and Barber, K. (2008) Multiproxy late Holocene peat records from Ireland: towards a regional palaeoclimate curve. *Journal of Quaternary Science*, **23**, 59-71.

- Bond, G., Kromer, B., Muscheler, R., Evans, M.N., Showers, W., Hoffman, S., Lottibond, R., Hajdas, I. and Bonani, G. (2001) Persistent solar influence on North Atlantic climate during the Holocene. *Science*, **294**, 2130-2136.
- Borcard, D., Legendre, P. and Drapeau, P. (1992) Partialling out the spatial component of ecological variation. *Ecology*, **73**, 1045-1055.
- Bowen, D.Q., Rose, J., McCabe, A.M. and Sutherland, D.G. (1986) Correlation of Quaternary glaciations in England, Ireland, Scotland and Wales. *Quaternary Science Reviews*, **5**, 299-340.
- Bowman, S. (1990) *Radiocarbon dating*. British Museum. London.
- Bronk Ramsey, C. (2001) Development of the Radiocarbon calibration program OxCal. *Proceedings of the 17th International 14C Conference*. *Radiocarbon*, **43**, 355-363.
- Brown, A.P. (1977) Late Devensian and Flandrian vegetational history of Bodmin Moor, Cornwall. *Philosophical Transactions of the Royal Society of London*, **B276**, 251-320.
- Brown, A.G. (1987) Long-term Sediment Storage in the Severn and Wye Catchments, In: Gregory, K.J., Lewin, J. and Thornes, J.B. (eds) *Palaeohydrology in Practice*, Wiley.
- Brown, A.G. (1998) Fluvial evidence of the Medieval Warm Period and the Late Medieval Climatic Deterioration, In: Benito, G., Baker, G. and Gregory, V.R. (eds), *Palaeohydrology and Environmental Change*. Wiley, 43-52.
- Brown, A.G. and Barber, K.E. (1985) Late Holocene palaeoecology and sedimentary history of a small lowland catchment in Central England. *Quaternary Research*, **24**, 87-102.
- Brown, A.G., Cooper, L., Salisbury, L.C.R. and Smith, D.N. (2001) Late Holocene channel changes of the Middle Trent: channel response to a thousand-year flood record. *Geomorphology*, **39**, 69-82.
- Brown, S.L., Warman, E.A., McGrorty, S., Yates, M., Pakeman, R.J., Boorman, L.A., Goss-Custard, J.D. and Gray, A.J. (1999) Sediment fluxes in intertidal biotopes: BIOTA II. *Marine Pollution Bulletin*, **37**, 173-181.
- Bryant, E.A. and Haslett, S.K. (2002) Was the AD1607 coastal flooding event in the Severn Estuary and Channel (UK) due to a tsunami? *Archaeology in the Severn Estuary*, **13**, 163-167.

- Bryne, R., Ingram, B.L., Starratt, S. and Malamud-Roam, F. (2001) Carbon-isotope, Diatom, and pollen Evidence for Late Holocene salinity change in a brackish marsh in the San Francisco Estuary. *Quaternary Research* **55**, 66-76.
- Buckland, P.C. and Sadler, J. (1985) The nature of late Flandrian alluviation in the Humberhead Levels. *The East Midland Geographer*, **8**, 239-251.
- Cant, D.J. and Walker, R.G.(1978) Fluvial processes and facies sequences in the sandy braided South Saskatchewan River. *Sedimentology*, **26**, 625-648.
- Carrión, J.S. (2002) Patterns and processes of Late Quaternary environmental change in a montane region of southwestern Europe. *Quaternary Science Reviews*, **21**, 2047-2066.
- Caseldine, C.J., Coles, B.J., Griffith, F.M. and Hatton, J.M. (2000) Conservation or Change? Human Influence on the Mid-Devon Landscape. In: Nicholson, R.A. and O'Connor, T.P. (eds) *People as an Agent of Environmental Change*, Symposia of the Association for Environmental Archaeology No.16, 60-70.
- Chambers, F.M., Barber, K.E., Maddy, D. and Brew, J. (1997) A 5500-year proxy-climate and vegetation record from blanket mire at Talla Moss, Borders, Scotland. *The Holocene*, **7**, 391-399.
- Charman, D.J., Blundell, A., Chiverrell, R.C., Hendon, D. and Langdon, P.G. (2006) Compilation of non-annually resolved Holocene proxy climate records: stacked Holocene peatland palaeo-water table reconstructions from northern Britain. *Quaternary Science Reviews*, **25**, 336-350.
- Chiverrell, R.C. (2001) A proxy record of late Holocene climate change from May Moss, northeast England. *Journal of Quaternary Science*, **16**, 9-29.
- Chmura, G.L. and Aharon, P. (1995) Stable carbon isotope signatures of sedimentary carbon in coastal wetlands as indicators of salinity regime. *Journal of Coastal Research*, **11**, 124-135.
- Collinson, J.D. (1996) Alluvial sediments, In: Reading, H.G. (ed), *Sedimentary Environments: Processes, Facies and Stratigraphy*, 3rd edn, pp 37-82.
- Cooper, S.R. (1999) Estuarine palaeoenvironmental reconstructions using diatoms. In: Stoemer, E.F. and Smol, J.P. *The Diatoms: Applications for the environmental and earth sciences*. Cambridge University Press, Cambridge, 352-373
- Coulthard, T.J, and Macklin, M.G. (2001) How sensitive are rivers to climate and land-use changes? A model-based approach. *Journal of Quaternary Science*, **16**, 347-351.

- Cronin, T., Willard, D., Karlsen, A., Ishman, S., Verardo, S. McGeehin, J., Kerhin, R., Holmes, C., Colman, S. and Zimmerman, A. (2000) Climatic variability in the eastern United States over the past millennium from Chesapeake Bay sediments. *Geology*, **28**, 3-6.
- Cronin, T.M., Thunell, R., Dwyer, G.S., Saenger, C., Mann, M.E., Vann, C. and Seal, R.R. (2005) Multiproxy evidence of Holocene climate variability from estuarine sediments, eastern North America. *Paleoceanography*, **20**, PA4006.
- Cullingford, R.A., Caseldine, C.J. and Gotts, P.E. (1980) Early Flandrian land and sea level changes in Lower Strathearn. *Nature*, **284**, 159-161.
- Dalrymple, R.W. and Zaitlin, B.A. (1994) High-resolution sequence stratigraphy of a complex, incised valley succession, Cobequid Bay – Salmon River estuary, Bay of Fundy, Canada. *Sedimentology*, **41**, 1069-1091.
- Dalrymple, R.W., Knight, R.J., Zaitlin, B.A. and Middleton, G.V. (1990) Dynamics and facies model of a macrotidal sand-bar complex, Cobequid Bay, Salmon River Estuary, Bay of Fundy, *Sedimentology*, **37**, 577-612.
- Dalrymple, R.W., Zaitlin, B.A. and Boyd, R. (1992) Estuarine facies models: conceptual basis and stratigraphic implications. *Journal of Sedimentary Petrology*, **62**, 1130-1146.
- Davis, O.K. (1992) Rapid climatic change in coastal southern California inferred from pollen analysis of San Joaquin Marsh. *Quaternary Research*, **37**, 89-100.
- Dawson, M.R. and Gardiner, V. (1987) River Terraces: the general model and a palaeohydrological and sedimentological interpretation of the terraces of the Lower Severn, In: Gregory, K.J., Lewin, J. and Thornes, J.B. (eds) *Palaeohydrology in Practice*. Wiley.
- De Vries, H. (1958) Variation in concentration of radiocarbon with time and location on earth. *Koninkijk Nederlandse Akademie von Wetenschappen, Amsterdam, Proceedings*, **B61**, 94-102.
- Dean, W.E. (1974) Determination of carbonate and organic matter in calcareous sediments and sedimentary rocks by loss on ignition: comparison with other methods. *Journal of Sedimentary Petrology*, **44**, 242-248.
- Dearing, J.A. (1986) Core correlation and total sediment influx. In: Berglund, B.J. (ed), *Handbook of Holocene Palaeoecology and Palaeohydrology*, 247-270. John Wiley and Sons, Chichester.

- Dearing, J.A. (1999) Magnetic Susceptibility. In: Walden, J., Oldfield, F. and Smith, J.P. (eds), *Environmental Magnetism: a practical guide*, 35-62. Technical Guide 6, Quaternary Research Association, London.
- Delworth, T. and Mann, M. (2000) Observed and simulated multi-decadal variability in the Northern Hemisphere. *Climate Dynamics*, **16**, 661-676.
- Denys, L. (1991-1992) A check-list of the diatoms in the Holocene deposits of the western Belgian coastal plain with a survey of their apparent ecological requirements. Professional Paper 246, In: *De Lescluzestraat*, **68**, B2600 Berchum, Belgium.
- Devoy, R.J.N. (1979) Sea level changes in the Thames Estuary. *Philosophical Transactions of the Royal Society of London B*, **285**, 388-407.
- Devoy, R.J.N. (1982) Analysis of the geological evidence for Holocene sea-level movements in southeast England. *Proceedings of the Geologists' Association*, **93**, 65-90.
- Donnelly, J.P., Cleary, P., Newby, P. and Ettinger, R. (2004) Coupling instrumental and geological records of sea-level change: evidence from southern New England of an increase in the rate of sea-level rise in the late 19th century. *Geophysical Research Letters*, **31**, L05203. doi: 10.1029/2003GL018933.
- Duller, G.A.T. (2004) Luminescence dating of Quaternary sediments: recent advances *Journal of Quaternary Science*, **19**(2), 183-192
- Dyer, K.R. (1972) Sedimentation in estuaries, In: Barnes, R.S.K. and Green, J. (eds), *The Estuarine Environment*. Applied Science Publications, London.
- Edgar, D.E. (1984) The role of geomorphic thresholds in determining alluvial channel morphology, In: Elliott, C.M. (ed.), *River meandering*. American Society of Civil Engineers, New Orleans, 44-54.
- Edmonds, E.A., Williams, B.J. and Taylor, R.T. (1979) Geology of Bideford and Lundy Island. *Memoir of the British Geological Survey for geological sheets 292, with 275, 276, 291 and part of 308, New Series*. HMSO, London.
- Edmonds, E. A., Whittaker, A. and Williams, B. J. (1985) Geology of the country around Ilfracombe and Barnstaple. Memoir of the British Geological Survey for geological sheets 277 and 293, New Series, HMSO, London.
- Edwards, R.J. (2001) Mid- to late Holocene relative sea-level change in Poole Harbour, southern England. *Journal of Quaternary Science*, **16**, 221-235.

- Edwards, R.J. (2006) Mid- to late-Holocene relative sea-level change in southwest Britain and the influence of sediment compaction. *The Holocene*, **16**(4), 575-587.
- Edwards, R.J. (2000) Reconstructing relative sea-level change using UK salt-marsh foraminifera. *Marine Geology*, **169**, 41-56.
- Evans, M.E. and Heller, F. (2003) *Environmental Magnetism: Principles and Applications of Enviromagnetics*. Elsevier Science, London.
- Fairbridge, R.W. (1980) The estuary: its definition and geodynamic cycle. In: Olausson, E. and Cato, I. (eds) *Chemistry and biochemistry of estuaries*. New York, Wiley, p.1-35.
- Fassbinder, J.W.E. and Stanjek, H. (1994) Magnetic properties of biogenic soil greigite (Fe₃S₄). *Geophysical Research Letters*, **21**, 2349-2352.
- Fletcher, C.H., Knebel, H.J. and Kraft, J.C. (1990) Holocene evolution of an estuarine coast and tidal wetland. *Geological Society of America, Bulletin*, **102**, 283-297.
- Fofonoff, P. and Millard Jr., R.C. (1983) Algorithms for computation of fundamental properties of seawater. *Unesco Technical Papers in Marine Science*, **44**.
- Foged, N (1974) *Freshwater Diatoms in Iceland*. Bibliotheca Phycologica, **15**. J. Cramer, Vaduz.
- Frankel, R.B. and Blakemore, R.P. (1989) Magnetite and magnetotaxis in microorganisms. *Bioelectromagnetics*, **10**, 223-237.
- French, J.R. (1993) Numerical simulation of vertical marsh growth and adjustment to accelerated sea-level rise, north Norfolk, UK. *Earth Surface Processes and Landforms*, **18**, 63-81.
- Frey, R.W. and Howard, J.D. (1986) Mesotidal estuarine sequences: a perspective from the Georgia Bight. *Journal of Sedimentary Petrology* **56**, 911-924.
- Fyfe, R.M. (2000) *Palaeochannels of the Exe catchment: their age and an assessment of their archaeological and palaeoenvironmental potential*. Unpublished PhD Thesis, University of Exeter.
- Fyfe, R.M., Brown, A.G. and Rippon, S.J. (2003) Mid to late Holocene vegetation history of Greater Exmoor, UK: estimating the spatial extent of human induced vegetation change. *Vegetation History and Archaeobotany*, **12**, 215-232.
- Gehrels, W.R. (1999) Middle and Late Holocene Sea-level changes in Eastern Maine reconstructed from Foraminiferal saltmarsh stratigraphy and AMS 14C dates on basal peat. *Quaternary Research*, **52**, 350-359.

- Gehrels, W.R. (2000) Using foraminiferal transfer functions to produce high-resolution sea-level records from salt-marsh deposits, Maine, USA. *Holocene*, **10**(3), 367-376.
- Gehrels, W.R., Belknap, D.F., Pearce, B.R. and Gong, B. (1995) Modeling the contribution of M₂ tidal amplification to the Holocene rise of mean high water in the Gulf of Maine and the Bay of Fundy. *Marine Geology*, **124**, 71-85.
- Gehrels, W.R., Belknap, D.F. and Kelley, J.T. (1996) Integrated high-precision analyses of Holocene relative sea-level changes: Lessons from the coast of Maine. *Geological Society of America Bulletin* **108**, 1073-1088.
- Gehrels, W.R., Roe, H.M. and Charman, D.J. (2001) Foraminifera, testate amoebae and diatoms as sea-level indicators in UK saltmarshes: a quantitative multiproxy approach. *Journal of Quaternary Science*, **16**(3), 201-220.
- Gehrels, W.R., Szkornik, K., Bartholdy, J., Kirby, J.R., Bradley, S.L., Marshall, W.A., Heinemeier, J. and Pedersen, J.B.T. (2006) Late Holocene sea-level changes and isostasy in western Denmark. *Quaternary Research*, **66**, 288-302.
- Gibbs, Z. (2000) *The origin of fine-grained magnetite in sediments*. Unpublished PhD Thesis, University of Liverpool.
- Gibson, J.R. and Najjar, R.G. (2000) The response of Chesapeake Bay salinity to climate-induced changes in streamflow. *Limnology and Oceanography*, **45**, 1764-1772.
- Godwin, H. (1948) Studies of the Post-Glacial History of British Vegetation, X. Correlation between Climate, Forest Composition, Prehistoric Agriculture and Peat Stratigraphy in Sub-Boreal and Sub-Atlantic Peats of the Somerset Levels. *Philosophical Transactions of the Royal Society of London, Series B, Biological Sciences*, **233** (600), 275-286.
- Godwin, H. and Willis, E.H. (1961) Cambridge University natural radiocarbon measurements III. *Radiocarbon*, **3**, 60-76.
- Gray, T. (ed) (1998) *Lost Chronicle of Barnstaple 1586-1611*. Devonshire Association, Exeter.
- Greensmith, J.T. and Tucker, E.V. (1986) Compaction and consolidation. In: Van der Plassche, O. (ed) *Sea-level research: a manual for the collection and evaluation of data*, 591-603. Geo Books, Norwich.
- Grimm, E. (1993) *TILIA: A pollen program for analysis and display*. Illinois State Museum, Springfield.
- Grimm, E.C. (2004) *TGView, version 2.0.2*. Illinois State Museum, Springfield.

- Gross, A. and Butcher, A. (1995) Adaption and investment in the age of the great storms: agricultural policy on the manors of the principal Lords of the Romney Marshes and the marshland fringe c.1250-1320, In: Eddison, J. (ed) *Romney Marsh: the debatable ground*, Oxford: Oxford University Committee for Archaeology, Monograph 41, 107-117.
- Grove, J.M. and Switsur, R. (1994) Glacial geological evidence for the medieval warm period. *Climatic Change*, **26**, 143-169.
- Haggart, B.A. (1986) Relative sea-level change in the Beaulieu Firth, Scotland, *Boreas*, **15**, 191-207.
- Hamilton, S. and Shennan, I. (2005) Late Holocene relative sea-level changes and the earthquake deformation cycle around upper Cook Inlet, Alaska. *Quaternary Science Reviews*, **24**, 1479-1498.
- Harms, J.C., McKenzie, D.B. and McCubbin, D.G. (1963) Stratification in modern sands of the Red River, Louisiana, *Journal of Geology*, **71**, 566-580.
- Hartley, B. (1996) *An Atlas of British Diatoms*. Biopress, Bristol.
- Hartley, B., Barber, H.G., Carter, J.R. and Sims, P.A. (1996) *An Atlas of British Diatoms*. Biopress, Bristol
- Haslett, S.K. and Bryant, E.A. (2004) The AD1607 coastal flood in the Bristol Channel and Severn Estuary: historical records from Devon and Cornwall (UK). *Archaeology in the Severn Estuary*, **15**, 81-89.
- Haslett, S.K., Davies, P., Curr, R.H.F., Davies, C.F.C., Kennington, K., King, C.P. and Margetts, A.J. (1998) Evaluating late-Holocene relative sea-level change in the Somerset Levels, southwest Britain. *The Holocene*, **8**, 197-207.
- Haslett, S.K., Howard, K.L., Margetts, A.J. and Davis, P. (2001) Holocene stratigraphy and evolution of the northern coastal plain of the Somerset Levels, UK. *Proceedings of the Cotteswold Naturalists' Field Club*, **XLII**, 42-52.
- Havelock, G.M. (2001) *Channel Equilibrium and Morphodynamics in a Norfolk Saltmarsh*. Unpublished MSc Thesis, University of Reading.
- Hawkins, C. (2005) *Vegetation History and land use change over the past 10,000 years in three study areas in lowland Devon: the Blackdown Hills, the Clyst Valley and the Hartland Peninsula*. Unpublished PhD thesis, University of Exeter.
- Healy, M.G. (1995) The lithostratigraphy and biostratigraphy of a Holocene coastal sediment sequence in Marazion Marsh, west Cornwall, UK, with reference to relative sea-level movements. *Marine Geology* **124**, 237-252.

- Hemphill-Haley (1995a) Diatom evidence for earthquake-induced subsidence and tsunami 300 years ago in southern coastal Washington. *Geological Society of America, Bulletin* **107**, 367-378.
- Hemphill-Haley, E. (1995b) Intertidal diatoms from Willapa Bay, Washington: application to studies of small-scale sea-level changes. *Northwest Science*, **69**(1), 29-45.
- Hemphill-Haley, E. (1996) Diatoms as an aid in identifying late-Holocene tsunami deposits. *The Holocene*, **6**, 439-448.
- Hendey, N.I. (1964) *An Introductory account of the smaller algae of British coastal waters, Bacillariophyceae (Diatoms)*. Fishery Investigation Series N., HMSO, London.
- Heyworth, A. and Kidson, C. (1982) Sea-level changes in southwest England and Wales. *Proceedings of the Geologists' Association*, **93**, 91-112.
- Hill, T.C.B., Woodland, W.A., Spencer, C.D. and Marriott, S.B. (2007) Holocene sea-level changes in the Severn Estuary, southwest England: a diatom-based sea-level transfer function for macrotidal settings. *The Holocene*, **17**(5), 639-648.
- Hilton, J. (1990) Greigite and the magnetic properties of sediments. *Limnology and Oceanography*, **35**, 497-508.
- Hinton, A.C. (1992) Palaeotidal changes within the area of the Wash during the Holocene. *Proceedings of the Geologists' Association*, **103**, 259-272.
- Hinton, A.C. (1995) Holocene tides of the Wash, U.K.: The influence of water-depth and coastline-shape changes on the record of sea-level change. *Marine Geology*, **124**, 87-111.
- Hinton, A.C. (1996) Tides in the Northeast Atlantic: considerations for modeling water depth changes. *Quaternary Science Reviews*, **15**, 873-894.
- Horton, B.P. (1999) The distribution of contemporary intertidal foraminifera at Cowpen Marsh, Tees Estuary, UK: implications for studies of Holocene sea-level changes. *Palaeogeography, Palaeoclimatology, Palaeoecology*, **149**, 127-149.
- Horton, B.P. and Edwards, R.J. (2005) The application of local and regional transfer functions to the reconstruction of Holocene sea levels, north Norfolk, England. *The Holocene*, **15**, 216-228.
- Horton, B.P., Edwards, R.J. and Lloyd, J.M. (1999) Reconstruction of former sea-levels using a foraminiferal-based transfer function: implications for sea-level studies. *Journal of Foraminiferal Research*, **29**, 117-129.

- Horton, B.P., Edwards, R.J. and Lloyd, J.M. (2000) Implications of a microfossil transfer function in Holocene sea-level studies. In: Shennan, I. and Andrews, J.E. (eds) *Holocene land-ocean interaction and environmental change around the western North Sea*. Geological Society Special Publication **166**, 41-54.
- Horton, B.P., Larcombe, P., Woodroffe, S.A., Whittaker, J.E., Wright, M.R. and Wynn, C. (2003) Contemporary foraminiferal distributions of a mangrove environment, Great Barrier Reef coastline, Australia: implications for sea-level reconstructions. *Marine Geology*, **198**, 225-243.
- Horton, B.P., Corbett, R., Culver, S.J., Edwards, R.J. and Hillier, C. (2006) Modern saltmarsh diatom distributions of the Outer Banks, North Carolina, and the development of a transfer function for high resolution reconstructions of sea level. *Estuarine, Coastal and Shelf Science*, **69**, 381-394.
- Horton, B.P., Zong, Y., Hillier, C and Engelhart, S. (2007) Diatoms from Indonesian mangroves and their suitability as sea-level indicators for tropical environments. *Marine Micropaleontology*, **63**, 155-168.
- Housley, R.A. (1988) The environmental context of Glastonbury Lake Village. *Somerset Levels Papers* **14**, 63-82.
- Howard, A.J. and Macklin, M.G. (1999) A generic geomorphological approach to archaeological interpretation and prospection in British river valleys: a guide for archaeologists investigating Holocene landscapes. *Antiquity*, **73**, 527-541.
- Howard, A.J., Macklin, M.G., Bailey, D.W., Mills, S. and Andreeson, R. (2004) Late-glacial and Holocene river development in the Teleorman Valley and the Southern Romanian Plain. *Journal of Quaternary Science*, **19**, 271-280.
- HR Wallingford (1990) *Barnstaple downstream study. Part I: An historical review of the Taw Estuary*. Report EX 1904.
- Hughes, M.K. and Diaz, H.F. (1994) Was there a 'Medieval Warm Period', and if so, where and when? *Climatic Change*, **26**, 109-142.
- Hustedt, F. (1930-1966) Die Kieselalgen Deutschlands, Oesterreich's und der Schweiz unter Berücksichtigung der übrigen Länder Europas sowie der angrenzenden Meeresgebiete. In: Rabenhorsts, L. (ed) *Kryptogamen-Flora von Deutschland, Osterreich, und der Schweiz*, **7**, Parts 1-3.
- Hustedt, F. (1953) Die Systematik der Diatomeen in ihren Beziehungen zur Geologie und Ökologie nebst einer Revision des Halobien-systems. *Svensk Botanisk Tidskrift*, **47**, 509-519.

- Hustedt, F. (1957) Die Diatomeenflora des Fluss Systems der Weser im Gebiet der Hansestadt Bremen. *Abhandlungen herausgegeben vom Naturwissenschaftlichen Verein zu Bremen*, **34**, 181-440.
- Hustedt, F. and Aleem, A.A. (1951) Littoral diatoms from the salstone, near Plymouth. *Journal of Marine Biological Association*, **30**, 177-196.
- Ingram, B.L., Ingle, J.C. and Conrad, M.E. (1996) Stable isotope record of late Holocene salinity and river discharge in San Francisco Bay, California. *Earth and Planetary Science Letters*, **141**, 237-247.
- Jacobs, Z. (2008) Luminescence chronologies for coastal and marine sediments. *Boreas*, **37**, 508-535.
- Jennings, S., Orford, J.D., Canti, M., Devoy, R.J.N. and Straker, V. (1998) The role of relative sea-level rise and changing sediment supply on Holocene gravel barrier development: the example of Porlock, Somerset, UK. *The Holocene*, **8**, 165-181.
- Johnstone, E. (2004) *River response to late quaternary environmental change: the Dyfi catchment, mid-Wales*. Unpublished Ph.D. Thesis, University of Wales, Aberystwyth.
- Jones, A.P., Tucker, M.E. and Hart, J.K. (1999) *The Description and Analysis of Quaternary Stratigraphic Field Sections*. Technical Guide 7, Quaternary Research Association, London.
- Juggins, S. (1992) Diatoms in the Thames Estuary, England: ecology, palaeoecology, and salinity transfer function. *Bibliotheca Diatomologica*, **Band 25**, 205pp.
- Kaye, C.A. and Barghoorn, E.S. (1964) Late Quaternary sea-level change and crustal rise at Boston, Massachusetts, with notes on the autocompaction of peat. *Geological Society of America Bulletin*, **75**, 63-80.
- Kellerhals, R., Church, M. and Bray, D.I. (1976) Classification of river processes. *Journal of the Hydraulics Division American Society of Civil Engineers*, **102**, HY7, 813-829.
- Kemp, A.C., Horton, B.P., Corbett, D.R., Culver, S.J., Edwards, R.J. and Van de Plassche, O. (2009) The relative utility of foraminifera and diatoms for reconstructing late Holocene sea-level change in North Carolina, USA. *Quaternary Research*, **71**, 9-21.
- Kidson, C. (1986) Sea-level changes in the Holocene. In: Van der Plassche, O. (ed) *Sea-level research: a manual for the collection and evaluation of data*, 27-64. Geo Books, Norwich.

- Kirby, R. (1996) *Hartland Point to Brean Down: Summary of existing knowledge of coastal trends and stability*. Ravensrodd Consultants.
- Knighton, D. (1998) *Fluvial Forms and Processes: a new perspective*. Arnold, London.
- Knighton, D. and Nanson, G.C. (1993) Anastomosis and the continuum of channel pattern. *Earth Surface Processes and Landforms*, **18**, 613-625.
- Knox, J.C. (1985) Responses of floods to Holocene climatic change in the Upper Mississippi Valley. *Quaternary Research*, **23**, 287-300.
- Knox, J.C. (1993) Large increases in flood magnitude in response to modest changes in climate. *Nature*, **361**, 430-435.
- Knox, J.C. (2003) North American palaeofloods and future floods: responses to climatic change. In: Gregory, K.J. and Benito, G. (eds), *Palaeohydrology: Understanding Global Change*. Wiley.
- Krammer, K. and Lange-Bertalot, H. (1986) *Bacillariophyceae. Süßwasserflora von Mitteleuropa, Band 2 Teil 1: Naviculaceae*. Gustav Fischer Verlag, Jena.
- Krammer, K. and Lange-Bertalot, H. (1988) *Bacillariophyceae. Süßwasserflora von Mitteleuropa, Band 2 Teil 2: Bacillariaceae, Epithemiaceae, Surirellaceae*. Gustav Fischer Verlag, Stuttgart.
- Krammer, K. and Lange-Bertalot, H. (1991a) *Bacillariophyceae. Süßwasserflora von Mitteleuropa, Band 2 Teil 3: Centrales, Fragilariaceae, Eunotiaceae*. Gustav Fischer Verlag, Jena/Stuttgart.
- Krammer, K. and Lange-Bertalot, H. (1991b) *Bacillariophyceae. Süßwasserflora von Mitteleuropa, Band 2 Teil 4: Achnanthes, kritische ergänzungen zu Navicula (lineolatae) und Gomphonema*. Gustav Fischer Verlag, Stuttgart/Jena.
- Lamb, A.L., Wilson, G.P. and Leng, M.J. (2006) A review of coastal palaeoclimate and relative sea-level reconstructions using $\delta^{13}\text{C}$ and C/N ratios in organic material. *Earth-Science Reviews* **75**, 29-57.
- Lamb, H.H. (1982) *Climate History and the Modern World*. Methuen, London.
- Lamb, H.H. (1984), In: Flohn, H. and Fantechi, R. (eds) *The Climate of Europe: Past, Present and Future*. Riedel, Dordrecht, 25-64.
- Langdon, P.G., Barber, K.E. and Hughes, P.D. (2003) A 7500-year peat-based palaeoclimatic reconstruction and evidence for an 1100-year cyclicity in bog surface wetness from Temple Hill Moss, Pentland Hills, southeast Scotland. *Quaternary Science Reviews*, **22**, 259-274.

- Lawrence, D.S.L., Allen, J.R.L. and Havelock, G.M. (2004) Salt-marsh morphodynamics: an investigation of tidal flows and marsh channel equilibrium. *Journal of Coastal Research*, **20**, 301-316.
- Lees, J. (1999) Evaluating magnetic parameters for use in source identification, classification and modelling of natural and environmental materials. In: Walden, J., Oldfield, F. and Smith, J. (eds), *Environmental Magnetism: A Practical Guide*. Quaternary Research Association, London.
- Lennon, G.W. (1963a) A frequency investigation of abnormally high tidal levels at certain west coast ports. *Proceedings of the Institution of Civil Engineers*, **25**, 451-484.
- Lennon, G.W. (1963b) The identification of weather conditions associated with the generation of major storm surges along the west coast of the British Isles. *Quarterly Journal of the Royal Meteorological Society*, **89**, 394-3811.
- Leorri, E. and Cearreta, A. (2009) Quantitative assessment of the salinity gradient within the estuarine systems in the southern Bay of Biscay using benthic foraminifera. *Continental Shelf Research*, **29**, 1226-1239.
- Leuschner, H.H., Sass-Klaassen, U., Jansma, E., Baillie, M.G.L. and Spurk, M. (2002) Subfossil European bog oaks: population dynamics and long-term growth depressions as indicators of changes in the Holocene hydro-regime and climate. *The Holocene*, **12**, 695-706.
- Lewin, J. and Macklin, M.G. (2003) Preservation potential for Late Quaternary river alluvium. *Journal of Quaternary Science*, **18**, 107-120.
- Lewin, J., Macklin, M.G. and Johnstone, E. (2005) Interpreting alluvial archives: sedimentological factors in the British Holocene fluvial record. *Quaternary Science Reviews*, **24**, 1873-1889.
- Long, A. (2000) The Mid and Late Holocene evolution of Romney Marsh and the Thames Estuary. *Archaeology in the Severn Estuary* 11, 55-68.
- Long, A.J. (1992) Coastal responses to changes in sea-level in the East Kent Fens and southeast England, UK, over the last 7500 years. *Proceedings of the Geologists' Association*, **103**, 187-199.
- Long, A.J. (2000) The Mid and Late Holocene evolution of Romney Marsh and the Thames Estuary. *Archaeology in the Severn Estuary*, **11**, 55-68.
- Long, A.J. and Hughes, P.D.M. (1995) Evolution of the Dungeness foreland during the last 4000 years. *Marine Geology*, **124**, 253-271.

- Long, A.J., Innes, J.B., Kirby, J.R., Lloyd, J.M., Rutherford, M.M., Shennan, I. and Tooley, M.J. (1998) Holocene sea-level change and coastal evolution in the Humber estuary, eastern England: an assessment of rapid coastal change. *The Holocene*, **8**, 229-247.
- Long, A.J., Scaife, R.G. and Edwards, R.J. (2000) Stratigraphic architecture, relative sea-level, and models of estuary development in southern England: new data from Southampton Water. In: *Pye, K. and Allen, J.R.L. (eds) Coastal and Estuarine Environments: sedimentology, geomorphology and geoarchaeology*. Geological Society, London, Special Publications, **175**, 253-279.
- Long, A.J., Woodroffe, S.A., Dawson, S., Roberts, D.H., Bryant, C.L. (2008) Late Holocene relative sea level rise and the Neoglacial history of the Greenland ice sheet. *Journal of Quaternary Science*, **24**, 345-359.
- Lowe, J.J. and Walker, M.J.C. (1997) *Reconstructing Quaternary Environments*. 2nd edn. Longman, Harlow.
- Macklin, M.G. & Lewin, J. (1986) Terraced fills of Pleistocene and Holocene age in the Rheidol Valley, Wales. *Journal of Quaternary Science*. **1**(1), 21-34.
- Macklin, M.G. and Lewin, J. (1993) Holocene river alluviation in Britain. *Zeitschrift für Geomorphologie Supplement-Band*, **88**, 109-122.
- Macklin, M.G. and Lewin, J. (2003) River sediments, great floods and centennial-scale Holocene climate change. *Journal of Quaternary Science*, **18**, 101-105.
- Macklin, M.G., Johnston, E. and Lewin, J. (2005) Pervasive and long-term forcing of Holocene river instability and flooding in Great Britain by centennial-scale climate change. *The Holocene*, **15**(7), 937-943.
- Macklin, M.G., Benito, G., Gregory, K.J., Johnstone, E., Lewin, J., Michczynska, D.J., Soja, R., Starkel, L. and Thorndycraft, V.R. (2006) Past hydrological events reflected in the Holocene fluvial record of Europe. *Catena*, **66**, 145-154.
- Maddy, D., Passmore, D.G. and Lewis, S. (2003) Fluvial morphology and sediments: Archives of past fluvial system response to global change. In: Gregory, K.J. and Benito, G. (eds), *Palaeohydrology: Understanding Global Change*. Wiley, 273-289.
- Madsen, A.T., Murray, A.S., Andersen, T.J., Pejrup, M. and Breuning-Madsen, H. (2005) Optically stimulated luminescence dating of young estuarine sediments: a comparison with ²¹⁰Pb and ¹³⁷Cs dating. *Marine Geology*, **214**, 251-268.
- Magny, M. (1998) Reconstruction of Holocene lake-level changes in the Jura (France): methods and results. In: Harrison, S.P., Frenzel, B., Huckried, U. and Weiss, M.

- (eds.) *Palaeohydrology as reflected in lake-level changes as climatic evidence for Holocene times*. Paläoklimaforschung 25. Akademie der Wissenschaften und Literatur, 67-85.
- Magny, M. (2004) Holocene climate variability as reflected by mid-European lake-level fluctuations and its probable impact on prehistoric human settlements. *Quaternary International*, **113**, 65-79.
- Magny, M., Begeot, C., Guiot, J., Peyron, O. (2003) Contrasting patterns of hydrological changes in Europe in response to Holocene climate cooling phases. *Quaternary Science Reviews*, **22**, 1589-1596.
- Maher, B.A. (1986) Characterization of soils by mineral magnetic measurements. *Physics of Earth and Planetary Interiors*, **42**, 76-92.
- Maher, B.A. (1988) Magnetic properties of some synthetic sub-micron magnetites. *Geophysical Journal of the Royal Astronomical Society*, **94**, 83-96.
- Makaske, B. (2001) Anastomosing rivers: a review of their classification, origin and sedimentary products. *Earth-Science Reviews*, **53**, 149-196.
- Malamud-Roam, F.P. and Ingram, B.L. (2004) Late Holocene $\delta^{13}\text{C}$ and pollen records of paleosalinity from tidal marshes in the San Francisco Bay estuary, California. *Quaternary Research*, **62**, 134-145.
- Malamud-Roam, F.P., Ingram, B.L., Hughes, M. and Florsheim, J.L. (2006) Holocene paleoclimate records from a large California estuarine system and its watershed region: linking watershed climate and bay conditions. *Quaternary Science Reviews*, **25**, 1570-1598.
- Manning, C. (2007) *Braunton Marsh Management Study 2007*. Taw Torridge Estuary Forum.
- Massey, A.C., Paul, M.A., Gehrels, W.R. and Charman, D.J. (2006) Autocompaction in Holocene coastal back-barrier sediments from south Devon, southwest England, UK. *Marine Geology*, **226**, 225-241.
- Massey, A.C., Gehrels, W.R., Charman, D.J., Milne, G.A., Peltier, W.R., Lambeck, K. and Selby, K.A. (2008) Relative sea-level change and postglacial isostatic adjustment along the coast of south Devon, United Kingdom. *Journal of Quaternary Science*, **23**, 415-433.
- Mauquoy, D. and Barber, K.E. (1999) A replicated 3000 year proxy-climate record from Coom Rigg Moss and Felecia Moss, The Border Mires, northern England. *Journal of Quaternary Science*, **14**, 263-275.

- May, M.D. (1999) *Vegetation and salinity changes over the last 2000 years at two islands in the northern San Francisco Estuary, California*. Unpublished M.A. Thesis, University of California, Berkeley, 55pp.
- May, V.J. and Hansom, J.D. (2003) *Coastal Geomorphology of Great Britain*. Geological Conservation Review Series, No. 28, Joint Nature Conservation Committee, Peterborough, 754pp.
- Merryfield, D.L. and Moore, P.D. (1974) Prehistoric human activity and blanket peat initiation on Exmoor. *Nature*, **250**, 439-441.
- Moore, P.D., Merryfield, D.L. and Price, M.D.R. (1984) The vegetation and development of blanket mires. In: Moore, P.D. (ed), *European Mires*, 203-235. Academic Press, London.
- Moore, A.J., Passmore, D.G. and Stevenson, A.C. (1999) High resolution palaeochannel records of Holocene Valley floor environments in the North Tyne basin, Northern England. In: Brown, A.G. and Quine, T.A. (eds), *Fluvial Processes and Environmental Change*, Wiley.
- Moskowitz, B.M., Frankel, R.B. and Bazilinski, D.A. (1993) Rock magnetic criteria for the detection of biogenic magnetite. *Earth and Planetary Science Letters*, **120**, 283-300.
- Najjar, R.G. (1999) The water balance of the Susquehanna River Basin and its response to climate change. *Journal of Hydrology*, **219**, 7-19.
- Nanson, G.C. (1986) Episodes of vertical accretion and catastrophic stripping: a model of disequilibrium flood-plain development. *Bulletin of the American Geological Society*, **97**, 1467-1475.
- Needham, S. (1989) River valleys as wetlands: the archaeological prospects, In: Coles, J.M. and Coles, B.J. (eds), *The Archaeology of Rural Wetlands*. WARP and English Heritage, 29-34.
- Nelson, A.R. and Kashima, K. (1993) Diatom zonation in southern Oregon tidal marshes relative to vascular plants, foraminifera and sea level. *Journal of Coastal Research*, **9**(3), 673-697.
- Nelson, A.R., Sawai, Y., Jennings, A.E., Bradley, L.A., Gerson, L., Sherrod, B.L., Sabeau, J. and Horton, B.P. (2008) Great-earthquake paleogeodesy and tsunamis of the past 2000 years at Alsea Bay, central Oregon coast, USA. *Quaternary Science Reviews*, **27**, 747-768.

- Nesje, A., Lie, O. and Dahl, S.O. (2000) Is the North Atlantic Oscillation reflected in Scandinavian glacier mass balance records? *Journal of Quaternary Science*, **15**, 587-601.
- Oldfield, F., (1994) Toward the discrimination of fine grained ferrimagnets by magnetic measurements in lake and near-shore marine sediments. *Journal of Geophysical Research*, **99**, 9045-9050.
- Oldfield, F., (1999) The rock magnetic identification of magnetic mineral and grain size assemblages. In: Walden, J., Oldfield, F. and Smith, J.P. (eds), *Environmental Magnetism: a practical guide*, 98-112. Technical Guide 6, Quaternary Research Association, London.
- Oldfield, F. and Yu, L. (1994) The influence of particle-size variations on the magnetic properties of sediments from the N.E. Irish Sea. *Sedimentology*, **41**, 1093-1108.
- Oldfield, F., Barnosky, C., Leopold, E.B. and Smith, J.P. (1983) Mineral magnetic studies of lake sediments: a brief review. *Hydrobiologia*, **103**, 37-44.
- Oldfield, F., Maher, B.A., Donoghue, J. and Pierce, J. (1985) Particle-size related mineral magnetic source-sediment linkages in the Rhode River catchment, Maryland, USA. *Journal of Geology*, **142**, 1035-1046.
- Oldfield, F., Maher, B.A. and Appleby, P.G. (1989). Sediment source variations and Pb-210 inventories in recent Potomac Estuary sediment cores. *Journal of Quaternary Science*, **4**, 189-200.
- Oldfield, F. (1991) Environmental magnetism – a personal perspective. *Quaternary Science Reviews*, **10**, 73-85.
- Oldfield, F., Darnley, I., Yates, G., France, D.E. and Hilton, J. (1992) Storage diagenesis versus sulphide authigenesis: possible implications in environmental magnetism. *Journal of Paleolimnology*, **7**, 179-189.
- Oldfield, F., Asioli, A., Accorsi, C.A., Mercuri, A.M., Juggins, S., Langone, L., Rolph, T., Trincardi, F., Wolff, G., Gibbs, Z., Vigliotti, L., Frignani, M., Van der Post, K. and Branch, N. (2003) A high resolution late Holocene palaeoenvironmental record from the central Adriatic Sea. *Quaternary Science Reviews*, **22**, 319-342.
- Oost, A.P., de Haas, H., Ijnsen, F., van der Boogert, J.K. and de Boer, P.L. (1993) The 18.6yr nodal cycle and its impact on tidal sedimentation. *Sedimentary Geology*, **87**, 1-11.
- Packham, J.R. and Willis, A.J. (2001) Braunton Burrows in context: a comparative management study. In: Houston, S.E. and Rooney, P.J. (eds), *Coastal dune*

- management: shared experience of European conservation practice*. Liverpool University Press.
- Palmer, A.J.M. and Abbott, W.H. (1986) Diatoms as indicators of sea-level change. In: Van der Plassche, O. (ed), *Sea-Level Research: a manual for the collection and evaluation of data*, 457-488. Geo Books, Norwich.
- Passmore, D.G. and Macklin, M.G. (2001) Holocene sediment budgets in an upland gravel bed river: the River South Tyne, northern England. In: Maddy, D., Macklin, M.G. and Woodward, J.C. (eds), *River Basin Sediment Systems: Archives of Environmental Change*. Balkema: Rotterdam, pp 423-444.
- Patterson, R.T., Hutchinson, I., Guilbault, J.-P. and Clague, J.J. (2000) A comparison of the vertical zonation of diatom, foraminifera, and macrophyte assemblages in a coastal marsh: implications for greater paleo-sea level resolution. *Micropaleontology*, **46**, 229-244.
- Patterson, R.T., Dalby, A.P., Roe, H.M., Guilbault, J.-P., Hutchinson, I. and Clague, J.J. (2005) Relative utility of foraminifera, diatoms and macrophytes as high resolution indicators of paleo-sea level in coastal British Columbia, Canada. *Quaternary Science Reviews*, **24**, 2002-2014.
- Paul, M.A. and Barras, B.F. (1998) A geotechnical correction for post-depositional sediment compression: examples from the Forth valley, Scotland. *Journal of Quaternary Science*, **13**, 171-176.
- Pearson, G.W., Pilcher, J.R., Baillie, M.G.L., Corbett, D.M. and Qua, F (1986) Highprecision ¹⁴C measurement of Irish oaks to show the natural ¹⁴C variations from AD 1840 to 5210 BC. *Radiocarbon*, **28**, 839-862.
- Peltier, W.R., Shennan, I., Drummond, R. and Horton, B.P. (2002) On the post-glacial isostatic adjustment of the British Isles and the shallow visco-elastic structure of the Earth. *Geophysical Journal International*, **148**, 443-475.
- Peterson, D.H., Cayan, D.R., DiLeo, J., Noble, M. and Dettinger., M. (1995) The role of climate in estuarine variability. *The American Scientist*, **83**, 58-67.
- Pethick, J.S. (1981) Long-term Accretion Rates on Tidal Salt Marshes. *Journal of Sedimentary Petrology*, **51**(2), 571-577.
- Pethick, J.S. (1984) *An Introduction to Coastal Geomorphology*. Arnold, London.
- Pethick, J.S. (2007) *The Taw-Torridge Estuaries: geomorphology and management report to the Taw-Torridge Estuaries Officers Group*. UNESCO Biosphere Reserve for North Devon

- Pizzuto, J.E. and Schwendt, A.E. (1997) Mathematical modelling of autocompaction of a Holocene transgressive valley-fill deposit, Wolfe Glade, Delaware. *Geology*, **25**, 57-60.
- Plater, A.J. and Shennan, I. (1992) Evidence of Holocene sea-level change from the Northumberland coast, eastern England. *Proceedings of the Geologists' Association*, **103**, 201-216.
- Prentice, I.C. (1986) Multivariate methods for data analysis. In: Berglund, B.E. (ed) *Handbook of Holocene Palaeoecology and Palaeohydrology*, 775-798. Wiley, London.
- Prescott, J.R. and Hutton, J.T. (1994) Cosmic ray contributions to dose rates for luminescence and ESR dating: large depths and long-term time variations. *Radiation Measurements*, **23**, 497-500.
- Pritchard, D.W. (1967) What is an estuary? Physical viewpoint. In: Laugh, G.H. (ed.) *Estuaries*. American Association for the advancement of science, Publication 83, p.3-5.
- Pye, K. (1992) Saltmarshes on the barrier coastline of North Norfolk, eastern England, In: Allen, J.R.L. and Pye, K. (eds), *Saltmarshes: Morphodynamics, Conservation and Engineering Significance*. Cambridge University Press, pp. 148-178.
- Pye, K. and French, P.W. (1993) *Erosion and accretion processes on British salt marshes, Vol.1, Introduction: Saltmarsh processes and morphology*. Cambridge Environmental Research Consultants.
- Ratcliffe, J. and Straker, V. (1996) *The early environment of Scilly*. Cornwall Archaeological Unit, Cornwall County Council: Truro, UK.
- Rees, J.G., Ridgway, J., Ellis, S., Knox, R.W.O'B., Newsham, R. and Parkes, A. (2000) Holocene sediment storage in the Humber Estuary. In: Shennan, I. and Andrews, J. (eds) *Holocene Land-Ocean interaction and Environmental change around the North Sea*. Geological Society Special Publications **166**, 119-143.
- Reimer, P.J., Baillie, M.G.L., Bard, E., Bayliss, A., Beck, J.W., Blackwell, P.G., Buck, C.E., Burr, G.S., Cutler, K.B., Damon, P.E., Edwards, R.L., Fairbanks, R.G., Friedrich, M., Guilderson, T.P., Herring, C., Hughen, K.A., Kromer, B., McCormac, F.G., Manning, S.W., Ramsey, C.B., Reimer, R.W., Remmele, S., Southon, J.R., Stuiver, M., Talamo, S., Taylor, F.W., van der Plicht, J., and Weyhenmeyer, C.E. (2004) IntCal04 Terrestrial radiocarbon age calibration, 0-26 cal kyr BP. *Radiocarbon*, **46**, 3, 1029-1058.

- Rijk, S. (1995a) *Agglutinated Foraminifera as indicators of Salt Marsh Development in relation to Late Holocene Sea Level Rise (Great Marshes at Barnstable, Massachusetts)*. Free University of Amsterdam. (Published PhD thesis.)
- Rijk, S. (1995b) Salinity Control on the distribution of salt marsh foraminifera (Great Marshes, Massachusetts). *Journal of Foraminiferal Research*, **25**, 156-166.
- Rijk, S. & Troelstra, S.R. (1997) Salt marsh foraminifera from the Great Marshes, Massachusetts: environmental controls. *Paleogeography, Palaeoclimatology, Palaeoecology*, **130**, 81-112.
- Risdon, T. (1620) *The Chorographical Description or Survey of the County of Devon and the City and County of Exeter*. Porcupines, Barnstaple (1970 facsimile reprint of 1811 edn, London: Printed for Rees & Curtis, Plymouth, 1811).
- Rittenour, T.M. (2008) Luminescence dating of fluvial deposits: applications to geomorphic, palaeoseismic and archaeological research. *Boreas*, **37**, 613-635.
- Rittenour, T.M., Goble, R.J. and Blum, M.D. (2003) An optical age chronology of Late Pleistocene fluvial deposits in the northern lower Mississippi valley. *Quaternary Science Reviews*, **22**, 1105-1110.
- Rittenour, T.M., Goble, R.J. and Blum, M.D. (2005) Development of an OSL chronology for Late Pleistocene channel belts in the lower Mississippi valley, USA. *Quaternary Science Reviews*, **24**, 2539-2554.
- Rittenour, T.M., Goble, R.J. and Blum, M.D. (2007) Fluvial evolution of the lower Mississippi valley during the last 100 k.y. glacial cycle: response to glaciation and sea-level change. *Geological Society of America Bulletin*, **119**, 586-608.
- Roberts, A.P. (1995) Magnetic properties of sedimentary greigite (Fe₃S₄). *Earth and Planetary Science Letters*.
- Roberts, H.M. and Plater, A.J. (2007) Reconstruction of Holocene foreland progradation using optically stimulated luminescence (OSL) dating: an example from Dungeness, UK. *The Holocene*, **17**, 495-505.
- Robinson, D.N. (1970) Coastal evolution in north-east Lincolnshire. *East Midland Geographer*, **5**, 62-70.
- Robinson, M.A. and Lambrick, G.H. (1984) Holocene alluviation and hydrology in the upper Thames basin. *Nature*, **308**, 809-814.
- Rockware Incorporated (1983-2004) *RockWorks 2004*, version 4.11.1. Golden, Colorado.
- Rumsby, B.T. and Macklin, M.G. (1996) River response to the last neoglacial (the 'Little Ice Age') in northern, central and western Europe, In: Branson, J.,

- Brown, A.G. and Gregory, K.J. (eds) *Global Continental Changes: The Context of Palaeohydrology*. Geological Society Special Publications, **115**, 217-233.
- Rybczyk, J.M., Callaway, J. and Day Jr., J.W. (1998) A relative elevation model (REM) for a subsiding coastal forested wetland receiving wastewater effluent. *Ecological Modeling*, **112**, 23-44.
- Sawai, Y., Nagumo, T. and Horton, B.P. (2004) Diatom-based transfer function along the Pacific coast of eastern Hokkaido, northern Japan – an aid in paleoseismic study along the coasts near Kurilesubduction zone. *Quaternary Science Reviews*, **23**, 2467-2484.
- Schumm, S.A. (1963) Sinuosity of alluvial rivers on the Great Plains. *Bulletin of the Geological Society of America*, **74**, 1089-1100.
- Schumm, S.A. (1981) Evolution and response of the fluvial system, sedimentologic implications. *Society of Economic paleontologists and Mineralogists Special Publication*, **31**, 19-29.
- Schumm, S.A. (1985) Patterns of alluvial rivers. *Annual Review of Earth and Planetary Sciences*, **13**, 5-27.
- Schumm, S.A. and Khan, H.R. (1972) Experimental study of channel patterns. *Bulletin of the Geological Society of America*, **83**, 1755-1770.
- Scott, D.B. and Greenberg, D.A. (1993) Relative sea-level rise and tidal development in the Fundy tidal system. *Canadian Journal of Earth Science*, **20**, 1554-1564.
- Selby, K.A. and Smith, D.E. (2007) Late Devensian and Holocene relative sea-level changes on the Isle of Skye, Scotland, UK. *Journal of Quaternary Science*, **22**, 119-139.
- Shennan, I. (1982) Interpretation of the Flandrian sea-level data from the Fenland, England. *Proceedings of the Geologists Association*, **93**, 53-63.
- Shennan, I. (1986) Flandrian sea-level changes in the Fenland, II: Tendencies of sea-level movement, altitudinal changes and local and regional factors. *Journal of Quaternary Science*, **1**, 77-89.
- Shennan, I. and Horton, B. (2002) Holocene land- and sea-level changes in Great Britain. *Journal of Quaternary Science*, **17**(5-6), 511-526.
- Shennan, I. and Waller, M. (1994) Depositional environments. In: Waller, M. *The Fenland Project, Number 9: Flandrian environmental change in Fenland*. East Anglian Archaeology Report No 70, Chelmsford, 35-46.
- Shennan, I., Tooley, M.J., Davis, M.J. and Haggart, B.A. (1983) Analysis and interpretation of Holocene sea-level data. *Nature*, **302**, 404-406.

- Shennan, I., Innes, J.B., Long, A.J. and Zong, Y. (1995) Holocene relative sea-level changes and coastal vegetation history at Kentra Moss, Argyll, northwest Scotland. *Marine Geology*, **124**, 43-59.
- Shennan, I., Long, A.J., Rutherford, M.M., Green, F.M., Innes, J.B., Lloyd, J.M., Zong, Y. and Walker, K.J. (1996) Tidal marsh stratigraphy, sea-level change and large earthquakes, I: A 5000 year record in Washington, USA. *Quaternary Science Reviews*, **15**, 1023-1059.
- Shennan, I., Horton, B., Innes, J., Gehrels, R., Lloyd, J., McArthur, J. and Rutherford, M. (2000a) Late Quaternary sea-level changes, crustal movements and coastal evolution in Northumberland, UK. *Journal of Quaternary Science*, **15**, 215-137.
- Shennan, I., Lambeck, K., Horton, B., Innes, J., Lloyd, J., McArthur, J. and Rutherford, M. (2000b) Holocene isostasy and relative sea-level changes on the east coast of England. In: Shennan, I. and Andrews, J. (eds) *Holocene land-ocean interaction and environmental change around the North Sea*. Geological Society, London, Special Publication, **166**, 275-298.
- Shennan, I., Lambeck, K., Flather, R., Horton, B., McArthur, J., Innes, J., Lloyd, J., Rutherford, M. and Wingfield, R. (2000c) Modelling western North Sea palaeogeographies and tidal changes during the Holocene. In: Shennan, I. and Andrews, J. (eds) *Holocene Land-Ocean interaction and Environmental change around the North Sea*. Geological Society, London, Special Publications, **166**, 299-319.
- Shennan, I., Peltier, W.R., Drummond, R. and Hortonm B.P. (2002) Global to local scale parameters determining relative sea-level changes and the post-glacial isostatic adjustment of Great Britain. *Quaternary Science Reviews*, **21**, 397-408.
- Shennan, I., Coulthard, T., Flather, R., Horton, B., Macklin, M., Rees, J.G. and Wright, M. (2003) Integration of shelf evolution and river basin models to simulate Holocene sediment dynamics of the Humber Estuary during periods of sea-level change and variations in catchment supply. In: Neal, C., Leeks, G.L., Millward, G.E., Harris, J.R.W., Huthnance, J.M. and Rees, J.G. (eds.) *Land ocean interaction: processes, functioning and environmental management: a UK perspective*. *Science of the Total Environment*, **314-316**, 737-754.
- Shennan, I., Bradley, S., Milne, G., Brooks, A., Bassett, S. and Hamilton, S. (2006) Relative sea-level changes, glacial isostatic modelling and ice-sheet reconstructions from the British Isles since the Last Glacial Maximum. *Journal of Quaternary Science*, **21**, 585-599.

- Sherrod, B.L. (1999) Gradient analysis of diatom assemblages in a Puget Sound salt marsh: can such assemblages be used for quantitative paleoecological reconstructions?, *149*, 213-226.
- Siddell, J., Wilkinson, K., Scaife, R. and Cameron, N. (2000) *The Holocene evolution of the London Thames*. London, Museum of London Archaeological Service Monograph 5.
- Simmons, I.G. (1964) Pollen Diagrams from Dartmoor. *New Phytologist*, **63**, 165-180.
- Smith, A.G. and Morgan, L.A. (1989) A succession to ombrotrophic bog in the Gwent Levels and its demise: a Welsh parallel to the peats of the Somerset Levels. *New Phytologist*, **112**, 145-167.
- Smith, J. (1999) An introduction to the magnetic properties of natural materials, In: Walden, J., Oldfield, F. and Smith, J. (eds.), *Environmental Magnetism: A Practical Guide*. Quaternary Research Association, London.
- Smith, D.G. and Smith, N.D. (1980) Sedimentation in anastomosing river systems: examples from alluvial valleys near Banff, Alberta. *Journal of Sedimentary Petrology*, **50**, 157-164..
- Smith, D.E., Haggart, B.A., Cullingford, R.A., Tipping, R.M., Wells, J.M., Mighall, T.M. and Dawson, S. (2003) Holocene relative sea-level change in the lower Nith valley and estuary. *Scottish Journal of Geology*, **39**, 97-120.
- Snowball, I.F. (1991) Magnetic hysteresis properties of greigite (Fe₃S₄) and a new occurrence in Holocene sediments from Swedish Lapland. *Physics of the Earth and Planetary Interiors*, **68**, 32-40.
- Snowball, I.F. (1994) Bacterial magnetite and the magnetic properties of sediments in a Swedish lake. *Earth and Planetary Science Letters*, **126**, 129-142.
- Snowball, I.F. and Thompson, R. (1988) The occurrence of greigite in sediments from Loch Lomond. *Journal of Quaternary Science*, **3**, 121-125.
- Stanley, J.D. (2001) Dating modern deltas: Progress, problems, and prognostics. *Annual Review of Earth and Planetary Sciences*, **29**, 257-294.
- Starkel, L. (2003) Short-term hydrological changes, In: Gregory, K.J. and Benito, G. (eds), *Palaeohydrology: Understanding Global Change*. Wiley, 337-356.
- Steel, T.J. and Pye, K. (1997) The development of saltmarsh tidal creek networks: evidence from the UK. *Proceedings of the Canadian Coastal Conference 1997*, pp 267-280.
- Stuiver, M. and Reimer, P.J. (1993) Extended ¹⁴C database and revised CALIB 3.0 ¹⁴C calibration program. *Radiocarbon*, **35**, 215-230.

- Sullivan, M.J. (1975) Diatom communities from a Delaware saltmarsh. *Journal of Phycology*, **11**, 384-390.
- Szkornik, K., Kirby, J.R. & Gehrels, W.R. (2006) Salt-marsh diatom distributions in Ho Bugt (western Denmark) and the development of a transfer function for reconstructing Holocene sea-level changes. *Marine Geology*, **235**, 137-150.
- Taylor, M.P. and Macklin, M.G. (1997) Holocene alluvial sedimentation and valley floor development: the River Swale, Catterick, North Yorkshire, UK. *Proceedings of the Yorkshire Geological Society*, **51**(4), 317-327.
- Taylor, M.P., Macklin, M.G. and Hudson-Edwards, K. (2000) River sedimentation and fluvial response to Holocene environmental change in the Yorkshire Ouse Basin, northern England. *The Holocene*, **10**, 201-212.
- Ter Braak, C.J.F. (1986) Canonical correspondence analysis: a new eigenvector technique for multivariate direct gradient analysis. *Ecology*, **67**, 1167-1179.
- Ter Braak, C.J.F. (1987) The analysis of vegetation-environment relationships by canonical correspondence analysis, *Vegetatio*, **69**, 69-77.
- Ter Braak, C.J.F. and Prentice, I.C. (1988) A theory of gradient analysis. *Advances in Ecological Research*, **18**, 271-317.
- Tooley, M.J. (1978) *Sea-level changes. North-west England during the Flandrian Stage*. Clarendon Press.
- Törnqvist, T.E., González, J.L., Newsom, L.E., Van der Borg, K., De Jong, A.F.M. and Kurnik, C.W. (2004) Deciphering Holocene sea-level history on the U.S. Gulf Coast: a high-resolution record from the Mississippi Delta. *Geological Society of America Bulletin*, **116**: 1026-1039.
- Tovey, N.K. and Paul, M.A. (2002) Modelling self-weight consolidation in Holocene sediments. *Bulletin of the International Association of Engineering Geologists*, **61**, 21-33.
- Troels-Smith, J. (1955) Characterization of unconsolidated sediments. *Danmarks Geologiske Undersøgelse, Series IV*, **3**, 38-73.
- Tucker, M.E. (1996) *Sedimentary Rocks in the Field* (2nd edition). Wiley, Chichester.
- Turney, C., Baillie, M., Clemens, S., Brown, D., Palmer, J., Pilcher, J., Reimer, P. and Leuschner, H.H. (2005) Testing solar forcing of pervasive Holocene climate cycles. *Journal of Quaternary Science*, **20**, 511-518.
- Uehara, K., Scourse, J.D., Horsburgh, K.J., Lambeck, K. and Purcell, A.P. (2006) Tidal evolution of the northwest European shelf seas from the Last Glacial Maximum to the present. *Journal of Geophysical Research-Oceans*, **111** (C9), C09025.

- Van Dam, H., Mertens, A. and Sinkeldam, J. (1994) A coded checklist and ecological indicator values of freshwater Diatoms from The Netherlands. *Netherlands Journal of Aquatic Ecology*, **28**(1), 117-133.
- Van de Plassche, O (1977) A manual for sample collection and evaluation of sea level data. Amsterdam, Free University, Institute for Earth Sciences, IGCP Project 61 (unpublished manuscript).
- Van de Plassche, O. (1986) Introduction in Van de Plassche, O. (ed), *Sea-level research: a manual for the collection and evaluation of data*. Geo Books, Norwich.
- Van den Berg, J.H. (1995) Prediction of alluvial channel pattern of perennial rivers. *Geomorphology*, **12**, 259-279.
- Van der Werff, A. (1958) L'importance de la recherche sur les diatomées par la paléobotanique. *Bulletin de la Société Botanique du Nord de la France*, **11**, 94-97.
- Van der Werff, A. and Huls, H. (1957-1974) *Diatomeenflora van Nederland*, 8 parts. Reprint 1976, Otto Koeltz Science Publications, Koenigstein.
- Vos, P.C. and de Wolf, H. (1988) Methodological aspects of paleoecological diatom research in coastal areas of the Netherlands. *Geologie en Mijnbouw*, **67**, 31-40.
- Vos, P.C. and de Wolf, H. (1993a) Diatoms as a tool for reconstructing sedimentary environments in coastal wetlands; methodological aspects. *Hydrobiologia*, **269/270**, 285-296.
- Vos, P.C. and de Wolf, H. (1993b) Reconstruction of sedimentary environments in Holocene coastal deposits of the southwest Netherlands; the Poortvliet boring, a case study of palaeoenvironmental diatom research. *Hydrobiologia* **269/270**, 297-306.
- Vos, P.C. and van Heeringen, R.M. (1997) Holocene geology and occupation history of the Province of Zeeland (SW Netherlands), In: Fischer, M.M. (ed) *Holocene Evolution of Zeeland (SW Netherlands)*.
- Walden, J. (1999a) Remanence measurements. In: Walden, J., Oldfield, F. and Smith, J.P. (eds), *Environmental Magnetism: a practical guide*, 63-88. Technical Guide 6, Quaternary Research Association, London.
- Walden, J. (1999b) Sample collection and preparation. In: Walden, J., Oldfield, F. and Smith, J.P. (eds), *Environmental Magnetism: a practical guide*, 26-34. Technical Guide 6, Quaternary Research Association, London.
- Walker, M. (2005) *Quaternary Dating Methods*. Wiley, Chichester.

- Waller, M.P. and Long, A.J. (2003) Holocene coastal evolution and sea-level change on the southern coast of England: a review. *Journal of Quaternary Science*, **18**(3-4), 351-359.
- Waller, M., Aldertan, A. and Switsur, R. (1994) Methods of Reconstruction. In: Waller, M. *The Fenland Project, Number 9: Flandrian environmental change in Fenland*, 18-34. East Anglian Archaeology Report No 70, Chelmsford.
- Wallinga, J. (2002) Optically stimulated luminescence dating of fluvial deposits: a review. *Boreas*, Vol.31, pp 303-322.
- Wallinga, J., Murray, A.S., Duller, G.A.T. and Tornqvist, T.E. (2001) Testing optically stimulated luminescence dating of sand-sized quartz and feldspar from fluvial deposits. *Earth and Planetary Science Letters*, **193**, 617-630.
- Wheeler, A.J., Oldfield, F. and Orford, J.D. (1999) Depositional and post-depositional controls on magnetic signals from saltmarshes on the north-west coast of Ireland. *Sedimentology*, **46**, 545-558.
- Willard, D.A., Cronin, T.M. and Verardo, S. (2003) Late-Holocene climate and ecosystem history from Chesapeake Bay sediment cores, USA. *The Holocene*, **13**, 201-214.
- Williams, H. (2003) Modeling shallow autocompaction in coastal marshes using cesium-137 fallout: preliminary results from the Trinity River Estuary, Texas. *Journal of Coastal Research*, **19**, 180-188.
- Wimble, G.A. (1986) *The palaeoecology of the lowland coastal raised mires of south Cumbria*. PhD thesis, University of Wales.
- Yang, B., Dalrymple, R.W., Gingras, M.K., Chun, S. and Lee, H. (2007) Up-estuary variation of sedimentary facies and ichnocoenoses in an open-mouthed, macrotidal, mixed-energy estuary, Gomso Bay, Korea. *Journal of Sedimentary Research*, **77**, 757-771.
- Zong, Y. (1997) Mid and Late Holocene sea-level changes in Roudsea Marsh, northwest England: a diatom biostratigraphical investigation. *The Holocene*, **7**(3), 311-323.
- Zong, Y. (1998) Diatom records and sedimentary responses to sea-level change during the last 8000 years in Roudsea Wood, northwest England. *The Holocene*, **8**(2), 219-228.
- Zong, Y. and Horton, B.P. (1998) Diatom zones across intertidal flats and coastal saltmarshes in Britain. *Diatom Research*, **13**, 375-394.

- Zong, Y. and Horton, B.P. (1999) Diatom-based tidal-level transfer functions as an aid in reconstructing Quaternary history of sea-level movements in the UK. *Journal of Quaternary Science*, **14**(2), 153-167.
- Zong, Y. and Tooley, M.J. (1996) Holocene sea-level changes and crustal movements in Morecambe Bay, northwest England. *Journal of Quaternary Science*, **11**, 43-58.
- Zong, Y., Lloyd, J.M., Leng, M.J., Yim, W.W.-S. and Huang, G. (2006) Reconstruction of Holocene monsoon history from the Pearl River Estuary, southern China, using diatoms and carbon isotope ratios. *The Holocene*, **16**, 251-263.